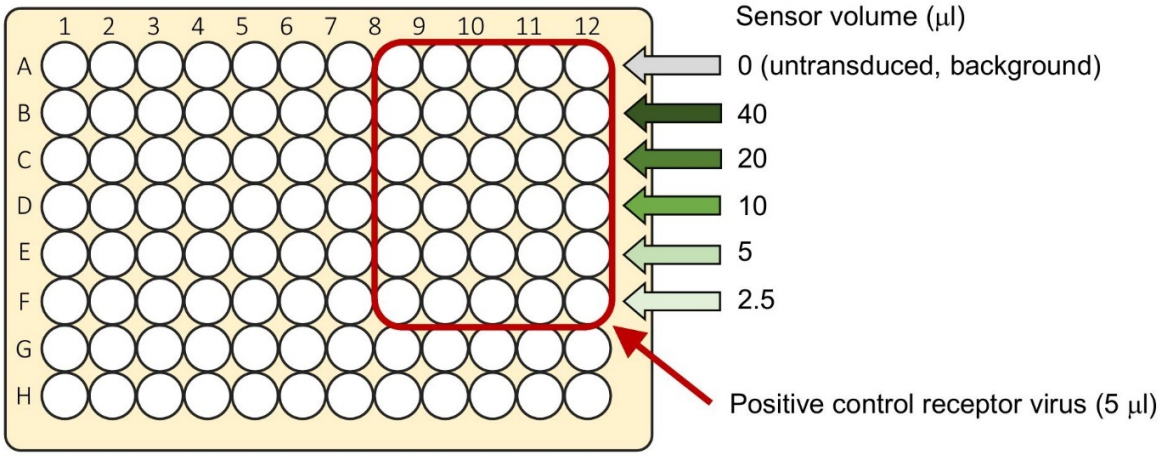
5. Cover plate to protect from light and let rest at room temperature for 30 minutes.
6. Incubate cells for 20-24 hours under normal growth conditions (5% CO_2, 37°C), protected from light.

Box 1. Optimizing amount of sensor by titration.

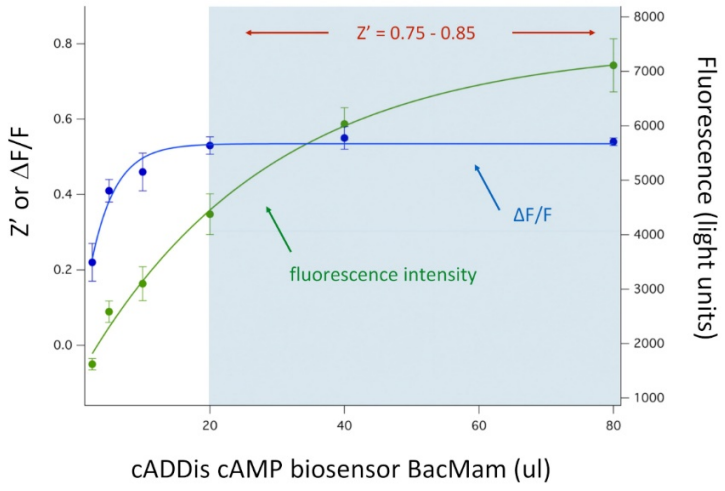
A titration series is used to determine the optimal amount of sensor.

Step 1. Set up the titration plate as illustrated below. Make up transduction mix as described in Cell Culture and Viral Transduction. Be sure to include control wells (untransduced cells, Row A) in order to calculate the signal-to-background ratio. In columns 9-12, add positive control receptor (supplied with kit). Include indicated volume of sensor and 0.6 µl 500 mM sodium butyrate and make up to 50 µl with cell culture medium.



Step 2. After 24 hours, measure baseline fluorescence intensity then add ligand and measure fluorescence as described in Assay for Signal Transduction.

Step 3. Select optimal sensor volume based on signal-to-background, response to ligand and cell health (sample data below). Signal-to-background ratio should be at least 5, and is the average fluorescence from wells with biosensor, compared with fluorescence from untransduced cells.



Assay for Signal Transduction

1. Replace culture medium with 150 µl assay buffer and leave at room temperature for 30 min. During this time, inspect cells for cell health.
2. Immediately before addition of stimulating compounds, measure the baseline fluorescence intensity in all the wells at multiple time points for five minutes. This baseline recording is necessary for the data normalization step in Data Normalization below.
3. Add stimulating compound to the wells in assay buffer in a volume of 50 µl, and immediately commence reading the fluorescence intensity. Measure repeatedly, with the read frequency appropriate for the time course of the response (see Timeframe of Response Measurement).
4. Continue reading fluorescence intensity until the response level has stabilized or decayed back to baseline.

Data Normalization

The raw data generated by the reader is fluorescence intensity in relative light units. It is standard practice in the biosensor field to normalize these data before they are further analyzed (Figure 4). The type of normalization used is normalization to baseline. Baseline means the fluorescence intensity before the addition of a stimulating ligand. (This is why the baseline is recorded, as described in Assay for Signal Transduction.) The average of the fluorescence intensity readings before ligand addition is taken as the baseline (Figure 4). Then the fluorescence intensity after ligand addition is divided by this mean baseline signal (Figure 4). This metric is described as "Fluorescence normalized to baseline" and is often termed F / ΔF in the biosensor literature. The data are handled in this way because it enables a convenient intra-well control, minimizing error due to any slight well-to-well differences in the number of cells or amount of sensor.

Biosensor responses can sometimes be difficult to interpret because of the use of downward sensors (which decrease in signal as the analyte increases) and also because some GPCRs signals are inhibitory (for example the decrease of cAMP produced by Gi). We advocate normalizing the data in such a way that the signal value reflects the concentration of the analyte being detected. In other words, the direction of the sensor data should be the same as the direction of the analyte concentration. This means that for downward sensors we convert the downward baseline-normalized fluorescence values to upward values. In this way, an increase of the signaling analyte is represented by an increase of the biosensor response value. The conversion can be done as follows:

$$\text{Upward} = 2 - \left(\frac{\text{F}}{\Delta\text{F}}\right)_{\text{Downward}}$$

This formula yields upward data with baseline equal to 1.

This normalization recommendation means that when the signal itself is inhibitory, e.g. inhibition of cAMP by Gi, the signal will decrease in response to the agonist. This results in the Y value of the time course decreasing over time (see for example Figure 5).

Timeframe of Response Measurement

The timeframe of the response varies considerably between the signaling molecules being measured, the receptor being tested, and the host cell type. Because it is being measured in live cells in real time, the signal is susceptible to the cellular mechanisms that change the signal over time. Some signaling analytes are transient - they are rapidly cleared by the cell and the duration of the signal is short (for example, Ca^{2+} and DAG, which can be cleared within a couple of minutes, Figure 6). For these analytes, it can be erroneously concluded there is no signal if the biosensor response is measured at 10 minutes as the first time point; by this time, Ca^{2+} and DAG are usually completely cleared (Figure 6). This exemplifies that some knowledge of the signaling time course is required when using the sensor for the first time. Fortunately, the typical time ranges are well established for the

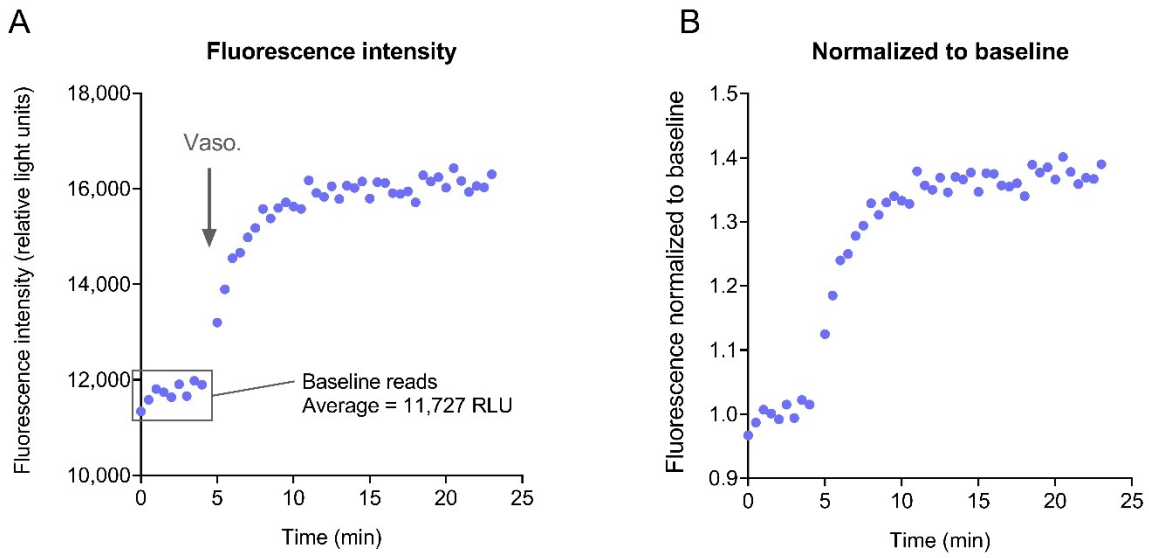


Figure 4. Biosensor data handling. Biosensor data are typically normalized to baseline, shown here for the cAMP biosensor, Red Up cADDis, detecting V_2 vasopressin-mediated cAMP production by 100 nM vasopressin in HEK293 cells. A) Time course of raw instrument data from a single well (fluorescence intensity from the BioTek Synergy Mx reader). First, the baseline response was read every 30 sec for 4 minutes. Then the ligand (vasopressin) was added and the plate read at 30 sec intervals for another 19 min. The data are then normalized to baseline as described in Data Normalization - the fluorescence intensity is divided by the baseline (average of the baseline fluorescence intensity values). This gives the normalized data in panel B.

familiar signaling molecules measured in this study (cAMP, DAG, PIP_2 and Ca^{2+}). The time ranges are given in Table 1 and illustrated in the graphs in Figures 4-6.

Another aspect of the timeframe is that it is desirable to record long enough to capture the entire time course curve shape (the waveform), particularly for rise-and-fall curve shapes. This means recording until the level of response has stabilized (or disappeared for transient responses). As detailed in ref. (37), fitting data to a waveform equation can provide estimates of regulation of signaling rate constants such as the rate of receptor desensitization. This requires the entire waveform to be collected, for example, for the level of the plateau to be well defined (Figure 6B and D). It is recommended the data be collected for as long as possible (given there is no extra cost using this continuous read modality), within the constraints of cell health, environmental control of the cells, and photobleaching.

Determining Amount of Biosensor in a Titration Experiment

The optimal amount of biosensor is dependent on numerous experimental variables including the cell type, plate format, and GPCR type. This variability is too great to permit a single amount of sensor to be recommended, however an initial titration experiment is done to determine the optimum number of virus units applied in the transduction step. A stock solution is supplied with commercially-available kits that is within range of the optimum for most applications. The titration experiment applies various volumes of this stock in order that the optimum volume can be determined. The experiment is detailed in Box 1.

cAMP biosensor properties

Gs Assay

In the cAMP signaling cascade, GPCRs stimulate cAMP production by first activating Gs-family G-proteins, which then go on to activate adenylyl cyclase, resulting in the production of cAMP. Numerous biosensors have

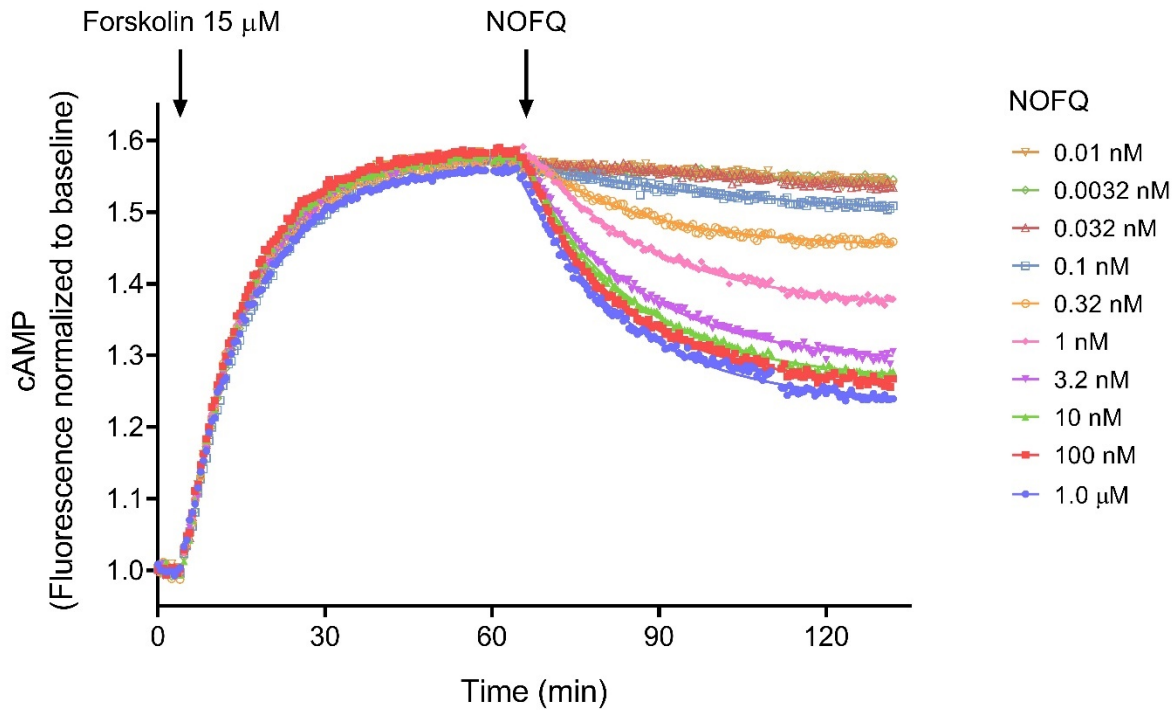


Figure 5. Gi signaling kinetics detected using a biosensor: Inhibition of cAMP by the nociceptin/orphanin FQ NOP receptor. The experiment consists of two phases. First, cAMP production is stimulated by forskolin, which directly activates adenylyl cyclase. This phase proceeds until the cAMP has plateaued, i.e. steady-state has been reached. Then the GPCR ligand is added and the decline of cAMP recorded. cAMP was measured using the Green Down cADDis biosensor (Table 1) in HEK293 cells transduced with the NOP receptor. Data were normalized to baseline as described in Data Normalization. (This involved taking the inverse of the baseline-normalized fluorescence values to convert this downward sensor response to an upward cAMP response.) Fluorescence intensity was measured every 30 seconds. The baseline period before addition of forkolin was 4 min and the NOP ligand NOFQ was added at 65 min.

been developed for detecting changes in cAMP concentration in living cells (13,38,60). These typically couple a protein that naturally binds cAMP with a second module that transduces cAMP binding into a light signal. Examples include the cADDis sensor family (61) ("cAMP difference detector in situ"). These sensors incorporate red or green fluorescent proteins into the cAMP-binding protein EPAC2 (Figure 2). Binding of cAMP causes an increase or decrease of fluorescence intensity, depending on the sensor variant (listed in Table 1). These sensors are very bright, and designed to be used in plate-based assays for drug discovery applications, such as lead optimization. The performance of the cADDis sensors has been evaluated using the Z' statistic. Typically, values of 0.6-0.9 have been observed. One important difference between biosensor assays and the more traditional endpoint measurements of cAMP is the absence (typically) of phosphodiesterase inhibitors when using biosensors. This enables the kinetics of cAMP to be detected in a more physiological context.

Representative data for the sensor Red Up cADDis are shown in Figure 4, for cAMP production via the V_2 vasopressin receptor stimulated by vasopressin. Before addition of the vasopressin, the average fluorescence intensity was 11,727 relative light units (RLU) (Figure 4A). After addition of vasopressin the fluorescence intensity increased. The time course shape was an exponential association curve - there was an initial rapid increase then the rate slowed then finally the fluorescence intensity approached a plateau (Figure 4A). The highest fluorescence intensity at the plateau was 16,431 RLU. The data were normalized to baseline as described in Data Normalization. The time course of baseline-normalized fluorescence is shown in Figure 4B, indicating an increase from 1.0 (the baseline) to 1.41 at the plateau.

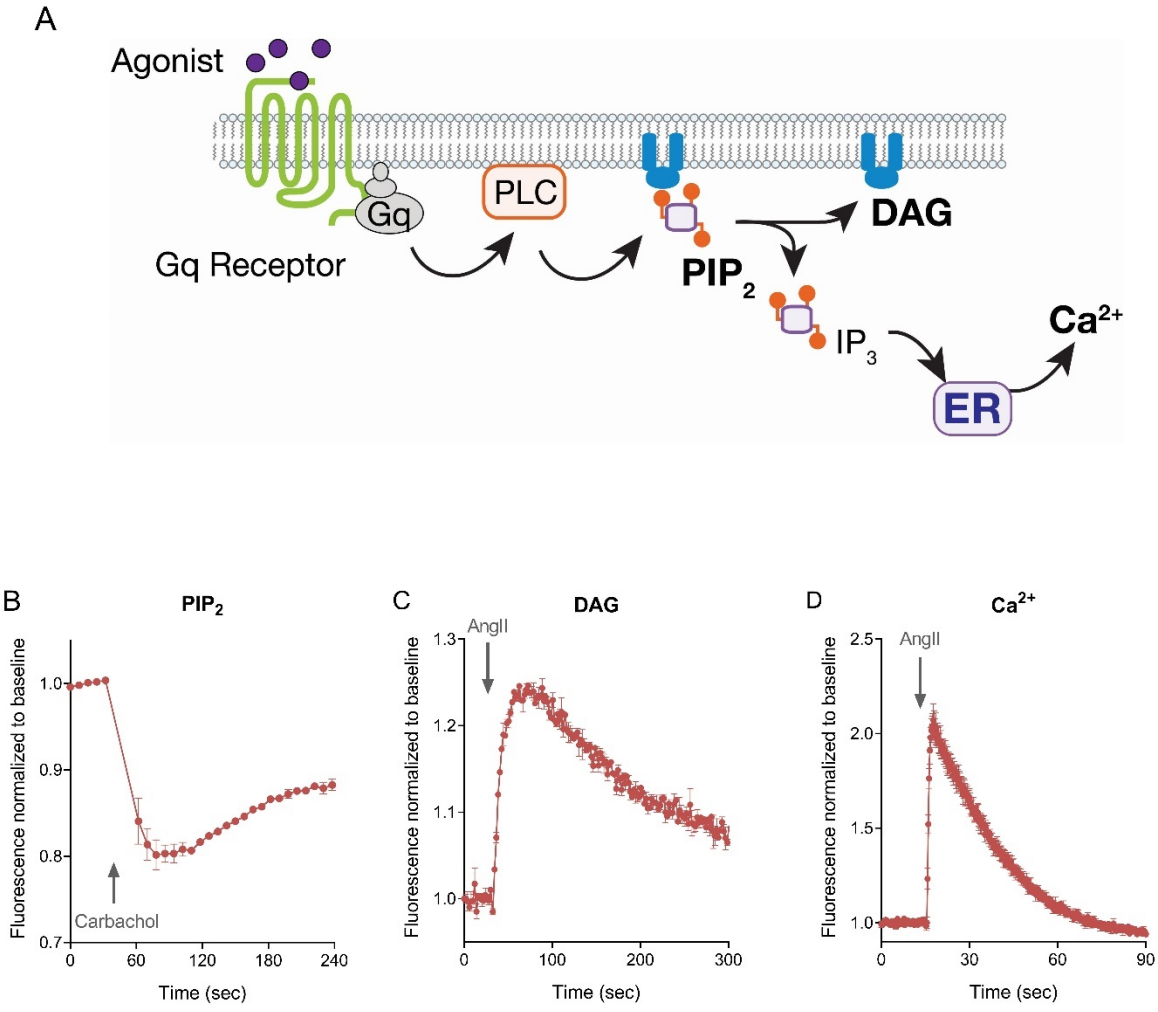


Figure 6. Biosensors for the Gq signaling pathway. GPCRs signal through Gq to mobilize Ca^{2+} into the cytoplasm from the endoplasmic reticulum (A). In this cascade, Gq activates the enzyme PLC, which converts PIP_2 to DAG and IP_3. IP_3 then binds and opens Ca^{2+} channels in the ER membrane, releasing Ca^{2+} into the cytoplasm. Biosensors have been developed for multiple signaling molecules in this pathway, including PIP_2, DAG and Ca^{2+} (13,38). Representative data are shown for these three biosensors in panels B-D. Note the level of PIP_2 decreases over time as it is being broken down by PLC. B, PIP_2 breakdown by carbachol (30 μM) via muscarinic receptors in HEK293 cells. C,D DAG generation and Ca^{2+} mobilization via AT_1 angiotensin receptor in HEK293 cells stimulated by angiotensin (32 μM).

The timeframe of the V_2 receptor response was about 20 minutes (Figure 4). The initial rise phase took place within the first 2 min and the plateau was reasonably well defined 20 min after ligand addition. The frequency of measurement was every 30 seconds in this experiment, which was sufficient to capture the waveform. For complete kinetic analysis, 30 second reads for 60 minutes is sufficient to capture the signaling dynamics for most Gs responses. In some cases, the curve shape is a rise-and-fall curve, where the fluorescence intensity rises to a peak then declines, either to a new plateau (Figure 8D) or to zero (Figure 8C).

Detailed protocols and videos can be found at the following links:

Green cADDis sensor: www.montanamolecular.com/live-cell-camp-assay-caddis/green-caddis-camp-protocol/

Red cADDis sensor: www.montanamolecular.com/live-cell-camp-assay-caddis/red-caddis-camp-protocol/

Gi Assay

As is well known, some GPCRs inhibit the production of cAMP. This results from the GPCR activating Gi-family G-proteins, which go on to inhibit adenylyl cyclase activity. cAMP biosensors have been used to record this inhibition of cAMP production resulting from Gi signaling. The assay requires the presence of a stimulating agent that generates a cAMP signal, which can then be inhibited by Gi-activated receptors. The stimulating agents typically used include forskolin, which binds adenylyl cyclase and activates it; and isoproterenol, which generates cAMP via the Gs pathway activated by the β_2 adrenergic receptor (endogenously expressed on most cell types, including HEK293 cells).

An example employing forskolin is shown in Figure 5, for the Gi-coupled nociceptin/orphanin FQ NOP receptor. Forskolin stimulates cAMP production, then upon addition of the receptor agonist NOFQ there is a dose-dependent reduction of cAMP (Figure 5). Traditionally in cAMP assays, forskolin and the receptor ligand are added simultaneously, or there is a short pre-incubation with forskolin. While this approach works for end-point assays, for kinetic analysis experiments it is best to pre-incubate with forskolin until a steady-state of cAMP has been reached, and then add the test compound. (Determining this is readily achievable using the continuous-read capability of the biosensors - the plate is simply left in the reader and the signal observed until the plateau level of cAMP response has been reached.) This is shown in the time course data in Figure 5. This greatly simplifies the kinetic data analysis because it removes the kinetics of forskolin activity from the equations (since this activity has reached steady-state when the test compound is added).

An alternative method is to employ a constitutively-active Gs G-protein to stimulate cAMP production (62). The day before assay, cells are co-transduced with the cAMP biosensor and a mutant Gs alpha protein that tonically activates adenylyl cyclase. There are pros and cons with this method. It is unfamiliar to most investigators and it requires more assay development to optimize expression of both biosensor and mutant Gs. However, for those investigators committed to quantifying the kinetics of Gi signaling, it offers the substantial benefit to assay workflow of avoiding the pre-incubation with the forskolin step; the test compound is simply applied by itself and Gi activity recorded by the reduction of the tonically-elevated cAMP produced by the mutant G-protein.

A detailed Gi assay protocol and video is at the following link: www.montanamolecular.com/live-cell-camp-assay-caddis/green-gi-caddis-camp-protocol/

Calcium Signaling Pathway Biosensors

GPCRs stimulate Ca^{2+} signaling pathways via Gq/11-family G-proteins. In this pathway, shown in Figure 6A, the G-protein activates the enzyme phospholipase C, which converts its substrate phosphatidylinositol 4,5-bisphosphate (PIP_2) to inositol 1,4,5-trisphosphate (IP_3) and diacyglycerol (DAG). IP_3 then binds to and opens Ca^{2+} channels in the endoplasmic reticulum, resulting in a rapid, large increase in cytoplasmic Ca^{2+} concentration. Numerous biosensors have been engineered to detect the signaling molecules in this pathway, including PIP_2, DAG and Ca^{2+} (13,38).

Three biosensors for this pathway are shown in Figure 6. The PIP_2 sensor (Figure 6A) is formed of dimerization-dependent green fluorescent proteins (48) (Green PIP_2, Table 1). The DAG sensor (Figure 6B) is formed of the DAG substrate PKC fused to a circularly permuted green fluorescent protein (63) (Green Up DAG, Table 1). The Ca^{2+} sensor GECO (Figure 6C), developed by Campbell and colleagues, is formed of calmodulin, the M13 peptide, and circularly permuted mApple (64) (Red GECO, Table 1). The choice of sensor will be dependent on issues including the research question, therapeutic relevance in a compound screen, sensitivity for detecting partial agonists, and assay performance for the GPCR target. Of interest, these sensors can be multiplexed, i.e. two sensors can be expressed in the same cells, and this allows simultaneous interrogation of two points on the same pathway (63).

The time course of the sensor response for all three sensors is both short and reversible (Figure 6B-D). These are transient responses, not accumulation responses, so care must be taken to collect the data in the appropriate time range. DAG and Ca^{2+} increase in response to agonist, whereas PIP_2 decreases because it is the substrate for PLC. The first phase is very rapid, occurring within seconds, so if possible time points should be collected on the second timescale (see Figures 6, 11 and 12). For accurate quantification of the kinetics by curve fitting (see Analyzing Signaling Time Course Data) we have used a recording frequency of 0.25 seconds using a plate reader (Figure 12). The DAG and Ca^{2+} response peaks and then rapidly declines. The PIP_2 response troughs and then rises. For DAG and Ca^{2+} the response returns either to baseline or close to it (Figure 6C,D), whereas for PIP_2 the response approaches a plateau (Figure 6B). The whole signaling event is complete within 2-5 minutes.

Detailed protocols and videos are available at the links in Table 1.

Arrestin Sensor

The arrestin proteins are principal regulators of GPCR signaling (14,18) . Arrestins can block G-protein signaling and in this way prevent overstimulation of the cell, through the classical process of receptor desensitization. In this process, the agonist-bound GPCR becomes phosphorylated by kinase enzymes and subsequently interacts with arrestin. Arrestins can also mediate downstream signaling, acting as scaffolding proteins to recruit signaling molecules such as extracellular signal–regulated kinase, or translocating the receptor to endosomes to enable persistent signaling (19,65).

Numerous assays for measuring the arrestin pathway have been created (66). Resonance energy-transfer sensors have been utilized, for example refs (11,67). The direct fluorescence modality described in this chapter is ideal for measuring the kinetics of receptor-arrestin interaction. We developed a sensor that directly reports receptor-arrestin interaction, in which the receptor interaction changes fluorescence intensity of a modified arrestin-3 (β arrestin-2) incorporating the fluorescent mNeonGreen protein (Figure 7A) (29). There is no time delay between the interaction event and the signal generation, the signal generation by the fluorescent protein occurring almost instantly. This is in contrast to enzyme complementation or reporter gene assays where there is a temporal disconnect between the interaction and the signal recording, and BRET-based assays where it can take time for sufficient light to build up to be measured robustly. The continuous read capability of the fluorescence modality enables the kinetics to be efficiently recorded. However, the absence of signal amplifying steps in this direct measurement of arrestin interaction impacts arrestin sensor sensitivity. Robust windows of response have been recorded in plate readers for GPCRs that strongly couple to arrestin (e.g. the AT_1 receptor), while the responses are smaller for GPCRs known to couple more weakly (β_2 adrenergic receptor) (29). Further optimization of the arrestin sensor is ongoing, and needed to increase the signal for weaker interactions.

Figure 7B shows the data obtained with the arrestin sensor and the AT_1 receptor, in response to AngII. Arrestin recruitment rises rapidly at first then approaches a plateau for this receptor. The rise phase occurs within a couple of minutes and the response reaches steady state within 20 minutes of application. A read interval of 30 seconds and a read time of up to 60 minutes captures the waveform of arrestin recruitment for most receptors examined. (In some cases the signal declines from a peak.) The robustness of the sensor response has been quantified using the Z' statistic. For the AT_1 receptor, Z' values approaching 0.9 have been obtained.

Analyzing Signaling Time Course Data

The goal of this section is to demonstrate how to measure the initial rate of signaling and the k_τ parameter (initial rate stimulated by agonist-bound receptor). This requires an explanation for why we use the initial rate analysis; a description of the curve shapes encountered in the time course data for GPCR signaling; and an overview of how the initial rate can be estimated by curve fitting.

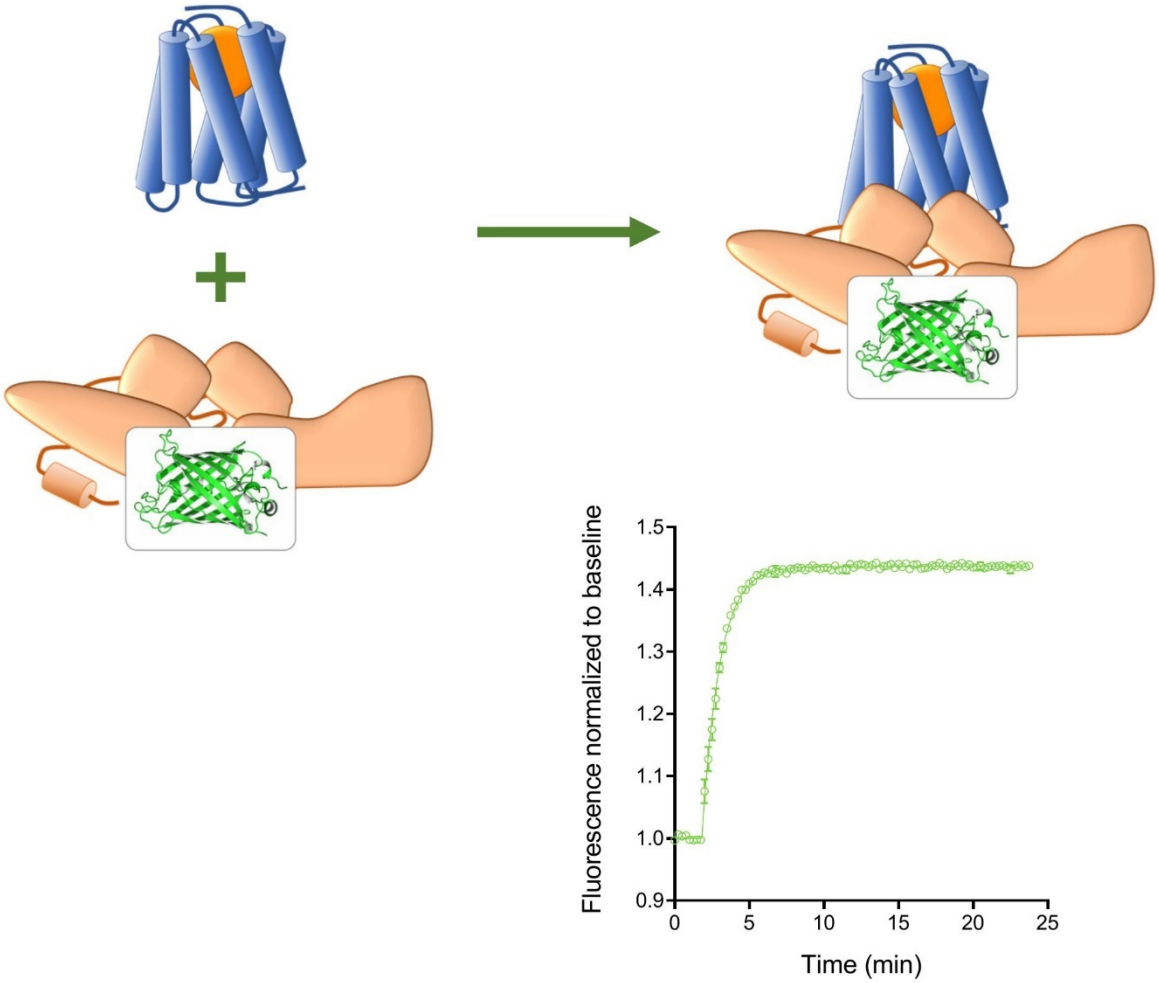


Figure 7. Arrestin biosensor. Arrestin-3 was engineered to incorporate a fluorescent protein (mNeonGreen) in a manner that interaction with receptor causes a decrease in fluorescence intensity (this being a downward sensor) (29). The graph shows the arrestin sensor response on interacting with the AT_1 receptor in HEK293 cells, stimulated by 32 μM AngII. The data have been normalized to baseline and converted to upward data, reflecting the increase of arrestin interaction with the receptor, as described in Data Normalization.

Why Use the Initial Rate?

The biosensor technology enables the time course of signaling to be measured in an efficient, streamlined manner. Now a data analysis method is required in order to reduce the time course data set to useful drug parameters that describe the kinetics of signaling. This reduction strategy is familiar in pharmacology generally. For example, concentration-response data are analyzed using the sigmoid curve equation, reducing the dataset to the pharmacological parameters EC_{50} and E_{max} (68). A useful parameter that can be extracted from time course data is the initial rate of signaling, analogous to the initial rate of enzyme activity (37). This parameter has several benefits. First, it is biologically-meaningful, being the initial burst of signaling by the receptor. Second, it can be measured regardless of the shape of the time course, providing a common metric across different responses (e.g. Ca^{2+} mobilization and arrestin recruitment, see below). Third, from a receptor theory perspective it is likely a pure efficacy parameter, being minimally impacted by regulation of signaling mechanisms that impact the later part of the time course. Finally, from a practical perspective the initial rate is a

familiar concept for investigators who learned the basics of enzyme kinetics in undergraduate biochemistry courses.

Time Course Curve Shapes

Kinetic data take the form of time course plots, where activity is measured over a range of time points. Analyzing time course data is more complicated than analyzing concentration-response data. The latter conform to just a single curve shape, the sigmoid curve, which is almost universally analyzed using the sigmoid curve equation. By contrast, time course data do not conform to a single shape. Fortunately, however, the number of shapes is limited to just four (37). Two of these are familiar, and all four are amenable to analysis in standard curve-fitting software. The four curve shapes for responses that initially increase are shown in Figure 8 and are:

1. The straight line. Response increases continuously over time, without limit (Figure 8A).
2. The association exponential curve. Response increases rapidly at first, then slows, then approaches a limit at which the level of the response remains constant over time (Figure 8B)
3. The rise-and-fall to baseline curve. Response rises to a peak, then falls, eventually declining to the baseline response before addition of ligand (Figure 8C).
4. The rise-and-fall to steady-state curve. Responses rises, peaks, then declines to a steady-state level that is above the baseline (Figure 8D).

Different formats of these curve shapes are often observed and a comprehensive list of the formats and equations is provided in the supplementary file Time course equation list. First, descending versions of these four curve shapes are observed when the receptor stimulates a decreases of signaling molecules / responses, e.g. inhibition of cAMP by Gi stimulation (Figure 5). Second, there is usually a baseline run-in period in biosensor assays (before the addition of receptor agonist) and this can be incorporated into the equation used to analyze the data (see below). Finally, occasionally the baseline drifts upwards or downwards over time and this too can be incorporated into the analysis (see Example 2: Ca^{2+} Mobilization via the AT_1 Receptor). These equations are available in Prism templates which can be downloaded from this Google Drive.

The time course curve shape is sculpted by regulation of signaling mechanisms (37,69-71). GPCR signaling is regulated, to limit the level of response and prevent over-stimulation of the cell. The canonical mechanisms are receptor desensitization (14,18) (involving receptor phosphorylation and arrestin binding) and signal degradation (for example, metabolism of second messengers, such as breakdown of cAMP by phosphodiesterases (72)). The shape is dependent on the number and nature of the regulation mechanisms (37). Without regulation, the signal increases indefinitely (the linear profile). A single regulation mechanism limits the signal to an association exponential curve - rather than continuing indefinitely, the signal level reaches a steady-state. When both mechanisms are in operation, the rise-and-fall curve results - the signal is transient, peaking then falling to zero. More complicated mechanisms result in the rise-and-fall to steady-state curve, including signaling by internalized receptors and receptor resensitization (37).

Equations Defining the Time Course Curve Shapes

Each of the curve shapes is defined by an equation that can be used to fit the data. The equation contains parameters that define the curve. The curve fitting procedure provides fitted values of these parameter values. These values are then used to calculate the initial rate. The equations are used in familiar curve fitting software, e.g. Prism (GraphPad Software, Inc.), SigmaPlot (Systat Software, Inc.) and XLfit (ID Business Solutions Ltd.). They are either built-in or can be entered as user-defined equations. In this chapter we exemplify the analysis methods using Prism version 8, but they can be applied using any suitable curve-fitting program. The general form of the equations are written below and a complete set of equations is provided in the supplementary file Time course equation list. Note the equations are likely to be formatted slightly differently depending on the software used. Note also the baseline (i.e. signal without ligand) is assumed to be constant over time in the

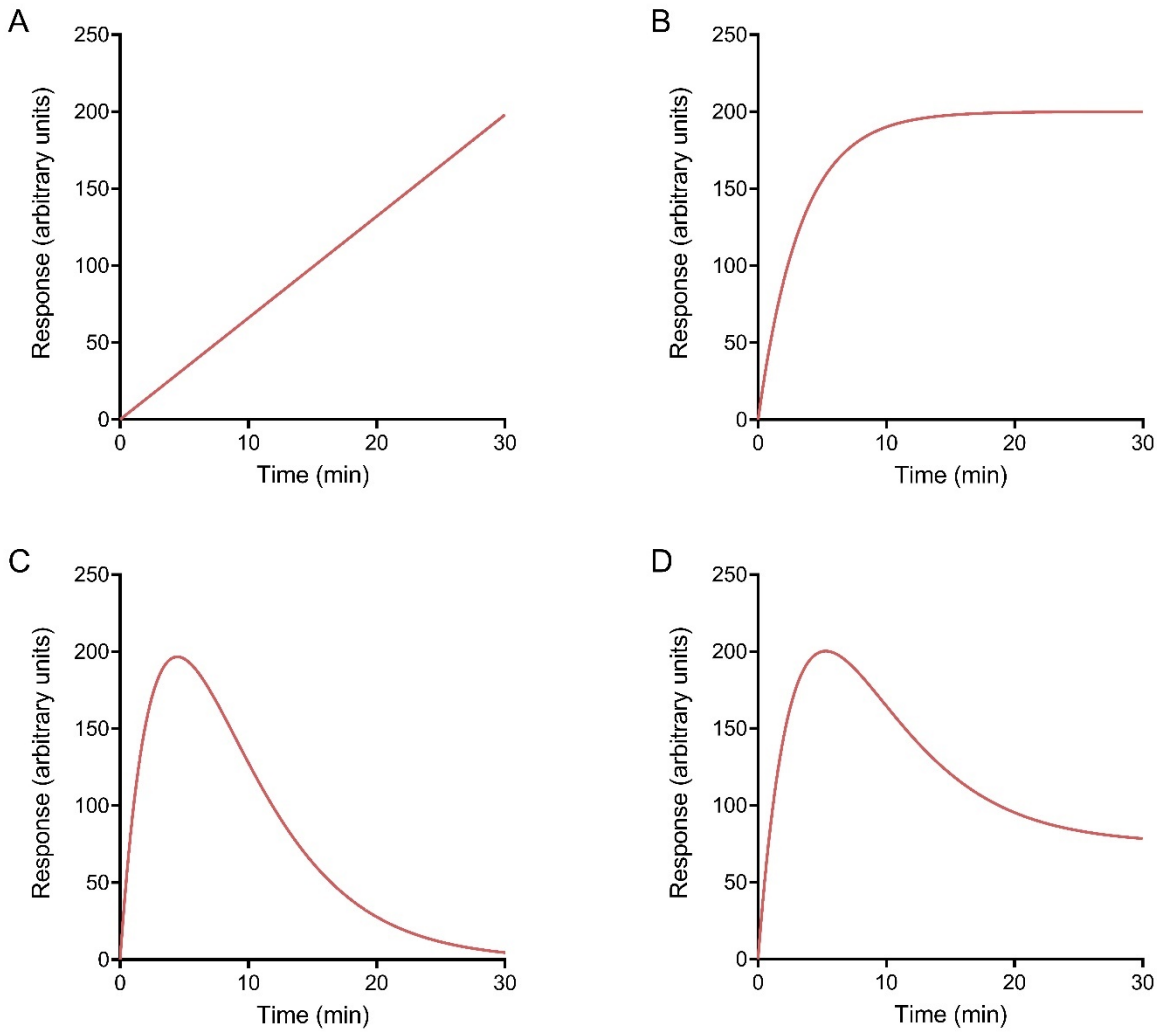


Figure 8. Time course profile shapes typically observed for GPCRs. For a comprehensive survey, see ref. (37). (a) Straight line. (b) Association exponential curve. (c) Rise-and-fall to baseline curve. (d) Rise-and-fall to steady-state curve. Data for (a) were simulated using Eq. 1 (Slope, 6.6 response units.min^{-1}), (b) with Eq. 2 (SteadyState, 200 response units; k, 0.30 min^{-1}), (c) with Eq. 3 (C, 120 response units.min^{-1}; k_1, 0.25 min^{-1}; k_2, 0.20 min^{-1}) and (d) with Eq. 4 (SteadyState, 75 response units; D, 25 (note is unitless); k_1, 0.25 min^{-1}; k_2, 0.20 min^{-1}). The Baseline parameter in each equation was set to zero.

equations immediately below. (Equations that allows for baseline drift, as may occur with photobleaching, are in Example 2: Ca^{2+} Mobilization via the AT_1 Receptor.) The equations are:

Straight line (Eq. 1):

$$Y = \text{Slope} \times t + \text{Baseline} \quad \text{Eq. 1}$$

where Y is response, Slope is the gradient of the line and t is the time of response measurement. Baseline is the response in the absence of ligand.

Association exponential curve (Eq. 2):

$$Y = \text{SteadyState} \times \left(1 - e^{-kt}\right) + \text{Baseline} \quad \text{Eq. 2}$$

where SteadyState is the steady-state response, specifically the ligand-specific response as time approaches infinity. Note the Y asymptote value (as time approaches infinity) is SteadyState + Baseline. k is the observed rate constant in units of t^{-1}.

Rise-and-fall to baseline curve (Eq. 3):

$$Y = \frac{C}{k_1 - k_2}\left(e^{-k_2 t} - e^{-k_1 t}\right) + \text{Baseline} \quad \text{Eq. 3}$$

where C is a fitting constant in units of Y units.t^{-1} and k_1 and k_2 are observed rate constants in units of t^{-1}.

Rise-and-fall to steady-state time curve (Eq. 4):

$$Y = \text{SteadyState} \times \left(1 - De^{-k_1 t} + (D-1)e^{-k_2 t}\right) + \text{Baseline} \quad \text{Eq. 4}$$

where D is a fitting constant (that is unitless).

Note the equations are for responses that initially rise over time. The corresponding equations for responses that initially fall over time are in the supplementary file Time course equation list.

Many of the equations are not included as built-in equations in curve fitting software and instead are entered as custom equations. This is easy to do in the program Prism and an overview of the custom equations and how they are entered is provided in the supplementary files Time course equation list and Loading equations into Prism from a file. Prism files containing all the equations can be downloaded from this Google Drive.

Curve Fitting Strategy for Measuring the Initial Rate

The familiar method for measuring the initial rate is to examine the time course and then select the "linear portion of the curve", that region of the time course at the earliest time points when the response increases linearly over time. Unfortunately, this method does not work well for GPCR signaling because the response rapidly deviates from linearity, owing to regulation of signaling mechanisms (37). A second issue is that manual selection of the linear time points is not suitable for high-throughput analysis and is prone to selection bias. An alternative method, described here, utilizes the whole time course data set and comprises two parts (37). First, the whole time course data set is fit to the relevant time course equation and the fitted parameter values obtained. Second, the fitted parameter values are entered into a formula that calculates the initial rate value. These initial rate values are then used to calculate k_τ. This process is summarized in Table 2 and exemplified below using biosensor time course data. Step-by-step guides for how to do the analysis in Prism are provided in supplementary files.

The formulas for calculating the initial rate from the curve fit parameter values are:

Straight line initial rate (Eq. 5):

$$\text{Initial rate} = \text{Slope} \quad \text{Eq. 5}$$

Association exponential curve (Eq. 6):

$$\text{Initial rate} = k \times \text{SteadyState} \quad \text{Eq. 6}$$

Rise-and-fall to baseline curve (Eq. 7):

$$\text{Initial rate} = C \quad \text{Eq. 7}$$

Rise-and-fall to steady-state time curve (Eq. 8):

$$\text{Initial rate} = \text{SteadyState} \times (Dk_1 - (D-1)k_2) \quad \text{Eq. 8}$$

Table 2. Steps for measuring the initial rate and k_τ by curve fitting

Step	Procedures
Prepare data for analysis	Express as fluorescence normalized to baseline If downward sensor is used, convert to upward data
Enter and graph data	Enter data into curve-fitting software Enter as the signal (y) versus time (x) Ensure graph is large enough for symbols to be discernable
Curve fitting the time course data	Fit data to relevant time course equation (Eq. 1-4) This provides estimates of the equation parameter values (rate constants, plateau's etc)
Calculation of initial rate	Use fitted parameter values to calculate initial rate (Eq. 5-8) Take care to use the correct parameters. The equations in software can be formatted differently than the general equations.
Determination of k_τ: Multiple concentrations method	Enter the initial rate (y) versus the ligand concentration (x) into the curve fitting program Fit to sigmoid dose response equation Constrain the bottom to be zero k_τ is the fitted value of the top of the curve
Determination of k_τ: Single concentration method	If a maximally-stimulating concentration of ligand is used, k_τ is simply the initial rate at that concentration.

Data Normalization and Entry Into Curve-Fitting Program

The steps involved in the initial rate determination are given in Table 2. The first step is normalizing the data to a format appropriate for the analysis. The raw fluorescence intensity data is normalized to baseline, as described in Data Normalization. If a downward sensor is used, the data are converted to upward data, as described in Data Normalization.

Next, the data are entered into the curve-fitting program. In the data table, the x values are time and the y values are the baseline-normalized fluorescence intensity data. The data for different ligand concentrations are entered in separate y columns. This is shown for Prism in the step-by-step analysis guides in the supplementary files.

Association Exponential Curve Fitting, Initial Rate Calculation and k_τ Determination

The most-commonly observed time course shape is the association exponential curve (Eq. 2). This waveform can be easily analyzed using equations built in to familiar curve-fitting software. Here we employ Prism (version 8). This program has a built-in association exponential equation analogous to Eq. 1. The basic equation is termed "One-phase association." We advocate the use of a slightly more advanced equation, also built into the program, termed "Plateau followed by one phase association." (73) This equation allows for a run-in time during which the baseline is measured prior to the application of ligand to the cells, the standard data collection method for biosensors. The equation (Eq. 9) is defined as follows:

$$Y = \text{if}\left(X < X0, Y0,\ Y0 + (\text{Plateau} - Y0)\left(1 - e^{-K(X - X0)}\right)\right) \quad \text{Eq. 9}$$

Y is the signal level, X is time, X0 is the signal initiation time (the time at which the signal starts to rise), Y0 is the baseline signal before application of ligand, Plateau is the total signal level at steady-state (the level at the right-hand plateau/asymptote as time approaches infinity), and K is the observed rate constant. Prism calculates a parameter termed "Span" which we will use – it is the Plateau minus the Y0 value and is equivalent to SteadyState in Eq. 2. (Also note that Y0 in the Prism-formatted Eq. 9 is the same as Baseline in Eq. 2.)

Example 1: cAMP Signaling

The data analysis is demonstrated using data for cAMP generated by the V_2 vasopressin receptor (Figure 9). cAMP generation was stimulated by oxytocin at multiple concentrations and cAMP detected using the Red Up cADDis sensor. The curve fitting protocol is described in detail in the supplementary file Association exponential analysis. In brief, data for each concentration of oxytocin are analyzed using the "Plateau followed by one phase association" equation. The value of X0, the signal start time, is floated in the analysis, i.e. it is a fitted rather than a fixed value. This is recommended, in order to accommodate imprecision in the precise ligand addition time, and to accommodate any delay between ligand addition and signal initiation. The initial value for X0 is entered manually. The analysis is then run, and the fitted values are then inspected (see supplementary file Association exponential analysis, page 16). For the data in Figure 9, this indicated the fit was reasonable for the higher concentrations ($R^2 > 0.9$ for 0.1 – 100 nM). The fit was poor for the lowest concentrations ($R^2 = 0.48$ - 0.74 for 0.0032 to 0.032 nM) because there was minimal signal generated.

The next step is the calculation of the initial rate. This is done using using Eq. 6.

$$\text{Initial rate} = k \times \text{SteadyState}$$

What we are doing here is multiplying the rate constant by the ligand-specific signal increment at the plateau. Note the SteadyState term is the plateau Y value *minus the background* – it isn't the plateau Y value. In terms of the Prism equation format, this equation is: Initial rate = K × Span. The values of K and Span are the fitted values from the curve fits. (Span is calculated from the fit parameters Y0 and Plateau, as Plateau – Y0). For example, in Figure 9 at 100 nM oxytocin, the K value is 0.37 min^{-1} and the Span value is 0.74. The initial rate is now calculated by multiplying K by Span, per Eq. 6. For 100 nM this gives the initial rate value of 0.27 normalized fluorescence units per min (NFU per min). This initial rate is illustrated by the dashed blue in in Figure 9. Initial rate values for the other concentrations are given in Figure 9.

The final step is the determination of k_τ, which is the initial rate at a maximally-effective concentration of ligand. This is done by analyzing the concentration-response for the initial rate, detailed in the supplementary file Association exponential analysis. The initial rate values are entered into a data table (y values). The corresponding ligand concentration is entered as the logarithm of the concentration (x values). The data are then fit to a standard sigmoid curve logistic equation by nonlinear regression ("log(agonist) vs. response -- Variable slope (four parameters)" (74)) (Figure 9). The "Bottom" parameter, the lower plateau, is fixed to zero, since by definition the initial rate is zero in the absence of ligand. From this fit the k_τ value can be determined - it is simply the value of "Top", the y value at the upper, right-hand plateau of the curve. This gives a k_τ value of 0.283 normalized fluorescence units.min^{-1} (Figure 9).

Example 2: Arrestin Recruitment

A second example of the analysis is arrestin recruitment via the AT_1 receptor. The arrestin sensor (see Arrestin Sensor) was used with five AT_1 receptor ligands to quantify kinetics of arrestin recruitment by full and partial agonists (Figure 10), as described in ref (29). Here ligands were tested at a single maximally-stimulating concentration (32 μM). This enables efficient assessment of ligand efficacy, i.e. maximal effect (though at the expense of measuring ligand potency). In this example of a downward sensor, data were were first normalized to be upward, to represent the stimulation of arrestin recruitment, using the equation from Data Normalization:

$$\text{Upward} = 2 - \left(\frac{F}{\Delta F}\right)_{\text{Downward}}$$

The upward time course data were then fit to the association exponential equation (Eq. 9), using Prism as described above (Example 1: cAMP Signaling). This yielded the fitted parameter values for the rate constant K and the steady-state response above background (SteadyState, or Span in Prism), values given in Figure 10). From these parameters the initial rate was calculated, by multiplying K by Span (Figure 10). The dashed lines in

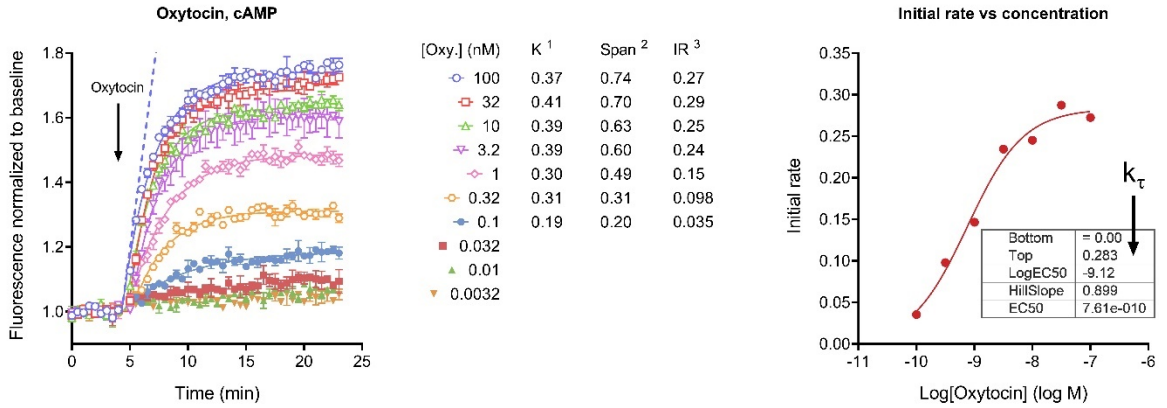


Figure 9. Initial rate analysis of oxytocin-stimulated cAMP accumulation via the V_2 vasopressin receptor, an example of association exponential time course analysis. Time course data on the left were fit to the "Plateau followed by one phase association" equation in Prism (73) (Eq. 9). The analysis gave the fitted values shown for K (the rate constant) and Span (the ligand-specific increment at the plateau). The initial rate (IR) was calculated by multiplying K by Span. The dashed blue line is the initial rate for 100 nM oxytocin. On the right, the initial rate is plotted against the logarithm of the concentration of oxytocin. The data were fit to the sigmoid curve equation "log(agonist) vs. response -- Variable slope (four parameters)" (74) with "Bottom" fixed to zero. The fit parameters are shown in the table. k_τ is equal to "Top." Detailed description of the curve fitting is in the supplementary file Association exponential analysis. 1, units are min^{-1}; 2, units are normalized fluorescence units; 3, units of normalized fluorescence units.min^{-1}. Data are from ref (37).

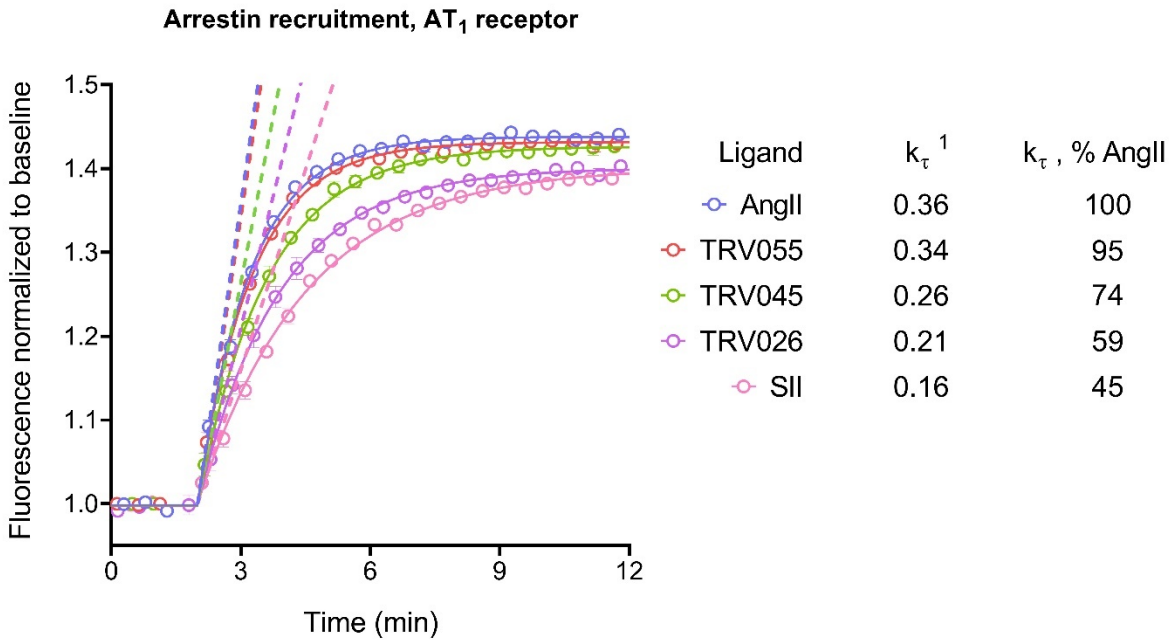
Figure 10 indicate the initial rate. From these values k_τ is determined. In this case, k_τ is simply equal to the initial rate because k_τ is the initial rate at a maximally-stimulating concentration of ligand, the concentration used in this experiment. The resulting k_τ values, given in Figure 10, ranged from 0.36 NFU per min for AngII to 0.16 NFU per min for SII. The value of SII indicates the ligand is a partial agonist; the SII-occupied receptor elicited arrestin recruitment at an initial rate only 45% of that produced by AngII. Interestingly, this partial agonism is not evident if an endpoint approach is used to quantify the data - by the time the signal has fully formed, at 10 min after ligand application (at the plateau), SII is almost as effective as AngII (Figure 10). This fact is relevant to the quantification of biased agonism (Simplifying Biased Agonism Assessment Using Signaling Kinetics).

Rise-and-Fall to Baseline Curve Fitting, Initial Rate Calculation and k_τ Determination

The rise-and-fall to baseline curve (Figure 8C) describes the time course for numerous biosensor responses. It is the familiar curve shape in Ca^{2+} mobilization assays. These data can be fit to determine the initial rate of signaling. The same general process is used as described above for the association exponential curve (Association Exponential Curve Fitting, Initial Rate Calculation and k_τ Determination). The time course data are fit to an equation, in this case Eq. 3, and the fitted parameter values used to calculate the initial rate and k_τ. Two examples are shown here, DAG production and Ca^{2+} mobilization (both via the AT_1 receptor). The latter employs an equation that accommodates a technical issue in biosensor experiments, baseline drift.

Example 1: DAG Production via the AT_1 Receptor

In this experiment, rather than a concentration-response being run, a single, maximally-stimulating concentration of ligand was used, to quantify ligand efficacy. In Figure 11, this is shown for the endogenous ligand AngII and for a synthetic ligand TRV055 (data from ref (29)). DAG was detected using the Red DAG sensor. Visual inspection indicates the response rises steeply, then peaks, followed by a decline back down to the baseline level before addition of ligand. The data were fit to Eq. 3. This equation is not a built-in equation in Prism and so needs loading in as a user-entered equation. The simplest way to load the equation is to load it



	AngII	TRV055	TRV045	TRV026	SII
X0	4.00	3.99	3.99	3.99	3.99
Y0	0.999	0.998	0.998	0.997	0.998
Plateau	1.44	1.43	1.43	1.40	1.40
K	0.818	0.791	0.619	0.523	0.397
Span	0.439	0.434	0.429	0.403	0.403

Figure 10. Initial rate analysis of arrestin recruitment to the AT_1 angiotensin receptor, an example of association exponential time course analysis. The five ligands were tested at a single concentration that was maximally-stimulating (32 μM). Time course data were fit to the "Plateau followed by one phase association" equation in Prism (73) (Eq. 9). The analysis gave the fitted values shown for K (the rate constant) and Span (the steady-state response above baseline). The initial rate (IR) was calculated by multiplying K by Span. The dashed lines indicate the initial rate. In this case, the initial rate is equal to k_τ because a maximally-stimulating concentration of ligand was used. 1, units of normalized fluorescence units.min^{-1}. Data are from ref (29).

from a file that already contains it, and such a file is provided in the supplementary file Rise-and-fall equations. The equation is loaded in as described in the supplementary file Loading equations into Prism from a file.

The equation used is named "[Pharmechanics] Baseline then rise-and-fall to baseline time course" and is formatted as follows (Eq. 10):

$$Y = \text{if}\left(X < X0, \text{Baseline}, \ \text{Baseline} + \frac{C}{k_1 - k_2}\left(e^{-k_2(X - X0)} - e^{-k_1(X - X0)}\right)\right) \quad \text{Eq. 10}$$

Note this equation is extended to include the run-in period before the start of the signal (at X0), using an IF statement, as described for Eq. 9 above. The AT_1 DAG data were fit to this equation (Figure 11). The fitting protocol is described in detail in the supplementary file Rise-and-fall to baseline exponential equation. The value of X0, the signal start time, was floated in the analysis, and its initial value was entered manually. The fit to the equation was reasonable (R^2 = 0.98 for both AngII and TRV055, Figure 11).

The value of the initial rate is then determined. This is particularly easy for the rise-and-fall to baseline equation - the initial rate is simply equal to the fitted parameter C. These initial rate values are indicated in Figure 11. Now the k_τ value can be determined. Since a maximally-stimulating concentration of ligand was used in this experiment, k_τ is equal to the initial rate at this concentration. In other words, k_τ is equal to the value of C (indicated in Figure 11). Now we can determine the relative efficacy of the two ligands AngII and TRV055 using

the k_τ value, by dividing the value by that for AngII. The resulting efficacy values are 100% for AngII (by definition) and 130% for TRV055 (Figure 11). This result indicates TRV055 had a higher efficacy than AngII in terms of the initial rate for Ca^{2+} mobilization, indicating TRV055 was a superagonist.

Example 2: Ca^{2+} Mobilization via the AT_1 Receptor

In this example, there was a slight drift of the baseline response over time. This is a common technical issue in biosensor experiments. It can arise from photobleaching or slight environmental changes over time. Fortunately, the analysis can be slightly modified to incorporate baseline drift.

The example is Ca^{2+} mobilization via the AT_1 receptor (29). In the experiment, five ligands were tested at a maximally-stimulating concentration, with Ca^{2+} detected using the Red GECO sensor. The ligands were AngII, TRV055, TRV045, TRV026 and SII. The time course data are shown in Figure 12. Close visual inspection indicates baseline drift - the response at late time points is slightly lower than the response before the addition of ligand. This can be handled by slight modification of the equation used to analyze the data. Eq. 10 is modified to incorporate a baseline drift term, giving Eq. 11:

$$YS = \text{Baseline} + \text{Drift} \times X0$$
$$Y = \text{if}\left(X < X0, \text{Baseline} + \text{Drift} \times X,\ YS + \text{Drift} \times (X - X0)\right) + \frac{C}{k_1 - k_2}\left(e^{-k_2(X - X0)} - e^{-k_1(X - X0)}\right)\right) \quad \text{Eq. 11}$$

"Drift" is the slope of the change of Baseline over time. Note Baseline is the Y value when X is zero, i.e. is the Y intercept. The equation is a user-defined equation that can be loaded from the file Rise-and-fall equations. The equation is loaded as described in the supplementary file Loading equations into Prism from a file.

The AT_1 Ca^{2+} mobilization data were fit to this equation (termed "[Pharmechanics] Baseline then rise-and-fall to baseline time course with drift" in Prism) (29). The fitting protocol is described in detail in the supplementary file Rise-and-fall to baseline exponential equation with baseline drift. The value of X0, the signal start time, was floated in the analysis, and its initial value was entered manually. The fit to the equation was reasonable ($R^2 >$ 0.97 for all five ligands). The k_τ value is equal to C, since C is the initial rate and a maximally-stimulating concentration of ligand was applied. These values are given in Figure 12. The k_τ values can be normalized to AngII to obtain a measure of relative efficacy (Figure 12). This showed TRV055 was slightly more efficacious than AngII (120%) and that the other ligands were partial agonists, with activity ranging from 9 - 33% (Figure 12). These data are used in the assessment of biased agonism for the AT_1 receptor, as described in Simplifying Biased Agonism Assessment Using Signaling Kinetics below.

Rise-and-Fall to Steady-State Curve Fitting

Often in rise-and-fall type responses the signal falls to a plateau that is above the baseline signal (as opposed to falling back to baseline) (Figure 8D) (37). This type of response can be analyzed with a modified form of the rise-and-fall equation (Eq. 4). The initial rate of the rise phase and k_τ can be determined by applying a formula to the fitted parameter values.

An example of this waveform is shown in Figure 13, the cAMP response to isoproterenol via the β_2 adrenoceptor endogenously expressed in HEK293 cells. A maximally-stimulating concentration of the agonist isoproterenol was used (20 μM). The data were fit to Eq. 4 using Prism. This equation is not built into the program so needs loading in as a user-defined equation. This can be done simply from the Rise-and-fall equations file, as described in the supplementary file Loading equations into Prism from a file. The equation is named "[Pharmechanics] Baseline then rise-and-fall to steady state time course" and is formatted as follows (Eq. 12):

$$Y = \text{if}\left(X < X0, \text{Baseline},\ \text{Baseline} + \text{SteadyState} \times \left(1 - De^{-k_1(X - X0)} + (D - 1)e^{-k_2(X - X0)}\right)\right) \quad \text{Eq. 12}$$

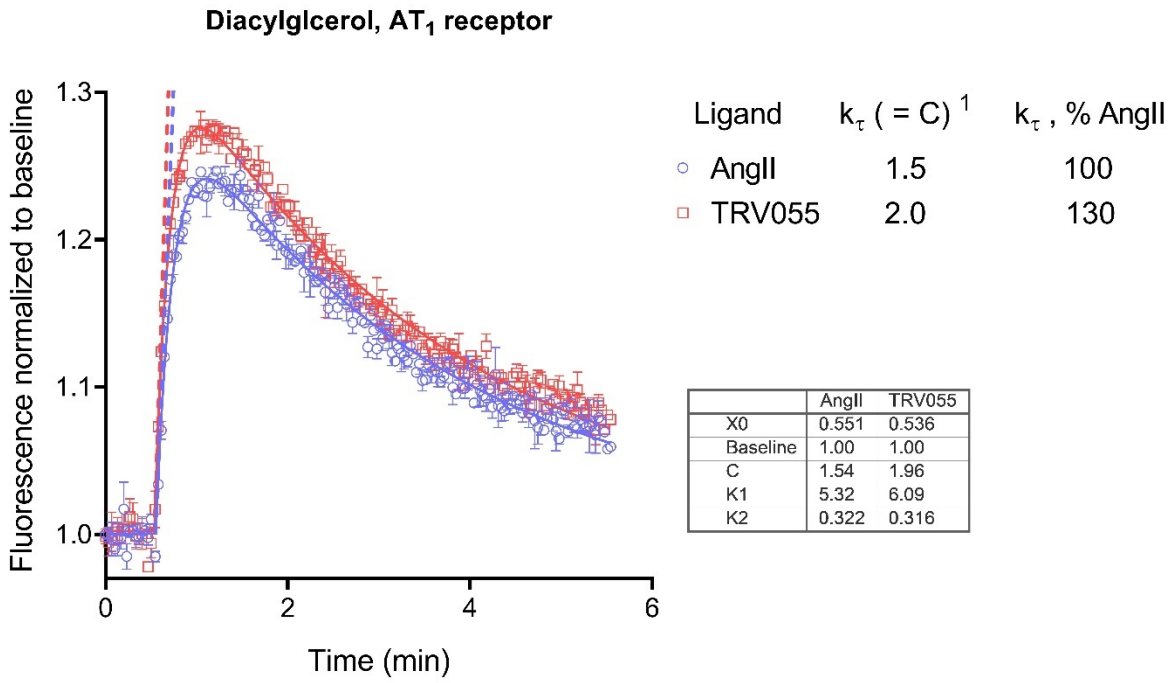


Figure 11. Initial rate analysis of diacylglycerol production by the AT_1 angiotensin receptor, an example of rise-and-fall to baseline time course analysis. Two ligands, AngII and TRV055, were tested at a single concentration that was maximally-stimulating (32 μM). Time course data were fit to Eq. 10 using Prism. This user-defined equation (called "[Pharmechanics] Baseline then rise-and-fall to baseline course") was loaded as described in the supplementary file Loading equations into Prism from a file. The fit parameters are shown in the table. The initial rate value is equal to the parameter C. The initial rate is indicated by the dashed lines. In this case, the initial rate is equal to k_τ because a maximally-stimulating concentration of ligand was used. Detailed description of the curve fitting is in the supplementary file Rise-and-fall to baseline exponential equation. 1, units of normalized fluorescence units.min^{-1}. Data are from ref (29).

Note this equation is extended to include the run-in period before the start of the signal (at X0) as described for Eq. 9 above (Association Exponential Curve Fitting, Initial Rate Calculation and k_τ Determination). The cAMP data were fit to this equation. A step-by-step guide is provided in the supplementary file Rise-and-fall to steady state analysis. The value of X0, the signal start time, was floated in the analysis, and its initial value was entered manually. The fit to the equation was good ($R^2 = 0.997$).

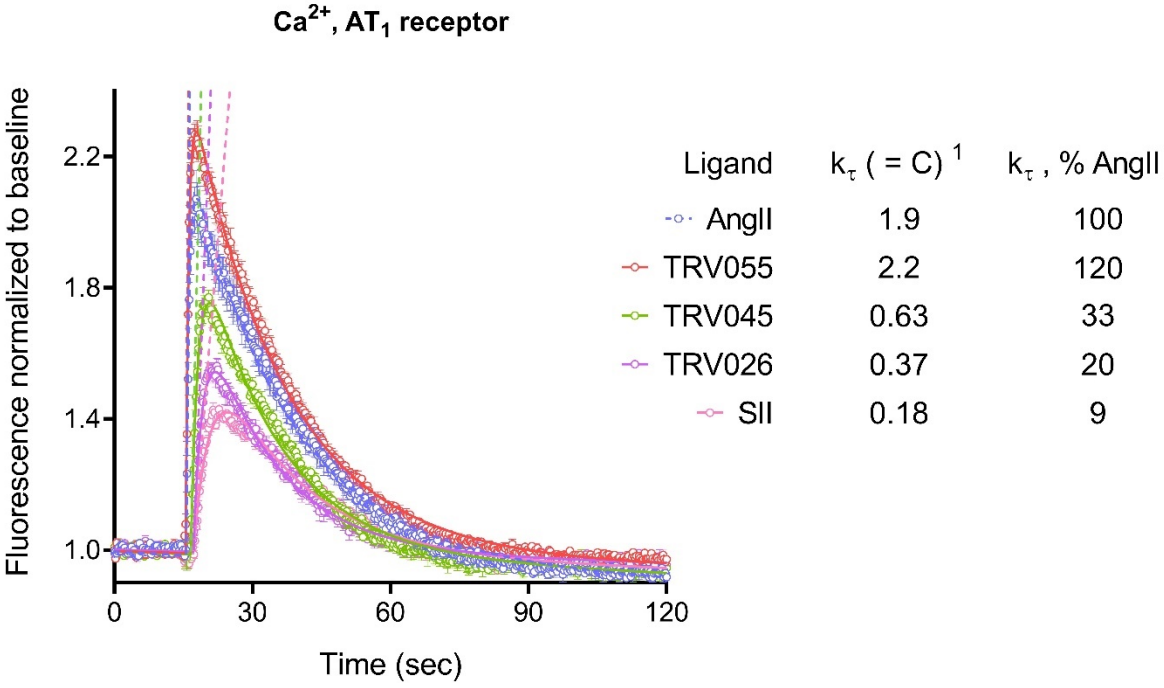
Now the initial rate value is determined. This requires application of a formula to the fitted parameter values. The formula is Eq. 8:

$$\text{Initial rate} = \text{SteadyState} \times (Dk_1 - (D-1)k_2)$$

Note SteadyState is the ligand-specific steady-state response (ligand-stimulated increment above baseline) and D is the fitting constant. Applying this formula to the data in Figure 13 gave an initial rate value of 0.36 NFU.min^{-1}. k_τ is equal to this initial rate, since a maximally-stimulating concentration of ligand was used.

Simplifying Biased Agonism Assessment Using Signaling Kinetics

GPCRs activate multiple signaling pathways and regulatory events. In GPCR drug discovery, it is desirable to activate pathways that mediate a desired therapeutic outcome, and to avoid or block stimulating pathways that lead to side effects and/or attenuate therapeutic efficacy. This pathway-selective activation by a ligand is



	AngII	TRV055	TRV045	TRV026	SII
X0	15.6	15.5	16.6	17.2	17.1
Baseline	0.994	0.996	0.995	1.00	0.997
Drift	-0.000724	-0.000379	-0.000569	-0.000339	-0.000463
C	1.88	2.19	0.625	0.373	0.176
K1	1.54	1.52	0.638	0.503	0.269
K2	0.0475	0.0492	0.0589	0.0638	0.0548

Figure 12. Initial rate analysis with baseline drift of Ca^{2+} mobilization by the AT_1 angiotensin receptor, an example of rise-and-fall to baseline time course with baseline drift analysis. The five ligands were tested at a single concentration that was maximally-stimulating (32 μM). Time course data were fit to Eq. 11 using Prism. This user-defined equation (called "[Pharmechanics] Baseline then rise-and-fall to zero time course with drift") was loaded as described in the in supplementary file Loading equations into Prism from a file. The fit parameters are shown in the table. The initial rate value is equal to the parameter C. The dashed lines indicate the initial rate. In this case, the initial rate is equal to k_τ because a maximally-stimulating concentration of ligand was used. Detailed description of the curve fitting is in the supplementary file Rise-and-fall to baseline exponential equation with baseline drift . 1, units of normalized fluorescence units.sec^{-1}. Data are from ref (29).

described as biased agonism (reviewed in refs. (31-35)). Broadly-speaking, GPCRs couple to two different signaling/regulatory limbs, G-proteins and arrestins (35). G-proteins activate signaling cascades that elicit the biological effect of the GPCR ligand. Arrestins usually block G-protein signaling, terminating the signal, but can also mediate signaling, often acting as scaffolding proteins that bring signaling partners together (75). Therapeutically, there are examples where it is potentially desirable to selectively activate one of these pathways over the other. For example, for the AT_1 receptor, ligands that selectively promote arrestin recruitment without activating G-protein can elicit increased cardiac performance compared with traditional antagonists that do not recruit arrestin (76).

k_τ Bias Ratio Calculation

Signaling bias is often quantified using ratios of efficacy for the different signaling pathways being compared. More specifically, the strength of signal transduction by the ligand-bound receptor down one pathway is divided by the strength transduction down the second pathway in the comparison (reviewed in ref. (31)). This approach

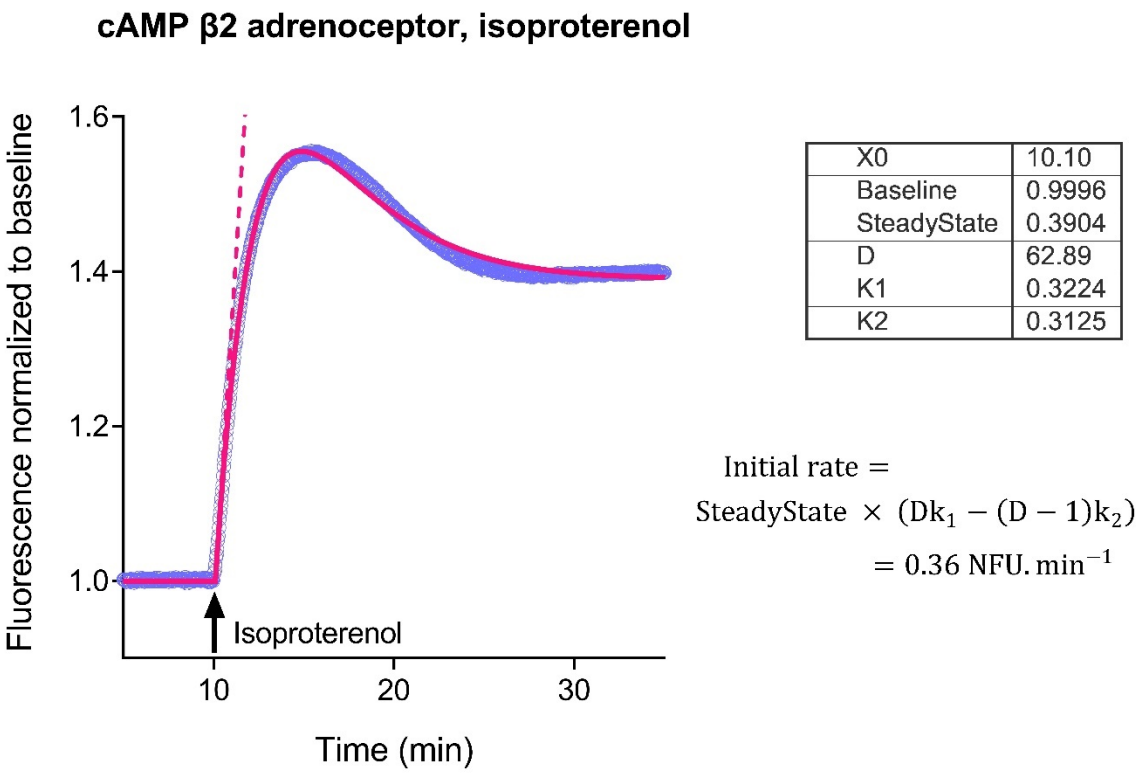


Figure 13. Initial rate analysis for a rise-and-fall to steady-state time course, cAMP accumulation stimulated by the β_2 adrenoceptor. The receptor was stimulated with a maximally-stimulating concentration of isoproterenol (20 µM). cAMP was detected with Green Down cADDis using the Hamamatsu FDSS reader at 2 second read frequency. The downward sensor data was normalized to baseline and converted to upward data as described in Data Normalization. Time course data were fit to Eq. 12 in Prism. This user-defined equation (called "[Pharmechanics] Baseline then rise-and-fall to steady state time course") was loaded as described in the supplementary file Loading equations into Prism from a file. The fit parameters are shown in the table. The initial rate value was calculated from the fitted parameter values using the formula shown. The initial rate is indicated by the dashed line. In this case, the initial rate is equal to k_τ because a maximally-stimulating concentration of ligand was used. Detailed description of the curve fitting is in the supplementary file Rise-and-fall to steady-state analysis. NFU is normalized fluorescence units.

is directly amenable to the initial rate measurement of signal transduction; k_τ is a direct measure of the strength of signal transduction by the ligand-bound receptor. Bias can simply be quantified as the ratio of the k_τ values.

This bias calculation is a simple, two-step process (29) and is exemplified here using the angiotensin AT_1 receptor data (Figure 14), comparing arrestin recruitment with Ca^{2+} mobilization (Figures 10 and 12). The first step is to tabulate the k_τ values for the pathways being compared (Figure 14). Next, the k_τ values are normalized to the k_τ value of a reference ligand. In this case, AngII was used as the reference ligand. The initial rate is expressed as a percentage of that for the reference (k_τ %) and this is done for the multiple pathways being compared (Figure 14, Step 2). For the AT_1 receptor, this yields the k_τ % values for arrestin and Ca^{2+} in Figure 14 (ranging from 45 - 100% for arrestin and 9-120% for calcium).

The next step is to compare the pathways by calculating the kinetic bias ratio (29). This is done by dividing the k_τ % value for one pathway by the k_τ % value for the other (Figure 14, Step 3). For the AT_1 receptor, this gives the k_τ % ratios in Figure 14. The highest arrestin : Ca^{2+} ratio in this set was 5.0, for SII. This result indicates SII is arrestin-biased by 5.0-fold, relative to AngII. The lowest value was 0.8 for TRV055. This value, being close to 1, indicates TRV055 is unbiased for the two pathways, relative to AngII. These bias estimates obtained using the k_τ method are in good agreement with established methods for quantifying bias (77).

It is important to note the k_τ method quantifies bias in terms of efficacy but not affinity. More specifically, k_τ defines the efficacy of the ligand-bound receptor to couple with an effector to generate a signal, but does not define the affinity of the ligand for the receptor-effector complex. Bias can be manifest at the level of affinity as well as efficacy; a ligand can bind with different affinity to the receptor in complex with different effectors (31).

Comparison with Existing Methods

Measuring biased agonism is not trivial. Major advances have been made in applying receptor theory to the data analysis and in training and educating investigators in the calculations. Numerous methods are now available, reviewed in ref. (31). However, challenges remain in quantifying biased agonism. There are three issues that the kinetic analysis presented here can help address. First, the bias estimate can be dependent on the time point at which it is measured (27,30). This problem emerges from the time-dependence of signaling; a ligand can be a partial agonist at one time point and a full agonist at a later time point, resulting in bias at the former time point and no bias at the latter. This is demonstrated by the AT_1 arrestin data in Figure 10 - at the early time points on the rise phase SII and TRV045 are partial agonist but later at the plateau the compounds are near-full agonists (relative to AngII). The initial rate approach solves this problem because the rate is the same at all time points. The second issue is the abstract scales that are used to quantify efficacy and biased agonism. The lack of intuitive meaning to these parameters makes it challenging to translate them to in vivo efficacy and to determine how large the bias effect is. The kinetic approach reduces this uncertainty because it is more intuitive - the initial rate is a biologically meaningful parameter and the bias ratio is simply the rate of one pathway relative to another (normalized to a reference ligand). Third, the data analysis methods and procedures involved in quantifying bias can be complex, often involving advanced curve fitting (such as simultaneous fits to multiple data sets) and multiple nested calculations (27,30,31). The kinetic method is simpler; once the initial rate is obtained, bias is simply the ratio of the initial rates for the pathways.

Conclusions

The timing of GPCR signaling is important in uncovering new mechanisms of signaling and regulation, revealing new spatiotemporal pharmacologic modalities potentially useful for new therapeutic development. Employing this kinetic dimension to drug discovery and receptor research requires straightforward methods to measure the time course of signaling, and tractable data analysis methods to reduce the time course data to meaningful drug parameters. This chapter describes how this can be done using genetically-encoded fluorescent biosensors. The continuous-read modality coupled with the exceptionally efficient workflow of the assay enables high-quality time course data recording. The data are ideally suited for analysis using an enzyme-based kinetic framework. This analysis has been reduced to practice so that any investigator familiar with basic curve-fitting analysis can employ it, as described in the step-by-step analysis guides. The drug parameter obtained, the initial rate of signaling by ligand-bound receptor, is intuitive and familiar, enabling a simplified and parsimonious calculation of biased agonism. These methods enable investigators to explore the kinetic dimension of GPCR signaling in their receptor research and drug discovery projects.

Acknowledgements

We are grateful to Anne Marie Quinn, Paul Tewson and Rose Quinn for reviewing and providing material for this chapter. Research reported in this chapter was funded by The National Institutes of Health under the following SBIR awards: R44DA050357, R44GM125390, R44NS082222 and National Science Foundation SBIR IIP-1430878.

1. Tabulate k_τ values

Compound	kτ (NFU per min)	
	Arrestin	Calcium
AngII	0.36	1.9
TRV055	0.34	2.2
TRV045	0.26	0.63
TRV026	0.21	0.37
SII	0.16	0.18

2. Normalize to control (AngII)

Compound	kτ (NFU per min)		kτ (% AngII)	
	Arrestin	Calcium	Arrestin	Calcium
AngII	0.36	1.9	100	100
TRV055	0.34	2.2	95	120
TRV045	0.26	0.63	74	33
TRV026	0.21	0.37	59	20
SII	0.16	0.18	45	9

3. Divide normalized k_τ value of one pathway by value of other pathway

Compound	kτ (NFU per min)		kτ (% AngII)		% kτ ratio
	Arrestin	Calcium	Arrestin	Calcium	
AngII	0.36	1.9	100	100	1.0
TRV055	0.34	2.2	95	120	0.8
TRV045	0.26	0.63	74	33	2.2
TRV026	0.21	0.37	59	20	3.0
SII	0.16	0.18	45	9	5.0

Figure 14. k_τ bias ratio calculation steps, exemplified using AT_1 arrestin and Ca^{2+} mobilization data (from Figures 10 and 12).

References

1. Fredriksson R., Lagerstrom M. C., Lundin L. G., Schioth H. B. The G-protein-coupled receptors in the human genome form five main families. Phylogenetic analysis, paralogon groups, and fingerprints. Mol Pharmacol. 2003;63:1256–1272. doi: 10.1124/mol.63.6.1256. doi. PubMed PMID: 12761335.

2. Sriram K., Insel P. A. GPCRs as targets for approved drugs: How many targets and how many drugs? Mol Pharmacol. 2018. doi: 10.1124/mol.117.111062. doi. PubMed PMID: 29298813.
3. Rask-Andersen M., Masuram S., Schioth H. B. The druggable genome: Evaluation of drug targets in clinical trials suggests major shifts in molecular class and indication. Annu Rev Pharmacol Toxicol. 2014;54:9–26. doi: 10.1146/annurev-pharmtox-011613-135943. doi. PubMed PMID: 24016212.
4. Salomon Y., Londos C., Rodbell M. A highly sensitive adenylate cyclase assay. Anal Biochem. 1974;58:541–548. doi: 10.1016/0003-2697(74)90222-x. doi. PubMed PMID: 4827395.
5. Berridge M. J., Dawson R. M., Downes C. P., Heslop J. P., Irvine R. F. Changes in the levels of inositol phosphates after agonist-dependent hydrolysis of membrane phosphoinositides. Biochem J. 1983;212:473–482. doi: 10.1042/bj2120473. doi. PubMed PMID: 6309146.
6. Wang, T., Li, Z., Cvijic, M. E., Zhang, L. & Sum, C. S. in *Assay Guidance Manual* (eds G. S. Sittampalam *et al.*) Available at: https://www.ncbi.nlm.nih.gov/books/NBK464633/ (2004).
7. Lohse M. J., et al. Optical techniques to analyze real-time activation and signaling of G-protein-coupled receptors. Trends Pharmacol Sci. 2008;29:159–165. doi: 10.1016/j.tips.2007.12.002. doi. PubMed PMID: 18262662.
8. Marullo S., Bouvier M. Resonance energy transfer approaches in molecular pharmacology and beyond. Trends Pharmacol Sci. 2007;28:362–365. doi: 10.1016/j.tips.2007.06.007. doi. PubMed PMID: 17629577.
9. Tsvetanova N. G., Irannejad R., von Zastrow M. G protein-coupled receptor (GPCR) signaling via heterotrimeric G proteins from endosomes. J Biol Chem. 2015;290:6689–6696. doi: 10.1074/jbc.R114.617951. doi. PubMed PMID: 25605726.
10. Ferrandon S., et al. Sustained cyclic AMP production by parathyroid hormone receptor endocytosis. Nat Chem Biol. 2009;5:734–742. doi: 10.1038/nchembio.206. doi. PubMed PMID: 19701185.
11. Namkung Y., et al. Functional selectivity profiling of the angiotensin II type 1 receptor using pathway-wide BRET signaling sensors. Sci Signal. 2018;11 doi: 10.1126/scisignal.aat1631. doi. PubMed PMID: 30514808.
12. Olsen R. H. J., et al. TRUPATH, an open-source biosensor platform for interrogating the GPCR transducerome. Nat Chem Biol. 2020. doi: 10.1038/s41589-020-0535-8. doi. PubMed PMID: 32367019.
13. Greenwald E. C., Mehta S., Zhang J. Genetically Encoded Fluorescent Biosensors Illuminate the Spatiotemporal Regulation of Signaling Networks. Chem Rev. 2018;118:11707–11794. doi: 10.1021/acs.chemrev.8b00333. doi. PubMed PMID: 30550275.
14. Moore C. A., Milano S. K., Benovic J. L. Regulation of receptor trafficking by GRKs and arrestins. Annu Rev Physiol. 2007;69:451–482. doi: 10.1146/annurev.physiol.69.022405.154712. doi. PubMed PMID: 17037978.
15. Kakiuchi S., Rall T. W. The influence of chemical agents on the accumulation of adenosine 3',5'-Phosphate in slices of rabbit cerebellum. Mol Pharmacol. 1968;4:367–378. PubMed PMID: 4298780.
16. Shear M., Insel P. A., Melmon K. L., Coffino P. Agonist-specific refractoriness induced by isoproterenol. Studies with mutant cells. J Biol Chem. 1976;251:7572–7576. PubMed PMID: 187593.
17. Exton J. H., Robison G. A., Sutherland E. W., Park C. R. Studies on the role of adenosine 3',5'-monophosphate in the hepatic actions of glucagon and catecholamines. J Biol Chem. 1971;246:6166–6177. PubMed PMID: 4331382.
18. Krupnick J. G., Benovic J. L. The role of receptor kinases and arrestins in G protein-coupled receptor regulation. Annu Rev Pharmacol Toxicol. 1998;38:289–319. doi: 10.1146/annurev.pharmtox.38.1.289. doi. PubMed PMID: 9597157.
19. Thomsen A. R. B., et al. GPCR-G Protein-beta-Arrestin Super-Complex Mediates Sustained G Protein Signaling. Cell. 2016;166:907–919. doi: 10.1016/j.cell.2016.07.004. doi. PubMed PMID: 27499021.
20. Calebiro D., et al. Persistent cAMP-signals triggered by internalized G-protein-coupled receptors. PLoS Biol. 2009;7:e1000172. doi: 10.1371/journal.pbio.1000172. doi. PubMed PMID: 19688034.
21. Mullershausen F., et al. Persistent signaling induced by FTY720-phosphate is mediated by internalized S1P1 receptors. Nat Chem Biol. 2009;5:428–434. doi: 10.1038/nchembio.173. doi. PubMed PMID: 19430484.
22. Stoeber M., et al. A Genetically Encoded Biosensor Reveals Location Bias of Opioid Drug Action. Neuron. 2018;98:963–976 e965. doi: 10.1016/j.neuron.2018.04.021. doi. PubMed PMID: 29754753.

23. Jensen D. D., et al. Neurokinin 1 receptor signaling in endosomes mediates sustained nociception and is a viable therapeutic target for prolonged pain relief. Sci Transl Med. 2017;9 doi: 10.1126/scitranslmed.aal3447. doi. PubMed PMID: 28566424.
24. Vilardaga J. P., Jean-Alphonse F. G., Gardella T. J. Endosomal generation of cAMP in GPCR signaling. Nat Chem Biol. 2014;10:700–706. doi: 10.1038/nchembio.1611. doi. PubMed PMID: 25271346.
25. Lobingier B. T., von Zastrow M. When trafficking and signaling mix: How subcellular location shapes G protein-coupled receptor activation of heterotrimeric G proteins. Traffic. 2019;20:130–136. doi: 10.1111/tra.12634. doi. PubMed PMID: 30578610.
26. Hothersall J. D., Brown A. J., Dale I., Rawlins P. Can residence time offer a useful strategy to target agonist drugs for sustained GPCR responses? Drug Discov Today. 2016;21:90–96. doi: 10.1016/j.drudis.2015.07.015. doi. PubMed PMID: 26226643.
27. Klein Herenbrink C., et al. The role of kinetic context in apparent biased agonism at GPCRs. Nat Commun. 2016;7:10842. doi: 10.1038/ncomms10842. doi. PubMed PMID: 26905976.
28. Zhu X., Finlay D. B., Glass M., Duffull S. B. Model-free and kinetic modelling approaches for characterising non-equilibrium pharmacological pathway activity: Internalisation of cannabinoid CB1 receptors. Br J Pharmacol. 2019;176:2593–2607. doi: 10.1111/bph.14684. doi. PubMed PMID: 30945265.
29. Hoare S. R. J., Tewson P. H., Quinn A. M., Hughes T. E. A kinetic method for measuring agonist efficacy and ligand bias using high resolution biosensors and a kinetic data analysis framework. Sci Rep. 2020;10:1766. doi: 10.1038/s41598-020-58421-9. doi. PubMed PMID: 32019973.
30. Thompson G. L., et al. Systematic analysis of factors influencing observations of biased agonism at the mu-opioid receptor. Biochem Pharmacol. 2016;113:70–87. doi: 10.1016/j.bcp.2016.05.014. doi. PubMed PMID: 27286929.
31. Kenakin T. Biased Receptor Signaling in Drug Discovery. Pharmacol Rev. 2019;71:267–315. doi: 10.1124/pr.118.016790. doi. PubMed PMID: 30914442.
32. Gesty-Palmer D., Luttrell L. M. Refining efficacy: exploiting functional selectivity for drug discovery. Adv Pharmacol. 2011;62:79–107. doi: 10.1016/B978-0-12-385952-5.00009-9. doi. PubMed PMID: 21907907.
33. Kenakin T., Christopoulos A. Signalling bias in new drug discovery: detection, quantification and therapeutic impact. Nat Rev Drug Discov. 2013;12:205–216. doi: 10.1038/nrd3954. doi. PubMed PMID: 23411724.
34. Violin J. D., Crombie A. L., Soergel D. G., Lark M. W. Biased ligands at G-protein-coupled receptors: promise and progress. Trends Pharmacol Sci. 2014;35:308–316. doi: 10.1016/j.tips.2014.04.007. doi. PubMed PMID: 24878326.
35. Gurevich V. V., Gurevich E. V. Biased GPCR signaling: Possible mechanisms and inherent limitations. Pharmacol Ther. 2020;107540 doi: 10.1016/j.pharmthera.2020.107540. doi. PubMed PMID: 32201315.
36. Hoare S. R. J., Pierre N., Moya A. G., Larson B. Kinetic operational models of agonism for G-protein-coupled receptors. J Theor Biol. 2018;446:168–204. doi: 10.1016/j.jtbi.2018.02.014. doi. PubMed PMID: 29486201.
37. Hoare S. R. J., Tewson P. H., Quinn A. M., Hughes T. E., Bridge L. J. Analyzing kinetic signaling data for G−protein−coupled receptors. Scientific Reports. 2020;10:12263. doi: 10.1038/s41598-020-67844-3. doi. PubMed PMID: 32704081.
38. Newman R. H., Fosbrink M. D., Zhang J. Genetically encodable fluorescent biosensors for tracking signaling dynamics in living cells. Chem Rev. 2011;111:3614–3666. doi: 10.1021/cr100002u. doi. PubMed PMID: 21456512.
39. Lakowicz, J. R. *Principles of Fluorescence Spectroscopy*. (Springer Science & Business Media, 2013).
40. Shrestha D., Jenei A., Nagy P., Vereb G., Szöllősi J. Understanding FRET as a research tool for cellular studies. Int. J. Mol. Sci. 2015;16:6718–6756. doi: 10.3390/ijms16046718. doi. PubMed PMID: 25815593.
41. Miyawaki A., et al. Fluorescent indicators for Ca2+ based on green fluorescent proteins and calmodulin. Nature. 1997;388:882–887. doi: 10.1038/42264. doi. PubMed PMID: 9278050.
42. Lam A. J., et al. Improving FRET dynamic range with bright green and red fluorescent proteins. Nat. Methods. 2012;9:1005–1012. doi: 10.1038/nmeth.2171. doi. PubMed PMID: 22961245.

43. Mastop M., et al. Characterization of a spectrally diverse set of fluorescent proteins as FRET acceptors for mTurquoise2. Sci. Rep. 2017;7:11999. doi: 10.1038/s41598-017-12212-x. doi. PubMed PMID: 28931898.
44. Kuner T., Augustine G. J. A genetically encoded ratiometric indicator for chloride: capturing chloride transients in cultured hippocampal neurons. Neuron. 2000;27:447–459. PubMed PMID: 11055428.
45. Sakaue-Sawano A., Miyawaki A. Visualizing spatiotemporal dynamics of multicellular cell-cycle progressions with fucci technology. Cold Spring Harb. Protoc. 2014;2014 doi: 10.1101/pdb.prot080408. doi. PubMed PMID: 24786503.
46. Harlen K. M., Roush E. C., Clayton J. E., Martinka S., Hughes T. E. Live-Cell Assays for Cell Stress Responses Reveal New Patterns of Cell Signaling Caused by Mutations in Rhodopsin, α-Synuclein and TDP-43. Front. Cell. Neurosci. 2019;13:535. doi: 10.3389/fncel.2019.00535. doi. PubMed PMID: 31920544.
47. Lambert T. J. FPbase: a community-editable fluorescent protein database. Nat. Methods. 2019;16:277–278. doi: 10.1038/s41592-019-0352-8. doi. PubMed PMID: 30886412.
48. Ding, Y. *et al.* Ratiometric biosensors based on dimerization-dependent fluorescent protein exchange. *Nature Publishing Group* **12**, 195-198- 193 p following 198, doi:10.1038/nmeth.3261 (2015).
49. Siegel M. S., Isacoff E. Y. A Genetically Encoded Optical Probe of Membrane Voltage. Neuron. 1997;19:735–741. PubMed PMID: 9354320.
50. Storace D., et al. Toward Better Genetically Encoded Sensors of Membrane Potential. Trends Neurosci. 2016;39:277–289. doi: 10.1016/j.tins.2016.02.005. doi. PubMed PMID: 27130905.
51. Baird G. S., Zacharias D. A., Tsien R. Y. Circular permutation and receptor insertion within green fluorescent proteins. Proc. Natl. Acad. Sci. U. S. A. 1999;96:11241–11246. PubMed PMID: 10500161.
52. Akerboom J., et al. Optimization of a GCaMP calcium indicator for neural activity imaging. J. Neurosci. 2012;32:13819–13840. PubMed PMID: 23035093.
53. Barnett L. M., Hughes T. E., Drobizhev M. Deciphering the molecular mechanism responsible for GCaMP6m's Ca2+-dependent change in fluorescence. PLoS One. 2017;12:e0170934. doi: 10.1371/journal.pone.0170934. doi. PubMed PMID: 28182677.
54. Ahrens M. B., Orger M. B., Robson D. N., Li J. M., Keller P. J. Whole-brain functional imaging at cellular resolution using light-sheet microscopy. Nat. Methods. 2013;10:413–420. doi: 10.1038/nmeth.2434. doi. PubMed PMID: 23524393.
55. Sofroniew N. J., Flickinger D., King J., Svoboda K. A large field of view two-photon mesoscope with subcellular resolution for in vivo imaging. bioRxiv. doi. 2016.
56. Molina R. S., et al. Understanding the Fluorescence Change in Red Genetically Encoded Calcium Ion Indicators. Biophys. J. 2019;116:1873–1886. doi: 10.1016/j.bpj.2019.04.007. doi. PubMed PMID: 31054773.
57. Shaner N. C., et al. A bright monomeric green fluorescent protein derived from Branchiostoma lanceolatum. Nat. Methods. 2013;10:407–409. doi: 10.1038/nmeth.2413. doi. PubMed PMID: 23524392.
58. Woehler A., Wlodarczyk J., Neher E. Signal/Noise Analysis of FRET-Based Sensors. Biophys. J. 2010;99:2344–2354. PubMed PMID: 20923670.
59. Arkin, M. R. *et al.* in *Assay Guidance Manual* (eds G. Sitta Sittampalam *et al.*) (Eli Lilly & Company and the National Center for Advancing Translational Sciences, 2012).
60. Willoughby D., Cooper D. M. F. Live-cell imaging of cAMP dynamics. Nat. Methods. 2008;5:29–36. doi: 10.1038/nmeth1135. doi. PubMed PMID: 18165805.
61. Tewson P. H., Martinka S., Shaner N. C., Hughes T. E., Quinn A. M. New DAG and cAMP Sensors Optimized for Live-Cell Assays in Automated Laboratories. J Biomol Screen. 2016;21:298–305. doi: 10.1177/1087057115618608. doi. PubMed PMID: 26657040.
62. Tewson P., et al. Assay for Detecting Galphai-Mediated Decreases in cAMP in Living Cells. SLAS Discov. 2018;23:898–906. doi: 10.1177/2472555218786238. doi. PubMed PMID: 29991302.
63. Tewson P., et al. Simultaneous detection of Ca2+ and diacylglycerol signaling in living cells. PLoS One. 2012;7:e42791. doi: 10.1371/journal.pone.0042791. doi. PubMed PMID: 22912738.
64. Zhao Y., et al. An expanded palette of genetically encoded Ca(2)(+) indicators. Science. 2011;333:1888–1891. doi: 10.1126/science.1208592. doi. PubMed PMID: 21903779.

65. Luttrell L. M., Gesty-Palmer D. Beyond desensitization: physiological relevance of arrestin-dependent signaling. Pharmacol Rev. 2010;62:305–330. doi: 10.1124/pr.109.002436. doi. PubMed PMID: 20427692.
66. Wang, T. *et al.* in *Assay Guidance Manual* (eds S. Markossian *et al.*) (2004).
67. Gillis A., et al. Low intrinsic efficacy for G protein activation can explain the improved side effect profiles of new opioid agonists. Sci Signal. 2020;13 doi: 10.1126/scisignal.aaz3140. doi. PubMed PMID: 32234959.
68. Kenakin T. Quantifying biological activity in chemical terms: a pharmacology primer to describe drug effect. ACS Chem Biol. 2009;4:249–260. doi: 10.1021/cb800299s. doi. PubMed PMID: 19193052.
69. Xin W., Tran T. M., Richter W., Clark R. B., Rich T. C. Roles of GRK and PDE4 activities in the regulation of beta2 adrenergic signaling. J Gen Physiol. 2008;131:349–364. doi: 10.1085/jgp.200709881. doi. PubMed PMID: 18347080.
70. Violin J. D., et al. beta2-adrenergic receptor signaling and desensitization elucidated by quantitative modeling of real time cAMP dynamics. J Biol Chem. 2008;283:2949–2961. doi: 10.1074/jbc.M707009200. doi. PubMed PMID: 18045878.
71. Rich T. C., et al. Cellular mechanisms underlying prostaglandin-induced transient cAMP signals near the plasma membrane of HEK-293 cells. Am J Physiol Cell Physiol. 2007;292:C319–331. doi: 10.1152/ajpcell.00121.2006. doi. PubMed PMID: 16899551.
72. Chang Y. Y. Cyclic 3',5'-adenosine monophosphate phosphodiesterase produced by the slime mold Dictyostelium discoideum. Science. 1968;161:57–59. PubMed PMID: 4298142.
73. Motulsky, H. J. *How to: Plateau followed by one phase association.* Available at: https://www.graphpad.com/guides/prism/latest/curve-fitting/reg_exponential_plateau_then_association.htm (2019).
74. Motulsky, H. J. *Equation: log(agonist) vs. response -- Variable slope.* Available at: https://www.graphpad.com/guides/prism/latest/curve-fitting/reg_dr_stim_variable.htm (2019).
75. Peterson Y. K., Luttrell L. M. The Diverse Roles of Arrestin Scaffolds in G Protein-Coupled Receptor Signaling. Pharmacol Rev. 2017;69:256–297. doi: 10.1124/pr.116.013367. doi. PubMed PMID: 28626043.
76. Violin J. D., et al. Selectively engaging beta-arrestins at the angiotensin II type 1 receptor reduces blood pressure and increases cardiac performance. J Pharmacol Exp Ther. 2010;335:572–579. doi: 10.1124/jpet.110.173005. doi. PubMed PMID: 20801892.
77. Rajagopal S., et al. Quantifying ligand bias at seven-transmembrane receptors. Mol Pharmacol. 2011;80:367–377. doi: 10.1124/mol.111.072801. doi. PubMed PMID: 21610196.

Cell Viability Assays

Terry L Riss, PhD,[1,*] Richard A Moravec, BS,[1] Andrew L Niles, MS,[1] Sarah Duellman, PhD,[1] Hélène A Benink, PhD,[1] Tracy J Worzella, MS,[1] and Lisa Minor[2,†]

Created: May 1, 2013; Updated: July 1, 2016.

Abstract

This chapter is an introductory overview of the most commonly used assay methods to estimate the number of viable cells in multi-well plates. This chapter describes assays where data are recorded using a plate-reader; it does not cover assay methods designed for flow cytometry or high content imaging. The assay methods covered include the use of different classes of colorimetric tetrazolium reagents, resazurin reduction and protease substrates generating a fluorescent signal, the luminogenic ATP assay, and a novel real-time assay to monitor live cells for days in culture. The assays described are based on measurement of a marker activity associated with viable cell number. These assays are used for measuring the results of cell proliferation, testing for cytotoxic effects of compounds, and for multiplexing as an internal control to determine viable cell number during other cell-based assays.

Introduction

Cell-based assays are often used for screening collections of compounds to determine if the test molecules have effects on cell proliferation or show direct cytotoxic effects that eventually lead to cell death. Cell-based assays also are widely used for measuring receptor binding and a variety of signal transduction events that may involve the expression of genetic reporters, trafficking of cellular components, or monitoring organelle function. Regardless of the type of cell-based assay being used, it is important to know how many viable cells are remaining at the end of the experiment. There are a variety of assay methods that can be used to estimate the number of viable eukaryotic cells. This chapter will provide an overview of some of the major methods used in multi-well formats where data are recorded using a plate reader. The methods described include: tetrazolium reduction, resazurin reduction, protease markers, and ATP detection. Methods for flow cytometry and high content imaging may be covered in different chapters in the future.

The tetrazolium reduction, resazurin reduction, and protease activity assays measure some aspect of general metabolism or an enzymatic activity as a marker of viable cells. All of these assays require incubation of a reagent with a population of viable cells to convert a substrate to a colored or fluorescent product that can be detected with a plate reader. Under most standard culture conditions, incubation of the substrate with viable cells will result in generating a signal that is proportional to the number of viable cells present. When cells die, they rapidly lose the ability to convert the substrate to product. That difference provides the basis for many of the commonly used cell viability assays. The ATP assay is somewhat different in that the addition of assay reagent immediately ruptures the cells, thus there is no incubation period of reagent with a viable cell population.

Author Affiliations: 1 Promega Corporation; Email: Terry.riss@promega.com; Email: Rich.moravec@promega.com; Email: Andrew.niles@promega.com; Email: Helene.benink@promega.com; Email: Tracy.worzella@promega.com. 2 In Vitro Strategies, LLC; Email: lisakminor@yahoo.com.

Corresponding author.

* Editor

† Editor

Tetrazolium Reduction Assays

A variety of tetrazolium compounds have been used to detect viable cells. The most commonly used compounds include: MTT, MTS, XTT, and WST-1. These compounds fall into two basic categories: 1) MTT which is positively charged and readily penetrates viable eukaryotic cells and 2) those such as MTS, XTT, and WST-1 which are negatively charged and do not readily penetrate cells. The latter class (MTS, XTT, WST-1) are typically used with an intermediate electron acceptor that can transfer electrons from the cytoplasm or plasma membrane to facilitate the reduction of the tetrazolium into the colored formazan product.

MTT Tetrazolium Assay Concept

The MTT (3-(4,5-dimethylthiazol-2-yl)-2,5-diphenyltetrazolium bromide) tetrazolium reduction assay was the first homogeneous cell viability assay developed for a 96-well format that was suitable for high throughput screening (HTS) (1). The MTT tetrazolium assay technology has been widely adopted and remains popular in academic labs as evidenced by thousands of published articles. The MTT substrate is prepared in a physiologically balanced solution, added to cells in culture, usually at a final concentration of 0.2 - 0.5mg/ml, and incubated for 1 to 4 hours. The quantity of formazan (presumably directly proportional to the number of viable cells) is measured by recording changes in absorbance at 570 nm using a plate reading spectrophotometer. A reference wavelength of 630 nm is sometimes used, but not necessary for most assay conditions.

Viable cells with active metabolism convert MTT into a purple colored formazan product with an absorbance maximum near 570 nm (Figure 1). When cells die, they lose the ability to convert MTT into formazan, thus color formation serves as a useful and convenient marker of only the viable cells. The exact cellular mechanism of MTT reduction into formazan is not well understood, but likely involves reaction with NADH or similar reducing molecules that transfer electrons to MTT (2). Speculation in the early literature involving specific mitochondrial enzymes has led to the assumption mentioned in numerous publications that MTT is measuring mitochondrial activity (3, 4).

The formazan product of the MTT tetrazolium accumulates as an insoluble precipitate inside cells as well as being deposited near the cell surface and in the culture medium. The formazan must be solubilized prior to recording absorbance readings. A variety of methods have been used to solubilize the formazan product, stabilize the color, avoid evaporation, and reduce interference by phenol red and other culture medium components (5-7). Various solubilization methods include using: acidified isopropanol, DMSO, dimethylformamide, SDS, and combinations of detergent and organic solvent (1, 5-7). Acidification of the solubilizing solution has the benefit of changing the color of phenol red to yellow color that may have less interference with absorbance readings. The pH of the solubilization solution can be adjusted to provide maximum absorbance if sensitivity is an issue (8); however, other assay technologies offer much greater sensitivity than MTT.

The amount of signal generated is dependent on several parameters including: the concentration of MTT, the length of the incubation period, the number of viable cells and their metabolic activity. All of these parameters should be considered when optimizing the assay conditions to generate a sufficient amount of product that can be detected above background.

The conversion of MTT to formazan by cells in culture is time dependent (Figure 2).

Longer incubation time will result in accumulation of color and increased sensitivity up to a point; however, the incubation time is limited because of the cytotoxic nature of the detection reagents which utilize energy (reducing equivalents such as NADH) from the cell to generate a signal. For cell populations in log phase growth, the amount of formazan product is generally proportional to the number of metabolically active viable cells as demonstrated by the linearity of response in Figure 2. Culture conditions that alter the metabolism of the cells will likely affect the rate of MTT reduction into formazan. For example, when adherent cells in culture

approach confluence and growth becomes contact inhibited, metabolism may slow down and the amount MTT reduction per cell will be lower. That situation will lead to a loss of linearity between absorbance and cell number. Other adverse culture conditions such as altered pH or depletion of essential nutrients such as glucose may lead to a change in the ability of cells to reduce MTT.

The MTT assay was developed as a non-radioactive alternative to tritiated thymidine incorporation into DNA for measuring cell proliferation (1). In many experimental situations, the MTT assay can directly substitute for the tritiated thymidine incorporation assay (Figure 3).

However, it is worth noting that MTT reduction is a marker reflecting viable cell metabolism and not specifically cell proliferation. Tetrazolium reduction assays are often erroneously described as measuring cell proliferation without the use of proper controls to confirm effects on metabolism (10).

Shortly after addition of MTT, the morphology of some cell types can be observed to change dramatically suggesting altered physiology (11 and Figure 4).

Toxicity of the MTT compound is likely related to the concentration added to cells. Optimizing the concentration may result in lower toxicity. Given the cytotoxic nature of MTT, the assay method must be considered as an endpoint assay. A recent report speculated that formazan crystals contribute to harming cells by puncturing membranes during exocytosis (12). The observation of extracellular formazan crystals many times the diameter of cells that grow longer over time make it seem unlikely that exocytosis of those large structures was involved (Figure 4 and 5).

Growing crystals may suggest that marginally soluble formazan accumulates where seed crystals have begun to deposit.

Reducing compounds are known to interfere with tetrazolium reduction assays. Chemicals such as ascorbic acid, or sulfhydryl-containing compounds including reduced glutathione, coenzyme A, and dithiothreitol, can reduce tetrazolium salts non-enzymatically and lead to increased absorbance values in assay wells (13-17). Culture medium at elevated pH or extended exposure of reagents to direct light also may cause an accelerated spontaneous reduction of tetrazolium salts and result in increased background absorbance values. Suspected chemical interference of test compounds can be confirmed by measuring absorbance values from control wells without cells incubated with culture medium containing MTT and various concentrations of the test compound.

Commercial Availability

Commercial kits containing solutions of MTT and a solubilization reagent as well as MTT reagent powder are available from several vendors. For example:

- CellTiter 96® Non-Radioactive Cell Proliferation Assay. Promega Corporation Cat.# G4000,
- Cell Growth Determination Kit, MTT based. Sigma-Aldrich Cat.# CGD1-1KT, and
- MTT Cell Growth Assay Kit. Millipore Cat.# CT02.
- Thiazolyl Blue Tetrazolium Bromide (MTT Powder). Sigma-Aldrich Cat.# M2128.

The concentration of the MTT solution and the nature of the solubilization reagent differ among various vendors. The amount of formazan signal generated will depend on variety of parameters including the cell type, number of cells per well, culture medium, etc. Although the commercially available kits are broadly applicable to a large number of cell types and assay conditions, the concentration of the MTT and the type of solubilization solution may need to be adjusted for optimal performance.

Reagent Preparation

MTT Solution

1. Dissolve MTT in Dulbecco's Phosphate Buffered Saline, pH=7.4 (DPBS) to 5 mg/ml.

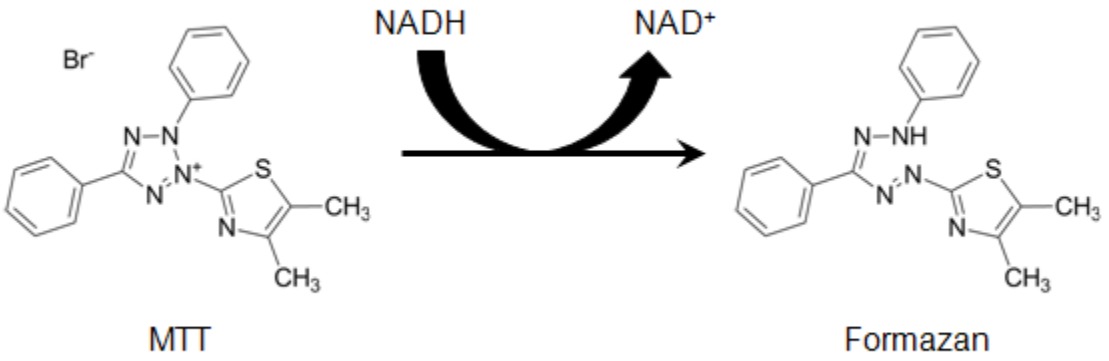


Figure 1: Structures of MTT and colored formazan product.

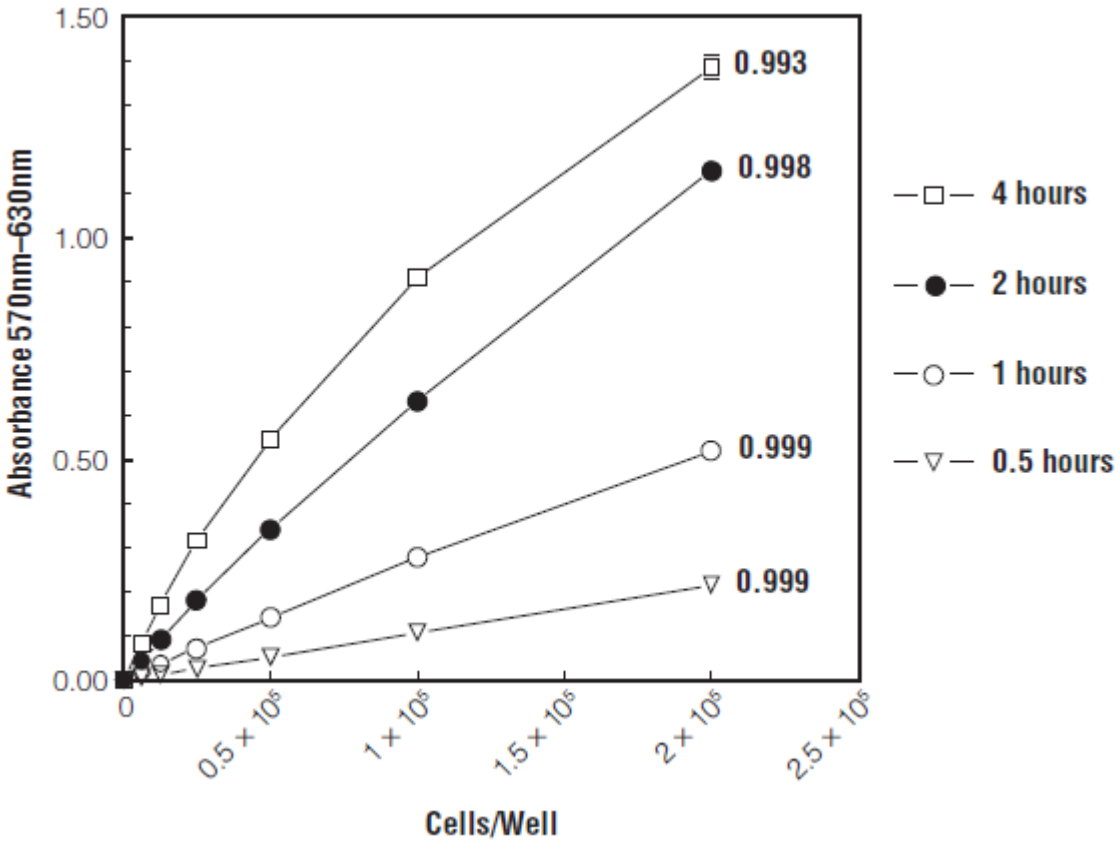


Figure 2: Direct correlation of formazan absorbance with B9 hybridoma cell number and time-dependent increase in absorbance. Note: there is little absorbance change between 2 and 4 hours. Adapted from CellTiter 96® Non-Radioactive Cell Proliferation Assay Technical Bulletin #112 (9).

2. Filter-sterilize the MTT solution through a 0.2 µM filter into a sterile, light protected container.
3. Store the MTT solution, protected from light, at 4°C for frequent use or at -20°C for long term storage.

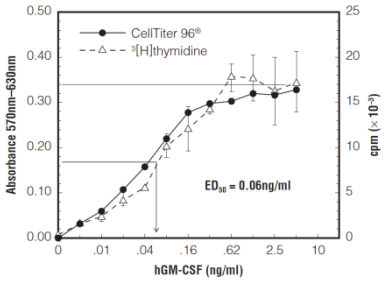


Figure 3: A comparison of using the MTT and ^{3}[H]thymidine incorporation assays of hGM-CSF-treated TF-1 cells. A blank absorbance value of 0.065 (from wells without cells but treated with MTT) was subtracted from all absorbance values. Adapted from CellTiter 96® Non-Radioactive Cell Proliferation Assay Technical Bulletin #112 (9).

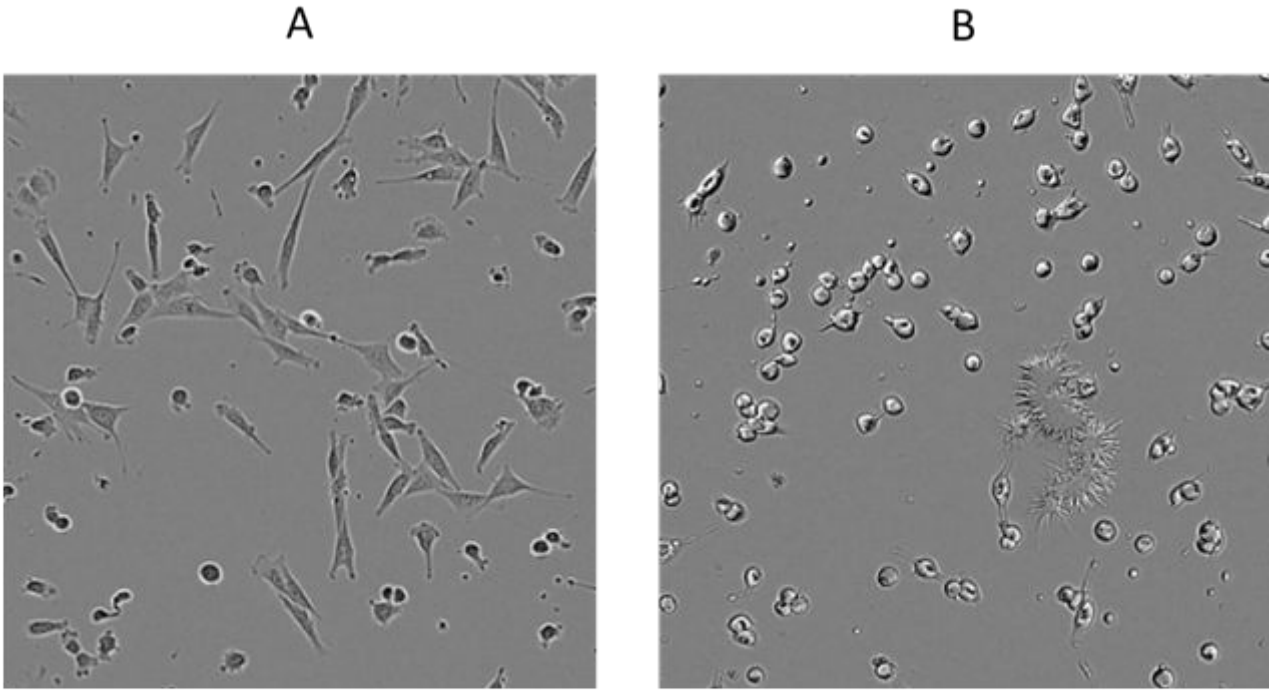


Figure 4: Change in NIH3T3 cell morphology after exposure to MTT (0.5 mg/ml). Panel A shows a field of cells photographed immediately after addition of the MTT solution. Panel B shows the same field of cells photographed after 4 hours of exposure to MTT. Panel B shows a change in cell morphology and the appearance of formazan crystals. Images were captured using the IncuCyte™ FLR from Essen Biosciences.

Solubilization Solution

1. Choose appropriate solvent resistant container and work in a ventilated fume hood.
2. Prepare 40% (vol/vol) dimethylformamide (DMF) in 2% (vol/vol) glacial acetic acid.
3. Add 16% (wt/vol) sodium dodecyl sulfate (SDS) and dissolve.
4. Adjust to pH = 4.7
5. Store at room temperature to avoid precipitation of SDS. If a precipitate forms, warm to 37°C and mix to solubilize SDS.

MTT Assay Protocol

1. Prepare cells and test compounds in 96-well plates containing a final volume of 100 µl/well.
2. Incubate for desired period of exposure.

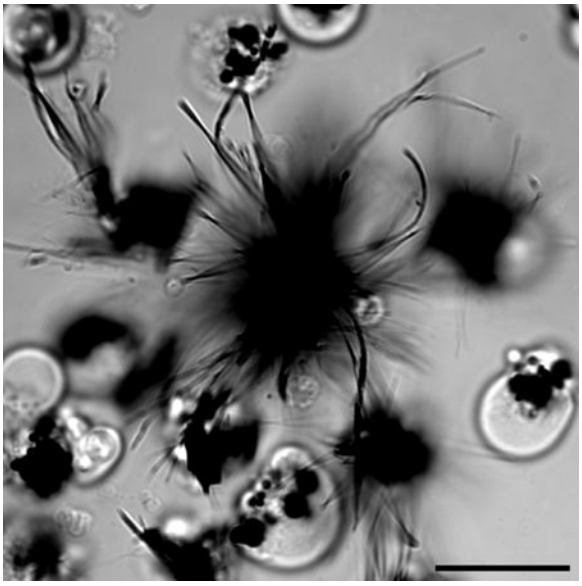


Figure 5: U937 cells incubated with MMT tetrazolium for 3 hours showing formazan crystals larger than the cells. Image was captured using an Olympus FV500 confocal microscope. Scale bar = 20 µm

3. Add 10 µl MTT Solution per well to achieve a final concentration of 0.45 mg/ml.
4. Incubate 1 to 4 hours at 37°C.
5. Add 100 µl Solubilization solution to each well to dissolve formazan crystals.
6. Mix to ensure complete solubilization.
7. Record absorbance at 570 nm.

MTS Tetrazolium Assay Concept

More recently developed tetrazolium reagents can be reduced by viable cells to generate formazan products that are directly soluble in cell culture medium. Tetrazolium compounds fitting this category include MTS, XTT, and the WST series (18-23). These improved tetrazolium reagents eliminate a liquid handling step during the assay procedure because a second addition of reagent to the assay plate is not needed to solubilize formazan precipitates, thus making the protocols more convenient. The negative charge of the formazan products that contribute to solubility in cell culture medium are thought to limit cell permeability of the tetrazolium (24). This set of tetrazolium reagents is used in combination with intermediate electron acceptor reagents such as phenazine methyl sulfate (PMS) or phenazine ethyl sulfate (PES) which can penetrate viable cells, become reduced in the cytoplasm or at the cell surface and exit the cells where they can convert the tetrazolium to the soluble formazan product (25). The general reaction scheme for this class of tetrazolium reagents is shown in Figure 6.

In general, this class of tetrazolium compounds is prepared at 1 to 2mg/ml concentration because they are not as soluble as MTT. The type and concentration of the intermediate electron acceptor used varies among commercially available reagents and in many products the identity of the intermediate electron acceptor is not disclosed. Because of the potential toxic nature of the intermediate electron acceptors, optimization may be advisable for different cell types and individual assay conditions. There may be a narrow range of concentrations of intermediate electron acceptor that result in optimal performance.

Commercial Availability

Commercial kits containing solutions of MTS, XTT, and WST-1 and an intermediate electron acceptor reagent are available from several vendors. For example:

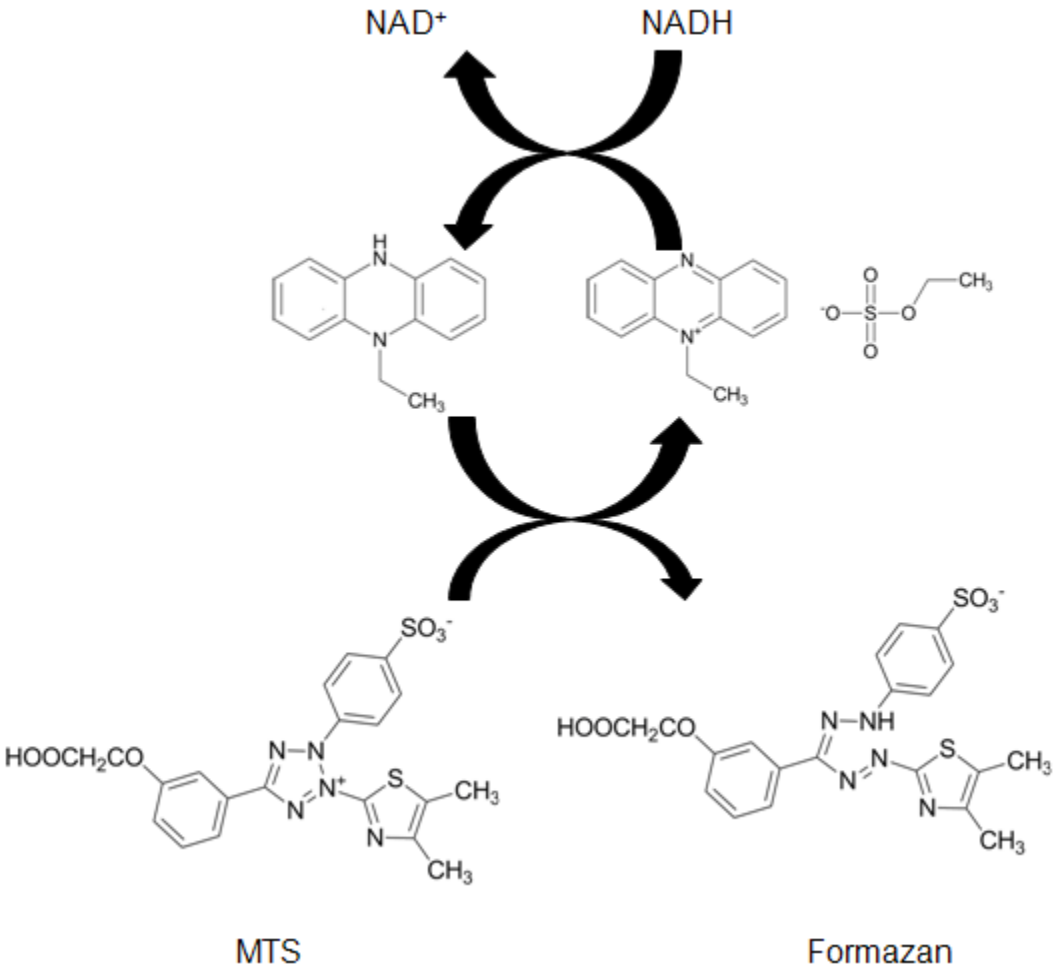


Figure 6: Intermediate electron acceptor pheazine ethyl sylfate (PES) transfers electron from NADH in the cytoplasm to reduce MTS in the culture medium into an aqueous soluble formazan.

- CellTiter 96® AQueous One Solution Cell Proliferation Assay. Promega Corporation Cat.# G3580,
- In Vitro Toxicology Assay Kit, XTT based. Sigma-Aldrich Cat.# TOX2-1KT,
- Cell Counting Kit-8 (WST-8 based). Dojindo Molecular Technologies, Inc. Cat.# CK04-01,
- MTS Reagent Powder. Promega Corporation Cat.# G1111,
- XTT sodium salt. Sigma-Aldrich Cat.# X4626.

Reagent Preparation

MTS Solution (containing PES)

1. Dissolve MTS powder in DPBS to 2 mg/ml to produce a clear golden-yellow solution.
2. Dissolve PES powder in MTS solution to 0.21 mg/ml.
3. Adjust to pH 6.0 to 6.5 using 1N HCl.
4. Filter-sterilize through a 0.2 µm filter into a sterile, light protected container.
5. Store the MTS solution containing PES protected from light at 4°C for frequent use or at -20°C for long term storage.

MTS Assay Protocol

1. Prepare cells and test compounds in 96-well plates containing a final volume of 100 µl/well. An optional set of wells can be prepared with medium only for background subtraction.
2. Incubate for desired period of exposure.
3. Add 20 µl MTS solution containing PES to each well (final concentration of MTS will be 0.33 mg/ml).
4. Incubate 1 to 4 hours at 37°C.
5. Record absorbance at 490 nm.

One of the advantages of the tetrazolium assays that produce an aqueous soluble formazan is that absorbance can be recorded form the assay plates periodically during early stages of incubation. Multiple readings may assist during assay development; but caution should be taken to return the plates to the incubator between readings to maintain a nearly constant environment. Extended incubations with the tetrazolium reagent beyond four hours should be avoided.

Whereas the background (culture medium and tetrazolium without cells) absorbance at 570 nm for an MTT assay may be 0.05, in general the background absorbance for the class of tetrazolium reagents is usually somewhat higher, in the range of 0.3 absorbance units and can depend on the type of culture medium and pH.

Resazurin Reduction Assay Concept

Resazurin is a cell permeable redox indicator that can be used to monitor viable cell number with protocols similar to those utilizing the tetrazolium compounds (26). Resazurin can be dissolved in physiological buffers (resulting in a deep blue colored solution) and added directly to cells in culture in a homogeneous format. Viable cells with active metabolism can reduce resazurin into the resorufin product which is pink and fluorescent (Figure 7).

Addition of an intermediate electron acceptor is not required for cellular resazurin reduction to occur, but it may accelerate signal generation. The quantity of resorufin produced is proportional to the number of viable cells which can be quantified using a microplate fluorometer equipped with a 560 nm excitation / 590 nm emission filter set. Resorufin also can be quantified by measuring a change in absorbance; however, absorbance detection is not often used because it is far less sensitive than measuring fluorescence. The resazurin reduction assay is slightly more sensitive than tetrazolium reduction assays and there are numerous reports using the resazurin reduction assay in a miniaturized format for HTS applications (27).

The incubation period required to generate an adequate fluorescent signal above background is usually 1to 4 hours and is dependent on the metabolic activity of the particular cell type, the cell density per well, and other assay conditions including the type of culture medium. The incubation period should be optimized and kept short enough to avoid reagent toxicity but long enough to provide adequate sensitivity.

The major advantages of the resazurin reduction assay are that it is relatively inexpensive, it uses a homogeneous format, and it is more sensitive that tetrazolium assays. In addition, resazurin assays can be multiplexed with other methods such as measuring caspase activity to gather more information about the mechanism leading to cytotoxicity (28 and Figure 8).

Multiplexing may require a sequential protocol to avoid color quenching by resazurin or direct chemical interference. For the multiplex example shown in Figure 8, resorufin fluorescence must be recorded first, followed by addition of the caspase reagent which contains detergent to lyse cells and reducing compounds to convert remaining resazurin and reduce interference with collecting the second fluorescent signal.

The disadvantages of the resazurin include the possibility of fluorescent interference from compounds being tested and the often overlooked direct toxic effects on the cells (Figure 9).

Some protocols describe exposing cells to resazurin for several hours or even days; however, in some systems, changes in cell morphology can be observed after only a few hours of exposure suggesting interference with normal cell function (29). It is possible that exposure of cells to resazurin depletes reduced forms of nucleotides resulting in cytotoxic effects. Exposure of cells to resazurin is known to reduce the amount of ATP measured as a marker of cell viability. Figure 10 shows a decrease in ATP content of HepG2 cells exposed to resazurin for 4 and 24 hours.

Commercial Availability

Commercial kits containing solutions of resazurin as well as resazurin powder are available from several vendors. For example:

- CellTiter-Blue® Cell Viability Assay. Promega Corporation Cat.# G8081,
- In Vitro Toxicology Assay Kit, Resazurin based. Sigma-Aldrich Cat.# TOX8-1KT,
- alamarBlue®—Rapid & Accurate Cell Health Indicator. Life Technologies, Inc. Cat.# DAL1100
- alamarBlue® AbD Serotech Cat.# BUF012B
- Resazurin sodium salt. Sigma-Aldrich Cat.# R7017-1G

Resazurin powder is readily available from chemical vendors; however, the resazurin dye content (% purity) and contamination with resorufin can lead to variability in assay results and the need to perform validation of each lot of reagent powder. Viability assay kits containing performance verified resazurin as the primary ingredient are available from different vendors; but the resazurin concentration and additional ingredients vary. The alamarBlue patent US 5,501,959 describes the use of poising agents to maintain the redox potential of the growth medium and prevent reduction of resazurin resulting in background signal (30). Preferred poising agents described include ferricyanide and ferrocyanide as well as methylene blue which can also serve as a redox indicator. The potential for undesired effects of additional ingredients in the proprietary alamarBlue formulation and the demonstrated performance equivalence of less complex formulations of highly purified resazurin in balanced saline solution should be considered when choosing an assay reagent.

Reagent Preparation

1. Dissolve high purity resazurin in DPBS (pH 7.4) to 0.15 mg/ml.
2. Filter-sterilize the resazurin solution through a 0.2 µm filter into a sterile, light protected container.
3. Store the resazurin solution protected from light at 4°C for frequent use or at -20°C for long term storage.

Resazurin Assay Protocol

1. Prepare cells and test compounds in opaque-walled 96-well plates containing a final volume of 100 µl/well. An optional set of wells can be prepared with medium only for background subtraction and instrument gain adjustment.
2. Incubate for desired period of exposure.
3. Add 20 µl resazurin solution to each well.
4. Incubate 1 to 4 hours at 37°C.
5. Record fluorescence using a 560 nm excitation / 590 nm emission filter set.

A general disadvantage of both the tetrazolium and resazurin reduction assay protocols is the requirement to incubate the substrate with viable cells at 37°C for an adequate period of time to generate a signal. Incubation of the tetrazolium or resazurin reagents with viable cells increases the possibility of artifacts resulting from chemical interactions among the assay chemistry, the compounds being tested, and the biochemistry of the cell. Incubation also introduces an extra plate handling step that is not required for the ATP assay protocol described later. Extra plate manipulation steps increase the possibility of errors and are not desirable for automated assays for HTS.

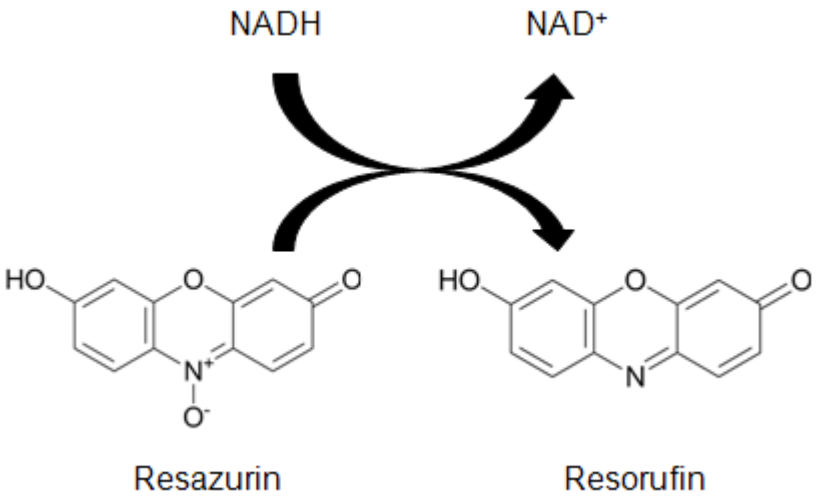


Figure 7: Structure of resazurin substrate and the pink fluorescent resorufin product resulting from reduction in viable cells.

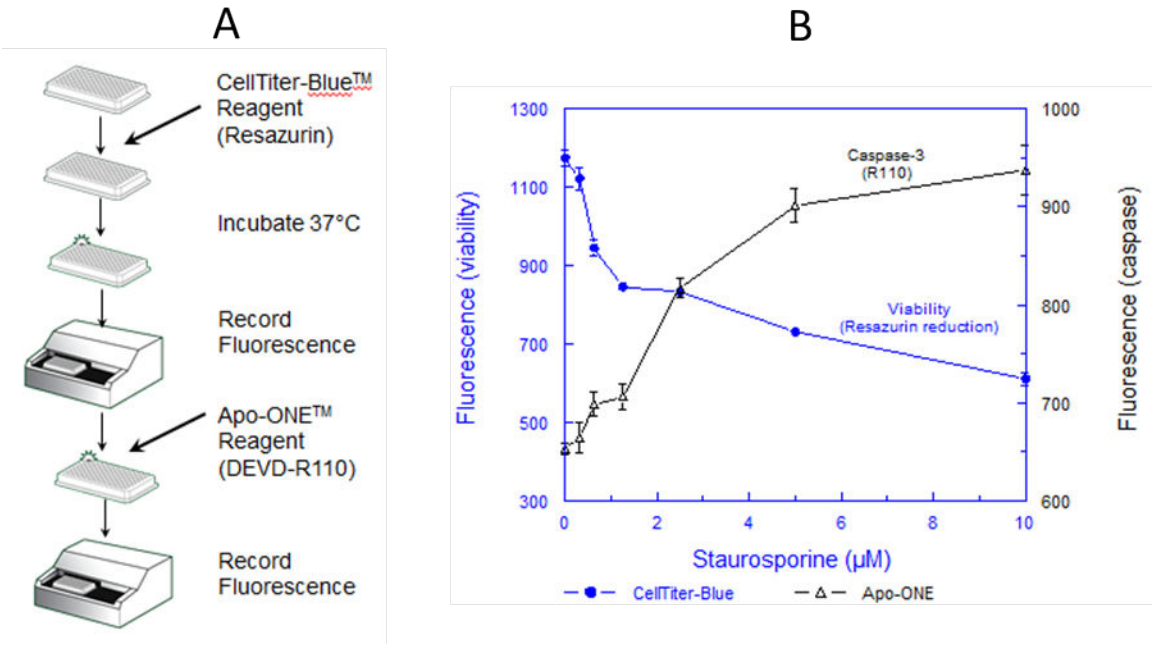


Figure 8: Panel A shows the steps of the sequential multiplex of a resazurin assay to measure viable cell number and a fluorometric caspase 3-assay to detect a marker of apoptosis. Panel B shows the results of treating PC3 (human prostate) cells with a range of concentrations of staurosporine for 20 hours. The resorufin (560/590 nm) and R110 fluorescence were captured at different wavelengths from the same sample as well.

Protease Viability Marker Assay Concept

Measurement of a conserved and constitutive protease activity within live cells has been shown to serve as a marker of cell viability. A cell permeable fluorogenic protease substrate (glycylphenylalanyl-aminofluorocoumarin; GF-AFC) has recently been developed to selectively detect protease activity that is restricted to viable cells (31). The GF-AFC substrate can penetrate live cells where cytoplasmic aminopeptidase activity removes the gly and phe amino acids to release aminofluorocoumarin (AFC) and generate a fluorescent signal proportional to the number of viable cells (Figure 11).

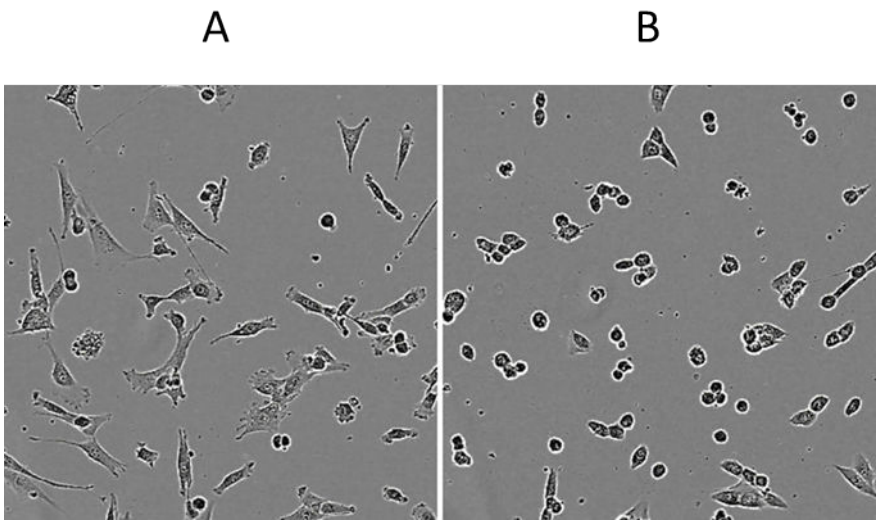


Figure 9: Change in NIH3T3 cell morphology after exposure to resazurin. Panel A shows a field of cells photographed immediately after addition of the resazurin solution. Panel B shows the same field of cells photographed after 4 hours of exposure to resazurin. Panel B shows a change in cell morphology. Images were captured using Incucyte from Essen Biosciences.

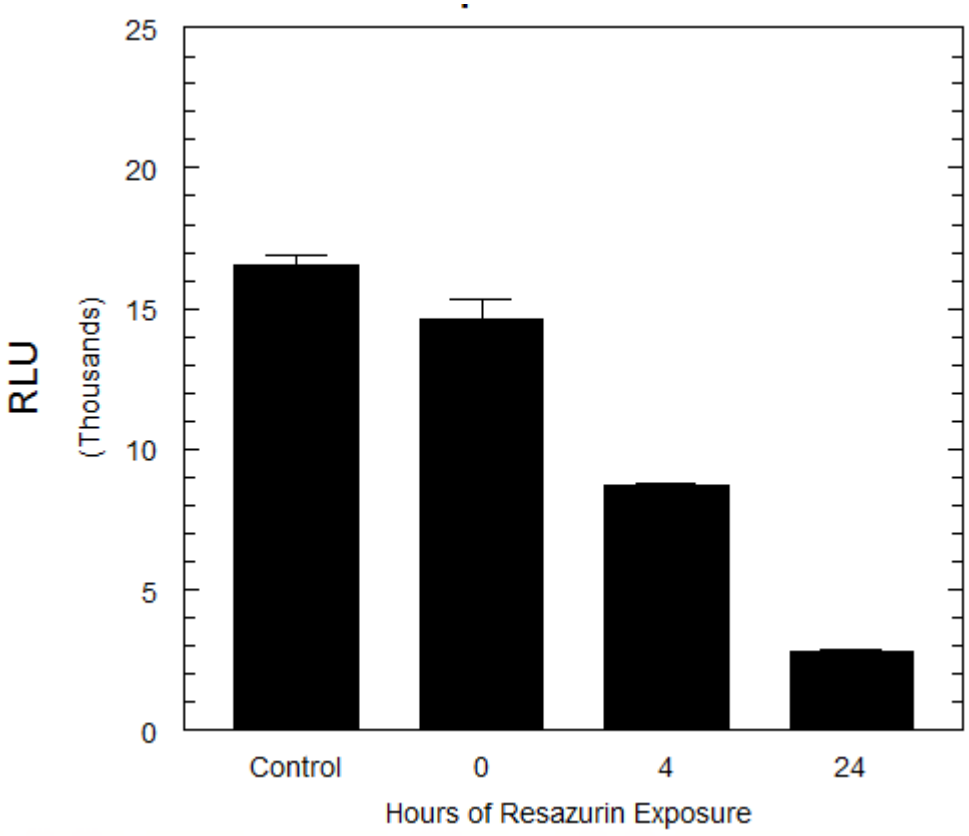


Figure 10: Viability (ATP content) of HepG2 cells exposed to resazurin for 0, 4, and 24 hours. Control wells did not contain resazurin. Zero hour wells contained resazurin and show quenching of luminescent signal following addition of the deeply blue colored resazurin reagent. ATP content was measured using the CellTiter-Glo® Assay.

As soon as the cells die, this protease activity rapidly disappears, thus making this protease activity a selective marker of the viable cell population. This assay approach is available as a commercial product from Promega Corporation (32). The components of the product include: GF-AFC 100mM in DMSO and an Assay Buffer for

dilution of the substrate. The signal generated from the protease assay approach has been shown to correlate well with other established methods of determining cell viability such as an ATP assay (Figure 12).

One of the advantages of the GF-AFC substrate is that it is relatively non-toxic to cells in culture (Figure 13).

In addition, long term exposure of the GF-AFC substrate to cells results in little change in viability measured using ATP as a marker. This is in direct contrast to the effects of exposing cells to tetrazolium or resazurin redox indicators which have been demonstrated to be toxic to cells as described above. The non-toxic nature of the GF-AFC substrate makes it an ideal candidate for multiplexing with other assay technologies using a sequential assay protocol. After recording fluorescence data from the live cell protease assay, the population of cells remains viable and can be used for subsequent assays as long as the fluorescent signal from AFC does not interfere. This property enables "on-the-fly" detection and follow-up of cytotoxic hits during screening campaigns. Wells containing hits can be subjected to an orthogonal method to detect viable cell number or an alternate assay method to detect the mechanism leading to cell death. Figure 14 shows an example of multiplexing the live cell protease marker and a luminescent caspase assay to detect apoptosis. In this example, the decrease in viability corresponds to an increase in caspase activity suggesting the mode of cell death is via apoptosis. An advantage of measuring this protease as a viability marker is that in general, the incubation time required to get an adequate signal is much shorter (30 min to 1 hour), compared to 1 to 4 hours required for the tetrazolium assays.

GF-AFC Reagent Preparation

1. Thaw the GF-AFC substrate and Assay Buffer components from the CellTiter-Fluor™ Cell Viability Assay kit following the detailed procedure in the Technical Bulletin #371 (32).
2. Transfer 10 µl of the GF-AFC Substrate into 10 ml of the Assay Buffer to prepare a 2X Reagent. Note: For multiplexing applications where total sample volume is a concern, a 10X Reagent can be prepared by adding 10 µl GF-AFC Substrate to 2 ml of Assay Buffer.
3. Mix by vortexing the contents until the GF-AFC substrate is thoroughly dissolved.

Storage: Store the CellTiter-Fluor™ Cell Viability Assay components at –20°C. The diluted CellTiter-Fluor™ Viability Reagent should be used within 24 hours if stored at room temperature. Unused GF-AFC Substrate and Assay Buffer can be stored at 4°C for up to 7 days with no appreciable loss of activity.

Live Cell Protease Assay Protocol

1. Set up opaque-walled 96-well assay plates containing cells in culture medium at desired density. An optional set of wells can be prepared with medium only for background subtraction and instrument gain adjustment.
2. Add test compounds and vehicle controls to appropriate wells so that the final volume is 100 µl in each well (25 µl for a 384-well plate).
3. Culture cells for the desired test exposure period.
4. Add CellTiter-Fluor™ Reagent in an equal volume (100 µl per well) to all wells, mix briefly by orbital shaking, then incubate for at least 30 minutes at 37°C. Note: Longer incubations may improve assay sensitivity and dynamic range. However, do not incubate more than 3 hours, and be sure to shield plates from ambient light.
5. Measure resulting fluorescence using a fluorometer (380–400 nm Ex/505 nm Em).

ATP Assay Concept

The measurement of ATP using firefly luciferase is the most commonly applied method for estimating the number of viable cells in HTS applications. Data from several example HTS assays using ATP assays are publically available on Pubchem (34). ATP has been widely accepted as a valid marker of viable cells. When cells lose membrane integrity, they lose the ability to synthesize ATP and endogenous ATPases rapidly deplete any

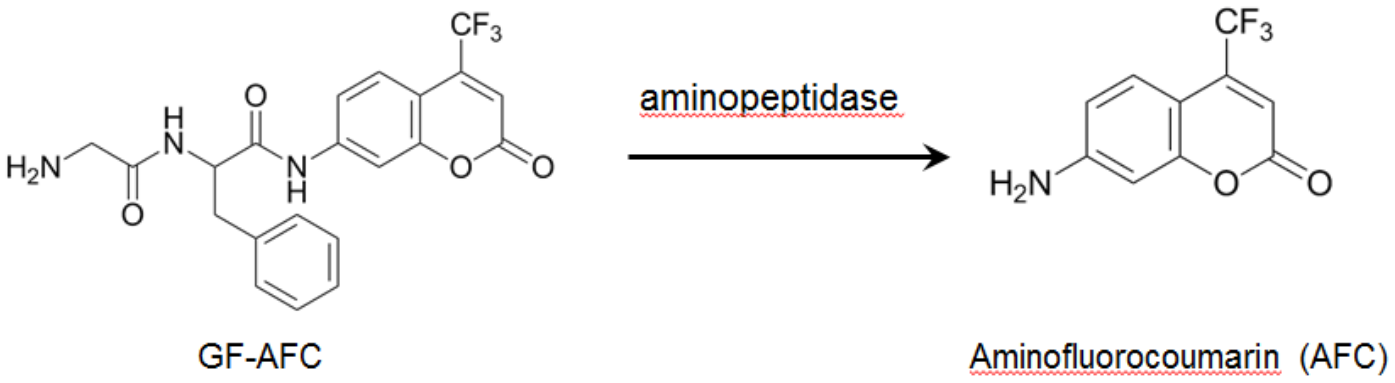


Figure 11: Cell permeable glycylphenylalanyl-aminofluoroumarin (GF-AFC) substrate is converted by cytoplasmic aminopeptidase activity to generate fluorescent aminofluorocoumarin (AFC).

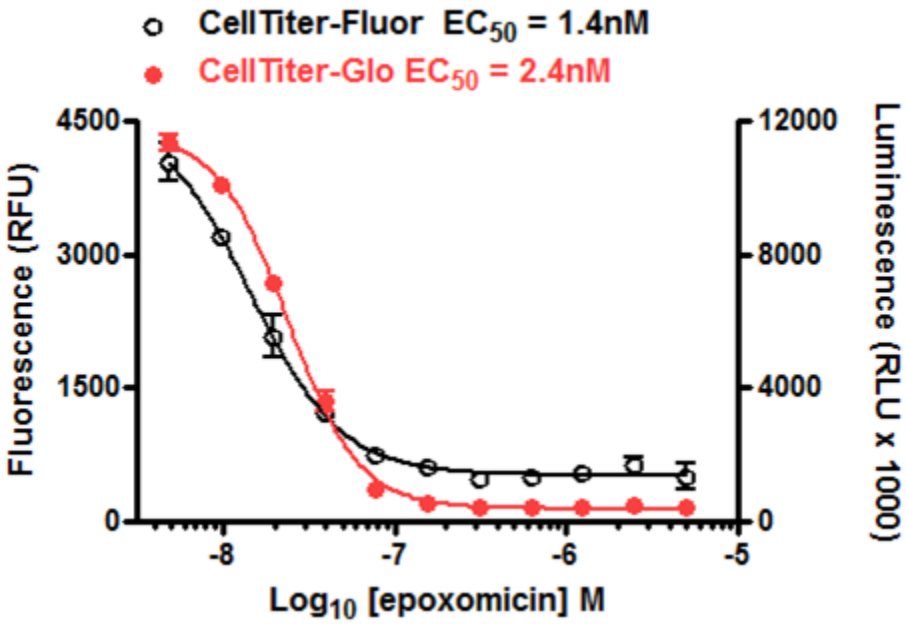


Figure 12: DU-145 cells treated with various concentrations of epoxomicin for 48 hours and assayed using GF-AFC reagent (CellTiter-Fluor™, open circles) and ATP detection (CellTiter-Glo® Assay, solid red circles). The similar EC_{50} values demonstrate good correlation between different methods to estimate viable cells.

remaining ATP from the cytoplasm. Although luciferase has been used to measure ATP for decades, recent advances in assay design have resulted in a single reagent addition homogeneous protocol that results in a luminescent signal that glows for hours. The most significant technological advancement was made under the direction of Keith Wood at Promega Corporation where directed evolution was used to select for stable molecules and generate improved versions of luciferase (35). The stable version of luciferase was the enabling technology that led to development of robust assays for HTS that can withstand harsh cell lysis conditions and are more resistant to luciferase inhibitors found in libraries of small molecules (36).

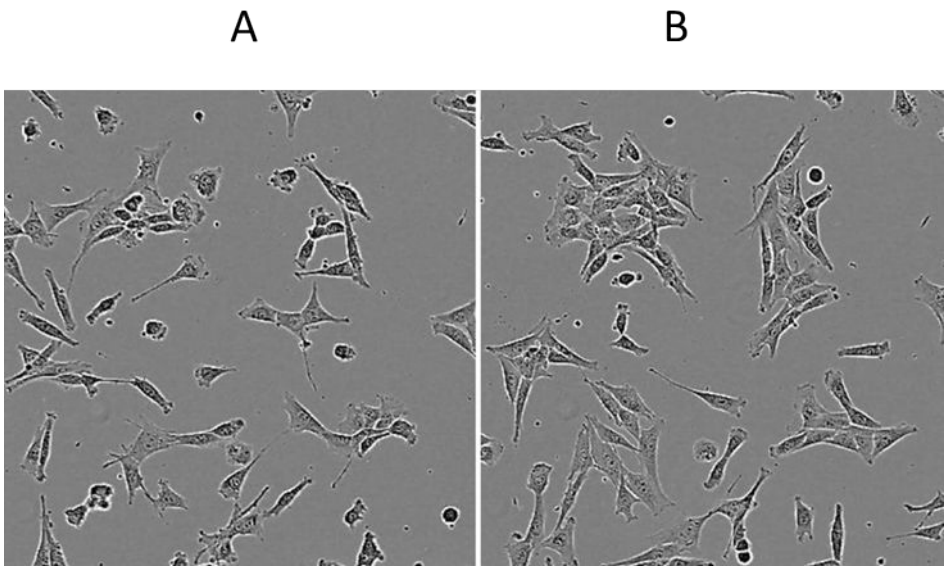


Figure 13: Morphology of NIH3T3 cells during exposure to GF-AFC reagent. Panel A shows a field of cells photographed immediately after additional of the GF-AFC reagent. Panel B shows the same cells photographed after 4 hours of exposure to GF-AFC. Panel B shows a little change in the cell morphology compared to the substantial changes and obvious toxicity shown for MTT and resazurin in the figures above. Images were captured using the IncuCyte^{TM} FLR from Essen Biosciences.

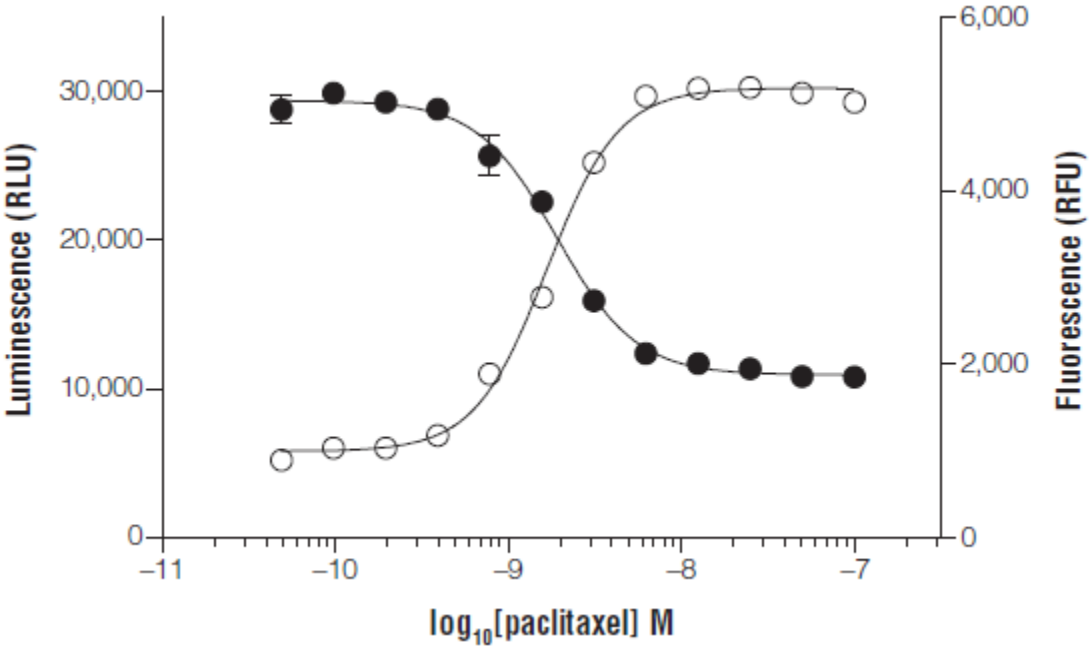


Figure 14: (Modified Figure 5 from TB371 32). Multiplex measurement of the live cell protease marker using GF-AFC (CellTiter-Fluor™ Assay) followed by measurement of caspase activity (Caspase-Glo® 3/7 Assay). The GF-AFC substrate was added to wells containing 10,000 cells/well, incubated for 30 minutes at 37°C and fluorescence (380–400nmEx/505nmEm) measured to estimate viable cell number. Following collection of the fluorescence data, caspase activity was measured using the luminogenic Caspase-Glo® 3/7 Reagent. Luminescence measured after 30-minutes incubation (Caspase-Glo TB323 33).

The ATP detection reagent contains detergent to lyse the cells, ATPase inhibitors to stabilize the ATP that is released from the lysed cells, luciferin as a substrate, and the stable form of luciferase to catalyze the reaction that generates photons of light. A simplified reaction scheme is shown in Figure 15.

The ATP assay is the fastest cell viability assay to use, the most sensitive, and is less prone to artifacts than other viability assay methods. The luminescent signal reaches a steady state and stabilizes within 10 minutes after addition of reagent and typically glows with a half-life greater than 5 hours. The ATP assay has the advantage that you do not have to rely on an incubation step with a population of viable cells to convert a substrate (such a tetrazolium or resazurin) into a colored compound. This also eliminates a plate handling step because you do not have to return cells to the incubator to generate signal.

The ATP assay chemistry can typically detect fewer than 10 cells per well and has been used widely in 1536-well format. The ATP assay sensitivity is usually limited by reproducibility of pipetting replicate samples rather than a result of the assay chemistry.

Commercial Availability

Commercial kits containing reagents to measure ATP are available from several vendors. For example:

- CellTiter-Glo® Luminescent Cell Viability Assay. Promega Corporation Cat.# G7570
- ATPLite™ 1 step, Perkin Elmer Cat.# 6016731,
- Adenosine 5′-triphosphate (ATP) bioluminescent somatic cell assay kit. Sigma-Aldrich Cat.# FLASC-1KT.

The most common version of the CellTiter-Glo® Assay kit contains a lyophilized CellTiter-Glo® Substrate and the CellTiter-Glo® Buffer which are both stored at –20°C; however, a bulk frozen liquid version of CellTiter-Glo® Assay also is available which eliminates the step of reconstituting the lyophilized Substrate. For more detailed information, refer to Promega Technical Bulletin #288 (37).

ATP Assay Reagent Preparation

1. Thaw the CellTiter-Glo® Buffer and CellTiter-Glo® Substrate and equilibrate to room temperature prior to use. For convenience the CellTiter-Glo® Buffer may be thawed and stored at room temperature for up to 48 hours prior to use.
2. Transfer the appropriate volume (10ml for Cat.# G7570) of CellTiter-Glo® Buffer into the amber bottle containing CellTiter-Glo® Substrate to reconstitute the lyophilized enzyme/substrate mixture. This forms the CellTiter-Glo® Reagent.
3. Mix by gently vortexing, swirling or inverting the contents to obtain a homogeneous solution. The CellTiter-Glo® Substrate should go into solution easily in less than 1 minute.

ATP Assay Protocol

1. Set up white opaque walled microwell assay plates containing cells in culture medium at desired density.
2. Add test compounds and vehicle controls to appropriate wells so that the final volume is 100 µl in each well for 96-well plate (25 µl for a 384-well plate).
3. Culture cells for the desired test exposure period.
4. Equilibrate plates to ambient temperature for 30 min to ensure uniform temperature across plate during luminescent assay.
5. Add CellTiter-Glo® Reagent in an equal volume (100 µl per well for 96-well plates or 25 µl per well for 384-well plates) to all wells.
6. Mix contents for 2 minutes on an orbital shaker to induce cell lysis.
7. Allow the plate to incubate at room temperature for 10 minutes to stabilize luminescent signal. Note: Uneven luminescent signal within standard plates can be caused by temperature gradients, uneven seeding of cells or edge effects in multiwall plates.
8. Record luminescence.

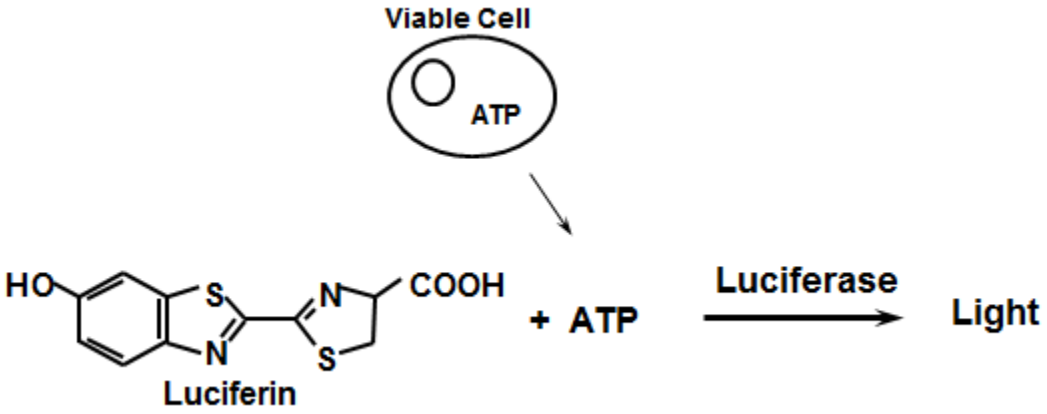


Figure 15: Simplified reaction scheme showing ATP and luciferin as substrates for luciferase to generate light.

Figure 16 shows the results of an example assay characterization experiment to determine the appropriate time to record viability data for a cell-based assay.

Real-Time Assay for Viable Cells

A recently developed approach for measuring viable cell number in "real time" utilizes an engineered luciferase derived from a marine shrimp and a small molecule pro-substrate (39). The pro-substrate and luciferase are added directly to the culture medium as a reagent. The pro-substrate is not a substrate for luciferase. Viable cells with an active metabolism reduce the pro-substrate into a substrate which diffuses into the culture medium where it is used by luciferase to generate a luminescent signal. Figure 17 shows an illustration of the assay concept.

The reagent is well tolerated by cells and is stable in complete cell culture medium at 37°C for at least 72 hours which enables measurements from the same sample for days without replenishing the pro-substrate. The assay can be performed in two formats: continuous-read or endpoint measurement. In the continuous-read format, the luminescent signal can be repeatedly recorded from the same sample wells over an extended period to measure the number of viable cells in "real time".

Figure 18 shows example results from a toxin dose-response assay using the real time format for 3 days. The cells in the vehicle control and the lowest concentrations of thapsigargin continue to grow and show an increase in luminescence over the three day period. Samples of cells treated with the highest concentrations of thapsigargin show a decrease in luminescence over time as the cells die.

For convenience, in the continuous read format, the reagents can be added to the cell suspension prior to dispensing into assay plates. This approach eliminates a pipetting step and a potential source of variability during delivery of assay reagent into samples. In the endpoint format, the reagent can be added to cells at any time during the experimental period. A steady state develops between viable cells reducing pro-substrate to convert it into the luciferase substrate, the appearance of the substrate in the culture medium and the luciferase enzymatic reaction using the substrate to generate light. For the endpoint format, luminescence can typically be recorded within 10 minutes to an hour after adding reagent to the cells, depending on assay conditions.

The substrate produced by viable cells is used rapidly by the luciferase, thus the luminescent signal diminishes soon after cell death. Figure 19 illustrates the decrease in luminescent signal following addition of digitonin to kill the cells.

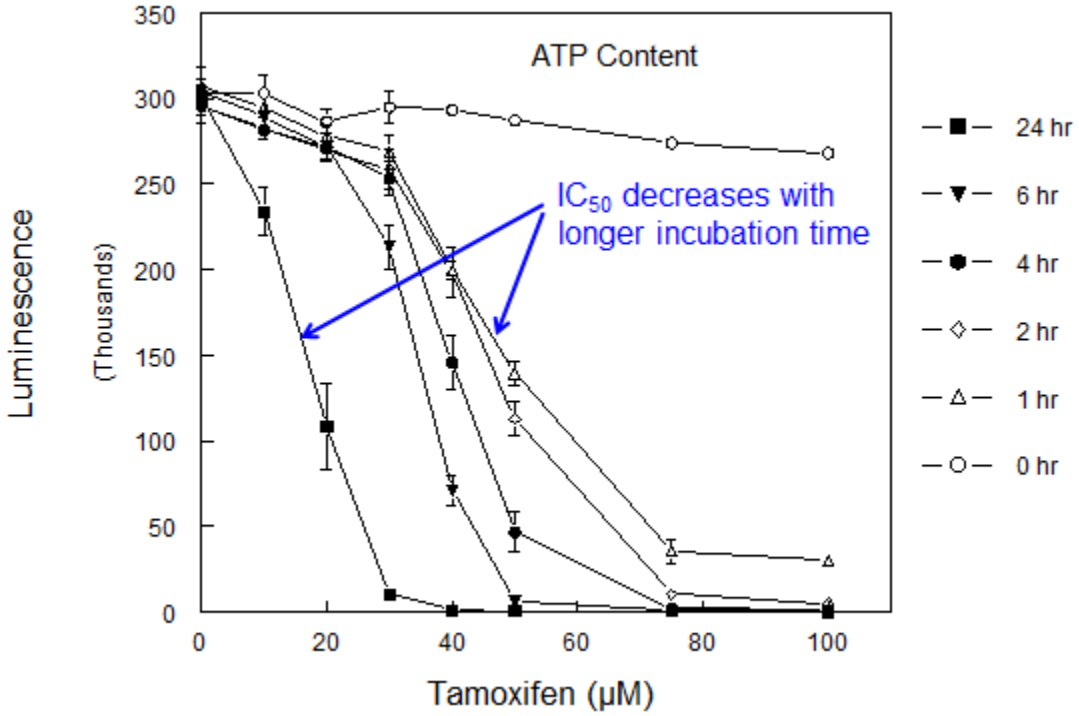


Figure 16: HepG2 cells (25,000 cells in 100ul medium/well) were cultured overnight in an opaque-walled 96 well plate then treated with 0-100uM tamoxifen in DMSO (final concentration of 0.2% DMSO) for various times. ATP content was measured by adding 100ul CellTiter-Glo® Reagent and recording luminescence after a 10min equilibration period. Data shown represent the mean +/- SD (n = 3). Modified from Figure 1 from Assay & Drug Devel Tech 2(1): 51, 2004 (38).

The rapid decrease in luminescent signal following cell death enables multiplexing of the real time viability assay with other luminescent assays that contain a lysis step that will kill cells. The decrease in luminescence from the real time viability assay following cell death is important to eliminate interference with subsequent luminescent assays that use firefly luciferase.

Multiplexing with the Real Time Viability Assay

Because the real time reagent does not contain detergent (i.e. is non-lytic) and is well tolerated by most cell types, after recording viability data, the remaining sample of cells can be used for many downstream applications. Multiplexing can be achieved with a variety of other assay chemistries including: most assays with a fluorescent detection method, the luminescent ATP assay as an orthogonal approach to confirm viability data with more than one method, a luminescent caspase-3/7 assay to measure apoptosis, firefly reporter assays to monitor gene expression, and extraction of RNA that can be used to monitor gene expression.

Figure 20 illustrates an example showing the effect of a dose-response of a proteasome inhibitor on the viability of cells measured at different times from the same samples using the real time viability assay followed by multiplex measurement of ATP as an orthogonal method to demonstrate concordance between the two viability assays. The sequential multiplexing example shows results from recording luminescence from a shrimp-derived luciferase followed by recording luminescence from a firefly-derived luciferase. The ATP assay contains detergent to lyse cells to release ATP as well as luciferin and a stable form of luciferase necessary to measure ATP (see general description above in this chapter). The detergent lysis step stops the ability of cells to generate a substrate for the shrimp luciferase and thus diminishes the luminescent signal from the real time viability assay. This sequential combination of reagents makes it possible to record two luminescent signals from two different luciferases from the same sample. The 48 hour data from the real time assay approach agrees well with the 48

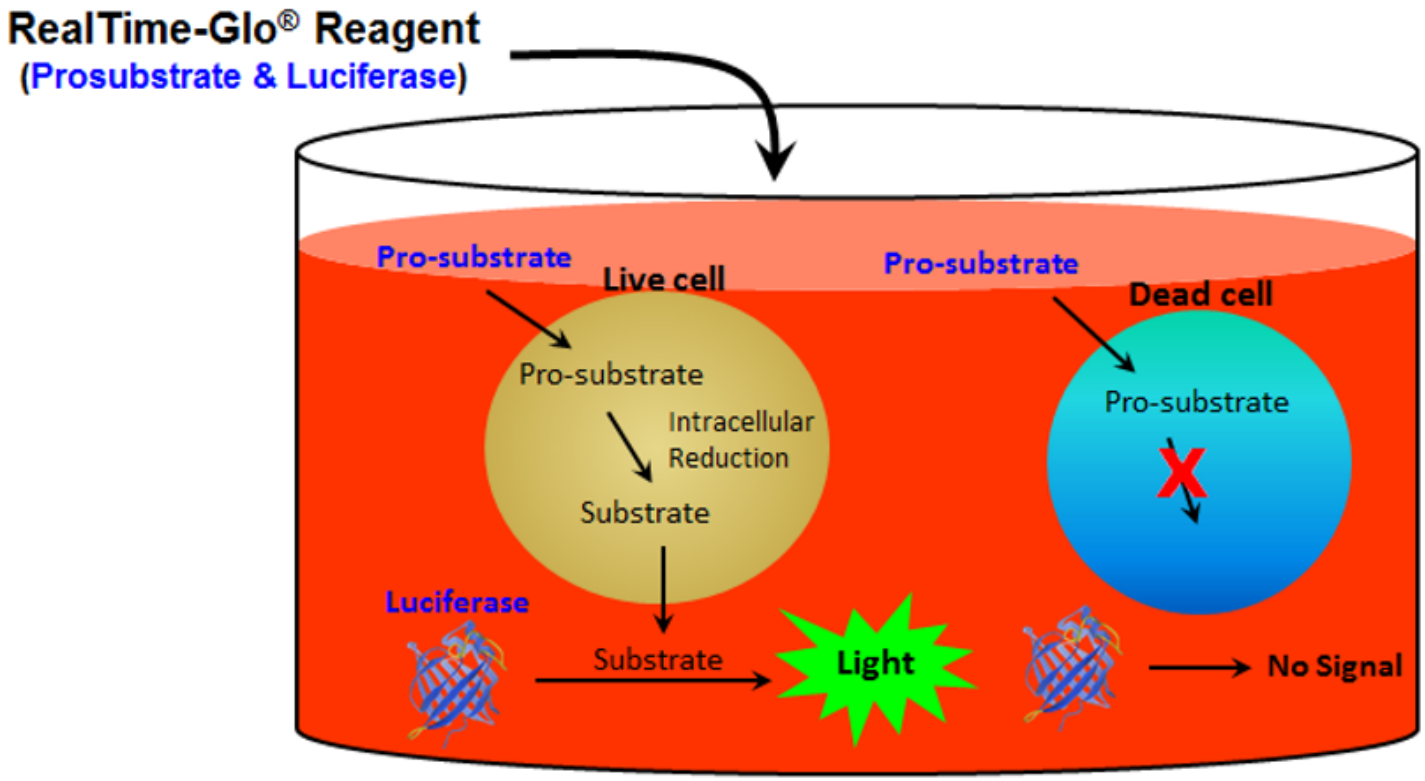


Figure 17: The real-time reagent components include a cell permeable pro-substrate and an engineered stable form of a shrimp-derived luciferase. The reagent components are added directly to cells in culture. Viable cells with an active metabolism reduce the pro-substrate to create a substrate for luciferase that generates light. Dead cells lacking metabolic activity do not generate luciferase substrate and thus do not contribute a luminescent signal.

hour data from the ATP assay, demonstrating concordance between these two methods. Similar agreement between assays has been observed from the combination of the real time viability assay and a constitutive firefly reporter gene assay (not shown).

Figure 21 shows another example of multiplexing the real time viability assay using the shrimp luciferase and a caspase-3/7 assay using firefly luciferase. A gradual decrease in viability and increase in caspase-3/7 activity was observed over the first ~30 hours. The decrease in caspase-3/7 activity at the longer incubations times is likely due to secondary necrosis of the cells resulting in loss of activity of the caspase enzyme. This assay combination exemplifies a special case where reagent chemical compatibility during multiplexing can be a problem. Caspase assay reagent formulations typically contain reducing agents (such as dithiothreitol) which can result in some chemical reduction of the pro-substrate into substrate. The substrate generated from chemical reduction of the pro-substrate can be used by the active shrimp luciferase and contribute to background luminescence. For those situations, the addition of a specific chemical inhibitor of the shrimp luciferase eliminates signal from that enzyme so the luminescence does not interfere with the signal from firefly luciferase used in a multiplexed secondary assay.

The real time viability assay enables monitoring for early cytotoxic events in populations of cells exposed to drugs. Analysis of RNA extracted from a population of cells that show the first signs of cell death (i.e. when most of the cells are still viable) can provide information about which stress response genes are expressed during experimental treatments. The real time viability assay reagent has been shown to have little effect on yield or integrity of RNA. That is in contrast to the ATP assay reagent which contains a high concentration of detergent to lyse cells resulting in poor recovery and loss of integrity of RNA. Figure 22 shows the results of extracting RNA from different sizes of individual 3D spheroids of HEK293 cells after measurement of cell viability using

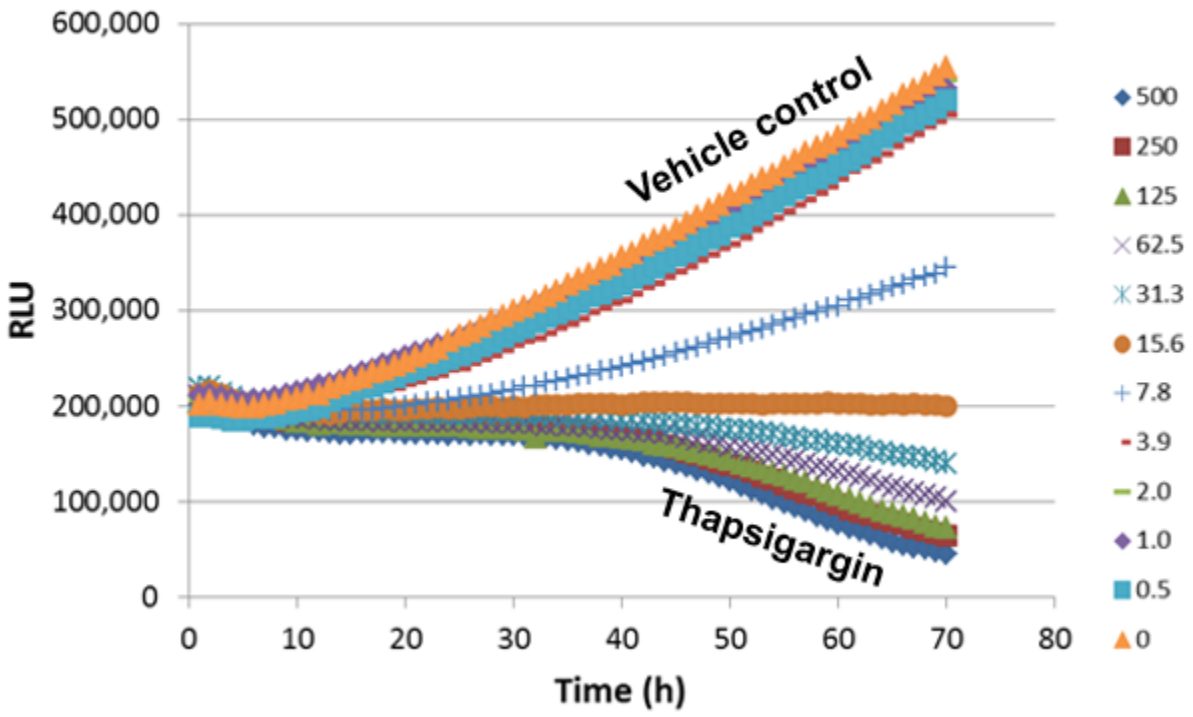


Figure 18: A549 cells (500/well) were plated in 40µL medium containing 2x RealTime-Glo™ reagents. A thapsigargin titration was prepared in medium at 2X concentrations and added to the plate at an equal volume. The final concentrations of thapsigargin ranged from 500nM - 0.5nM. The vehicle control was 0.1% DMSO. Luminescence was monitored every hour for 72 hours using a Tecan Infinite® 200 Multimode Reader with Gas Control Module (37°C and 5% CO_2).

the real time assay reagent. RNA was extracted using either a manual or an automated method. For each method, the presence or absence of the real time reagent did not affect the recovery of RNA from spheroids. In addition, the RIN values (used as an indicator of the integrity of the RNA) were in the excellent range (~8 to 9.5) and were not affected by the presence of the real time cell viability assay reagent.

A limitation of the real time assay format results from the eventual depletion of pro-substrate by metabolically active cells. In general, the luminescent signal generated correlates with the number of metabolically active viable cells; however, the length of time the luminescent signal will be linear with cell number will depend on the number of cells per well and their overall metabolic activity. Figure 23 shows luminescent signals recorded every hour for 72 hours from wells initially seeded with 750, 1500, 3000, or 6000 K562 cells/well in a 384-well plate. The signal from 750 and 1500 cells/well remain linear over the 3 day period, whereas the signal from higher cell numbers per well lose linearity after different times of incubation. It is recommended that the maximum incubation time to maintain linearity should be empirically determined for each cell type and seeding density.

Commercial Availability

Commercial kits containing the pro-substrate and the engineered shrimp-derived luciferase are available from Promega Corporation. RealTime-Glo™ MT Cell Viability Assay, Cat.# G9711 (100 reactions); G9712 (10x100 reactions); G9713 (1000 reactions)

Reagent Preparation and Real Time Viability Assay Protocol

The MT Cell Viability Substrate and the NanoLuc® Enzyme are both supplied at 1000X the final recommended concentration.

For continuous read mode:

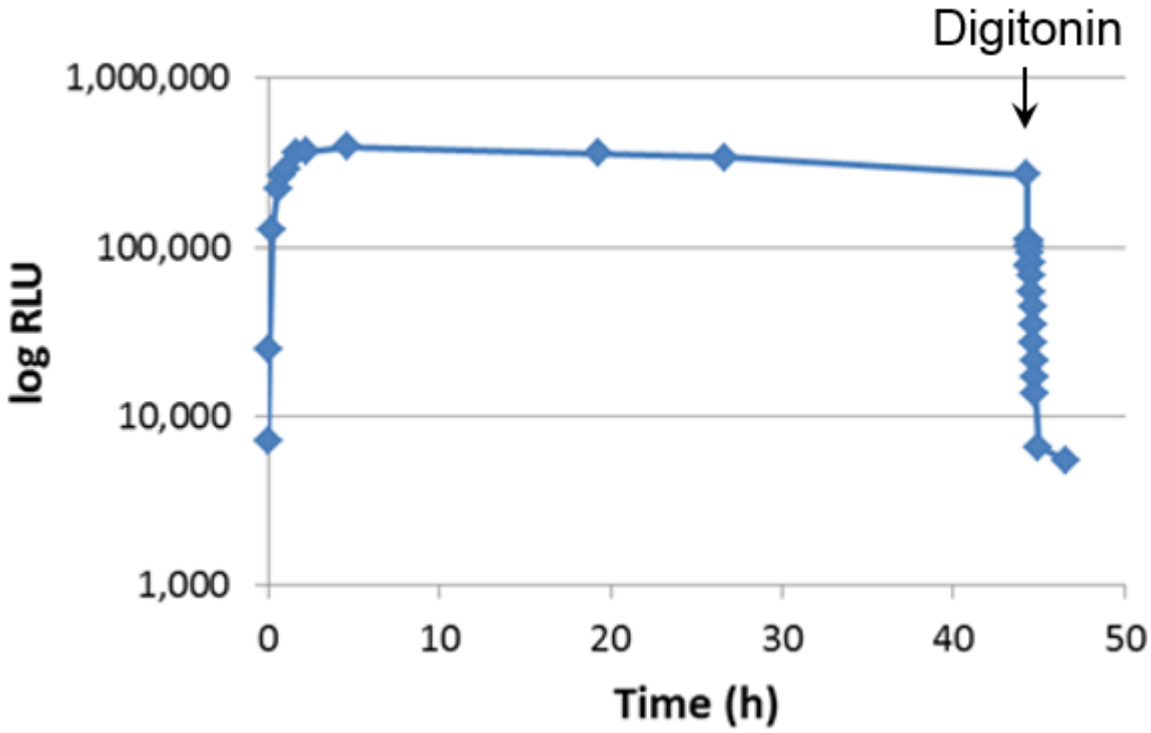


Figure 19: iCell cardiomyocytes (Cellular Dynamics, Inc.) were plated and grown in medium containing RealTime-Glo™ reagents (pro-substrate and NanoLuc luciferase) in a 37°C/5% CO_2 humidified incubator. At various time points, the luminescence signal was monitored on a Tecan M1000Pro plate reader. After 2 days, digitonin was added to a final concentration of 200 µg/ml. The luminescence was read continually, starting immediately after digitonin addition.

1. Equilibrate the MT Cell Viability Substrate and the NanoLuc® Enzyme to 37°C.
2. Harvest cells and adjust to desired cell density to be used in the assay.
3. Add MT Cell Viability Substrate and the NanoLuc® Enzyme to the cell suspension.
4. Dispense cell suspension containing MT Cell Viability Substrate and the NanoLuc® Enzyme into white opaque walled multiwell plates suitable for luminescence measurements.
5. Add test compound and incubate for desired length of time.
6. Record luminescence.

For endpoint mode:

1. Harvest cells and adjust to desired cell density to be used in the assay.
2. Add test compound to cells and incubate for desired length of time.
3. Equilibrate the MT Cell Viability Substrate and the NanoLuc® Enzyme to 37°C.
4. Dilute MT Cell Viability Substrate and the NanoLuc® Enzyme in cell culture medium to form 2X RealTime-Glo™ Reagent.
5. Add an equal volume of 2X RealTime-Glo™ Reagent to cells.
6. Incubate at 37°C for 10-60 min.
7. Record luminescence.

Conclusion

There are a variety of assay technologies available that use standard plate readers to measure metabolic markers to estimate the number of viable cells in culture. Each cell viability assay has its own set of advantages and disadvantages. The ATP detection assay is by far the most sensitive, has fewer steps, is the fastest to perform, and has the least amount of interference, whereas the tetrazolium or resazurin reduction assays offer less expensive

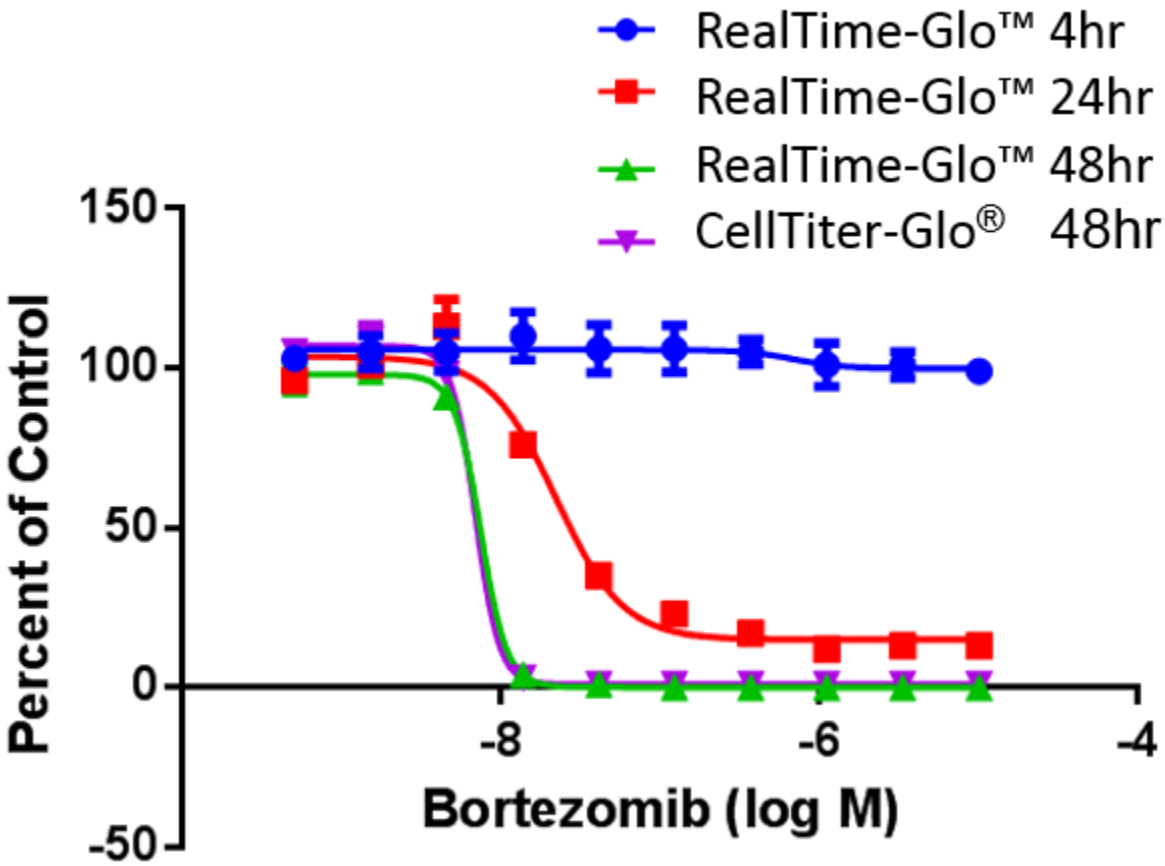


Figure 20: K562 cells in complete medium (RPMI medium supplemented with 10% FBS and Pen/Strep) containing the RealTime-Glo™ Reagent were seeded at 2500 cells in 50µl/well into 96 well opaque white plates. Bortezomib dilutions were prepared from DMSO stock as 2X final concentration in complete culture medium and 50µl were added to appropriate wells. The vehicle control was 0.6% DMSO in complete culture medium. Luminescence from the real time viability assay was recorded after 4, 24 and 48 hours incubation, then 100µl/well of the CellTiter-Glo® 2.0 Reagent was added to each well, the plate was stored at room temperature for 30 min to ensure cell lysis, then luminescence recorded. The values represent the mean ± SD of 4 replicates and were normalized to 100% assigned to the vehicle control for each assay.

alternatives that may achieve adequate performance depending on experimental design. The fluorogenic cell permeable protease substrate is far less cytotoxic than the tetrazolium and resazurin compounds while enabling many possibilities for multiplexing other assays to serve as orthogonal or confirmatory methods. The recently developed cell viability assay, based on generating a substrate for the shrimp luciferase, provides the opportunity for capturing data repeatedly in real time and offers many possibilities for multiplexing with other assays. Regardless of the assay method chosen, the major factors critical for reproducibility and success include: 1) using a tightly controlled and consistent source of cells to set up experiments and 2) performing appropriate characterization of reagent concentration and incubation time for each experimental model system.

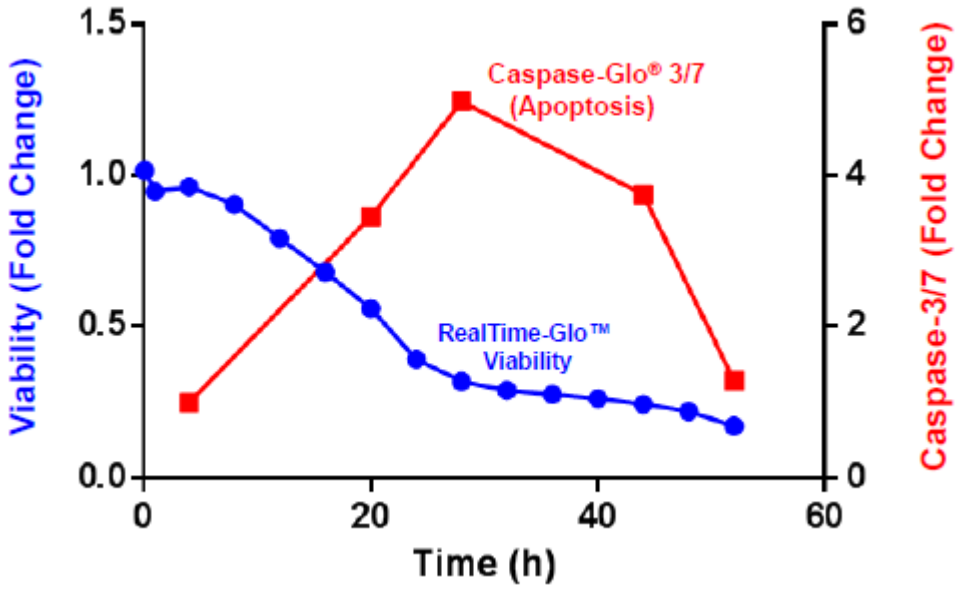


Figure 21: THP1 cells were grown in medium containing the RealTime-Glo™ Assay Reagent and treated with 1µM doxorubicin. Luminescence was recorded every 4 hours to monitor changes in cell viability. At selected times, Caspase-Glo® 3/7 Assay Reagent supplemented with a specific inhibitor for the shrimp luciferase was added to parallel wells. The plates were incubated at room temperature for 1 hour, then luminescence recorded from the firefly-derived luciferase in the caspase detection reagent.

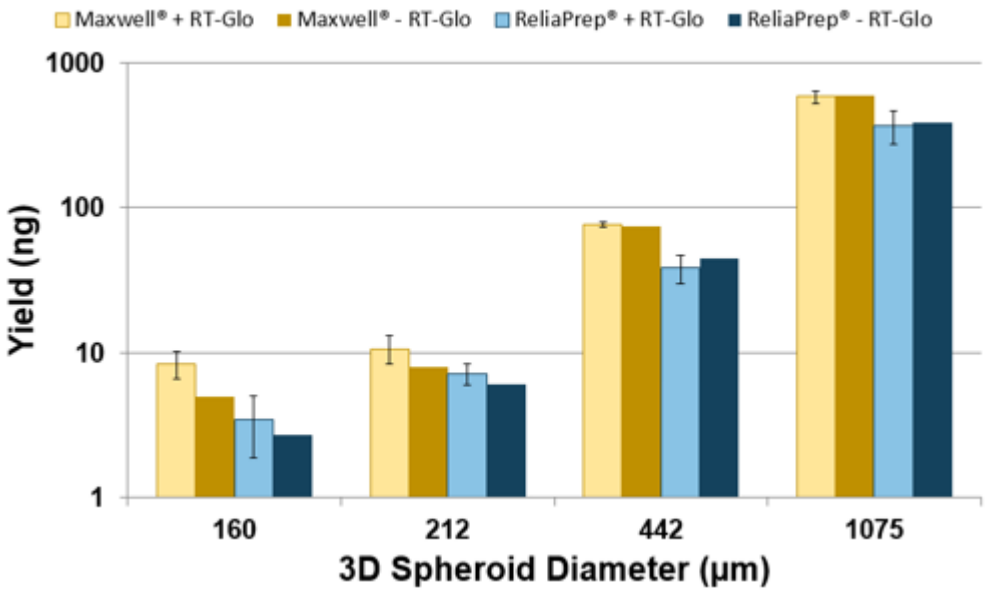


Figure 22: HEK293 spheroids of different sizes were prepared using the GravityPLUS™ Hanging Drop System from InSphero. RealTime-Glo™ MT Cell Viability Assay was used to measure viability of different sizes of HEK293 cell spheroids followed by RNA extraction of the same samples using a manual method (ReliaPrep™ RNA Tissue Miniprep System) and an automated method (Maxwell® 16 LEV simply RNA Tissue Kit). Each RNA extraction method was done in the presence and absence of RealTime-Glo™ Reagent for each of the different sizes of spheroid. Each bar represents the mean +/- SD of 3 spheroids.

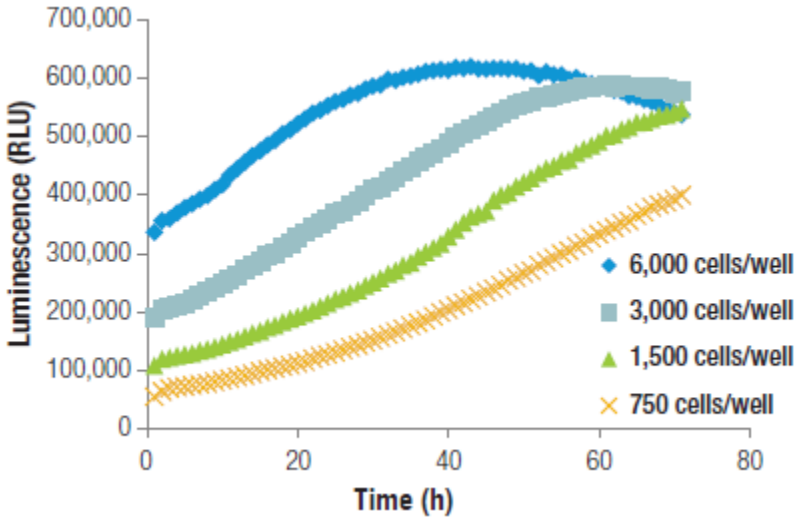


Figure 23: K562 cells were seeded at 750, 1500, 3000 or 6000 cells/well in a 384-well opaque white plate in 80µL of RPMI medium supplemented with 10% FBS and Pen/Strep that contained the RealTime-Glo™ Reagent. Luminescence was monitored every hour for 72 hours using a Tecan Infinite® 200 Multimode Reader with Gas Control Module (37°C and 5% CO_2).

References

1. Mosmann T. Rapid colorimetric assay for cellular growth and survival: Application to proliferation and cytotoxicity assays. J. Immunol. Meth. 1983;65:55–63. PubMed PMID: 6606682.
2. Marshall NJ, Goodwin CJ, Holt SJ. A critical assessment of the use of microculture tetrazolium assays to measure cell growth and function. Growth Regul. 1995;5(2):69–84. PubMed PMID: 7627094.
3. Berridge MV, Tan AS. Characterization of the cellular reduction of 3-(4,5-dimethylthiazol-2-yl)-2,5-diphenyltetrazolium bromide (MTT): subcellular localization, substrate dependence, and involvement of mitochondrial electron transport in MTT reduction. Arch Biochem Biophys. 1993;303(2):474–82. PubMed PMID: 8390225.
4. Berridge M., Tan A., McCoy K., Wang R. The Biochemical and Cellular Basis of Cell Proliferation Assays that Use Tetrazolium Salts. Biochemica. 1996;4:14–19.
5. Tada H, Shiho O, Kuroshima K, et al. An improved colorimetric assay for interleukin 2. J. Immunol. Methods. 1986;93:157–65. PubMed PMID: 3490518.
6. Hansen MB, Nielsen SE, Berg K. Re-examination and further development of a precise and rapid dye method for measuring cell growth/cell kill. J. Immunol. Methods. 1989;119:203–210. PubMed PMID: 2470825.
7. Denizot F, Lang R. Rapid colorimetric assay for cell growth and survival. Modifications to the tetrazolium dye procedure giving improved sensitivity and reliability. J. Immunol. Meth. 1986;89:271–277. PubMed PMID: 3486233.
8. Plumb JA, Milroy R, Kaye SB. 1989. Effects of the pH dependence of 3-(4,5-dimethylthiazol-2-yl)-2,5-diphenyl-tetrazolium bromide-formazan absorption on chemosensitivity determined by a novel tetrazolium-based assay. Cancer Res 15;49(16):4435-40.
9. CellTiter 96® Non-Radioactive Cell Proliferation Assay Technical Bulletin #112. Online at [Available at: http://www.promega.com/~/media/Files/Resources/Protocols/Technical%20Bulletins/0/CellTiter%2096%20Non-Radioactive%20Cell%20Proliferation%20Assay%20Protocol.pdf]
10. Huyck L, Ampe C, Van Troys M. The XTT cell proliferation assay applied to cell layers embedded in three-dimensional matrix. Assay Drug Dev Tech. 2012;10(4):382–392. PubMed PMID: 22574651.
11. Squatrito R, Connor J, Buller R. Comparison of a novel redox dye cell growth assay to the ATP bioluminescence assay. Gynecologic Oncology. 1995;58:101–105. PubMed PMID: 7789873.

12. Lü L, Zhang L, Wai MS, Yew DT, Xu J. Exocytosis of MTT formazan could exacerbate cell injury. Toxicol In Vitro. 2012;26(4):636–44. Epub 2012 Feb 28. PubMed PMID: 22401948.
13. Ulukaya E, Colakogullari M, Wood E J. Interference by anti-cancer chemotherapeutic agents in the MTT-tumor chemosensitivity assay. Chemotherapy. 2004;50(1):43–50. PubMed PMID: 15084806.
14. Chakrabarti R, Kundu S, Kumar S, Chakrabarti R. Vitamin A as an enzyme that catalyzes the reduction of MTT to formazan by vitamin C. J Cellular Biochem. 2000;80(1):133–138. PubMed PMID: 11029760.
15. Bernas T, Dobrucki J. Mitochondrial and nonmitochondrial reduction of MTT: interaction of MTT with TMRE, JC-1, and NAO mitochondrial fluorescent probes. Cytometry. 2002;47(4):236–42. PubMed PMID: 11933013.
16. Pagliacci M, Spinozzi F, Migliorati G, et al. Genistein inhibits tumour cell growth in vitro but enhances mitochondrial reduction of tetrazolium salts: a further pitfall in the use of the MTT assay for evaluating cell growth and survival. Eur J Cancer. 1993;29:1573–1577. PubMed PMID: 8217365.
17. Collier A, Pritsos C. The mitochondrial uncoupler dicumerol disrupts the MTT assay. Biochem Pharm. 2003;66:281–287. PubMed PMID: 12826270.
18. Cory A, Owen T, Barltrop J, Cory JG. Use of an aqueous soluble tetrazolium/formazan assay for cell growth assays in culture. Cancer Commun. 1991;3(7):207–212. PubMed PMID: 1867954.
19. Barltrop J, Owen T. 5-(3-carboxymethoxyphenyl)-2-(4,5-dimethylthiazoly)-3-(4-sulfophenyl)tetrazolium, inner salt (MTS) and related analogs of 3-(4,5-dimethylthiazolyl)-2,5-diphenyltetrazolium bromide (MTT) reducing to purple water-soluble formazans as cell-viability indicators. Bioorg Med Chem Lett. 1991;1:611–614.
20. Paull KD, Shoemaker RH, Boyd MR, et al. The synthesis of XTT: A new tetrazolium reagent that is bioreducible to a water-soluble formazan. J Heterocyclic Chem. 1988;25:911–914.
21. Ishiyama M, Shiga M, Sasamoto K, Mizoguchi M, He P. A new sulfonated tetrazolium salt that produces a highly water-soluble formazan dye. Chem Pharm Bull (Tokyo). 1993;41:1118–1122.
22. Tominaga H, Ishiyama M, Ohseto F, et al. A water-soluble tetrazolium salt useful for colorimetric cell viability assay. Anal Commun. 1999;36:47–50.
23. Goodwin CJ, Holt SJ, Downes S, Marshall NJ. 1995. Microculture tetrazolium assays: a comparison between two new tetrazolium salts, XTT and MTS. J Immunol Methods 13;179(1):95-103.
24. Scudiero DA, Shoemaker RH, Paull KD, Monks A, Tierney S, Nofziger TH, Currens MJ, Seniff D, Boyd MR. Evaluation of a soluble tetrazolium/formazan assay for cell growth and drug sensitivity in culture using human and other tumor cell lines. Cancer Res. 1988;48(17):4827–33. PubMed PMID: 3409223.
25. Berridge MV, Herst PM, Tan AS. Tetrazolium dyes as tools in cell biology: New insights into their cellular reduction. Biotechnology Annual Review. 2005;11:127–152. PubMed PMID: 16216776.
26. Ahmed SA, Gogal RM, Walsh JE. A new rapid and simple nonradioactive assay to monitor and determine the proliferation of lymphocytes: An alternative to [3H]thymidine incorporation assays. J Immunol Meth. 1994;170:211–224. PubMed PMID: 8157999.
27. Shum D, Radu C, Kim E, Cajuste M, Shao Y, Seshan VE, Djaballah H. A high density assay format for the detection of novel cytotoxic agents in large chemical libraries. J Enz Inhib Med Chem. 2008;23(6):931–945. PubMed PMID: 18608772.
28. Wesierska-Gadek J, Gueorguieva M, Ranftler C, Zerza-Schnitzhofer G. A new multiplex assay allowing simultaneous detection of the inhibition of cell proliferation and induction of cell death. J Cell Biochem. 2005;96(1):1–7. PubMed PMID: 16052484.
29. Invitrogen alamarBlue Assay manual. Online at [Available at: http://tools.invitrogen.com/content/sfs/manuals/PI-DAL1025-1100_TI%20alamarBlue%20Rev%201.1.pdf].
30. Lancaster MV and Fields RD. Antibiotic and cytotoxic drug susceptibility assays using resazurin and poising agents. US Patent 5,501,959. Issued March 26, 1996.
31. Niles AL, Moravec RA, Hesselberth PE, Scurria MA, Daily WJ, Riss TL. A homogeneous assay to measure live and dead cells in the same sample by detecting different protease markers. Anal Biochem. 2007;366:197–206. PubMed PMID: 17512890.

32. CellTiter-Fluor® Technical Bulletin. Online at Available at: http://www.promega.com/~/media/Files/Resources/Protocols/Technical%20Bulletins/101/CellTiter-Fluor%20Cell%20Viability%20Assay%20Protocol.pdf
33. Caspase-Glo® Technical Bulletin. Online at Available at: http://www.promega.com/~/media/Files/Resources/Protocols/Technical%20Bulletins/101/Caspase-Glo%203%207%20Assay%20Protocol.pdf
34. PubChem BioAssay: http://pubchem.ncbi.nlm.nih.gov/assay/
35. Hall MP, Gruber MG, Hannah RR, Jennens-Clough ML, Wood KV. 1998. Stabilization of firefly luciferase using directed evolution. In: Bioluminescence and Chemiluminescence—Perspectives for the 21st Century. Roda A, Pazzagli M, Kricka LJ, Stanley PE (eds.), pp. 392–395. John Wiley & Sons, Chichester, UK.
36. Auld DS, Zhang Y-A, Southall NT, et al. A basis for reduced chemical library inhibition of firefly luciferase obtained from directed evolution. J Med Chem. 2009;52:1450–1458. PubMed PMID: 19215089.
37. CellTiter-Glo® Technical Bulletin #288. Online at Available at: http://www.promega.com/~/media/Files/Resources/Protocols/Technical%20Bulletins/101/Caspase-Glo%203%207%20Assay%20Protocol.pdf.
38. Riss TL, Moravec RA. Use of multiple assay endpoints to investigate the effects of incubation time, dose of toxin, and plating density in cell-based cytotoxicity assays. Assay Drug Dev Technol. 2004;2(1):51–62. PubMed PMID: 15090210.
39. Duellman SJ, Zhou W, Meisenheimer P, Vidugiris G, Cali JJ, Gautam P, Wennerberg K, Vidugiriene J. Bioluminescent, Nonlytic, Real-Time Cell Viability Assay and Use in Inhibitor Screening. Assay Drug Dev Tech. 2015;13(8):456–65. PubMed PMID: 26383544.
40. RealTime-Glo MT Cell Viability Assay Technical Manual. Online at Available at: http://www.promega.com/~/media/files/resources/protocols/technical%20manuals/101/realtimeglo%20mt%20cell%20viability%20assay%20protocol.pdf

Cytotoxicity Assays: *In Vitro* Methods to Measure Dead Cells

Terry Riss, PhD,[✉1] Andrew Niles, MS,[1] Rich Moravec, BS,[1] Natashia Karassina, MS,[1] and Jolanta Vidugiriene, PhD[1]

Created: May 1, 2019.

Abstract

Membrane integrity is the feature most often used to detect whether eukaryotic cells cultured *in vitro* are alive or dead. Cells that have lost membrane integrity and allow movement of otherwise non-permeable molecules are classified as non-viable or dead. Detection of dead cells is accomplished by measuring movement of molecules either into or out of cells across membranes that have become leaky and cannot be repaired. A major class of molecules that serve as indicators of dead cells include markers that exist in the cytoplasm of viable cells, but leak into the surrounding culture medium upon loss of membrane integrity. The marker can exist naturally such as an enzyme, or be introduced artificially, such as loading radioactive [^{51}Cr] or a fluorescent marker into viable cells. Artificially introduced markers enable selective detection of target cell cytotoxicity for experiments using more than one population of cells such as cell mediated cytotoxicity. A second class of molecules that serves as an indicator of dead cells is referred to as "vital dyes". These dyes typically are not permeable to viable cells, but can enter dead cells through damaged membranes. Examples include trypan blue and many fluorogenic DNA binding dyes. Addition of these molecules to cells in culture results in selective staining of the dead cells.

Introduction

This chapter will describe common methods for measuring dead cells in culture using a plate reader that can be applied to high-throughput screening. This is an introductory review focused on the most frequently used methods for measuring the number of dead cells using a plate reader. We will describe basic assay methods and factors to consider when choosing an assay as well as the advantages and disadvantages of different methods. A separate chapter will describe HTS assays to measure apoptosis.

For all assays using cultured cells as a model system, it is valuable to know how many live and dead cells are present during or after the end of the experiment. This becomes especially important when cells are incubated for a period of time adequate to enable growth and division and thus change the total number of cells present. Relating live and dead cell numbers by a normalization process improves the statistical robustness of the assay. However, the use of cell number as an internal control is often overlooked in many cell-based assays such as reporter assays to detect expression of stress response genes or testing for other stress related events.

A frequent use of cells in culture is for a commonly used cytotoxicity assay where cells are exposed to a test compound and after some period of incubation, a marker is measured to reflect the number of viable cells present compared to positive (toxin) and negative (vehicle) control treatments. In addition to estimating the number of live cells, it can be of great value to measure the number of dead cells that have accumulated over the course of the experiment and to be able to distinguish between cytotoxicity and cytostasis or growth arrest. In some cases, estimating the number of accumulated dead cells may be more sensitive than measuring a decrease in a marker used to estimate viable cell number.

The two commonly used methods of estimating dead cells take advantage of the loss of membrane integrity and the ability of indicator molecules to partition into a compartment not achievable if the cell membrane is intact.

Author Affiliation: 1 Promega Corporation; Email: terry.riss@promega.com; Email: andrew.niles@promega.com; Email: rich.moravec@promega.com; Email: natasha.karassina@promega.com; Email: jvidugir@promega.com.

✉ Corresponding author.

As illustrated in the diagram in **Figure 1**, assays used to detect dead cells include measuring the leakage of a component (usually an enzyme marker) from the cytoplasm into the culture medium or the penetration of an otherwise non-permeable dye into cells with a compromised membrane. This chapter will describe options for both general approaches for measuring dead cells.

Dyes That Selectively Penetrate Dead Cells

Trypan blue

The selective staining of dead cells with trypan blue and microscopic examination on a hemocytometer is one of the most frequently used routine methods to determine the cell number and percent viability in a population of cells. The general concept is that trypan blue is excluded from live cells, but penetrates dead cells with a damaged plasma membrane. Longer incubations with solutions of trypan blue may result in faint staining of the viable cells in the population, possibly due to slow uptake of dye molecules. The mechanism of selective staining of dead cells may actually involve impermeability of aggregates of trypan blue (1). There are several sources for published protocols or instructional videos describing the use of trypan blue and the many details associated with correctly using a hemocytometer (2).

Counting cells using a hemocytometer

Cell Counting Using the Trypan Blue Exclusion Method

Counting of cells using Trypan Blue and a haemocytometer

The trypan blue staining technique is usually performed on a single sample (such as when passaging a stock culture flask of cells) or relatively small numbers of samples from simple experiments. The main disadvantages of this technique are: the error involved with measuring a single sample, the subjective judgement of the user to determine what is a dead cell or stained debris, inconsistency among operators, and the time and manual labor involved with measuring multiple samples (3). There are benchtop instruments designed to automate imaging and improve the biased analysis steps of this basic staining technique using trypan blue or other fluorescent vital dyes (Bio Rad TC10 / TC20 Automated Cell Counter; Olympus Cell Counter model R1; ThermoFisher Scientific Countess II Automated Cell Counter (fluorescent); Roche Cedex HiRes Analyzer; Nexcelom Bioscience Cellometer Auto T4); however, the primary intent of these automated instruments is to establish reliable and reproducible counting of live and dead cells prior to seeding into microwell plates and not for high-throughput studies so they will not be discussed further in this chapter.

Fluorescent DNA Binding Dyes That Penetrate Dead Cells

There is a large number of nucleic acid binding dyes that can be used to stain cells for microscopy or flow cytometry but have limitations for use with assays using plate readers to detect signal. Many dyes have somewhat similar properties which make it difficult to choose the most appropriate probe for a particular purpose. A general description of many of the nucleic acid binding dyes can be found in the following link to The Molecular Probes Handbook found on the ThermoFisher Scientific website.

There are many fluorescent DNA binding dyes to select from which are generally considered to be non-permeable to viable cells and can be used for detection of the accumulation of dead cells in culture using a multi-well plate format; however, there are a variety of factors to consider when selecting the most appropriate dye for assay development. The most important and practical factors to consider when choosing a dye include: the emission wavelength, selectivity for staining DNA, cell permeability, solubility at the vendor-recommended concentration, detection sensitivity and cytotoxicity. Fluorogenic DNA dyes that readily pass through the intact cell membrane and stain the nucleus of live cells should be avoided for consideration for measuring dead cells.

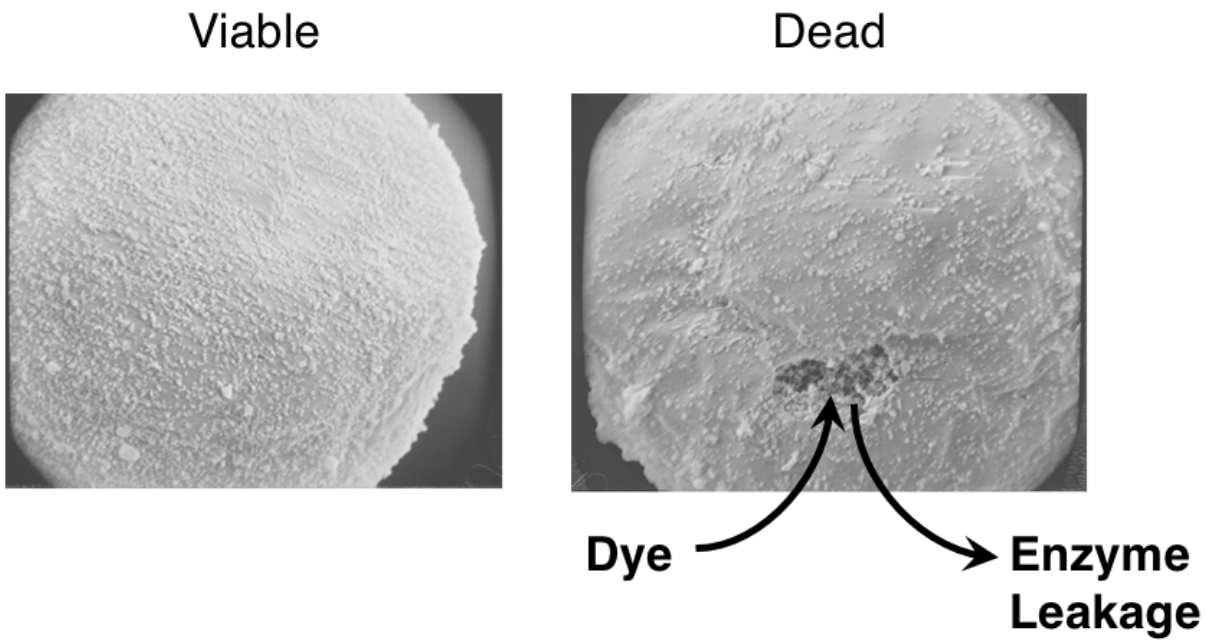


Figure 1. Illustrates scanning electron micrographs of isolated rat hepatocytes. The left image is meant to depict an intact live cell and the image on the right depicts a dead cell with a damaged membrane. The loss of membrane integrity enables leakage of dead cell markers such as enzymes from the cytoplasm into the surrounding culture medium and penetration of materials (vital dyes) that normally are non-permeable to live cells.

Chiaraviglio and Kirby (4) have recently reported on the evaluation of non-permeable DNA-binding dye fluorescence as a real-time readout of eukaryotic cell toxicity in a high-throughput screening format. They include a useful table summarizing the properties for many nucleic acid binding dyes as well as demonstrating the ability to multiplex fluorescent dead cell assays with other cell-based methods.

An important factor to consider when choosing any fluorescent dye is the emission wavelength spectrum. Knowledge of the excitation and emission spectra and the extent of any spectral overlap can be used to predict compatibility of two fluorescent assays and to select an appropriate filter set to avoid overlap of emission of different fluorophores. For example, a green-emitting DNA binding dye would be a logical candidate to multiplex with an assay detecting a red fluorescent protein. A table listing filter sets used for many of the nucleic acid binding dyes is included in the Chiaraviglio and Kirby reference (4). The ability to multiplex more than one fluorescent or luminescent assay provides flexibility during assay design. Measuring the number of dead cells is often used as a multiplexed internal control for other cell-based screening assays. Sequential multiplexing by recording data from a fluorogenic assay prior to addition of a second luminogenic assay chemistry can expand the possibilities for multiplexing.

The DNA binding dyes can be considered to be environmental sensors, meaning they change fluorescent properties after binding to various molecules. The various nucleic acid binding dyes may exhibit between a 20- to 1000-fold increase in fluorescence upon binding to double stranded DNA. That fold-increase can contribute to the relative sensitivity of detection of the number of dead cells. In most experimental conditions using a growing population of cultured cells *in vitro*, the quantity of DNA is proportional to the total number of cells present; however, changing culture conditions to induce rapid cell growth, to starve cells of nutrients, or induce differentiation to result in multinucleation may have a greater influence to change the amount of nucleic acid present in cells. The ideal situation for quantitatively detecting dead cells is for the dye to selectively bind to double stranded DNA. If the dye binds to double stranded RNA which may change under stimulatory or stressful culture conditions, using dyes that also bind to RNA can lead to artifacts and misinterpretation of results.

Even slight adverse effects of DNA binding dyes can limit their usefulness for real-time assay protocols where the dye is exposed to cells for extended periods of time. Dyes that cause cytotoxicity upon long term exposure to cells may be the result of partial permeability. Membrane permeability may depend on the cell type, the overall health of the cells or whether the dyes are substrates for efflux pumps that result in expulsion from the cytoplasm even if the dye does enter the cell. Reagent toxicity is not a problem if the dye is going to be used to stain cells for an endpoint assay protocol; however, cytotoxicity is critical to consider if cells will be cultured in the presence of the dye for an extended period to perform a real-time assay.

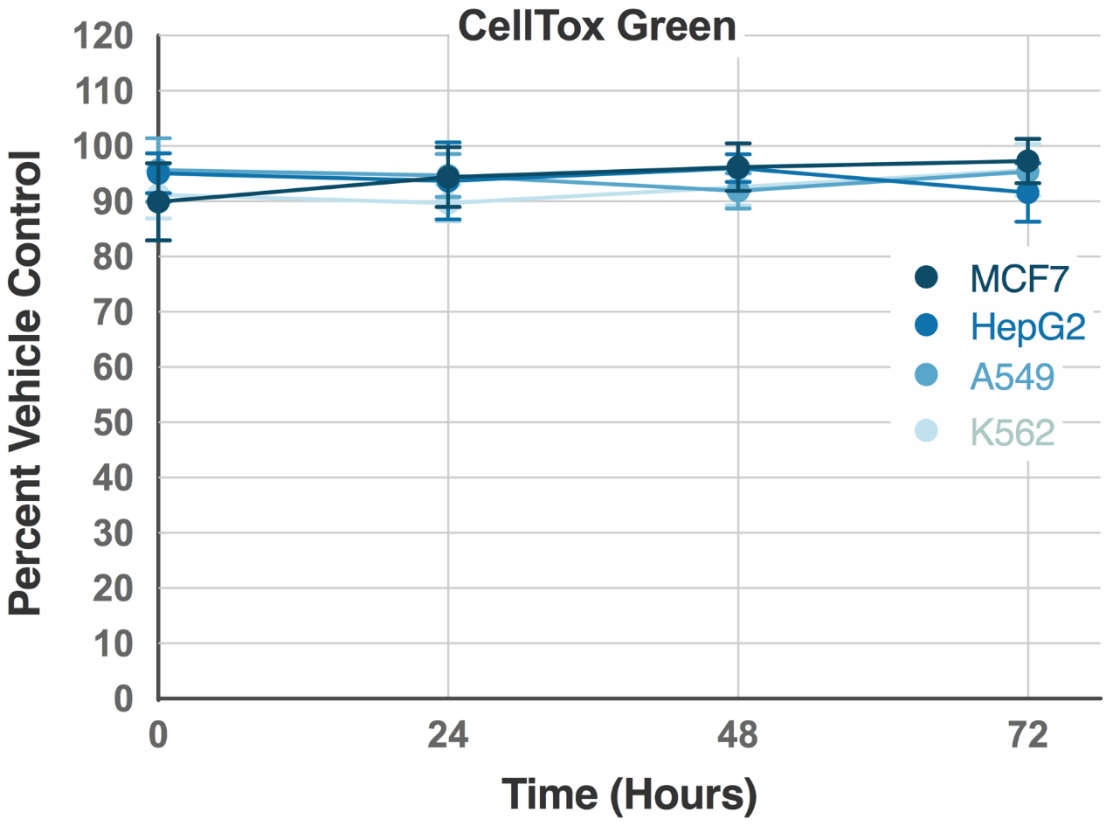
The use of DNA binding dyes for long term real-time detection of the accumulation of dead cells must consider if there is any influence of the assay reagent on the health or responsiveness of the cell model system. For example, for some cell viability assays, it is well known that reagents to estimate viable cell number (e.g. MTT and resazurin) can be toxic to the population of cells, even during a few hours of exposure (5). Similar reagent cytotoxicity effects are known for the DNA binding dyes. **Figure 2** shows the effects of three different DNA binding dyes continuously exposed to four different cell types for 72 hours before measuring cell viability using an ATP assay.

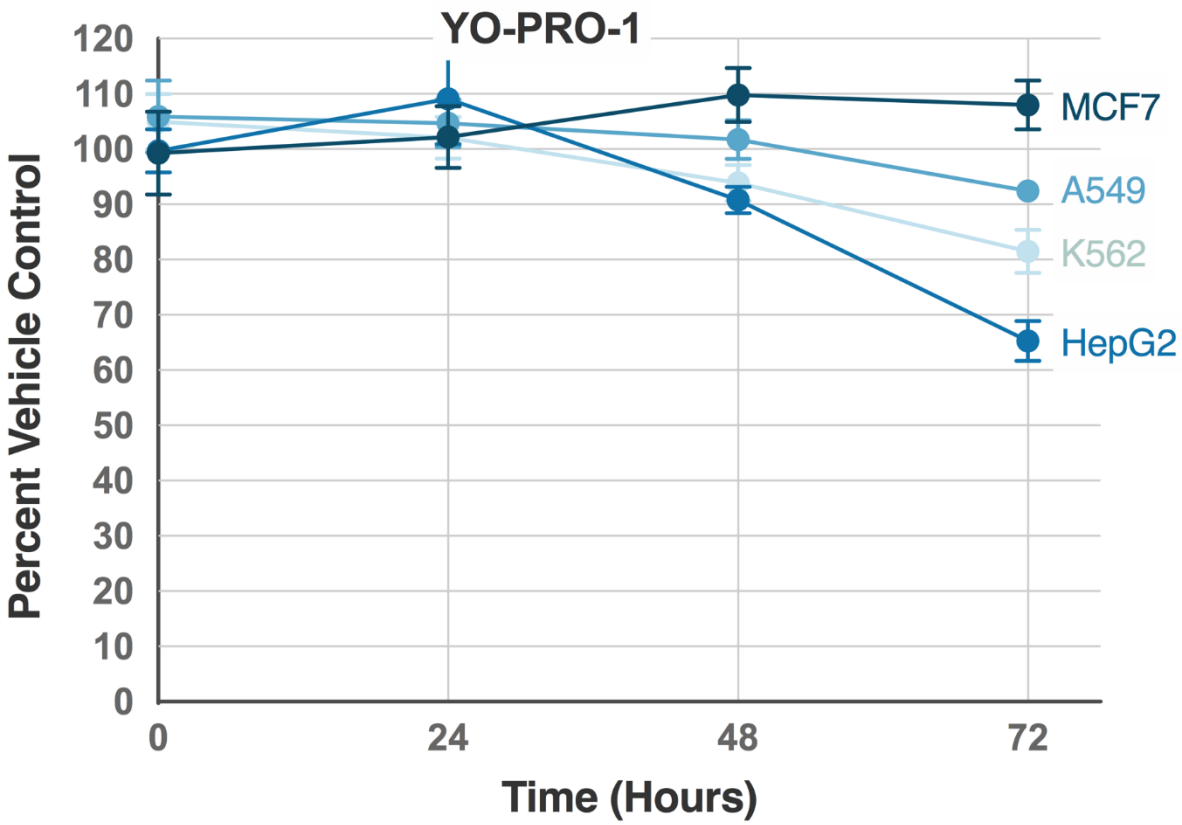
The data suggest similar nucleic acid binding dyes may have different effects on cell viability and those effects can be cell type specific. Understanding the mechanism and use of these DNA dyes is therefore important to determine the best probe for the desired assay design. Like all potential toxins, the cytotoxic effect of assay reagent components can be expected to depend on the concentration, the duration of exposure, and the susceptibility of individual cell types. Appropriate controls (vehicle only without dye) are recommended to validate each dye and cell type combination to determine if there is a cytotoxic effect of the assay reagent. It is suggested to use the vendor recommended concentration as a starting point and test a range of concentrations of dyes with each cell model system to confirm there is not an artefactual cytotoxic or cytostatic effect.

Commercial Availability

Several examples of DNA binding dyes classified as nonpermeable to live cells are commercially available.

- Propidium iodide: 1 mg/mL in water; ThermoFisher Catalog No. P3566
- Hoechst 33342: 10 mg/ml in water; ThermoFisher Catalog No. H3570
- SYTOX Green Nucleic Acid Stain: 5 mM Solution in DMSO; ThermoFisher Catalog No. S7020
- YOYO-1 Iodide (491/509) - 1 mM Solution in DMSO; ThermoFisher Catalog No. Y3601
- TO-PRO-3 Iodide (642/661) - 1 mM Solution in DMSO; ThermoFisher Catalog No. T3605
- DRAQ7 far-red fluorescent DNA dye; Biostatus Catalog No. DR70250
- GelRed 10,000X in DMSO; Biotium Catalog No. 41002
- CellTox Green Cytotoxicity Assay: 1000X in DMSO; Promega Corporation Catalog No. G8741


CellTox Green
Percent Vehicle Control
120
110
100
90
80
70
60
50
40
30
20
10
0
0
24
48
72
Time (Hours)
MCF7
HepG2
A549
K562


YO-PRO-1
Percent Vehicle Control
120
110
100
90
80
70
60
50
40
30
20
10
0
0
24
48
72
Time (Hours)
MCF7
A549
K562
HepG2

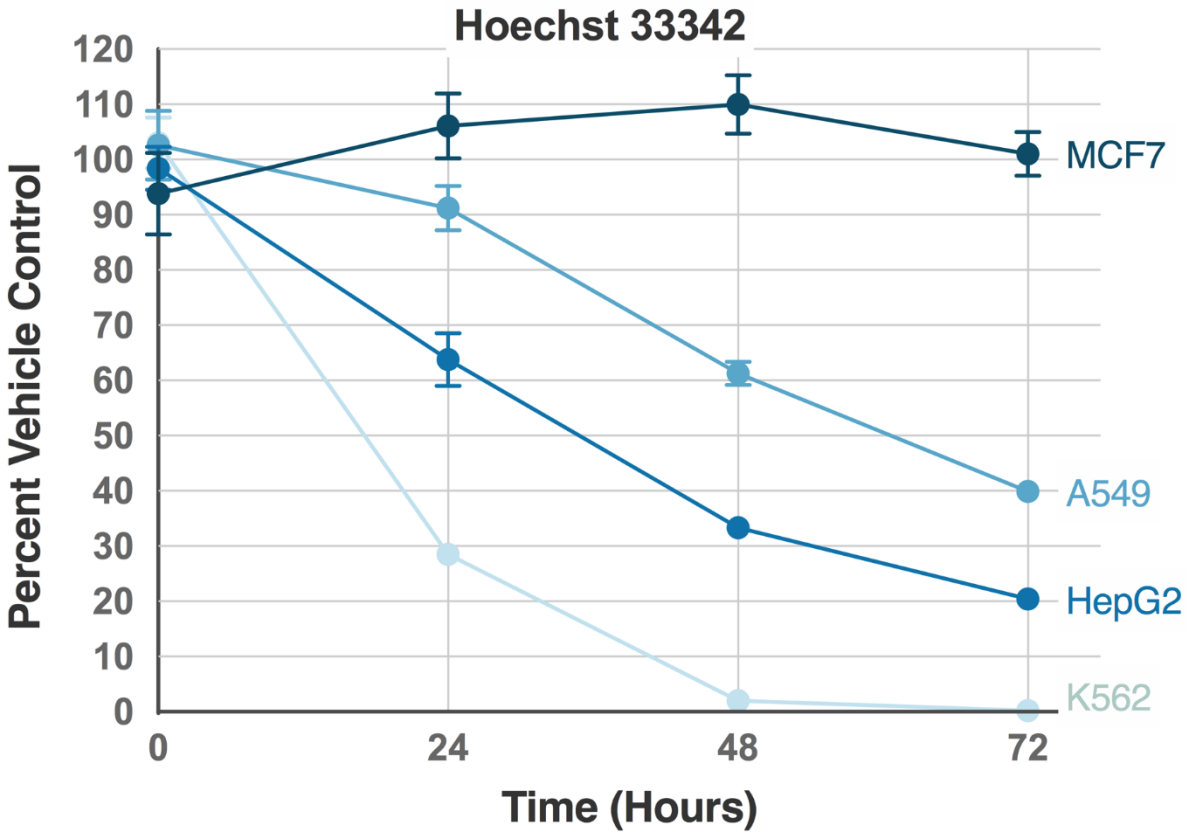


Figure 2. Effect of DNA binding dyes on cell viability. Four different cell types were treated with the vendor recommended concentration of DNA binding dye and cell viability assayed at various times up to three days using ATP content as the marker.

Protocols and Sample Data

The following example protocols are based on using the CellTox Green Cytotoxicity Assay which contains a non-permeable asymmetric cyanine dye which binds the minor groove to stain DNA of dead cells. The CellTox Green Dye is optimally excited at 512nm with a peak emission at 532nm. The filter recommendations for detection are 485 ± 20nm$_{Ex}$ and 520 ± 20nm$_{Em}$. For a complete detailed description of protocols including: reagent preparation, determination of linear range, detection sensitivity for individual cell types, and endpoint or homogeneous assay protocols, refer to Promega Technical Manual #375.

The components of the CellTox Green Cytotoxicity Assay kit are provided frozen and include:

- 20 µl CellTox Green Dye, 1,000X
- 10 ml Assay Buffer
- 0.5 ml Lysis Solution

The DNA binding dye is provided frozen as a 1000X reagent dissolved in DMSO. Thaw the tube in a 37°C water bath, vortex to mix contents, and centrifuge briefly to collect all the liquid in the bottom of the tube.

The general goal of the protocol is to create a 1:1000 dilution of the DNA binding dye in the sample of cultured cells to be measured. There are optional protocols to prepare a working dilution in a balanced salt solution (Assay Buffer) and achieve a final 1:1000 dilution of dye depending on whether you choose to run the assay in a real-time mode (record data periodically over 1-3 days in culture) or an endpoint mode (measure once at the end of the experiment).

General Protocol / Real-Time Assay

1. Add 10 µl of CellTox Green DNA binding dye per 5 ml of cell suspension in culture medium prior to seeding cells in the assay plates. That approach achieves a 1:500 dilution of dye in culture medium and allows for addition of test compounds (or vehicle control) as a 2X preparation in an equal volume of culture medium.
2. Mix the tube containing the suspension of cells by inversion or gently vortex to ensure dye homogeneity prior to seeding into assay plates.
3. Seed cell suspension in opaque walled assay plates (to avoid fluorescent signal crosstalk) with desired volume and cell number.
4. Add test compound treatment (and vehicle controls) to each well using a volume of medium equivalent to that used to seed the cells so the final concentration of dye is a 1:1000 dilution of the original component.
5. Measure fluorescence intensity at 485–500nm$_{Ex}$ / 520–530nm$_{Em}$ at any time from 0 to 72 hours.
6. Return the plate to the cell culture incubator between reads.

The following example in **Figure 3** illustrates results from a real-time assay showing an increase in fluorescence with both higher Terfenadine concentration and longer incubation time. The increase in fluorescence indicates the accumulation of dead cells over a three day incubation. Cells treated with 100 µM toxin are stained within a few hours and maintain most of the fluorescent intensity over the three day period.

Optional Protocol / Endpoint Assay

Addition of DNA binding dye can be used as an endpoint assay at the end of an experiment to stain dead cells and estimate how many are present. To assist in mixing of reagent and to avoid pipetting extremely small volumes, it is convenient to create a 1:500 dilution of dye in Assay Buffer and add a 1:1 vol:vol ratio of diluted dye reagent to the sample of cells in culture medium. Simply add the dye to a plate containing samples of cells exposed to test compound (and appropriate "no cell" and "no treatment/vehicle only" controls), mix using a plate shaker, wait 15 min, and record fluorescence intensity at 485–500nm$_{Ex}$ / 520–530nm$_{Em}$.

Optional Protocol / Multiplex Assay

The DNA binding dye in CellTox Green is functionally inert to the viable cell population which enables subsequent measurement of other parameters using a variety of compatible assay chemistries. One limitation to consider during multiplex assay design is the total volume available in the sample well. If you are performing a multiplex assay that requires addition of other reagents, you can include the DNA dye in the suspension of cells before dispensing into the assay plate or you can add a smaller volume of a more concentrated DNA dye reagent as long as the final concentration in the assay well is 1:1000 of the original dye component. For any lytic endpoint assay that will result in the second (multiplexed) reagent lysing the cells, the fluorescence value corresponding to the number of dead cells must be recorded first. The following example in **Figure 4** shows a multiplex combination of assays by first recording the fluorescence resulting from the DNA binding dye to indicate the number of dead cells, followed by subsequent addition of a luminogenic reagent to quantify ATP as a marker for the number of viable cells. The multiplex combination of orthogonal assays to detect complementary cell health markers can be used to confirm overall results.

Multiplex Assay Protocol

1. Perform DNA binding dye detection of dead cells using either real-time or endpoint assay format as described above.
2. Add a 1:1 vol:vol ratio of CellTiter-Glo Reagent to the samples containing CellTox Green Dye and experimentally treated cells.

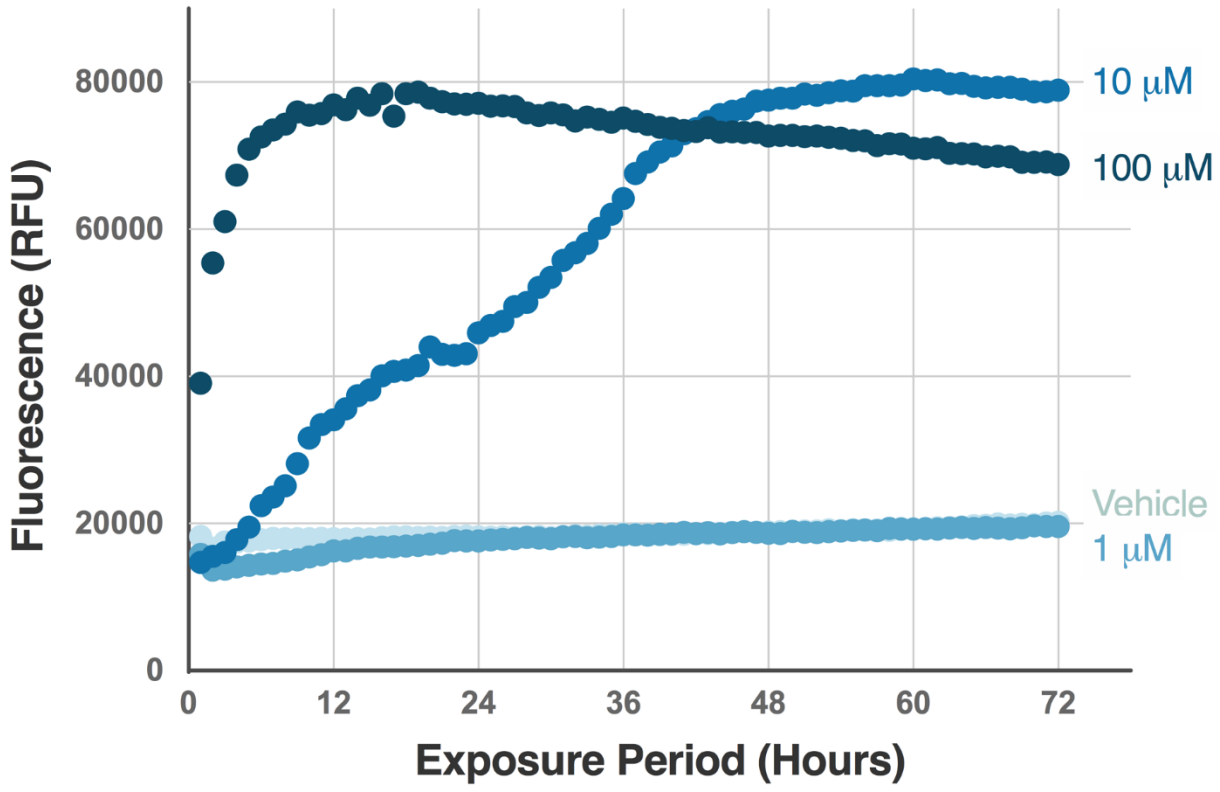


Figure 3. HepG2 cells treated with various doses of Terfenadine. CellTox Green Dye was added at time of Terfenadine dosing. Fluorescence was measured every hour over a three day incubation in a plate reader with an environmental chamber to control temperature at (37°C) and CO2 (5%). Increasing fluorescence indicates increase in number of dead cells in the culture well.

3. Place the plate on an orbital shaker and shake at 500–700 rpm to facilitate cell lysis and ATP extraction from the cells.
4. Measure luminescence after 5–10 minutes.

Optional Protocol to Estimate Total Number of Cells

The total number of live plus dead cells at the end of an experiment can be estimated by including a detergent (Lysis Solution) with the DNA binding dye reagent to lyse and stain all of the cells present.

1. Prepare a dilution of reagent by adding 20 µl CellTox Green Dye, 1,000X and 40 µl Lysis Solution (9% w/v Triton X-100) to 10 ml of Assay Buffer to create a 1:500 dilution of dye and a 1:250 dilution of Lysis Solution.
2. Mix the tube containing the combined reagent by inversion or gently vortex to ensure homogeneity of the dye and detergent prior to adding to assay plates.
3. Add a 1:1 vol:vol ratio of the combined reagent to the sample of cells to be measured.
4. Mix the plate on an orbital shaker (700–900 rpm) for 1 minute to ensure homogeneity.
5. Incubate at room temperature for 15 minutes, shielded from ambient light.
6. Measure fluorescence intensity at 485–500nm$_{Ex}$ / 520–530nm$_{Em}$.

Controls for DNA Binding Dye Experiments

Background control (without cells). To determine background fluorescence, record fluorescence values from samples containing the recommended concentration of DNA binding dye in complete culture medium without cells.

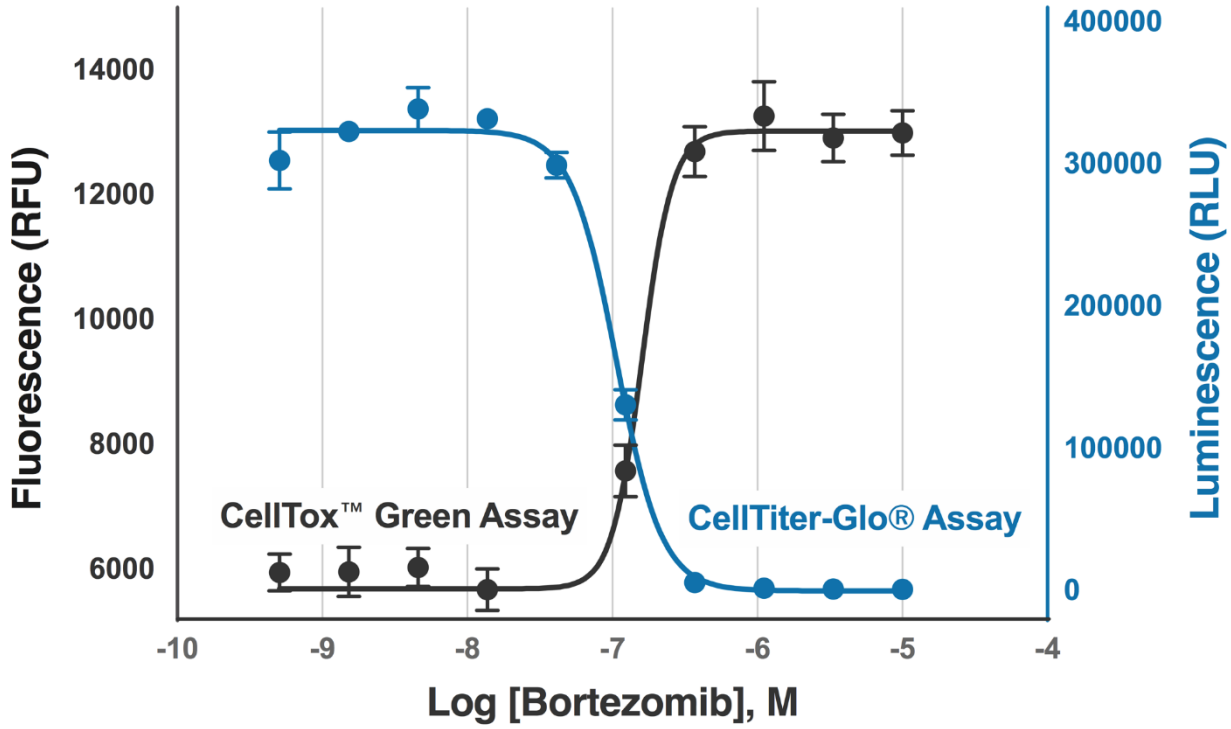


Figure 4. Multiplexing allows complementary measures of cell health. CellTox Green reagent was applied to bortezomib-treated K562 cells after 48 hours of exposure. Bortezomib is a known proteasome inhibitor chosen as a model toxin. Fluorescence associated with cytotoxicity was measured, then CellTiter-Glo Reagent was added and luminescence associated with the amount of ATP as a marker of viable cell number was measured.

Negative control (untreated cells). To establish a negative control, measure fluorescence from samples containing cells in complete culture medium treated with the same amount of vehicle/buffer used to deliver test compounds and containing the same concentration of DNA binding dye used for test samples.

Positive control (total cell number). To determine a value for the positive control representing all of the cells in the sample, a detergent (Lysis Solution: a 1:250 dilution of 9% wt:vol Triton X-100) is used to lyse the cells and enable staining of the entire population. To prepare positive control samples, add 4 µl of Lysis Solution per 100 µl of cells in culture medium, mix the samples using a plate shaker as described above, allow the samples to stand at ambient temperature and record fluorescence. Note: The dynamic range of the plate-reading fluorometer should be validated to ensure it is capable of reading over the complete range of fluorescence for the chosen cell number and probe concentration.

Troubleshooting / DNA Binding Dye

- The optimal concentration of DNA binding dye for staining may vary among cell types and culture conditions. It is recommended to test a range of concentrations to optimize detection sensitivity.
- Use appropriate controls including wells containing complete culture medium and vehicle only (without cells) to determine the background fluorescence.
- Culture medium containing phenol red can quench overall fluorescence. The endpoint assay protocol that uses the provided Assay Buffer can reduce quenching and increase the signal-to-background ratio. The Assay Buffer should not be used to deliver the CellTox Green Dye for the kinetic real-time mode using longer incubation times.
- Confirm appropriate filter selection is in place in the plate reading fluorometer.
- Use opaque-walled 96-, 384-, or 1536-well tissue culture plates compatible with fluorometer.

- DNA intercalating compounds (doxorubicin, actinomycin D, daunorubicin, etc.) may compete for binding of the DNA dye, thus reducing staining and leading to underestimation of cytotoxicity.
- Extended incubations (more than 24 hours) can cause evaporation of culture medium and may lead to edge effects. Using only the inner wells of assay plates may mitigate this problem.
- Monitoring the viable, dead and total cell number over the course of an experiment, enables determination of cytostatic vs cytotoxic effects of test compounds. Vehicle-treated control cells may continue to proliferate over the course of an experiment.
- A general precaution for all DNA binding dyes is to protect the reagent from light.
- Animal-derived products such as Matrigel Matrix which is a tumor extract may contain DNA and result in high background levels.
- Use of DNA binding dyes to test for cytotoxicity resulting from transfection experiments is not recommended. Residual DNA from transfection mixture may result in high background fluorescence.

Markers That Leak Out of the Cytoplasm of Dead Cells into Culture Medium

Introduction

The presence of dead cells that have lost membrane integrity can be detected by measuring markers that leak from the cytoplasm into the culture medium. The most common marker used for this type of assay is lactate dehydrogenase (6, 7). Lactate dehydrogenase (LDH) catalyzes the conversion of pyruvate to lactate and in the process, converts NAD^+ to NADH. The reducing capacity of NADH can be used to reduce a variety of substrate molecules into products that are either colored, fluorescent, or luminogenic. **Figure 5** illustrates the general scheme and assay chemistry used to detect LDH-release from the cytoplasm of dead cells. An excess amount of lactate and NAD+ as substrates are delivered in a reagent mixture to drive LDH to generate pyruvate and NADH. The reducing power of NADH is used to convert the substrate (resazurin) into the fluorogenic product (resorufin). Colorimetric versions of this assay chemistry have used a tetrazolium compound as the diaphorase substrate which is converted into an intensely colored formazan product that can be measured using a spectrophotometer. Similarly, a luminometric assay can use a "pro-luciferin" substrate which is converted into a luciferin product that is linked to a firefly luciferase reaction to generate a luminescent signal. The colorimetric version of the assay was developed decades ago and lacks detection sensitivity. In addition, because of buffer incompatibility with live cells, it requires removal of culture supernatant to a different container to perform the assay. The fluorescent assay protocol is homogeneous and more sensitive than the colorimetric version. Advances in formulating the reagent to be compatible with viable cells enabled a homogeneous fluorescent protocol to be developed. The luminogenic version of the assay is far more sensitive than the fluorogenic version that enables sampling of 2-5 µl of culture supernatant at various times which can be stored frozen for future analysis of the trends of LDH release over time.

Other enzymes that do not use the NADH cycling assay chemistry also have been used as markers of dead cells. Examples include enzymes such as adenylate kinase (AK) and glyceraldehyde-3-phosphate dehydrogenase (GAPDH) that can produce ATP by providing a reaction cocktail containing the necessary ingredients to generate a cycling assay chemistry (8, 9); however, those enzymes may be less stable than LDH and lose enzymatic activity sooner after release from dead cells.

Another option is to measure protease activity as a marker that is released from dead cells with damaged membranes (10). Aminopeptidase activity can be measured using substrates containing a short sequence of amino acids (alanine-alanine-phenylalanine) conjugated via a peptide bond to either rhodamine 110 or aminoluciferin. Enzymatic removal of the amino acids can generate free rhodamine-110 for a fluorescent assay or free aminoluciferin which can be used by firefly luciferase to generate light (11).

Another optional assay approach is to load cells to contain a measurable marker. Loading target cells with an artificial measurable marker such as pro-fluorescent Calcein-AM (12) or radioactive ^{51}Cr (13) has been used to measure cytotoxicity, mostly for assays that involve mixtures of more than one cell type (e.g. effector and target cells in antibody dependent cell mediated cytotoxicity assays). Target cells incubated with ^{51}Cr will take up the radioactive marker which becomes bound as protein complexes in the cytoplasm of live cells. Similarly, calcein-AM is taken up by live cells where cytoplasmic esterase activity removes the AM group to generate fluorescent calcein which is retained in live cells. Upon cell death and loss of membrane integrity, the fluorescent calcein or the radioactive ^{51}Cr is released from the cytoplasm into the culture medium where they can be quantified relative to the background spontaneous release from the viable cell population. The disadvantages of this approach include: the extra handling step to label the target cells prior to performing an assay, spontaneous release from the live cell population, and the safety and cost issues associated with using and disposing of radioactivity.

Still another cytotoxicity assay option is to genetically engineer cells to express luciferase as a marker (14). When cells die, the luminescence declines because the luciferase activity diminishes once cytoplasmic components are released into the culture medium. An advantage of this approach is the ability to selectively measure death of one type of cell in a mixed cell culture model such as antibody dependent cell mediated cytotoxicity assays. Disadvantages include the need to engineer cells to express luciferase and the assay measures a decrease in luminescent signal with increased cell killing which may make it difficult to detect small changes in the number of dead cells.

Commercial Availability

- Calcein-AM; ThermoFisher Scientific Catalog No. C1430
- CytoTox 96 Non-Radioactive Cytotoxicity Assay; Promega Corporation Catalog No. G1780
- CytoTox-ONE Homogeneous Membrane Integrity Assay; Promega Corporation Catalog No. G7890
- LDH-Glo Cytotoxicity Assay; Promega Corporation Catalog No. J2380.
- CytoTox-Glo Cytotoxicity Assay; Promega Corporation Catalog No. G9290
- Cytotoxicity Detection Kit (LDH); Millipore-Sigma (Roche) Catalog No. 11644793001
- In Vitro Toxicology Assay Kit, Lactic Dehydrogenase based; Sigma Catalog No. TOX7-1KT
- Pierce LDH Cytotoxicity Assay Kit; ThermoFisher Scientific Catalog No. 88953
- aCella-TOX Glyceraldehyde-3 Phosphate Dehydrogenase; Cell Technology Catalog No. CLATOX100-3
- Vybrant Cytotoxicity Assay Kit (Glucose-6-Phosphate Dehydrogenase Release Assay); ThermoFisher Scientific Catalog No. V23111

Example Protocol / Homogeneous Fluorescent LDH-Release Assay

The following example protocol is based on using the CytoTox-ONE Homogeneous Membrane Integrity Assay. For a detailed description of protocols including: reagent preparation, determination of linear range, detection sensitivity, and a detailed troubleshooting section, refer to Promega Technical Bulletin #306.

1. Prepare opaque-walled assay plates containing cells in culture medium.
2. Include control wells for: no cells (medium only), no treatment (cells with same amount of vehicle used to deliver test compounds), and maximum LDH release controls from detergent lysed cells (to determine value for 100% cytotoxicity).
3. Add test compounds and vehicle controls to appropriate wells.
4. Culture cells for desired test exposure period (usually 24-72 hours).
5. Remove assay plates from 37°C incubator and equilibrate to 22°C (approximately 20–30 minutes) so all wells reach the same temperature.

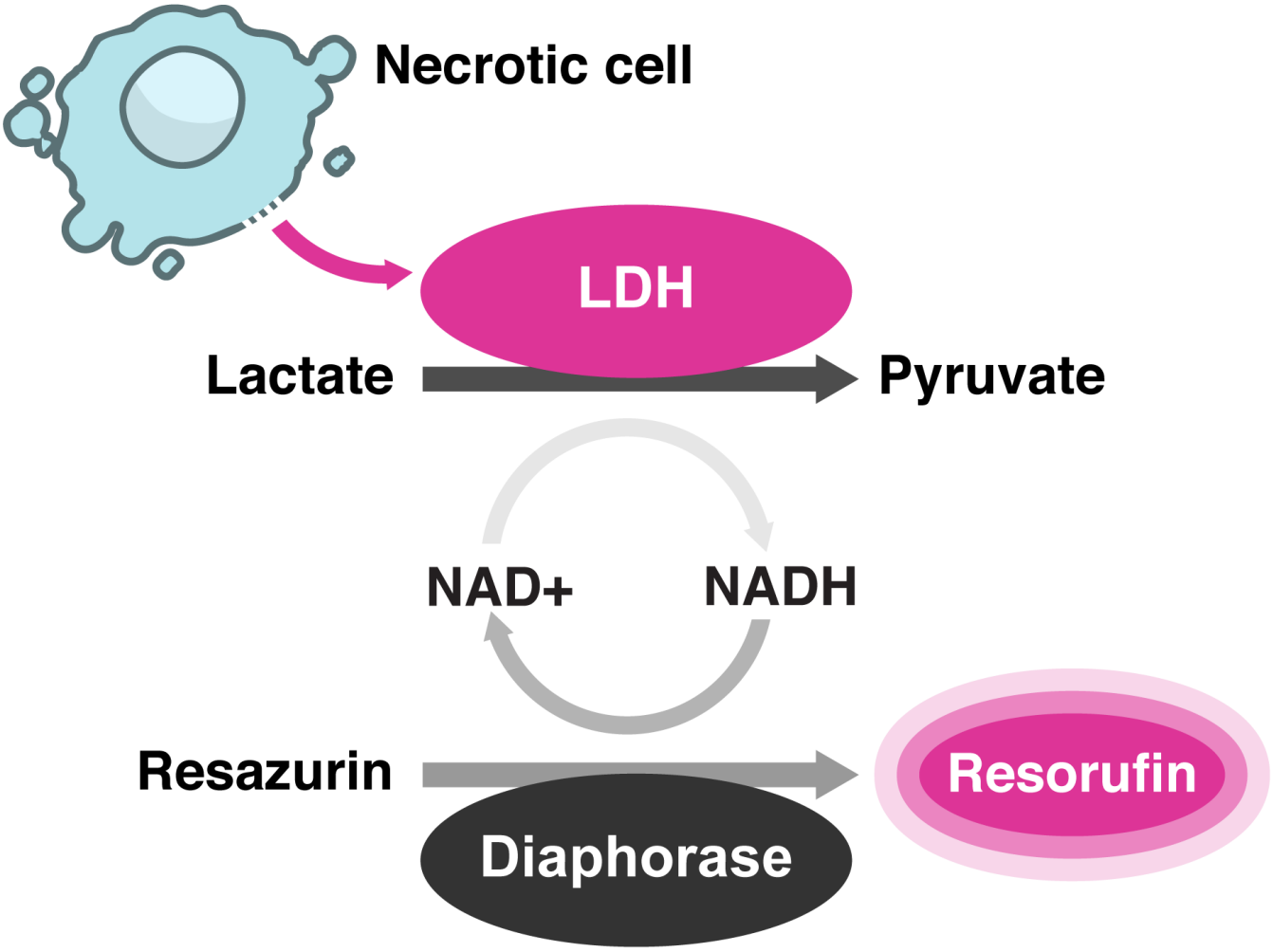


Figure 5. A schematic representation of the fluorogenic LDH-release assay chemistry. LDH from dead cells that leaked into the culture medium catalyzes the conversion of lactate to pyruvate and in the process generates NADH. In the presence of the diaphorase (reductase) enzyme, the NADH can reduce resazurin into the fluorogenic resorufin product that can be measured using a plate reading fluorometer.

6. Add 2 µl of Lysis Solution (9% w/v Triton X-100) per 100 µl volume to the wells prepared for maximum LDH release control. (Note: If a larger pipetting volume is desired, use 10 µl of a 1:5 dilution of Lysis Solution.)
7. Add a volume of CytoTox-ONE Reagent equal to the volume of culture medium present in each well.
8. Mix for 30 seconds using a plate shaker.
9. Incubate at 22°C for 10 minutes.
10. Add Stop Solution (50 µl per 100 µl of CytoTox-ONE Reagent added) to each well. (Note: This step is optional, but recommended to stabilize the fluorescent signal and provide better consistency among replicate samples.)
11. Mix the contents of the wells for 10 seconds using an orbital shaker and record resorufin fluorescence using an excitation wavelength of 560nm and an emission wavelength of 590nm.

Figure 6 shows example data from the LDH-release (CytoTox-ONE) assay. The effect of TNFα treatment on murine L929 cells was measured using the homogeneous (add-mix-measure) fluorescent LDH-release assay and a luminescent ATP assay as orthogonal methods using different endpoints to measure cell health. The half

maximal response values correlate well for the LDH-release (dead cell) and the ATP content (viable cell number) assays.

Optional Protocol to Assist with Multiplexing

For assays that measure markers such as LDH released into the culture medium, an optional approach is to transfer an aliquot of culture supernatant into a separate suitable multi-well plate to perform the assay. Although this approach is a non-homogeneous protocol for the LDH-release assay, the advantage is that the population of cells remaining in the original assay plate can be used for multiplexing with another assay. The sample transfer approach can enable multiplexing in situations where two assay chemistries are not compatible or there is spectral overlap between fluorophores used for two different assays. Splitting the sample also has the result of reducing the volume of medium in the original well which may be required for multiplexing with assay reagents that recommend adding a 1:1 vol:vol ratio of reagent to culture medium. The extreme detection sensitivity of the luminescent version of the LDH-release assay provides an additional option of repeated sampling of 2-5 µl from the test wells at several different times to enable gathering kinetic data on the progress of cell death, while leaving the original sample of cells intact.

Controls for LDH-release Experiments

A negative control (background fluorescence) should be determined by adding the LDH detection reagent to replicate wells containing culture medium without cells and the same vehicle used to deliver test compound to experimental wells.

A 100% cell lysis positive control is recommended to determine the maximum amount of LDH present. Cells can be lysed to release LDH using an appropriate amount of a compound known to be toxic to the type of cells used in the experiment or a detergent. The CytoTox-ONE Homogeneous Membrane Integrity Assay described in the protocol above includes a Lysis Solution, which is a 9% (weight/volume) solution of Triton X-100 in water.

Troubleshooting

- Animal sera used to supplement culture medium contains endogenous LDH activity and will contribute to background signal. Different lots and different types of sera contain different amounts of LDH activity. Using serum-free medium, reducing the percent of serum, or choosing a different lot or type can reduce background values.
- The apparent half-life of LDH released from cells into the surrounding medium is approximately 9 hours; however, the half-life may depend on the mechanism of cell death and should be confirmed for each cell culture model used. If treated cells die (or if Lysis Solution is added) at the beginning of an experimental exposure period, the quantity of active LDH remaining in the culture medium at the end of the experiment may underestimate the quantity of LDH present in untreated cells. Performing 100% lysis of a set of control wells at the beginning and end of the incubation period is recommended. A further complication that should be considered is the amount of cell growth during the experiment. If the indicator cells are growing throughout the duration of the experiment, untreated control wells will have more cells and thus will have more LDH activity present at the end of the exposure period.
- Pyruvate-supplemented media such as Ham's F12, Iscove's, and some formulations of DMEM may cause a reduction in the fluorescent signal due to product inhibition of the LDH enzymatic reaction catalyzing conversion of lactate to pyruvate.
- The presence of strong reducing compounds may interfere with the resazurin-resorufin assay chemistry.
- Measuring death of a specific population of cells can be challenging when there is more than one cell type present. Although LDH-release has been used for detecting target cell killing in mixtures of target and effector cells, additional controls must be used to account for spontaneous release of LDH from dying

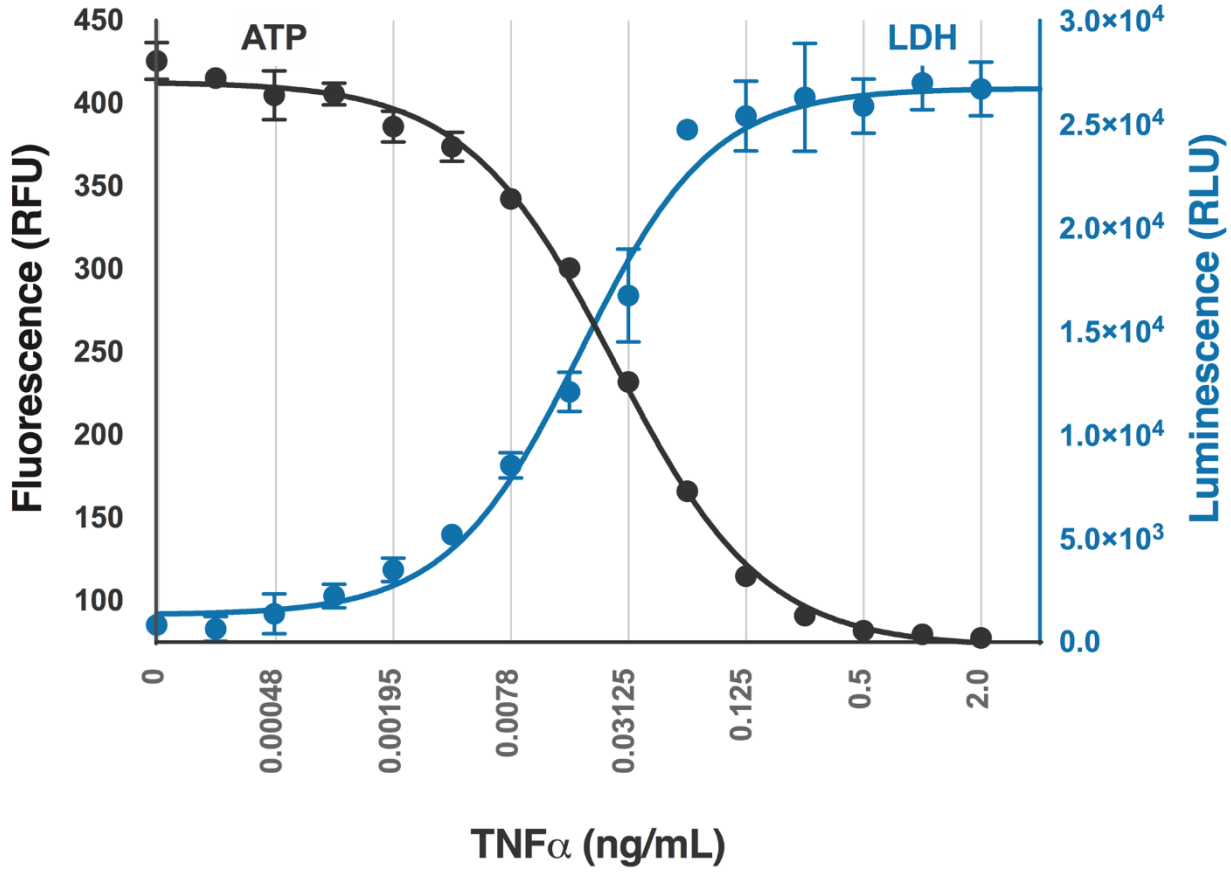


Figure 6. Murine L929 cells were seeded at 2,000 cells per well in a 384-well opaque walled plate in serum-supplemented medium, cultured for 24 hours, then various amounts of TNFα were added and incubated overnight. Either CytoTox-ONE Reagent (to measure LDH-release representing dead cells) or CellTiter-Glo Reagent (to measure ATP as a marker of viable cells) was added to parallel sets of wells, and fluorescence (560Ex / 590Em) or luminescence values, respectively, were recorded. The values represent the mean ± SD of 4 replicate samples.

effector cells. This can be especially cumbersome to implement when several different ratios of effector to target cells are used for experiments.

Conclusion

There are many different types of assays available to measure the accumulation of dead cells in culture. Finding the best "fit for purpose" method will depend on several factors including the cell model system, desired throughput, cost for reagents and instrumentation availability. Regardless of the method chosen to measure the accumulation of dead cells, it is recommended to validate the chosen assay method and appropriate positive controls with each cell type and consider the possibility of selective reagent toxicity among different types of cells. Dyes that are claimed to be non-toxic should be confirmed for each cell culture model system and duration of exposure. It is also recommended to use orthogonal assays (using a multiplex approach on the same sample if possible) to confirm assay performance using another method measuring a separate marker. Recently developed options for recording the accumulation of dead cells in real time from the same sample show promise for broad acceptance and will provide much flexibility for multiplexing and the early phases of assay development.

References

1. Owen SC, Doak AK, Ganesh AN, Nedyalkova L, McLaughlin CK, Shoichet BK, et al. Colloidal drug formulations can explain "bell-shaped" concentration-response curves. ACS Chem Biol. 2014;9(3):777-84.

Epub 2014/01/09. doi: 10.1021/cb4007584. PubMed PMID: 24397822; PubMed Central PMCID: PMCPMC3985758.
2. Freshney RI. Culture of animal cells: Wiley Online Library; 2005.
3. Piccinini F, Tesei A, Arienti C, Bevilacqua A. Cell counting and viability assessment of 2d and 3d cell cultures: expected reliability of the trypan blue assay. Biological procedures online. 2017;19(1):8. PubMed PMID: 28814944.
4. Chiaraviglio L, Kirby JE. Evaluation of impermeant, DNA-binding dye fluorescence as a real-time readout of eukaryotic cell toxicity in a high throughput screening format. Assay Drug Dev Technol. 2014;12(4):219-28. Epub 2014/05/17. doi: 10.1089/adt.2014.577. PubMed PMID: 24831788; PubMed Central PMCID: PMCPMC4026211.
5. Riss TL, Moravec RA, Niles AL, Duellman S, Benink HA, Worzella TJ, et al. Cell Viability Assays. In: Sittampalam GS, Coussens NP, Brimacombe K, Grossman A, Arkin M, Auld D, et al., editors. Assay Guidance Manual. Bethesda (MD)2004.
6. Korzeniewski C, Callewaert DM. An enzyme-release assay for natural cytotoxicity. J Immunol Methods. 1983;64(3):313–20. Epub 1983/11/25. PubMed PMID: 6199426.
7. Decker T, Lohmann-Matthes ML. A quick and simple method for the quantitation of lactate dehydrogenase release in measurements of cellular cytotoxicity and tumor necrosis factor (TNF) activity. J Immunol Methods. 1988;115(1):61–9. Epub 1988/11/25. PubMed PMID: 3192948.
8. Olsson T, Gulliksson H, Palmeborn M, Bergstrom K, Thore A. Leakage of adenylate kinase from stored blood cells. J Appl Biochem. 1983;5(6):437–45. Epub 1983/12/01. PubMed PMID: 6088465.
9. Squirrell D, Murphy J. Rapid detection of very low numbers of micro-organisms using adenylate kinase as a cell marker. A practical guide to industrial uses of ATP luminescence in rapid microbiology. 1997:107-13.
10. Niles AL, Moravec RA, Eric Hesselberth P, Scurria MA, Daily WJ, Riss TL. A homogeneous assay to measure live and dead cells in the same sample by detecting different protease markers. Anal Biochem. 2007;366(2):197–206. doi: 10.1016/j.ab.2007.04.007. Epub 2007/05/22. PubMed PMID: 17512890.
11. Cho MH, Niles A, Huang R, Inglese J, Austin CP, Riss T, et al. A bioluminescent cytotoxicity assay for assessment of membrane integrity using a proteolytic biomarker. Toxicol In Vitro. 2008;22(4):1099-106. Epub 2008/04/11. doi: 10.1016/j.tiv.2008.02.013. PubMed PMID: 18400464; PubMed Central PMCID: PMCPMC2386563.
12. Papadopoulos NG, Dedoussis GV, Spanakos G, Gritzapis AD, Baxevanis CN, Papamichail M. An improved fluorescence assay for the determination of lymphocyte-mediated cytotoxicity using flow cytometry. J Immunol Methods. 1994;177(1-2):101–11. Epub 1994/12/28. PubMed PMID: 7822816.
13. Brunner KT, Mauel J, Cerottini JC, Chapuis B. Quantitative assay of the lytic action of immune lymphoid cells on 51-Cr-labelled allogeneic target cells in vitro; inhibition by isoantibody and by drugs. Immunology. 1968;14(2):181-96. Epub 1968/02/01. PubMed PMID: 4966657; PubMed Central PMCID: PMCPMC1409286.
14. Nazarian AA, Archibeque IL, Nguyen YH, Wang P, Sinclair AM, Powers DA. Characterization of bispecific T-cell Engager (BiTE) antibodies with a high-capacity T-cell dependent cellular cytotoxicity (TDCC) assay. J Biomol Screen. 2015;20(4):519–27. doi: 10.1177/1087057114561405. Epub 2014/12/06. PubMed PMID: 25477202.

Apoptosis Marker Assays for HTS

Terry L. Riss, PhD,[1] Martha A. O'Brien, PhD,[1] Richard A. Moravec, BS,[1] Kevin Kupcho, BS,[1] and Andrew L. Niles, MS[1]

Created: July 1, 2021.

Abstract

A variety of assays are available to detect apoptosis; however, few are conveniently adapted for high-throughput screening (HTS) using a multimode plate reader. The markers most commonly used for *in vitro* detection of apoptosis include caspase-3/7 activity and phosphatidylserine (PS) exposure on the outer leaflet of the cell membrane. Caspase-3/7 activity is routinely measured using consensus tetrapeptide substrates in lytic cell-based assays to generate a fluorescent or luminescent signal measured with a plate reader. PS exposure historically has been measured using flow cytometry to detect binding of fluorescently-tagged annexin V; however, sample throughput and washing steps to remove unbound fluorescent probe have limited broad adoption of the flow cytometric approach for HTS. Recently, recombinant annexin V fusion proteins engineered to contain subunits of a shrimp-derived luciferase have been used to develop a no-wash enzyme complementation approach for detecting PS exposure using a multimode plate reader. This homogeneous annexin V-binding assay approach has broadened the availability of assays compatible with ultraHTS.

Abbreviations

AFC	aminofluorocoumarin
AMC	aminomethylcoumarin
BiT	binary technology
caspase	cysteine-aspartic protease
DEVD	Asp-Glu-Val-Asp
dUTP	2′-Deoxyuridine, 5′-Triphosphate
ELISA	enzyme-linked immunosorbent assay
FITC	fluorescein isothiocyanate
FMK	fluoromethylketone
HTS	high throughput screening

Author Affiliation: 1 Promega Corporation; Email: terry.riss@promega.com.

Table continued from previous page.

LgBiT	Large BiT
LOPAC	library of pharmaceutically active compounds
PARP	poly ADP ribose polymerase
pNA	*p*-nitroaniline
PS	phosphatidylserine
R110	rhodamine 110
RFU	relative fluorescence units
RLU	relative luminescence units
SmBiT	Small BiT
TUNEL	terminal deoxynucleotidyl transferase dUTP nick end labeling

Introduction

This chapter is not meant to be a thorough review of cell death or apoptosis detection assays, but will describe the basic methods for the measurement of caspase activity and phosphatidylserine (PS) exposure that can be used in a high-throughput screening (HTS) format to detect markers consistent with apoptosis (1).

Apoptosis is a form of programmed cell death that is critical for carrying out normal developmental and physiological processes. Deregulated apoptosis is associated with many disease states. Too much cell death occurs in many degenerative diseases and too little cell death occurs in some kinds of cancer when the apoptotic process has become inhibited or non-functional leading to continued net proliferation of tumor cells. Much has been learned about the complex signaling events in the extrinsic and intrinsic pathways that modulate apoptosis. There is much interest in attempting to further understand the process of apoptosis by investigating individual members of the signaling pathways as potential targets for therapeutic development. Phenotypic screening campaigns to identify compounds that induce apoptosis often precede efforts to identify the individual target interactions. Despite the interest in individual target interaction, there remains a need to efficiently screen large chemical libraries by measuring markers to detect apoptosis.

Historically, apoptosis was detected based on changes in cell morphology. Some of those hallmark changes include: membrane blebbing, cell shrinkage, nuclear fragmentation and chromatin condensation. The process of apoptosis also results in discrete patterns of DNA fragmentation. Assays developed for detection of DNA fragmentation as a marker of late stage apoptosis included the terminal deoxynucleotidyl transferase dUTP nick end labeling (TUNEL) assay and ELISA methods. The TUNEL assay is a method for detecting DNA fragmentation by labeling the 3′- hydroxyl termini in the double-strand DNA breaks generated during apoptosis

and the ELISA approach relies on antibody detection of DNA fragments. However, both of those approaches are not amenable to HTS because they require multi-step procedures including wash steps.

Caspase Activity Detection

Most apoptosis involves the activation of a cascade of cysteine-aspartic proteases (caspases) that mediate upstream signaling events ultimately leading to the activation of executioner caspases involved with destroying the cell.

Executioner caspases are involved with the terminal proteolytic events of the apoptotic process. Those events include breaking down the cytoskeleton that leads to morphological changes observed during apoptosis and inactivating repair enzymes such as poly ADP ribose polymerase (PARP) which was among the first substrates recognized to be cleaved by "caspase" (2-4).

With few exceptions, if a cell has active executioner caspase activity, it is beyond the point of no return in the apoptotic process. Thus, measuring executioner caspase-3/7 activity has become the most popular assay performed in an HTS format using a standard multimode plate-reader to detect the process of apoptosis.

Early in apoptosis research, the protease now called caspase-3 was shown to cut PARP at the C-terminal end of a DEVD amino acid sequence generating ~p89 and p24 fragments and resulting in inactivation of the DNA damage repair properties of PARP. This caspase activity is sometimes referred to as DEVDase activity.

Research into the cleavage site specificities of the various members of the caspase family of proteases lead to identification of four amino acid recognition sequences useful as selective substrates (5). Those four amino acid long substrates are typically *N*-terminally blocked with a protecting group to prevent aminopeptidase activity from liberating the reporting group, thus increasing substrate selectivity. The most commonly used artificial substrate for detecting caspase-3 or 7 activity include DEVD linked via a peptide bond to either a chromophore (*p*-nitroaniline, pNA), a fluorophore (aminomethylcoumarin (AMC), aminofluorocoumarin (AFC), or rhodamine 110; R110) or aminoluciferin as a reporter (6). The inherent reagent background signal and the reporting molecule dynamic response influence detection sensitivity and usefulness for HTS. The choice of the fluorogenic reporting molecule (e.g. AMC, AFC, R110, or a far red emitting dye) can affect the overall performance of the protease assay and can also serve to enable opportunities for multiplexing with other fluorescent assays. For example, the coumarin class of fluorophores are excited by light in the UV region (e.g. AMC = 340nmEx / 440nmEm) which is more likely to result in fluorescent interference from compounds in small molecule libraries. The R110 fluorophore contains 2 amine groups, both of which form peptide bonds with the peptide substrate forming $(Z\text{-DEVD})_2$-R110. Although it is generally not an issue for detecting the presence or absence of caspase-3/7 activity, the cleavage of two peptides from a single R110 fluorophore may raise questions during interpretation of results. For additional details regarding fluorescence interference, please refer to the Assay Guidance Manual chapter Interference with Fluorescence and Absorbance by Simeonov and Davis (7). Interference with luminescent assays also needs to be considered. For example, small molecule libraries contain known colored compounds that can result in signal quenching and luciferase inhibitors that may interfere with the detection assay chemistry. For a detailed description of luciferase inhibitors, see the Assay Guidance Manual chapter Interferences with Luciferase Reporter Enzymes by Auld and Inglese (8).

The luminogenic protease substrate is about 20-50-fold more sensitive than the fluorogenic versions (and far more sensitive than the colorimetric pNA format) which has enabled miniaturization of caspase-3/7 assays to high density plate formats used for HTS. Figure 1 was copied from the Technical Manual of the Caspase-Glo-3/7 Assay and shows the general scheme for the luminogenic assay. Caspase-3/7 activity cleaves at the *C*-terminal side of aspartic acid to release aminoluciferin that is subsequently used as a substrate for firefly luciferase to generate photons. The light is quantified as relative luminescence units (RLU) using a standard plate reading luminometer.

The caspase assay can be applied to cells grown as a monolayer, in suspension, or as a 3D culture model system. The luminescent assay detection sensitivity is adequate for using small numbers of cells in 96-, 384- or 1536-well plate formats. Figure 2 shows Panel B of Figure 6 from O'Brien et al., 2005 (6) illustrating the detection sensitivity of the luminescent assay is about 20-fold better than a fluorescent approach for Jurkat cells. The general assay performance and relative detection sensitivity for each cell line and well format should be empirically determined and validated in the user's lab.

Several results of "Cellular Toxicity (caspase-3)" from National Center for Advancing Translational Sciences (NCATS) labs validating the luminescent caspase-3/7 assay approach have been posted to the PubChem database. The uHTS approach in the 1536 well format using several different cell lines (HepG2, Jurkat, HUV-EC-C, SHSY5Y, BJ, MRC-5, Mesangial, SK-N-SH, FSKstim, H-4-II-E, HEK293, N2a,NIH 3T3, Renal Proximal Tubule) has been reported as AID654-AID667 (e.g. for HepG2 https://pubchem.ncbi.nlm.nih.gov/bioassay/654). The PubChem database also contains results from a cell-based screening bioassay of 325,733 compounds demonstrating its utility for implementing an automated HTS campaign (Luminescence Cell-Based Primary HTS to Identify Inhibitors of A1 Apoptosis: AID2462, https://pubchem.ncbi.nlm.nih.gov/bioassay/2462). A further example from screening 9667 compounds as part of the U.S. Tox21 Program is PubChem AID1347037 (Caspase-3/7 induction in CHO-K1 cells by small molecules, qHTS assay; https://pubchem.ncbi.nlm.nih.gov/bioassay/1347037).

The luminescent assay detection chemistry is not affected by the presence of routine concentrations of DMSO used as a vehicle to deliver test compounds. Figure 3 (reproduction of Figure 9 from O'Brien et al., 2005) shows results comparing the effects of 0.1%, 1% or 10% DMSO added to assays containing two concentrations of caspase-3. Although there was a slight increase in the background (no caspase, white bars) samples containing 10% DMSO, routine concentrations of DMSO did not have a substantial effect on the results.

Protocol to Detect Caspase-3/7 Activity as a Marker of Apoptosis

A detailed protocol is included in Promega Technical Bulletin #323 (https://www.promega.com/Resources/Protocols/Technical%20Bulletins/101/Caspase%20Glo%2037%20Assay%20Protocol/?fq=caspase-glo%203%207).

1. Choose opaque walled white plates for best results when using luminescent assays. Clear bottom plates are optional and recommended for viewing cells with a microscope during the experiment.
2. Reproducible results among different days, different end users, etc. require a standard operating procedure to produce a consistent source of cells for each experiment (9).
3. Prepare assay plates containing replicates of: blanks (complete medium without cells); negative control (cells treated with vehicle only); and positive controls (wells containing cells treated with a compound known to cause apoptosis in the cell model being used).
4. Dispense a uniform number of cells in each well (except for blanks) and allow the plates to equilibrate prior to addition of test compounds, positive control samples and vehicle controls.
5. Add test compounds and positive control samples dissolved in the same solvent and volume as the vehicle control. **Note:** Some potentially useful positive control compounds, their mode of action and a recommended concentration are included in Table 1.
6. Incubate assay plate using empirically determined conditions for desired time. (**Note**: The process of apoptosis is a series of transient kinetic events. Detection of apoptosis markers can occur in less than 1 hour or more than a day depending on the model system and culture conditions. The optimum incubation time should be determined empirically for each model system. In addition, heterogeneity among individuals in the population of cells can be expected. When using an endpoint assay, choosing a consistent time to record data can be critical to achieve reproducible results.)

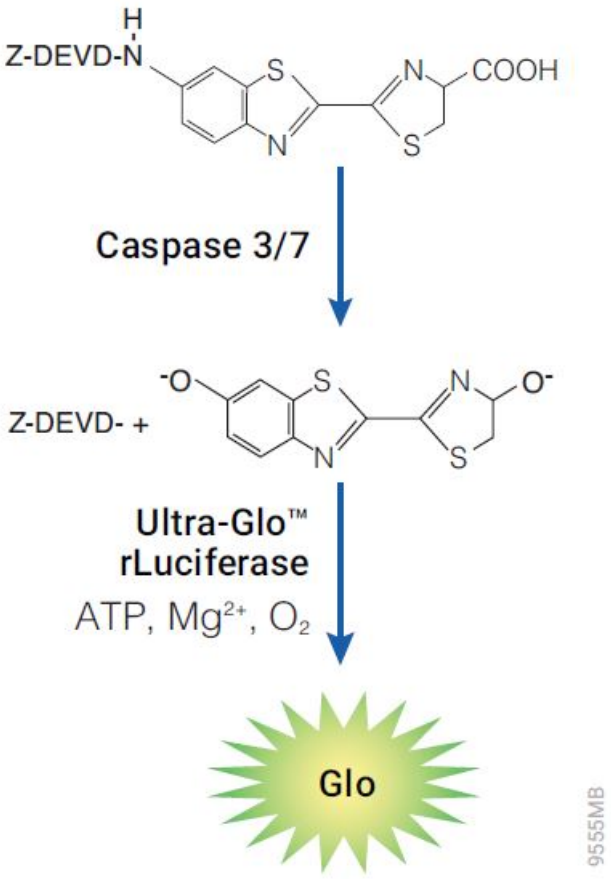


Figure 1. Schematic diagram of the Caspase-Glo 3/7 Assay technology. Following caspase cleavage of the DEVD-proluciferin substrate, a substrate for luciferase (aminoluciferin) is released and in the presence of luciferase, ATP, O_2 and Mg^{2+}, results in the luciferase reaction and the production of light.

Reprinted with permission from Promega Corporation.

7. Prepare the assay reagent by addition of the Buffer to the lyophilized substrate and allow the reagent to equilibrate to room temperature prior to use. Follow detailed instructions provided in the vendor Technical Bulletin. The reconstituted caspase-3/7 reagent requires storage at 4°C to maintain activity. The reagent can be stored at 4°C for up to 3 days with no loss of activity.
8. Remove assay plates containing cells from the incubator and allow plates to equilibrate to room temperature to ensure a consistent temperature among all assay wells. (**Note**: Most luminescent assays are designed to rely on the rate of the luciferase enzyme to produce photons of light and that enzymatic rate is dependent on temperature.)
9. Add a volume of assay reagent equal to the volume of medium in each assay well.
10. Mix the contents of all wells using a plate shaker at 300–500 rpm for 30 seconds. (**Note**: An appropriate plate shaker designed to mix the contents of the wells is necessary. Plate shakers may not be effective at mixing the contents of high density 1536-well plates.)
11. Incubate the plate at room temperature protected from direct light for 30 minutes to 3 hours. (**Note**: The optimal incubation period should be determined empirically and be consistent each time the assay is performed. If the room temperature fluctuates, use a constant-temperature incubator.) (**Note:** Cell culture models of 3D spheroids may require longer incubation in the presence of the detergent-containing assay reagent to completely lyse all the cells.)

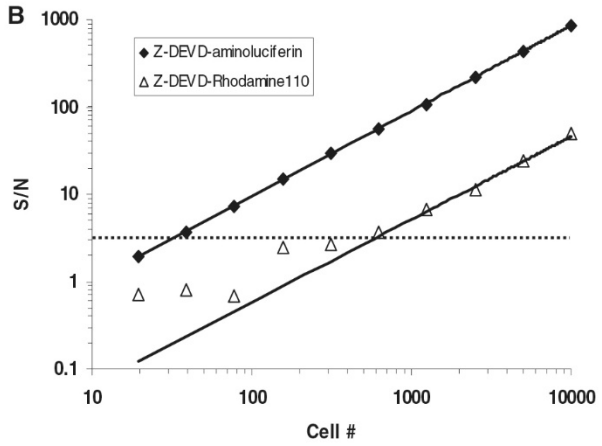


Figure 2. A comparison between bioluminescent and fluorescent caspase assays. The bioluminescent and fluorescent assays were run simultaneously using the same anti-Fas treated Jurkat cells serially diluted in 96-well plates. After addition of the appropriate substrate reagents, readings were taken at 1 h. Results were plotted as S/N. Background RLUs or RFLUs were determined from wells containing culture medium without cells. The limit of detection is defined as the number of cells giving an S/N ratio ≥3 (dotted line). For the fluorescent results, only the points above the limit of detection were used to determine the linear trend because values below the limit of detection deviate significantly from the linear trend.

Reprinted with permission from O'Brian et al., (6) Journal of Biomolecular Screening, Sage Publishing.

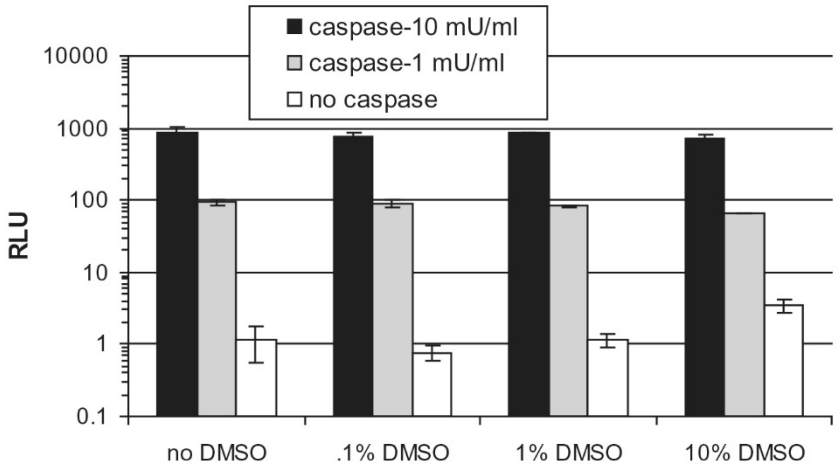


Figure 3. DMSO tolerance of the luminescent caspase assay. DMSO was tested at 0.1%, 1%, and 10% with 2 concentrations of caspase-3 (10mU/mL and 1 mU/mL) for its effects on the luminescent signal. 10 mU of caspase-3 = 1 ng.

Reprinted with permission from O'Brian et al., (6) Journal of Biomolecular Screening, Sage Publishing.

12. Measure the luminescence of each sample in a plate-reading luminometer as directed by the luminometer manufacturer. It is recommended to follow the basic guidelines for reporting nonclinical data as described in Dahlin et al., 2019 (10).

The luminescent caspase-3/7 assay also has been demonstrated to be suitable for use with 3D culture models. Figure 4 shows data from measurement of caspase-3/7 activity from HCT116 cell 3D microtissues formed using the hanging drop method, then treated with Panobinostat for various times up to 3 days. Note that the caspase-3/7 activity after 72 hours incubation is lower than the values at 48 hours. That is consistent with cells

undergoing apoptosis at an earlier time followed by subsequent loss of caspase-3/7 activity when cells undergo secondary necrosis and release cytoplasmic contents into the culture medium. These time course data highlight the importance of understanding the kinetics of the onset of apoptosis and empirically determining the length of compound treatment prior to using lytic endpoint assays. The use of a kinetic real-time assay approach (described later in this chapter) is helpful for efficiently establishing optimal test compound exposure times prior to implementing a lytic endpoint assay.

Figure 5 shows example results from screening 640 compounds from the LOPAC library to detect inhibitors of the luminogenic caspase-3/7 assay in the presence of 1mU recombinant caspase-3. The data demonstrate adequate performance of the luminescent assay approach for HTS. The Z' factors for controls are: no caspase (Z' = 0.72), 1mU caspase + Z-VAD-FMK inhibitor (Z' = 0.54) and 1mU caspase + Ac-DEVD-CHO inhibitor (Z' = 0.52). The dotted line represents two standard deviations below the mean of all the LOPAC compounds tested. The open triangles that have been circled represent 6 hits below the dotted line in this scenario.

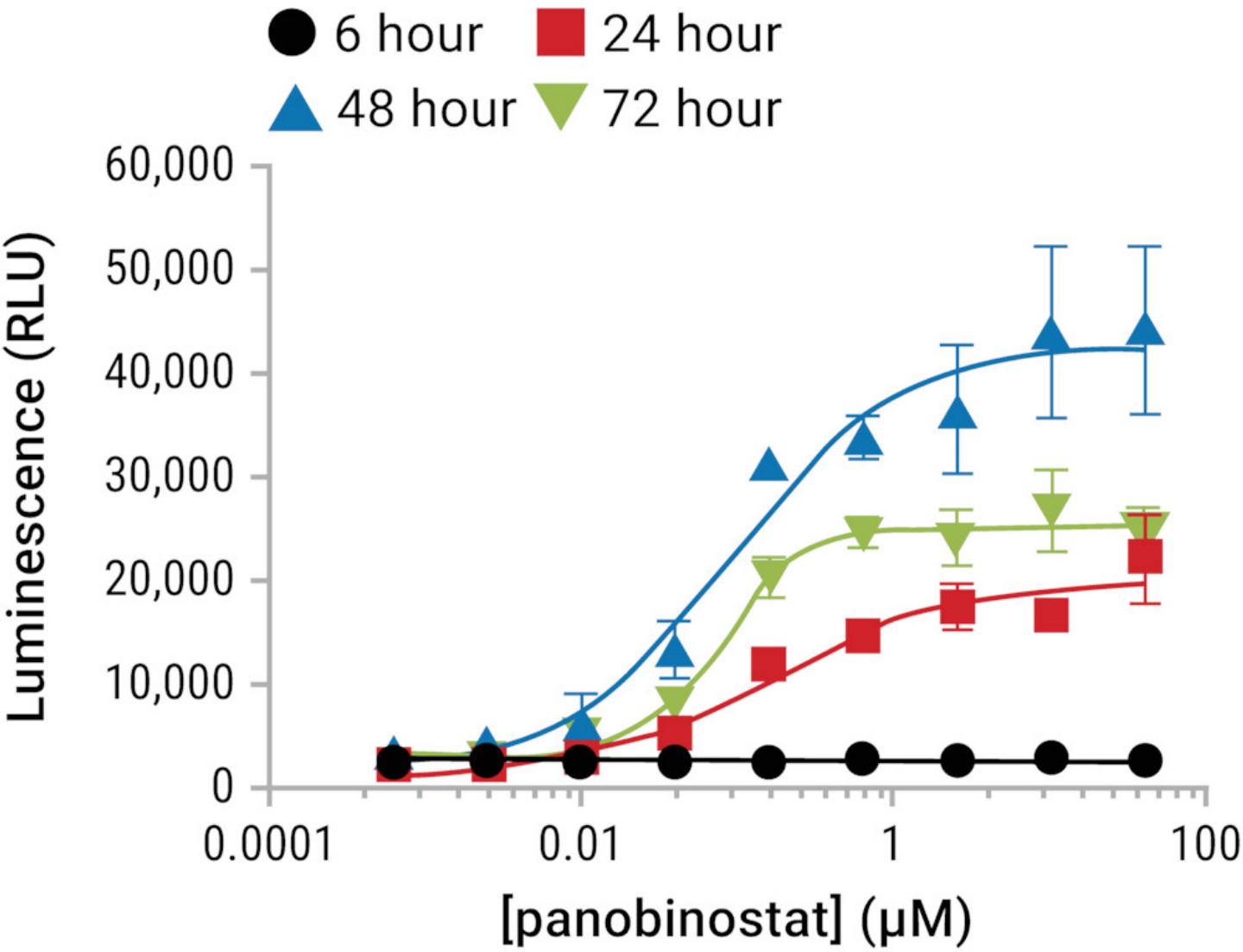


Figure 4. Caspase-3/7 activity resulting from treatment of 3D microtissues with panobinostat in a time course experiment. HCT116 cell microtissues were created using the InSphero GravityPLUS Hanging Drop System, transferred to Gravity Trap plates, then treated with panobinostat for up to 72 hours. At indicated time points, samples were transferred to solid white Corning 96 well plates (Cat. No. 3917), Caspase-Glo 3/7 Reagent was added to the wells and shaken for 30 minutes prior to recording luminescence. The values represent the mean ± SD from 3 technical replicates.

Reprinted with permission from Promega Corporation.

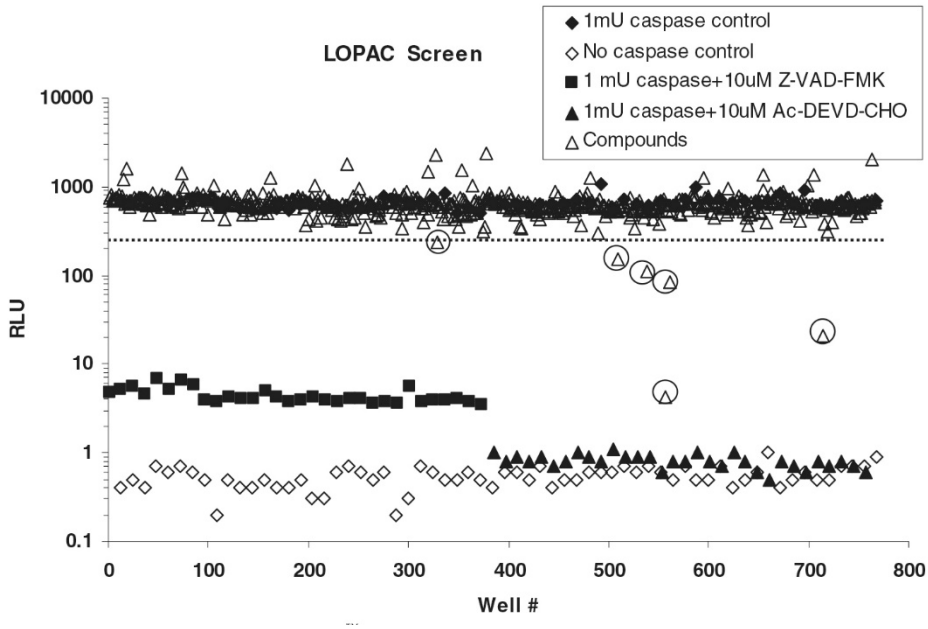


Figure 5. Screen for caspase-3/7 inhibitors using the LOPAC collection. The luminescent caspase assay was tested for compound interference using 640 compounds. The compounds were tested at a final concentration of 10 µM in 1% DMSO. The controls for the screen were caspase (1 mU/well or 1 ng/mL), no caspase, and caspase +Z-VAD-FMK (10 µM) or caspase +Ac-DEVD-CHO (10 µM). Hits were defined as compounds that gave RLU values 2 standard deviations or more below the mean of all samples (dotted line). Circles denote the 6 hits detected in this screen.

Reprinted with permission from O'Brian et al., (6) Journal of Biomolecular Screening, Sage Publishing.

Table 1. Example compounds frequently used as positive controls to induce apoptosis

Positive Control Compound	Mode of Action	Recommended Concentration
Panobinostat	HDAC inhibitor	10µM
Staurosporine	Kinase inhibitor	20µM
Bortezomib	Proteasome inhibitor	10µM
Doxorubicin	DNA intercalator/damager	10µM
Camptothecin	Topoisomerase inhibitor	10µM
Paclitaxel	Microtubule poison	10µM

Detection of PS Exposure as a Marker of Apoptosis

One of the signaling events facilitated by caspases is the activation of lipid scramblases that result in PS exposure on the outer leaflet of the cell membrane. That event is involved with producing the "eat me signal" and recognition of apoptotic cells by phagocytes, ultimately resulting in engulfment and destruction of the apoptotic cells *in vivo*. In contrast, all cells that undergo apoptosis *in vitro* eventually undergo secondary necrosis exhibiting a loss of membrane integrity which must be considered when seeking to selectively measure apoptosis rather than general necrotic cell death.

Measurement of PS exposure on the cell surface prior to loss of membrane integrity by secondary necrosis is a frequently reported method used to assay for detection of apoptosis (11). The protein annexin V is known to bind to PS in the presence of calcium. Fluorescently-labeled annexin V has been used as a tool for detection of apoptosis for over 20 years, primarily using flow cytometry for detection (12). However, the protocol steps for

sample preparation and washing away the unbound fluorescent annexin V as well as comparatively low-throughput of flow cytometry have limited the widespread adoption of annexin V binding for HTS applications.

When cells undergo secondary necrosis and lose membrane integrity, annexin V can enter the cell and bind to PS remaining on membrane components in the cytoplasmic compartment. To distinguish annexin V binding to apoptotic cells versus necrotic cells, a vital DNA binding dye can be used as a control to stain the cells that have lost membrane integrity. The vital dye does not penetrate viable cells or cells in the early stages of apoptosis when membrane integrity remains intact, thus only necrotic cells are stained. Historically, a combination of annexin V-FITC and propidium iodide (which are available from several vendors) have been used as reagents to detect apoptosis and secondary necrosis using flow cytometry.

A homogeneous HTS-compatible assay protocol has recently been developed for detecting PS exposure and secondary necrosis in real-time using a standard multimode plate reader (13). Instead of using annexin conjugated to a fluorophore, the reagent contains two recombinant annexin V fusion proteins containing different subunits of a luciferase (annexin V-LgBiT and annexin V-SmBiT) that was engineered from a marine shrimp (14). Addition of the two annexin V fusion proteins and a luciferase substrate to samples of viable cells does not produce a signal above background (Figure 6). However, when cells undergo apoptosis and expose PS on the outer leaflet of the cell membrane, the two annexin V fusion proteins (containing either a large or small subunit of the NanoBiT luciferase) bind in close proximity, the luciferase domains can interact to reconstitute an active enzyme and produce photons of light. When cells proceed to secondary necrosis, the DNA binding dye (labeled as Necrosis Detection Reagent in Figure 6) can enter the cell and stain the nucleus green.

The kinetic real-time aspect of the assay comes from the fact that the Detection Reagent can be added to the cells once at time zero and incubated up to 48 hours with periodic recording of luminescence and fluorescence to monitor the onset of apoptosis and secondary necrosis, respectively.

Figure 7 illustrates that different cell types and different apoptosis-inducing treatments result in different kinetics for the onset of PS exposure (marker consistent with the process of apoptosis) and loss of membrane integrity (necrosis). The detection reagent was added once at time zero and the assay plate incubated in a multi-mode plate reader equipped with an environmental chamber programmed to record luminescence and fluorescence every hour for two days. The aqua-colored circles represent luminescence indicating PS exposure. The green squares represent fluorescence resulting from loss of membrane integrity (necrosis) and binding of the vital dye to DNA.

Figure 7 Panel A shows a relatively rapid onset of apoptosis (~1.5 hours) in TRAIL-treated DLD-1 cells whereas substantial PS exposure in HepG2 cells treated with paclitaxel does not occur until ~16 hours (Panel C). The gradual increase in signals is the result of heterogeneity among individuals in the population of cells in the sample wells. Figure 7 Panel D illustrates the effects of digitonin which causes loss of membrane integrity without initiating a preceding apoptotic process. The changes in luminescence and fluorescence from the same sample well provide a real-time indication of markers consistent with apoptosis and secondary necrosis. This contrasts with the endpoint caspase-3/7 assay described above that lysis the cells upon addition of assay reagent and restricts multiplexing options.

Figure 8 illustrates that up to 1% DMSO does not substantially change the RLU values or calculated EC_{50} values from the luminescent annexin V assay applied to cells treated with various concentrations of recombinant TRAIL.

Figure 9 illustrates similar kinetics for the appearance of two orthogonal markers of apoptosis, PS exposure and caspace-3/7 activity. Data showing the increase in PS exposure were recorded repeatedly from a single plate using the kinetic real-time assay approach (Panel A). The appearance of caspase-3/7 activity was measured from a set of parallel plates using the luminescent lytic endpoint assay (Panel B).

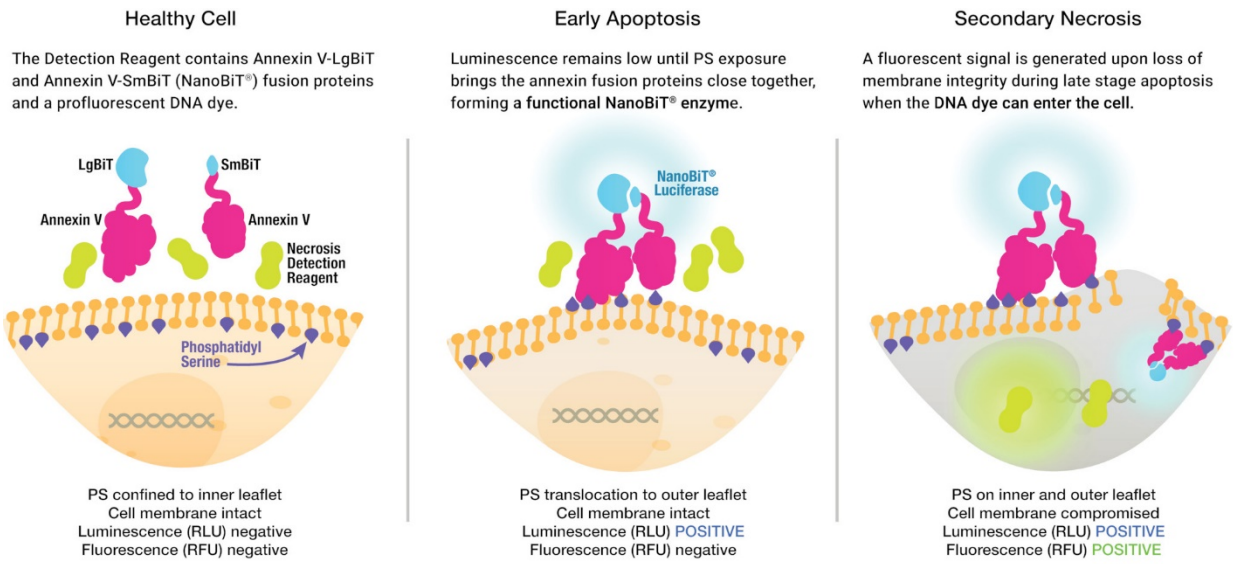


Figure 6. A diagram depicting no luminescent or fluorescent signal from a normal viable cell (left), progressing to an apoptotic cell with an intact cell membrane generating a luminescent signal, but no fluorescent signal (center) and a cell with secondary necrosis generating both luminescent and fluorescent signals (right).

Reprinted with permission from Promega Corporation.

Protocol to Detect PS Exposure as a Marker of Apoptosis

Detailed directions for use of the RealTime-Glo Annexin V Apoptosis and Necrosis Assay are described in Promega Technical Manual #507 (https://www.promega.com/Resources/Protocols/Technical%20Manuals/500/RealTime%20Glo%20Annexin%20V%20Apoptosis%20and%20Necrosis%20Assay%20Protocol/?fq=realtime%20glo%20annexin%20v). It is recommended to prepare the 2X Detection Reagent immediately before use; however, the 2X Detection Reagent can be stored at room temperature, 4°C or 37°C for up to 18 hours with no detectable loss in functionality.

Choose opaque walled white plates for best results when using luminescent assays. Clear bottom plates are optional for viewing cells with a microscope during the experiment. The assay detection sensitivity is adequate for using a 96 or 384 well plate format. The recommended volumes mentioned below are for 384 well plates.

1. Harvest cells (suspension or anchorage-dependent) and resuspend the cell pellet to 200,000 cells/ml in prewarmed complete medium.
2. Add 12.5µl of a 200,000 cells/ml suspension to appropriate wells of 384-well plates (2500 cells/well) or 12.5µl of complete cell culture medium to a set of wells for no cells, no-compound controls. **Note**: If cells are attachment-dependent, return the assay plate (with the lid on) to a humidified tissue culture incubator to allow cells to attach and recover for a minimum of 3–4 hours. Alternatively, cells may be plated the night before dosing to allow the cells to attach overnight. This equilibration/attachment period is unnecessary for cells that grow in suspension.
3. Add 12.5µl of appropriate dilutions of test compounds, positive control compounds or medium only (no cell vehicle controls) to chosen wells. **Note:** All wells should now contain 25µl.
4. Prepare 2X Detection Reagent according to vendor recommendations. The reconstituted annexin reagent is stable for up to 18 hours at ambient temperature which is sufficient for a standard 8 hour shift.
5. Add 25µl of the 2X Detection Reagent in complete medium to all wells. All wells should now contain a final assay volume of 50µl for a 384-well plate.
6. Shake the assay plate on a plate shaker for approximately 30 seconds at 500–700rpm to mix.

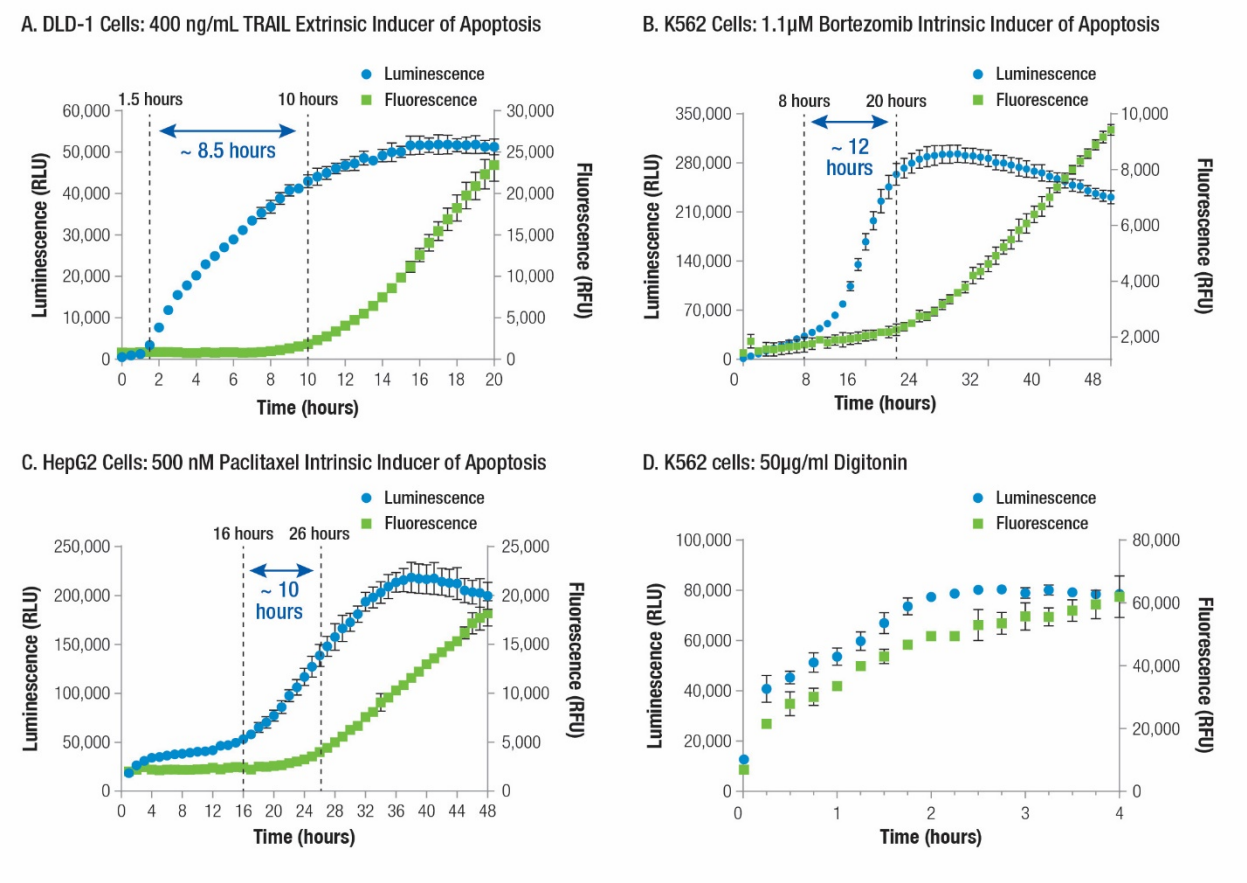


Figure 7. Sequentially repeated measures of luminescence (RLU) and fluorescence (RFU) resolve the kinetic effects of different cytotoxic stimuli and help establish mechanism of action. Panel A. DLD-1 cells treated with 400ng/ml rhTRAIL. Panel B. K562 cells treated with 1.1µM bortezomib. Panel C. HepG2 cells treated with 500nM paclitaxel. Panel D. K562 cells treated with 50µg/ml digitonin. Background-subtracted luminescence (blue circles) and fluorescence (green squares) readings are shown. For Panels A–C, there is a significant time delay between the emergence of PS:Annexin V binding and the loss of membrane integrity, results that are indicative of an apoptotic phenotype leading to secondary necrosis. In Panel D, luminescence and fluorescence signals emerge concurrently, suggesting a non-apoptotic phenotype. Data represent the mean of 4 readings for each replicate ± SD.

Reprinted with permission from Promega Corporation.

7. Incubate plate using standard cell culture conditions and record luminescence and fluorescence repeatedly from the same samples at desired times.

Data Calculation

Subtract the average luminescence signal from the no-cell, no-compound background controls (a measure of intrinsic reagent and instrument luminescence) from all sample luminescence values to obtain net RLU. **Note:** Although it will depend on the cell culture model system, if cultures are handled properly, there should be less than 5% apoptotic cells in vehicle treated controls.

Subtract the average fluorescence signal from the no-cell, no-compound background controls (a measure of intrinsic reagent and instrument fluorescence) from all sample fluorescence values to obtain net relative fluorescence units.

Graph net luminescence (resulting from PS:Annexin V binding) and net fluorescence (resulting from changes in membrane integrity) versus compound concentration (include the untreated control in the analysis when possible) for each time point using commercially available curve-fit software (e.g. GraphPad Prism, SigmaPlot,

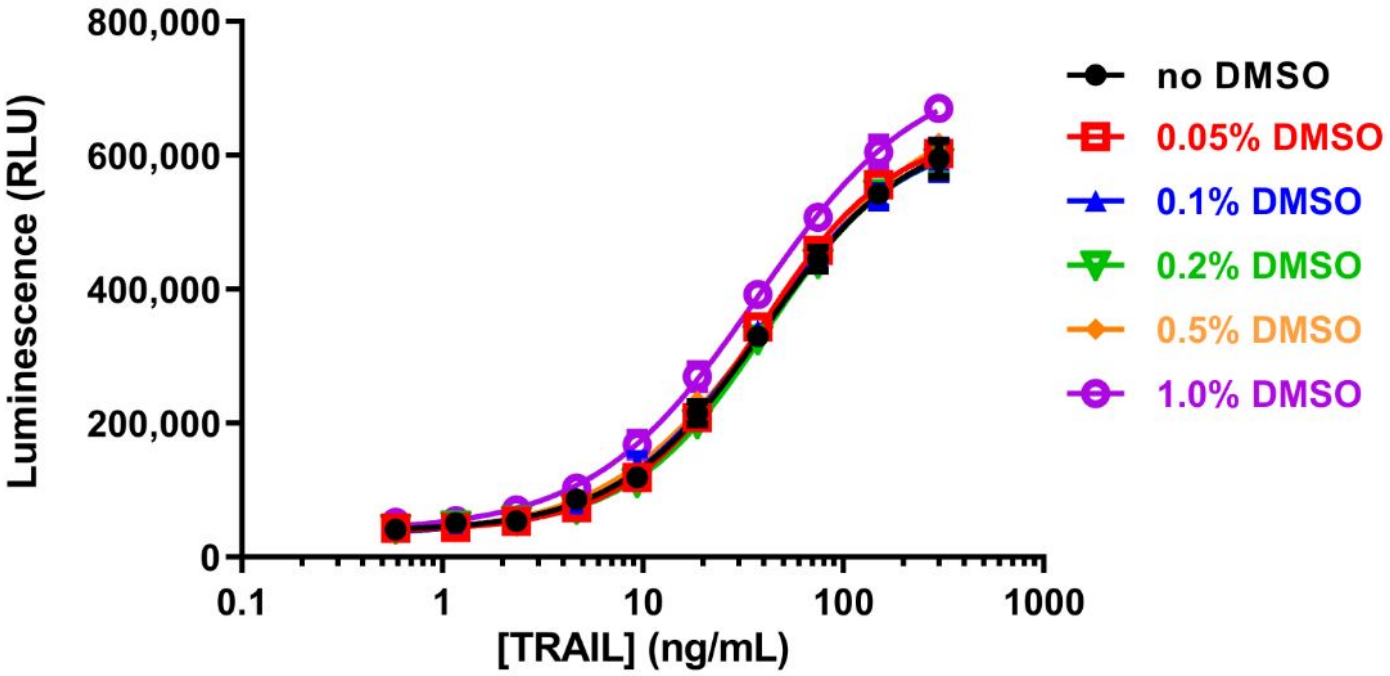


Figure 8. Various concentrations of TRAIL were added to 10,000 DLD-1 cells/well cultured in McCoy's 5A medium + 10% FBS. Samples were incubated for 6.5 hours in the presence of the listed concentrations of DMSO. The RealTime-Glo Annexin V Apoptosis and Necrosis Assay reagent was added and luminescence recorded. The plotted values represent the mean ± SD of four technical replicates.

etc.). It is instructive to graph net luminescence and net fluorescence signals versus time at a specific compound concentration.

The luminogenic annexin V-PS binding assay can be multiplexed with the luminogenic caspase-3/7 assay to measure two different orthogonal markers of apoptosis in the same sample of cells. This multiplex is possible because of the different assay chemistries of the luciferases from different species. For this multiplex to be successful, data from the real-time annexin V-PS assay must be recorded first. The caspase-3/7 assay detection reagent will disrupt the luminescent signal from the shrimp-derived NanoBiT luciferase in the annexin V-PS binding assay and provide the necessary substrate to enable generation of the luminescent signal from the firefly-derived luciferase in the caspase-3/7 assay. Figure 10 shows an example of data from multiplexing the two assays. The results for the annexin V assay to detect PS exposure on the cell membrane and the caspase-3/7 assay to detect executioner protease activity are in agreement.

Any change to the contents of the culture medium (such as the presence of reagents for multiplexing) or handling of the sample needs to be considered and the assay protocol validated for any change. For example, if the temperature of the plate is altered by recording values of the first assay, it may change the values of a secondary luciferase assay (because luminescence is reporting the rate of the luciferase enzyme). The statistical advantage of measuring two different signals from the same sample instead of creating and assaying a parallel sample also needs to be considered.

Figure 11 provides evidence that the presence of RealTime-Glo Annexin V Apoptosis and Necrosis Assay Reagent does not have a substantial effect on the signal or performance of the luminescent caspase-3/7 assay. The signal from the luminescent caspase-3/7 assay is similar in samples with or without the presence of the RealTime-Glo Annexin V Apoptosis and Necrosis Assay Reagent.

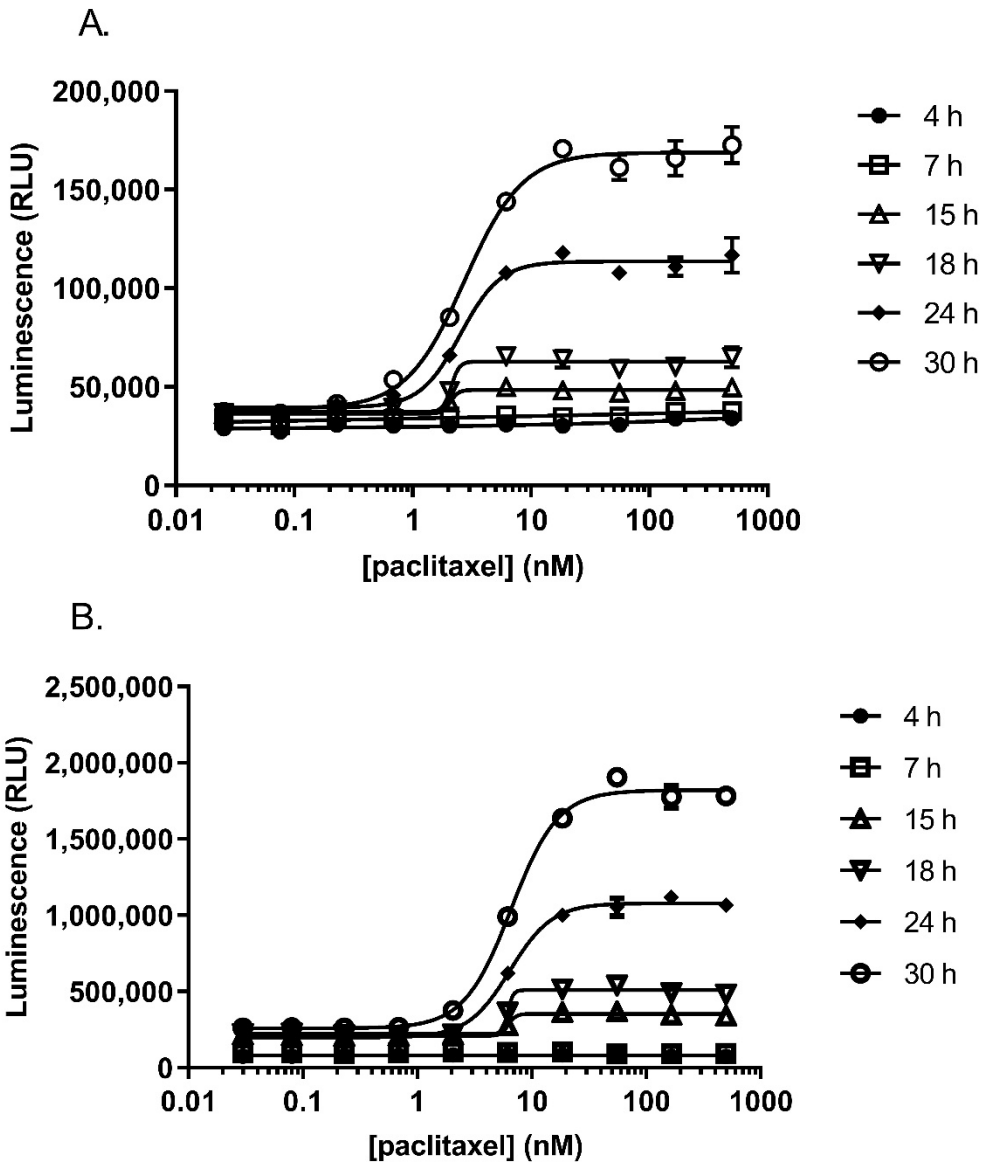


Figure 9. A kinetic comparison between PS exposure (Panel A) and caspase activation (Panel B) after paclitaxel treatment of HepG2 cells. Annexin-binding luminescence was collected by sequential measurements of the same plate over a 30 hour time course (A). Caspase activity data were collected from parallel plates using lytic endpoints (Panel B). The values represent the mean ± SD of four technical replicates for each dose.

This figure was modified from Kupcho et al., (13) A real-time, bioluminescent annexin V assay for the assessment of apoptosis. Apoptosis (2019) 24:184–197 under the terms of the Creative Commons Attribution 4.0 International License (http://creativecommons.org/licenses/by/4.0/), which permits unrestricted use, distribution, and reproduction in any medium.

Figure 12 shows an example of multiplexing a fluorescent cell viability assay with the luminescent annexin v assay. The fluorescent cell viability assay uses a cell permeable Gly-Phe-AFC protease substrate to measure an aminopeptidase activity selectively present in viable cells. Details of the fluorogenic assay are described in the AGM chapter on cell viability assays (15). (https://www.ncbi.nlm.nih.gov/books/NBK144065/pdf/Bookshelf_NBK144065.pdf). The signal magnitude and potency values from the multiplex and control assays are similar suggesting compatibility of the two reagents in a multiplex format.

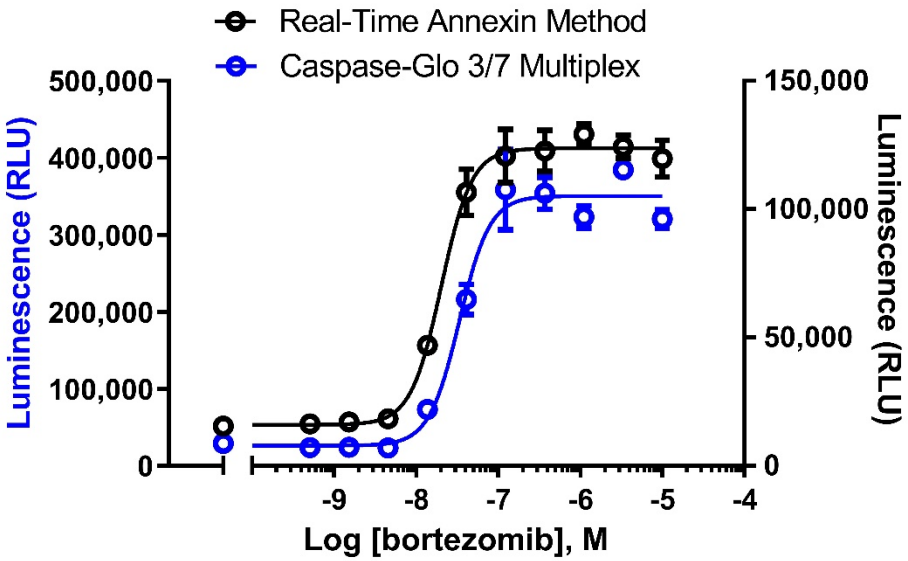


Figure 10. Sequential multiplex of orthogonal assays to measure different markers to confirm the occurrence of apoptosis. K562 cells (10,000/well in 100µl RPMI1640 + 10% FBS) were seeded in assay plates and treated with various concentrations of bortezomib. The RealTime-Glo Annexin V Apoptosis and Necrosis Assay reagent (100µl) was added at time zero and luminescence recorded at 18 hours (black circles). The Caspase-Glo 3/7 Assay reagent was added, the samples were mixed and incubated at room temperature for 30 minutes and luminescence recorded (blue circles). The values represent the mean ± SD of four technical replicates.

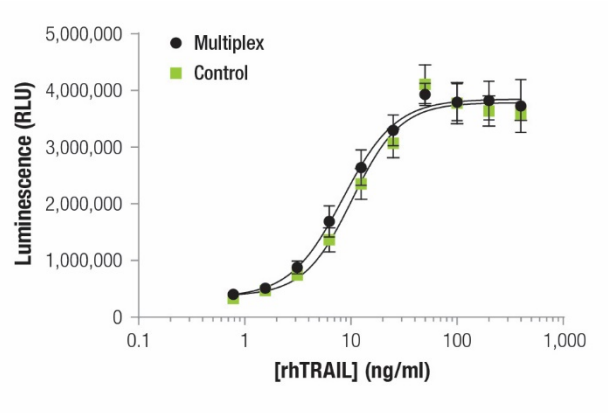


Figure 11. The effect of the RealTime-Glo Annexin V Apoptosis and Necrosis Assay reagent on subsequent multiplex using the Caspase-Glo 3/7 Assay. DLD-1 cells were exposed to serial dilutions of rhTRAIL either in the presence (black circles) or absence (green squares) of the RealTime-Glo Annexin V Apoptosis and Necrosis Assay Reagent. The plate was incubated at 37°C/5% CO_2 for 6.5 hours then the Caspase-Glo 3/7 Reagent was added to all wells and the assay performed as described above. Data represent the mean ± SD from four technical replicates. Additional details are shown in TM507.

Reprinted with permission from Promega Corporation.

Commercial Reagents

Caspase-3/7: Commercial kits with colorimetric and fluorogenic caspase-3/7 substrates containing pNA, AMC, or AFC are available from several vendors; however, they are not listed here because the detection sensitivity is generally inadequate for HTS. Commercial kits with fluorogenic caspase-3/7 substrates containing R110 also are available from several vendors (examples shown below); however, the luminogenic reagent kit is available only from Promega Corporation.

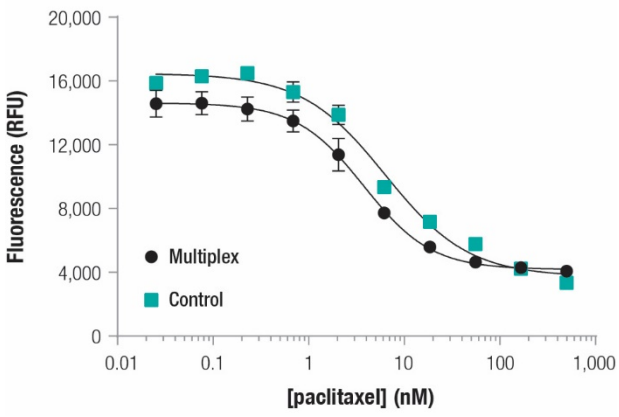


Figure 12. Example multiplex data with the RealTime-Glo Annexin V Apoptosis and Necrosis Assay and CellTiter-Fluor Cell Viability Assay. HepG2 cells were exposed to serial dilutions of paclitaxel in the presence (black circles) or absence (green squares) of the RealTime-Glo Annexin V Apoptosis and Necrosis Assay Reagent. The plate was incubated at 37°C/5% CO_2 for 48-hours prior to adding the CellTiter-Fluor Reagent using the multiplex format and recording fluorescence indicating viable cell number. Data represent the mean ± SD from four technical replicates.

Reprinted with permission from Promega Corporation.

Fluorogenic

- EnzChek Caspase-3 Assay Kit, Thermo Fisher Catalog Number E13184
- Apo-ONE Homogeneous Caspase-3/7 Assay; Promega Corp. Catalog Number G7791
- EarlyTox Caspase-3/7 R110 Assay Kit: Molecular Devices Catalog Number R8347
- NucView 488 Caspase-3 Enzyme Substrate, 1 mM in DMSO. Biotium Catalog Number 10402

Luminogenic

- Caspase-Glo 3/7 Assay, Promega Corporation Cat.# G8092

Phosphatidyl Serine: Annexin V is available conjugated to several different fluorophores (at least seven from Thermo Fisher); however, they are designed for microscopic imaging and flow cytometry and are not recommended for fluorescent plate readers. Many kits also contain a vital dye such as propidium iodide as a control to detect secondary necrosis as described above.

Fluorescent

- Annexin V Alexa Fluor 488 Conjugate, Thermo Fisher Catalog Number A13201
- Annexin V-FITC Apoptosis Detection Kit, Millipore Sigma Catalog Number APOAF-50TST
- Cell Meter APC-Annexin V Binding Apoptosis Assay Kit, ATT Bioquest Catalog Number 22837
- FITC Annexin V Apoptosis Detection Kit with PI, Biolegend Catalog Number 640914
- Annexin V-FITC Apoptosis Staining / Detection Kit, Abcam Catalog Number ab14085

Luminogenic

- RealTime-Glo Annexin V Apoptosis and Necrosis Assay, Promega Corp. Catalog Number JA1012

Conclusion

Although the assays described in this chapter may be “fit-for-purpose” and identify “hits” by detecting an apoptotic marker, we need to keep in mind that no assays are perfect. Confirming the occurrence of apoptosis by using more than one method has historically been a requirement for peer reviewed journals. There are many different marker assays that can serve to confirm the presence of apoptosis. However, care should be taken to not

choose a confirmatory marker that is selective for either intrinsic (e.g. mitochondrial polarization changes and caspase-9 release) or extrinsic pathways (e.g. caspase-8 association with a member of the death receptor family) because diverse members of small molecule libraries may be selective for only one pathway. Observing gross cell morphology or using antibodies to detect neo-epitopes resulting from caspase cleavage of target proteins are options to confirm the occurrence of apoptosis. Detecting cleaved PARP or cleaved caspase can be accomplished using Western blotting or immunocytochemistry approaches (4); however, those assays are labor intensive for large numbers of samples. Assays such as TUNEL or ELISA to detect DNA fragmentation are options to confirm apoptosis; however, they also require many procedural steps and may not be practical for follow-up of 100s of hits. A logical approach to confirm the results of a high-throughput screen for apoptosis modulators is to repeat the original assay in combination with a multiplexed method detecting an orthogonal marker. An example of multiplexing two homogeneous orthogonal assays compatible with HTS is shown in Figure 10.

Apoptosis is a process of programmed cell death that is of interest to the drug development community because members of the signaling cascade leading to cell suicide are potential targets for development of therapeutics to treat degenerative diseases or cancer. Although there are a variety of methods to detect markers indicative of apoptosis, not all methods are easily adaptable for HTS. Easy homogeneous methods to detect markers of apoptosis in a high throughput format are valuable for initial phenotypic screening. The apoptosis marker assays most frequently reported in the literature are caspase-3/7 activity and PS exposure on the surface of cells detected by annexin V binding. Both of those methods do not require prior engineering of cells to express an artificial reporter or sensor molecule. Measuring caspase-3/7 activity in an HTS setting can be done using homogeneous fluorogenic or luminogenic methods, with the latter providing much greater sensitivity enabling miniaturization. Measuring PS exposure historically has relied on flow cytometry; however, recently a homogeneous procedure based on enzyme complementation has been developed that enables detecting the onset of apoptosis in real-time using a plate reading luminometer. The real-time method enables monitoring the progress of apoptosis in heterogeneous populations of cells and can provide useful information for development of assays that measure orthogonal endpoints. This chapter provides a brief description of those two homogeneous HTS assay methods and includes references and links to detailed Technical Manuals describing assay protocols.

References

1. Kromer G, Galluzzi L, Vandenabeele P, Abrams J, Alnemri ES, Baehrecke EH, Blagosklonny MV, El-Deiry WS, Golstein P, Green DR, Hengartner M, Knight RA, Kumar S, Lipton SA, Malorni W. Nun˜ez GPeter ME, Tschopp J, Yuan J, Piacentini M, Zhivotovsky B, Melino G. Classification of cell death: recommendations of the Nomenclature Committee on Cell Death 2009. Cell Death and Differentiation. 2009;16:3–11.
2. Lazebnik YA, Kaugmann SH, Desnoyers S, Poirier GG, Earnshaw WC. Cleavage of poly (ADP-ribose) polymerase by a proteinase with properties like ICE. Nature. 1994;371(6495):346–7.
3. Duriez PJ, Shah GM. Cleavage of poly (ADP-ribose) polymerase: a sensitive parameter to study cell death. Biochem Cell Biol. 1997;75(4):337–9.
4. O'Brien MA, Moravec RA, Riss TL. Poly (ADP-ribose) polymerase cleavage monitored in situ in apoptotic cells. BioTechniques. 2001;30(4):886–91.
5. Thornberry NA, Rano TA, Peterson EP, Rasperi DM, Timkey T, Garcia-Calvo M, Houtzageri VM, Nordstromi PA, Royi S, Vaillancourti JP, Chapman KT, Nicholson DW. 1997; A combinatorial approach defines specificities of members of the caspase family and granzyme B. Functional relationships established for key mediators of apoptosis. J. Biol. Chem. 1997;272(29):17907–11.
6. O'Brien MA, Daily WJ, Hesselberth E, Moravec RA, Scurria MA, Klaubert DH, Bulleit RF, Wood KV. Homogeneous, bioluminescent protease assays: Caspase-3 as a model. J Biomol Screen. 2005;10(2):137–48.
7. Simeonov A, Davis MI. Interference with Fluorescence and Absorbance. In: Markossian S, Sittampalam GS, Grossman A, et al., editors. Assay Guidance Manual [Internet]. Bethesda (MD): Eli Lilly & Company and the National Center for Advancing Translational Sciences; 2004-.

8. Auld DS, Inglese J. Interferences with Luciferase Reporter Enzymes. In: Markossian S, Sittampalam GS, Grossman A, et al., editors. Assay Guidance Manual [Internet]. Bethesda (MD): Eli Lilly & Company and the National Center for Advancing Translational Sciences; 2004.
9. Eskes C, Boström A-C, Bowe G, Coecke S, Hartung T, Hendriks G, Pamies D, Piton A, Rovida C. Good cell culture practices & in vitro toxicology. Toxicology in Vitro. 2017;45:272–7.
10. Dahlin JL, Sittampalam GS, Coussens NP, et al. Basic Guidelines for Reporting Non-Clinical Data. 2019 Oct 1 In: Markossian S, Sittampalam GS, Grossman A, et al., editors. Assay Guidance Manual [Internet]. Bethesda (MD): Eli Lilly & Company and the National Center for Advancing Translational Sciences; 2004.
11. Martin SJ, Reutelingsperger CP, McGahon AJ, Rader JA, van Schie RC, LaFace DM, Green DR. Early redistribution of plasma membrane phosphatidylserine is a general feature of apoptosis regardless of the initiating stimulus: Inhibition by overexpression of Bcl-2 and Abl. J. Exp. Med. 1995;182:1545–56.
12. Vermes I, Haanen C, Steffens-Nakken H, Reutelingsperger C. A novel assay for apoptosis. Flow cytometric detection of phosphatidylserine expression on early apoptotic cells using fluorescein labelled Annexin V. J Immunol Methods. 1995;184(1):39–51.
13. Kupcho K, Shultz J, Hurst R, Hartnett J, Zhou W, Machleidt T, Grailer J, Worzella T, Riss T, Lazar D. Cali J, Niles A. A real-time, bioluminescent annexin V assay for the assessment of apoptosis. Apoptosis. 2019;24:184–197. doi: 10.1007/s10495-018-1502-7.
14. Hall MP, Unch J, Binkowski BF, Valley MP, Butler BL, Wood MG, Otto P, Zimmerman K, Vidugiris G, Machleidt T, Robers MB, Benink HA, Eggers CY, Slater MR, Mesienheimer PL, Klaubert DH, Fan F, Encell LP, Wood KV. Engineered luciferase reporter from a deep sea shrimp utilizing a novel imidazopyrazinone substrate. ACS Chem Biol. 2012;7:1848–57.
15. Riss TL, Moravec RA, Niles AL, et al. Cell Viability Assays. 2013 May 1 [Updated 2016 Jul 1]. In: Markossian S, Sittampalam GS, Grossman A, et al., editors. Assay Guidance Manual [Internet]. Bethesda (MD): Eli Lilly & Company and the National Center for Advancing Translational Sciences; 2004.

Pluripotent Stem Cell Culture Scale-Out

Debra L. Johnson,[1] Robert Scott,[1] and Rhonda Newman[1]

Created: June 1, 2021.

Abstract

Culture systems for human pluripotent stem cell (hPSC) expansion help enable the generation of a nearly unlimited pool of cells for use in downstream differentiation, disease modeling, drug discovery, and therapeutic applications. Monolayer culture is desirable in many circumstances due to the long history of validated assays and differentiation protocols. General culture protocols typically focus on methods for small plate formats (e.g., 6-well plate) yielding approximately 20 million hPSCs per plate. However, for some high-throughput screening and therapeutic applications, hPSCs expanded to a scale exceeding 1 billion cells may be required. This chapter provides a method for scale-out of hPSCs in monolayer cell culture conditions using commercially available cell culture media systems in conjunction with large surface area vessels. This scale-out procedure uses cell therapy grade reagents, which make application of cells and cell products to patients possible. It also provides insight into how to monitor cell health, assess pluripotency in normal stem cell cultures, and evaluates the capability to cryopreserve high cell densities.

Author Affiliation: 1 Thermo Fisher Scientific.

Overview and Flowchart of Assay Guidelines

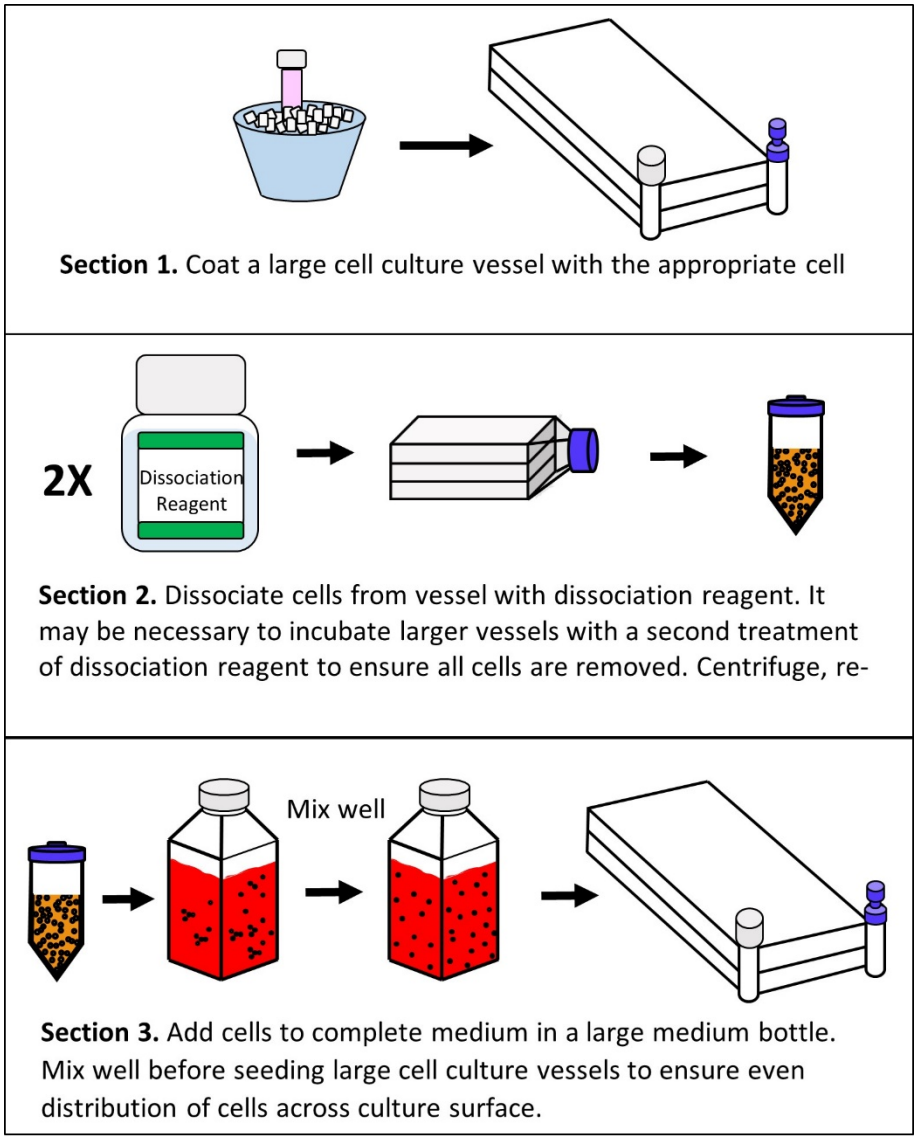


Figure 1. Workflow Diagram for Seeding of EasyFill Cell Factory from Triple Flask.

Introduction

Expanding large quantities of human pluripotent stem cells (hPSCs), while avoiding aberrant differentiation is critical for consistency in downstream applications. Most hPSC studies and differentiation protocols have been conducted and developed in monolayer cell culture systems, which limit the amount of cells that can be reasonably produced due mainly to space constraints. Development of large-scale tissue culture plastics and feeder-independent culture media have greatly improved our ability to expand hPSCs for large-scale applications. For expansion of hPSCs in a clinically compliant manner, media systems such as animal origin-free Gibco Cell Therapy Systems (CTS) Essential 8 provide Good Manufacturing Practices (GMP) grade materials and proper documentation for using cells and their products for application in patients. For applications that do not require cell therapy grade materials, the use of broadly versatile Gibco StemFlex Medium can be used.

Monolayer cell culture provides several advantages for stem cell assays, including uniform treatment with small molecules and growth factors, which facilitate directed differentiation to the desired cell type for downstream

application (1). Monolayer cell culture also enables simplistic, more complete medium exchanges and eliminates shear stress from agitation caused by growing cells in suspension (2). Furthermore, monolayer cell culture provides investigators with the ability to easily assess cell health via observation of normal stem cell morphology, which is represented by high nuclear-to-cytoplasmic ratios and condensation of colonies. Automated monolayer culture has also recently been developed for stem cells, leading to reduced labor costs and more reproducible cell culture (3).

While monolayer scale-out provides the user with many advantages, it is important that the user also consider scale-up (i.e.,suspension culture) with various size spinner flasks and bioreactors. The details of scale-up in suspension will not be considered in this chapter, but further information can be found at the following references: 4, 5, 6 and 7. Users should choose the most appropriate scale-out or scale-up method based on their desired assay type, endpoints to be measured, and available equipment in the laboratory.

In this chapter, we introduce strategies and a protocol for successful scale-out of human induced pluripotent stem cells (hiPSCs) in a monolayer culture system using Cell Therapy Systems (CTS) grade reagents. hiPSCs were cultured in the Nunc TripleFlask and the Nunc Easy Fill Cell Factory allowing for growth of large quantities of cells. We examined the use CTS Essential 8 Medium with recombinant human Vitronectin-N coated culture vessels. Using a defined, animal-origin-free medium and coating matrix like the combination presented here is preferred for clinical manufacturing purposes. We also confirmed this protocol using the animal derived Geltrex Basement Membrane Matrix and Gibco StemFlex Medium. After expansion in both systems, cells were assessed for maintenance of normal hPSC properties, including morphology with high nuclear to cytoplasmic ratio, presence of extracellular and intracellular markers of pluripotency, as well as normal karyotype. Cells scaled-out using this protocol maintain normal characteristics of hPSCs required for consistency in downstream applications.

Stem Cell Culture Considerations

How to Choose an Appropriate Culture Medium

A variety of culture media exist for expansion of human pluripotent stem cells in feeder-free conditions. Considerations for selection of the appropriate medium largely depends upon the proposed end use. For instance, if the cells expanded will be utilized in research use only (RUO) applications, then one may utilize a more robust medium that includes animal derived components (e.g., StemFlex Medium, mTeSR1, etc.). However, as research moves to more translational and clinical applications, general regulatory guidance from the US Food and Drug Administration (USFDA) indicates that cGMP manufactured, clinical grade reagents should be used whenever available as ancillary reagents to minimize downstream risk of patient exposure to adventitious agents. Thus, utilizing cGMP manufactured formulations composed of xeno-free and/or recombinant, animal origin free (AOF) components becomes critical. Cell Therapy Systems (CTS) reagents provided by Thermo Fisher Scientific provide cGMP manufactured, xeno-free and/or AOF medium formulations with full traceability and additional safety testing for components like endotoxin and mycoplasma. CTS Essential 8 Medium is an AOF version of the more classical xeno-free Essential 8, affording improved safety when used for clinical applications.

Another cell therapy grade media type is the StemFit Basic Series from Ajinomoto. We did not test this media type in this chapter, but the following references can provide more information: 8, 9 and 10.

How to Choose an Extracellular Matrix

Just as is the case for cell culture medium selection, selection of the appropriate matrix largely depends upon the proposed end use. One commonly used, undefined matrix is the solubilized form of basement membrane extract from murine Engelbreth-Holm-Swarm (EHS) tumors. This matrix is called Geltrex (from Thermo Fisher

Scientific), Matrigel or Cultrex (distributed from a range of vendors). This extract contains a multitude of extracellular matrix components, including but not limited to laminin, collagen IV, heparin sulfate proteoglycans, and entactin. Such an undefined matrix can be used in conjunction with a many types of cell culture media formulations for RUO applications (11, 12). As research moves to more translational and clinical applications, the guidance of using fully defined or recombinant matrices applies to minimize risk of patient exposure to adventitious reagents. Recombinantly expressed proteins including vitronectin or laminins in the full-length or truncated versions should be utilized. A truncated version of CTS vitronectin is optimal for such applications as it meets the criteria for use in clinical applications and it is a cost-effective solution for scale-out of cell cultures (13). However, for applications that might increase cellular stress, such as genome editing, a cell therapy grade rh-Laminin (Biolaminin 521 CTG) from BioLamina affords greater clonal cell survival but is offered at an increased cost.

Another parameter affecting potential consideration of extracellular matrix is temperature tolerance which is important in ensuring consistency in coating of vessels and thus is critical for scale-out of hPSC cultures. Geltrex, Matrigel, and Cultrex require special handing as they must remain on ice at all times to prevent premature gelling. These matrices should furthermore be diluted in pre-chilled (4^{o}C) solution. Improper handling of these matrices can result in an uneven coating on the cell culture surface, which may result in aberrant differentiation. Such handling risks occur less frequently with vitronectin and laminin-based coating solutions. It is important to follow the manufacturer's instructions for proper handling of extracellular matrices as these reagents have been validated and verified to perform under their specified conditions only.

How to Choose an Appropriate ROCK Inhibitor Cocktail

One obstacle for single cell passaging of stem cells is that they are very susceptible to cell death when dissociated from a culture surface and from other cells. To increase cell survival, Rho-associated protein kinases (ROCK) inhibitors are added to the culture medium to improve cell attachment and cell spreading (14). Passaging using non-enzymatic treatments such as EDTA or citrate does not require the inclusion of ROCK inhibitors. Also, plating cells on rh-Laminin 521 does not require a ROCK inhibitor as laminin is a very favorable substrate for cell growth. When utilizing, ROCK inhibitors, they should be included at the time of seeding to minimize apoptosis and then removed 18-24 hours post passage via simple media exchange.

There are a range of ROCK inhibitors and ROCK inhibitor containing cocktails that can be utilized for such applications including but not limited to Y-27632, thiazovivin, and the more recently reported Chroman 1, and associated CEPT cocktail (15). While ROCK inhibitors can improve cell survival post-passaging, inclusion of antioxidants and free radical scavengers to the formulation can further boost cell survival. One such proprietary formulation is RevitaCell Supplement which contains a ROCK inhibitor with higher kinase specificity relative to Y-27632 and thiazovivin. This specific kinase utilized in this formulation is designed to minimize off-target impact on other kinases. RevitaCell Supplement also contains antioxidants and free radical scavengers. This supplement has been shown to support hPSCs in stressful conditions such as cryopreservation recovery, passaging, and single cell sorting for clonal expansion (16, 17). Furthermore, a CTS version of RevitaCell Supplement is available with full traceability of components, increased safety assessment, and proven use in clinical applications.

How to Choose a Dissociation Reagent

Dissociation reagents can be provided either as an undefined composition or as fully defined reagents. An example of a dissociation reagent with an undefined composition is Accutase which is an extract of proteolytic and collagenolytic enzymes from the gut of crustaceans. Such a passaging reagent can be utilized in research use only applications and it is appropriate where small clusters of 2-3 cells are acceptable as substantially long incubation times are necessary for single-cell dissociation. If your research is translational or based on clinical applications, non-enzymatic passaging of hPSCs using EDTA or citrate based-buffers should be utilized for

passaging cells as clumps. In instances where even cell seeding is required such as high throughput screening or large vessel expansion applications utilization of recombinant trypsin solutions is ideal. In this chapter, we use CTS TrypLE Select which is clinically compliant, stable at room temperature, and allows for single cell passaging of cultures for greater confidence in scale-out applications.

How to Choose a Cell Culture Vessel

The quantities of cells necessary to seed large-scale cell culture vessels require some initial passages to be conducted in smaller scale culture vessels. These can include flasks of various sizes, multilayer flasks, or roller bottles. The selection of culture vessel for these early steps depends largely on the capabilities and physical constraints of the facility being used. Flasks made of the same material and surface treatment as the final large-scale vessels are recommended, as this will minimize any cell adaptation period after passaging into the large-scale vessel. Multilayer tissue culture flasks (e.g., Nunc TripleFlasks, Corning Multi-Flasks, and EMD Millipore Millicell HY Flask) are an optimal choice due to their similarity to the large-scale culture vessels and their minimal footprint during incubation.

After passage in a smaller multi-layer flask, larger vessels like the Nunc Cell Factory or Corning CellStack can be seeded. There are several different methods that can be used when filling large-scale cell culture vessels including direct pouring, the use of tubing and a peristaltic pump system, or using a medium bag on a gravity feed setup. All systems must be used with the aseptic technique. In this chapter we use the direct pour method, which does not require any extra equipment or materials. More information on use of a peristaltic pump system or using bagged medium can be found at the following hyperlink: https://assets.thermofisher.com/TFS-Assets/BPD/brochures/cell-factory-aseptic-filling-brochure.pdf

Importance of Tracking Cell Passaging

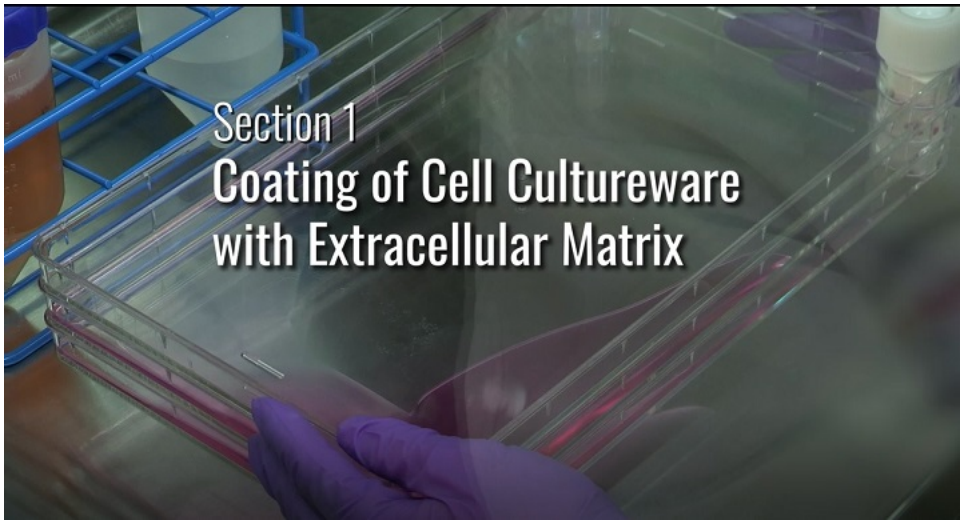
Previous reports have documented the presence of chromosomal aberrations in iPSCs and hPSCs that have been grown in culture (18, 19). It is important to keep a record of how many times your cells have been removed from a tissue culture surface and seeded again or passaged and assess genome integrity utilizing G-band karyotyping and/or Karyostat assays periodically (i.e., every 5-10 passages). It is recommended to keep the passage number below 60. It is also important to maintain a passaging schedule so that your cells are passaged at about the same confluency every time. If a detailed schedule is followed, a deviation in cell growth can indicate that the cells are unhealthy or that there is a problem with the culture system such as contamination.

Stem cells should be passaged when they are between 70-85% confluent. Similar to other cells in culture, it is important to passage the cells when they have exited the lag phase of growth and before they have entered a stationary phase of growth. This period of time is referred to as the log phase and this is when cells are least susceptible to damage.

Assay Protocol: Scale-out of hPSCs in Monolayer Culture Conditions

This protocol was developed using cell therapy grade products to simulate procedures used in large scale manufacturing of cells or products for patient therapies. Cells cultured under these conditions meet regulatory guidance from the USFDA which indicates that cGMP manufactured, clinical grade reagents should be used to minimize downstream risk of patient exposure to reagents derived from animals. Adjustments to coating matrices, media, dissociation and other reagents can be made based on the workflow required.

Section 1 – Coating Cell Culture Vessels with Extracellular Matrix



Video of section 1 starts at 0:00:05

Download video

1 Pre-coat culture vessel with desired extracellular matrix according to manufacturer's instructions (Figure 1, Step 1). In this protocol, we used CTS Vitronectin Recombinant Protein, truncated at a concentration of 0.9 µg/cm^2 or Geltrex at a 1:100 dilution.

Format	Diluted Matrix Volume
TripleFlask	120 mL
Cell Factory 1 Stack	115 mL
Cell Factory 2 Stack	230 mL
Cell Factory 4 Stack*	460 mL
Cell Factory 10 Stack*	1.15 L

* Four stack and 10 stack Nunc Cell Factory Systems are too large to view under a standard bright field microscope. It is recommended to also coat a smaller cell culture vessel (e.g. 75 cm^2 flask) at this time. This vessel should be seeded and used as a proxy to monitor cell health inside the larger cell culture vessels.

Section 2 – Passaging of Large-scale Cell Culture



Video of section 2 starts at 0:02:02

Download video

1. Pour spent medium from the culture vessel containing healthy, pluripotent stem cells.
2. Rinse the vessel once with recommended volume of CTS Dulbecco's Phosphate-Buffered Saline with no calcium or magnesium (DPBS (-/-)). See table for recommended volumes.

Format	CTS DPBS (-/-)
TripleFlask	80 mL
Cell Factory 1 Stack	100 mL
Cell Factory 2 Stack	200 mL
Cell Factory 4 Stack	400 mL
Cell Factory 10 Stack	1 L

3. Add recommended volume of room temperature CTS TrypLE Select (Figure 1, Step 2). See table for recommended volumes. Tilt the vessel to evenly distribute the reagent.

Format	CTS TrypLE Select
TripleFlask	25 mL
Cell Factory 1 Stack	30 mL

Table continued from previous page.

Format	CTS TrypLE Select
Cell Factory 2 Stack	60 mL
Cell Factory 4 Stack	120 mL
Cell Factory 10 Stack	300 mL

4. Incubate the vessel on an even surface in the laminar flow hood for 6 minutes. Do not shake or roughly handle the TripleFlask or EasyFill Cell Factory during this time as this will affect viability.
5. After incubation, gently rock the cell culture vessel back and forth 4-6 times.
6. Pour CTS TrypLE Select containing disassociated cells out of culture vessel and into a centrifuge bottle containing recommended volume of DMEM/F12 medium. TrypLE does not require neutralization and therefore, unsupplemented DMEM/F12 can be used in this step.

Format	DMEM/F12
TripleFlask	60 mL
Cell Factory 1 Stack	75 mL
Cell Factory 2 Stack	150 mL
Cell Factory 4 Stack	300 mL
Cell Factory 10 Stack	760 mL

7. If a large amount of cells remain attached to the cell culture surface, quickly add more room temperature CTS TrypLE Select to the vessel (Figure 1, Step 2). See table for recommended volumes. Tilt the vessel so that the liquid is evenly distributed across the culture surface.
8. Incubate the vessel in the laminar flow hood for 3-5 minutes. After incubation, gently tilt the vessel to one side. Cells should be detached and now in suspension. Do not shake or harshly rock the vessel as this can reduce the amount of viable cells.
9. Gently rock the cell culture vessel back and forth 4-6 times.
10. Pour the cell suspension into the conical tube containing cells and DMEM/F12 from step 6.
11. Rinse the culture vessel with DMEM/F12 to remove the remaining cells in the culture vessel.
12. Centrifuge conical tube(s) at 200xg for 6 minutes at room temperature.

Section 3 – Seeding Large-scale Cell culture vessels



Video of section 3 starts at 0:07:05

Download video

1. Pour off the supernatant leaving about 3 mL of DMEM/F12. Rock the tube gently back and forth to loosen the pellet.
2. Add recommended amount of resuspension medium (e.g., StemFlex or CTS Essential 8 Medium +/- CTS RevitaCell Supplement) to re-suspend the cells in the conical tube. Pipette up and down 10-15 times to break up large cell clumps.

Format	Volume of Medium for Resuspension*
TripleFlask	50 mL
Cell Factory 1 Stack	60 mL
Cell Factory 2 Stack	120 mL
Cell Factory 4 Stack	250 mL
Cell Factory 10 Stack	630 mL

* Adding Gibco CTS RevitaCell Supplement to the re-suspension medium can improve post passage cell viability.

3. Determine the cell number and percent viability using a Countess II Automated Cell Counter or similar automated or manual cell counting method. Resuspension volumes may need to be adjusted based on cell yield and the counting range of the cell counter.
4. Add the appropriate number of cells to plating medium (e.g., CTS Essential 8 Medium + CTS RevitaCell Supplement or StemFlex + RevitaCell Supplement) volume. It is recommended to add the cells to the

medium in a separate media bottle and mixing that bottle before adding to the culture vessel. This ensures proper mixing of the cells and even distribution of cells on the culture surface (Figure 1, Step 3).

Culture vessel	Number of Viable Cells Added		Volume of Plating Medium
	12,500 cells/cm^2	25,000 cells/cm^2	
TripleFlask	6,250,000	12,500,000	200 mL
Cell Factory 1 Stack	7,900,000	15,800,000	200 mL
Cell Factory 2 Stack	15,800,000	31,600,000	300 mL
Cell Factory 4 Stack	31,600,000	63,200,000	600 mL
Cell Factory 10 Stack	79,000,000	158,000,000	1.5 L

5. Immediately prior to plating cells, pour diluted extracellular matrix out of the Cell Factory and discard. Work quickly so that the coated culture surface does not dry out.
6. Transfer the cell suspension to the pre-coated culture vessel. NOTE: If using substrates such as Geltrex Basement Membrane Matrix or recombinant Vitronectin-N, then inclusion of 1X RevitaCell Supplement for the first 18-24 hours post-passage is recommended, whereas if using rhLaminin-521 inclusion of RevitaCell Supplement is not required as rhLaminin-521 affords greater cell survivability.
7. Ensure that the layers of larger culture vessels receive equal amounts of cells in suspension by standing the cell factory on the end opposite the fill ports to allow the liquid to equilibrate across layers before lying flat. Return the vessel to the normal, flat position and move the vessel in several side-to-side and back and forth motions to disperse the cells across the surface of each layer.
8. Place cell culture vessel in the 37°C, 5% CO_2 incubator and incubate the cells overnight. It is important the culture vessel is on a flat, level surface to prevent growth medium from pooling at one end and ensure an even distribution of cells across the surface.
9. Feed the hPSCs with fresh growth medium (e.g., CTS Essential 8 Medium or StemFlex) without RevitaCell Supplement the day after passaging, followed by every day medium exchanges for CTS Essential 8 Medium cultures or every-other-day for StemFlex Medium cultures. NOTE: It is normal to see cell debris and small colonies after passage. It is also normal to see large amounts of DNA that has been released from cells that did not survive passage when using recombinant trypsin solutions as a dissociation reagent. DNA that is released from cells sticks together forming a substance that looks like white, stringy mucus. It is possible to add DNase to the medium after passaging to reduce the extra-cellular DNA present. Numerous DNase enzymes are available on the market for this purpose and optimal DNase enzyme working concentration should be determined for each cell line.
10. Cells should be passaged upon reaching ~85% confluency to maintain optimum cell health of cultures.

Viable Cell Counts

Harvesting from large-scale culture vessels produces vast cell numbers with relatively high viability. Figure 2A shows the viable cell number obtained from the Nunc TripleFlask and from the Nunc Cell Factory. Data were collected from two different users and averaged together. Various hPSC lines grow with small differences in

morphology and compactness of the colonies. Thus, we utilized two human induced pluripotent stem cell (hiPSC) lines which spanned the typical range of morphology and compactness. We consistently harvested more WTC-11 cells than Gibco Episomal iPSC Line. This is presumably due to the different morphology in the WTC-11 which pack more tightly than the Gibco Episomal iPSC Line. Actual cell yield will depend on the cell line chosen. Viability remained high (Figure 2B) despite the fact that we incubated with the dissociation reagent twice during cell passage. Note: The WTC-11 cell line was obtained from the NIGMS Human Genetic Cell Repository at the Coriell Institute for Medical Research: G25256.

Monitoring Cell Health in Large-Scale Culture

Visualizing Morphology

Monitoring cell health in culture is critical for consistent and accurate results. However, observing cells in large-scale culture vessels can be difficult. The largest cell culture vessels cannot be viewed under standard bright field microscopes. It is highly recommended to coat a smaller cell culture vessel with extracellular matrix at the same time you coat your larger vessel used for hPSC scale-out. You should seed this smaller vessel with the same number of cells per square centimeter of culture area and the same volume of liquid per square centimeter of culture area as the larger vessel. The smaller vessel will allow you to monitor cell health, proper colony formation, and check for contamination.

There are certain microscopes that can be easily modified to view larger culture vessels. This is done by removing any accessories from the stage and the light source if necessary. Then, using an alternative light source if the included one is removed, the cells can be visualized through the microscope objective. A step-by-step guide, including pictures, can be found at the following hyperlink:

http://tools.thermofisher.com/content/sfs/brochures/Visualize-cells-in-Nunc-Cell-Factory-AQLSPCFVISUALIZE-EN.pdf

Both the TripleFlask and the 2 layer Cell Factory are small enough to fit on the stage of a standard inverted bright field microscope allowing the user to view the bottom layer of plastic and the cells that have attached to it. Figure 3A shows hPSC colony formation over a four day period inside a TripleFlask. Twenty-four hours after plating, the cells have a spiked appearance. This morphology change is due to the presence of RevitaCell Supplement which acts as a Rho kinase inhibitor. These inhibitors are known to cause reversible changes to cell morphology (20). When the supplement is removed 18-24 hours after addition, the cells begin to pack closely to each other. Over the next several days, stem cell colonies form with smooth, round edges. Cells follow a similar pattern of colony development when plated in the Cell Factory (Figure 3B). We observed very large and very tightly packed colonies in these two large-scale culture vessels.

Glucose, Lactate, Ammonia and pH Measurements

Measuring the spent medium metabolites or pH in large cell culture vessels is an alternative method for determining cell growth rates and the appropriate time to split your cell culture. It has been demonstrated that lactate levels higher than 1g/L can reduce stem cell growth (21). The accumulation of lactate can also decrease growth rates despite regulating pH (22).

To examine spent medium iPSC culture, WTC-11 cells were plated at a range of 5,000- 40,000 cells/cm^2 in a 6 well plate on a recombinant human Vitronectin-N coated surface. They were expanded over a 3 day time period in CTS Essential 8 medium with medium exchange every 24 hours. Following the last 24 hours, the cells were scanned for confluency using the IncuCyte Live Cell Analysis System and spent medium was removed and centrifuged. The supernatant was analyzed using the Cedex Bio HT Analyzer (Roche). A strong correlation occurs between cell confluency and a reduction in glucose or between confluency and an increase in lactate

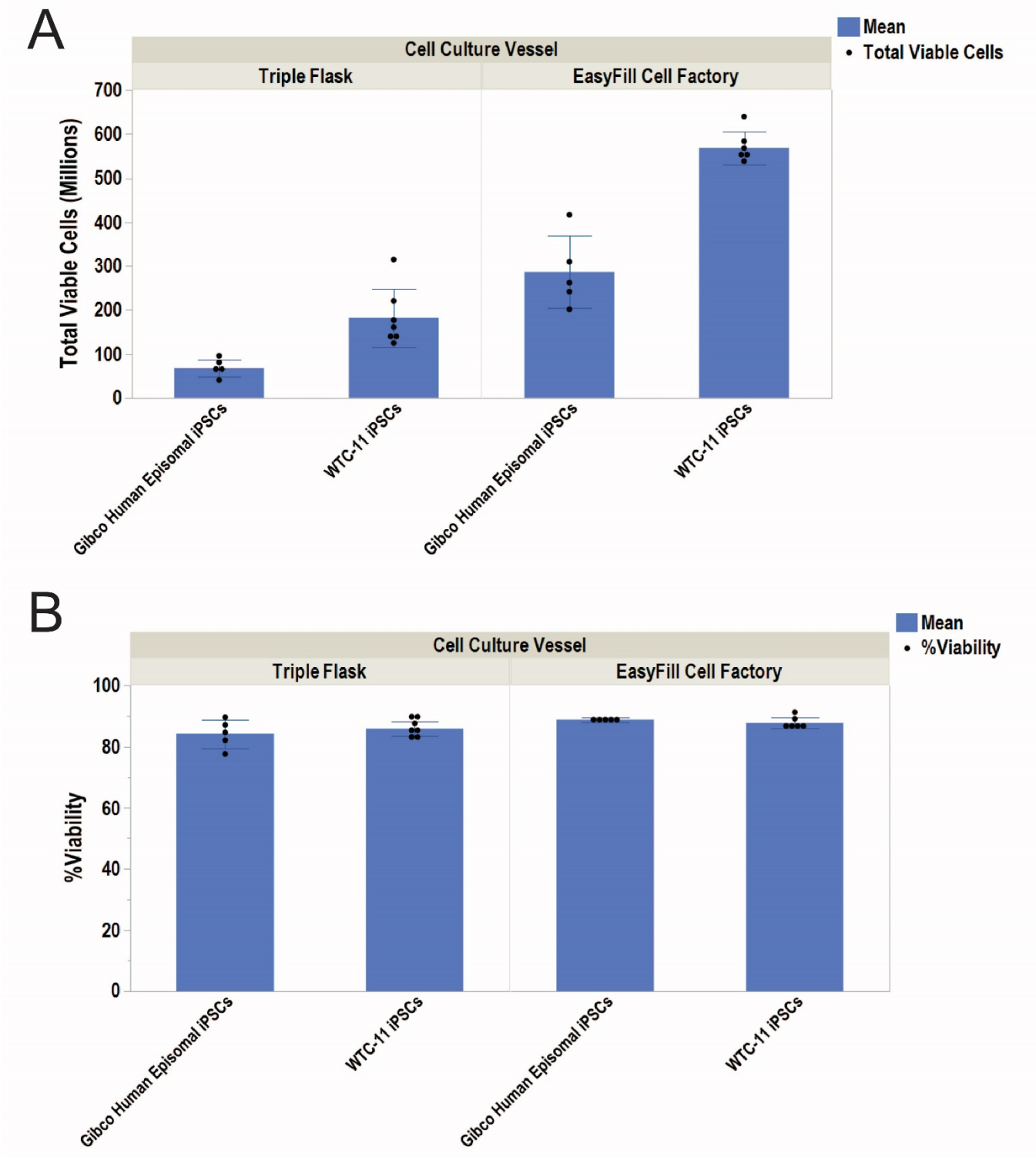


Figure 2. Assessment of (A) Viable Cell Counts and (B) Percent Viable Cells Following Expansion in TripleFlask and EasyFill Cell Factory (2-Layer). Human iPSCs were expanded using CTS Essential 8 Medium on recombinant human Vitronectin-N coated cultureware. After single passage expansion in the various vessel types to ~85% confluency, cells were harvested and counted using Trypan Blue exclusion in conjunction with the Countess II Automated Cell Counter. Differences in the range of cell yields between two iPSC cell lines, Gibco Human Episomal iPSCs and WTC-11, are highlighted. Differences in cell yield are due to differences in colony compactness. WTC-11 cells grow in tightly packed colonies allowing for higher cell numbers. The means and standard deviations of each dataset are highlighted with data points indicating the counts from individual flasks ($n \geq 5$).

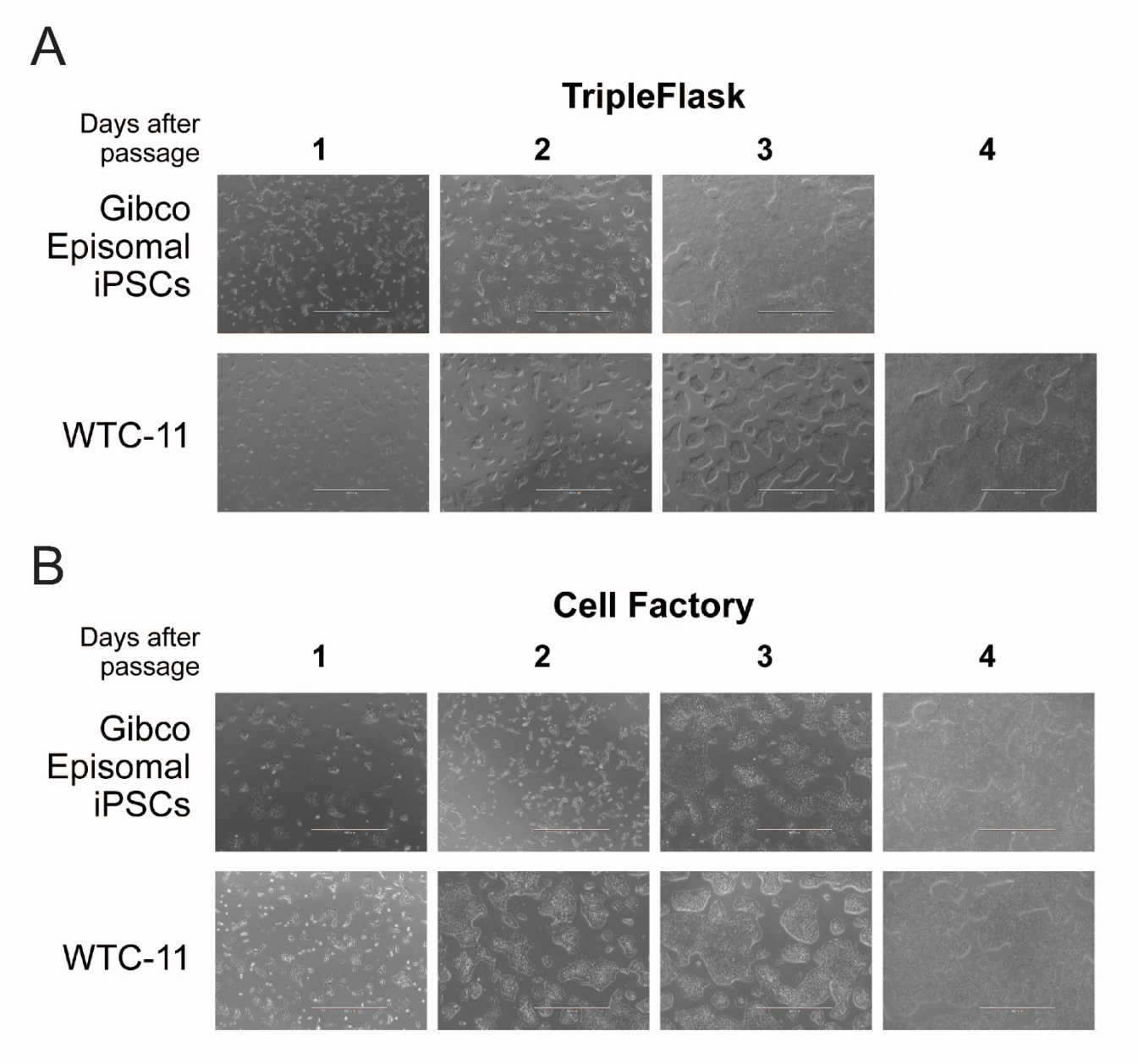


Figure 3. Representative phase contrast images of hiPSCs following seeding and expansion in Triple Flask and EasyFill Cell Factory. Human iPSCs were expanded using CTS Essential 8 Medium on recombinant human Vitronectin-N coated culture vessels. A) After seeding stem cells into a TripleFlask vessel in the presence of CTS RevitaCell Supplement, cells initially have a spiked morphology. Upon medium exchange and further expansion, cells condense and colony-like morphology with smooth, round edges is observed on day 3 and 4 of culture. B) Cells seeded into a Cell Factory follow a similar time course developing large, tightly packed colonies at day 4. Please note that different cell lines will reach confluency at different rates. Scale bar is 1000 µm.

(Figure 4). There is also a correlation between confluency and ammonia levels and confluency and pH. Using one or several of these correlations, you can analyze the spent medium and get an accurate estimate of cell confluency in vessels that cannot be viewed under a microscope. A standard curve will need to be generated for each cell type in each medium type.

Characterizing spent medium can be done using commercially available reagents. These offer a quick, low-cost way to ensure your cells are not passaged too soon or that they do not exceed ~85% confluency. Ideally cells should not be passaged before they reach at least 70% confluency and before they reach 90% confluency.

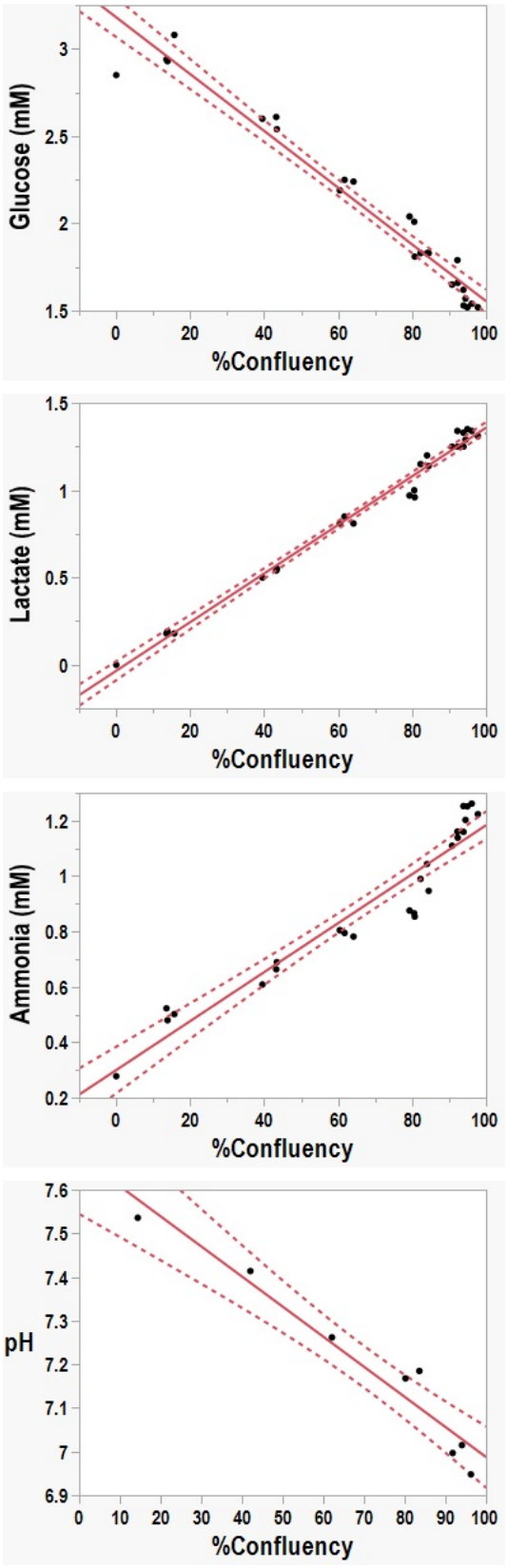


Figure 4. Spent Media Measurements in Large-Scale Cell Culture Vessels. WTC-11 Cells were plated on recombinant human Vitronectin-N coated culture vessels at different seeding densities and cultured for 3 days with daily feeding using CTS Essential 8 Medium. On day 3, they were scanned for confluency and spent medium from that day was analyzed. There is a clear correlation between cell number and spent medium components. This characterization allows indirect measurement of cell confluency in large-

scale culture vessels. This correlation is specific for each cell type, medium used, and incubation condition. Dotted lines represent 95% confidence intervals. Each dot represents a biological replicate.

Analysis of Pluripotency and Cell Quality

Immunofluorescent Labeling of Pluripotent Markers- Immunofluorescence of transcription factors or cell surface antigens is a relatively fast and easy way to determine the homogeneity and pluripotency of your stem cell population. Many of these proteins have been characterized in depth and indicate "stemness" or the potential to differentiate (23, 24). OCT4 and SOX2 are critical transcription factors for proper development of mammalian embryos. The presence of these factors supports self-renewal but does not impair differentiation and their expression levels are commonly used to identify pluripotent populations. The surface antigens TRA-1-60 and SSEA-4 are also expressed by pluripotent stem cells (25). TRA-1-60 antibodies recognize a specific epitope which is present in stem cells as a part of a mucin-type O-glycan structure (26). SSEA-4 is a ganglioside consisting of a glycosphingolipid containing a terminal sialic acid residue (27). All four of these markers, OCT4, SOX2, TRA-1-60, and SSEA-4, can also be used for quantitative flow cytometry analysis or qualitative immunocytochemistry analysis.

WTC-11 and Gibco Episomal iPSCs were grown in TripleFlasks and Cell Factories. After two passage expansion in TripeFlasks followed by two passages in Cell Factories, the cells were plated in 6 well dishes at 75,000 cells/cm^2 in the presence of RevitaCell supplement. In this work, we used the Invitrogen Pluripotent Stem Cell 4-Marker Immunocytochemistry Kit which multiplexes labeling of OCT4, SOX2, SSEA4, and TRA-1-60 in the presence of the DNA stain DAPI. One day after plating, the cells were fixed and permeabilized using the Image-iT Fixation/Permeabilization Kit, immunolabeled, and analyzed on the EVOS FL2 Imaging System.

Figure 5 shows representative images of the cells after 2 passages in a TripleFlask and 2 passages in a Cell Factory. After large-scale expansion, OCT4 and SOX2 are highly expressed and localized to the nucleus while TRA-1-60 and SSEA-4 show a more diffuse labeling pattern. These markers were readily observed in both Gibco Episomal iPSCs and WTC-11. Notice that there is dimmer labeling towards the center of densely packed colonies. We routinely see this labeling pattern which is an artifact of immunofluorescent labeling rather than lower levels of Oct4 or Sox2 expression which can be confirmed using flow cytometry. Densely packed colonies prevent access to epitopes for antibody binding. The presence of OCT4, SOX2, TRA-1-60, and SSEA-4 indicate that, regardless of the increase in cell culture vessel size, consistent expression of pluripotency markers is maintained during the scale-out process.

PluriTest Analysis – The PluriTest pluripotency assay provides a bioinformatics approach to assess pluripotency. It uses an extensive reference library, comparing the transcriptional profile in your samples to a variety of cell and tissue types. This comparison produces two scores; the pluripotency score (PluriCor), indicating strength of pluripotency expression, and the novelty score (NovelCor), showing the model fit for that particular assessment. Two detailed protocols describing PluriTest analysis have been published by Müller et al. (28, 29) which provide valuable insight. Data from the PluriTest is represented in graph form like the one shown in Table 1. The red and blue cloud on the graph represent the empirical distribution function of hPSCs and differentiated cells respectively. The red and blue clouds are used as a reference for sample comparison. The red cloud represents hPSCs and the blue cloud represents differentiated cells. The empirical distribution functions are generated from approximately 450 genome-wide transcriptional profiles of stem cells cultured under feeder and feeder-free culture conditions, differentiated cell types, and developing tissues.

PluriTest was performed on WTC-11 cells and Gibco Episomal iPSCs that had been cultured in large vessels. To do this analysis, the cells were dissociated from the cell culture surface and processed to obtain a viable cell count. Two million cells were added to a cryopreservation tube. They were pelleted using centrifugation and the medium was aspirated. The pellet was temporarily stored at -80^{o}C and then shipped under dry ice conditions to

be processed by Thermo Fisher Scientific Pluritest Services in Carlsbad, CA, USA. After two passages in Cell Factories, the PluriCor was high and NovelCor was low signifying these samples were pluripotent (Table 1).

G-Banding – Giemsa Banding (G-banding) provides a visual representation of chromosomes in metaphase. It can be used to detect gross chromosomal abnormalities and abnormal chromosomal structures (30, 31). After scale-out of WTC-11 and Gibco Episomal iPSCs, the cells were harvested and plated at 600,000 cells in a flask with a surface area of 25 cm^2. When the cells reached approximately 50% confluency, the flask was filled with fresh medium, tightly sealed and shipped at ambient temperature to Cell Line Genetics for G-banding analysis (Madison, WI, USA). Figure 6 shows both cell lines displayed normal karyotype indicating that scale-out did not produce any changes in chromosomal structure.

Karyostat Analysis – Karyostat arrays provide researchers with a quick and effective method to determine if their stem cells carry chromosomal aberrations. It is a very thorough, whole-genome analysis. This assay has a resolution similar to G-banding and is able to detect aberrations greater than 2 megabase pairs for chromosomal gains and to detect any deletions greater than 1 megabase pair (32).

For the Karyostat analysis in this chapter, we cultured Gibco Episomal iPSCs and WTC-11 cells in the TripleFlask for two passages and in the Cell Factory for two additional passages. Following the same procedure as described for the PluriTest analysis, cells were harvested, pelleted, and stored at -80°C. They were shipped in dry ice conditions to Thermo Fisher Scientific KaryoStat Karyotyping Services in Carlsbad, CA, USA. Upon receipt the cells are processed to isolate genomic DNA and thus the result achieved is based upon the population of cells as a whole rather than 20 metaphase cells as is performed for G-Band analysis.

Whole genome views of the Karyostat are represented in a KaryoView in Figure 7. While Gibco Episomal iPSCs do not have any chromosomal aberrations (Figure 7A), WTC-11 did show a chromosomal loss detected on the Y-chromosome at position p11.2 (Figure 7B). This chromosomal loss was confirmed in the parental line and was not caused by large-scale cell culture. This example illustrates the need to examine more than one indicator of stem cell state when assessing overall iPSC quality.

Considerations for cryopreservation – Effective cryopreservation methods are essential for large-scale cell culture and for therapeutic applications of stem cells. Numerous publications have addressed this issue (33, 34). To successfully cryopreserve cells a number of factors should be optimized, including freezing conditions, proper storage, and proper thawing (35).

To ensure that cells could be preserved following expansion in large-scale cell culture vessels, we grew Gibco Episomal iPSCs and WTC-11 cells in Cell Factories and then harvested them for cryopreservation. The cells were dissociated following the methods described in Section 2 of this chapter. After centrifugation, viable cells were re-suspended in 1 mL of pre-chilled CTS PSC Cryomedium, placed on ice, and counted. A range of different cell numbers were added to 1 mL of CTS PSC Cryomedium in a 2 mL cryopreservation tube. This range included 5 million, 10 million, 20 million and 50 million cells. The cryopreservation tubes were quickly transferred to a pre-chilled Mr. Frosty Freezing Container and stored in a -80°C freezer for 24 hours. Cryopreservation tubes were then transferred to the cryogenic storage Dewar and stored for several days. To assess viability, cells were quickly thawed in a 37°C water bath until a small sliver of ice remained in the cryopreservation vial. Thawed cells were gently triturated with a p1000 micro-pipette. The cell suspension was transferred to a 15 mL conical tube. Two mL of complete medium was then added dropwise to the 15 mL conical while gently agitating. This slow addition of medium reduces osmotic shock and increases percent cell viability. Cell suspensions were mixed using gentle inversion and then centrifuged at 200 x g for 4 minutes. Medium was aspirated from the cell pellet and the pellet was re-suspended in complete medium containing RevitaCell Supplement.

Cells were plated at a density of 40,000 cells/cm^2 in a 96 well plate that had been previously coated with recombinant human Vitronectin-N. The plate was placed in an incubator at 37°C with 5% CO_2. After 24 hours,

medium was replaced with PrestoBlue Viability Reagent diluted in complete medium. The plate was incubated for 2 hours and then assessed using the SpectraMax M5 (Molecular Devices). Cells preserved up to 50 million cells/mL of cryopreservation medium demonstrated acceptable recovery from cryopreservation (Figure 8). There are numerous reagents and methods that can be used to measure cell viability. The user should choose the reagent that will work best with their application and other available laboratory equipment (36).

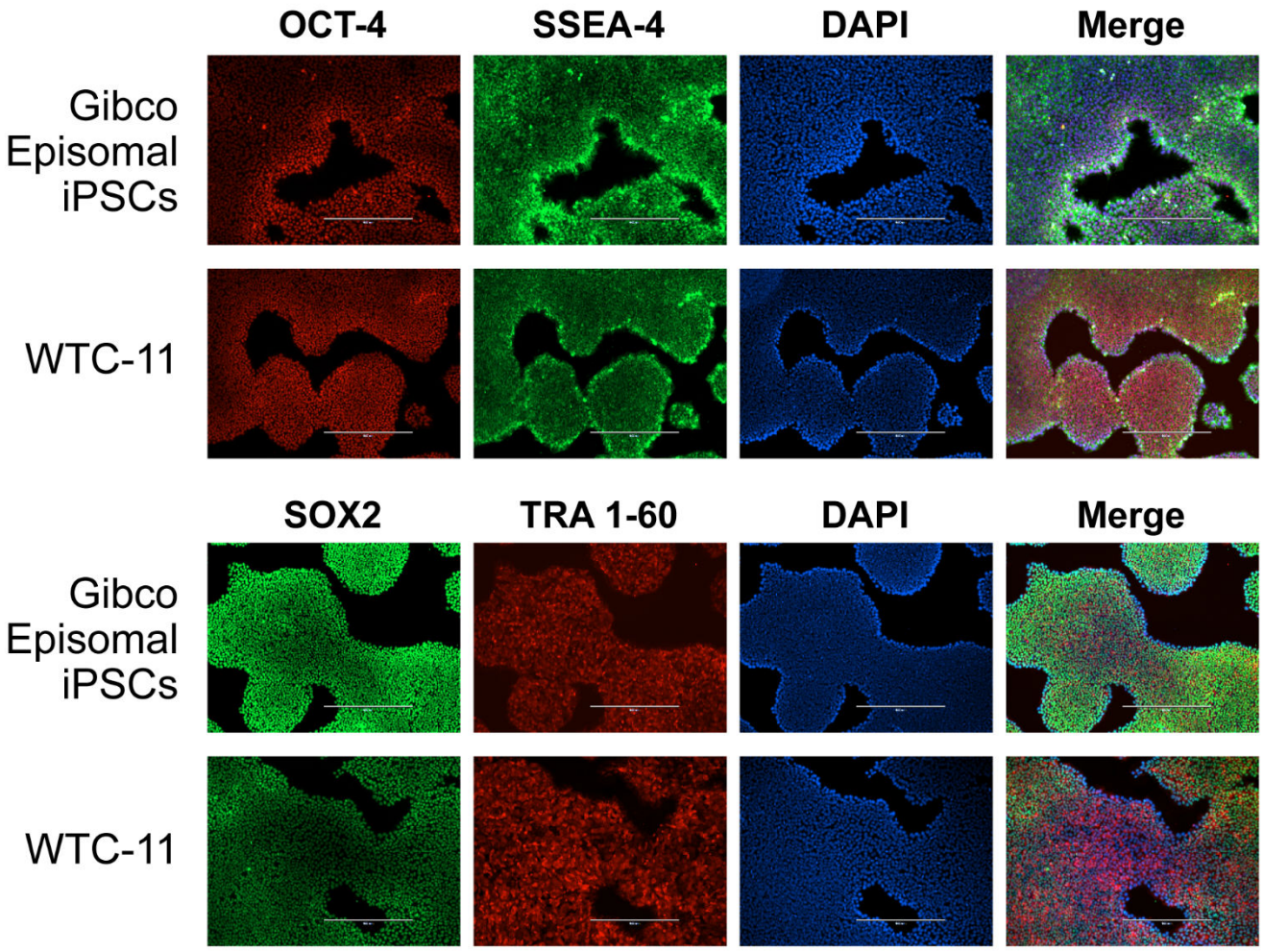


Figure 5. Immunocytochemistry labeling of cells after scale-out. Human iPSCs were expanded in 6 well plates using CTS Essential 8 Medium on recombinant human Vitronectin-N. Following expansion of induced pluripotent stem cells and embryonic stem cells, the cells were labeled for four different pluripotent markers. Transcription factors OCT4 and SOX2 were abundant in the nuclei. SSEA-4 and TRA-1-60 were both shown to be extracellular, consistent with the presence of these proteins on the plasma membrane. Scale bar is equal to 400 μm.

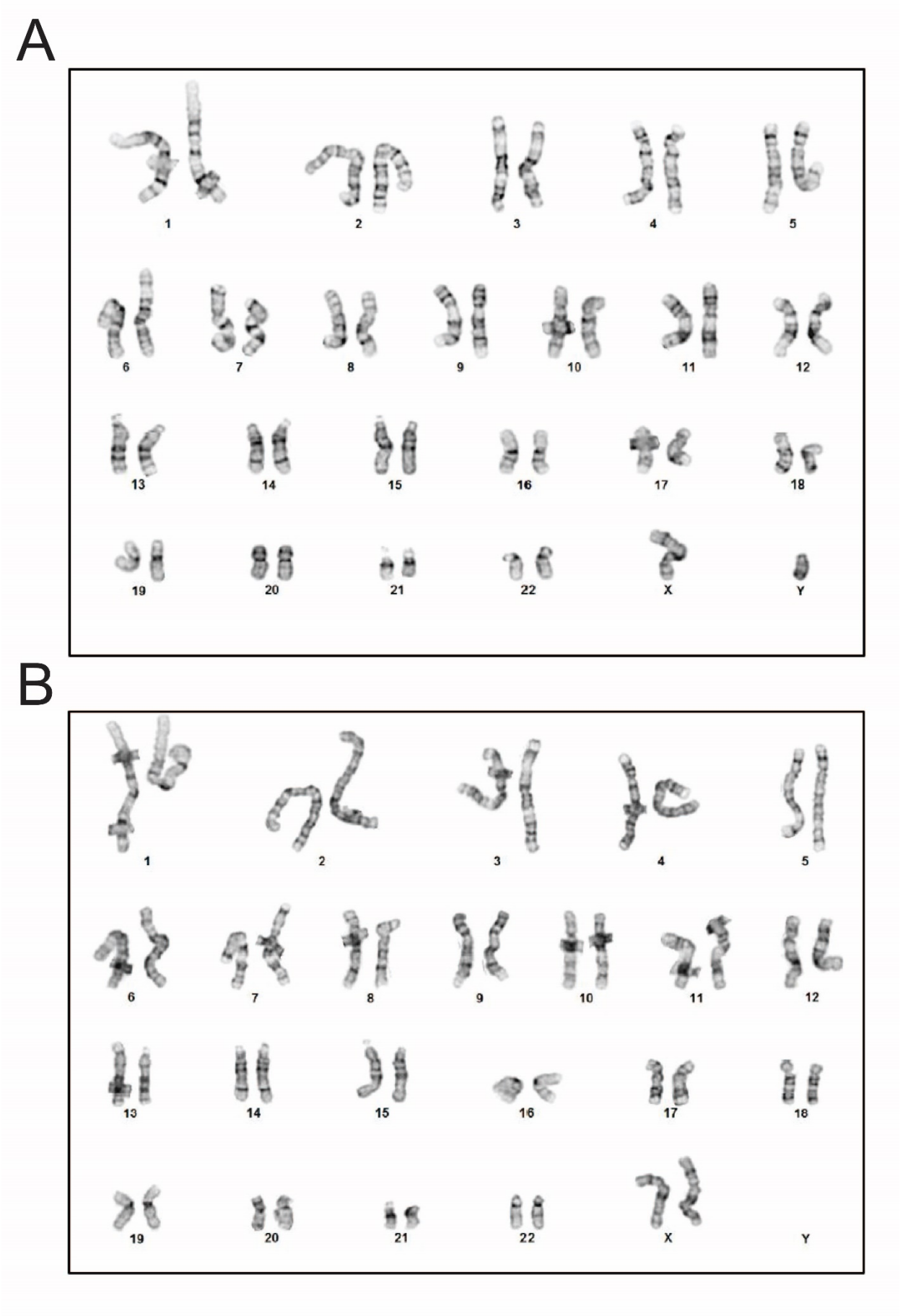


Figure 6. G-Band Karyotype Assessment of Cells Grown at Large-Scale. Human iPSCs were expanded using CTS Essential 8

Medium on recombinant human Vitronectin-N coated cultureware. Cells were grown in Cell Factories and then passaged into 25cm^2 flasks. After expansion, live cell cultures were sent to Cell Line Genetics for G-band Karyotype analysis. A) WTC-11 and B) Gibco Episomal iPSCs both displayed a normal human karyotype after large-scale cell culture with cytogenetic analysis being completed for 20 G-band metaphase cells per line. Representative G-banding pattern is shown.

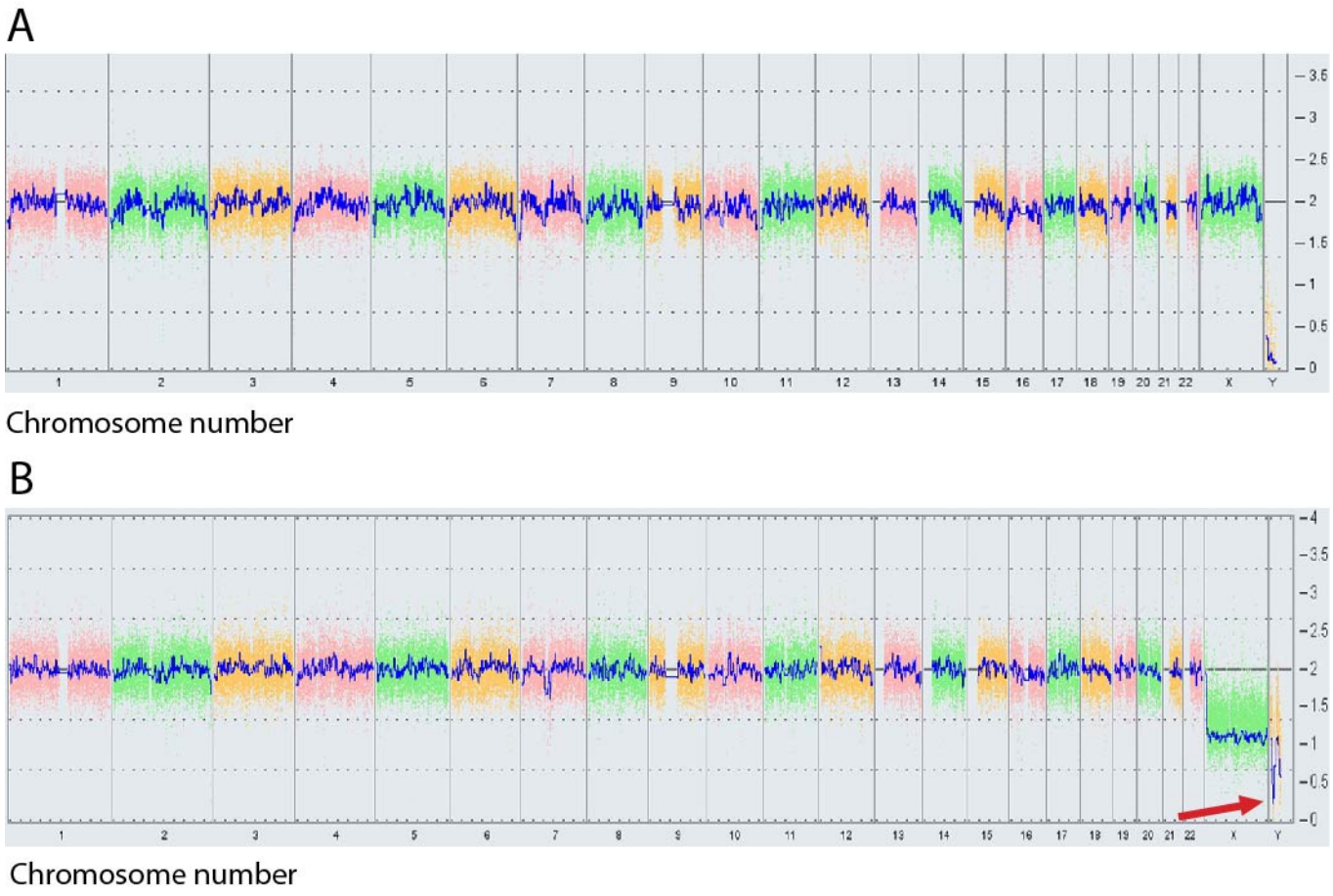


Figure 7. Whole Genome View of Karyostat Analysis. The whole genome view displays all somatic and sex chromosomes in one frame with the y-axis representing the copy number. The chromosome number can be found on the x-axis. A value of 2 on the y-axis represents a normal copy number state (CN = 2). A value of 3 on the y-axis represents chromosomal gain (CN = 3). A value of 1 on the y-axis represents a chromosomal loss (CN = 1). The pink, green and yellow colors indicate the raw signal for each individual chromosome probe, while the blue signal represents the normalized probe signal which is used to identify copy number and aberrations. Human iPSCs were expanded using CTS Essential 8 Medium on recombinant human Vitronectin-N coated cultureware. A) Gibco Episomal iPSCs did not show any chromosomal aberrations. B) WTC-11 iPSCs do have chromosomal loss detected on the Y-chromosome at position p11.2 (red arrow). This loss was not due to the scale-out process as this loss was also detected in the parental line before scale-out.

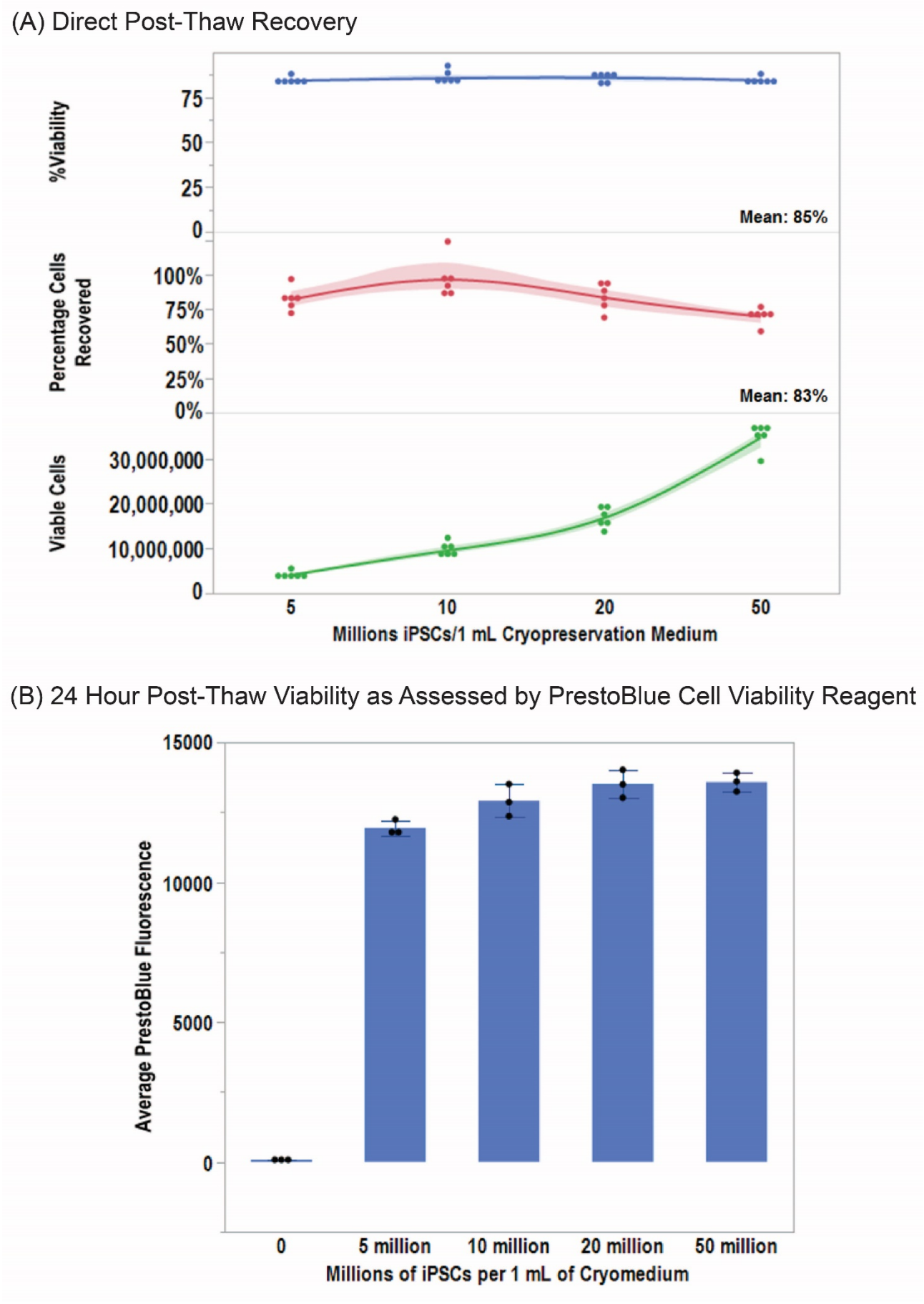
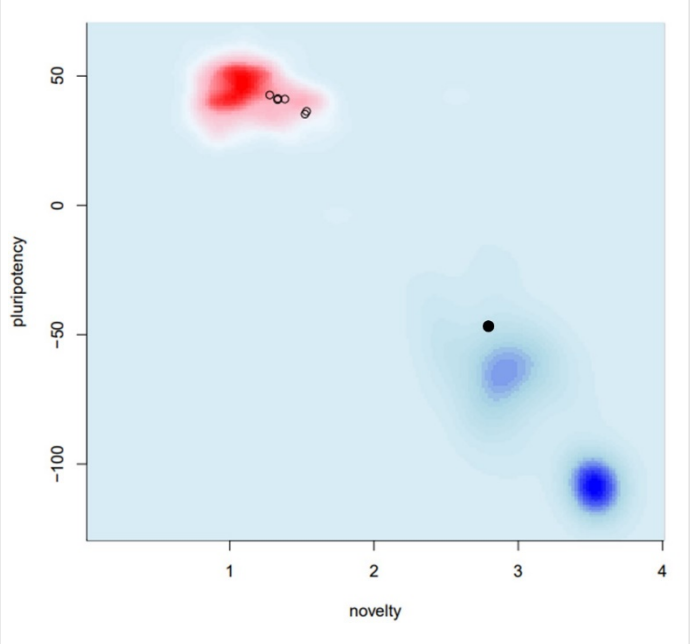


Figure 8. Assessment of Cryopreservation of iPSCs at High Cell Densities. Human iPSCs were expanded using CTS Essential 8

Medium on recombinant human Vitronectin-N coated cultureware. iPSCs were harvested after reaching approximately 80% confluency. They were cryopreserved at 5-50 million viable cells/mL in CTS PSC Cryomedium. Following cryogenic storage for several days, the cells were then thawed and (A) direct post-thaw recovery was determined as assessed by Trypan blue exclusion and number of viable cells recovered, followed by (B) assessment of 24 hour post-thaw viability as assessed by PrestoBlue fluorescence. Acceptable recovery was noted up to 50 million viable iPSCs per mL of CTS PSC Cryomedium. In panel A, trend lines are indicated with metrics from independent vials denoted by the individual data points (n = 6). The means of the overall dataset for %viability and %viable cells recovered are denoted in the bottom, right hand corner of the plots. In panel B, the means and standard deviations of each dataset are denoted with datapoints indicating average Prestoblue Fluorescence from wells seeded using cells cryopreserved at each of the denoted densities (n = 3).

Table 1. PluriTest Assay Results. Human iPSCs were expanded using CTS Essential 8 Medium on recombinant human Vitronectin-N coated cultureware. iPSCs cultured in large-scale culture vessels were analyzed with the PluriTest. Two samples of each cell type were measured for pluripotency score (PluriCor) and the novelty score (NovelCor) and are represented in the graph by open circles. The red and blue clouds on the plot represent empirical density distributions for hPSCs and differentiated cells respectively. The red and blue clouds are used as a reference for sample comparison. The red cloud represents hPSCs and the blue cloud represents differentiated cells. The empirical distribution functions are generated from approximately 450 genome-wide transcriptional profiles of stem cells, differentiated cell types, and developing tissues. The non-iPSC sample is near the blue cloud and is represented with a solid black dot. All samples passed the PluriTest indicating that large-scale cell culture does not affect pluripotency.

Sample ID	PluriTest Result	PluriCor	NovelCor
WTC-11	Pass	36.33	1.53
WTC-11	Pass	35.29	1.52
Gibco Episomal iPSCs	Pass	40.87	1.33
Gibco Episomal iPSCs	Pass	42.68	1.28
iPSC_Control	Pass	41.32	1.33
Non_iPSC	Fail	-46.37	2.80



Conclusion

Pluripotent stem cells are valuable resources that provide the ability to do controlled differentiation, disease modeling, drug discovery, and generate novel, cell-based therapies. The development of animal-origin-free workflows and large cell culture vessels have increased our power to produce large amounts of stem cells that are

useful in clinical and translational research. In the past, these applications were limited by culture vessel size and therefore in growth area which made large-scale expansion challenging. The sensitive nature of these types of cells, however, mean special care must be taken to ensure the cells behave in any large-scale growth vessels as they would in previous small-scale experiments. Using the protocols outlined above, we have shown that large-scale cell culture vessels can be used to expand large quantities of high quality pluripotent cells.

References

1. McKee C., Perez-Cruet M., Chavez F., Chaudhry G. R. Simplified three-dimensional culutre system for long term expansion of embryonic stem cells. World J Stem Cells. 2015.:1064–1077. pp. PubMed PMID: 26328022.
2. Tohyama S., Fujita J., Fujita C., Yamaguchi M., Kanaami S., Ohno R., Sakamoto K., Kodama M., Kurokawa J., Kanazawa H., Seki T., Kishino Y., Okada M., Nakajima K., Tanosaki S., Someya S., Hirano A., Kawaguchi S., Kobayashi E., Fukuda K. Efficient Large-Scale 2D Culture System for Human Induced Pluripotent Stem Cells and Differentiated Cardiomyocytes. Stem Cell Reports. 2017.:1406–1414. pp. PubMed PMID: 28988990.
3. Konagaya S., Ando T., Yamauchi T., Suemori H., Iwata H. Long-term maintenance of human. Nature Scientific Reports. 2015. PubMed PMID: 26573336.
4. Wang Y., Chou B.-K., Dowey S., He C., Gerecht S., Cheng L. Scalable Expansion of human induced pluripotent stem cells in the defined xeno-free E8 medium under adherent and suspension culture conditions. Stem Cell Research. 2013.:1103–1116. pp. PubMed PMID: 23973800.
5. Meng G., Liu S., Poon A., Rancourt D. E. Optimizing Human Induced Pluripotent Stem Cell Expansion in Stirred-Suspension Culture. Stem Cells and Development. 2017. PubMed PMID: 29017378.
6. Manstein F., Halloin C., Zweigerdt R. Human Pluripotent Stem Cell Expansion in Stirred Tank Bioreactors. Methods in Molecular Biology. 2019.:79–91. pp. PubMed PMID: 31124106.
7. Li X., Ma R., Liang L., Wang L., Zhang Y., Wang X., Liu X., Li Z., Fang J., Wu J., Wang Y., Li W., Hu B., Wang L., Zhou Q., Hao J. A fully defined static suspension culture system for large-scale human embryonic stem cell production. Cell Death & Disease. 2018. PubMed PMID: 30166524.
8. Nakagawa M., Taniguchi Y., Senda S., Takizawa N., Ichisaka T., Asano K., Morizane A., Doi D., Takahashi J., Nishizawa M., Yoshida Y., Toyoda T., Osafune K., Sekiguchi K., Yamanaka S. A Novel Efficient Feeder-Free Culture. Scientific Reports. 2014. PubMed PMID: 24399248.
9. Morizane R., Bonventre J. V. Generation of nephron progenitor cells and kidney organoids from human pluripotent stem cells. Nature Protocols. 2016.:195–207. pp. PubMed PMID: 28005067.
10. Gupta N., Susa K., Yoda Y., Bonventre J. V., Valerius M. T., Morizane R. CRISPR/Cas9-based Targeted Genome Editing for the Development of Monogenic Diseases Models With Human Pluripotent Stem Cells. Current Protocols in Stem Cell Biology. 2018. PubMed PMID: 30040245.
11. Aalders J., Van den Vreken N., Popovic M., Mishra S., Heindryckx B., Hengel J. v. Robust Protocol for Feeder-Free Adaptation of Cryopreserved Human Pluripotent Stem Cells. In Vitro Cell Dev Biol Anim. 2019.:777–783. pp. PubMed PMID: 31664691.
12. B. GroB. M. Sgodda, A. Rasche, G. Schambach, B. Gohring, B. Schelelberger, B. Greber, T. Linden, D. Reinhardt, J. Cantz and H. Klusmann, "Improved Generation of Patient-Specific Induced Pluripotent Stem Cells Using a Chemically-Defined and Matrigel-Based Approach. Current Molecular Medicine. 2013.
13. Badenes S. M., Fernandes T. G., Cordeiro C. S., Boucher S., Kuninger D., Vemuri M. C., Diogo M. M., Cabral J. M. Defined Essential 8 Medium and Vitronectin Efficiently Support Scalable Xeno-Free Expansion of Human Induced Pluripotent Stem Cells in Stirred Microcarriers. PLOS ONE. 2016.
14. Watanabe K., Ueno M., Kamiya D., Nishiyama A., Matsumura M., Wataya T., Takahashi J. B., Nishikawa S., Nishikawa S.-i., Muguruma K., Sasai Y. A ROCK Inhibitor Permits Survival of Dissociated Human Embryonic Stem Cells. Nature Biotechnology. 2007.:681–686. pp. PubMed PMID: 17529971.
15. Chen Y., Tristan C. A., Chen L., Javanovic V. M., Malley C., Chu P.-H., Ryu S., Deng T., Ormanoglu P., Tao D., Fang Y., Slamecka J., LeClair C. A., Michael S., Austin C. P., Simeonov A., Singec I. A Versatile

Polypharmacology Platform Promotes Cytoprotection and Viability of Human Pluripotent and Differentiated Cells. bioRxiv. 2019.
16. Chen Y.-H., Pruett-Miller S. M. Improving Single-Cell Cloning Workflow for Gene Editing in Human Pluripotent Stem Cells. Stem Cell Res. 2018.:186–192. pp. PubMed PMID: 30099335.
17. Ye H., Wang Q. Efficient Generation of Non-Integration and Feeder-Free Induced Pluripotent Stem Cells From Human Peripheral Blood Cells by Sendai Virus. Cell Physiol Biochem. 2018.:1318–1331. pp. PubMed PMID: 30355953.
18. Paterson S., Loring J. Genomic Instability in Puripotent Stem Cells: Implications for Clinical Applications. J Biol Chem. 2014.:4578–4584. pp.
19. Mayshar Y., Ben-David U., Lavon N., Biancotti J.-C., Yakir B., Clark A., Plath K., Lowry W., Benvenisty N. Identification and Classification of Chromosomal Aberrations in Human Induced Pluripotent Stem Cells. Cell Stem Cell. 2010.:521–531. pp. PubMed PMID: 20887957.
20. Holm F., Nikdin H., Kjartansdottir K. R., Gaudenzi G., Fried K., Aspenstrom P., Hermanson O., Bergstrom-Tengzelius R. Passaging Techniques and ROCK Inhibitor Exert Reversible Effects on Morphology and Pluripotency Marker Gene Expression of Human Embryonic Stem Cell Lines. Stem Cells and Development. 2013. PubMed PMID: 23421967.
21. Chen X., Chen A., Woo T. L., Choo A. B., Reuveny S., Oh S. K. Investigations into the Metabolism of Two-Dimensional Colony and Suspended Microcarrier Cultures of Human Cells in Serum-Free Media. Stem Cells and Development. 2010.:1781–1792. pp. PubMed PMID: 20380517.
22. Horiguchi Y. Urabe, K. Kimura and Y. Sakai, "Effects of glucose, lactate and basic FGF as limiting factors on the expansion of human induced pluripotent stem cells. Journal of Bioscience and Bioengineering. 2018.:111–115. pp. PubMed PMID: 28864123.
23. Rizzino and E. L. Wuebben, "Sox2/Oct4: A delicately balanced partnership in pluripotent stem cells and embryogenesis," Biochimica et Biophysica Acta (BBA) - Gene Regulatory Mechanisms, pp. 780-791, 2016.
24. Trusler O., Huang Z., Goodwin J., Laslett A. L. Cell surface markers for the identification and study of human naivepluripotent stem cells. Stem Cell Research. 2018.:36–43. pp. PubMed PMID: 29227830.
25. Collier J., Panula S. P., Schell J. P., Chovanec P., Reyes A. P., Petropoulos S., Corcoran A. E., Walker R., Douagi I., Lanner F., Rugg-Gunn P. J. Comprehensive Cell Surface Protein Profiling Identifies Specific Markers of Human Naive and Primed Pluripotent States. Cell Stem Cell. 2017.:874–890. pp. PubMed PMID: 28343983.
26. Natunen S., Satomaa T., Pitkanen V., Salo H., Mikkola M., Natunen J., Otonkoski T., Valmu L. The binding specificity of the marker antibodies Tra-1-60 and Tra-1-81 reveals a novel pluripotency-associated type 1 lactosamine epitope. Glycobiology. 2011.:1125–1130. pp. PubMed PMID: 21159783.
27. Sivasubramaniyan K., Harichandan A., Schilback K., Mack A. F., Bedke J., Stenzl A., Kanz L., Niederfellner G., Buhring H.-J. Expression of stage-specific embryonic antigen-4 (SSEA-4) defines spontaneous loss of epithelial phenotype in human solid tumor cells. Glycobiology. 2015.:902–917. pp. PubMed PMID: 25978997.
28. F.-J. Muller, B. Brandl and J. F. Loring, "Assessment of human pluripotent stem cells with PluriTest," StemBook, 2012.
29. Muller F.-J., Schuldt B. M., Williams R., Mason D., Altun G., Papapetrou E. P., Danner S., Goldmann J. E., Herbst A., Schmidt N. O., Aldenhoff J., Laurent L. C., Loring J. F. A bioinformatic assay for pluripotency in human cells. Nature Methods. 2011. PubMed PMID: 21378979.
30. J. Bayani and J. A. Squire, "Traditional Banding of Chromosomes for Cytogenetic Analysis," Current Protocols, 2004.
31. C. M. Moore and R. G. Best, "Chromosome Preparation and Banding," Encyclopedia of Life Sciences, 2001.
32. MacArthur C. D., Pradhan S., Wetton N., Zarrabi A., Dargitz C., Sridharan M., Jackson S., Pickle L., Lakshmipathy U. Generation and comprehensive characterization of induced pluripotent stem cells for translational research. Regenerative Medicine. 2019.:505–524. pp. PubMed PMID: 31115261.
33. Li Y., Ma T. Bioprocessing of Cryopreservation for Large-Scale Banking of Human Pluripotent Stem Cells. BioResearch Open Access. 2012. PubMed PMID: 23515461.

34. Ausubel L. J., Lopez P. M., Couture L. A. "GMP scale-up and banking of pluripotent stem cells for cellular therapy applications.," Human Pluripotent Stem Cells. Methods in Molecular Biology. 2011.
35. Cohen R. I., Thompson M. I., Ehrhardt R. O. Standardized cryopreservation of pluripotent stem cells. Current Protocols in Stem Cell Biology. 2014. PubMed PMID: 24510767.
36. T. L. Riss, R. A. Moravec, A. L. Niles, S. Duellman, H. A. Benink, T. J. Worzella and L. Minor, "Cell Viability Assays," Assay Guidance Manual, 2013.

Authentication of Human and Mouse Cell Lines by Short Tandem Repeat (STR) DNA Genotype Analysis

Jamie L. Almeida[1] and Christopher T. Korch[2,3]

Created: January 17, 2023.

Abstract

The earliest mammalian cell lines, established by Earle et al. in 1943, were derived from the subcutaneous tissue of a C3H mouse strain and many cell lines still used today were derived from the L strain in those early studies [31]. Several years later, HeLa, the first human cell line was established and since then there has been an increase in the use of human and mouse cell lines as models for cell biology, genetics, diseases such as cancer, for the production of viruses and vaccine development, and as tools for synthesizing recombinant proteins for use as therapeutics. Unfortunately, this accelerated use of cell lines and the lack of best practices in tissue culture have led to increases in cellular cross-contamination, which has resulted in spurious results. Now the simple molecular genotyping technique Short Tandem Repeat (STR) DNA genotyping of human and mouse cell lines is available. If applied routinely in cell culture management this technique, in combination with others, can greatly improve the detection of cellular cross-contamination resulting in more reproducible and meaningful research.

This Assay Guidance Manual (AGM) chapter is an extensive update of the 2013 version entitled *Authentication of Human Cell Lines by STR DNA Profiling Analysis* by Yvonne Reid, Douglas Storts, Terry Riss, and Lisa Minor [68]. This new document is targeted primarily at researchers who will need to interpret STR genotyping data generated in their laboratory or received from a core facility or commercial testing laboratory for the authentication of mouse and human cell lines. These testing facilities should consult the ANSI-ATCC ASN-0002 revised in 2021 for more detailed guidelines for evaluation and interpretation of STR data [49].

Introduction

Historical Background of Human STR Genotyping

Ever since 1951 there has been a progressive increase in the use of cultured cells as models, substrates, and tools for both basic research and industrial applications. The rapid growth in areas such as cell biology, genomics, and proteomics has triggered a remarkable increase in cell culture activities, resulting in an increase in the potential risk of cross-contamination of cell cultures, which results in the original cells in the culture being replaced by the contaminating cells.

Interspecies and intraspecies cross-contamination among cultured cell lines is a persistent problem and has occurred at frequencies ranging from 6 to 100% [6, 47, 57, 60]. Detection is particularly difficult if co-cultivated cells express similar phenotypes. At one point, the number of cell lines contaminated with HeLa, a cell line derived from an invasive cervical adenocarcinoma in 1951 [39, 44, 53], represented one-third of all human tumor cell lines developed for research in cancer and cell biology. Stanley Gartler showed in 1967-1968 that 18 extensively used cell lines were all derived from HeLa cells [36, 37]. Currently, at least 209 cell lines in the Cellosaurus database are misidentified and have been shown to be HeLa (A. Bairoch, personal communication

Author Affiliations: 1 National Institute of Standards and Technology, Biosystems and Biomaterials Division, 100 Bureau Drive, Gaithersburg, MD 20899, USA; Email: jamie.almeida@nist.gov. 2 Division of Medical Oncology, University of Colorado Anschutz Medical Campus, Campus Mailstop 8117, 12801 E. 17th Avenue, Aurora, CO 80045, USA; Email: christopher.korch@cuanschutz.edu. 3 Division of Endocrinology, University of Colorado Anschutz Medical Campus, Campus Mailstop 8117, 12801 E. 17th Avenue, Aurora, CO 80045, USA; Email: christopher.korch@cuanschutz.edu.

Corresponding author.

2021) [9, 10, 61, 62]. In 1999, Drexler et al. found that 15% of 117 hematopoietic cell lines received from original investigators or a secondary source were cross-contaminated with other cell lines [27]. From the same cell line repository, MacLeod et al. reported that 18% of a collection of 252 cell lines were misidentified [54]. More recent reports have shown many cross-contaminated cell lines purportedly representing, for example, breast [46] and prostate cancers [71, 78-81], thyroid cancer [72], adenoid cystic carcinoma [66], and esophagus[15]. Reviewing published reports of the identities of 3,630 human cell lines, Korch and Varella-Garcia reported an average of 22.5% or 2 of 9 cell lines were misidentified [47]. Cross-contamination of cell lines has persisted as a result of mishandling and a lack of attention to best practices in tissue culture [11, 42, 47, 82]. As Lewis L. Coriell foresaw in 1962 "Like death and taxes, contamination or the threat of contamination is always with us" [24].

The discovery of DNA hypervariable regions within genomes has made it possible to identify each human cell line derived from a single donor. In 1985 Alec Jeffreys and others [43, 59] demonstrated that hypervariable regions, which consist of variable number tandem repeat (VNTR) units from minisatellite DNA, are distributed throughout the genome and can be used to produce a DNA "fingerprint". These DNA fingerprints are very complex and not easily interpretable. However, subsequent advances in the technology have given rise to the use of Short Tandem Repeats (STR) of microsatellite regions which consist of repeats of core sequences of 1-6 bp ideally located on different chromosomes. The core sequences of these human microsatellite DNAs can serve as hotspots for homologous recombination events which are believed to maintain the variability of these loci [83].

Advances in molecular biology have now made it possible, using STR genotyping (a.k.a. STR DNA profiling), to uniquely identify not only human [7, 27, 49, 54, 58] tissue and cell line samples, but also cell lines derived from African green monkeys [4], dogs [14, 63], rats [17], and mice [3, 5]. In addition, the PCR assays described by Cooper et al. allow the detection of DNA from several commonly cultured mammalian species [23], although to identify the genotype it is necessary to carry out human STR analysis.

Most human cell lines established before 2000 have not been authenticated by comparing their genotypes with those of DNA extracted from tissue samples from which the cell lines were derived, in part because such original samples were not retained. One exception is the melanoma cell line M14, which in 2014 was authenticated by comparing its STR genotype with that of DNA from the patient's serum from 1975 and from a lymphoblastoid cell line derived from the same donor [46]. Because of the high incidence of misidentified cell lines, many researchers are now genotyping samples of the original tissue (e.g., donor blood, tumor cells, xenografts, patient-derived tumor xenografts, FFPE sections) to confirm that the cell lines are derived from the claimed tissue samples [50, 73, 74].

In addition to the STR genotyping, it is important to highlight the other checkpoints for quality cell line management. Mycoplasma frequently contaminate mammalian tissue cultures [28, 30, 55] to the point that in 2014 seven percent of the sequences in the 1000 Genome Project were found to be contaminated with mycoplasma DNA sequences [51] and their presence has previously been shown to affect cell behavior [29]. Therefore, screening for mycoplasma DNA is critical when culturing cells. By combining the above DNA assays, researchers can now not only ascertain whether human cell lines and tissues are derived from a single, specific individual, but also whether their cultures are misidentified or cross-contaminated with the same species or with different mammalian species or mycoplasma. This Assay Guidance Manual (AGM) chapter aims to provide researchers with an understanding of STR analysis of human and mouse cell lines.

NOTE: Please download the pdf version of this chapter for a higher-resolution rendering of these figures.

Principles of PCR Amplification of STR Loci and Identification of PCR Products by Capillary Electrophoresis

Figure 1 outlines a laboratory procedure for authenticating cell lines upon establishment or receipt in a laboratory. Ideally, the STR profiles of cell lines are compared to those of tissue samples at the genome level to

determine whether they are derived from the original donor and therefore can be used to model a specific biological process. Table 1 illustrates how to determine at which stage of handling human cell lines and tissue samples during cell line establishment can become misidentified and by what process this occurred. Unfortunately, this cannot be done for most older cell lines because donor tissue samples have not been retained.

Currently, up to 26 STR loci can be examined. To perform STR genotyping, PCR primers are designed to amplify each selected STR loci so that each of the alleles are distinguishable by size. One primer of each pair is labeled with a fluorescent dye. The range of sizes for each STR locus is determined by number of variants that differ in length. Figure 2 below illustrates this process for human STR locus D7S820. From the length of the PCR amplicons, the number of repeats in an STR locus can be deduced and, if necessary, confirmed by sequencing. Capillary electrophoresis (CE) allows length determination of STR PCR products to an accuracy of approximately 0.5 nucleotide by comparison with an internal size standard (ISS). Furthermore, comparing the STR allele length to an allelic ladder allows for accurate allele call determination based on the actual number of repeats.

In STR genotype analysis, the most commonly used human STR loci consist of tetranucleotide repeats (e.g. GATA), but some kits include a few STR loci that have pentanucleotide repeats (e.g. CATGA). The resulting PCR products usually differ by units of four base pair repeats. The alleles can be simply whole numbers (e.g., with 5, 6, 7, 8, 9, 10, 11, 12 repeats as illustrated in Figure 2). In addition, there are variants with partial repeats due to insertions/deletions which lead to a microvariant (less than a full repeat). For example, $(GATA)_7$ GATA is an 8-repeat allele, and $(GATA)_7$ GATA GA is an 8-repeat allele with an extra 2 bp, which would result in a microvariant repeat of an 8.2 allele. Microvariants that have an additional 1, 2, or 3 bp are indicated by these alleles being designated by a number after a decimal, for example, alleles 8.1, 8.2, and 8.3, respectively. In the case of tetranucleotide repeats, there would not be an 8.4 allele since that would be equivalent to a 9-repeat allele.

The PCR amplifications for different STR loci can be combined, i.e., multiplexed, so that a single PCR can test several STR loci. The amplicon loci size ranges with the same dye label are designed so that they do not overlap with amplicons for other STR loci using the shared dye. The PCRs can be further multiplexed by using different fluorescent dyes. Some current capillary instruments can separate up to eight different dyes spectrographically, which allows a great expansion of the number of loci that can be compared by analyzing 3-5 STR loci per dye.

Figure 3 illustrates this separation of the peaks associated with different fluorescent dyes (top panel) and as seen when deconvoluted in their separate channels (middle four panels). Currently, up to six different dyes are commonly used in a multiplex PCR. As a result, most human STR genotyping kits test 16-26 different STR loci.

The main advantage of genotyping STR loci is that in human populations each locus has many different sequence variants, which is also seen in other mammals. Table 2 (modified from the 2021 revision of the ASN-0002 standard [49]) lists the chromosomal positions, sequence motifs of STR loci, and the number of variants (differentiated by fragment length or sequence) of the 13 STR loci recommended for authentication of human research samples (tissues and cell lines). Unlike single nucleotide polymorphisms (SNPs) with at most four different variants, there are between 19 and 94 different alleles distinguishable by length and up to an additional 57 alleles, which have identical lengths but are distinguishable by their sequence, at these 13 STR loci (see NIST STRBase for detailed information). This enormous variability provides much greater power of distinguishing between individual human samples with only a single 13-locus multiplexed assay than the same number of SNP assays. In summary, the polymorphism or informativeness of these STR markers, which display many variations in the number of the repeating units between alleles and among loci, can be used to distinguish between unrelated cell lines and in some cases variants of the same cell line.

In a normal diploid cell, there are two alleles at a given locus on a chromosome; one allele derived from the mother (M) and the other allele is derived from the father (F). The inheritance of human STR alleles is illustrated in Figure 4. A progeny from these two parents could inherit either two copies of the 9-repeat allele, one from

each parent, and would only show a single peak for the 9-repeat allele, thus being homozygous at the D7S820 locus. Alternatively, as shown in Figure 4, the child inherited the 11-repeat allele from the mother and the 10-repeat allele from the father and thus is heterozygous at this locus.

In contrast to the majority of normal non-germline cells that have two copies of all autosomal chromosomes and all the genes on those chromosomes, cultured cells and tissue samples from tumors, even human pluripotent stem cells (hPSCs) may lose or gain copies of chromosomal segments or even of whole chromosomes [12]. Consequently, populations of cultured cells, which are often passaged (sub-cultured) by small dilutions of a culture, may show loss of heterozygosity (LOH) at diallelic loci due to some cells in the culture having lost an allele. Initially, this may show up by allelic imbalances between the STR alleles with one allele peak being taller than the other (see Figure 5). With time, this imbalance can change to the point that the minor allele is not detected in the culture. Alternatively, the imbalance can be restored to balance or even changed to where the major allele becomes the minor allele as described by Parson et al. [64].

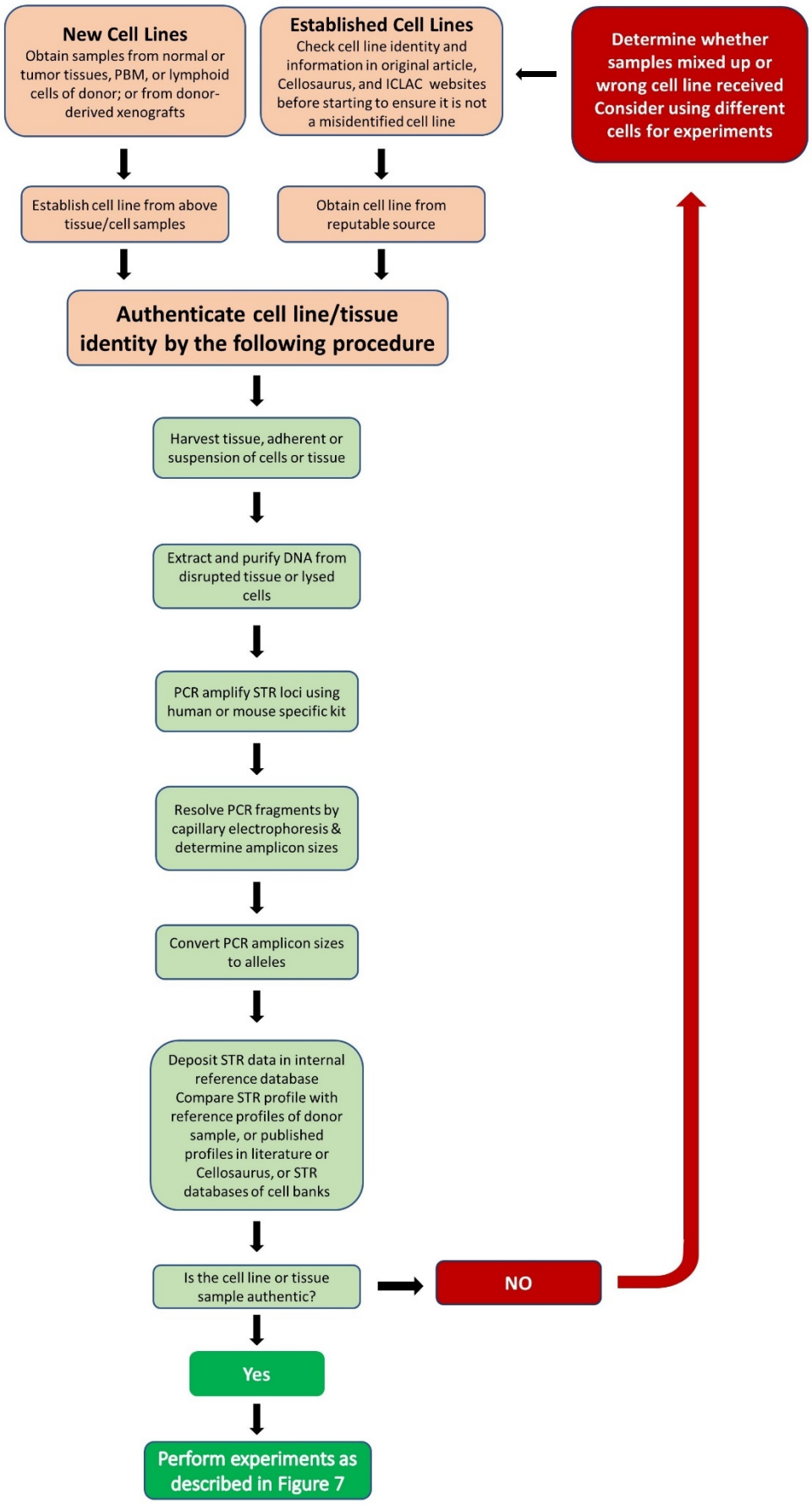


Figure 1. Standard Laboratory Procedure for Establishing Cell Lines. Flow chart of the STR DNA genotype analysis procedure for

establishing and authenticating cell line identities.

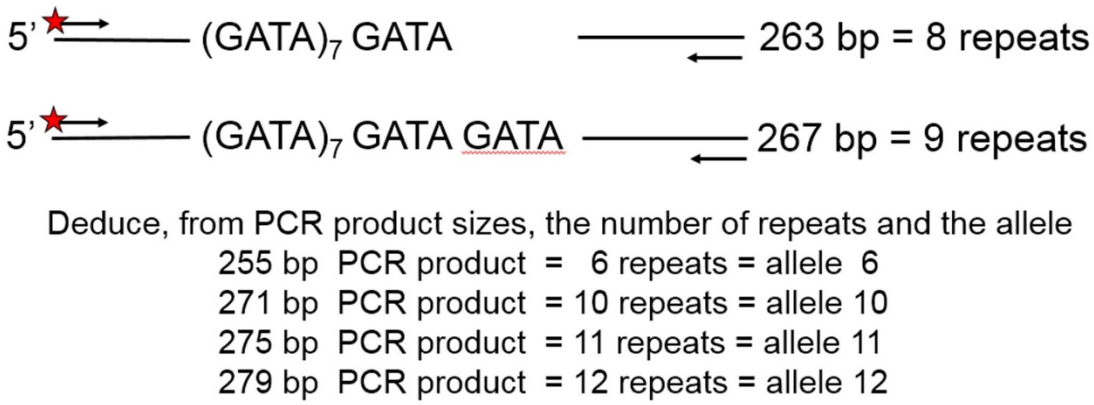


Figure 2. Example of Analysis of STR alleles by Sizing of PCR Amplicons. Determination of alleles by sizing of PCR amplicons of the human STR locus D7S820 on chromosome 7 with different tetranucleotide STR repeat sequences. Allele 8 has 8 repeats, allele 9 has 9 repeats, etc. Modified version from reference [49].

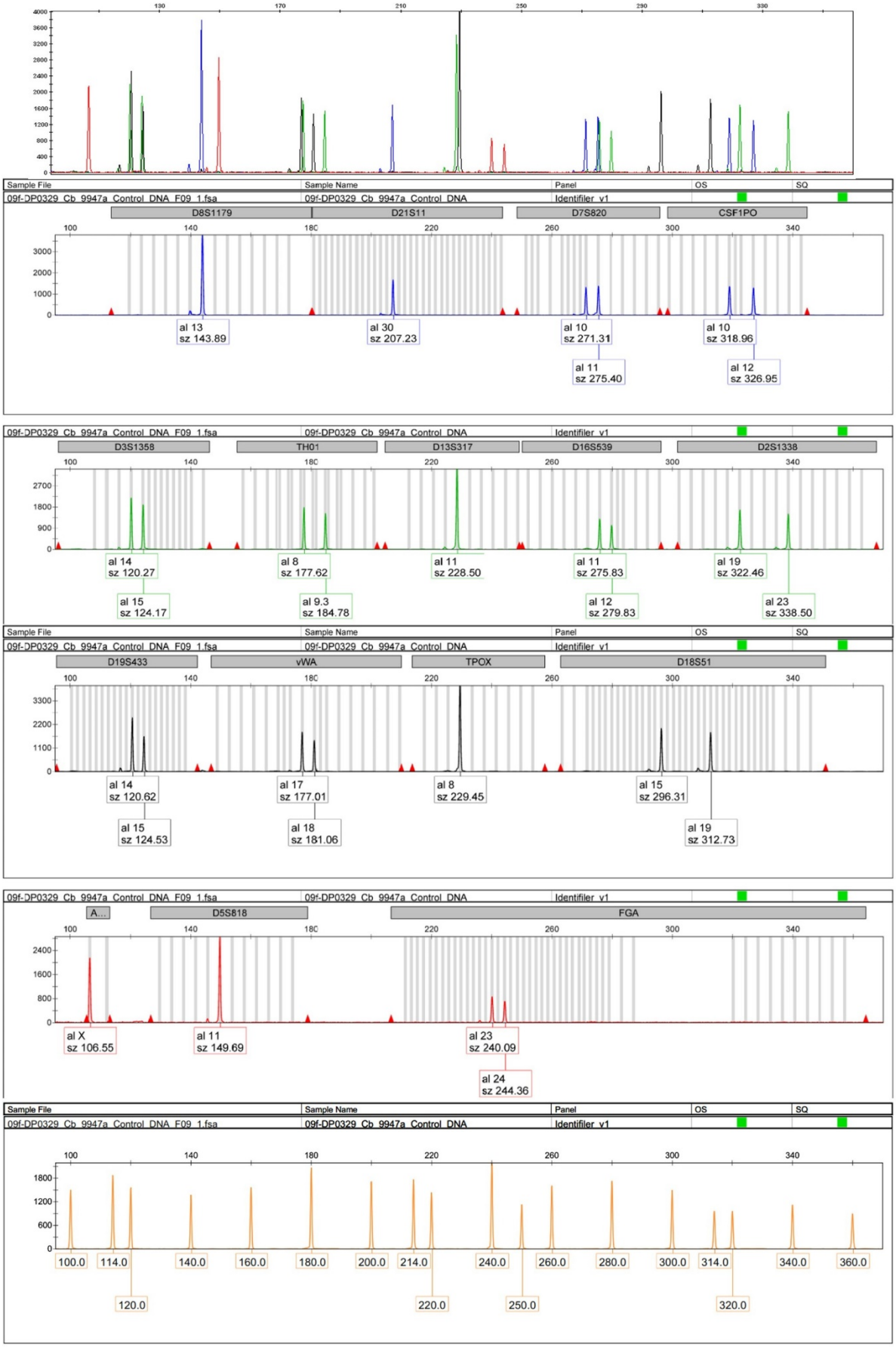


Figure 3. Example of Human STR Profile. Electropherogram of cell line 9947a control DNA using the Thermo Fisher Applied

Biosystems AmpFLSTR Identifiler PCR Amplification Kit (Cat No. 4322288). This figure illustrates how the amplified PCR products tagged with different fluorophores (see top panel) are separated by both their sizes and deconvoluted by the attached fluorophores (next four panels). The last panel is the reference size ladder (not included in top panel). Data courtesy of CTK.

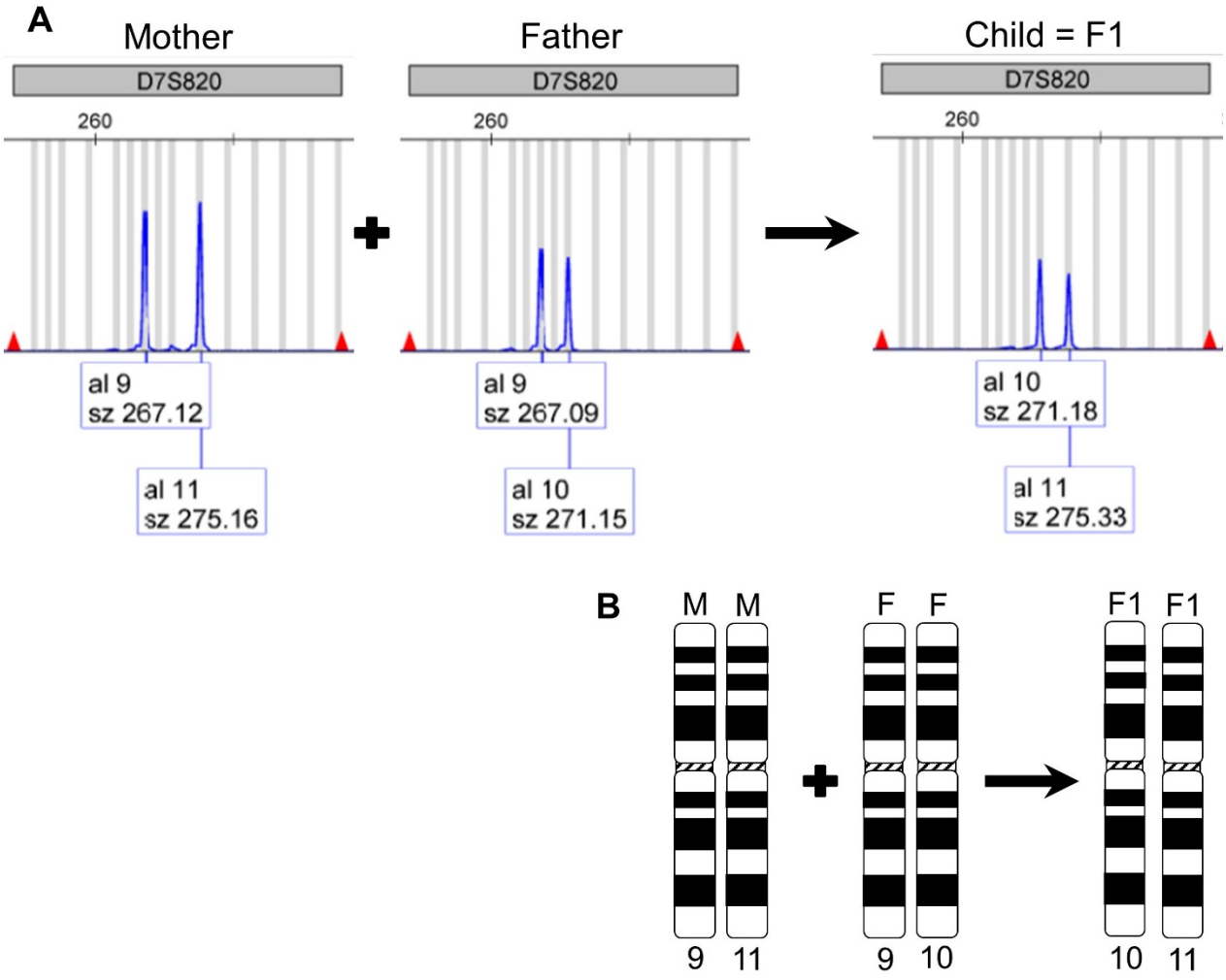


Figure 4. Inheritance of Human STR Alleles. (A) A mother with STR alleles 9 & 11 in D7S820 and a father with STR alleles 9 & 10 in the same locus can have a child (F1) with alleles 10 & 11 in D7S820. Note, the vertical gray bars indicate the positions of known D7S820 alleles as determined by the allelic ladder relative to the ISS. (B) A diagram of the parental and child's chromosomal karyotypes for the D7S820 alleles.

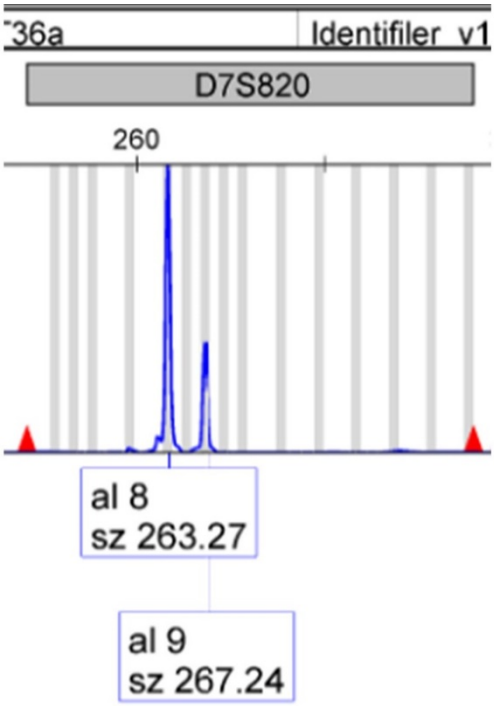


Figure 5. Allelic Imbalance. Cell line sample showing allelic imbalance at the human D7S820 locus. Data courtesy of CTK.

Table 1. Use of STR Profiles to Determine Scenario by which Human Cell Lines and Tissue Samples Become Misidentified *

Scenario	Sample Origin			Cell Line Status
	Donor / Patient	Biopsy / Tumor	Model System Cell Line or Xenograft	
1	**STR Profile A**	**STR Profile A**	**STR Profile A**	**Authenticated**
2	**STR Profile A**	**STR Profile A**	**STR Profile B**	**Misidentified due to cross-contamination or mix-up of cell lines during culturing**
3	**STR Profile A**	**STR Profile B**	**STR Profile B**	**Mis-attributed donor due to biopsy mix-up**

* This table is a modification of one presented in the 2021 revision of the ASN-0002 standard [49].

Table 2. Characteristics of the 13 human reference STR loci used for cell line and tissue authentication*

STR Loci	Chromosome Position	STR Repeat Sequences Simplified	Number of Known Alleles by Length	Additional STR Alleles by Sequence
CSF1PO	5q33.1	[AGRT] $_{5-17}$	29	2
D3S1358	3p21.31	[TCTA] [TCTG]$_{1-4}$ [NN]$_{0-1}$ [TCTA] $_{7-19}$ & 15 microvariants	33	18
D5S818	5q23.2	[ASAT] $_{4-20}$ & 6 microvariants	23	3
D7S820	7q21.11	[GATA] $_{5-16}$ & 21 microvariants	34	1
D8S1179	8q24.13	[TSTR] $_{6-20}$ & 16 microvariants	31	13
D13S317	13q31.1	[TATC] $_{5-17}$ & 8 microvariants	21	6
D16S539	16q24.1	[GATA] $_{4-17}$	29	0
D18S51	18q21.33	[AGAA] $_{8-40}$ [AGAR]n & 41 microvariants	73	5

Table 2. continued from previous page.

STR Loci	Chromosome Position	STR Repeat Sequences Simplified	Number of Known Alleles by Length	Additional STR Alleles by Sequence
D21S11	21q21.1	[TCTR] $_{12-46}$ + intervening bp & 64 microvariants	59	57
FGA	4q31.3	[YTYY] $_{13-51}$ & 66 microvariants	94	8
TH01	11p15.5	[AAYG] $_{3-14}$ & 12 microvariants	24	0
TPOX	2p25.3	[AATG] $_{4-16}$ & 6 microvariants	19	0
vWA	12p13.31	[TCTR] $_{10-25}$	22	24

* This table is a modification of one presented in the 2021 revision of the ASN-0002 standard [49].

Characteristics, Utility, and Advantages of Human STR Markers

STR loci selected for cell line authentication are chosen because they display the greatest possible variations for discriminating among human cell lines with the fewest PCR targets and can readily detect cross-contaminating cells. The criteria for selecting STR loci for human cell line authentication include the following characteristics.

- High discriminating power due to each locus having many alleles
- High observed heterozygosity >70% in human populations
- Robust and reproducible PCR results
- Low stutter characteristics
- Low mutation rate
- Allele sizes of PCR products fall in the range of 90-500 bp, which allows easier genotyping of degraded DNA that often falls in this size range.

Advantages of Identification of Cell Lines and Tissue by STR Genotyping

STR analysis is a universally accepted forensic method for human cell line authentication, because it is robust in its ability to identify unique human cell lines, easy to perform, accessible to scientists, and affordable. Some other advantages of STR analysis include:

- Target sequence consists of microsatellite DNA
- Typically uses 1-2 ng of genomic DNA
- 1 or 2 size fragments; discrete alleles allow digital record of data
- Highly variable within populations, thus highly informative
- Banding pattern is reproducible
- Easily PCR amplifiable allowing for high throughput
- Multiplexing of relatively few PCRs produces highly informative data
- Small amplicon size ranges allow multiplexing
- Allelic ladders simplify interpretation
- Small product sizes (less than 500 bp) are compatible with some degraded DNA samples, such as those extracted from Formalin Fixed Paraffin Embedded (FFPE) samples. Commercially, there are special kits available for very degraded samples that produce DNA fragments shorter than those made with the kits used for general STR genotyping.
- Rapid processing is attainable.

Below in Step 5 - NIST Protocol for Authentication of Mouse Samples by STR Analysis we provide an example of how to use a human STR genotyping kit.

Authentication of Mouse Samples by STR Analysis

Introduction

Authentication of mouse cell lines and tissue samples present a rather unique problem; namely, many mouse strains are inbred to be as isogenic as possible. As a consequence, in contrast to human samples, it is very difficult to differentiate between individual cell lines and tissue samples from these strains since they were often derived from clones of the same individual. A group at the National Institute of Standards and Technology has developed a mouse cell line authentication method using mouse-specific STR loci that allows the identification of many different mouse strains derived from these inbred lines and from non-inbred strains [1-3, 5]. The method was validated by the Mouse Cell Line Authentication Consortium in an interlaboratory study to test 50 commonly used mouse cell lines [3] and individual, unique profiles were obtained from non-related cell lines. This method is licensed and currently available through several cell line authentication service providers.

Mouse STR Markers

A multiplex PCR assay that targets eighteen mouse-specific tetranucleotide STR markers and two human STR markers, for contamination detection, was developed for mouse cell line authentication. The eighteen mouse loci in this assay include 1-1, 1-2, 2-1, 3-2, 4-2, 5-5, 6-4, 6-7, 7-1, 8-1, 11-2, 12-1, 13-1, 15-3, 17-2, 18-3, 19-2, and X-1.

These mouse loci mainly consist of simple tetranucleotide repeats as shown in Table 3; however, there are a few loci that exhibit more complex repeats, such as marker 7-1. In cases like STR 7-1, two samples could present the same fragment length at this marker but have very different sequences. Sequencing is a useful tool when more resolution is needed to discriminate between two samples. In addition to repeat motifs, Table 3 also lists known allele ranges and associated fragment lengths for each STR marker. Note that microvariants are present in the allele ranges and are very common in mouse STR profiles.

Figure 6 presents an electropherogram of an STR of the mouse cell line P19. The two marker regions in gray in the second and third panels are for two human loci (D4S2408, and D8S1106) as described in Step 5, wherein we outline a standardized method for the authentication of mouse cell lines by STR genotyping. This link has detailed information on mouse cell line P19 and a higher resolution image of the electropherogram.

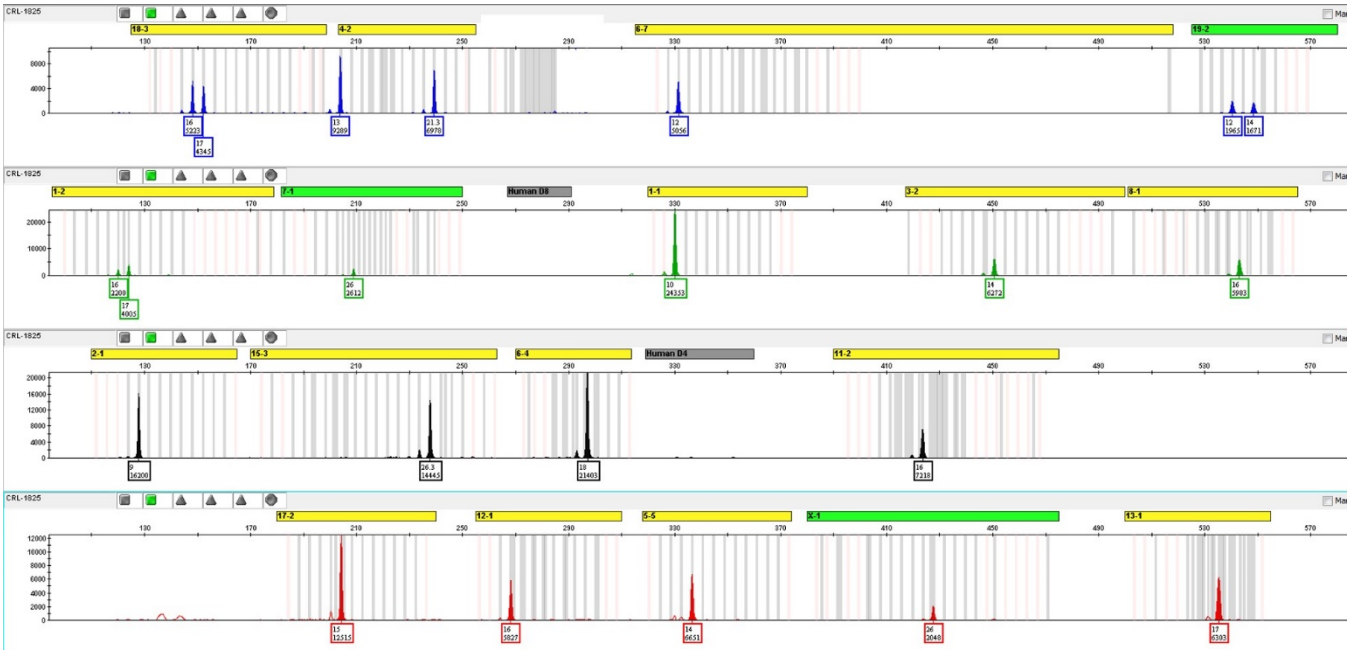


Figure 6. Electropherogram of P19 Mouse Cell Line STR Profile (ATCC# CRL-1825)

Table 3. Characteristics of the 18 Mouse STR Loci [2, 3]

STR Marker	Repeat Motif	Known Allele Range	Fragment Length Range (bp)
1-1	$[ATAC]_n$	10-19	330-366
1-2	$[TAGA]_n[TGAT]_n[AGAT]_n$	12-30.1	104-178
2-1	$[ATAC]_n$	8-17.1	124-162
3-2	$[TATC]_n$	9-25	430-495
4-2	$[GATA]_n[GATG]_n[ATAG]_n$	13-23.3	204-264
5-5	$[TATC]_n$	11-22	324-369
6-4	$[AGAT]_n[GATA]_n$	12.2-21	275-309
6-7	$[CTAT]_n$	11-26	327-388
7-1	$[ATCT]_n[TTAT]_n[N1]_{14}[TC]_n[N2]_6[ATTT]_n$	19.2-33.2	183-239
8-1	$[TATG]_n$	6-19	503-555
11-2	$[ATCT]_n$	12-26.2	407-466
12-1	$[AGAT]_n[GATA]_n$	15-24.1	264-302
13-1	$[TCTA]_n$	11-20.1	511-549
15-3	$[TAGA]_n$	12-31.3	178-258
17-2	$[CTAT]_n$	11-22	188-232
18-3	$[ATCT]_n$	13-28	136-197
19-2	$[CTAT]_n$	10-16	532-557
X-1	$[ATAG]_n[ATGA]_n[TAGA]_n$	15.2-37	385-472

STR DNA genotyping assays for authentication of human and mouse cell line identities and detection of cross-contaminating intraspecies cells

Targeted user group for this AGM chapter on STR analysis

This AGM chapter will outline for researchers how to STR genotype human and mouse DNA samples and how to interpret the test results. A much fuller explanation of STR genotype analysis is presented in the ANSI- ATCC ASN-0002 Standard protocol revised in 2021 [49], which contains many more examples and explanations of various aspects of STR genotype analysis of cell lines. In contrast to this AGM chapter, the ASN-0002-2021 Standard is targeted to both the technical personnel performing the assay and the researcher interpreting the results. The principles and main steps of the STR assays described herein are applicable to the authentication of cell lines by identification using STR genotyping.

STR analysis can be performed in most laboratories that have the capabilities to execute molecular techniques if they have access to a capillary gel electrophoresis instrument and appropriate data collection software (for example through a core laboratory) for data analysis. In most cases however, laboratories submit DNA samples or even cell line cultures to core facilities or commercial DNA testing laboratories for testing, which send the results back to the researcher. Different levels of analyses of the data are often offered as an additional service.

It can be useful for the research labs to learn how to interpret the data themselves so they can understand the significance and reliability of the data. This understanding is a principal goal of this AGM chapter. Therefore, if the labs choose to perform the STR assays in-house or to receive the raw STR data, the genotypes can be determined either with commercially available software or with the free NCBI software package OSIRIS. This procedure is an easy, low cost, and reliable method for the authentication of human and mouse cell lines using the commercially available kits and/or services.

DISCLAIMER

Certain commercial equipment, instruments, or materials (or suppliers, or software, etc.) are identified in this AGM chapter to foster understanding. Such identification does not imply recommendation or endorsement by the National Institute of Standards and Technology, the authors, or the National Center for Advancing Translational Sciences (NCATS). Also, it does not imply that the materials or equipment identified are necessarily the best available for the purpose. Below we use a Promega STR genotyping kit and software packages from different vendors only to exemplify the STR procedure, but we do not advocate the use of any one product over another. Refer to the manufacturers' manuals for detailed instructions on using the specific kits and instruments that are available.

Outline of STR Genotyping Assay Steps

STR genotyping encompasses seven of the nine following laboratory steps depending on the whether the samples are of human (Steps 1-4 & 7-8) or mouse (Steps 1-2, 5-8) origin.

1. Collection of human or mouse samples of cell line cultures, tissue samples (e.g., from related fresh or frozen tumor samples, FFPE sections, xenografts, peripheral blood mononuclear cells, serum) for DNA extraction;
2. DNA extraction, purification, and quantification from one or more of the above samples;
3. Choosing a kit for the authentication of human DNA samples;

4. Multiplex PCR amplification of human STR loci, usually in a single reaction for each DNA sample. Included are both a negative control PCR without DNA and a PCR with DNA from a reference sample with known alleles;
5. Choosing a kit for the authentication of mouse DNA samples;
6. Multiplex PCR amplification of mouse STR loci, usually in a single reaction for each DNA sample. Included are both a negative control PCR without DNA and a PCR with DNA from a reference sample with known alleles;
7. Capillary gel electrophoresis (CE) to separate the different STR amplicons that are tagged with different fluorophores. In the 1990s and early 2000s slab gels were used, but they did not provide as accurate sizing of amplicons that current CE instruments do;

   To each sample a size ladder of fragments with a different fluorophore is added to determine the sizes of allelic amplicons. In addition, an allelic ladder containing amplicons of known allele sizes is electrophoresed with a size ladder in the same experiment in order to identify STR alleles in the test samples;
8. Allele calling software (e.g., Gene Mapper from Applied Biosystems/Thermo Fisher Scientific, Gene Marker from SoftGenetics, or OSIRIS from the National Library of Medicine/National Center for Biotechnology Information) is used to identify the alleles present in each sample and to confirm that no alleles are present in the No DNA control sample, and that the alleles in the reference sample and allelic ladder are called correctly;

After the collection of the STR data, the data are analyzed and interpreted by comparing the allele calls of each of the test samples to reference profiles as described in the Data Analysis and Interpretation section. For example, a cell line profile is compared to STR profiles for the cell line in an STR database (e.g., Cellosaurus, one available from cell line repositories, a published profile by the originator of cell line, an in-house database) or ideally to an STR profile of DNA isolated from a sample of tissue (fresh, frozen, FFPE, xenograft, blood) from which the cell line was established. This allows determination whether the cell line or tissue (e.g., xenograft patient-derived tumor xenograft) sample being used for experiments is from the original donor.

Step 1 - Compiling cell line information and management prior to use

When a cell line is first received into the laboratory it is essential to capture as much information as possible on its history, growth, and functional characteristics, including what is known about its true identity. This information is important for tracking the behavior of a cell line during culturing, its characterization, whether it is appropriate for the experiments, if it is known to be or has been misidentified prior to being received by a laboratory, or a culture of it has become cross-contaminated during the experiments (see Figure 1), and finally for correctly reporting which cell line and/or tissue samples were used for the reported experiments.

Cellosaurus [9, 10] is a rich resource with descriptions for 130,952 cell lines, including 97,714 from humans, 22,740 from mouse, 2,493 from rat, and 863 from dog (version 39, October 2021). The International Cell Line Authentication Committee (ICLAC) is continuously updating its register of misidentified cell lines (mostly human samples, see ICLAC.org/cross-contamination/ and [22]) and this information is incorporated into the Cellosaurus database. Therefore, prior to using any cell line for research, both of these resources should be consulted for the latest information about its identity and characteristics, so as not to waste effort and research funds on using misidentified cell lines. The following information should be compiled from these resources and/or from the original publications:

- Name of cell line
- Cellosaurus ID number if available

- Name of cell line source
- Name of cell line originator
- Date cell line was established
- Reference(s) describing the establishment of the cell line
- Tissue of origin
- Species
- Population doubling levels
- Unique characteristics and function
- Complete growth medium
- Doubling time

After collecting this information, it should be stored in an in-house laboratory database or commercial software package (e.g., the cell line tracking software Find Cell by Find Genomics, [86]) for consultation when troubleshooting abnormal observations or planning to use the cell line or tissue sample for subsequent experiments. Figure 7 outlines a plan and standardized procedures which should be established in-house for managing the cells during expansion and their use for experiments, such as the creation of a Seed stock (Master Cell Bank) and a Distribution stock (Working Cell Bank).

Upon thawing, spot approximately 20 µL of cell suspension containing 1 x 10^6 cells / mL from the donor vial directly onto FTA paper for subsequent STR analysis to establish the baseline STR profile. Alternatively, freeze at -20°C a similar or larger aliquot of cells in a microfuge tube for subsequent DNA extraction and STR analysis. The baseline STR profile from the original donor material should be determined prior to starting experiments and then used to compare against all subsequent STR DNA profiles performed on the various cell banks.

The remaining cells are expanded to create a Seed stock from which a Distribution stock is prepared. Representative vials from both the Seed and Distribution stocks are subjected to another round of STR DNA profile analysis in addition to other quality control procedures. The STR DNA profiles for both Seed and Distribution stocks are compared to the baseline profile of the original donor material.

STR DNA profile analysis involves the simultaneous amplification of STR markers plus a locus for gender determination. The amplicons from the PCR are resolved by capillary electrophoresis and sized using internal size standards (ISS). The sized fragments are then converted into alleles with comparison to the allelic ladders and the assigned alleles are converted to numeric values which are used to create a baseline profile. The baseline DNA profiles are used to create a reference database. All subsequent STR DNA profile analyses performed on the various cell line samples are compared to the baseline profile of that cell line in the reference database. The STR DNA profile should also be compared to profiles of other cell lines in Cellosaurus and any in-house reference database to determine if the results from these quality control tests meet the acceptance criteria between the cell line and its original tissue (or its derivatives).

Step 2 - Extraction, Purification, and Quantification of DNA

DNA for STR genotyping can be extracted from adherent or suspension cultures. The cell suspension is either spotted directly onto FTA paper or may be used for liquid DNA extraction of genomic/total DNA (gDNA). Assuming a commercial DNA extraction kit will be used, follow the manufacturer's instructions. It is recommended to select a kit that eliminates RNA for reliable DNA quantification.

If the DNA extraction procedure uses spin columns, cells can simply be harvested in their growth medium (for adherent cells by first scraping them off the flask or plate surface), by decanting the cell suspension into a 15 or 50 mL sterile polypropylene centrifuge tube, centrifuging the tube to pellet the cells, resuspending the cells in about 1 mL of residual medium, further concentrating the cells into about 25-50µL of residual medium in a 1.7 mL microfuge tube, and proceeding with cell lysis and DNA purification per kit protocol.

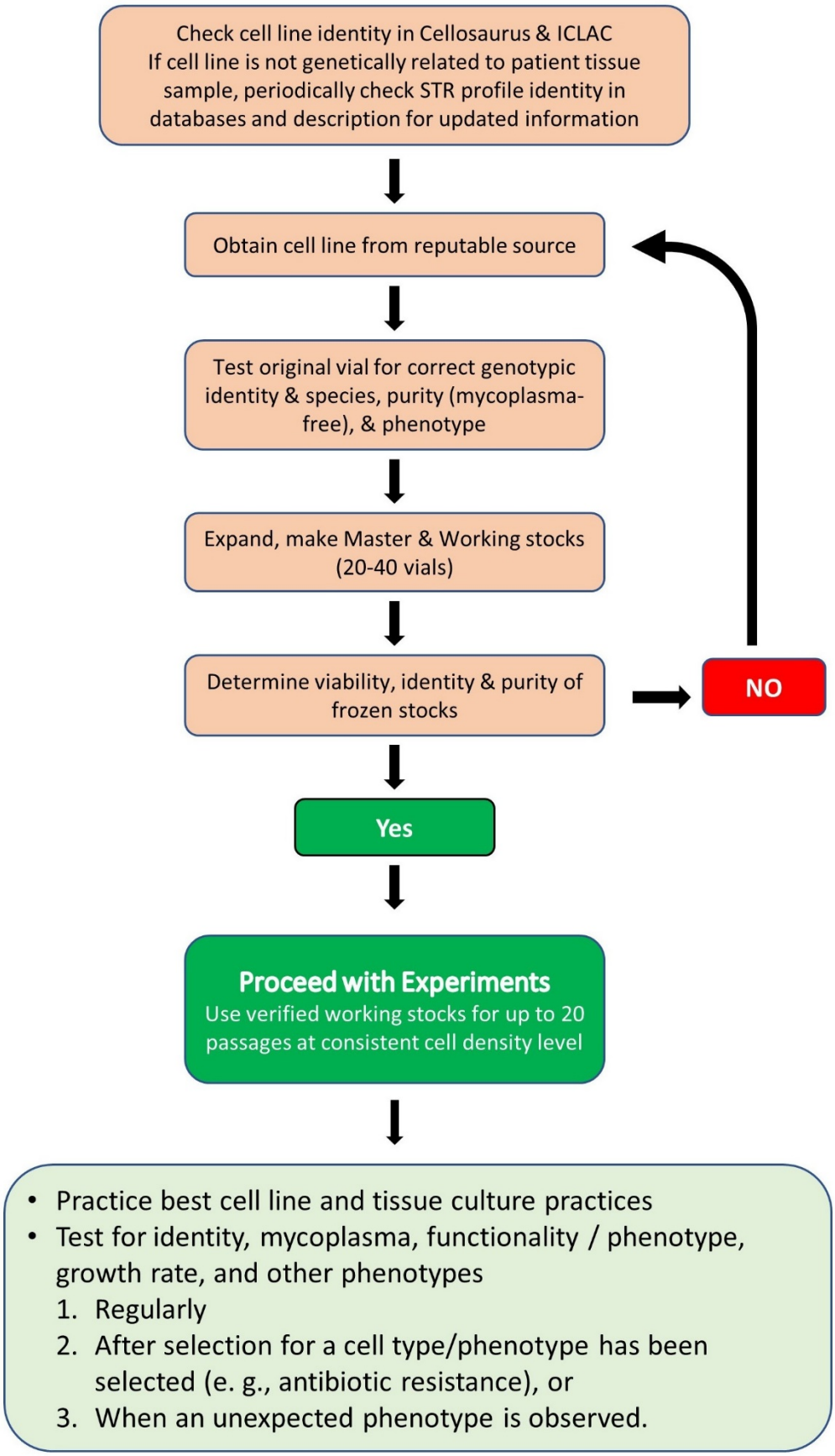


Figure 7. Standard Laboratory Procedure for Handling Cell Lines. Follow this procedure to ensure the use of valid cell lines and tissue

samples by cell line authentication.

For extracting DNA from solid tissue samples (e.g., xenografts or tumor tissue), the tissue sample can be disrupted using a "bead-beating" based method with the appropriate type of beads or granules recommended by the manufacturer of the bead beating instrument. The extraction buffer of the selected gDNA isolation kit can be used for resuspending the tissues before "bead-beating", followed by purifying the DNA using a purification procedure of the gDNA kit that is normally used for cell suspensions. The length of the extracted DNA obtained by bead beating may be about 10 kb in length, which is shorter than that obtained for DNA from cell suspensions (20+ kb).

Estimation of the DNA concentration is critical for uniform amplification of the various PCR amplicons in the multiplex PCR reaction and interpretation of CE data. A DNA-specific fluorescence-based assay is a reliable method for determining DNA concentrations. Absorbance measurements in triplicate at 260 nm for double stranded DNA are commonly used and rely on the 260/280 ratio being approximately 1.8 and the 260/230 ratio being between 2.0 and 2.2. Note that the presence of RNA in the sample can seriously inflate the apparent DNA concentration and may result in using insufficient amounts of DNA and an unsatisfactory result.

If this occurs, check DNA concentrations by agarose gel electrophoresis (see the Troubleshooting section below). Genomic DNA concentrations can be estimated using a 0.75% agarose gel with a nucleic acid stain (e.g., ethidium bromide in the gel and running buffer) along with a DNA mass ladder concentration standard (sample of DNA fragments of known sizes and amounts), preferably one with a broad range of evenly spaced concentrations and sizes. Instead of ethidium bromide, other, more expensive "safe" fluorescent dyes may be used to stain the DNA bands after electrophoresis. This will allow for semi-quantification of the DNA concentration by comparing the fluorescence of the sample band with that of the standard and for the detection of the presence of RNA in the sample, which would interfere with spectrometric quantification of the DNA in the sample. This technique, described in Appendix J of the ASN-0002-2021 standard, can be used to verify microliter spectrophotometric measurements, which may be subject to artifactually elevated readings. The success and amplicon yield of an STR PCR can be evaluated as above using instead a 1.75-2.0% agarose gel (see section below on Troubleshooting of PCR Step).

Note: Isolate DNA with FTA paper using cells harvested in log-phase of growth cycle; when cells are in the exponential growth phase, they are the most viable. A useful protocol is available from Promega.

Note: Use best practices in tissue culture to prevent cross-contamination of cells. When culturing and passaging cells, add a simple step for monitoring and subsequent troubleshooting cell identity questions, it is possible to concentrate an aliquot of unused cell suspensions from passaged cultures in a microfuge tube and freeze it at -20°C. This can be done at a predetermined frequency, e.g., once every or every other week or every predetermined passage. These aliquots offer the possibility of extracting DNA for STR analysis at different time points when one suspects a cross-contamination may have occurred and thus determine when the cell line became cross-contaminated and the results became no longer valid.

Step 3 - Commercially-available Human STR Analysis Kits

Human STR analysis was developed for forensic uses and several STR analysis kits are commercially available from different manufacturers. These are well validated for normal human testing. The most widely available are those from Promega Corporation, Thermo Fisher Scientific/Applied Biosystem, and Qiagen. These and many other kits are listed in the 2021 revision of the ASN-0002 standard [49]. These kits are also used for authentication of human tissues and cell lines, but as discussed below, cell lines present some unique differences that are not encountered with normal tissue samples.

For the authentication of cell lines, the 2021 revision of the ASN-0002 standard [49] recommends the testing of a common gender determining locus (amelogenin) and the following 13 STR loci as a minimum number needed for the identification of cell lines and tissue samples:

- Amelogenin (gender determination gene on the short arms of the X and Y chromosomes, with the X-linked allele being 6 base pairs shorter than the Y-linked allele), and
- The following STR loci: CSF1PO, D3S1358, D5S818, D7S820, D8S1179, D13S317, D16S539, D18S51, D21S11, FGA, TH01, TPOX, and vWA, which are dispersed on different human chromosomes.

For determining the gender of the human tissue donor, the amelogenin is the most commonly used gene. Copies of this gene are present on both the X and the Y chromosomes. *AMELX* is located in the Xp22.1-Xp22.3 region and *AMELY* is in the Yp 11.2 region. In intron 3 of *AMELX,* there is a 6 bp deletion of AAAGTG, while in *AMELY* these 6 bp are present. Primers have been designed to co-amplify this region from both chromosomes and by PCR two products are produced that differ by 6 bp. A normal germline DNA sample from a female will produce only the shorter product from the two X chromosomes; while PCR of a germline DNA sample from a normal male will produce two amplicons that differ by 6 bp, one from the X chromosome and one from the Y chromosome.

As discussed extensively in the ASN-0002 2021 revision [49], males can infrequently lose this portion of the Y chromosome (6 of 29,432) and as a consequence appear by this amelogenin PCR test to be genetically female although they are not infertile. On comparing a large collection of cell lines, Liang-Chu reported finding that about 45% of cell lines reportedly derived from males did not have the *AMELY* allele [52]. Unfortunately, the identities of most older cell lines have not been confirmed by STR or other genetic analyses to be from the purported donor, so the true identities of these *AMELY*-minus cell lines cannot be validated. As a consequence, although this locus is useful to identify a cell line as being derived from a male donor, the absence of the *AMELY* allele does not prove that the cell line was derived from a female. An example of this is the cell line M14, which is derived from a melanoma on a male patient. This cell line was thought to be from a female (and called MDA-MB-435 or more correctly MDA-MB-435S), since it did not have an *AMELY* allele and had two X chromosomes. However, it has been clearly shown that despite being extensively used as a model of female breast cancer, it was actually from a male donor and a large part of the Y chromosome (including the *AMELY* locus and the centromere) had been lost [46] and the X chromosome had been duplicated. To partially address such genetic changes, some newer STR kits have added other Y-linked loci to their STR kits and some forensic STR kits are designed specifically to test for different segments of the Y chromosome (e.g., AGCU ScienTech Inc. AGCU Expressmarker 16+18Y STR kit with 18 Y-STR loci or the Promega VersaPlex 27PY System with three Y-STR loci, or Applied Biosystems Yfiler Plus PCR Amplification Kit with 27 STR loci).

Step 4 - Authentication Protocol for Human Samples by STR Analysis

This technology is capable of discriminating between two human cell lines originating from different individuals, with random probabilities of identity (POI) ranging between 1×10^{-15} and 3×10^{-15} (see Chapter 10 in reference [19] for calculation method).

As mentioned above, different kits from various suppliers can be used with assorted markers for the analysis of STRs of purified DNA. A commonly used kit is the Powerflex 18D (Cat. No. DC1802) from Promega Corporation. Using the DNA isolated as described above, this kit allows co-amplification and four-color fluorescent detection of eighteen loci; namely, amelogenin, CSF1PO, D3S1358, D5S818, D7S820, D8S1179, D13S317, D16S539, D18S51, D21S11, FGA, TH01, TPOX, vWA plus four additional loci: D2S1338, D19S433, Penta D, and Penta E. A fifth fluorescent dye is used for the size ladder. The system is optimized for analysis of common laboratory cell suspension samples and other samples as outlined above from almost any source of human DNA. Ideally, the isolated gDNA should consist of fragments greater than 1 kb in length. Genomic DNA from FFPE samples is often shorter than this minimum and may require modification of the protocols below. As

mentioned previously, other STR genotyping kits are available such as the AmpFLSTR Identifiler kit from Thermo Fisher Scientific/Applied Biosystems that tests for all loci above, except Penta D and Penta E (STR profile shown in Figure 3).

The PowerPlex 18D System is compatible with the ABI PRISM 3100 and 3100-Avant and Applied Biosystems 3130, 3130xl, 3500, 3500xL, 3730, 3730XL, SeqStudio, and Promega's Spectrum Compact CE System Genetic Analyzers. For specific and detailed protocols, refer to the user manuals available from the kit and instrument manufacturers.

Materials

- GeneAmp PCR System 9700 thermal cycler (Applied Biosystems) or equivalent.
- MicroAmp optical 96-well reaction plate (Applied Biosystems) or equivalent.
- Microcentrifuge with rotor(s) specific for 1.7 mL and 0.2 mL tubes and for 96-well plates.
- Aerosol-resistant pipet tips.
- Microfuge tubes 1.5 mL with frosted caps and 0.2 mL PCR tubes with domed caps (or equivalent). Note that if left in the original plastic bags they are usually sufficiently clean to avoid contamination of samples by DNA. Handle with clean forceps and gloves.
- NOTE - Do not autoclave the plastic ware as the heat can deform tubes and contaminate the plastic.
- 1.2 mm Micro-Punch and cutting mat.

Table 4A and Table 4B provide a listing of the pre- and post-amplification components and long-term storage instruction for the human STR profiling kit PowerPlex 18D System.

Table 4A. Human PowerPlex 18D System Pre-amplification Components and Storage

Pre-amplification components*	Volumes provided	Long-term storage temperature
PowerPlex D 5X master mix containing buffer and the hotstart DNA polymerase	1 mL	Store at -30 °C to -10 °C
PowerPlex 18D 5X primer pair mix	1 mL	Store at -30 °C to -10 °C; light sensitive, store in dark
2800M control DNA, 10 ng/µL	25 µL	2 °C to 10 °C
Water, amplification grade	5 x 1,250 µL	Room temperature (18 °C to 22 °C)

* Recommend that the pre-amplification and post-amplification reagents and equipment are stored and used in different laboratory locations. Use different pipettors, aerosol-absorbing pipette filter tips, and racks at these two locations. To prevent contamination of the kit reagents, do not use the same pipettors for the reagents that is used to pipette aliquots of the DNA solution.

Table 4B. Human PowerPlex 18D System Post-amplification Components and Storage

Post-amplification components*	Volumes provided	Long-term storage temperature
PowerPlex 18D allelic ladder mix	100 µL	Store at -30 °C to -10 °C; light sensitive, store in dark
CC5 internal lane standard 500	2 x 300 µL	Store at -30 °C to -10 °C; light sensitive, store in dark
Note: The matrix standard required for the initial setup of the color separation matrix is not a component of kit above.		

Table 4B. continued from previous page.

Post-amplification components*	Volumes provided	Long-term storage temperature
PowerPlex 5-Dye Matrix standard 3100/3130		Suitable for genetic analyzers: ABI PRISM 3100, 3100-Avant Genetic Analyzers, Applied Biosystems 3130, 3130xl, 3500, 3500xL, 3730, 3730XL, SeqStudio, and the Promega Spectrum Compact CE System

* Recommend that the pre-amplification and post-amplification reagents and equipment are stored and used in different laboratory locations. Use different pipettors, aerosol-absorbing pipette filter tips, and racks at these two locations. To prevent contamination of the kit reagents, do not use the same pipettors for the reagents that is used to pipette aliquots of the DNA solution. Available separately, the proper panel and bins text files for the use with GeneMapper ID software is available for download at: www.promega.com/geneticidtools/panels_bins/

Amplification setup

1. Completely thaw and vortex the PowerPlex D 5X Master Mix and PowerPlex 18D 5X Primer Pair Mix.
2. Determine the number of reactions needed. Note: Include negative and positive controls and add enough for an additional 1 or 2 reactions to compensate for pipetting errors.
3. For reaction assembly, label a clean 0.2 mL MicroAmp plate or individual 0.2 mL PCR tubes with domed caps (or equivalent) for each reaction.
4. Vortex the PCR amplification master mix and the primer mix for 10 seconds.
5. Depending on the type of DNA, add reagents in the order listed in Table 5A for FTA samples or Table 5B for DNA purified from tissue or cell lines to each sterile tube or well.
6. Add either 25 µL PCR amplification mix to each of the reaction tubes containing FTA disks (Table 5A) or combine 1 ng of purified DNA up to a maximum volume of 15 µL with the individual mixtures in Table 5B.
7. For the positive amplification control:
    a. Vortex the tube of 2800M Control DNA.
    b. Dilute 2800 M Control DNA to a concentration of 5 ng/µL.
    c. Pipet 1 µL of diluted Control DNA into reaction well or tube containing 25 µL of PCR amplification mix.
    d. For the negative amplification control use either a reaction well or tube containing 25 µL amplification mix without DNA or a reaction well containing 25 µL amplification mix with an FTA disk without DNA.
8. Seal the plate or individual tubes and briefly centrifuge the plate/tubes to bring the disks to the bottom of the wells.

Note 1: The number of cells spotted onto the FTA card and the amount of Control DNA used to obtain positive results must be empirically predetermined.

Note 2: Ensure that the cells are uniformly suspended with no clumps of cells present prior to applying to the FTA card, otherwise different punches of the same FTA card can produce variable profiles.

Note 3: Individual 0.2 mL PCR tubes with domed caps (or equivalent) are less wasteful than 96-well plates when only a few reactions are to be performed and their use can reduce the chances of sample contamination.

Table 5A. Human PCR Amplification Setup Reaction Volumes for Samples on FTA® Cards

PCR Amplification Mix Components	Volume per reaction	X	Number of reactions	=	Final volume
Water, amplification grade	Up to 15 µL	×		=	

Table 5A. continued from previous page.

PCR Amplification Mix Components	Volume per reaction	X	Number of reactions	=	Final volume
PowerPlex D 5X Master Mix (see above)	5 µL	×		=	
PowerPlex 18D 5X Primer Pair mix	5 µL	×		=	
Total Reaction Volume	**25 µL**	×		=	

* Recommend that the pre-amplification and post-amplification reagents and equipment are stored and used in different laboratory locations. Use different pipettors, aerosol-absorbing pipette filter tips, and racks at these two locations. To prevent contamination of the kit reagents, do not use the same pipettors for the reagents that is used to pipette aliquots of the DNA solution.

Table 5B. Human PCR Amplification Setup Reaction Volumes Using Samples of Purified DNA

PCR Amplification Mix Components	Volume per reaction	x	Number of reactions	=	Final volume
PowerPlex D 5X Master Mix (see above)	5 µL	×		=	
PowerPlex 18D 5X Primer Pair mix	5 µL	×		=	
Water, amplification grade	Up to final volume	×		=	
DNA solution (1 ng)	Up to 15 µL	**x**		=	
Total Reaction Volume	**25 µL**	×		=	

* Recommend that the pre-amplification and post-amplification reagents and equipment are stored and used in different laboratory locations. Use different pipettors, aerosol-absorbing pipette filter tips, and racks at these two locations. To prevent contamination of the kit reagents, do not use the same pipettors for the reagents that is used to pipette aliquots of the DNA solution.

Thermal cycling

1. Place the MicroAmp plate or individual tubes in the thermal cycler.
2. Select and run the recommended protocol provided in Table 6.
3. Store amplified samples at 4°C or freeze after completion of the thermal cycling protocol.
4. Optimize the cycle number and injection conditions of the protocol based on the kits and instruments used, starting from the conditions recommended by the manufacturers of the kits and instruments. Also, be aware that some thermal cyclers have variable ramp speeds and this can affect the yield and quality of the PCR products.

NOTES

The temperatures of these steps and the number of recommended cycles may vary between different kits from different manufacturers.

The duration of Step 4 is used to drive the complete addition of an Adenine (A) nucleotide by the terminal transferase activity of the DNA polymerase to the 3' end of the PCR amplicons. The addition of this terminal A will depend on the kit and DNA polymerase used and the amount of DNA in the PCR. Excessive DNA can cause incomplete A addition. The optimal time for Step 4 should be validated for the kit being used to minimize the presence of N-1 bp products. Many laboratories use 40-60 minutes for this step.

Table 6. Example of Thermal Cycling Protocol

Steps	Temperature	Duration	Cycles
1	96 °C	2 min	1 cycle
2	94 °C	10 sec	27 cycles
3	60 °C	1 min	
4	60 °C	20 minutes	1 cycle
5	4 °C	Final hold up to 24 hours. Analyze thereafter or freeze at -20°C for longer storage.	

Step 5 - NIST Protocol for Authentication of Mouse Samples by STR Analysis

In addition to the mouse STR loci described above, two human STR markers, D4S2408 and D8S1106 (Table 7), which were previously described to identify both human and African green monkey DNA [4, 41] are included in the NIST STR genotyping method for mouse samples to check for the presence of human DNA in the samples. The mouse-specific primers target STR markers found on 16 different chromosomes, with redundancy at chromosomes 1 (>164 Mb apart) and 6 (>90 Mb apart). In humans, alleles greater than 50 Mb apart are considered unlinked [18]. The forward primers are labeled at the 5' end with one of the following fluorescent dyes: 6-FAM, VIC, NED, or PET dye (Table 7).

To promote complete adenylation and reduce troublesome artifacts during data analysis, a guanine base (G) or a "PIGtail" sequence (note the underlined sequence GTTTCTT of the reverse primers, Table 7) was added to the 5' end of the unlabeled reverse primer [16]. Highly purified primers should be ordered (e.g., HPLC-purified) to reduce the artifacts produced during capillary electrophoresis (e. g., dye blobs). Using 100 µM primer stock solutions, prepare the multiplex primer mixture by adding to a single tube containing 20.5 µL of TE (10 mM Tris-HCl pH8.0, 1 mM EDTA) the amounts of the forward and reverse primers for each STR marker indicated in Table 8.

Qiagen Type-It Microsatellite PCR Kit (Cat. No. 206243) was used in the interlaboratory study to validate this method [3]. The internal lane size standard, GeneScan LIZ 600 v2.0 (Thermo Fisher Scientific Cat. No. 4408399) was used to assign fragment length to amplicons and the calibrants, used in lieu of a mouse allelic ladder, were successfully used for accurate allele call determination. A five-dye matrix standard, DS-33 (Thermo Fisher Cat. No. 4345833) was used to perform spectral calibrations on the Genetic Analyzers prior to running amplified products. The NIST Reference Material 8399 for a Mouse Allelic Ladder will be released soon.

Table 7. Multiplex PCR primers for Mouse Cell Line Authentication [2, 3]

Marker	Species	Chromosome Location	Forward Primer (5'-3')	Reverse Primer (5'-3')
1-1	mouse	Chr 1, NC_000067.7: 169186184-169186538	[VIC]-CCCTTCACTCCTTCATTCCA	GTTTCTTTGAGCCTAAGGACCTGGACA
1-2	mouse	Chr 1, NC_000067.7: 4359489-4359820	[VIC]-TCTTTAAAAATCAAACAGGCAAA	GTTTCTTGGGGAGGTTGGGGTGTATAA
2-1	mouse	Chr 2, NC_000068.8: 123931409-123931564	[NED]-ACAACTTCAAACTTTGCTGGAA	GTTTCTTTCCTGCTTAGCTTGTCATTTCC
3-2	mouse	Chr 3, NC_000069.7: 3583578-3584020	[VIC]-TGAGCTACCATGTGGGTACA	GTTTCTTCACACACACACACAAAGATGGA
4-2	mouse	Chr 4, NC_000070.7: 81986558-81986794	[6FAM]-AAGCTTCTCTGGCCATTTGA	GTTCATAAACTTCAAGCAATGACA

Table 7. continued from previous page.

Marker	Species	Chromosome Location	Forward Primer (5'-3')	Reverse Primer (5'-3')
5-5	mouse	Chr 5: NC_000071.7: 112789408 -112789749	[PET]-CGTTTTACCTGGCTGACACA	GTTTCTTTGGTTTAAAACTCAATACCAAACAA
6-4	mouse	Chr 6, NC_000072.7: 141967700-141967993	[NED]-TTTGCAACAGCTCAGTTTCC	GTTTCTTAATCGCTGGCAGATCTTAGG
6-7	mouse	Chr 6, NC_000072.7: 51578323-51578669	[6FAM]-AGTCCACCCAGTGCATTCTC	GTTTCTTCATGTGGCTGGTATGCTGTT
7-1	mouse	Chr 7, NC_000073.7: 3459093-3459299	[VIC]-ACACCAGTTGGGGACTAGGA	GTTTCTTAACTGGTGCTGGGTCTGAAC
8-1	mouse	Chr 8, NC_000074.7: 4343688-4344225	[VIC]-AGTAATATCCTGGTCCTGGCC	GTTTCTTGAGCTCACTATGTAGCTATTGGA
11-2	mouse	Chr 11, NC_000077.7: 3268934-3269352	[NED]-AAGGCAGGGGAATTCACAGT	GTTTCTTTCTCACCATTGCAGTCCTGA
12-1	mouse	Chr 12, NC_000078.7: 38530945-38531211	[PET]-TTTCAAAATTGTCATTGAACACA	GTTTCTTTGGTCCTTCAGTATCATCCTTG
13-1	mouse	Chr 13, NC_000079.7: 3707170-3707698	[PET]-AACTCCCACTGCTTCTTGGT	GTTTCTTGCCAAAGTAAACCCTTCTCCC
15-3	mouse	Chr 15, NC_000081.7: 4959715-4959932	[NED]-TCTGGGCGTGTCTGTCATAA	GTTTCTTAGGCTATCTAAACTTGACATGCT
17-2	mouse	Chr 17, NC_000083.7: 5104174-5104375	[PET]-CTCTTCTCCATCCGTCCATC	GTTTCTTATGGCTCTTGCCACAAATCT
18-3	mouse	Chr 18, NC_000084.7: 63244973-63245122	[6FAM]-TCTTTCTCCTTTTGTGTCATGC	GTTTCTTGCTAAATAACTAAGCAAGTGAACAGA
19-2	mouse	Chr 19, NC_000085.7: 4110814-4111352	[6FAM]-AGGCTAGCACTGTTCCTTGT	GTTTCTTACTCAGCACCTTCCATCCTG
X-1	mouse	Chr X, NC_000086.8: 110003461-110003885	[PET]-AACAAAAATGTCCCTCAATGC	GTTTCTTAAGGTATATATCAAGATGGCATTATCA
D4S2408	human	Chr 4, NC_000004.12: 31302712-31303035	[NED]-TCATTTCCATAGGGTAAGTGAAAA	GTTTCTTGCCATGGGGATAAAATCAGA
D8S1106	human	Chr 8, NC_000008.11: 12978351-12978648	[VIC]-TCTGCTGATTGTGCCCATTG	GTTTCTTATTGGCTGGTTAGTGACACA

Table 8. Preparation of Mouse Multiplex Primer Mixture (100 µL total volume). Scale up as necessary

STR Marker	Final Primer Concentration in 25 µL PCR reaction (nM)	Volume of 100 µM Forward primer (µL)	Volume of 100 µM Reverse primer (µL)
1-1	150	1.5	1.5
1-2	225	2.25	2.25
2-1	125	1.25	1.25
3-2	200	2	2
4-2	200	2	2
5-5	250	2.5	2.5
6-4	200	2	2

Table 8. continued from previous page.

STR Marker	Final Primer Concentration in 25 µL PCR reaction (nM)	Volume of 100 µM Forward primer (µL)	Volume of 100 µM Reverse primer (µL)
6-7	200	2	2
7-1	200	2	2
8-1	200	2	2
11-2	200	2	2
12-1	200	2	2
13-1	250	2.5	2.5
15-3	100	1	1
17-2	200	2	2
18-3	150	1.5	1.5
19-2	200	2	2
X-1	275	2.75	2.75
D4S2408	250	2.5	2.5
D8S1106	200	2	2
Total volume of primers (µL)		**79.5**	
Volume of TE in µL added to q.s. to 100 µL		**20.5**	

Step 6 - Authentication Protocol for Mouse Samples by STR Analysis

Use the above mixture of primers (Table 8, for additional information see Almeida et al. [2, 3]) for the PCR amplifications of the mouse STR analyses as described below. Table 9 and Table 10 describe the pre- and post-amplification solutions and components and their recommended storage conditions for these STR reactions.

Table 9. Mouse Microsatellite PCR Qiagen Type-It Kit Pre-amplification Components and Storage

Pre-amplification components*	Volumes provided	Long-term storage temperature
Qiagen Type-It Microsatellite PCR 2X master mix containing buffer and the hotstart DNA polymerase	3 x 0.85 mL	Store at -20 °C
Water, amplification grade	2 x 1.9 mL	Room temperature (18 °C to 22 °C)
Mouse primer multiplex mix (see Tables 3, 7, and 8) **	0.1 mL	Store at 4 °C, light sensitive, store in dark

* Recommend that the pre-amplification and post-amplification reagents and equipment are stored and used in different laboratory locations. Use different pipettors, aerosol-absorbing pipette filter tips, and racks at these two locations. To prevent contamination of the kit reagents, do not use the same pipettors for the reagents that is used to pipette aliquots of the DNA solution.
** Not included in the Qiagen Type-It Microsatellite PCR Kit.

Table 10. Mouse PCR Post-amplification Components and Storage

Post-amplification components*	Volumes provided	Long-term storage temperature
NIST mouse allelic ladder (RM 8399)	0.1 mL	Store in aliquots at -20 °C; Light sensitive, store in dark
GeneScan 600 LIZ internal lane size standard v2.0	2 x 0.2 mL	Store at 4 °C; light sensitive, store in dark

Table 10. continued from previous page.

Post-amplification components*	Volumes provided	Long-term storage temperature
DS-33 Matrix Standard Kit (Dye Set G5)	1 tube	Store at 4 °C, protect from light, do not freeze.

* Recommend that the pre-amplification and post-amplification reagents and equipment are stored and used in different laboratory locations. Use different pipettors, aerosol-absorbing pipette filter tips, and racks at these two locations. To prevent contamination of the kit reagents, do not use the same pipettors for the reagents that is used to pipette aliquots of the DNA solution.
Available separately for download are the proper panel and bins text files for the use with GeneMapper and GeneMarker software (https://doi.org/10.1371/journal.pone.0218412.s004).

Amplification setup for mouse STR assay

1. Completely thaw the Master Mix and PCR grade water from the Qiagen Type-It Microsatellite PCR Kit (Cat. No. 206243).
2. Determine the number of reactions needed. Note: Include a negative control, two positive controls (one mouse and one human), and an additional 2 samples for pipetting error (use Table 11 below).
3. Prepare PCR master mix of components detailed in Table 11 and vortex for 10 seconds. Briefly spin down.
4. Aliquot 24 µL of master mix into each 0.2 mL tube or well in 96-well plate, or equivalent.
5. Add 1 µL of quantified mouse DNA at 2 ng/µL to appropriate sample tube/well. For the negative control add 1 µL of water to the reaction. For positive controls add 1 µL of 2 ng/µL of mouse DNA with a known STR profile to one tube and 1 µL of 2 ng/µL of human DNA sample as a contamination control to a separate tube.
6. Mix briefly and spin down sample to the bottom of the tube or plate.

Table 11. Amplification Setup for Mouse PCR Reaction Volumes

PCR Amplification Mix Components	Volume per reaction	×	Number of reactions	=	Final volume
Water, amplification grade	9 µL	×		=	
Type-It Microsatellite PCR Master Mix (2X)	12.5 µL	×		=	
Mouse Multiplex Primer Mix	2.5 µL	×		=	
Total Volume	**24 µL**	×		=	

* Recommend that the pre-amplification and post-amplification reagents and equipment are stored and used in different laboratory locations. Use different pipettors, aerosol-absorbing pipette filter tips, and racks at these two locations. To prevent contamination of the kit reagents, do not use the same pipettors for the reagents that is used to pipette aliquots of the DNA solution.

Thermal cycling

1. Place the 0.2 mL tubes or 96 well plate on the thermal cycler.
2. Select and run the recommended protocol provided in Table 12. Ramp rate should be set to 3.35 °C/sec, if possible. The assay must be validated on the specific thermal cycler being used and the selected ramp rate.
3. Store amplified samples at 4°C after completion of the thermal cycling protocol.

Table 12. Mouse Multiplex PCR Thermal Cycling Protocol

Steps	Temperature	Duration	Cycles
1	95 °C	5 minutes	1 cycle

Table 12. continued from previous page.

Steps	Temperature	Duration	Cycles
2	95 °C	30 seconds	29 cycles
3	59 °C	90 seconds	
4	72 °C	30 seconds	
5	60 °C	90 minutes	1 cycle
6	4-10 °C	Indefinite	Final hold

Step 7 - Detection of Amplified Fragments using Automated Capillary Gel Electrophoresis Instruments

Each forward primer used in these multiplex PCR assays for cell line authentication has a fluorescent dye molecule covalently linked at its 5' end. Multiple sets of primers with different "color" fluorescent labels are used to analyze numerous different loci in a single multiplexed PCR reaction. Following the PCR step, internal size standards and deionized formamide are added to the reaction mixture, heat denatured, centrifuged to remove bubbles, and the DNAs are separated by size via capillary gel electrophoresis.

Several different automated capillary gel electrophoresis instruments can be used, such as Thermo Fisher Scientific / Applied Biosystems 3500, 3500XL, 3730, 3730XL, 3130, 3130XL, SeqStudio Genetic Analyzer, or Promega Spectrum Compact CE or Spectrum CE Systems.

Once the data are collected, the software (such as GeneMapper (versions 4, 5, or 6), GeneMapper ID-X from Thermo Fisher Scientific / Applied Biosystems, OSIRIS from the National Library of Medicine, and GeneMarker from SoftGenetics) is used to size the amplicons based on the internal size standard. STR genotyping of each cell line is performed by converting amplicons size to alleles by comparing to allelic ladders [7, 21, 49]. See Table 13 for a listing of the reagents and equipment that can be used in this assay.

Table 13. Detection of Amplified Fragment

Material	Manufacturer	Catalog Number
Dry heating block or thermal cycler for heat denaturation of PCR amplicons	N/A	N/A
Water bath	N/A	N/A
Ice-water bath or crushed iced	N/A	N/A
Centrifuge compatible with 96-well plates	N/A	N/A
Aerosol-resistant pipet tips	N/A	N/A
36 cm 3500/3500*xL* capillary array or 50 cm capillary array for ABI 3130 or ABI 3730	Life Technologies	4404687
96-well retainer and base set (standard)	Life Technologies	4410228
POP-4 polymer in a pouch for the Applied Biosystems 3500 or 3500*xL* Genetic Analyzer Alternatively, POP-7 polymer (or equivalent) can be used on other Applied Biosystems Genetic Analyzers (e.g., 3130, 3730) with a 50 cm capillary	Life Technologies	4393710
Anode buffer container	Life Technologies	4393927
Cathode buffer container	Life Technologies	4408256
Conditioning reagent pouch for the Applied Biosystems 3500 or 3500xL Genetic Analyzer or equivalent buffer	Life Technologies	4393718
Hi-Di formamide	Life Technologies	4311320

Table 13. continued from previous page.

Material	Manufacturer	Catalog Number
PowerPlex 5-Dye Matrix Standards, 3100/3130	Promega Corporation	DG4700
DS-33 Matrix Standard Kit G5 dye set	Thermo Fisher Scientific	4345833
GeneScan 600 LIZ dye internal size standard	Thermo Fisher Scientific	4408399
Mouse Allelic Ladder (Research Grade Material, soon to be Reference Material)	NIST	RM8399

Sample preparation

1. Preparation of loading cocktail:

   For human STR genotyping, combine and mix the internal size standard (e.g., Promega CC5 Internal Lane Standard 500 with the Promega Powerplex 18D kit or GeneScan 600 LIZ with an Applied Biosystems kit, Figure 8) and Hi-Di formamide as for example:

   (1 µL CC5 ILS 500) × (number of samples) + (10 µL Hi-DiTM formamide) × (number of samples) = amount of loading cocktail

   For mouse STR genotyping, combine and mix 0.5 µL GeneScan 600 LIZ internal size standard with 9.5 µL of Hi-Di formamide for each sample (prepare a master mix of this for all samples).

   Note: the amount of internal lane size standard (ISS) for both human and mouse STR genotyping may need to be adjusted so the ISS peaks are of sufficient signal intensities that their sizes are correctly called, as illustrated in Figure 8 and the bottom panel of Figure 3, and described in more detail in the section Evaluation of Internal Lane Size Standards (ISS) and Allelic Ladders.

2. Vortex loading cocktail (formamide/lane standard mix).
3. Pipet 11 µL of loading cocktail into each well for human samples (10 µL of loading cocktail for mouse).
4. Add 1 µL of amplified sample or negative control to appropriate well. For each injection, add 1µl of PowerPlex 18D Allelic Ladder Mix to a single well for human samples or 1 µL of mouse allelic ladder.
5. Cover wells with appropriate septa.
6. Centrifuge plate(s) briefly to remove bubbles from the wells.
7. Denature samples at 95°C for 3 minutes just prior to loading instrument.
8. Immediately chill plate on crushed ice or an ice-water bath for 3 minutes.

Instrument preparation and use

Detect amplified fragments using one of the capillary gel electrophoresis instruments specified above. Refer to the User Guide for use and care of the instrument and the manufacturer's (e.g., Promega) for a detailed protocol of data analysis.

Step 8 – Allele Calling

To analyze human STR data produced with an STR kit, such as the PowerPlex 18D kit, the GeneMapper ID-X software version 1.2 or later can be used in combination with specific Panel, Bins, and Stutter text files, which can be obtained from www.promega.com/geneticidtools/panels_bins/. This will allow the automatic assignment of human genotypes by the software analysis of the fragment electrophoretic data .fsa files. Alternatively, the calling of the STR alleles can be determined using one of the Applied Biosystems gel electrophoresis instruments (e.g., 3130, 3500, 3730, SeqStudio) or the Promega Spectrum Compact CE System genetic analyzers in

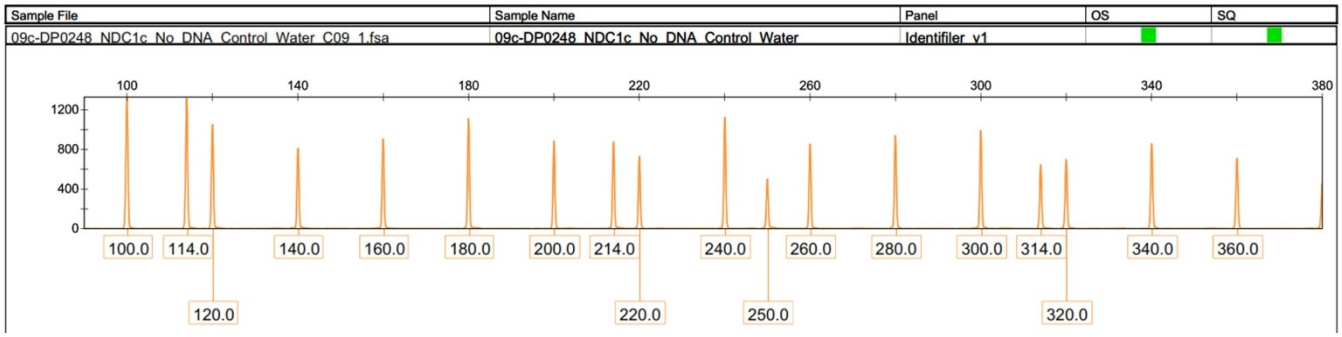


Figure 8. Suitable Internal Size Standard (ISS). This example of an ISS shows peaks of DNA fragments 100 to 360 nucleotides in length from the Applied Biosystems GeneScan 600 LIZ size standard.

combination with one of the following programs: GeneMapper version 5 for Windows 7 or version 6 for Windows 10 from Applied Biosystems, GeneMarker for Windows 7/8/10 from Softgenetics, or OSIRIS from the National Center for Biotechnology Information at the NIH National Library of Medicine (NLM).

Software analysis using GeneMapper, GeneMapper ID-X, and GeneMarker have been previously used in the validation for mouse cell line authentication [3]. Bins and panels for the mouse multiplex assay can be accessed from Almeida et al. [3] in their supplemental section (S4 File), or can be downloaded in a zip file. Using the mouse allelic ladder, align the bins for the associated platform (specific array, polymer, and instrument) prior to data analysis.

Supplemental File 1 illustrates how to adjust allele calling software settings for optimal visualization of STR genotyping data using, for example, GeneMapper 6 Software for human STR kits.

Data Analysis and Interpretation

Interpretation of Human and Mouse Sample STR Genotyping Data

Researchers should compile from their in-house STR genotyping experiment or receive from the STR testing facility the following information: a table in CSV or XLSX format of the STR results for each sample, plus that for the three controls that were run for quality purposes: 1) the allelic ladder, 2) the positive control DNA sample(s), and 3) the No DNA negative control. In addition, they should print out or obtain PDF copies of the electropherograms of the analyzed data of the samples and all the controls so the data can be closely examined. The negative control will show whether the reaction mixture was contaminated with extraneous DNA and how well the analysis software corrects for background noise, the positive control and the allelic ladder (see Figure 8) will show whether the allele calling was correct. If an external facility was used, these controls should be evaluated by them prior to distributing the data to the researcher. Receiving all the data, will allow the researcher to confirm that the results do not show any technical errors or artifacts, such as those mentioned above or below in the Data Analysis and Interpretation and Criteria for Determining Quality STR Profile Analysis for Reliable and Interpretable Results.

Because of the LOH seen in cultured cell lines, unlike reporting of forensic STR data, the cell line STR profiles should only report the actual peaks seen; namely, single peaks in the STR profiles should be reported as single alleles (e.g., 9) and not double alleles (not 9,9 and not X,X for a female). The doubling of alleles, as done in forensic STR analysis, is based on an assumption that the samples are normal diploid cells. However, this doubling can bias (both in favor and against) matching cell line STR profiles and thus confuse the identification of both pure cell line cultures and of mixed cell line cultures. The counting of only the alleles seen is standard

practice as demonstrated not only in the two versions of the ANSI-ATCC STR profiling standard [7, 49], but also it is the procedure done by others [8, 21, 33, 52, 58, 69, 85].

On receipt of the data, the researcher must compare the results with STR profiles of the original sample or those expected for the tested sample. There are several algorithms for comparing two STR profiles. These are discussed in great detail in Chapter 6 and Appendix E of the revised ASN-0002 standard [49]. In 1999, Tanabe et al. [77] modified the Sørensen formula [75] to its presently used format as described by Capes-Davis et al. [21]. Originally, Sørensen divided the number of shared characteristics by the average number of characteristics for the two samples. In the Tanabe version of the formula, the number of shared alleles is instead multiplied by 2, the product of which is divided by the total number alleles in the two samples at shared loci. Loci which were not tested in both samples or loci that gave no alleles ("no-calls") are not included in the calculation of percent match.

$$\text{Tanabe \% Match} = \left[\frac{2 \times (\text{No. of STR alleles shared between Query and Reference Profiles})}{(\text{No. of STR alleles in the Query Profile}) + (\text{No. of STR alleles in the Reference Profile})}\right] \times 100\%$$

In 2001, Masters et al. [58] proposed a simpler formula for calculating a % Match. In this formula, the number of shared alleles at shared loci (neither of which had any no-calls) is divided by the number of alleles in the query at shared loci as shown here.

$$\text{Masters \% Match} = \left[\frac{(\text{No. of STR alleles shared between Query and Reference Profiles})}{(\text{No. of STR alleles in the Query Profile})}\right] \times 100\%$$

Subsequently, Capes-Davis et al. evaluated the use of an alternative version of the Masters et al. In this % Match algorithm the denominator is instead the number of alleles in the reference profiles as shown below.

$$\text{Alt Masters \% Match} = \left[\frac{(\text{No. of STR alleles shared between Query and Reference Profiles})}{(\text{No. of STR alleles in the Reference Profile})}\right] \times 100\%$$

Between 2001 and 2020, alternative algorithms have been proposed as described in Appendix E of ASN-0002 of 2021 [49]. In all of the above algorithms it should be understood that the profile with the fewest alleles limits the percent match. This becomes important where one sample has significantly more alleles than the other sample(s). Cases where this is more likely to occur are when: (a) a mixture of two cell lines is compared to a pure sample of a cell line, (b) one of the samples being compared has undergone extensive loss of heterozygosity (LOH) due to genetic drift as commonly occurs in cancer cell lines, or (c) the cell line shows extra peaks due to being genetically unstable, for example, because it has a defect in the DNA mismatch repair system and manifests microsatellite instability (MSI; see Parson et al. [64]). To deal with these situations it is best to compare samples using all three algorithms. The Cellosaurus website provides these options in their CLASTR cell line comparison tool for human, mouse, and dog STR profiles.

Masters et al. [58] using their original algorithm proposed that a score of 80% or greater would identify human samples with identical or closely related profiles. This threshold value has been often incorrectly interpreted to mean that two cell line samples with ≥80% match are the same or even identical. These comparisons only mean that the samples are most likely related because they were derived from the same donor.

Bady et al. [8] and another group [52, 85] recognized that this cut-off level was insufficient for identifying related human samples when using data from only eight STR loci and recommended using results from a minimum 15 STR loci when comparing samples, preferably with cut-off scores of >90% be used "to be absolutely certain of a match" as stated by Yu et al. [85]. The revised standard ASN-0002 of 2021 recommends that at least 13 human STR loci be used with a match score of <70% indicating two samples are very unlikely to be from the same donor and strongly suggest one of the samples is misidentified. Scores between 70% and 79% for cell lines known to be related could be because some significant genetic drift has occurred (e.g., due to MSI), or that one of the samples is a mixture of two or more cell lines. It may be possible to resolve such a mixture into its component cell lines by using the Alt – Masters % Match algorithm.

After the publication in 2011 of the first version of ANSI-ATCC ASN-0002 standard [7], a score of 80-89% for eight STR loci including the amelogenin locus in the scoring algorithm was used to indicate that two human samples were likely to be from the same donor and a score ≥ 90% indicated that the samples were most likely from the same donor. These scoring criteria have been revised in the 2021 revision of this standard for cell line authentication by STR profiling [49]. Currently, a minimum of thirteen core STR loci is needed to uniquely identify a human cell line. The thirteen loci are: CSF1PO, D3S1358, D5S818, D7S820, D8S1179, D13S317, D16S539, D18S51, D21S11, FGA, TH01, TPOX, vWA. The amelogenin locus is not to be included in the scoring of match, but only to identify potentially misidentified cell lines, for example, those that are purportedly from a female, but which bear an *AMELY* allele.

Cautionary Note

Using the match algorithms described above, a common guideline has been if the human STR profiles have match scores of ≥80% at 13 or more STR loci (not counting the amelogenin loci on the X and Y human sex chromosomes), then the two samples are derived from the same donor. It is important to note that it does not mean that to two samples are identical. The 13 STR loci encompass only a very small portion of the human genome (< 0.0004%) and therefore many changes in the genome from the original sample can have occurred and still the two samples may show a 100% matching STR profiles. For instance, Kleensang et al. reported that two aliquots of the same batch of the breast cancer cell line MCF-7 (obtained from a commercial cell line repository), which differed by only 3 passages and which had identical STR profiles at 8 loci, showed considerable differences in phenotypes [45]. Ben-David et al. expanded this understanding of the genetic drifting process for the same cell line [13]. Therefore, it is important to understand that such scores only indicate that two samples are related by having been derived from the same donor, but that they are not necessarily identical and can have genetically drifted (and therefore phenotypically) significantly from one another and altered their utility as cell line models.

Using CLASTR of Cellosaurus to Find Related Cell Lines

The Cellosaurus database of cell line information for 139,592 cell lines includes (as of August 24, 2022) the STR profiles for 8,159 human cell lines, 78 for mouse cell lines, and 36 for dog cell lines. These profiles can be compared using the CLASTR search algorithm of Robin et al. [69].

Figure 9 shows how human STR data are entered into CLASTR search template. The STR data can be entered manually, directly from the Cellosaurus database, or from a separate spreadsheet file. Three optional algorithms can be used with different filters for cutoff level, number of STR loci, and the number of returns. The result of searching for matches are shown in a table, Figure 10 shows the CLASTR search results for the HeLa-derived human cell line HEp-2 [HeLa] [48] (electropherogram data not shown).

Figure 11 shows the CLASTR search template for mouse STR data and Figure 12 shows the search results using the STR data of the mouse cell line P19 taken from the electropherogram in Figure 6.

Common Features of Cell Line STR Profiles

A unique cell line will have a unique STR profile that is different from that of an unrelated cell line as illustrated in Figure 13.

Figure 14 shows how cell lines derived from different tissues from the same individual have the same STR profile.

However, data interpretations of STR profiles on human and mouse cell lines, especially those derived from tumor tissue, often present certain nuances such as:

- Loss of heterozygosity (LOH), also known as allele drop-out (ADO)
- Peak imbalance

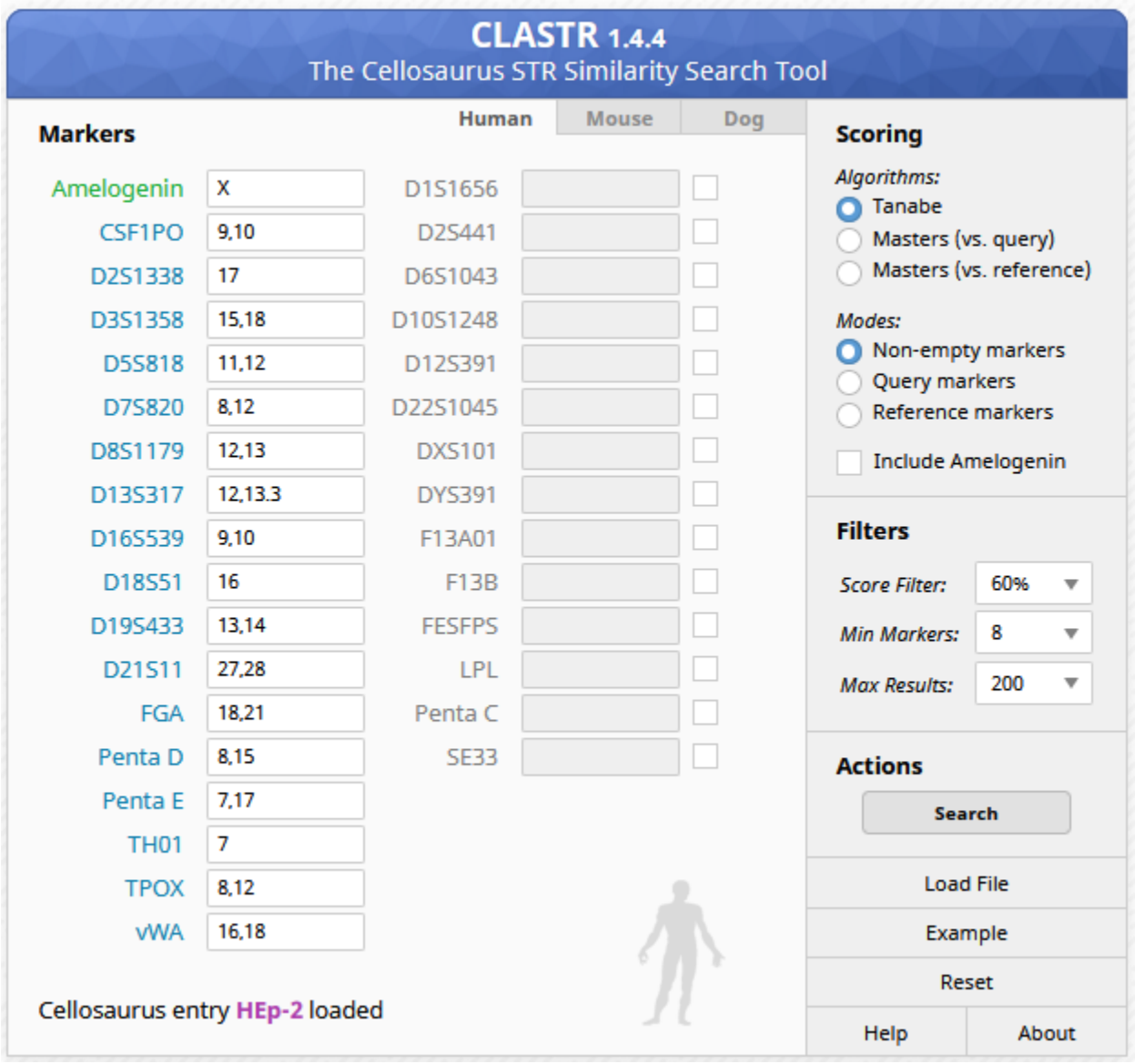


Figure 9. CLASTR Search Tool Input of Human STR Data. Date is for the HeLa-derived cell line HEp-2.

- Novel out-of-range alleles
- Multiple peaks at several loci

Loss of Heterozygosity (LOH)

The incidence of genetic instability in STR markers used to evaluate human cancers is not uncommon [32, 58, 70]. Most human cell lines are derived from a cancer, which differ genetically from normal tissue. Moreover, cell lines are capable of undergoing additional genetic changes while in culture. In a study of 24 lung samples, there were complete deletions of alleles at multiple loci when compared to normal tissue [65]. Figure 14 compares the allelic STR profiles of two samples from the same donor. Several loci show some degree of allelic imbalances. Figure 15 compares the STR profile of the DNA from serum of the donor with the cell line MDA-MB-435S (M14) from this donor's melanoma and illustrates the loss of alleles at three STR loci.

Furthermore, great care should be taken when evaluating STR profile of biopsy tissue (which may contain normal tissue) when comparing it to the STR profile(s) of cell line(s) derived from a tumor of that same tissue.

Results of similarity search on the 7647 human cell lines with STR profiles in Cellosaurus release 38.0

Export table

Accession	Name	Nº Markers	Score	Amel	CSF1PO	D2S1338	D3S1358	D5S818	D7S820	D8S1179	D13S317	D16S539	D18S51	D19S433	D21S11	FGA	Penta D	Penta E	TH01	TPOX	vWA
NA	Query	NA	NA	X	9,10	17	15,18	11,12	8,12	12,13	12,13.3	9,10	16	13,14	27,28	18,21	8,15	7,17	7	8,12	16,18
CVCL_M022	CM-319	8	100.00%		9,10			11,12	8,12		12,13.3	9,10							7	8,12	16,18
CVCL_1905 *Best*	FL	8	100.00%	X	9,10			11,12	8,12		12,13.3	9,10							7	8,12	16,18
CVCL_1815	Girardi Heart cl one 2	8	100.00%	X	9,10			11,12	8,12		12,13.3	9,10							7	8,12	16,18
CVCL_1816	Girardi Heart cl one 7	8	100.00%	X	9,10			11,12	8,12		12,13.3	9,10							7	8,12	16,18
CVCL_1277	HeLa NR1	8	100.00%	X	9,10			11,12	8,12		12,13.3	9,10							7	8,12	16,18
CVCL_JG57	HeLa/CMV-Luc	8	100.00%	X	9,10			11,12	8,12		12,13.3	9,10							7	8,12	16,18
CVCL_2485	HeLa9903	8	100.00%	X	9,10			11,12	8,12		12,13.3	9,10							7	8,12	16,18
CVCL_B053	HeLaRC32	8	100.00%	X	9,10			11,12	8,12		12,13.3	9,10							7	8,12	16,18
CVCL_1278	HeLaSF	8	100.00%	X	9,10			11,12	8,12		12,13.3	9,10							7	8,12	16,18
CVCL_2940	HEp-2C	8	100.00%	X	9,10			11,12	8,12		12,13.3	9,10							7	8,12	16,18
CVCL_D680	KB 16	8	100.00%	X	9,10			11,12	8,12		12,13.3	9,10							7	8,12	16,18
CVCL_D681	KB 18	8	100.00%	X	9,10			11,12	8,12		12,13.3	9,10							7	8,12	16,18
CVCL_0581 *Best*	WRL 68	8	100.00%	X	9,10			11,12	8,12		12,13.3	9,10							7	8,12	16,18
CVCL_2260	1-5c-4	10	100.00%	X	9,10		15,18	11,12	8,12		12,13.3	9,10				18,21			7	8,12	16,18
CVCL_1908 *Best*	L-132	10	100.00%	X	9,10		15,18	11,12	8,12		12,13.3	9,10				18,21			7	8,12	16,18
CVCL_1907	Intestine 407	12	100.00%	X	9,10			11,12	8,12	12,13	12,13.3	9,10	16		27,28	18,21			7	8,12	16,18

Figure 10. CLASTR Search Results for Matches to STR Profile for the Human HeLa-derived HEp-2 Cell Line. Note that several matches have accession numbers in red font, which indicates these are misidentified cell lines. HEp-2 was one of many cell lines shown in 1968 by Gartler [37] to be derived from the cervical adenocarcinoma HeLa cells and yet it is still frequently used under its false identity of being derived from a laryngeal cancer [48].

The STR profile due to the presence of the normal tissue may differ from that of the cell line that is eventually established from the tumor.

Peak Imbalance

Many tumor cell lines are aneuploid with varying copies of individual chromosomes and total chromosome numbers exceeding 46. For instance, in the case of M14, a melanoma cell line that is often misidentified as a breast cancer cell line, has been reported to have on average 66 chromosomes [46]. ML14 is a lymphoblastoid cell line that was established by transfection of lymphocytes with Epstein-Barr virus (EBV) from the same donor as M14. EBV is known to cause cells to fuse, which may result in fused cells being tetraploid initially. With culturing, the cells start to slowly lose some of the chromosomes. A sample of ML40 has a near tetraploid complement of chromosomes with an average of 89 chromosomes (Figure 16).

Aneuploidy is also common in mouse cell lines where total chromosome numbers exceed 40. It has been shown in mouse embryonic stem cell lines [67, 76], and in a separate study Didion et al. demonstrated that 42% of normal and cancer mouse cell lines tested had evidence of aneuploidy [26]. The normal cell lines that contained chromosomal abnormalities confirmed that this is not just a problem found in cancer cell lines, but is caused from cells growing in culture. It is possible that fluctuating aneuploidy can affect the apparent allelic balances in STR profiles.

Peak imbalance is a common feature of cancer cells (see Figure 5, 13, 14, 16). The favored amplification of one allele over another may be due to genetic duplications, aneuploidy, or chimeric (mixed) cell populations [25, 32, 65] in which some cells in the culture have lost a copy of an STR locus. This characteristic brings a unique feature to cell line identification that is not commonly seen in DNA from normal tissue (see Figure 3) or forensic samples. Cell lines often show allelic imbalances, as illustrated by the CSF1PO, D5S818, D16S539 and TPOX loci of K562 in Figure 13, the D13S317 locus in the HFAE-2 profile in Figure 14, and TH01 locus in MDA-MB-435S in the bottom panel of Figure 16.

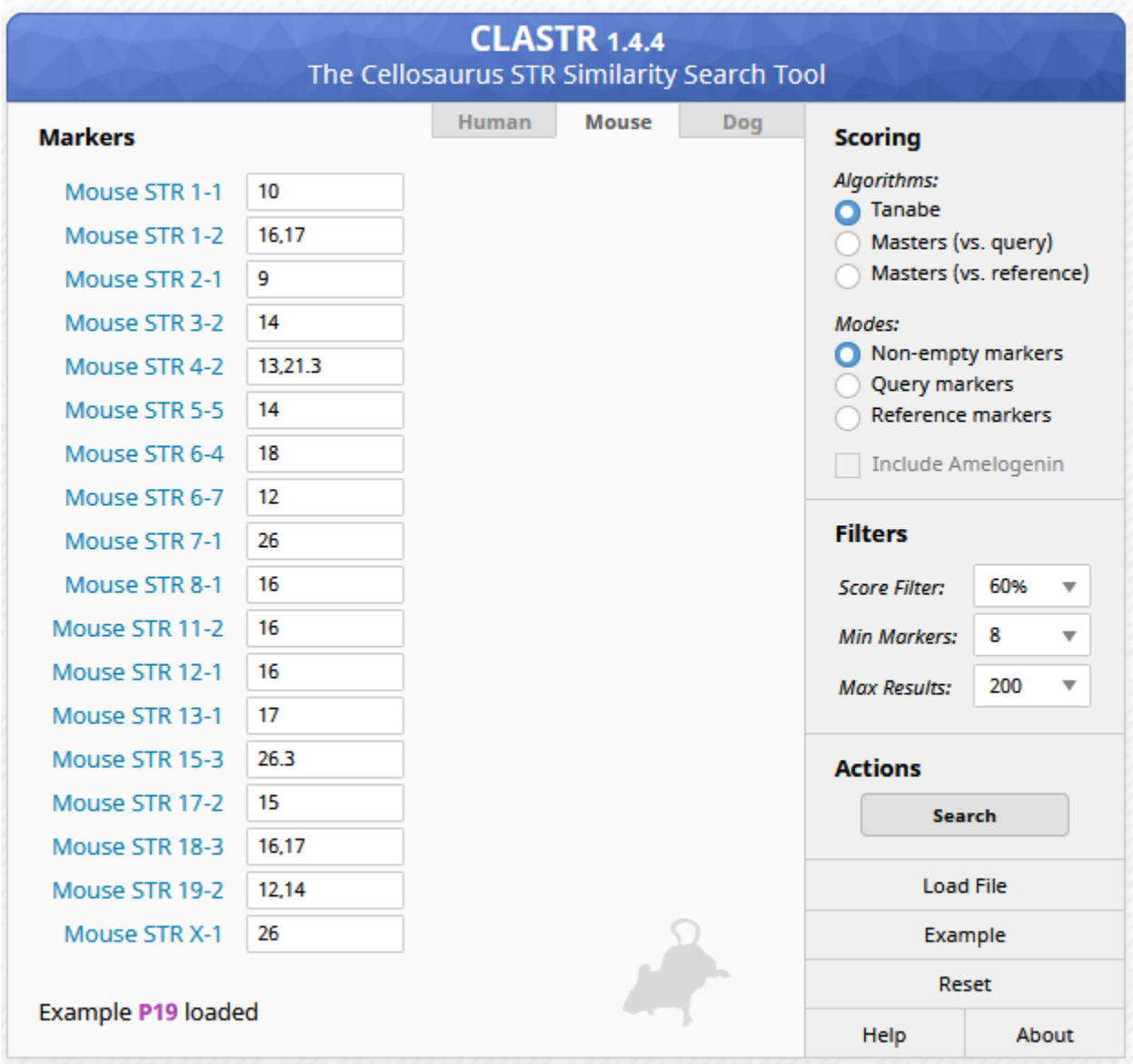


Figure 11. CLASTR Search Tool Input of Human STR Data. Data is for mouse P19 cell line taken from Figure 6.

Results of similarity search on the 74 mouse cell lines with STR profiles in Cellosaurus release 38.0

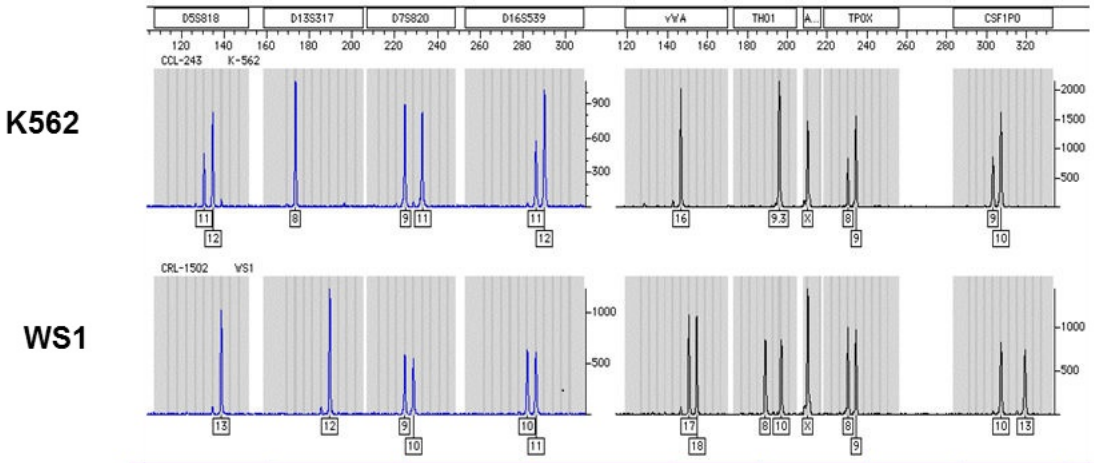
Export table

Accession	Name	Nº Markers	Score	STR 1-1	STR 1-2	STR 2-1	STR 3-2	STR 4-2	STR 5-5	STR 6-4	STR 6-7	STR 7-1	STR 8-1	STR 11-2	STR 12-1	STR 13-1	STR 15-3	STR 17-2	STR 18-3	STR 19-2	STR X-1
NA	Query	NA	NA	10	16,17	9	14	13,21.3	14	18	12	26	16	16	16	17	26.3	15	16,17	12,14	26
CVCL_2153	P19	18	100.00%	10	16,17	9	14	13,21.3	14	18	12	26	16	16	16	17	26.3	15	16,17	12,14	26
CVCL_3984	A-9	18	70.83%	10	17,18	9	14	20.3,21.3	14,15	17,18	12	26,27	16	15,16,17	16	17	25.3	15	16	12	26,27
CVCL_0462	NCTC clone 929	18	70.83%	10	17	9	13,14	20.3	14	17,18	12	25,26,27	16	15,16	16	17	24.3,25.3, 26.3	15	16	12	26,27

Figure 12. CLASTR Search Results for STR Profile for the Mouse P19 Cell Line

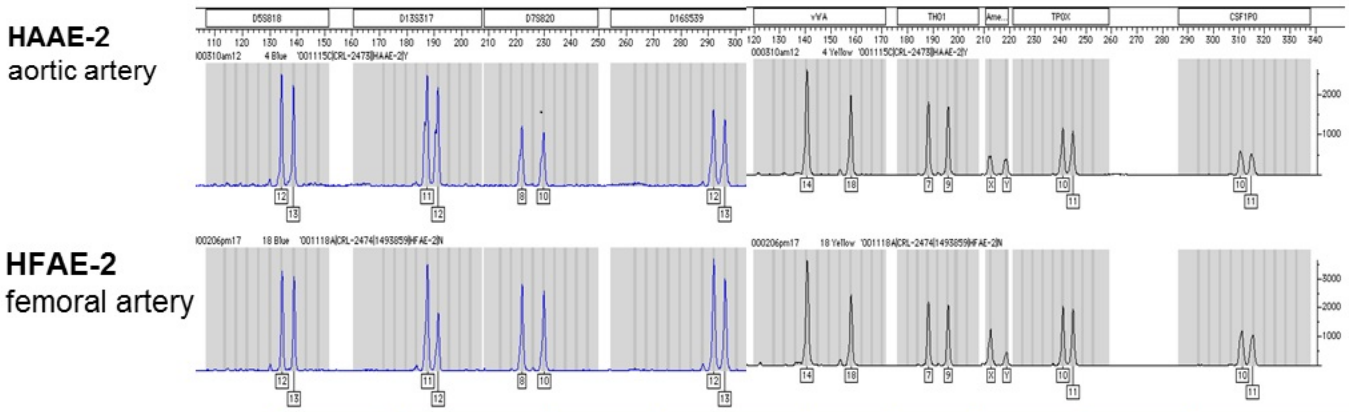
Novel, Out-of-Range Alleles

On rarer occasions, some peaks do not align with the allelic ladder and fall between loci ranges (see peak encircled in red, Figure 17). It may be a 15-repeat allele of the D7S820 locus from its position and such an allele is listed on the NIST website. The identity of such out-of-range peaks should be confirmed by PCR amplification



	D5S818	D13S317	D7S820	D16S539	vWA	THO1	Amel.	TPOX	CSF1PO
K562	11, 12	8	9, 11	11, 12	16	9.3	X	8, 9	9, 10
WS1	13	12	9, 10	10, 11	17, 18	8, 10	X	8, 9	10, 13

Figure 13. Electropherogram of Two Unrelated Human Cell Lines. K562 (chronic myelogenous leukemia) and WS1 (skin fibroblast) were obtained from two unrelated individuals. STR profile is different between the two cell lines. STR analysis performed with PowerPlex 1.2. Allele numerical values are used to create database. The new STR genotyping standard protocol recommends the use of at least 13 STR loci [49]. Courtesy of Reid et al. [68].



	D5S818	D13S317	D7S820	D16S539	vWA	THO1	Amel.	TPOX	CSF1PO
HAAE-2	12,13	11,12	8,10	12,13	14,18	7,9	X,Y	10,11	10,11
HFAE-2	12,13	11,12	8,10	12,13	14,18	7,9	X,Y	10,11	10,11

Figure 14. Electropherogram of Two Related Human Cell Lines. HAAE-2 (human aortic artery) and HFAE-2 (femoral artery) were obtained from the same individual. STR profiles are identical between the two cell lines. STR analysis was performed using the Promega PowerPlex 1.2 kit. Allele numerical values are used to create a database entry. Courtesy of Reid et al. [68].

of the alleles in question (i.e., D7S820 and D16S539 in Figure 17) by using monoplex PCR reactions with primers specific for the two loci (D7S820 and D16S539) to determine which primer pair produces the out-of-range allele.

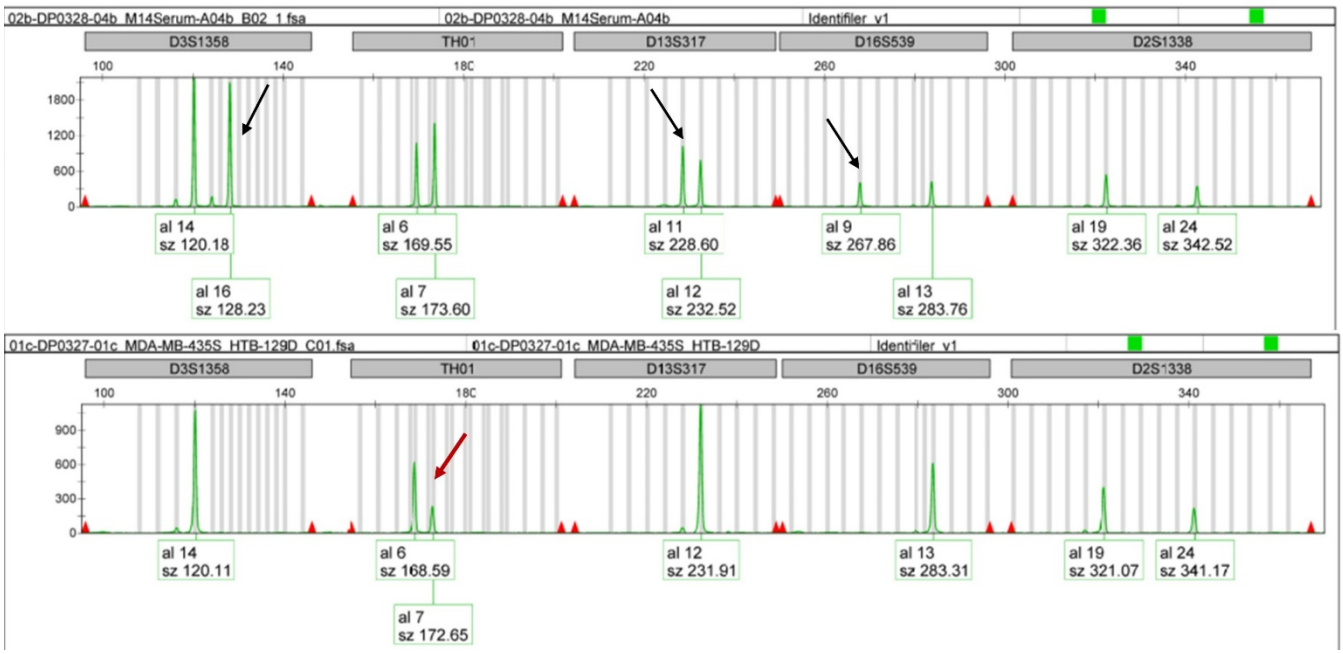


Figure 15. Comparison of STR Profiles of Patient Serum DNA vs Misidentified Cell Line DNA Showing Allelic Imbalance and Losses. Comparison of partial STR profiles for DNA from serum from male melanoma patient M14 (top) and misidentified cell line MDA-MB-435S (bottom) shown to be derived from M14 cell line [46]. Notice in the bottom panel the allelic imbalance of the TH01 alleles (red arrow). MDA-MB-435S cells (bottom panel) have lost three alleles from the D3S1358, D13S317, and D16S539 loci that are present in the STR profile of DNA from M14 serum (black arrows in top panel).

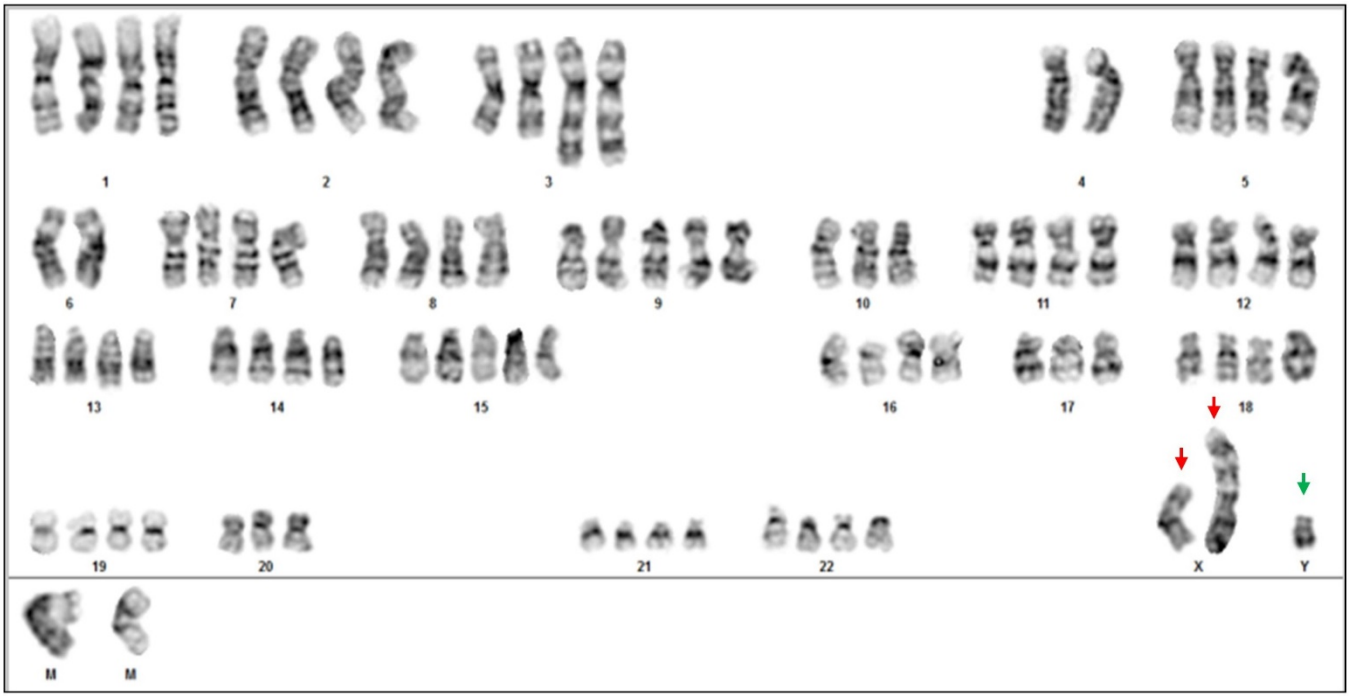


Figure 16. Metaphase Karyogram of the Lymphoblastoid Cell Line ML14 [46]. Notice there are four copies of most of the human chromosomes, two versions of the X chromosome, and two marker chromosomes (M) of unknown origin. Image courtesy of Dr. Marileila Varella-Garcia.

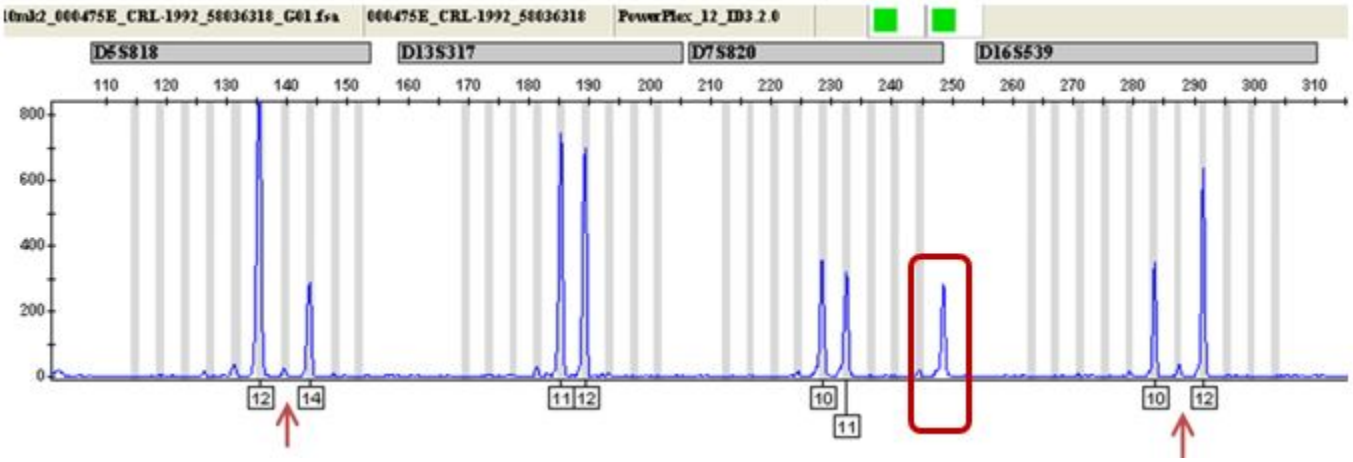


Figure 17. Examples of Allelic Imbalance and Novel Out-of-Range Allele. At the D5S818 and D16S539 loci (red arrows), an off-ladder allele between the D7S820 and the D16S539 loci, and stutter peaks. The red arrows point to stutter peaks in the D5S818 and D16S539 loci. These small peaks are a PCR artifact and contain one less repeat than the true alleles and usually represent less than 15% of the height of the true allele peak. An off-ladder peak is circled in red. Courtesy of Reid et al. [68].

Multiple Peaks at Several Loci

Another relatively common occurrence of STR typing of cancer cell lines is multiple peaks at several loci. Three or more peaks at one or two loci may be due to somatic mutation, trisomy, or gene duplications. The most common somatic mutations of STR loci are caused by microsatellite instability (MSI) due to defects in the cell's DNA mismatch repair (MMR) system. Events with more than three peaks at more than three loci may be due to cross contamination with cells from a different human cell line (see Figure 18 as an example for cellular cross contamination, and Appendix F and Figures H.5 and H.15 in the ASN-0002-2021 Standard [49]). In either event, an independent method should be used to eliminate cell line mixtures.

Several approaches to discern whether a cell line is cross-contaminated with another cell line or whether MSI is the cause of a gain of alleles at one more STR loci include:

- Retrieve the earliest aliquot of the original batch of the cell line to see whether it also has multiple peaks. This would indicate whether the multiple peaks are a "feature" of the cell line or have arisen during subsequent culturing. Repeat culturing to see whether the additional alleles appear.
- Attempt to subculture from a single, or as few as possible cells, and see whether such subcultures present different profiles or similar mixed profile. If the former, then the culture is probably a mixture of cells, if the latter, then the culture may be unstable due to a defective DNA MMR system.
- If the additional shorter peaks only differ from the taller peaks by plus or minus single repeat units this suggests MSI is involved.
- Using the Cellosaurus search tool CLASTR, search for potential matches to different cell lines using the Master versus Reference algorithm. This approach can potentially identify the profiles of the components of a mixture of two cell lines (see this discussion of the algorithms), and thus identify the cell lines in the mixture and the source of the extra peaks. Figure 19 shows the CLASTR search results for the purported thyroid cell line BHP18-21 (CVCL_6282) which has three or more alleles at 7 of 9 STR loci (query line). This suggests that the cell line is actually a mixture of two or more lines. On comparing the STR profile using the Masters vs Reference algorithm, it is clear that alleles of both the TPC-1 (CVCL_6298) thyroid cell line and the melanoma cell line M14 (CVCL_1395) are shared and that these two lines are derived from the same person and have cross-contaminated several other cell lines.
- MSI causes gains or losses of single repeats in STR alleles as described by Parson et al. [64] and illustrated Appendix F of the ASN-0002-2021 Standard [49]. On comparing the STR profile with a reference profile,

note whether the additional peaks differ by plus or minus single repeats (i.e., ± 4 bp) and using the Masters vs Reference algorithm determine whether the complex profile matches a single cell line or multiple different lines. If the profile shows only gains or losses by single repeats and the match is to a single cell line (including multiple variants of it), this suggests that the extra peaks are due to MSI. This can be confirmed by testing for MSI using either in-lab designed assay (see supplemental information in Korch et al. [46]) or a commercial kit (e.g., Promega MSI Analysis System, Version 1.2, Cat. No. MD1641) or described in Appendix F of the ASN-0002-2021 [49].

Criteria for Determining Quality STR Profile Analysis for Reliable and Interpretable Results

Validation of Procedure

Method validation is the process of demonstrating that a laboratory procedure is robust, reliable, and reproducible in the hands of the laboratory personnel performing the test. The factors for method validation include precision, accuracy, limit detection, specificity, linearity, range, robustness, and system suitability. For more information on method validation of STR Systems, refer to ANSI-ATCC ASN-0002 2021 revision [49], STRBase Validation Information to Aid Forensic DNA Laboratories, and Promega's Validation of STR Systems Reference Manuals here and here.

Setting Appropriate Analytical Peak Heights and Peak Thresholds

Each laboratory should determine the analytical threshold or the level at which valid signals are above baseline noise. Data falling below this threshold may not be suitable for allele calls; however, data above the threshold should be of sufficient quality to determine an allele call.

The genetic material for some tumor cell lines is very complex and this could lead to difficulty in distinguishing true low-level peaks from technical artifacts, including noise. There are no set rules for establishing threshold values; consequently, each laboratory must establish empirically peak-height thresholds for "calling" alleles as part of its validation process. Only peak-heights, expressed in relative fluorescent units (RFU), that exceed the analytical threshold value can be accepted.

The threshold may be determined experimentally on the basis of observed signal-to-noise ratios or be a predetermined value established by manufacturers (for the ABI 3500 the recommended cut-off level is 150 RFU; while that for the ABI 3730 or 3130 instrument is generally about 50 RFU) or through in-house validation of the available kit and instrument. The lower threshold is a measure of the procedure sensitivity. The upper threshold is essential when reviewing data from samples with high DNA quantities. Samples with high RFU values can oversaturate the instrument's ability to detect the sample and lead to artifacts that can make it difficult to interpret the results. These include reducing the efficiency of the terminal transferase reaction to produce fragments with and without a terminal A (see Figure 24 for illustration of incomplete adenylation by the terminal transferase activity of the DNA polymerase). Figure 20 is an example of a real allele that is a 9.3-repeat allele at the D7S820 locus, which could be confused for incomplete adenylation of a 10-repeat allele. Additional artifacts include very intense peaks which can appear as split doublets and signal spill-over into a different fluorophore channel. Thus, these extra artifactual peaks may be incorrectly interpreted as real peaks (i.e. alleles) especially when working with samples that are in the early stages of cellular cross-contamination.

Another factor for optimal display of the STR allele peaks is the size range of analysis. In the GeneMapper software this must be set correctly so as not to include the residual peaks that appear first at the beginning of each sample profile and each panel must be set to automatically adjust the peaks to fit optimally. This procedure is described in the 2021 revision of the ANSI-ATCC ASN-0002 standard [49] and may be described in the manuals for the analysis software being used.



Figure 18. Electropherogram of Cellular Cross-contamination. Multiple peaks at D5S818, D13S317, D7S820, D16S539, vWA, CSF1PO loci (indicated by the red arrows). STR typing of human cell lines with PowerPlex 1.2. Courtesy of Reid et al. [68].

Accession No.	Cell Line Name	No. Loci	Score (%)	Amel	D3S1358	D5S818	D7S820	D8S1179	D13S317	D18S51	D21S11	FGA	vWA
NA	Query = BHP 18-21	NA	NA	X	14,16,17	8,10,11,13	8,10,11	11,13,17	11,12	13,16,17	30,31.2	20,21	14,16,18
CVCL_6282	BHP 18-21	9	100.00%	X	14,16,17	8,10,11,13	8,10,11	11,13,17	11,12	13,16,17	30,31.2	20,21	14,16,18
CVCL_6298	**TPC-1 = thyroid**	**9**	**100.00%**	**X**	**16,17**	**8,10**	**11**	**11,17**	**11,12**	**13,16**	**30,31.2**	**20,21**	**14,18**
CVCL_6278	BHP 10-3	9	100.00%	X	16,17	8,10	11	11,17	11,12	13,16	30,31.2	20,21	14,18
CVCL_6285	BHP 7-13	9	100.00%	X	16,17	8,10	11	11,17	11,12	13,16	30,31.2	20,21	14,18
CVCL_6283	BHP 2-7	8	100.00%	X	16,17	8,10	11		11,12	13,16	30,31.2	20,21	14,18
CVCL_1395	**M14 = cutaneous melanoma**	**9**	**92.86%**	**X**	**14,16**	**11,12**	**8,10**	**13**	**12**	**13,17**	**30**	**21**	**16,18**
CVCL_6279	BHP 14-9	9	92.86%	X	14,16	11,12	8,10	13	12	13,17	30	21	16,18
CVCL_6280	BHP 15-3	9	92.86%	X	14,16	11,12	8,10	13	12	13,17	30	21	16,18
CVCL_6281	BHP 17-10	9	92.86%	X	14,16	11,12	8,10	13	12	13,17	30	21	16,18
CVCL_6284	BHP 5-16	9	92.86%	X	14,16	11,12	8,10	13	12	13,17	30	21	16,18
CVCL_0467	NPA	9	92.31%	X	14,16	11,12	8	13	12	13,17	30	21	16,18
CVCL_0417	MDA-MB-435	9	92.31%	X	14	11,12	8,10	13	12	13,17	30	21	16,18
CVCL_0622	MDA-MB-435S	9	92.31%	X	14	11,12	8,10	13	12	13,17	30	21	16,18
CVCL_1910	MDA-N	9	92.31%	X	14	11,12	8,10	13	12	13,17	30	21	16,18
CVCL_3448	MuM-2C	9	84.62%	X	14,16	11,12	8,10	13	12	13,18	30	21	18
CVCL_6934	OCM-1	9	84.62%	X	14,16	11,12	8,10	13	12	13,18	30	21	18
CVCL_6935	OCM-1A	9	84.62%	X	14,16	11,12	8,10	13	12	13,18	30	21	18

Figure 19. Matches to Mixed "Thyroid" Cell Line BHP18-21 Using the Alt Masters % Match Algorithm. This is a selection of the CLASTR search results. Note that the CVCL IDs for true cell lines TPC-1 and M14 are in blue font, while all others are in red, which are false cell lines. Most of these are derived from M14, such as the cross-contaminated series of "thyroid" cell lines (BHP 2-7, 7-13, 10-3) and NPA, "breast" cell lines MDA-MB-435S and NDA-N, and the "uveal" melanoma cell lines MUM-2C and OCM-1. The thyroid cell line TPC-1 had cross-contaminated the thyroid cell lines NPA and the BHP series 5-16. 14-9, 15-3, and 17-10.

Use of Appropriate Positive and Negative Controls

Including controls during the STR profile analysis is very important as it allows the technician to identify and troubleshoot possible problems, such as DNA contamination of the PCR reagents, and thus ensure whether the data are accurate and reliable.

During the amplification process, positive and negative controls are used. A positive control is a DNA sample with a known STR profile that is added to the sample set. The positive control confirms that the analysis processes are working accurately. A positive control DNA is usually provided in the manufacturer's STR kits. A negative control, which could be a reagent blank with either water or buffer substituted for DNA, is also performed and treated exactly in the same manner as other samples. This allows the technician to determining if the reagents and/or techniques used may have introduced contaminating DNA.

Evaluation of Internal Lane Size Standards (ISS) and Allelic Ladders

All commercial STR kits include allelic ladders and internal size standards (ISS). Each sample during a run is assessed at completion for the correct calling of the ISS peaks. In general, the peaks from an ISS are uniform in size or intensity. In some ISS there may be peaks of different heights/intensities so that they can be easily identified. Lack of uniformity or miscalled peaks can indicate problems with the sample, injection, and/or run conditions. The ISS is valuable in determining the accuracy of a capillary electrophoresis run. Temperature

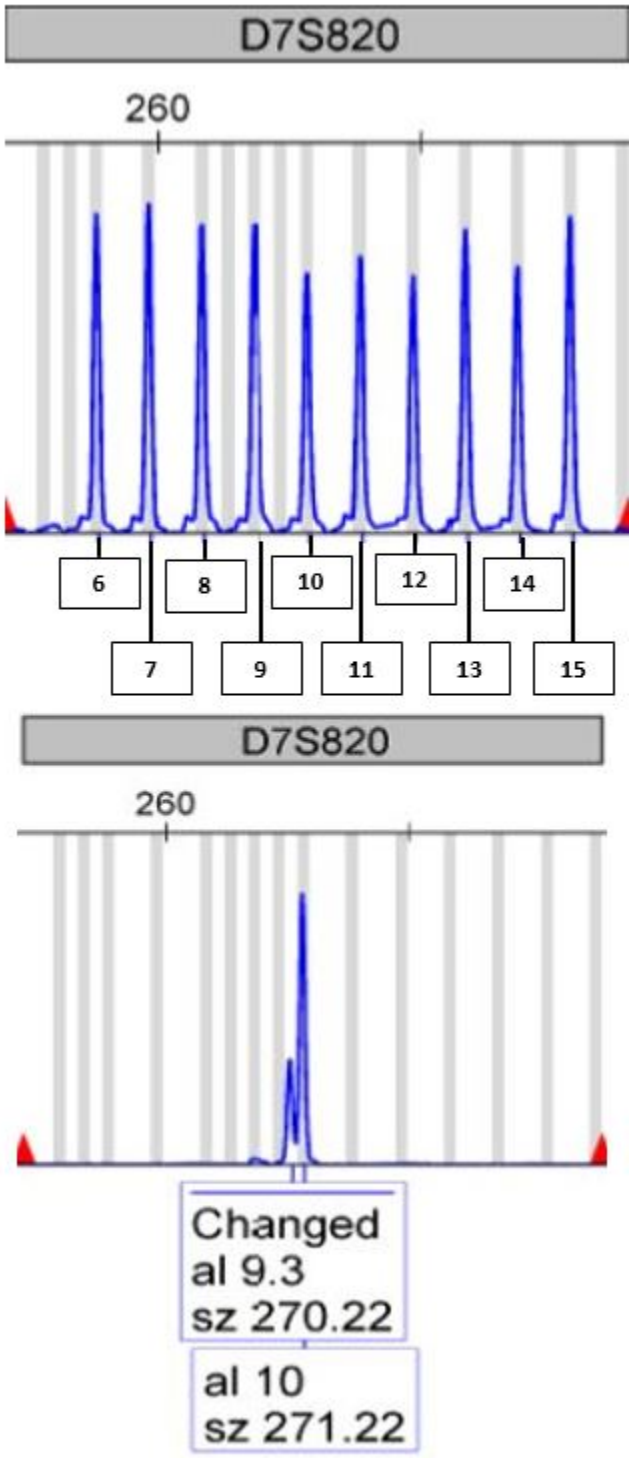


Figure 20. Example of D7S820 Microvariant Allele. On comparison of an off-ladder allele with the allelic ladder (top panel) at the D7S820 locus of the cell line SKMEL28. Based on its length it is a 9.3 allele, one base shorter than the 10-repeat allele. It should not be confused with an allele that is due to incomplete addition of the terminal A (see section on artifacts).

variations during electrophoresis can cause the in-run precision to exceed 1 base pair and evaluation of the ISS can assist analysts in identifying this issue.

In the new ASN-0002-2021 [49], Figures 5.5, H.8a, and H.8b show examples of good, poor and unusable ISS profiles which prevent their use in profiling. Also, high amounts of sample can reduce the signal strength of the

ISS, which is probably due to the increased amounts of salt in the sample which compete with the DNA amplicons for uptake (see Figures 5.5, 5.6, 5.7 in ASN-0002-2021 [49]).

Allelic ladders should be assessed to ensure that all peaks have been correctly called (top panel in Figure 20). Ladder peaks that have not been called or have been miscalled can indicate a problem with the ladder sample, injection, and/or run.

Detection and interpretation of off-ladder alleles and microvariants

Allelic ladder (AL) standards are a collection of labeled DNA fragments that represent the most common alleles at each locus and were established through the evaluation of STR and sequencing data from several hundred individuals. Alleles within the STR loci are known to differ significantly between individuals and the AL included in STR kits do not represent all possible known alleles. The bins of the allele calling software identifies known peaks that are in the range of alleles for a locus. Older versions of the allele bins data may not include more recently identified alleles. In this case, the software calls such unknown alleles within this range as off-ladder (OL) peaks / alleles. A well-known microvariant is the 13.3 allele of the D13S317 locus of HeLa cells (Figure 21). This allele, very infrequently seen in forensic and other cell lines, was often mis-called as a 14-repeat allele or an OL allele. This miscalling was probably due to the lower resolution of the slab-gel electrophoresis equipment used in the 1990s and the absence of a bin for this distinct allele. Peaks between loci ranges are usually not called (see Figure 17).

While off-ladder alleles have been well documented with forensic STR testing, some may not have been previously characterized. The National Institute of Standards and Technology (NIST) website has a listing of human off-ladder alleles and can be used as a reference in these instances. If it is determined that an allele has not been characterized, it may be advisable to rerun the sample to confirm that it is not an artifact. If repeatable, unlabeled primers for the possible loci (D7S820 and D16S539 for the allele between these two loci in Figure 17 or for the D13S317 for the 13.3 allele in Figure 21) can be used to PCR amplify and sequence the amplicons in question to ascertain the cause of the OL size.

Microvariants are incomplete repeats at a particular locus and are expressed as a partial representation of the repeat motif. Generally, microvariants may be off by 1, 2, or 3 bases and are designated by the whole number of repeats plus .1, .2, or .3, respectively. Note that there are only these variations and there are not any alleles with the ".4 " designation, because most of the STR alleles in the various STR kits are tetranucleotide repeats and any allele with 4 extra nucleotides is the next full-size allele (i.e., a "14.4" allele migrates as a 15-repeat allele). There are exceptions to this as shown by the sequencing of the different alleles. This is discussed extensively elsewhere [19, 49] and on the NIST website.

Detection and Interpretation of Data Artifacts

There are several artifacts during STR profile analysis that can lead to misinterpretation of the data. Identification and resolution of these artifacts are explained in great detail in the 2021 revision of the ANSI/ATCC ASN-0002 standard [49].

- Stutter peaks
- Dye blobs
- Incomplete adenylation
- Dye pull-up or bleed-through

Stutter peaks (products)

Stutter products are a common amplification artifact caused by strand slippage of the polymerase and is associated with STR analysis [40, 84]. Stutter products are often observed as one repeat unit shorter in length

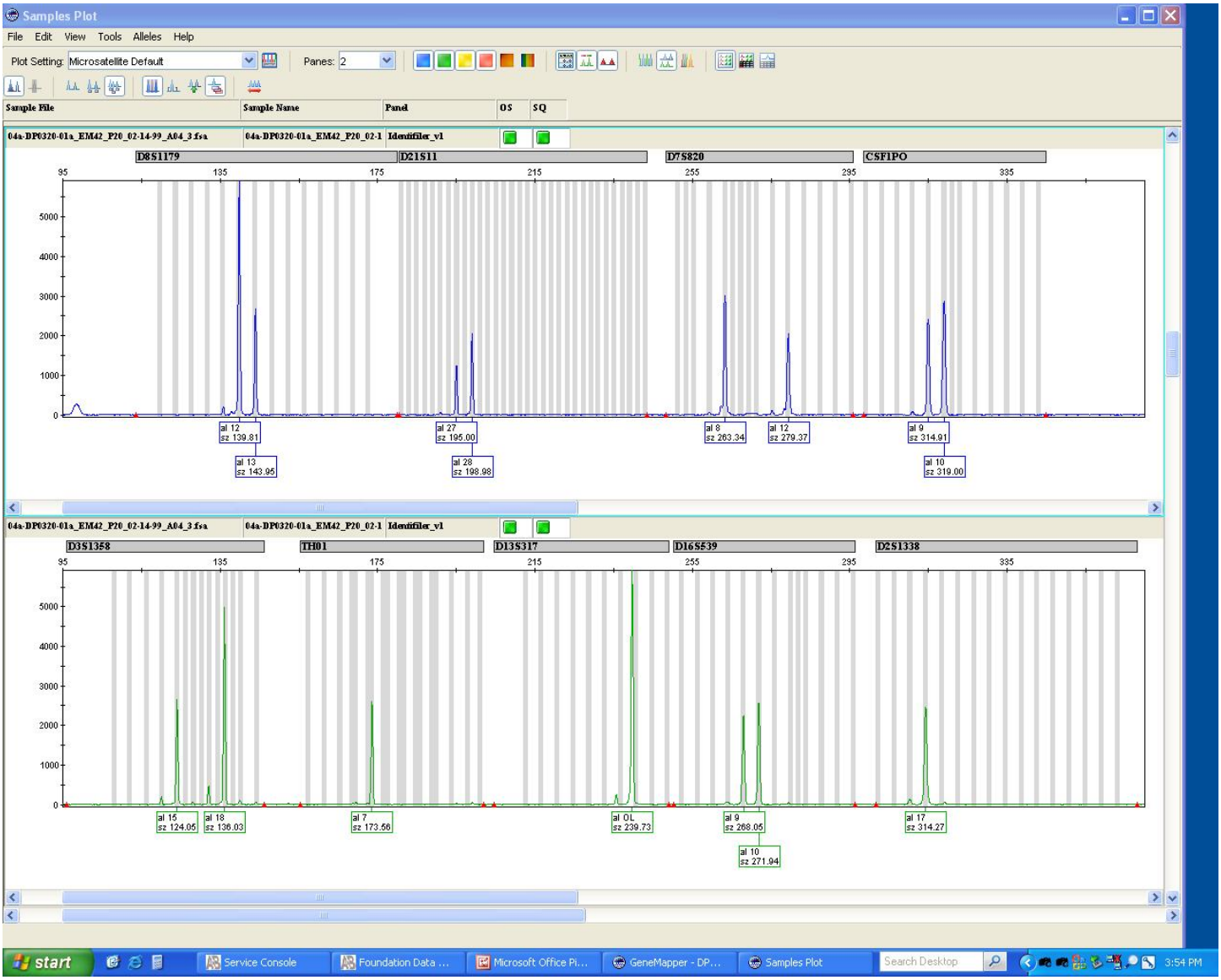


Figure 21. Example of D13S317 Microvariant Allele. The 13.3 off-ladder allele of D13S317 locus of HeLa cells, which has often mistakenly been called as a 14-repeat allele in earlier analyses.

(N-1) than the true allele peak. Other stutter products (N-2 or N+1 repeats) if seen, are the exception. Frequently, alleles with a greater number of repeat units will exhibit a higher percent stutter. The pattern and intensity of stutters may differ slightly between primer sets for the same loci (see Figure 22 and either Promega's manual on troubleshooting PowerPlex 18D System, or the manual from the manufacturer of the kit being used).

Dye blobs

Dye blobs, which appear as broad peaks that are not as sharp as normal peaks, may occur in STR analysis (Figure 23). Evidence suggests that the fluorescent dye tags attached to the primers begin to break down over time. Disassociated primer dyes can appear in the sample analysis range and mask true data. Dye blobs are usually wider than real peaks and typically only seen in one color. The example of a dye blob in Figure 23 is probably evident because the signal strength of the peaks in the panel are relatively weak; with stronger peaks the dye blob might have been hidden in the background noise. Follow the manufacturer's specifications for storage of amplification kits to avoid problems associated with free dyes. If problems persist, clean-up or re-amplify sample.

Figure 22. Stutter Peaks. Stutter peaks (red arrows) appear to run ahead of the main peaks (or true allele) by 1 repeat unit (4 bp). In cell lines, they can be mistaken for or co-migrate with real allele peaks. The 12-repeat allele in this figure is probably a stutter peak and not a real allele. Courtesy of Reid et al. [68].

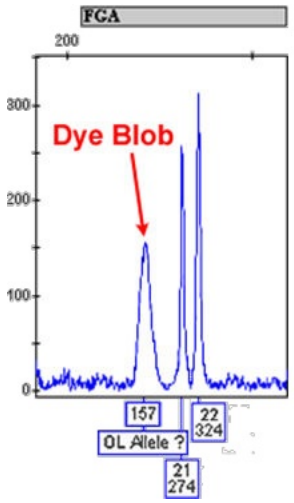


Figure 23. Dye Blob. Note, it produces a broad peak. Courtesy of Reid et al. [68].

Incomplete adenylation of PCR amplicons

Non-template addition occurs when Taq DNA polymerase adds an additional base, usually adenine (A), to the 3' end of the amplicon during the PCR amplification process [18]. If incomplete adenylation occurs, split peaks, which differ in length by one base, are evident during CE analysis and result in an amplicon with +A and -A peaks (Figure 24). This type of artifact leads to broad or double peaks and makes it difficult for the software to accurately call the real allele. It is important to note that some authentic microvariant alleles at certain loci can migrate at the same position as these incomplete adenylation peaks and thus produce confusing results. They can look similar to the double peaks in Figure 20, but the double peaks due to incomplete terminal A addition will be evident at several loci and not just at one locus. The use of excess genomic DNA and / or too short of a final extension time in the PCR can result in the elevated levels of the N-1 base stutter peak. In such cases it can be difficult to distinguish this peak from a true allele. Therefore, use of validated commercial kits approved for forensic analyses, accurate quantification of the DNA sample, and optimization of the final extension times will ensure optimal STR peak formation.

Dye pull-up or bleed-through

Dye pull-up, sometimes referred to as bleed-through, represents a failure of the analysis software to discriminate between the different dye colors used during the generation of the data. Oversaturated data due to excessive signal strength can cause the dyes to “bleed” over or pull-up into another color space. If pull-up occurs, inject less of the sample, dilute the sample and reinject it, or re-amplify the sample with less DNA. Reoccurring pull-up (due to too much DNA) may indicate that the quantification method or the amount of DNA used for amplification should be reevaluated. If the peaks are very high due to too much DNA, there are three approaches that can resolve this issue. The PCR reactions can be diluted by either adding additional volumes of formamide or diluting the PCR reaction before mixing an aliquot with formamide. Alternatively, the injection time and / or voltage could be reduced and the samples re-run on the capillary electrophoresis instrument. The latter may require assay validation by the laboratory.

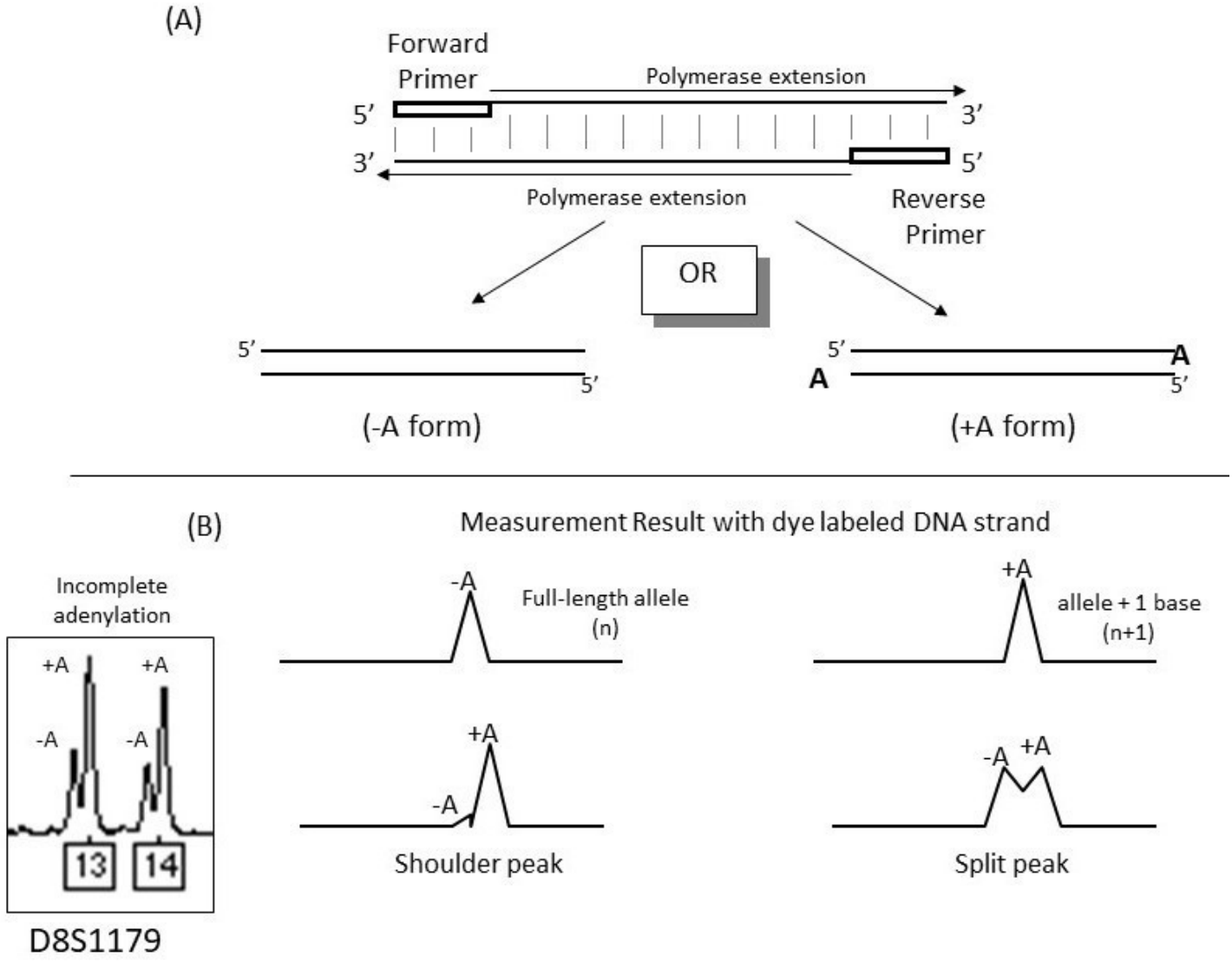


Figure 24. Schematic of Incomplete Adenylation of PCR Amplicons. Schematic of non-template nucleotide addition shown (A) with illustrated size difference. (B) Some DNA polymerases add an extra nucleotide beyond the 3′-end of the target sequence extension product. The amount of non-template addition is dependent on the DNA polymerase, sequence of the 5′-end of the opposing primer, DNA concentration, and extension time. In the case of dye-labeled PCR products where the fluorescent dye is on the forward primer, the reverse primer sequence is the critical one affecting the level of adenylation. Courtesy of John M. Butler, NIST [18].

If DNA was accurately quantified and the concentration is in the target range it may be necessary to perform a new spectral calibration of the capillary electrophoresis instrument and re-run the samples.

In some cases, even after the ideal amount of DNA was processed for STR genotyping, other peaks arise that are not artifacts, but are actual alleles that fall outside of bins (or known alleles) in the data analysis software. These peaks are called off-ladder alleles; see above for discussion of these type of alleles.

Services for STR Genotyping of Cell Lines

Over the past few years, several institutions have started offering STR typing of human cell lines. When choosing a testing laboratory, considerations should be made based on experience of testing laboratory personnel to perform and interpret the data from STR analysis. The following are some types of institutions who currently offer STR typing services.

- Cell Banks
- Commercial genetic identification laboratories
- Paternity testing labs
- Universities
- Core labs

Troubleshooting

The revised ANSI-ATCC ASN00002-2021 standard for cell line authentication contains extensive troubleshooting guidelines [49]. Below are three sets of best practices and troubleshooting suggestions to assist in obtaining optimal STR genotyping results.

Best Practices for Avoiding Misidentified and Cross-contaminated Cell Lines

Below are some procedures that can help reduce usage of cross-contaminated and misidentified cell lines:

- Good documentation and tracking of cell line handling using in-house programs or the cell line tracking and inventory software, such as Find Cell by Find Genomics.
- Consult the Cellosaurus and the ICLAC websites for descriptions of misidentified and false cell lines to avoid using them.
- Obtain cell lines from reputable, cell line repositories which authenticate their cell lines. Beware of unreliable sources of cell lines which have simply cut-and-pasted cell line descriptions from the websites of the well-known repositories.
- If generating cell lines etc. within your laboratory, freeze samples (biopsy, blood or serum, buccal smear, xenografts, FFPE) in liquid nitrogen for eventual STR genotyping and further genetic studies (e.g., next generation sequencing).
- Quarantine cell lines upon receipt and test to ensure they are mycoplasma free. Perform the Cooper et al. PCR test for common mammalian species in sample [23].
- Train all laboratory personnel who handle cell lines on proper cell handling techniques as described in these publications: [20, 22, 35, 38].
- Write up standard cell line handling and testing protocols to be followed by all lab personnel, including how to interpret STR profiles and the significance of STR profile match scores.
- Stress the use of good aseptic techniques.
- Devote one reservoir of medium for each cell line.
- Aliquot stock solutions/reagents.
- Label flasks (name of cell line, passage number, date of transfer (use barcoded flasks when available).
- Work with one cell line at a time in biological safety cabinet.
- Handle the slower growing cultures before the faster growing cultures.
- Clean biological safety cabinet between each cell line.
- Allow a minimum of 5 minutes between each cell line with the laminar flow fan running.
- Quarantine “dirty” cell lines (i.e., ones that have not been tested for the presence of mycoplasma and have not been authenticated for their identity) separately from “clean” cell lines before using them.
- Manageable work load to reduce accidental mixing-up of cell lines.
- Clean laboratory regularly to reduce bioburden.
- Legible handwriting (printed labels) to avoid mislabeling of samples.
- Routinely monitor for cell line identity and characteristics to check for potential contamination.
- Use seed stock (create master stocks) see Figure 1 and Figure 7.
- Create a clean, orderly working environment, which includes ensuring tissue culture hoods are neither cluttered nor used to store equipment and reagents.

- Review and approve laboratory notebooks frequently by the laboratory principal investigator.
- Authenticate cell lines regularly and a) after selection of cells (antibiotic selection or drug resistance), b) when unexpected phenotypes are observed, c) at end of a project, and d) before submission of grant applications and manuscripts. See 20 steps in the suggested Cell Line Policy available on the ICLAC website (see ICLAC links below).

Preventing Contamination During PCR

This section is for the laboratory performing the PCR and electrophoretic steps of the STR analysis. Preventing contamination during PCR is of critical importance to ensure that you are getting meaningful results. The

following list provides some suggestions of how to reduce and/or prevent contamination during PCR.

- Separate pre-amplification (low copy) space from post-amplification (high copy) space.
- Use separate lab coat, gloves, tubes, pipette tips in pre-amplification room from post-amplification room.
- Use aerosol-resistant pipette tips.
- Use a different pipette tip for each pipetting (even of the same reagent) when pipetting all your reagents, even the same master mix to each tube.
- Keep pre-amplification and post-amplification reagents in separate rooms.
- Prepare amplification reactions in a room dedicated for reaction setup.
- Use a separate aliquot of molecular grade water stock for each round of PCR*.
- Prepare your PCR mix in a hood with laminar flow. Decontaminate it with 10% bleach, 70% ethanol, and/or solutions for decontaminating surfaces of RNases and DNases (e.g., RNaseZap or RNaseAway or NucleoClean decontamination spray).
- Keep your tubes closed during the procedure, even your master mix tube**.
- Be sure that your tubes are closed when discarding the pipette tip!!! Aerosols are dangerous!!!
- Open the tubes only when necessary.

NOTES

* Molecular-grade and HPLC-grade water are usually DNA-free and do not pose the risk of residual DEPC in these water sources that could inhibit the PCR. Working in a PCR hood, aliquot these waters into sterile 15 and / or 50 mL polypropylene capped centrifuge tubes for ease of handling and minimization of contamination. Test aliquots for purity before use in PCR experiments.

** For the PCRs, individual PCR tubes with attached domed caps can be used instead of 96-well plates for setting up the PCRs. The caps can be left partially closed between each addition and then fully closed after the final addition. Although strip caps are available for 96-well plates, they are not easily handled in a manner that would avoid sample mix up and cross-contamination.

Troubleshooting of PCR Step

When first validating the PCR of STR alleles and on occasions when the PCR amplification of STR alleles may fail to produce any amplicons detectable by capillary electrophoresis, a useful troubleshooting technique is to analyze the yield of PCR reactions by agarose gel electrophoresis in the laboratory. This will be more rapid and less expensive than submitting samples to a facility for analysis.

Causes of unsuccessful PCRs, besides omission of a PCR reagent or an aliquot of sample DNA, include insufficient gDNA in the sample due to inaccurate DNA quantification or the DNA is not from the correct species for the STR genotyping kit.

To troubleshoot the multiplex STR PCRs, electrophorese an aliquot (1/3 or ½) of the reaction on a 1.75% - 2.0% agarose gel made and run with 1X TBE buffer containing 0.3 μg of ethidium bromide per mL of buffer. The

image in Figure 25 shows an agarose gel with No DNA control reaction and the positive control DNA 9947a in the bottom half of the gel and results of PCR amplification of STR alleles from DNA isolated from seven cell lines in the top half of the gel. Note that the No DNA control shows only the presence of the dye labeled primers; whereas, the other samples show multiple, closely migrating bands above the dye labeled primers.

Non-commercial Kits and Inappropriate Authentication Methods

Commercial vs Home-brew STR Genotyping Kits

Commercially available kits for human STR genotyping are recommended due to the extensive validation they have undergone on behalf of the forensics community. Some laboratories have developed their own STR assays [56]; however, they have not undergone as rigorous testing as the commercial kits and may not produce high quality results. Therefore, commercial kits are preferred and lists of different kits are available on the NIST website and in the 2021 ASN-0002 revised edition [49].

Inappropriate Authentication Methods of Cell Lines and Tissue Samples

Korch and colleagues [46, 47], and Appendix D in the 2021 revision of the ASN-0002 standard [49] discuss both earlier methods of authentication of cell lines and tissue samples as well as inappropriate methods that have been too frequently used in the literature. The two most common invalid methods are by visual examination of cellular morphology and/or transcript or protein expression. Visually it is very difficult to distinguish between many cell lines and all of these types of observations can be strongly affected by growth conditions.

Next-generation transcriptome comparisons [34] can be useful for monitoring differences between aliquots of samples of the same cell line to ascertain whether the data can be usefully compared and whether an unknown cell line has contaminated a culture. However, such sequence data are not useful to identify cell lines using the Cellosaurus or similar databases which use only STR data based on genomic DNA. Also, in the case where a copy of a gene is not expressed for any number of reasons, the % match from transcriptomic date will be lower than that obtained from STR genotyping of genomic DNA.

Glossary of Terms

Please refer to the "Genetics Terms" section of the "Glossary of Quantitative Biology Terms" for a list of terms and definitions used in this chapter and to the Glossary of terms in the 2021 revision of the ASN-0002 Standards [49].

License

All Assay Guidance Manual content, except where otherwise noted, is licensed under a Creative Commons Attribution- NonCommercial-ShareAlike 3.0 Unported license (CC BY-NC-SA 3.0), which permits copying, distribution, transmission, and adaptation of the work, provided the original work and any copyrighted figures and data are properly cited and not used for commercial purposes. Any altered, transformed, or adapted form of the work may only be distributed under the same or similar license to this one.

Acknowledgements

We would like to thank Drs. Yvonne A Reid, Wilhelm G Dirks, and Amanda Capes-Davis for their suggestions and comments on an earlier draft of this AGM chapter and Drs Reid, Douglas Storts, and their colleagues for permission to use some figures from the 2013 AGM chapter [68] for this 2023 AGM chapter describing the authentication of cell lines by STR genotyping. We are also grateful to Dr. Marileila Varella-Garcia for use of her karyotype of the lymphoblastoid cell line ML14.

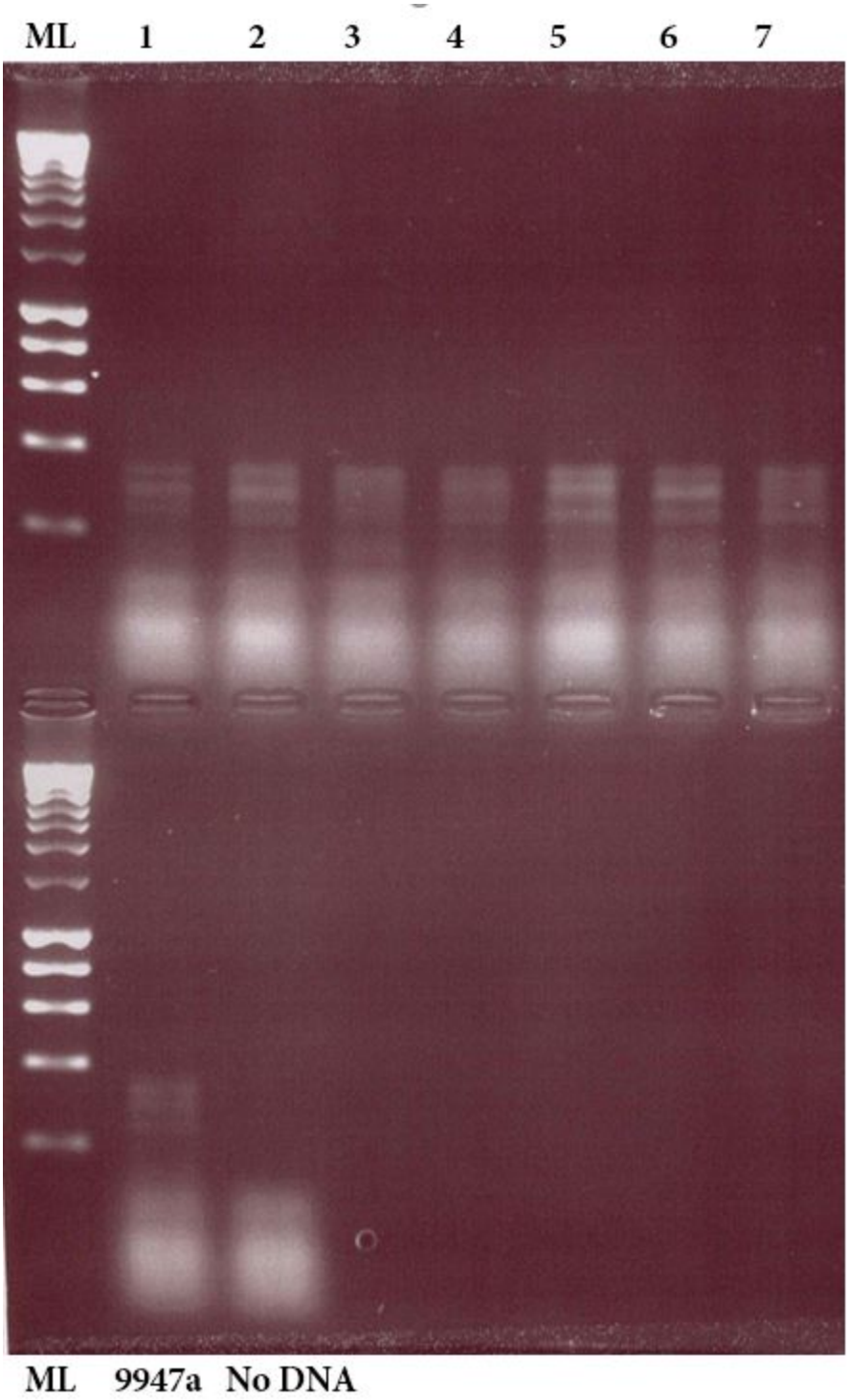


Figure 25. Agarose Gel of STR Profiling Reactions. Lane ML is the Bioline DNA 1 kb HyperLadder mass ladder in both the top and bottom set of lanes. Samples 1-7 are aliquots of the STR profiling reactions from 7 different cell line DNA samples. 9947a is the STR reaction with the positive control DNA and No DNA is the negative control STR reaction. Copyright CTK.

Useful Resources

The International Cell Line Authentication Committee (ICLAC) maintains a register of misidentified cell lines. See Step 1 for additional information about this organization. Links to additional guidelines for handling and authenticating cell lines include:

- Guide to Human Cell Line Authentication
- Advice to Scientists
- Cell Line Policy for Research Institutions

See this list of commercially available STR Multiplex Kits and the 2021 Revision of the ANSI-ATCC ASN-0002, Appendices A and B [49].

The Find Cell program by Find Genomics allows maintaining a database of cell lines being used in a laboratory [86].

Links to Cell Line Repositories with Human STR Genotypes and Search Tools

This list is derived from Chapter 6 and Appendix I of the 2021 revision of the ANSI-ATCC ASN-0002 Standard [49].

- **American Type Culture Collection (ATCC)** – A searchable database of human cell line STR profiles.
- **Catalogue of Somatic Mutations in Cancer (COSMIC)** - Collection of STR profiles for 1,103 cell lines, but does not have a search tool.
- **Cellosaurus Cell Line Knowledge Database and CLASTR Search Tool** – See Step 1 for details.
- **Childhood Cancer Repository of Cell lines and Xenografts STR database of the Children's Oncology Group (COG)** contains a compilation of searchable STR data from this repository plus many profiles from the ATCC, DSMZ, JCRB, RIKEN.
- **CLDB AND HyperCLDB (version 4.0.201701)** – Searchable collection of human STR genotypes.
- **CLIMA 2.1 - The Cell Line Integrated Molecular Authentication Database 2.1 (version 2.1.201505)** – This resource provides a large collection of searchable STR genotyping data.
- **European Collection of Authenticated Cell Cultures (ECACC)** – This is culture collections of the Public Health England has a searchable collection of human STR genotypes and is a source of authenticated cell lines and induced pluripotent stem cells.
- **Leibniz Institute DSMZ - Deutsche Sammlung von Mikroorganismen und Zellkulturen: The Leibniz Institute DSMZ - German Collection of Microorganisms and Cell Cultures.** This searchable STR database of human cell lines is a compilation of some data from four repositories (ATCC, DSMZ, JCRB, and RIKEN) and reports profiles with different match scores.
- **Japanese Collection of Research Bioresources (JCRB)** - This organization is part of the Japanese National Institutes of Biomedical Innovation, Health and Nutrition. The STR profiles of many of their cell lines are in the database of STR profiles compiled by the DSMZ.
- **Korean Cell Line Bank (KCLB)** – The cell line repository of the Cancer Research Institute of the Seoul National University College of Medicine contains with cell lines from the JCRB and numerous laboratories, including SNU cell lines. Much of the cell line data are available in the Cellosaurus website.
- **NCBI Biosample Human Cell Line Database** - The NCBI BioSample database serves as a central and freely disseminated public repository for authenticated human cell line records. It cannot be searched for STR match, but does contain actual electropherograms of STR profiles, which can be examined herein.
- **Rikagaku Kenkyūsho (RIKEN)** – This nationwide group of Japanese research institutions maintains a cell line repository. Many of the cell line STR profiles are accessible in the databases of STR profiles maintained by the DSMZ and Cellosaurus.

References

1. Almeida JL, Cole KD. 2017. Mouse Cell Line Authentication USA patent US 9,556,482, .
2. Almeida JL, Cole KD. 2020. Mouse Cell Line Authentication. . USA patent US 10,745,753.
3. Almeida JL, Dakic A, Kindig K, Kone M, Letham DLD, Langdon S, Peat R, Holding-Pillai J, Hall EM, Ladd M, Shaffer MD, Berg H, Li J, Wigger G, Lund S, Steffen CR, Fransway BB, Geraghty B, Natoli M, Bauer B,

Gollin SM, Lewis DW, Reid Y. Interlaboratory study to validate a STR profiling method for intraspecies identification of mouse cell lines. PLoS One. 2019;14:e0218412. PMID. PubMed PMID: 31220119.
4. Almeida JL, Hill CR, Cole KD. Authentication of African green monkey cell lines using human short tandem repeat markers. BMC Biotechnol. 2011;11:102. PMID. PubMed PMID: 22059503.
5. Almeida JL, Hill CR, Cole KD. Mouse cell line authentication. Cytotechnology. 2014;66:133–147. PMID. PubMed PMID: 23430347.
6. Anonymous. Identity crisis. Nature. 2009;457:935–936. PMID. PubMed PMID: 19225471.
7. ATCC SDO. 2011. ASN-0002. Authentication of Human Cell Lines: Standardization of STR Profiling. ANSI eStandards Store, by ATCC-Standards Development Organization (SDO). Available at: https://webstore.ansi.org/standards/atcc/ansiatccasn00022011. Accessed: September, 2021.
8. Bady P, Diserens AC, Castella V, Kalt S, Heinimann K, Hamou MF, Delorenzi M, Hegi ME. DNA fingerprinting of glioma cell lines and considerations on similarity measurements. Neuro Oncol. 2012;14:701–711. PMID. PubMed PMID: 22570425.
9. Bairoch A. The Cellosaurus, a cell-line knowledge resource. J Biomol Tech. 2018;29:25–38. PMID. PubMed PMID: 29805321.
10. Bairoch A. 2018. The Cellosaurus: a cell line knowledge resource, by The CALIPHO group at the Swiss Institute of Bioinformatics, Geneva, Switzerland. Available at: https://web.expasy.org/cellosaurus/. Accessed: October 2021.
11. Baust JM, Buehring GC, Campbell L, Elmore E, Harbell JW, Nims RW, Price P, Reid YA, Simione F. Best practices in cell culture: an overview. In Vitro Cell Dev Biol Anim. 2017;53:669–672. PMID. PubMed PMID: 28808859.
12. Ben-David U. Genomic instability, driver genes and cell selection: Projections from cancer to stem cells. Biochim Biophys Acta. 2015;1849:427–435. PMID. PubMed PMID: 25132386.
13. Ben-David U, Siranosian B, Ha G, Tang H, Oren Y, Hinohara K, Strathdee CA, Dempster J, Lyons NJ, Burns R, Nag A, Kugener G, Cimini B, Tsvetkov P, Maruvka YE, O'Rourke R, Garrity A, Tubelli AA, Bandopadhayay P, Tsherniak A, Vazquez F, Wong B, Birger C, Ghandi M, Thorner AR, Bittker JA, Meyerson M, Getz G, Beroukhim R, Golub TR. Genetic and transcriptional evolution alters cancer cell line drug response. Nature. 2018;560:325–330. PMID. PubMed PMID: 30089904.
14. Berger B, Heinrich J, Niederstätter H, Hecht W, Morf N, Hellmann A, Rohleder U, Schleenbecker U, Berger C, Parson W. Forensic characterization and statistical considerations of the CaDNAP 13-STR panel in 1,184 domestic dogs from Germany, Austria, and Switzerland. Forensic Sci Int Genet. 2019;42:90–98. PMID. PubMed PMID: 31277051.
15. Boonstra JJ, van Marion R, Beer DG, Lin L, Chaves P, Ribeiro C, Pereira AD, Roque L, Darnton SJ, Altorki NK, Schrump DS, Klimstra DS, Tang LH, Eshleman JR, Alvarez H, Shimada Y, van Dekken H, Tilanus HW, Dinjens WN. Verification and unmasking of widely used human esophageal adenocarcinoma cell lines. J Natl Cancer Inst. 2010;102:271–274. PMID. PubMed PMID: 20075370.
16. Brownstein MJ, Carpten JD, Smith JR. Modulation of non-templated nucleotide addition by Taq DNA polymerase: primer modifications that facilitate genotyping. Biotechniques. 1996;20:1004–1006, 1008-1010. PMID. PubMed PMID: 8780871.
17. Bryda EC, Riley LK. Multiplex microsatellite marker panels for genetic monitoring of common rat strains. J Am Assoc Lab Anim Sci. 2008;47:37–41. PMID. PubMed PMID: 18459711.
18. Butler JM. 2005. Forensic DNA Typing: Biology, technology, and genetics of STR markers, 2nd ed. Elsevier Academic Press, Amsterdam.
19. Butler JM. 2015. Advanced Topics in Forensic DNA Typing: Interpretation. Academic Press, Elsevier, Inc, Oxford, UK; San Diego, CA, USA.
20. Capes-Davis A, Freshney RI. 2021. Freshney's Culture of Animal Cells: A Manual of Basic Technique and Specialized Applications, Eighth ed. Wiley.
21. Capes-Davis A, Reid YA, Kline MC, Storts DR, Strauss E, Dirks WG, Drexler HG, MacLeod RA, Sykes G, Kohara A, Nakamura Y, Elmore E, Nims RW, Alston-Roberts C, Barallon R, Los GV, Nardone RM, Price PJ,

Steuer A, Thomson J, Masters JR, Kerrigan L. Match criteria for human cell line authentication: where do we draw the line? Int J Cancer. 2013;132:2510–2519. PMID. PubMed PMID: 23136038.
22. Capes-Davis A, Theodosopoulos G, Atkin I, Drexler HG, Kohara A, MacLeod RA, Masters JR, Nakamura Y, Reid YA, Reddel RR, Freshney RI. Check your cultures! A list of cross-contaminated or misidentified cell lines. Int J Cancer. 2010;127:1–8. PMID. PubMed PMID: 20143388.
23. Cooper JK, Sykes G, King S, Cottrill K, Ivanova NV, Hanner R, Ikonomi P. Species identification in cell culture: a two-pronged molecular approach. In Vitro Cell Dev Biol Anim. 2007;43:344–351. PMID. PubMed PMID: 17934781.
24. Coriell LL. Detection and elimination of contaminating organisms. Natl Cancer Inst Monogr. 1962;7:33–53. PMID. PubMed PMID: 13881339.
25. Dang Z, Li L, Kong X, Zhang G, Liu Q, Li H, Li L, Zhang R, Cui W, Wang Y. Evaluation of allelic alterations in short tandem repeats in papillary thyroid cancer. Mol Genet Genomic Med. 2020;8:e1164. PMID. PubMed PMID: 32043756.
26. Didion JP, Buus RJ, Naghashfar Z, Threadgill DW, Morse HC 3rd, de Villena FP. SNP array profiling of mouse cell lines identifies their strains of origin and reveals cross-contamination and widespread aneuploidy. BMC Genomics. 2014;15:847. PMID. PubMed PMID: 25277546.
27. Drexler HG, Dirks WG, MacLeod RA. False human hematopoietic cell lines: cross-contaminations and misinterpretations. Leukemia. 1999;13:1601–1607. PMID. PubMed PMID: 10516762.
28. Drexler HG, Dirks WG, MacLeod RA, Uphoff CC. False and mycoplasma-contaminated leukemia-lymphoma cell lines: time for a reappraisal. Int J Cancer. 2017;140:1209–1214. PMID. PubMed PMID: 27870004.
29. Drexler HG, Uphoff CC. Mycoplasma contamination of cell cultures: Incidence, sources, effects, detection, elimination, prevention. Cytotechnology. 2002;39:75–90. PMID. PubMed PMID: 19003295.
30. Drexler HG, Uphoff CC, Dirks WG, MacLeod RA. Mix-ups and mycoplasma: the enemies within. Leuk Res. 2002;26:329–333. PMID. PubMed PMID: 11839374.
31. Earle WR, Schilling EL, Stark TH, Strauss NP, Brown MF, Shelton E. Production of malignancy in vitro. IV. The mouse fibroblast cultures and changes seen in the living cells. JNCI: Journal of the National Cancer Institute. 1943;4:165–212. PMID.
32. Edelmann J, Lessig R, Hering S, Horn LC. 2004. Loss of heterozygosity and microsatellite instability of forensically used STR markers in human cervical carcinoma. International Congress Series 1261:499-501. PMID:
33. Eltonsy N, Gabisi V, Li X, Russe KB, Mills GB, Stemke-Hale K. Detection algorithm for the validation of human cell lines. Int J Cancer. 2012;131:E1024–1030. PMID. PubMed PMID: 22419365.
34. Fasterius E, Raso C, Kennedy S, Rauch N, Lundin P, Kolch W, Uhlen M, Al-Khalili Szigyarto C. A novel RNA sequencing data analysis method for cell line authentication. PLoS One. 2017;12:e0171435. PMID. PubMed PMID: 28192450.
35. Freshney RI. 2016. Culture of Animal Cells: A Manual of Basic Technique and Specialized Applications. Wiley.
36. Gartler SM. Genetic markers as tracers in cell culture. Natl Cancer Inst Monogr. 1967;26:167–195. PMID. PubMed PMID: 4864103.
37. Gartler SM. Apparent Hela cell contamination of human heteroploid cell lines. Nature. 1968;217:750–751. PMID. PubMed PMID: 5641128.
38. Geraghty RJ, Capes-Davis A, Davis JM, Downward J, Freshney RI, Knezevic I, Lovell-Badge R, Masters JR, Meredith J, Stacey GN, Thraves P, Vias M. Guidelines for the use of cell lines in biomedical research. Br J Cancer. 2014;111:1021–1046. PMID. PubMed PMID: 25117809.
39. Gey GO, Coffman WD, Kubicek MT. Tissue culture studies of the proliferative capacity of cervical carcinoma and normal epithelium. Cancer Res. 1952;12:264–265. PMID.
40. Hauge XY, Litt M. A study of the origin of 'shadow bands' seen when typing dinucleotide repeat polymorphisms by the PCR. Hum Mol Genet. 1993;2:411–415. PMID. PubMed PMID: 8504301.

41. Hill CR, Butler JM, Vallone PM. A 26plex autosomal STR assay to aid human identity testing*. J Forensic Sci. 2009;54:1008–1015. PMID. PubMed PMID: 19627417.
42. Horbach S, Halffman W. The ghosts of HeLa: How cell line misidentification contaminates the scientific literature. PLoS One. 2017;12:e0186281. PMID. PubMed PMID: 29023500.
43. Jeffreys AJ, Wilson V, Thein SL. Individual-specific 'fingerprints' of human DNA. Nature. 1985;316:76–79. PMID. PubMed PMID: 2989708.
44. Jones HW Jr, McKusick VA, Harper PS, Wuu KD. George Otto Gey. (1899-1970). The HeLa cell and a reappraisal of its origin. Obstet Gynecol. 1971;38:945–949. PMID. PubMed PMID: 4942173.
45. Kleensang A, Vantangoli MM, Odwin-DaCosta S, Andersen ME, Boekelheide K, Bouhifd M, Fornace AJ Jr, Li HH, Livi CB, Madnick S, Maertens A, Rosenberg M, Yager JD, Zhaog L, Hartung T. Genetic variability in a frozen batch of MCF-7 cells invisible in routine authentication affecting cell function. Sci Rep. 2016;6:28994. PMID. PubMed PMID: 27456714.
46. Korch C, Hall EM, Dirks WG, Ewing M, Faries M, Varella-Garcia M, Robinson S, Storts D, Turner JA, Wang Y, Burnett EC, Healy L, Kniss D, Neve RM, Nims RW, Reid YA, Robinson WA, Capes-Davis A. Authentication of M14 melanoma cell line proves misidentification of MDA-MB-435 breast cancer cell line. Int J Cancer. 2018;142:561–572. PMID. PubMed PMID: 28940260.
47. Korch C, Varella-Garcia M. 2018. Tackling the Human Cell Line and Tissue Misidentification Problem Is Needed for Reproducible Biomedical Research. Adv Mol Pathol 1:209-228.e236. PMID: 10.1016/j.yamp.2018.07.003
48. Korch CT, Capes-Davis A. The Extensive and Expensive Impacts of HEp-2 [HeLa], Intestine 407 [HeLa], and Other False Cell Lines in Journal Publications. SLAS Discov. 2021;26:1268–1279. PMID. PubMed PMID: 34697958.
49. Korch CT, Hall EM, Dirks WG, Sykes GR, Capes-Davis A, Butler JM, Neve RM, Nims RW, Storts DR, Tian F, Nardone RM. 2021. Human Cell Line Authentication. Standardization of Short Tandem Repeat (STR) Profiling. ASN-0002 Revised 2021, by American National Standards Institute - American Type Culture Collection Standards Development Organization. Available at: https://webstore.ansi.org/Standards/ATCC/ansiatccasn00022021. Accessed: September, 2021.
50. Landa I, Pozdeyev N, Korch C, Marlow LA, Smallridge RC, Copland JA, Henderson YC, Lai SY, Clayman GL, Onoda N, Tan AC, Garcia-Rendueles MER, Knauf JA, Haugen BR, Fagin JA, Schweppe RE. Comprehensive Genetic Characterization of Human Thyroid Cancer Cell Lines: A Validated Panel for Preclinical Studies. Clin Cancer Res. 2019;25:3141–3151. PMID. PubMed PMID: 30737244.
51. Langdon WB. Mycoplasma contamination in the 1000 Genomes Project. BioData Min. 2014;7:3. PMID. PubMed PMID: 24872843.
52. Liang-Chu MM, Yu M, Haverty PM, Koeman J, Ziegle J, Lee M, Bourgon R, Neve RM. Human biosample authentication using the high-throughput, cost-effective SNPtrace(TM) system. PLoS One. 2015;10:e0116218. PMID. PubMed PMID: 25714623.
53. Lucey BP, Nelson-Rees WA, Hutchins GM. Henrietta Lacks, HeLa cells, and cell culture contamination. Arch Pathol Lab Med. 2009;133:1463–1467. PMID. PubMed PMID: 19722756.
54. MacLeod RA, Dirks WG, Matsuo Y, Kaufmann M, Milch H, Drexler HG. Widespread intraspecies cross-contamination of human tumor cell lines arising at source. Int J Cancer. 1999;83:555–563. PMID. PubMed PMID: 10508494.
55. MacLeod RA, Nagel S, Scherr M, Schneider B, Dirks WG, Uphoff CC, Quentmeier H, Drexler HG. Human leukemia and lymphoma cell lines as models and resources. Curr Med Chem. 2008;15:339–359. PMID. PubMed PMID: 18288989.
56. Marlow LA, Rohl SD, Miller JL, Knauf JA, Fagin JA, Ryder M, Milosevic D, Netzel BC, Grebe SK, Reddi HV, Smallridge RC, Copland JA. Methodology, Criteria, and Characterization of Patient-Matched Thyroid Cell Lines and Patient-Derived Tumor Xenografts. J Clin Endocrinol Metab. 2018;103:3169–3182. PMID. PubMed PMID: 29846633.
57. Masters JR. Cell-line authentication: End the scandal of false cell lines. Nature. 2012;492:186. PMID. PubMed PMID: 23235867.

58. Masters JR, Thomson JA, Daly-Burns B, Reid YA, Dirks WG, Packer P, Toji LH, Ohno T, Tanabe H, Arlett CF, Kelland LR, Harrison M, Virmani A, Ward TH, Ayres KL, Debenham PG. Short tandem repeat profiling provides an international reference standard for human cell lines. PNAS. 2001;98:8012–8017. PMID. PubMed PMID: 11416159.
59. Nakamura Y, Leppert M, O'Connell P, Wolff R, Holm T, Culver M, Martin C, Fujimoto E, Hoff M, Kumlin E, et al. Variable number of tandem repeat (VNTR) markers for human gene mapping. Science. 1987;235:1616–1622. PMID. PubMed PMID: 3029872.
60. Nelson-Rees WA. The identification and monitoring of cell line specificity. Prog Clin Biol Res. 1978;26:25–79. PMID. PubMed PMID: 218226.
61. Nelson-Rees WA, Daniels DW, Flandermeyer RR. Cross-contamination of cells in culture. Science. 1981;212:446–452. PMID. PubMed PMID: 6451928.
62. Nelson-Rees WA, Flandermeyer RR. HeLa cultures defined. Science. 1976;191:96–98. PMID. PubMed PMID: 1246601.
63. O'Donoghue LE, Rivest JP, Duval DL. Polymerase chain reaction-based species verification and microsatellite analysis for canine cell line validation. J Vet Diagn Invest. 2011;23:780–785. PMID. PubMed PMID: 21908323.
64. Parson W, Kirchebner R, Muhlmann R, Renner K, Kofler A, Schmidt S, Kofler R. Cancer cell line identification by short tandem repeat profiling: power and limitations. FASEB J. 2005;19:434–436. PMID. PubMed PMID: 15637111.
65. Peloso G, Grignani P, Rosso R, Previderè C. 2003. Forensic evaluation of tetranucleotide STR instability in lung cancer. International Congress Series 1239:719-721. PMID:
66. Phuchareon J, Ohta Y, Woo JM, Eisele DW, Tetsu O. Genetic profiling reveals cross-contamination and misidentification of 6 adenoid cystic carcinoma cell lines: ACC2, ACC3, ACCM, ACCNS, ACCS and CAC2. PLoS One. 2009;4:e6040. PMID. PubMed PMID: 19557180.
67. Rebuzzini P, Neri T, Zuccotti M, Redi CA, Garagna S. Chromosome number variation in three mouse embryonic stem cell lines during culture. Cytotechnology. 2008;58:17–23. PMID. PubMed PMID: 19002773.
68. Reid Y, Storts D, Riss T, Minor L. 2013. Authentication of Human Cell Lines by STR DNA Profiling Analysis. Assay Guidance Manual. PMID: 23805434
69. Robin T, Capes-Davis A, Bairoch A. CLASTR: The Cellosaurus STR similarity search tool - A precious help for cell line authentication. Int J Cancer. 2020;146:1299–1306. PMID. PubMed PMID: 31444973.
70. Rubocki RJ, Duffy KJ, Shepard KL, McCue BJ, Shepherd SJ, Wisecarver JL. Loss of heterozygosity detected in a short tandem repeat (STR) locus commonly used for human DNA identification. J Forensic Sci. 2000;45:1087–1089. PMID. PubMed PMID: 11005185.
71. Schmelz M, Cress AE, Barrera J, McDaniel KM, Davis TL, Fuchs L, Dalkin BL, Nagle RB. 2004. Erratum: PEAZ-1: A new human prostate neoplastic epithelial cell line. Prostate. 2001;48:79–92. Accessed: September 2021.
72. Schweppe RE, Klopper JP, Korch C, Pugazhenthi U, Benezra M, Knauf JA, Fagin JA, Marlow LA, Copland JA, Smallridge RC, Haugen BR. Deoxyribonucleic acid profiling analysis of 40 human thyroid cancer cell lines reveals cross-contamination resulting in cell line redundancy and misidentification. J Clin Endocrinol Metab. 2008;93:4331–4341. PMID. PubMed PMID: 18713817.
73. Schweppe RE, Korch C. Challenges and Advances in the Development of Cell Lines and Xenografts. Advances in Molecular Pathology. 2018;1:239–251. PMID.
74. Schweppe RE, Pozdeyev N, Pike LA, Korch C, Zhou Q, Sams SB, Sharma V, Pugazhenthi U, Raeburn C, Albuja-Cruz MB, Reigan P, LaBarbera DV, Landa I, Knauf JA, Fagin JA, Haugen BR. Establishment and Characterization of Four Novel Thyroid Cancer Cell Lines and PDX Models Expressing the RET/PTC1 Rearrangement, BRAFV600E, or RASQ61R as Drivers. Mol Cancer Res. 2019;17:1036–1048. PMID. PubMed PMID: 30733375.
75. Sørensen T. A method of establishing groups of equal amplitudes in plant sociology based on similarity of species content and its application to analyses of the vegetation on Danish commons. Kongelige Danske

Videnskabernes Selskab. Det Kongelige Danske Videnskabernes Selskab Biologiske Skrifter. 1948;5:1–34. PMID.
76. Sugawara A, Goto K, Sotomaru Y, Sofuni T, Ito T. Current status of chromosomal abnormalities in mouse embryonic stem cell lines used in Japan. Comp Med. 2006;56:31–34. PMID. PubMed PMID: 16521857.
77. Tanabe H, Takada Y, Minegishi D, Kurematsu M, Masui T, Mizusawa H. 1999. Cell line individualization by STR multiplex system in the cell bank found cross-contamination between ECV304 and EJ-1/T24. Available at: https://www.jstage.jst.go.jp/article/jtca1981/18/4/18_329/_article/-char/en. Accessed: September, 2021.
78. van Bokhoven A. 2004. Models for prostate cancer. Molecular characterization and critical appraisal of human prostate carcinoma cell lines. PhD. University Medical Centre St. Radboud, Nijmegen, The Netherlands, Nijmegen, The Netherlands.
79. van Bokhoven A, Caires A, Maria MD, Schulte AP, Lucia MS, Nordeen SK, Miller GJ, Varella-Garcia M. Spectral karyotype (SKY) analysis of human prostate carcinoma cell lines. Prostate. 2003;57:226–244. PMID. PubMed PMID: 14518030.
80. van Bokhoven A, Varella-Garcia M, Korch C, Hessels D, Miller GJ. Widely used prostate carcinoma cell lines share common origins. Prostate. 2001;47:36–51. PMID. PubMed PMID: 11304728.
81. van Bokhoven A, Varella-Garcia M, Korch C, Miller GJ. TSU-Pr1 and JCA-1 cells are derivatives of T24 bladder carcinoma cells and are not of prostatic origin. Cancer Res. 2001;61:6340–6344. PMID. PubMed PMID: 11522622.
82. Vaughan L, Glänzel W, Korch C, Capes-Davis A. Widespread use of misidentified cell line KB (HeLa): Incorrect attribution and its impact revealed through mining the scientific literature. Cancer Res. 2017;77:2784–2788. PMID. PubMed PMID: 28455420.
83. Wahls WP, Wallace LJ, Moore PD. Hypervariable minisatellite DNA is a hotspot for homologous recombination in human cells. Cell. 1990;60:95–103. PMID. PubMed PMID: 2295091.
84. Walsh PS, Fildes NJ, Reynolds R. Sequence analysis and characterization of stutter products at the tetranucleotide repeat locus vWA. Nucleic Acids Res. 1996;24:2807–2812. PMID. PubMed PMID: 8759015.
85. Yu M, Selvaraj SK, Liang-Chu MM, Aghajani S, Busse M, Yuan J, Lee G, Peale F, Klijn C, Bourgon R, Kaminker JS, Neve RM. A resource for cell line authentication, annotation and quality control. Nature. 2015;520:307–311. PMID. PubMed PMID: 25877200.
86. Zaaijer S, Groen SC, Sanjana NE. Tracking cell lineages to improve research reproducibility. Nat Biotechnol. 2021;39:666–670. PMID. PubMed PMID: 34012093.

In vitro 3D Spheroids and Microtissues: ATP-based Cell Viability and Toxicity Assays

Monika Kijanska, Dr[1] and Jens Kelm, Dr[2]

Created: January 21, 2016.

Abstract

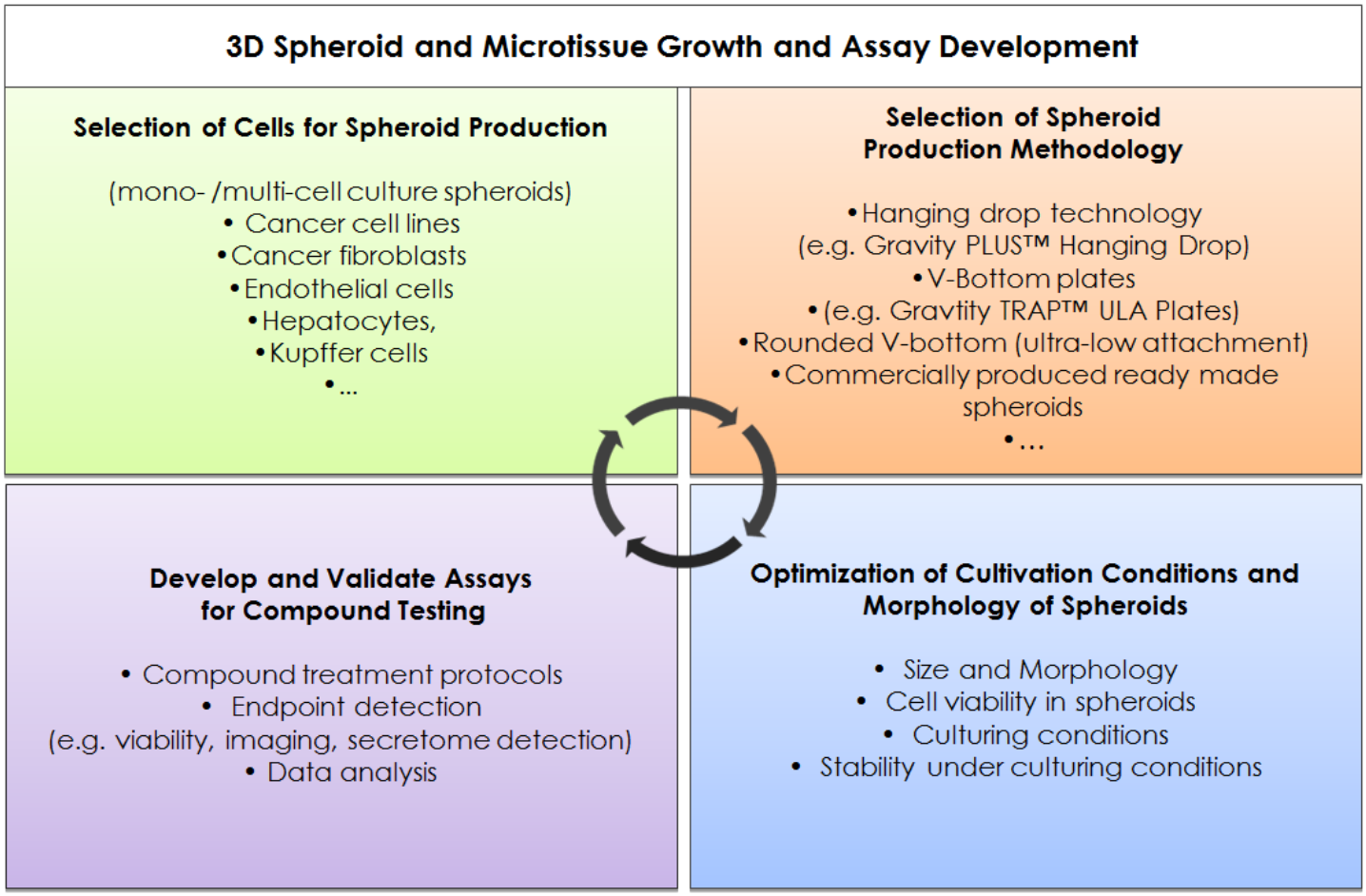
In vitro models continuously evolve to more closely mimic and predict biological responses of living organisms. Just in the past years many novel three dimensional (3D) organotypic models, which resemble tissue structure, function and even disease progression, have been developed. However, application of more complex models and technologies may increase the risk of compromising assay robustness and reproducibility. Consequently, the first developmental stage of cell-based assays is to combine complex tissue models with standard assays - a combination that already provides more physiologically insightful information when compared to two-dimensional (2D) systems. The final goal should be to exploit the full potential of tissue-like *in vitro* models by investigating them with modern assays such as –Omics and imaging technologies. Furthermore, organotypic models will allow for a design of novel assay concepts that utilize the whole tool box of models and endpoints.

In this chapter we focus on assessment of spheroid viability by measuring intracellular ATP content. This primary assay performed on 3D cell culture system is a powerful tool to predict with high confidence health, growth and energy status of tissue of interest. The 3D spheroid model is particularly useful to mimic solid-tumors from a physiologically relevant architectural perspective, when they are grown with multiple cell types prevalent in these tumors. However, this assay is equally applicable for other non-spheroid 3D tissue models to quantify viability and toxicity.

Author Affiliations: 1 InSphero AG; Email: monika.kijanska@insphero.com. 2 InSphero AG; Email: jens.kelm@insphero.com.

Corresponding author.

Flow Chart: 3D Spheroid and Microtissue Growth and Assay Development



Introduction

In recent decades cell-based assays to investigate cell biology, drug efficacy, metabolism and toxicology were dominated by technologies employing cells grown on flat plastic surfaces (2D) or in single cell suspension (1). However, biology of cells is extensively influenced by the environmental context such as cell-cell contacts, cell-matrix interactions, cell polarity or oxygen profiles.

For many years biology of avascular tumor has been recognized by cancer researchers to be particularly well mimicked by three dimensional (3D) cell cultures (2)(3). For instance, one of the earliest 3D-acknowledged effects correlating with *in vivo* clinical observations was development of multicellular resistance (MCR) to anticancer drugs in 3D culture formats. As highlighted by Desoize and Jardillier, cancer cells embedded within a 3D environment had lower sensitivity to anticancer drugs, e.g. upon Vinblastine exposure human lung carcinoma (A549) monolayer culture exhibited the IC_{50} value of 0.008 µmol/l, whereas the IC_{50} value of spheroid culture was 53 µmol/l (4). Importantly, drug sensitivity is a net effect of multiple factors and is highly regulated by hypoxia, which occurs in the oxygen-deficient areas of the tumor with limited access to the capillary network. Low oxygen partial pressure can lead to either higher drug sensitivity or elevated drug resistance of the tumor, depending on the drug mechanism and structure. Additionally, extracellular acidification is yet another factor influencing response to either basic (e.g. Doxorubicin) or acidic (e.g. Chlorambucil) drugs. In this case, the uptake of basic drugs is decreased, whereas the uptake of acidic drugs is increased, resulting in higher drug resistance or higher drug sensitivity, respectively (5)(6). Therefore, tumor cells cultured in 3D formats, which are

exposed to complex and heterogenic environmental context, are more relevant tool to study tumor biology and responsiveness than standard 2D cell culture.

Another example of cells with well documented influence of culturing conditions on physiology are hepatocytes. Hepatocytes are characterized by their polygonal shape and multi-polarization with at least two basolateral and two apical surfaces. Changes in cell form limit cell–cell and cell–matrix interactions, consequently leading to reduced polarization, reduced bile canaliculi formation and a loss of important signaling pathways. Dedifferentiation of hepatocytes observed in 2D monolayer cell culture results in reduction of liver-specific functions, such as metabolic competence for detoxification, due to down-regulation of phase I and II enzymes. Therefore, maintenance of hepatocyte shape and function is of the utmost importance in hepatotoxicity studies. To tackle this problem, 3D liver models employing scaffolds, hydrogels and the cellular self-assembly approach have been created. Additionally, variety of different cell types, such as HepG2, HepaRG and primary hepatocytes, is currently used to investigate liver functions. For an in depth overview of current *in vitro* liver models and application please see Godoy et al. 2013 (7).

However, a decision about application of a cell-based methodology depends not only on its physiological properties, but also on its automation-compatibility, high throughput processing and feasibility to couple it with established endpoint. A number of technologies have been developed to create 3D tissue-mimicking environment on microscale *in vitro*, with embedding cells within a hydrogel or preventing of cellular adhesion to an artificial matrix and concomitant enforced cell re-aggregation being the main ones (Table 1) (8)(9)(10)(11)(12). Both scaffold-free technologies have been used successfully to create a 3D context of cancer cells, as they allow for reconstitution of cell type-specific extracellular environment. The concept of the hanging drop technology is one of the oldest ones and it provides the benefit of aggregation of defined types and number of cells. Already used by Ross Granville Harrison, the hanging drop has proven to be a universal technology to produce a wide variety of either disease models or primary tissues (7)(13)(14)(15)(16).

A paradigm of 3D spheroid/microtissue growth and assay development summarized in Flow Chart 1, shows interplay between selection of the most suitable cell type(s) and the 3D culturing technique, followed by optimization of spheroid culturing conditions and morphology, and between the assay development and the choice of the endpoint. Tailored combinations of the above elements offer experimental freedom that makes the 3D *in vitro* testing systems fit to the purpose, and increase the amount of extracted biologically-relevant information.

Table 1: Overview of the three basic cell culture concepts that are employed to coax cells into a 3D environment.

Scaffold-free	• cells produce their own ECM • no scaffold-associated growth factors/undefined components • no scaffold-associated batch-to-batch variations • possibility to co-culture different cell types • cellular aggregation in hanging drops or in ultra-low attachment plates • HTS-applicable **Examples:** Multicellular tumor spheroids (14)(39) Colorectal cancer spheroids (40) Human liver heterotypic microtissues (26) Celebral organoids (41) Myocardial microtissues (42)(23) Neurospheres (43) Kidney organoids (44)
Hydrogels/sponges/membranes	• mimic soft tissue stiffness and ECM composition • natural tissue-derived (batch-to batch variations, biological contaminants, e.g. growth factors) or synthetic • gel maintenance conditions may limit application **Examples:** Mini-guts (45)
Scaffolds/matrices	• added (biodegradable) cellular, acellular or composite materials • mimick ECM • diversified pore geometry, mechanistic properties, size and transparency • regenaretive medicine/implants **Examples:** Pre-vascularized scaffolds for bone regeneration (46)

1. *In Vitro* Toxicity and Drug Efficacy Testing in a 3D Spheroid Model

1.1. *In Vitro* Toxicity and Drug Efficacy Assay Concept

An increasing need for robust and reliable *in vitro* models for toxicity and drug efficacy testing is potentiated not only by the urge to make the process of bring therapeutics from the bench to the bedside faster and more cost-effective, but also by increasing regulatory and safety challenges. However, one of the major concerns of *in vitro* toxicity/efficacy testing remains its predictive power and translation into *in vivo* situations. As discussed in the introductory section, 3D cell culture formats such as spheroids, present a powerful alternative to standard 2D cell culture for *in vitro* studies (17)(18). The 3D spheroid model is particularly useful to mimic solid-tumors from a physiologically relevant architectural perspective, when they are grown with multiple cell types prevalent in these tumors.

The choice of the 3D model and the end point for toxicity/efficacy testing should depend on both the physiological question to be answered and the scale of the screen. In general, treatment with a toxicant can affect cellular and/or 3D cell culture morphology, viability, metabolic activity (such as oxygen consumption or metabolic enzyme activation), or tissue-specific function. Here, the spectrum of possible tissue-specific end points is constantly widening, together with the development of specialized 3D tissue models (19)(20)(21)(22)

(23)(24)(25). In case of liver microtissues of co-cultured hepatocytes and non-parenchymal cells (NPCs), established approaches include monitoring albumin and urea secretion, bile acid secretion, Kupffer cell-dependent IL-6 and TNFα secretion, to list a few (26). Contractile responsiveness of the myocardial microtissue model or glucose-stimulated insulin secretion by pancreatic microislets add yet further options to the growing list of functionality tests. Additionally, cultivated 3D cell culture models can be further analyzed using transcriptomic and proteomic methods, allowing for RNA and protein expression profiling upon toxicant exposure.

Although very powerful and promising, the use and predictivity of the 3D models has to be carefully validated for each given application, and conditions of cultivation and sample collection need to be standardized and controlled (27)(28). For screening purposes 3D cell culture models can be treated with many classes of substances (e.g. small molecules, biologicals, siRNA/RNAi). It is good practice to include an appropriate model- or cellular process-specific control compound of known toxic effect, such us Chlorpromazine for drug-induced hepatotoxicity, Aflatoxin B for apoptotic cell death induction or Trovafloxacine for inflammation-mediated toxicity (26).

In this section we will describe an exemplary experimental design to test the toxic effects over a range of concentrations of compounds dissolved in tissue culture-grade dimethyl sulfoxide (DMSO, 0.5% v/v) on liver microtissues of primary hepatocytes co-cultured with primary NPCs, produced in a hanging drop technology (Figure 1) (26). Analogously, such an experimental set up can be applied to evaluate anticancer efficacy of drugs in spheroids derived from cancer cell lines, such as HEY - human ovarian cancer cell line, as presented in Figure 2. The effect of the toxic agents on microtissue morphology, cell viability and tissue functionality can be further investigated, depending on the study goal, endpoint of interest and compatibility with the screening approach.

1.1.1. Sample Protocol for a Commercially Available 3D Spheroid System

The GravityPLUS™ Hanging Drop System is designed to generate organotypic microtissues in the process of scaffold-free aggregation of cells and to enable for their prolonged cultivation and multiple compound re-dosing. Microtissues are formed within 2-4 days from cell suspensions in hanging drops on the GravityPLUS™ Plates and are subsequently harvested into the ultra-low adhesive GravityTRAP™ ULA Plates. The unique design of GravityTRAP™ ULA wells allows for numerous media exchange without microtissue disturbance as well as for microtissue imaging. This 96-well platform is compatible with liquid handling stations and suitable for HT-screening applications. Commercially available hanging drop system and microtissues for hepatotoxicity testing include:

- GravityPLUS™ 10x Kit (96-well), includes 10 GravityPLUS™ and 10 GravityTRAP™ ULA plates (InSphero, Cat.# CS-06-001)
- GravityTRAP™ ULA Plate (InSphero, Cat.# CS-09-001)
- 3D InSight™ Human Liver Microtissues from primary hepatocytes, co-culture with non-parenchymal cells (96x) (InSphero, Cat.# MT-02-002-04)
- 3D InSight™ Human Liver Microtissues from primary hepatocytes (96x) (InSphero, Cat.# MT-02-002-01)
- 3D InSight™ Rat liver microtissues formed by primary hepatocytes (96x) (InSphero, Cat.# MT-02-001-01)
- 3D InSight™ Rat liver microtissues from primary hepatocytes, co-culture with nonparenchymal cells (96x) (InSphero, Cat.# MT-02-001-04)
- 3D InSight™ Human Pancreatic Microislets (96x) (InSphero, Cat.# MT-04-001-01)

1.1.2. Compound Preparation

1. To adjust 0.5% DMSO (v/v) final concentration in culture medium, prepare a 200 X top compound concentration stock in DMSO.

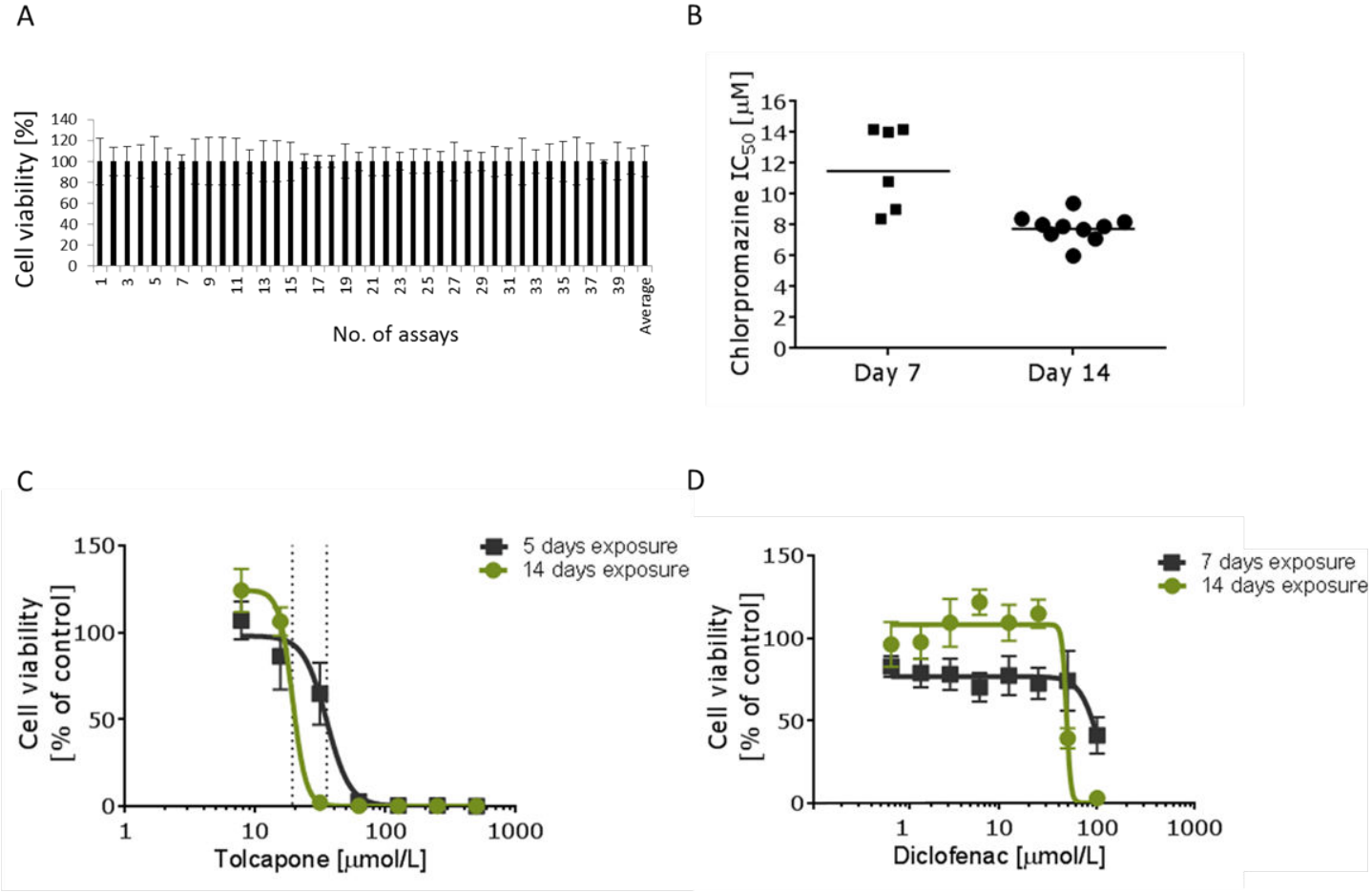


Figure 1: Toxicity testing in 3D heterotypic human liver microtissues - reproducibility and sensitivity of the ATP assay. (A) The human liver microtissues (hLiMTs) of co-cultured primary hepatocytes and primary NPCs were cultured for 14 days and their intra-tissue ATP content was assessed with Promega CellTiter-Glo® assay. In each assay (n = 40) average relative light units (RLU) from triplicates (3 microtissues) was set to 100%, the relative standard deviation (SD) of the mean is depicted. Average relative SD from 40 assays is 14.6%. (B) Reproducibility of IC_{50} values of Chlorpromazine after 7 days- and 14 days-long treatment of hLiMTs. Presented are results of independent experiments and their geometric mean. Note the reproducible shift to lower IC_{50} values after increased exposure time. (C) hLiMTs were exposed to increasing concentrations of Tolcapone and of Diclofenac (D) during shorter (5 days and 7 days, respectively; 1 re-dosing) or longer (14 days; 2 re-dosing) incubation. Note the shift to lower IC_{50} values after increased exposure time. Source: InSphero AG.

2. Prepare 6 dilutions of the compound stock in DMSO using sterile V-bottom microplate (e.g. Greiner Bio-one, Cat.#651161). Choose the dilution factor depending on the range of concentrations to be tested in the assay.
3. Transfer 2.5 µl of each compound dilution to the corresponding well on a deep well plate (e.g. Axygen®, Cat.# 391-01-111) as presented in Figure 3 (upper panel). For each re-dosing prepare a separate deep well plate.
4. For vehicle control, pipette 2.5 µl of DMSO to columns 3 and 4 on a deep well plate.
5. Seal deep well plates with aluminum plate sealer (e.g. Greiner Bio-One, Cat.# 67609) and store in – 20°C for future re-dosing.

1.1.3. Compound Exposure Protocol

1. Thaw deep well plates with compound(s) to be tested and add to each experimental well 497.5 µl of pre-warmed culture medium, thereby generating 1 X top concentration of the compound and its corresponding dilutions in culture medium with 0.5% DMSO (v/v).

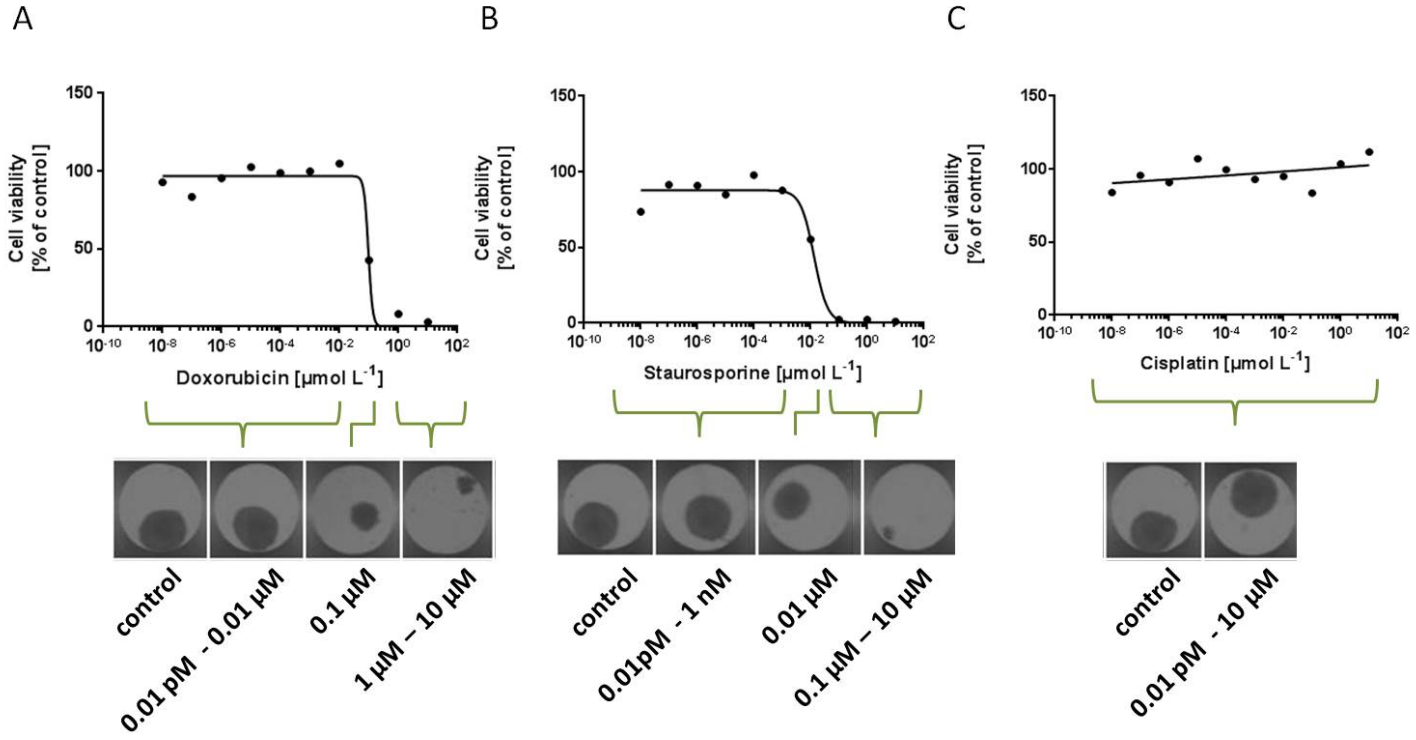


Figure 2: Anticancer drug efficacy testing in tumor microtissues - correlation between cell viability and tumor microtissue size suppression. Tumor microtissues grown from human ovarian cell line (HEY) were exposed to increasing concentrations of Doxorubicin (A), Staurosporine (B) and Cisplatin (C) for 10 days and their intra-tissue ATP content was assessed with Promega CellTiter-Glo® assay. Representative images of control and compound-treated microtissues show dose-dependent decrease of microtissue size upon treatment with Doxorubicin (A) and Staurosporine (B) which corresponds to decrease of microtissue viability as measured with the ATP assay. Cisplatin treatment (C) neither surpressed microtissue vibility nor had an impact on size of spheroids. Source: InSphero AG.

2. Gently aspirate culture medium from the GravityTRAP™ ULA Plate, leaving microtissues in the remnant volume of the medium in the V-shaped bottom of the well
3. Thoroughly mix medium with compound in the deep well plate and dose 70 µl per microtissue in required number of replicates (Figure 3, middle panel).
4. To control the DMSO effect on microtissues, add 70 µl of culture medium per well to column 2 on the Gravity GravityTRAP™ ULA Plate (Figure 1, middle panel).
5. Repeat dosing at required time intervals.
6. Determine toxicity and cell viability using CellTiter-Glo® 3D Cell Viability Assay or other suitable methods available.

1.2. Conclusion/Summary

Testing toxicity/drug efficacy in 3D cell culture formats presents multiple advantages over conventional 2D cell culture system. Firstly, cells aggregated into a 3D structure exhibit native tissue-mimicking organization, metabolic characteristics and specialized functions, and retain them for significantly longer periods of time, therefore enabling prolonged and repeated exposure. This in turn allows for detection of effects caused by longer exposure of lower compound concentrations, which appears frequently *in vivo.* For example, longer exposure tends to shift IC_{50} values towards lower compound concentrations, hence increasing sensitivity of the assay and better prediction of false negative compounds (Figure 1). Additionally, a comparison between shorter and longer toxic exposures may give an idea about sensitization of the system to a given treatment. Secondly, several

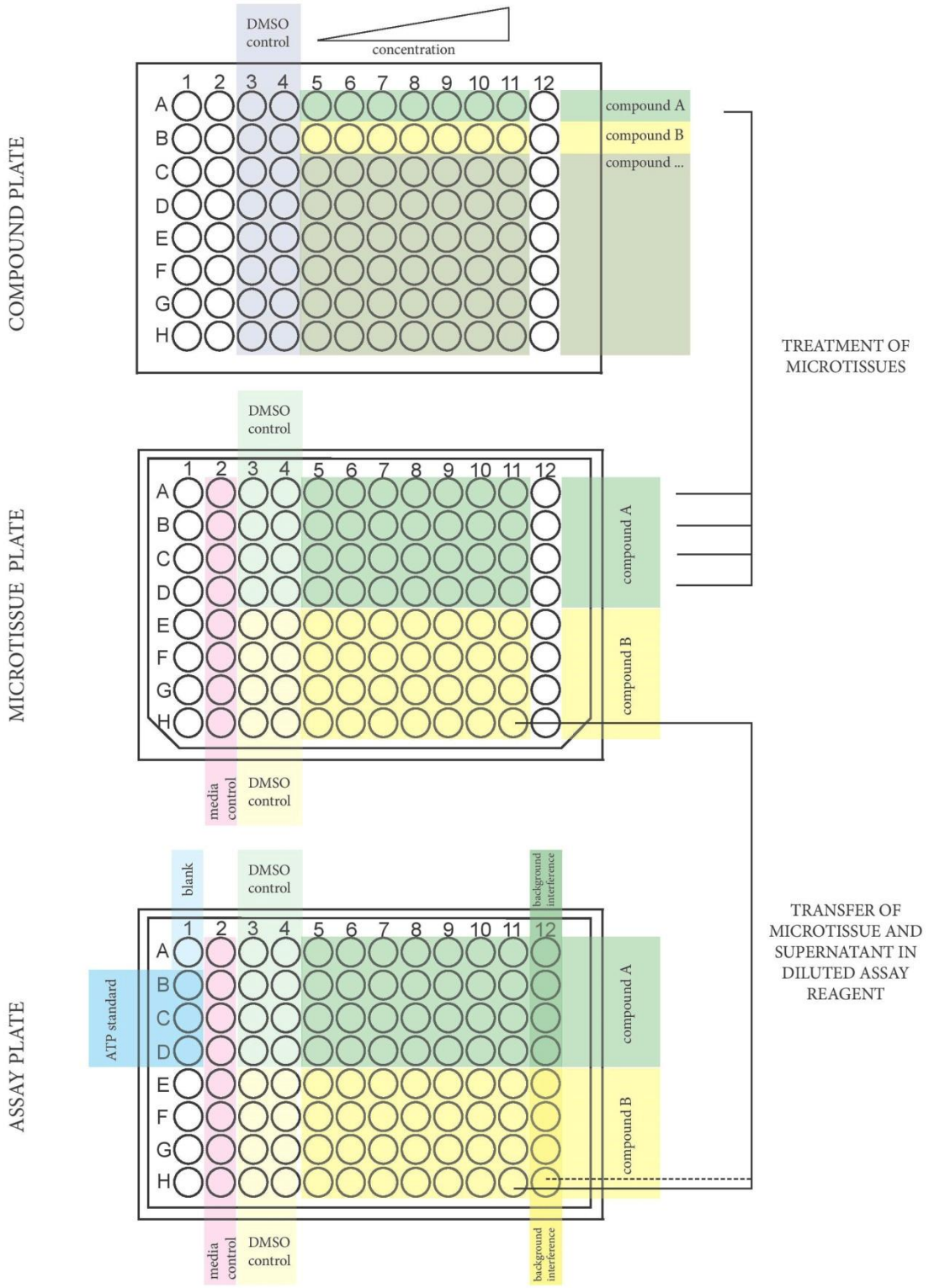


Figure 3: Schematic plate layout of compound-treated spheroids and of ATP measurement. Upper panel: compound deep-well plate layout. Each row contains vehicle control (column 3 and 4) and 7 compound concentrations (column 5 – 11; top concentration: column 11). Application of deep well plates reduces pipetting steps to generate 200 X dilutions of the compound and allows for dosing

of experimental replicates from the same reservoir. Middle panel: dosing of microtisues in 96-well format. **Microtissues cultured in GravityTRAP™ ULA Plate are exposed to treatment with 2 compounds. Each compound concentration is tested in quadruplicate, whereas the vehicle control in octuplicate. Culture medium control is included in column 2**. Lower panel: assay plate layout for ATP measurement. Microtissues suspended in 40 µl of diluted CellTiter-Glo® Cell Viability Assay are transferred from the **GravityTRAP™ Plate into the assay plate (column 2 to 11).** Assay blank (A1), standard curve (A1 – D1) and the control for background interference (column 12) are included in the assay plate.

commercially available solutions allow for 3D cell culture cultivation in HT-friendly 96- or 384-well format with multiple re-dosing of tested compounds. On the assay development side, an appealing concept of multiplexing endpoints to generate simultaneous data-reach readouts is currently under development and shall provide more experimental flexibility.

2. 3D Microtissue Viability Assay

2.1. ATP Assay Concept

The frequently chosen primary assay for determination of 3D cell culture viability is quantification of a luminescent signal generated by conversion of luciferin by luciferase as a function of cytoplasmic ATP concentration (29)(30). Initially, architecture of the 3D cellular aggregates – their size, composition and penetration barrier, presented a challenge to assays originally tailored for the 2D cell culture models. However, by optimization of detergent composition and lysis conditions, ATP assays suitable for variable 3D cell culture formats (such as spheroids and hydrogel-based systems), have been developed (31)(30)(32)(33)(34). Available bioluminescent ATP detection assay are robust, sensitive, and scalable to high-throughput screens, and offer relatively simple work-flow and data analysis. In contrast, standard colorimetric methods based on resazurin reduction (Alamar blue assay) or tetrazolium reduction (MTT assay), frequently used to assess number of viable cells in 2D cell culture, have been found not applicable to 3D spheroids/microtissues and collagen matrices (30)(29)(35)(36). 3D matrices and tight cell-cell junctions can affect uptake and diffusion kinetics of a dye, therefore changing readout of the assay and making results more difficult to interpret (35)(36). In parallel, development of live imagining assays linking changes of spheroid's size and morphology or localization/expression of fluorescent markers to viability of cells in 3D formats are under constant development (37)(38).

The protocol below describes how to measure viability of cells aggregated into spheroids (e.g. heterotypic liver microtissues and tumor microtissues) using CellTiter-Glo® 3D Cell Viability Assay quantifying intra-tissue ATP content (Figure 1 and Figure 2). This protocol can be easily adjusted to an automated pipetting station.

2.1.1. Commercial Availability

Recommended single-reagent assay for multi-well plate format:

- CellTiter-Glo® 3D Cell Viability Assay, Promega Corporation, Cat.# G9681, G9682, G9683

CellTiter-Glo® 3D Cell Viability Assay combines the enhanced penetration and lytic activity required for efficient lysis of 3D cell culture with generation of the stable ATP-dependent luminescent signal. This thereby reduces the complexity of processing multiple assay plates and HTS applications (30).

2.1.2. ATP Assay preparation

CellTiter-Glo® 3D Cell Viability Assay is provided as a ready-to-use solution and no additional preparation is required. The reagent should be equilibrated to room temperature before use. For stability and storage conditions please refer to the manufacturer's guidelines (www.promega.com).

To perform the assay on microtissues cultured in 96-well GravityTRAP™ ULA Plates, mix 1:1 the required volume of CellTiter-Glo® 3D Cell Viability Assay (20 µl per well) and PBS without calcium and magnesium (e.g. PAN-Biotech, Cat.# P04-36500)

2.1.3. ATP Assay Protocol

1. Equilibrate GravityTRAP™ ULA Plates with cultured micro-tissues to room temperature.
2. Prepare 96-opaque well microplate, hereinafter refer to as assay plate (e.g. Greiner Bio-One, Cat.# 675075), by pipetting into dedicated wells (Figure 3, lower panel):
   a. Blank – 40 µl of diluted CellTiter-Glo® 3D Cell Viability Assay
   b. *Optional:* Standard curve – depending on the type of microtissue and the detection range of luminometer available, mix 20 µl of CellTiter-Glo® 3D Cell Viability Assay with 20 µl of 1 µM ATP (e.g. for human liver microtussies of ~ 300 µm diameter) or with 5 µM ATP (e.g. for more metabolically active or bigger microtissues), and with corresponding ATP dilutions.
   c. *Optional:* To check background interference of the compound tested in the cytotoxicity assay, pipet 5 µl of a culture medium from wells containing microtissues treated with the highest concentration of the compound into wells on the assay plate containing 20 µl CellTiter-Glo® 3D Cell Viability Assay and 20 µl of 1 µM ATP .
3. Gently remove the culture medium from the GravityTRAP™ ULA Plate by placing the pipette tip at an inner ledge of the well, leaving intact the microtissues in the remnant volume of the medium in the V-shaped bottom of the well.
4. Dispense 40 µl of diluted CellTiter-Glo® 3D Cell Viability Assay into each well of the GravityTRAP™ ULA Plate.
5. Mix and transfer content of each well from the GravityTRAP™ ULA Plate into the corresponding well on the assay plate.
6. Protect the lysate from light by covering the assay plate with aluminum foil or with aluminum platesealer (e.g. Greiner Bio-One, Cat.# 67609).
7. For effective MT lysis keep the plates on an orbital shaker for 20 minat room temperature.
8. Record luminescence with a microplate luminometer using a program recommended by the manufacturer.

2.1.4. Data analysis

The absolute ATP concentration of microtissue can be calculated from the standard curve included on the same assay plate. However, for *in vitro* testing of cell toxicity of chemicals, it is often more applicable to calculate relative ATP levels of microtissues exposed to treatment as a percentage of vehicle-treated control microtissues (Figure 1, Figure 2). During prolonged cultivation of microtissues, certain cytotoxicity and a decrease in ATP levels of DMSO controls can be observed with respect to maintenance medium controls.

2.2. Conclusions/Summary

The type and number of cells integrated into the 3D structure as well as cultivation conditions (cell culture media compositions, time of cultivation, media exchange/re-dosing scheme) may affect physiological characteristics of the model and its responsiveness to the treatment. Therefore, standardization of intrinsic characteristics of 3D cell culture formats and extrinsic culturing parameters and protocols is crucial for further development of 3D *in vitro* assay portfolio.

Measurement of cytoplasmic ATP content is a common method for cellular viability determination in both 2D and 3D cell culture, and is a routine endpoint in toxicology/drug efficacy studies. However, 3D culture formats are characterized by development of compact structures with tight cell-cell junctions and extracellular matrix, presenting additional obstacle for effective lysis and reagent accessibility. Therefore, to allow for effective ATP

release from cells, the time of lysis combined with physical disruption of the 3D structure should be determined empirically for each 3D cell culture format.

Ready-to-use assay kits, such as CellTiter-Glo® Cell Viability Assay, facilitate time-effective and standardized processing of multiple assay plates by combining lysis and luminescent signal generation into one step. However, for the best assay performance special care should be taken to ensure both the highest system reproducibility and operational reproducibility (e.g. mixing and transfer of the reagent with 3D culture from culturing plates to the assay plates, avoiding a temperature gradient within the plate and ATP contamination). Additionally, special care should be taken to ensure that the ATP levels of either large or metabolically active 3D cultures correlate with the dynamic range of luminescence output of the assay.

References

1. Abbott A. Biology ' s new dimension. 2003;424(August).
2. Hirschhaeuser F, Menne H, Dittfeld C, West J, Mueller-Klieser W, Kunz-Schughart L a. Multicellular tumor spheroids: an underestimated tool is catching up again. J Biotechnol [Internet]. 2010 Jul 1 [cited 2014 Jul 16];148(1):3–15. Available from: http://www.ncbi.nlm.nih.gov/pubmed/20097238
3. Sutherland RM, Durand RE. Growth and cellular characteristics of multicell spheroids. Recent Results Cancer Res.[Internet] 1984;95:24–49.Available fromhttp://www.ncbi.nlm.nih.gov/pubmed/6396760 PubMed PMID: 6396760.
4. Desoize B, Jardillier J. Multicellular resistance: a paradigm for clinical resistance? Crit Rev Oncol Hematol. [Internet] 2000;36(2-3):193–207.Available fromhttp://www.ncbi.nlm.nih.gov/pubmed/11033306 PubMed PMID: 11033306.
5. William R., Wilson MPH. Targeting hypoxia in cancer therapy. Nat Rev Cancer. 2011;11:393–410. PubMed PMID: 21606941.
6. Matthew D. Halla, Catherine Martinb, David J.P. Fergusonb, Roger M. Phillipsc, Trevor W. Hambleya. Comparative efficacy of novel platinum(IV) compounds with established chemotherapeutic drugs in solid tumour models. Biochem Pharmacol. 2004;67(1):17–30. PubMed PMID: 14667925.
7. Godoy P, Hewitt NJ, Albrecht U, Andersen ME, Ansari N, Bhattacharya S, et al. Recent advances in 2D and 3D in vitro systems using primary hepatocytes, alternative hepatocyte sources and non-parenchymal liver cells and their use in investigating mechanisms of hepatotoxicity, cell signaling and ADME. [Internet]. Archives of toxicology. 2013 [cited 2014 Jul 10]. 1315-530 p. Available from: http://www.pubmedcentral.nih.gov/articlerender.fcgi?artid=3753504&tool=pmcentrez&rendertype=abstract
8. Lin R-Z, Lin R-Z, Chang H-Y. Recent advances in three-dimensional multicellular spheroid culture for biomedical research. Biotechnol J [Internet]. 2008 Oct [cited 2011 Jul 24];3(9-10):1172–84. Available from: http://www.ncbi.nlm.nih.gov/pubmed/18566957
9. Tibbitt Mark W., Anseth KS. Hydrogels as Extracellular Matrix Mimics for 3D Cell Culture. Biotechnol Bioeng.[Internet] 2009;103(4):655–63.Available fromhttp://www.ncbi.nlm.nih.gov/pmc/articles/PMC2997742/ PubMed PMID: 19472329.
10. Jeanie L., Drury DJM. Hydrogels for tissue engineering: scaffold design variables and applications. Biomaterials. 2003;24(24):4337–51. PubMed PMID: 12922147.
11. Khademhosseini A, Langer R, Borenstein JT, Vacanti JP. Microscale technologies for tissue engineering and biology. Proc Natl Acad Sci U S A. 2006;103(8):2480–7. PubMed PMID: 16477028.
12. Singh M, Close DA, Mukundan S, Johnston PA, Sant S. Production of Uniform 3D Microtumors in Hydrogel Microwell Arrays for Measurement of Viability, Morphology, and Signaling Pathway Activation. Assay Drug Dev Technol.[Internet] 2015;(November)150814092825009Available fromhttp://online.liebertpub.com/doi/10.1089/adt.2015.662 PubMed PMID: 26274587.
13. Rose G. Harrison, M. J. Greenman FPM andC. MJ. Observations of the living developing nerve fiber. Anat Rec. 1907;1(5):116–28.

14. Kelm JM, Timmins NE, Brown CJ, Fussenegger M, Nielsen LK. Method for generation of homogeneous multicellular tumor spheroids applicable to a wide variety of cell types. Biotechnol Bioeng [Internet]. 2003 Jul 20 [cited 2011 Jul 5];83(2):173–80. Available from: http://www.ncbi.nlm.nih.gov/pubmed/12768623
15. Kelm JM, Fussenegger M. Microscale tissue engineering using gravity-enforced cell assembly. Trends Biotechnol [Internet]. 2004 Apr [cited 2011 Jun 20];22(4):195–202. Available from: http://www.ncbi.nlm.nih.gov/pubmed/15038925
16. Kelm JM, Fussenegger M. Scaffold-free cell delivery for use in regenerative medicine. Adv Drug Deliv Rev [Internet]. Elsevier B.V.; 2010 Jun 15 [cited 2011 Aug 30];62(7-8):753–64. Available from: http://www.ncbi.nlm.nih.gov/pubmed/20153387
17. Grainger DW. Cell-based drug testing; this world is not flat. Adv Drug Deliv Rev [Internet]. 2014 Apr [cited 2014 Jun 5];69-70:vii – xi. Available from: http://www.ncbi.nlm.nih.gov/pubmed/24709443
18. Hartung T. 3D - A new dimension of in vitro research. Adv Drug Deliv Rev [Internet]. Elsevier B.V.; 2014 Apr [cited 2014 Jun 12];69-70:vi. Available from: http://www.ncbi.nlm.nih.gov/pubmed/24721291
19. Riss T. How to Choose a Cell Health Assay Choosing the Right Cell Health Assay Depends on What You Want to Measure. Illum A Cell Notes Publ. 2014;(January).
20. Thoma CR, Zimmermann M, Agarkova I, Kelm JM, Krek W. 3D cell culture systems modeling tumor growth determinants in cancer target discovery. Adv Drug Deliv Rev [Internet]. Elsevier B.V.; 2014 Apr 20 [cited 2014 May 28];69-70C:29–41. Available from: http://www.ncbi.nlm.nih.gov/pubmed/24636868
21. Ranga A, Gjorevski N, Lutolf MP. Drug discovery through stem cell-based organoid models. Adv Drug Deliv Rev [Internet]. Elsevier B.V.; 2014 Apr 20 [cited 2014 May 27];69-70C:19–28. Available from: http://www.ncbi.nlm.nih.gov/pubmed/24582599
22. Mathes SH, Ruffner H, Graf-Hausner U. The use of skin models in drug development. Adv Drug Deliv Rev [Internet]. Elsevier B.V.; 2014 Apr 20 [cited 2014 Jun 12];69-70C:81–102. Available from: http://www.ncbi.nlm.nih.gov/pubmed/24378581
23. Emmert MY, Hitchcock RW, Hoerstrup SP. Cell therapy, 3D culture systems and tissue engineering for cardiac regeneration. Adv Drug Deliv Rev [Internet]. Elsevier B.V.; 2014 Apr 20 [cited 2014 Jun 1];69-70C:254–69. Available from: http://www.ncbi.nlm.nih.gov/pubmed/24378579
24. Giese C, Marx U. Human immunity in vitro - Solving immunogenicity and more. Adv Drug Deliv Rev [Internet]. Elsevier B.V.; 2014 Apr 20 [cited 2014 May 27];69-70C:103–22. Available from: http://www.ncbi.nlm.nih.gov/pubmed/24447895
25. Kim D-H, Kim P, Suh K, Kyu Choi S, Ho Lee S, Kim B. Modulation of adhesion and growth of cardiac myocytes by surface nanotopography. Conf Proc IEEE Eng Med Biol Soc. 2005;4:4091–4. PubMed PMID: 17281132.
26. Messner S, Agarkova I, Moritz W, Kelm JM. Multi-cell type human liver microtissues for hepatotoxicity testing. Arch Toxicol [Internet]. 2013 Jan [cited 2013 Feb 13];87(1):209–13. Available from: http://www.pubmedcentral.nih.gov/articlerender.fcgi?artid=3535351&tool=pmcentrez&rendertype=abstract
27. Roth A, Singer T. The application of 3D cell models to support drug safety assessment: Opportunities & challenges. Adv Drug Deliv Rev [Internet]. Elsevier B.V.; 2014 Apr 20 [cited 2014 Jun 12];69-70C:179–89. Available from: http://www.ncbi.nlm.nih.gov/pubmed/24378580
28. Astashkina A, Grainger DW. Critical analysis of 3-D organoid in vitro cell culture models for high-throughput drug candidate toxicity assessments. Adv Drug Deliv Rev [Internet]. Elsevier B.V.; 2014 Mar [cited 2014 Mar 9]; Available from: http://linkinghub.elsevier.com/retrieve/pii/S0169409X14000301
29. Riss TL, Niles AL, Minor L. Cell Viability Assays Assay Guidance Manual. Assay Guid Man. 2013;
30. Riss TL, Valley MP, Kupcho KR, Zimprich CA, Leippe D, Niles AL, et al. Validation of In Vitro Assays to Measure Cytotoxicity in 3D Cell Cultures. 2014;2014.
31. Messner S, Agarkova I, Moritz W, Kelm JM. Multi-cell type human liver microtissues for hepatotoxicity testing. Arch Toxicol [Internet]. 2012 Nov 11 [cited 2012 Nov 13];87(1):209–13. Available from: http://www.pubmedcentral.nih.gov/articlerender.fcgi?artid=3535351&tool=pmcentrez&rendertype=abstract

32. Rimann M, Laternser S, Gvozdenovic A, Muff R, Fuchs B, Kelm JM, et al. An in vitro osteosarcoma 3D microtissue model for drug development. J Biotechnol [Internet]. Elsevier B.V.; 2014 Nov 10 [cited 2015 May 19];189:129–35. Available from: http://www.ncbi.nlm.nih.gov/pubmed/25234575
33. Fey SJ, Wrzesinski K. Determination of Drug Toxicity Using 3D Spheroids Constructed From an Immortal Human Hepatocyte Cell Line. Toxicol Sci [Internet]. 2012 Jun [cited 2013 Feb 6];127(2):403–11. Available from: http://www.pubmedcentral.nih.gov/articlerender.fcgi?artid=3355318&tool=pmcentrez&rendertype=abstract
34. Rimann M, Angres B, Patocchi-Tenzer I, Braum S, Graf-Hausner U. Automation of 3D Cell Culture Using Chemically Defined Hydrogels. J Lab Autom.[Internet] 2013.:1–7.Available fromhttp://www.ncbi.nlm.nih.gov/pubmed/24132162 PubMed PMID: 24132162.
35. Bonniera F., Keatinga M.E., Wróbelb T.P., Majznerb K., Baranskac M., Garcia-Munoza A. A. Blancod HJB. No Title. Toxicol Vitr. 2015;29(1):124–31.
36. Walzl A, Unger C, Kramer N, Unterleuthner D, Scherzer M, Hengstschläger M, et al. The Resazurin Reduction Assay Can Distinguish Cytotoxic from Cytostatic Compounds in Spheroid Screening Assays. J Biomol Screen.[Internet] 2014;19(7):1047–59.Available fromhttp://www.ncbi.nlm.nih.gov/pubmed/24758920 PubMed PMID: 24758920.
37. Sirenko O, Mitlo T, Hesley J, Luke S, Owens W, Cromwell EF. High-Content Assays for Characterizing the Viability and Morphology of 3D Cancer Spheroid Cultures. Assay Drug Dev Technol [Internet]. 2015 Sep [cited 2015 Sep 14];13(7):402–14. Available from: http://www.ncbi.nlm.nih.gov/pubmed/26317884
38. Anastasov N, Höfig I, Radulović V, Ströbel S, Salomon M, Lichtenberg J, et al. A 3D-microtissue-based phenotypic screening of radiation resistant tumor cells with synchronized chemotherapeutic treatment. BMC Cancer [Internet]. 2015 Jan [cited 2015 Jun 15];15:466. Available from: http://www.pubmedcentral.nih.gov/articlerender.fcgi?artid=4460881&tool=pmcentrez&rendertype=abstract
39. Alessandri K, Sarangi BR, Gurchenkov VV, Sinha B, Kießling TR, Fetler L, et al. Cellular capsules as a tool for multicellular spheroid production and for investigating the mechanics of tumor progression in vitro. Proc Natl Acad Sci U S A [Internet]. 2013 Sep 10 [cited 2014 Jan 24];110(37):14843–8. Available from: http://www.ncbi.nlm.nih.gov/pubmed/23980147
40. Rajcevic U, Knol JC, Piersma S, Bougnaud S, Fack F, Sundlisaeter E, et al. Colorectal cancer derived organotypic spheroids maintain essential tissue characteristics but adapt their metabolism in culture. Proteome Sci [Internet]. 2014 Jan [cited 2014 Aug 4];12:39. Available from: http://www.pubmedcentral.nih.gov/articlerender.fcgi?artid=4114130&tool=pmcentrez&rendertype=abstract
41. Lancaster M a, Renner M, Martin C-A, Wenzel D, Bicknell LS, Hurles ME, et al. Cerebral organoids model human brain development and microcephaly. Nature [Internet]. Nature Publishing Group; 2013 Sep 19 [cited 2014 Mar 19];501(7467):373–9. Available from: http://www.pubmedcentral.nih.gov/articlerender.fcgi?artid=3817409&tool=pmcentrez&rendertype=abstract
42. Kelm JM, Ehler E, Nielsen LK, Schlatter S, Perriard J-C, Fussenegger M. Design of artificial myocardial microtissues. Tissue Eng.[Internet] 2004;10(1-2):201–14.Available fromhttp://www.ncbi.nlm.nih.gov/pubmed/15009946 PubMed PMID: 15009946.
43. Moors M, Rockel TD, Abel J, Cline JE, Gassmann K, Schreiber T, et al. Human neurospheres as three-dimensional cellular systems for developmental neurotoxicity testing. Environ Health Perspect [Internet]. 2009 Jul [cited 2013 Apr 15];117(7):1131–8. Available from: http://www.pubmedcentral.nih.gov/articlerender.fcgi?artid=2717141&tool=pmcentrez&rendertype=abstract
44. Alexander N. Combes*, Jamie A. Davies† MHL. Cell-cell interactions driving kidney morphogenesis. Curr Top Dev Biol. 2015;112:467–508. PubMed PMID: 25733149.
45. Sato T, Clevers H. Growing self-organizing mini-guts from a single intestinal stem cell: mechanism and applications. Science [Internet]. 2013 Jun 7 [cited 2014 Mar 20];340(6137):1190–4. Available from: http://www.ncbi.nlm.nih.gov/pubmed/23744940
46. Giada D. G. Barabaschi, Vijayan Manoharan, Qing Li LEB. Engineering Pre-vascularized Scaffolds for Bone RegenerationNo Title. Eng Miner Load Bear Tissues. 2015;881:79–94.

Cell-Based RNAi Assay Development for HTS

Scott Martin,[1] Gene Buehler,[1] Kok Long Ang,[2] Farhana Feroze, Gopinath Ganji, and Yue Li

Created: May 1, 2012; Updated: May 1, 2013.

Abstract

Gene silencing through RNA interference (RNAi) has become a powerful tool for understanding gene function. RNAi screens are primarily conducted using synthetic small interfering RNA (siRNA) or plasmid-encoded short hairpin RNA (shRNA). In this chapter, some considerations for design, optimization, validation, analysis and hit selection criteria in RNAi screens are discussed. A special emphasis is placed on pitfalls associated with off-target effects, which represent a primary limitation to the successful application of this technology.

Introduction

RNA interference (RNAi) is a gene silencing mechanism initiated by short double-stranded RNA (dsRNA) of ~21nt in length (for a recent review see 1). Two major classes of dsRNAs harness this pathway for post-transcriptional gene regulation, including siRNAs and microRNAs (miRNAs). siRNAs direct the cleavage of mRNA transcripts that contain full sequence complementarity. Cleavage is mediated by a single strand of the siRNA duplex termed the guide strand, after loading into the RNA-induced silencing complex (RISC). Notably, the documented occurrence of naturally occurring cleavage complexes is not common in mammalian cells. Rather, it is miRNAs that use the innate RNAi machinery. miRNAs interact with transcripts possessing partial complementarity, primarily within target 3′ untranslated regions (UTRs), resulting in transcript degradation and/or translation inhibition (Figure 1).

Experimentally, the ability to harness the RNAi pathway through the use of siRNAs/shRNAs (Figure 2) has paved the way for genome-wide high throughput screens. Many large-scale RNAi screens have been reported. Common variations include drug modifier screens, which combine the use of RNAi and a drug to identify genes that affect drug response, viability screens to look for vulnerabilities within specific cellular backgrounds, pathway reporter assays, pathogen-host screens to look for genes that affect pathogen spread and host response, and image-based phenotypic screens to report on genes associated with a wide variety of processes, including protein localization and disease-specific phenotypes. Many reviews cover the RNAi biology, experimental parameters and considerations for performing screens (for example, 2-11). See table 1 for a brief summary of the differences between siRNA and shRNA reagents.

In the following sections, we have compiled our experience around RNAi-based LOF screens in mammalian cells to offer a few guidelines on best practices. As with any technology, this chapter will benefit from growing expertise and improvements in technology and methods.

Author Affiliations: 1 National Center for Advancing Translational Sciences. 2 Eli Lilly & Company, Indianapolis, IN.

Corresponding author.

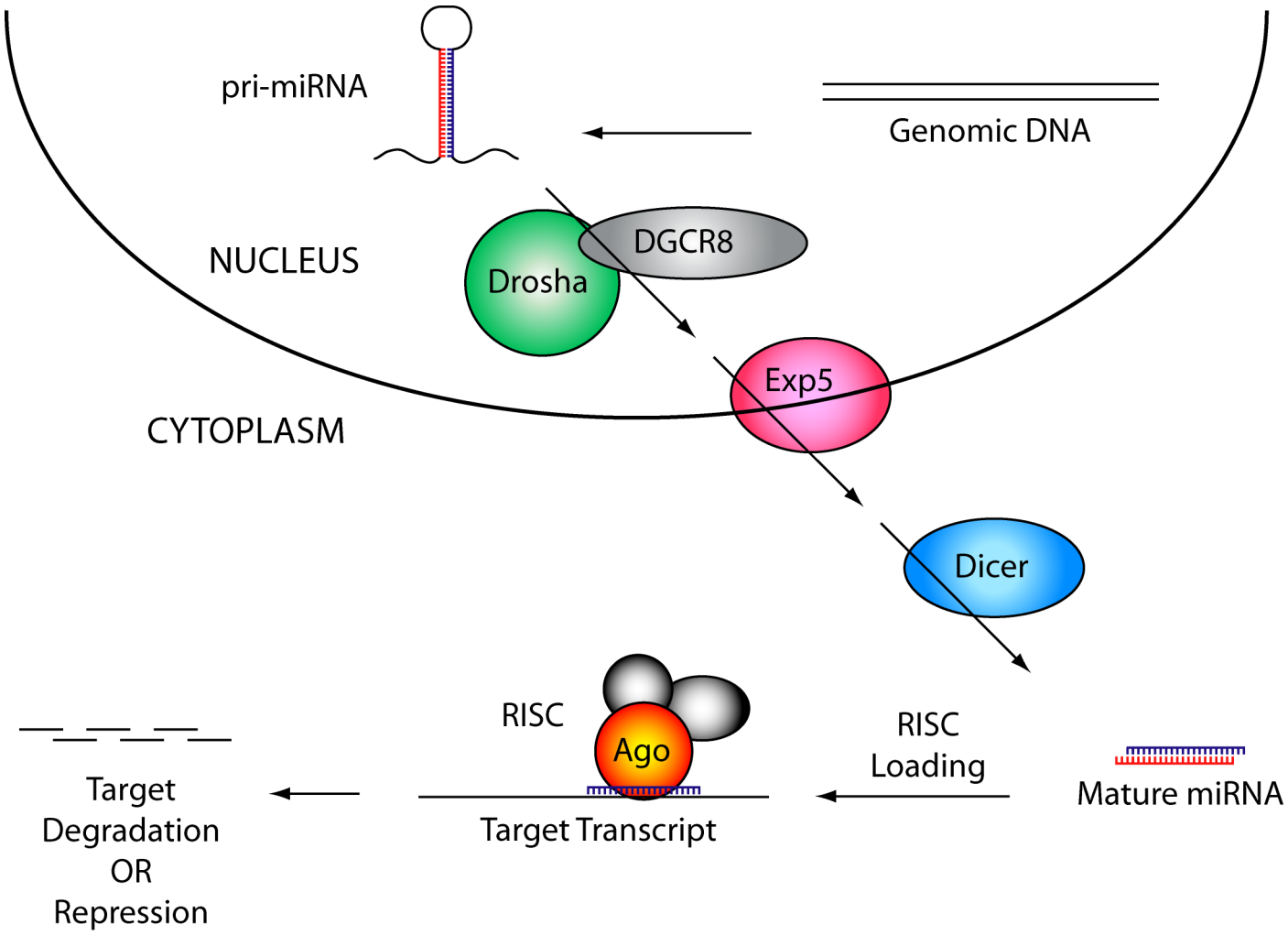


Figure 1. Simplified schematic of RNAi in mammalian cells. RNAi in mammalian cells is primarily mediated by endogenous miRNAs. miRNAs are expressed as primary hairpin-containing transcripts that are processed in the nucleus and cytoplasm to yield mature miRNA duplexes of ~22 nt in length. A single strand of the duplex is then loaded into an argonaute-containing silencing complex (RISC), which then guides the complex to target mRNA transcripts with partial sequence complementarity within their 3'UTRs. This interaction leads to degradation and/or translational repression.

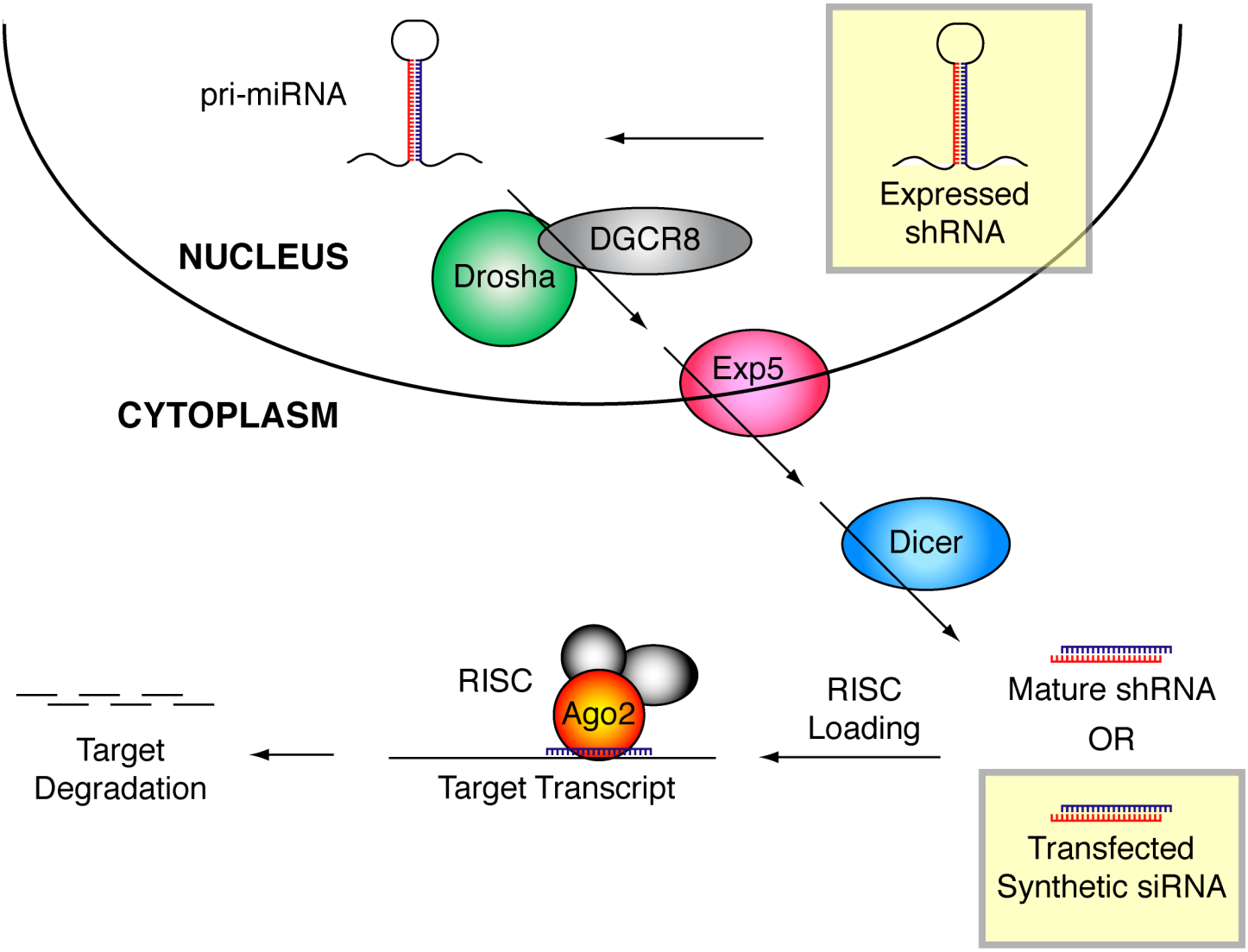


Figure 2. siRNAs and shRNAs harness the RNAi pathway for loss-of-function studies. shRNAs are encoded by plasmids and processed much like miRNAs to yield mature duplexes of ~22 nt in length. Alternatively, synthetic siRNAs can be introduced directly into the cell using transfection reagents. siRNAs and mature shRNAs are incorporated into a similar, if not identical, RISC complex as mature miRNAs. The loaded siRNA/shRNA strand then guides RISC to target mRNAs with full sequence complementarity, resulting in the site-specific cleavage target mRNA. Importantly, siRNA and shRNA guide strands can interact with the 3'UTRs of unintended targets through only limited stretches of sequence complementarity, much like miRNAs. These types of unintentional off-target effects can dominate the results of RNAi screens.

Table 1: Comparison of siRNA and shRNA-lentivirus

siRNA	shRNA-lentivirus
Short-term target KD (< 1 week)	Long-term target KD
Minimal library maintenance	Significant library maintenance
Some cell types are not transfected efficiently	Infection is generally more effective than transfection, thus larger repertoire of cells can be used
Dosing to control cellular concentration	Difficult to control cellular concentration, though inducible system possible
Chemical modifications possible	Stable target KD cell line can be generated.
More consistent quality of reagent	Titer of shRNA-lentiviral particles can be more variable

Off-Target Effects

The ability of siRNAs/shRNAs to knockdown intended targets while minimizing or controlling for off-target effects (OTEs) is critical for the meaningful interpretation of RNAi screens. Off-target effects arise from mechanisms that can be either independent or dependent upon the siRNA/shRNA sequence. Sequence-independent effects can relate to experimental conditions (e.g., transfection reagents), inhibition of endogenous miRNA activity, or stimulation of pathways associated with the immune response. Sequence-dependent effects primarily concern the unintentional silencing of targets sharing partial complementarity with RNAi effector molecules through miRNA-like interactions. There are a number of approaches toward controlling and accounting for both types of off-target effects (discussed below).

Sequence-Dependent Off-Target Effects: Interactions between siRNAs/shRNAs and non-targeted mRNAs

Although RNAi reagents can cause sequence-independent effects, the primary source of trouble for RNAi screeners are sequence-dependent off-target effects. Off-target effects originate from partial complementarity between RNAi effectors and off-target transcripts, in much the same way as those exhibited by endogenous miRNAs. In fact, like miRNA targets, off-targeted transcripts are enriched in those containing perfect pairing between their 3′ UTRs and hexamer (nts 2–7) and heptamer (nts 2–8) sequences within 5′ ends of RNAi effectors (12,13). These stretches of sequence are known as "seed sequences". Some studies have found these effects to be non-titratable, with dose responses mirroring that of on-target transcripts (14). Others have found these effects to be concentration-dependent, whereby the use of low siRNA concentrations can significantly mitigate off-target interactions (15). Sequence-dependent off-target effects can have profound consequences. For example, Lin and colleagues determined that the top three "hits" from a siRNA-based screen for targets affecting the hypoxia-related HIF-1 pathway resulted from off-target effects (16). For two of these three "hits," activity could be traced to interactions within the 3′ UTR of *HIF-1A* itself. Additionally, Schultz and coworkers found that all active siRNAs in a TGF-β assay reduced TGFBR1 and TGFBR2 (17).

How bad is the problem with seed-driven OTEs? It has been estimated that in a genome-wide screen using 4 siRNAs per gene, and an estimated 20 true positives in the assay, that 3,362 off-target genes would score with 1 active siRNA, 259 would score with 2 of 4 active siRNAs, and 9 would score with 3 of 4 (18). This is a sobering estimate given that the vast majority of published RNAi screen are conducted with only a single reagent per gene (pool of 4 siRNAs), and the typical bar for follow-up validation is to require that 2 members of the pool, or sometimes even 1, exhibit activity. Those approaches seem insufficient, and lead to published hit lists that are loaded with false positives, especially in cases where a simple laundry list of actives from the primary screen are presented. An additional illustration of this problem can be found in recently published host-virus screens. For example, a meta-analysis of 3 genome-wide siRNA screens conducted in human cells to look for host genes associated with HIV revealed strikingly little overlap (19). Notably, only 3 genes were called in all 3 screens, and the pair-wise comparison of any two screens revealed only 3%-6% overlap. However, pathway analysis revealed greater similarities between the screens, and certainly false negatives (e.g, arising from reagent deficiencies) and differences in experimental set up (e.g., cell lines and assay endpoints) are significant contributors to the lack of agreement. However, even when comparing different siRNA libraries under the same exact experimental conditions there is virtually no correlation (Figure 3). In fact, the correlation between siRNAs having the same seed is much greater than siRNAs designed to target the same gene (20, Figure 4), emphasizing the prevalence and impact of seed-driven OTEs in RNAi screen data.

There are a number of ways to help minimize the impact of sequence-dependent off-target effects. For starters, an attempt should be made to use siRNAs at relatively low concentrations. Early studies used siRNAs at ≥ 100nM, but it should be possible to routinely use them at 10 nM – 50 nM without loss of on-target potency. Other ways to reduce OTEs, relate to siRNA design features and chemical modifications. For example, siRNAs

are now commercially available with chemical modifications to the passenger strand, which eliminate their loading into RISC, and the subsequent off-target effects that may result. Redundancy (the use of multiple reagents per gene) is another way to minimize the impact of off-target effects by requiring multiple active reagents per gene for that gene to be considered a candidate active. There are also informatic approaches to identify and even interpret off-target effects within RNAi screens. These will be discussed in more detail below. Despite all of these considerations, the occurrence of sequence-dependent off-target effects is unavoidable.

Loss-of-Function Screens Using siRNA

siRNA Reagents

The following choices of reagents need to be made prior to running any screens.

- **Scale**: Focused libraries (pathway collection, gene family, disease-specific library, etc.), druggable genome, or genome-wide. A variety of vendors offer these reagents (e.g., Qiagen, Dharmacon, Ambion, Sigma).
- **Format**: Some vendors provide pools of siRNAs against a given gene in an effort to guarantee knockdown. Others provide libraries in a single siRNA per well format. Recently, a variety of chemically modified siRNAs have become available. These modifications reduce off-target effects, especially arising from the passenger strand, and should be used.
- In light of the issue with OTEs, the use of multiple reagents per gene in a screen will increase the chances of identifying true positives. This is illustrated in the meta-analysis of HIV screen for example, in which genes called in 2 or 3 of the screens were more enriched in relevant pathways (19). Screening multiple reagents per gene can be a more expensive option and increase the scale of the screen. However, it is common practice to screen one reagent per gene in duplicate or triplicate. Given that the majority of variance arises from false negatives and positives (see figures 3 and 4) and that the correlation between replicates in a well-optimized assay can be quite high (see the pilot screens section below), it would seem wise to invest more in redundancy than replicates, if a choice must be made (i.e., 3 different reagents per gene can be screened for the same cost as 1 reagent per gene in triplicate), provided that an assay has been demonstrated to be highly reproducible.
- **Negative and positive controls**: Negative and positive controls should be embedded in every assay plate. Negative controls are available from a number of vendors and are designed to lack homology with known transcripts. Positive controls should affect the assay under investigation (e.g., block the spread of virus in a virus assay). In cases where a good positive control does not exist, siRNAs should be chosen to at least report on the quality of transfection (e.g., lethal siRNAs that target essential genes or siRNAs that target the reporter used in a given assay, like GFP or luciferase). It is also important to note that negative controls are most likely not truly negative in any given assay.

Assay Optimization

Optimization needs to be done for all screens. Table 2 lists some important parameters for consideration in RNAi optimization.

A few essential parameters (and their purpose) are worth highlighting:

- General guidelines for cell-based assays such as growth media, seeding density, growth rate, incubation time, etc. can be found in the Cell-Based Assay section in this manual.
- Timing: Typical siRNA screen range from 48 h to 120 h. siRNA can reach maximal silencing of mRNA transcripts within 12h – 24h, but concomitant loss or protein will depend on protein half-life. If stimuli is to be added (e.g., drug or virus), it is typical to add it 48 h – 72 h post-transfection to ensure protein knockdown for a majority of genes prior to treatment. It is also important to remember that loss of

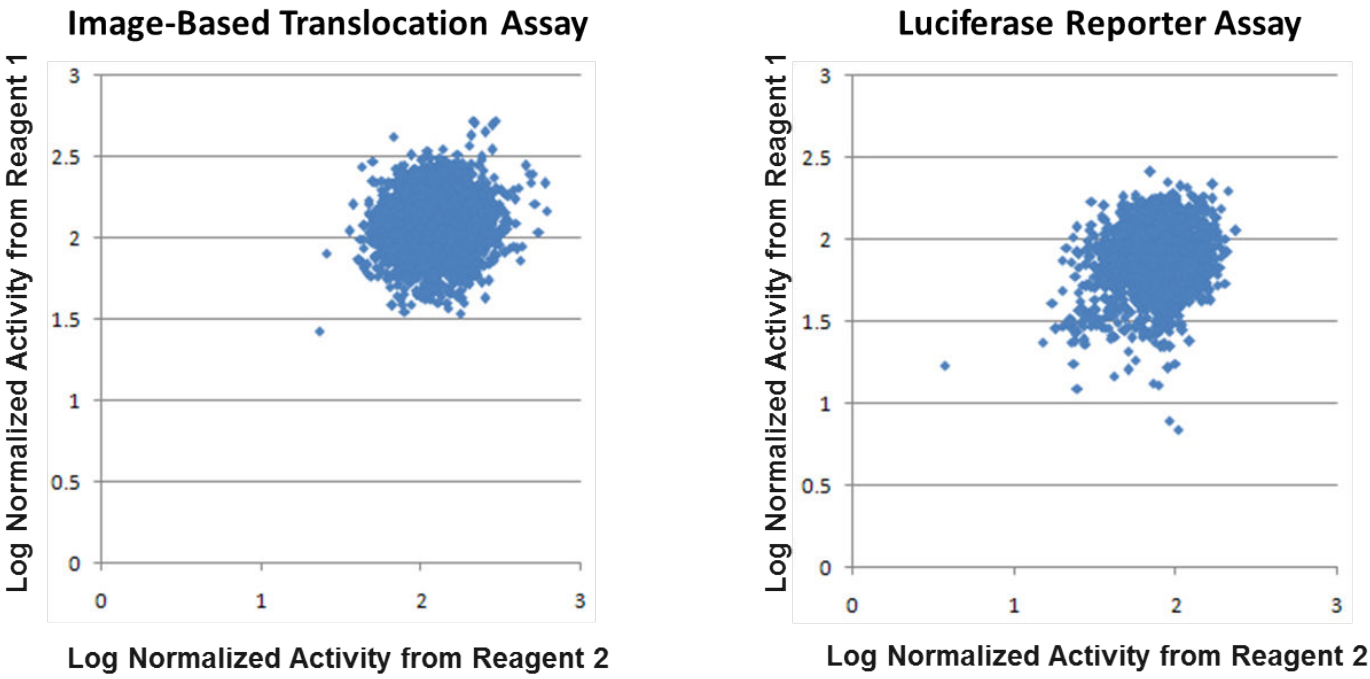


Figure 3. Comparing different siRNA reagents under the same exact experimental conditions. Two different screens show very little correlation between different siRNAs desigend to target the same gene.

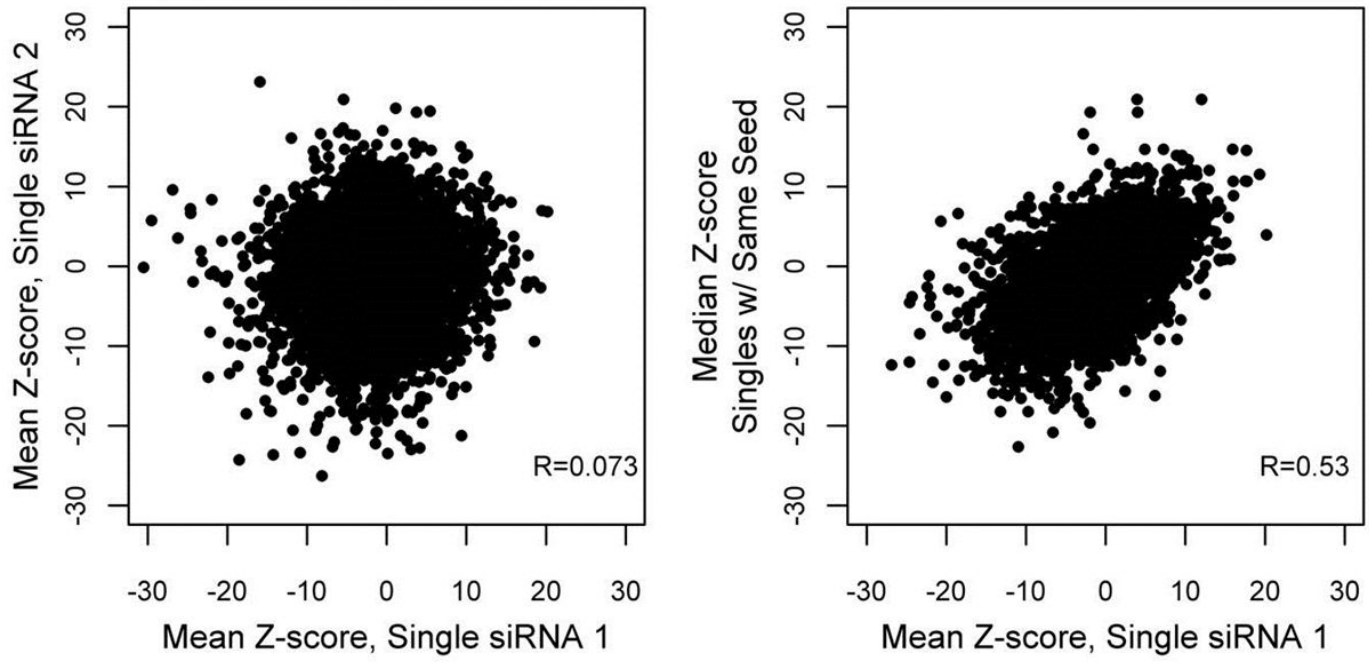


Figure 4. The correlation between siRNAs having the same seed is much greater than siRNAs designed to target the same gene (20). This is clear evidence that seed-dependent OTEs are the primary reason for a lack of agreement between siRNAs designed to target the same gene.

silencing will begin to occur around ~96 h, so careful considerations must be made when designing an assay.

- Transfection efficiency (below are some of the most important parameters for RNAi optimization, with reverse transfection being the preferred method for screening). See the "siRNA Transfection Optimization Experiments" section below.
  - Cell seeding density (e.g., for a viability-based experiment, you would not want to reach confluence prior to the assay endpoint).
  - Choice of transfection reagent and the amount
  - siRNA concentration (typically 10nM – 50nM)
- Determination of KD efficiency along with transfection efficiency should constitute an essential part of assay development and optimization. The extent of KD can be determined by qRT-PCR quantification of target transcript level after si/shRNA treatment. Transfection efficiency can be gauged with positive controls where a phenotypic effect (such as cell killing or reporter gene knockdown) is observed. It is ideal to use a positive control that is sensitive to knockdown efficiency, meaning that the effects are not observed under suboptimal transfection conditions. The use of such controls would also allow evaluation of both transfection and KD efficiency after a large scale screening to check performance.
- Choice of controls
  - Positive controls: cells with gene specific si/shRNAs transfected that will result in a significant change to the assay readout. For example si/shRNAs targeting UBB or PLK1 can be used as positive controls in cell proliferation or apoptosis assays. These controls can be informative in evaluating transfection efficiency and KD efficiency.
  - Negative controls: cells with non-silencing si/shRNAs (NS), also known as non-targeting control (NTC), transfected but without significant effect on the assay readout. It is also recommended to include the following as negative controls, although there may not be enough real estate in screen plates for these to be included throughout the screen:
    - Non-transfected (NT) cells: cultured cells only, without transfection/infection
    - Mock-transfected (MT) cells: cells with transfection reagent only, without si/shRNA
  - It is important to verify that transfection conditions do not significant alter the assay. For example, drug efficacy should be the same in cells transfected with negative control siRNA versus NT cells in a drug modifier screen. Similarly, cell transfected with negative control siRNA should not respond differently to virus than NT cells.
- Assay z'-factors: After identifying optimal transfection conditions, it is important to evaluate the assay z'-factor to understand if the assay signal window and variation are at an acceptable level. Although, a factor of 0.5 is widely accepted for small molecule screens, lower assay z'-factors are generally accepted and expected for RNAi screens.

Table 2: Important parameters in RNAi-assay optimization

Parameter	Key Factors
Cell line for screening	transfection efficiency, growth rate, assay sensitivity
Cell growth media	should not interfere with readout or transfection efficiency
[si/shRNA]	concentration must produce effective silencing and limit off-target effects
Plate format	medium evaporation, machine readout, barcode
Negative control si/shRNA	should have no effect on assay readout
Positive control si/shRNA	Should have large measurable effect on assay readout
Transfection reagent	should be effective in introducing RNAi reagent into cells with low toxicity and affect on assay
Transfection reagent diluent	should not interfere with assay readout, or transfection efficiency
Transfection reagent ratio	Toxicity vs. efficiency

Table 2 continued from previous page.

Parameter	Key Factors
Transfection reagent incubation time	enough time to complex RNAi reagent and transfection reagent
Mechanism for addition of transfection reagent	minimize well-to-well, plate-to-plate variability
Complexing time	enough time to complex RNAi reagent and transfection reagent
Cell volume added	well-to-well, plate-to-plate variability
Cell number added	optimize to give greater dynamic range at readout
Mechanism for addition of cells	minimize well-to-well, plate-to-plate variability
Mechanism for addition of readout reagent	minimize well-to-well, plate-to-plate variability
Incubation time for readout reagent	optimized to give greater dynamic range at readout
Readout method	sensitivity, accuracy

siRNA Transfection Optimization Experiments

A convenient first step in optimizing siRNA transfection conditions is to use viability assays with lethal control siRNAs. Two examples of a 96-well plate layout for transfection optimization are shown below (Figure 5). The bottom line is that a number of variables, including cell seeding density and transfection reagent identity/concentration, should be assessed.

The optimal condition is determined mainly by:

1. Negative controls should closed mimic NT; while the positive controls should achieve maximal effect as determined by the optimization experiments. Knockdown efficiency using the best condition should be verified by real-time PCR with previously validated siRNAs.
2. Controls should not exhibit high variance, which would indicate significant variation in transfection efficiency.
3. Performing experiments in clear bottom plates is also an excellent way to visualize transfection efficiency, as virtually all cells in a given well should be visibly affected by transfection with lethal controls (e.g., cell rounding).
4. After identifying potential conditions via lethal control experiments, those conditions should still be tested with assay-specific positive controls.

Pilot Screens

Pilot screens should be performed when conducting large-scale siRNA screens. Pilot screens will help inform on assay reproducibility and data distribution. Pilot screens can be conducted with defined subsets of the genome-wide library such as the kinome. Replicate screens conducted at the same time should exhibit large correlation (r^2~0.8) and even replicate screens conducted at different times (e.g., weeks or day apart) should be highly reproducible (see Figure 6). Pilot screen will also indicate how the data will be distributed in the larger screening campaign (e.g., normal, log-normal, or non-normal) and help indicate problems. For example, a very active screen, even if reproducible, may make it impossible to find anything of true significance in the assay, if one determines significance based on the screen population, and not a comparison to a single negative control (see hit selection below). Pilot screens can also indicate edge effects and other assay artifacts (Figure 7).

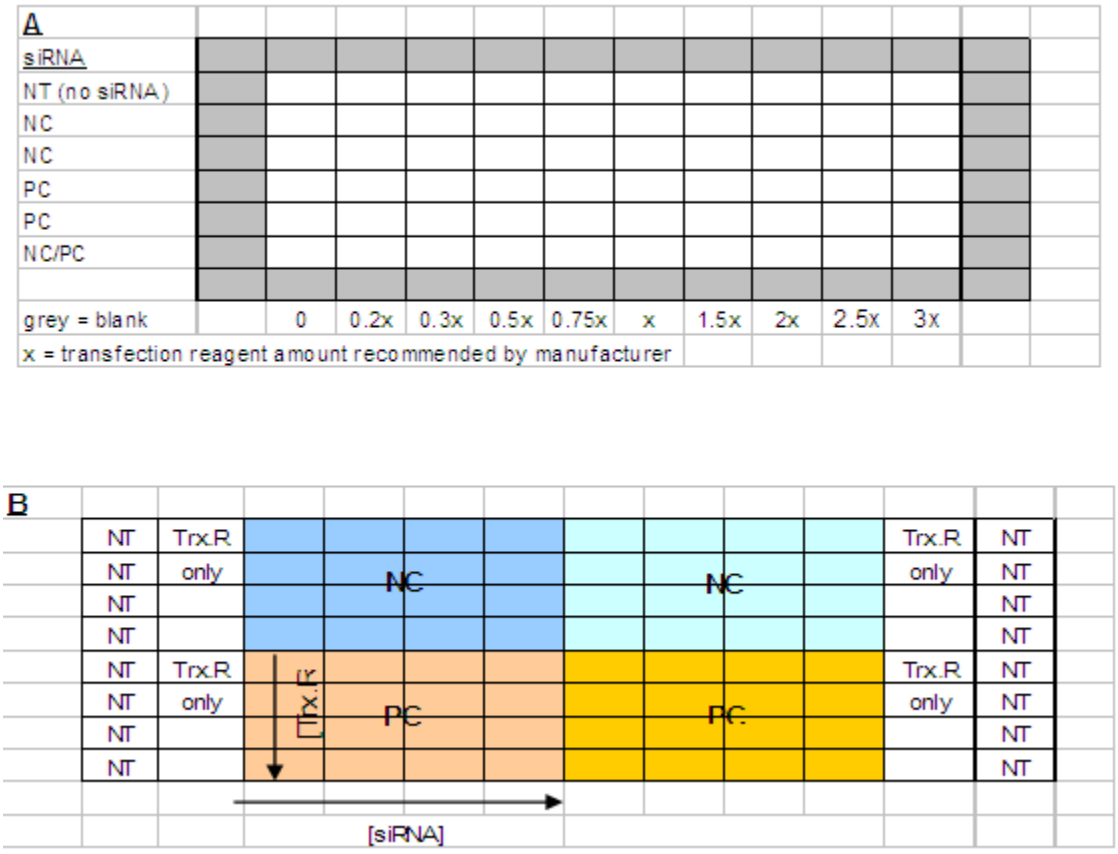


Figure 5. siRNA optimization plate layout examples. (A) has a wider range of transfection reagent concentrations to judge, given a fixed siRNA concentration (the edge wells are intentionally left blank); while in (B) the concentrations of siRNA and transfection reagent are optimized together. Different cell seeding density can also be tested along with the two factors in different plates. NC-negative control; PC-positive control; TRx.R – transfection reagent. In (B) each of the four blocks (4x4) in the center is a factorial design of siRNA and transfection reagent concentrations

RNAi Screen Design and Quality Control

Plate Design: When designing the plates one should consider including a sufficient number of control replicates to help evaluate data quality. The number of wells for each type of control within the plate should be ≥ 4 for 96-well plates (preferably 8 wells); or ≥ 8 for 384-well plates (preferably 16 wells). See Figure 8 for a sample screen plate layout.

Note**:** Plate layouts and available wells may limit the incorporation of MT or NT controls. However, control plates should always be included in screen batches to show that negative control transfected cells respond similar to MT and NT.

Replicates and Redundancy: Ideally, one would incorporate numerous, different reagents per gene (redundancy) and biological replicates. Given the issues with siRNA screening, it has been suggested that 4-6 reagents per gene be screened in the primary campaign (21). Unfortunately, many off-the-shelf libraries, whether whole genome or focused, come with one reagent per gene (pool) or 3 singles per gene, requiring multiple expensive purchases to achieve that threshold. Notably, it is much easier to acquire ≥4 reagents per gene when constructing a custom library in conjunction with a vendor. Performing replicate screens can be another approach to honing in on the most reproducible actives. For example, in the meta-analysis of HIV screens by Bushman and colleagues (19), simulations using the estimated variance for one of the siRNA screens predicted that of the top 300 hits only half would be shared between two replicate screens. Increasing the number of

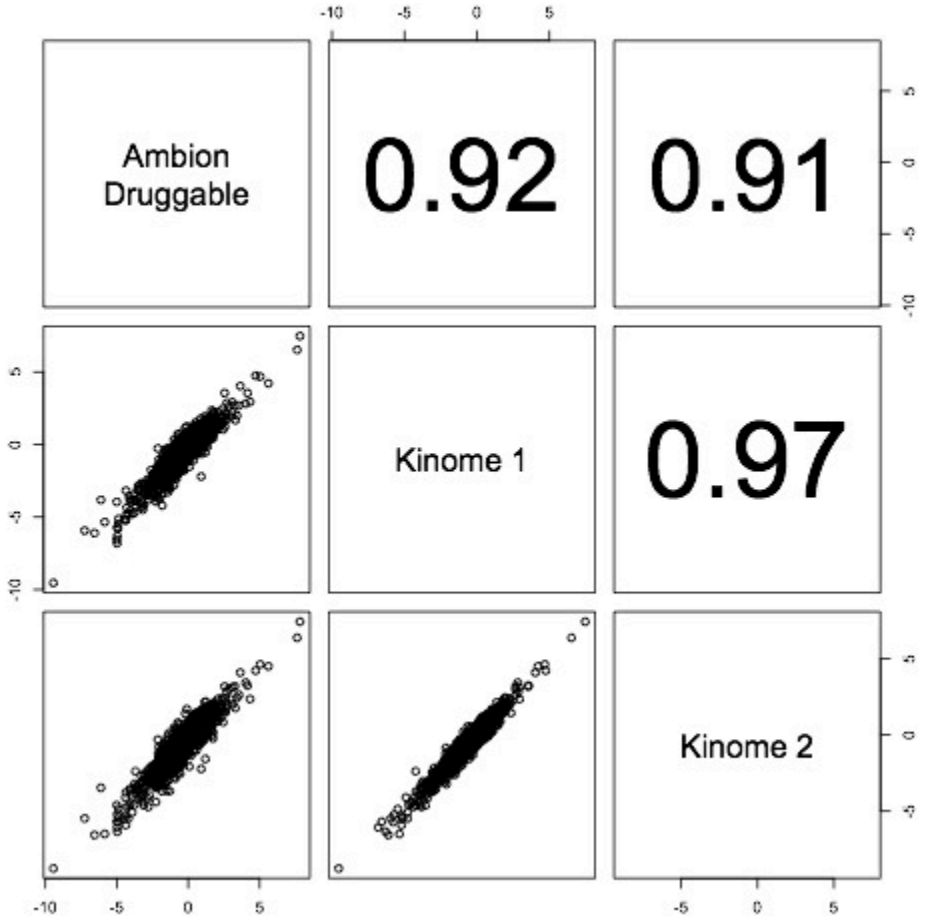


Figure 6. An example of a highly reproducible assay. Pilot kinome screens conducted on separate occasions indicate highly reproducible assay conditions - a prerequisite for conducting an RNAi screen. Using siRNA sequences in pilot screens that are also represented in the large-scale campaign ensures that assay performance remained unchanged (compare "Ambion Druggable" to Kinome 1 and 2).

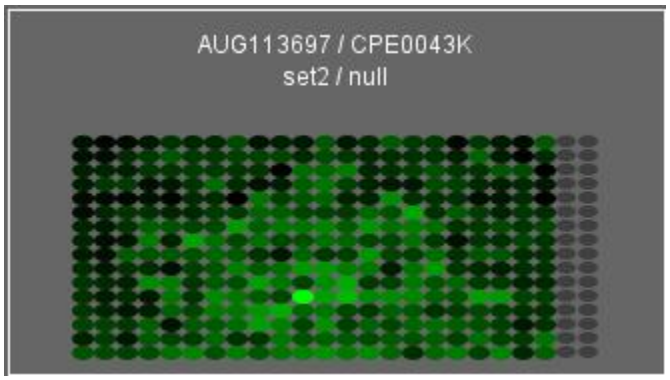


Figure 7. Pilot screens can indicate technical problems such as positional biases. Here, the assay signal is clearly biased toward the middle of the plate. This also emphasizes the value of data visualization.

replicates to ten would increase the overlap to 240 genes. However, the cost of running multiple reagents per gene ten times is prohibitive, requiring enough reagents (e.g., plates, tips, cell culture, transfection reagent, assay reagent, etc.) to run ~2400 384-well plates. Given cost and throughput realities, choices must be made. For a

highly reproducible assay, as determined in the pilot phase of a screening campaign, it is a given that most of the variance will come from a lack of agreement between reagents designed to target the same gene (false positives and negatives) and one may wish to devote more resources to redundancy as compared to replicates. If pilot screens indicate a high variance and very little overlap between replicates, then many replicates or a complete overhaul of the assay will be required. For smaller, focused screens, it should be practical to run multiple reagents per gene in duplicate and beyond if necessary (the correlation between replicates can dictate the ideal number of replicates).

Quality Control

Uniformity: Uniformity within-plate or from plate to plate is also a key factor to check for quality control. Heat maps are recommended to visualize each screen plate as they help to identify geometric effects due to experimental errors or systematic problems. Section II of this manual has guidelines on within-plate variation evaluation. Given the steps involved and the cell-based nature of RNAi experiments, CVs (coefficient of variation) ranging from ~15% to > 30% of the sample population are common. A scatter plot of pate-wise CVs versus the plate index may reveal plate-to-plate differences. In general most plates would be expected to yield similar CVs, but undoubtedly there will be biased plates in a given library given that libraries are not always randomly distributed (e.g., a plate may be rich in ribosomal proteins). If there are outlier plates in terms of CV, it will be important to inspect the source of those differences on a case by case basis. A replicate of that plate will ultimately determine if the aberrant CV is in fact a reflection of the biology occurring on the plate, or an assay artifact. Additionally, B-score normalization may help to minimize systematic row and column variations.

Control Variation: Scatter plots of common control wells across plates also help to evaluate plate-plate variation (Figure 9).

Assay Z'-factors: In HTS, a scatter plot of Z prime factors for every plate versus the plate index will reveal the plate-plate differences and may help to troubleshoot any existing problems, or flag plates for redo.

Transfection / Infection Efficiency: In many cases, the ratios between the negative control and positive control will inform on transfection/infection efficiency. For example, in a cell viability assay, the ratio of the potent positive control versus the negative controls can ideally be <5%, which can be interpreted as high (> 95%) transfection/infection efficiency. While there is no theoretically defined threshold value, often these ratios will depend on the type of assays and potency of controls. In some assays, comparing positive and negative controls will not obviously inform on transfection efficiency or homogeneity. In those cases, it may be advisable to run a control plate with siRNAs that will inform upon efficiency and heterogeneity of transfection.

Replicates: To evaluate the reproducibility between replicate plates (or within plate replicates), one can use Lin's Concordance Correlation Coefficient (Lin's CCC 22, 23), Bland-Altman test (24) and Pearson correlation coefficients. Please consult your statistician for the most applicable method.

siRNA Hit Selection

Normalization and Hit Selection: Data is typically normalized to controls (e.g., the median of the negative control wells on each plate) or median plate activity (although the presence of biased plates may make this less appropriate). Although normalizing to the plate median may initially seem more attractive than normalizing to a negative control (which could have assay activity due to off-target effects), this will cause problems during follow-up experiments. After selections are made for follow-up, any validation experiments will be biased as will the plate median, making it impossible to compare result between primary and secondary experiments. Therefore, we consider it preferable to control for plate to plate variation by normalizing to a negative control. Please consult your statistician for most suitable method. Hit selection in large-scale siRNA screens is usually performed by converting normalized values into z-scores, or MAD-based z-scores, and then selecting actives that cross a selected threshold (e.g., 2 z-scores or MAD scores from the screen median). To apply these types of

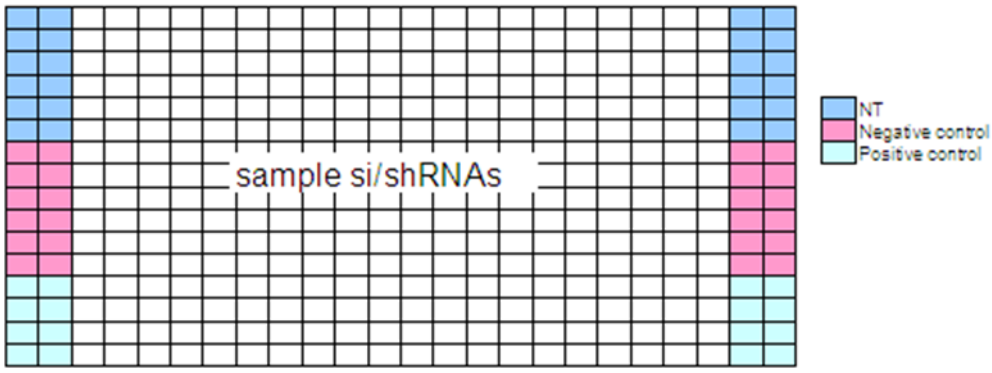


Figure 8. Experimental plate layout example shown in 384-well format.

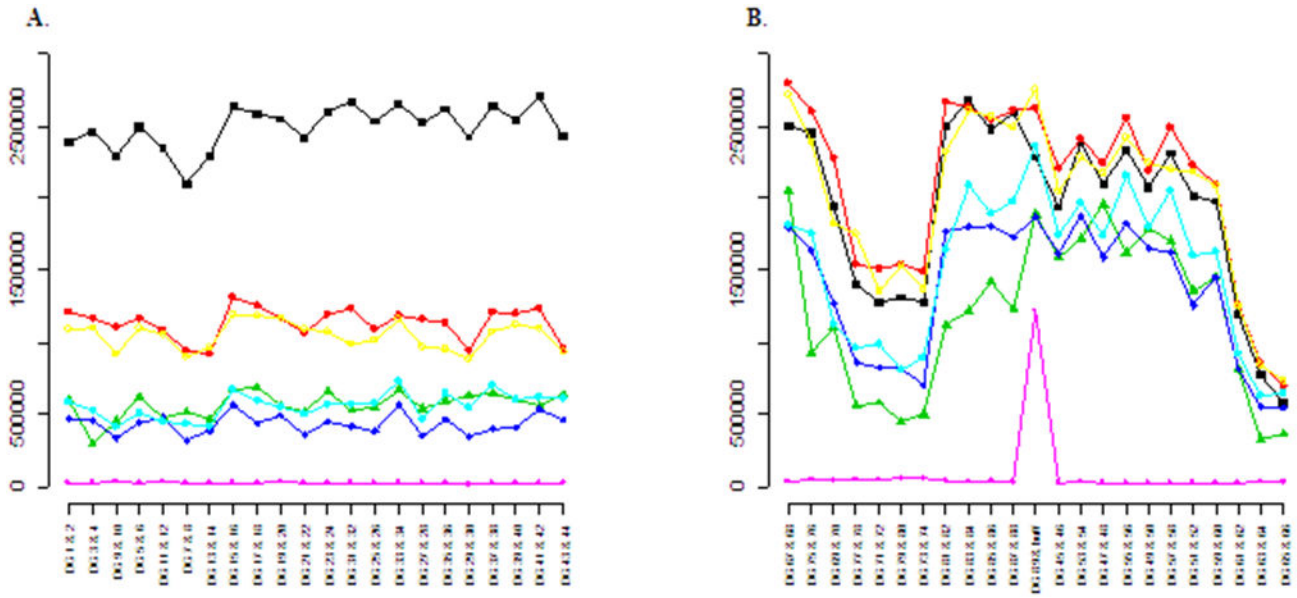


Figure 9. Scatter plots from two exemplar screens. Plots A and B show plate to plate variability as assessed by controls (different colors for different controls). It can be seen that the signals (Y-axis) for each kind of control are similar from plate to plate when analyzing all plates (X-axis) indicating low plate-plate variation while in plot B there is dramatic change from plate to plate, which could be corrected by some appropriate normalization method if the variation is consistent for all kinds of controls, or one needs to consider dropping some plate/wells with inconsistent variation.

methods it is important that the data be normally distributed. Comparison to negative control using a specified cutoff with statistical and/or biological significance (e.g. > 50% loss of cell viability) may be more appropriate for smaller screens. However, using cutoffs based on departure from negative control for larger screens may lead to too many "hits". For example, it may be historically accepted that a 30% reduction in the spread of a particular virus is biological relevant and significant. However, a 30% reduction may only score one standard deviation from the screen median, meaning that ~15% of a normally distributed population would be considered active. Alternatively, the biologically significant reduction of 30% may represent a very significant departure from the screen median, and be a very appropriate threshold. For smaller screens with large number of replicates, statistical tests (such as two sample t-test) can be used with appropriate multiple testing correction (e.g. Tukey's, or Dunnett) if necessary.

Hits selected from screens using reagent redundancy are typically restricted to those genes with multiple active reagents. For example, one could require that 2 or more of 4 siRNAs total cross a specified threshold. A corresponding p-value and FDR can also be associated with those criteria. Similarly, redundant siRNA analysis

(RSA) considers the activity of each siRNA for a given gene in an assay and generates a corresponding rank and p-value (21). Other non-parametric methods like sum of ranks can also be employed. Consult your statistician, and be sure that hits selected for follow-up are actually grounded in the screen data.

Primary screen data can and should be filtered for off-target effects. For example, by screening a large library of non-pooled siRNAs, one can analyze the data for biased seed sequences (20, Figure 10). siRNAs containing these seeds can be demoted in hit selection. Similarly, the top active siRNAs can be filtered for those containing known miRNA seed sequences with the assumption that these seeds will be highly promiscuous in terms of off-target profiles. In addition to flagging potentially biased siRNAs, there are also tools to even interpret the underlying OTEs (25, 26).

Pathway analysis can also reveal enrichments in the data and prioritize hits for follow-up. A variety of commercial and open software are available. A potential caveat is that this type of analysis is biased towards well-annotated genes.

Follow-up Assays

The detailed follow up plan for hits identified in a screen would depend on the nature of the investigation and the goal(s) of the study. That said, a few general suggestions are described below.

- Test additional siRNAs for targets of interest. These siRNAs should constitute different sequences than those in the primary screen. It has been traditionally accepted that 2 active siRNAs constitutes a validated active, but given the estimates described above, and the continued reports describing lack of correlation between published screens using similar systems, 2 active siRNAs seems to be an inadequate standard. However, any candidate can be examined in additional follow-up experiments for more rigorous validation.
- Target gene KD can be validated. Knockdown can be measured by QPCR over 24h or 48h. Best practices for carrying out QPCR experiments can be found elsewhere in the current or future versions of the QB manual. siRNA efficacy can also be assessed by Western blotting or immunofluorescence when possible. Clearly, a siRNA that yields a phenotype, but does not yield KD is a false positive. However, demonstrating KD does not prove that the observed phenotype is due to the on-target knockdown of that gene (i.e., an siRNA that is effective against its target has no bearing on its ability to down-regulate other transcripts and cannot be interpreted as validation). Furthermore, the number of siRNAs that have no effect on their intended target is relatively small, making it unlikely that QPCR will be a cost effective method for eliminating false-positives.
- Rescue: The current gold standard in RNAi hit validation is rescue of phenotypes by introducing siRNA-resistant cDNA. Another approach is to knockout the gene of interest by using TALEN or similar technologies. This knockout should recapitulate the siRNA-induced phenotype and can also be rescued by subsequent re-expression of the gene via cDNA. Although these experiments can be excellent validation, they can also be technically challenging and suffer from their own pitfalls.
- Test control siRNAs that retain the seed region of the original siRNA, but not its ability to cleave the transcript of interest. Recent reports have described control siRNAs where the seed region is maintained, but bases 9-11 are altered (27). The intent is to maintain the seed-driven off-target effects of a given siRNA, while eliminating its on-target effect. This initial study showed promise in separating false from true positives.

Secondary assays: This is recommended to eliminate assay artifacts and characterize target biology in more detail. Therefore, the exact nature of the assay may differ as a function of target pathway, biological process and disease biology. Validated high-content assays maybe particularly useful in this regard. These are described elsewhere in the QB manual.

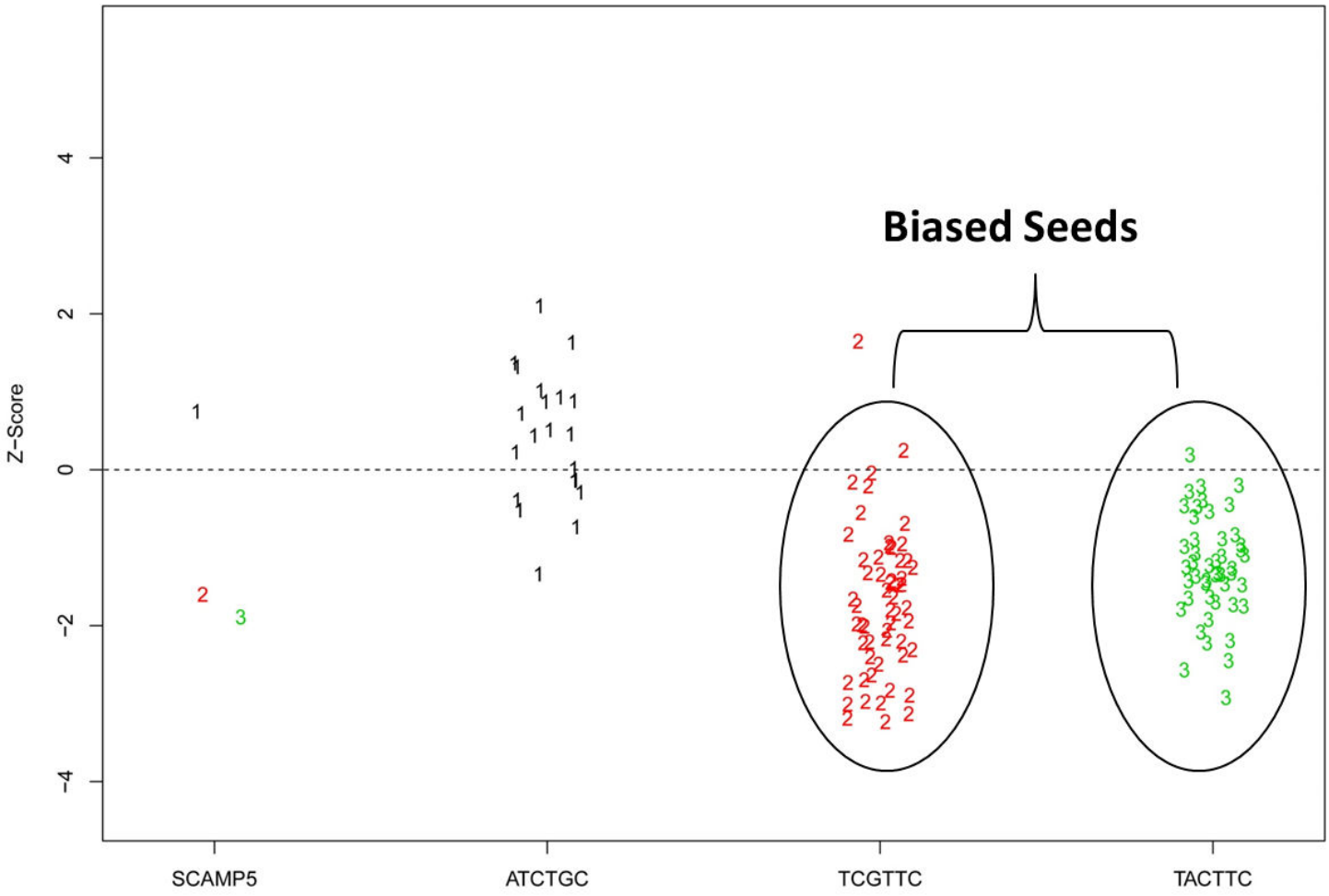


Figure 10. Screening a large library of non-pooled siRNAs enables determination of biased seed sequences (20). Two siRNAs targeting SCAMP5 appear to significantly down-regulate the assay response. However, siRNAs containing the same hexamer sequences exhibit a clear bias towards down-regulating the assay. Therefore, the SCAMP5 siRNAs would be flagged as highly suspicious and are most likely OTEs.

RNAi Synthetic Lethality Screens

Synthetic Lethality Screens

A variation of a LOF screen is a synthetic lethality (or, synthetic lethal) screen which combines the use of RNAi and a drug (at single concentration or multiple concentrations) to identify knockdown events that would modulate drug response such as sensitizers that enhance drug effect. This offers a powerful approach to identify genetic determinants of drug response, especially in cancer. Most of the assay optimization and follow-up assays for si/shRNA described in part B apply here. The extra optimization and differences in data analysis will be discussed below.

Assay Optimization

In synthetic lethality screens, the incubation time of the drug, its potency and stability also need to be evaluated. Drug dose and time response (DDTR) experiments can be carried out to optimize these conditions in either 96-well or 384-well plates. For instance, in a 96-well plate, 10-point drug dilutions with NT and negative controls (at fixed si/shRNA concentration) can be applied along each row excluding the two edge columns (Figure 11). Assay

readouts need to be monitored over a period of time, say from Day 1 to Day 6. The result of such an experiment is mentioned below.

Example: A DDTR experiment for one drug was done from Day 1 to Day 6 to determine the appropriate drug incubation time for subsequent siRNA synthetic lethality screens. Data from Day 3 to Day 6 in Figure 8 (data from Day 1 and Day 2 data was not informative for curve fitting). Sigmoidal dose response curves of NT and NS were obtained from the experimental plates designed as above and IC_{50} values were estimated for each day. From Figure 12, we can see that:

- NS and NT produce almost exactly the same dose response curves over the various concentrations sampled
- IC_{50} values of the drug (either from NT or NS curves, see vertical drop lines in Figure 12) tend to stabilize from Day 4 (for NT, Day 3: 44.59nM, Day 4: 35.78nM, Day 5: 36.54nM, Day 6: 31.77nM)
- Signal window between the zero concentration and the highest concentration of the drug tends to stabilize from Day 5 (Z prime factor calculated using NT at concentration zero and 200 nM: Day 3-0.42; Day 4-0.89; Day 5-0.73; Day 6-0.73).

Therefore 5 days of drug treatment would be recommended.

Design of Synthetic Lethality Screens

There are two main designs for synthetic lethality screens: single and multiple concentrations of drug. The hit selection strategy will vary accordingly.

- **Single-concentration experiment** - Typically drug concentrations less than the IC_{50} are chosen (e.g. IC_{10} and/or $_{IC30}$). At each point including zero, we recommend at least three replicates (may reduce to duplicates in a high-throughput screen).
- **Multiple-concentration experiment** - A full dose response curve of the drug is used. We recommend 7 doses with duplicates as a minimum. For larger scale screens where number of points and replicates are an issue, we would suggest increased dose points, provided they are chosen carefully to cover the full range of dose response.

  Note: Several advantages exist with a RNAi synthetic lethality screen run with multiple concentrations. Non-linear curve fitting to identify biologically more relevant hits that demonstrate a 'shift' in DDR is made possible. Replicates are not as major an issue and achieving exact dose effect is not a concern due to curve fitting. In our experience, it is likely to produce more robust screen actives (less false-positives) and reduce follow-up steps.

In synthetic lethality screens, other necessary considerations are:

- Monitoring drug dose response in a large scale screen, such as control charting on drug potency (Quantitative Biology).
- Choice of sensitizer control (positive control) which may be targets related to drug MOA.
- Inclusion of extra control plates (see Appendix) along with other library plates in the screen to assess the quality of the screen especially HTS.

Hit Selection in Synthetic Lethality Screens

Normalization methods basically are the same as described earlier for LOF screens. The basic idea of synthetic lethality experiments is to identify hits that result in maximum chemosensitization. Therefore, we suggest the following hit selection process:

	1	2	3	4	5	6	7	8	9	10	11	12
A	NT	NT	NT	NT	NT	NT	NT	NT	NT	NT	NT	NT
B	NT	NT	NT	NT	NT	NT	NT	NT	NT	NT	NT	NT
C	NT	NT	NT	NT	NT	NT	NT	NT	NT	NT	NT	NT
D	NT	NT	NT	NT	NT	NT	NT	NT	NT	NT	NT	NT
E	NS	NS	NS	NS	NS	NS	NS	NS	NS	NS	NS	NS
F	NS	NS	NS	NS	NS	NS	NS	NS	NS	NS	NS	NS
G	NS	NS	NS	NS	NS	NS	NS	NS	NS	NS	NS	NS
H	NS	NS	NS	NS	NS	NS	NS	NS	NS	NS	NS	NS

Drug dilution

Figure 11. 96-well plate layout for DDTR. NT: non-transfected; NS: non-silencing siRNA (negative control)

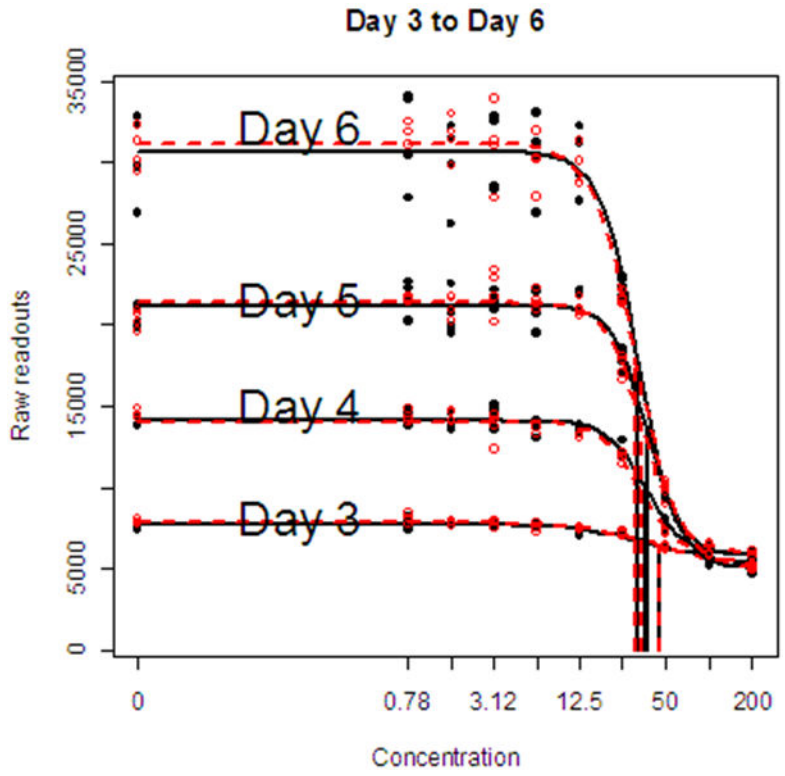


Figure 12. DDTR example of one experiment with four replicates from Day 1 to Day 6 (Data from Day 1 and 2 was not for curve fitting and is not shown); black solid lines and solid points are for NT, red dash lines and bullet points for NS.

1. When using a cell growth or death assay, we suggest excluding si/shRNA hits that are result in high cytotoxicity without drug. This is to prevent confounding interpretation around drug potentiation (These hits can be tested separately for any sensitization effect). As an example, in our experience, we have excluded hits that cause >60% loss of viability from the following analysis. Other threshold values can also be obtained by using population-based methods suggested by statisticians (such as 2 or 3 standard deviations from the mean).
2. After the first step,
    - In a single-concentration experiment with sufficient replicates, one can use statistical models (such as linear models) to pick statistically significant hits that demonstrate significant interaction of drug and siRNA. Furthermore, to rank hits, we suggest a non-parametric metric based on the

interaction between RNAi, drug and the combination, called "potentiation score", based on the idea of independent events, calculated as shown below for inhibition assays, such as cell viability:

$$P = \frac{NS(T)}{NS(UT)} \times \frac{siRNAOnly(UT)}{NS(UT)} \Big/ \frac{Combination}{NS(UT)}$$

Or, for activation assays, such as cell apoptosis:

$$P = \frac{Combination}{NS(UT)} \Big/ \frac{NS(T)}{NS(UT)} \times \frac{siRNAOnly(UT)}{NS(UT)}$$

"UT" here refers to the untreated condition; the "drug only" and "combination" are at the same drug dose point. P >1 indicates that the combination effect is more than the product of two individual effects. The threshold values can be determined using population-based methods. An example of hits in single-concentration experiment is illustrated in Figure 13.

- In a multiple-concentration experiment, sigmoidal curve comparison is done between RNAi with and without small molecule. Using cell viability assay as an example, hits that demonstrate a significant left shift of dose response curves (Figure 14) would be of interest. One should first exclude those response curves above the negative controls (to avoid transfection artifacts) and then look for a decrease of IC_{50}/EC_{50} values. Statistical tests like t-test between IC_{50}/EC_{50} estimates, F test for two curve fittings, or information criteria can be used for testing significance (GraphPad Prism Manual). In general, we recommend hits that show at least a 2-fold EC_{50} shift with respect to the negative control.
- Apart from the follow-up mentioned above we recommend confirmation of sensitization in a multiple dose format (10-point with replicates). If available, testing related compounds for specificity is suggested.

Loss-of-Function Screens Using shRNA

General Considerations for shRNA-Lentivirus Infection

Many of the same consideration for siRNA screening can be applied to arrayed shRNA screening. However, optimization of shRNA-lentivirus infection for each cell line is a more involved process than siRNA. There are various parameters that should be considered when optimizing infection.

1. Determination of cell seeding density from performing a simple growth curve experiment
2. Determination of puromycin concentration by performing a 10-point dose response curve, ranging from 0.1 mg/ml to 10 mg/ml (a typical concentration ranges between 2-5 mg/ml)
3. Time course for puromycin treatment
4. Effect of protamine sulfate to cells
5. The amount of virus to be used for maximal infection. A detailed protocol on viral infection can be found at http://www.broad.mit.edu/genome_bio/trc/publicProtocols.html. Furthermore, infectability can be measured for each cell line using a cell count assay:

$$\text{Infectibility} = \left[\frac{(\#\text{ of infected cells with puromycin }) - (\#\text{ of non-infected cells with puromycin*})}{(\text{ Total \# of cells without puromycin})} \right] \times 100$$

*Refers to background (killing) i.e. just cells with puromycin added

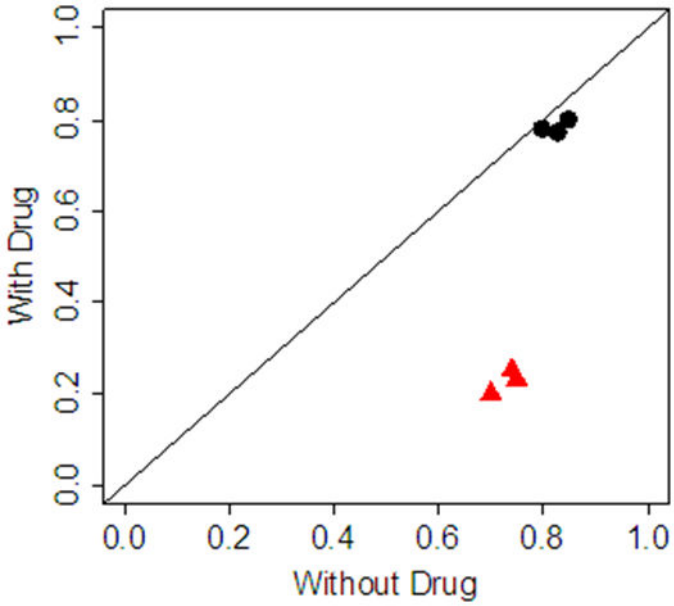


Figure 13. A hit from single-dose synthetic lethality screen in a cell proliferation assay. The black round points are for negative controls (NS), showing not much different effect w/ or w/o drug; the off-diagonal red triangle points are for the hit, which does not have much of an effect on its own but has significantly more effect with drug.

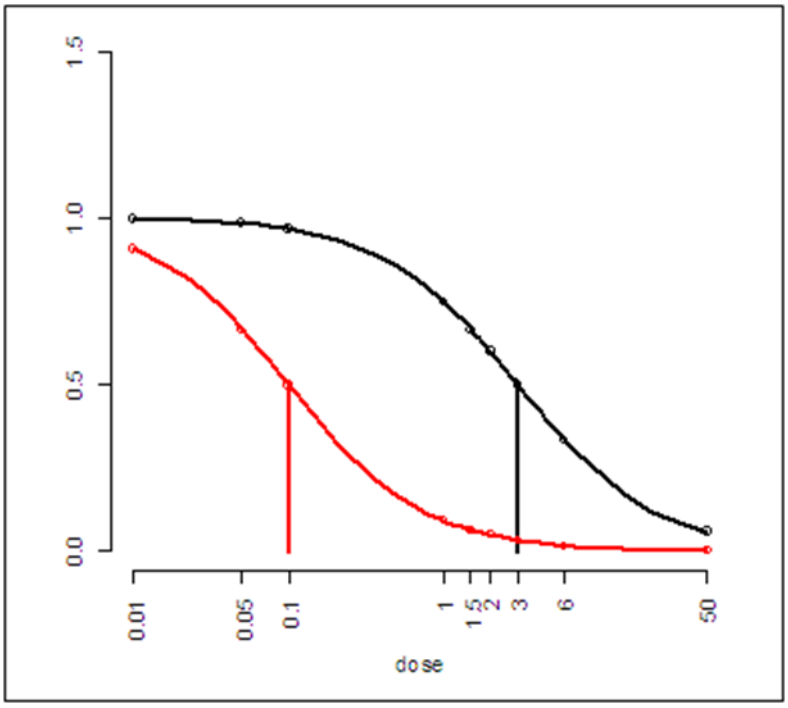


Figure 14. A hit in multiple-dose synthetic lethality siRNA screen in a cell viability assay. The decrease of IC50 value of the red dose response curve (the siRNA with the drug) compared to the black curve (negative control, NS with the drug) is observed (the dropping lines indicate the positions of IC50 values).

shRNA-Lentivirus Infection Protocol

Viral infection in 96-well microplate format. This step is similar for determination of viral titer.

1. Seed cells of interest overnight in a total volume of 50 µl of growth media

2. Add 40 µl of growth media with 2X of protamine sulfate (16 mg/ml) to cells. This volume is dependent of the viral supernatant added in below in Step 3.
3. Add 2-10 µl of viral supernatant to mix above. This volume is dependent on the viral titer. The final volume of steps 2 and 3 is 50 µl. Incubate at 37°C overnight.
4. Add 2X puromycin (4 mg/ml) in 100 µl of growth media and incubate for 37°C overnight.
5. Wash off puromycin and replace with normal growth media.
6. Incubate for 2-4 days depending on the assays.

Pooled shRNA Screening

Pooled shRNAs enable large-scale screens without the need for HTS infrastructure. Pooled screens are conducted by transducing cells with a soup of shRNA-containing lentiviral particles, which can comprise 1000s of unique shRNAs. Pooled screens are performed under positive or negative selection. In positive selection, a selective pressure is applied, and the identity of shRNAs in selected cells is identified. In negative selection screens, a control population of transduced cells is compared to a treated population, and shRNAs that are lost or enriched in the treated arm are identified. Pooled shRNA libraries are commercially available and corresponding protocols are provided in detail. Some general considerations include infecting cells at a low MOI (0.1 – 0.3) to ensure no more than one integrant per cell, transducing at a reasonable fold representation (e.g., 100 – 1000 fold representation for each shRNA in the pool), and maintaining adequate representation throughout all steps of the screening process. For example, harvesting genomic DNA from a number of cells that at leasts corresponds to the intended number of viral integrants. This will ensure that all shRNAs in the experiment population are represented.

Appendix

shRNA-lentivirus system

shRNA can be delivered into cells either by transfection of plasmids expressing shRNA of the gene of interest or by infection of viral-packaged shRNA of the gene of interest in the form of lentiviral vectors. The following optimization of delivery of shRNA into cells is focused on the lentiviral shRNA vectors. The lentiviral library used here is created from a pLKO1 vector that carries a puromycin resistance gene and shRNA expression is driven from a human U6 promoter (5). The puromycin resistance gene has been used as a selection marker for infected cells harboring the shRNA vectors.

Cell based phenotypic RNAi assays using shRNA lentiviral vectors involves (1) viral production where shRNA vectors are packaged into lentivirus and (2) viral infection where the lentivirus harboring the shRNA vectors are transduced into the cells of interest.

Optimization of shRNA-lentivirus production

The production of shRNA-lentivirus involves the packaging of the shRNA vector into lentivirus and requires transfection of two plasmids which forms the packaging system, pCMVD8.9 (28, 29) and pHCMV-G (30). In the transfection process, the key factors to be optimized are the seeding density, transfection reagents used, concentration of plasmids and the ratio of transfection reagent to plasmids. For concentration of plasmids, the usual practice includes concentration ranging from 100 ng to 200 ng. The plasmid concentration to transfection reagent ratio to be tested usual includes 2:1, 3:1 and 3:2. Viral production can be performed using the protocol published by the Broad institute at http://www.broad.mit.edu/genome_bio/trc/publicProtocols.html.

GFP control vector is used for optimization purpose and can be viewed briefly under the microscope to assess fluorescence. The number of infectious units in the viral supernatant calculated as IU/ml is assessed by infecting cells with generally 2 ml of virus and counting survival of cells after puromycin treatment. The viral titer

determination is important to assess the amount of virus to be used in infection for cell based assay. An acceptable range for viral titer is 2 x 106 to 2 x 107. A variety of commercial kits (p24 ELISA) are now available to determine titer.

shRNA-lentivirus production protocol (96-well microplate format)

1. Dilute D8.9 to 9 ng/ml, vsv-g to 1 ng/ml and shRNA to 25 ng/ml.
2. Add 6 µl per well (150 ng) of shRNA and 5 ml each of D8.9 (45 ng) and vsv-g (5 ng) to the shRNA.
3. Dilute transfection reagent (e.g. Fugene 6 from Roche) in Opti-Mem to a volume of 14 ml per well, that is, 0.6 ml of reagent to 13.4 ml of Opti-Mem. The final ratio of transfection reagent:vDNA should be 3 ml:1mg.
4. Add diluted transfection reagent (e.g. Fugene 6 from Roche) to the plasmid mix to a final volume of 30 ml per well and incubate for 30-45 minutes at room temperature.
5. Transfer Fugene/DNA complex to HEK293T cells grown overnight seeded at 25000 cells per well in low antibiotic growth media. Incubate for 18 hours at 37°C.
6. Replace media with 170 ml of high serum growth media and incubate for further 24 hours at 37°C.
7. Harvest 150 ml of viral supernatant and add 170 ml of high serum growth media and incubate for another 24 hours at 37°C.
8. Harvest another 150 ml of viral supernatant and discard cells.
9. Pool viral supernatant and use for infection.

Examples of plate layout for control plates to quality control RNAi synthetic lethality screens.

Acknowledgements

The authors would like to acknowledge collaborations with Translational Genomics Research Institute (Phoenix, AZ) and Genome Institute of Singapore (Singapore) that have led to joint learnings in adopting best practices for executing RNAi screens. We would like to acknowledge Seppo Karrila (Lilly Singapore Center for Drug Discovery) for introducing the potentiation score method. We also thank Pat Solenberg and Wayne Blosser (Eli Lilly and Company) for critical review and recommendations of content.

Abbreviations

- RNAi - RNA Interference
- siRNA - Small Interfering RNA
- shRNA - Short Hairpin RNA
- miRNA - Micro-RNA
- dsRNA - Double-Stranded RNA
- KD - Knock-Down
- HTS - High Throughput Screen/Screening
- LOF - Loss-Of-Function
- QC - Quality Control
- NS - Non-Silencing
- NT - Non-Transfected
- NTC - Non-Targeting Control
- MT - Mock-Transfected
- NC - Negative Control
- PC - Positive Control
- CV - Coefficient of Variation
- SW - Signal Window

- Lin's CCC - Lin's Concordance Correlation Coefficient
- DDTR - Drug Dose Time Response
- UT/T - (Drug) Untreated/Treated

References

Publications:

1. Kettling RF. The many faces of RNAi. Developmental Cell. 2011;20(2):148–161. PubMed PMID: 21316584.
2. Mohr SE, Perrimon N. RNAi screening: new approaches, understandings, and organisms. WIREs RNA. 2012;3:145–158. PubMed PMID: 21953743.
3. Panda D, Cherry S. Cell-based genomic screening: elucidating virus-host interactions. Current Opinion in Virology. 2012;2:784–792. PubMed PMID: 23122855.
4. Chatterjee-Kishore M. From genome to phenome--RNAi library screening and hit characterization using signaling pathway analysis. Current Opinion in Drug Discovery & Development. 2006;9(2):231–239. PubMed PMID: 16566293.
5. Echeverri CJ, Beachy PA, Baum B, Boutros M, Buchholz F, Chanda SK, Downward J, Ellenberg J, Fraser AG, Hacohen N, Hahn WC, Jackson AL, Kiger A, Linsley PS, Lum L, Ma Y, Mathey-Prevot B, Root DE, Sabatini DM, Taipale J, Perrimon N, Bernards R. Minimizing the risk of reporting false positives in large-scale RNAi screens. Nature Methods. 2006;3(10):777–779. PubMed PMID: 16990807.
6. Echeverri CJ, Perrimon N. High-throughput RNAi screening in cultured cells: a user's guide. Nature Review Genetics. 2006;7(5):373–384. PubMed PMID: 16607398.
7. Fuchs F, Boutros M. Cellular phenotyping by RNAi. Briefings in Functional Genomics and Proteomics. 2006;5(1):52–56. PubMed PMID: 16769679.
8. Moffat J, Sabatini DM. Building mammalian signaling pathways with RNAi screens. Nature Reviews Molecular Cell Biology. 2006;7(3):177–187. PubMed PMID: 16496020.
9. Root DE, Hacohen N, Hahn WC, Lander ES, Sabatini DM. Genome-scale loss-of-function screening with a lentiviral RNAi library. Nature Methods. 2006;3(9):715–719. PubMed PMID: 16929317.
10. Sachse C, Krausz E, Kronke A, Hannus M, Walsh A, Grabner A, Ovcharenko D, Dorris D, Trudel C, Sonnichsen B, Echeverri CJ. High-throughput RNA interference strategies for target discovery and validation by using synthetic short interfering RNAs: functional genomics investigations of biological pathways. Methods in Enzymology. 2005;392:242–277. PubMed PMID: 15644186.
11. Willingham AT, Deveraux QL, Hampton GM, Aza-Blanc P. RNAi and HTS: exploring cancer by systematic loss-of-function. Oncogene. 2004;23(51):8392–8400. PubMed PMID: 15517021.
12. Birmingham A, Anderson EM, Reynolds A, Ilsley-Tyree D, Leake D, et al. 3'UTR seed matches, but not overall identity, are associated with RNAi off-targets. Nature Methods. 2006;3:199–204. PubMed PMID: 16489337.
13. Jackson AL, Burchard J, Leake D, Reynolds A, Schelter J, et al. Position-specific chemical modification of siRNAs reduces "off-target" transcript silencing. RNA. 2006;12:1197–11205. PubMed PMID: 16682562.
14. Jackson AL, Bartz SR, Schelter J, Kobayashi SV, Burchard J, et al. (2003). Expression profiling reveals off-target gene regulation by RNAi. Nature Biotechnology 21:635–3.7
15. Semizarov D, Frost L, Sarthy A, Kroeger P, Halbert DN, Fesik SW. Specificity of short interfering RNA determined through gene expression signatures. PNAS. 2003;100:6347–52. PubMed PMID: 12746500.
16. Lin X, Ruan X, Anderson MG, McDowell JA, Kroeger PE, et al. siRNA-mediated off-target gene silencing triggered by a 7 nt complementation. Nucleic Acids Research. 2005;33:4527–4535. PubMed PMID: 16091630.
17. Schultz N, Marenstein DR, DeAngelis DS, Wang WQ, Nelander S, Jacobsen A, Marks DS, Massaque J, and Sander C. (2011). Off-target effects dominate a large-scale RNAi screen for modulators of the TGF-β pathway and reveal microRNA regulation of TGFBR2. Silence 2: 1758-907X-2-3.

18. Sigoillot FD, King RW. Vigilance and validation: Keys to success in RNAi screening. ACS Chemical Biology. 2011;6:47–60. PubMed PMID: 21142076.
19. Busman FD, Malani N, Fernandes J, D'Orso I, Cagney G, Diamond TL, et al. Host cell factors in HIV replication: Meta-Analysis of genome-wide studies. PLoS Pathogens. 2009;5:e1000437. PubMed PMID: 19478882.
20. Marine S, Bahl A, Ferrer M, Buehler E. Common seed analysis to identify off-target effects in siRNA screens. Journal of Biomolecular Screening. 2012;17:370–378. PubMed PMID: 22086724.
21. Konig R, Chiang C, Tu BP, Yan SF, DeJesus PD, Romero A, Berguer T, et al. A probability-based approach for the analysis of large-scale RNAi screens. Nature Methods. 2007;4:847–849. PubMed PMID: 17828270.
22. Lin LI. A concordance correlation coefficient to evaluate reproducibility. Biometrics. 1989;45:255–268. PubMed PMID: 2720055.
23. Lin LI. A note on the concordance correlation coefficient. Biometrics. 2000;56:324–325.
24. Bland JM, Altaman DG. Statistical methods for assessing agreement between two methods of clinical measurement. Lancet. 1986;I:307–310. PubMed PMID: 2868172.
25. Buehler E, Khan AA, Marine S, Rajaram M, Bahl A, Burchard J, Ferrer M. siRNA off-target effects in genome-wide screens identify signaling pathway members. Scientific Reports. 2012;2:428. article. PubMed PMID: 22645644.
26. Sigoillot FD, Lyman S, Huckins JF, Adamson B, Chung E, Quattrochi B, King RW. A bioinformatics method identifies prominent off-targeted transcripts in RNAi screens. Nature Methods. 2012;19:363–366. PubMed PMID: 22343343.
27. Buehler E, Chen YC, Martin SE. C911: A bench-level control for sequence specific siRNA off-target effects. PLoS One. 2012;7:e51942. PubMed PMID: 23251657.
28. Naldini L, Blömer U, Gage FH, Trono D, Verma IM. Efficient transfer, integration, and sustained long-term expression of the transgene in adult rat brains injected with a lentiviral vector. PNAS. 1996;93:11382–11388. PubMed PMID: 8876144.
29. Zufferey R, Nagy D, Mandel RJ, Naldini L, Trono D. Multiply attenuated lentiviral vector achieves efficient gene delivery in vivo. Nature Biotechnology. 1997;15:871–875. PubMed PMID: 9306402.
30. Yee J, Miyanohara A, LaPorte P, Bouic K, Burns JC, Friedmann T. A General Method for the Generation of High-Titer, Pantropic Retroviral Vectors: Highly Efficient Infection of Primary Hepatocytes. PNAS. 1994;91:9564–9568. PubMed PMID: 7937806.

Additional References:

Berns K, Horlings HM, Hennessy BT, Madiredjo M, Hijmans EM, Beelen K, Linn SC, Gonzalez-Angulo AM, Stemke-Hale K, Hauptmann M, Beijersbergen RL, Mills GB, van de Vijver MJ, Bernards R. A functional genetic approach identifies the PI3K pathway as a major determinant of trastuzumab resistance in breast cancer. Cancer Cell. 2007 Oct;12(4):395–402. PubMed PMID: 17936563.

Brideau C., Gunter B., Pikounis B., Liaw A. Improved statistical methods for hit selection in high-throughput screening. Journal of Biomolecular Screening. 2003;8:634–647. PubMed PMID: 14711389.

Brummelkamp TR, Fabius AW, Mullenders J, Madiredjo M, Velds A, Kerkhoven RM, Bernards R, Beijersbergen RL. An shRNA barcode screen provides insight into cancer cell vulnerability to MDM2 inhibitors. Nat Chem Biol. 2006 Apr;2(4):202–6. Epub 2006 Feb 13. PubMed PMID: 16474381.

Eggert US, Kiger AA, Richter C, Perlman ZE, Perrimon N, Mitchison TJ, Field CM. Parallel chemical genetic and genome-wide RNAi screens identify cytokinesis inhibitors and targets. PLoS Biol. 2004 Dec;2(12):e379. Epub 2004 Oct 5. PubMed PMID: 15547975.

Epping MT, Wang L, Plumb JA, Lieb M, Gronemeyer H, Brown R, Bernards R. A functional genetic screen identifies retinoic acid signaling as a target of histone deacetylase inhibitors. Proc Natl Acad Sci U S A. 2007 Nov 6;104(45):17777–82. Epub 2007 Oct 29. PubMed PMID: 17968018.

Gunter B., Brideau C., Pikounis B., Liaw A. Statistical and graphical methods for quality control determination of high-throughput screening data. Journal of Biomolecular Screening. 2003;8:624–633. PubMed PMID: 14711388.

Iversen PW., Eastwood BJ., Sittampalam S., Cox KL. A comparison of assay performance measures in screening assays: signal window, Z' factor and assay variability ratio. Journal of Biomolecular Screening. 2006;11:1–6. PubMed PMID: 16490779.

Malo N., Hanley JA., Cerquozzi S., Pelletier J., Naddon R. Statistical practice in high-throughput screening data analysis. Nature Biotechnology. 2006;24:167–175. PubMed PMID: 16465162.

Root DE, Hacohen N, Hahn WC, Lander ES, Sabatini DM. Genome-scale loss-of-function screening with a lentiviral RNAi library. Nature Methods. 2006;3(9):715–719. PubMed PMID: 16929317.

Sachse C, Krausz E, Kronke A, Hannus M, Walsh A, Grabner A, Ovcharenko D, Dorris D, Trudel C, Sonnichsen B, Echeverri CJ. High-throughput RNA interference strategies for target discovery and validation by using synthetic short interfering RNAs: functional genomics investigations of biological pathways. Methods in Enzymology. 2005;392:242–277. PubMed PMID: 15644186.

Whitehurst AW, Bodemann BO, Cardenas J, Ferguson D, Girard L, Peyton M, Minna JD, Michnoff C, Hao W, Roth MG, Xie XJ, White MA. Synthetic lethal screen identification of chemosensitizer loci in cancer cells. Nature. 2007 Apr 12;446(7137):815–9. PubMed PMID: 17429401.

Willingham AT, Deveraux QL, Hampton GM, Aza-Blanc P. RNAi and HTS: exploring cancer by systematic loss-of-function. Oncogene. 2004;23(51):8392–8400. PubMed PMID: 15517021.

Web sites:

1. Minimum Information About an RNAi Experiment (MIARE) - http://miare.sourceforge.net/HomePage

2. GraphPad Prism Manual - http://www.broad.mit.edu/genome_bio/trc/publicProtocols.html

FLIPR™ Assays for GPCR and Ion Channel Targets

Michelle R. Arkin,[1] Patrick R. Connor,[2] Renee Emkey,[2] Kim E. Garbison,[2] Beverly A. Heinz,[2] Todd R. Wiernicki,[2] Paul A. Johnston,[3] Ramani A. Kandasamy, Nancy B. Rankl, and Sitta Sittampalam[4]

Created: May 1, 2012; Updated: October 1, 2012.

Abstract

Calcium ions (Ca2+) play a key role in cellular homeostasis involving calcium channel and GPCR function, which plays a critical role in many disease pathologies. Fluorescent Imaging Plate Reader (FLIPRTM) technology to measure Ca2+ flux in cells was an important development in the early 1990's and has played a significant role in HTS and lead optimization applications. In this chapter, the basic concepts in using the FLIPR instrument and assay development and optimization to measure Ca2+ flux in cells are described. Although this chapter is devoted to Ca2+ channel based assay development, the FLIPRTM is also useful for measuring potassium and other ion flux in cells with appropriate fluorescent dyes.

Overview: FLIPR™ Assay Development

Reagents Needed:

Cell line(s) expressing GPCRs, ion Channels, and coupling proteins.

Control cell line without target.

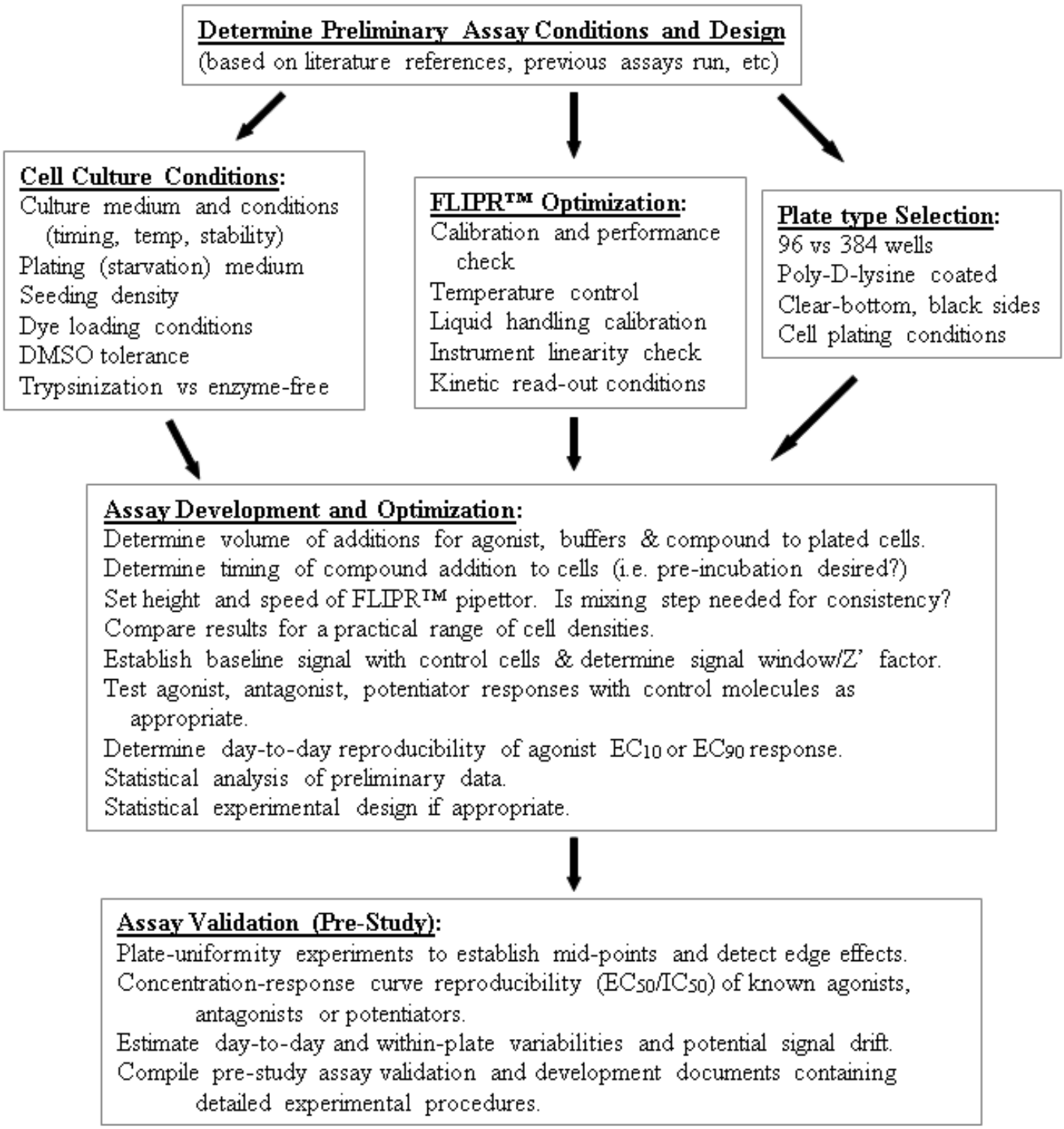
Suitable fluorescent dye (e.g. Fluo-3AMA, Calcein 4, etc).

Suitable agonist or ion channel modulators.

Standard antagonists, potentiators, and control compounds.

Appropriate buffer solutions, additives, etc.

Author Affiliations: 1 University of California San Francisco, CA. 2 Eli Lilly & Company, IN. 3 University of Pittsburgh, PA. 4 National Center for Advancing Translational Sciences (NIH), MD.



Introduction

The introduction of FLIPR™ (Fluorescence Imaging Plate Reader) in the 1990's provided biologists with a fast and easy method of detecting G-protein coupled receptor (GPCR) activation through changes in intracellular calcium (Ca^{2+}) concentration. By coupling receptors to G_q proteins which stimulate intracellular calcium flux upon binding, a functional response can be measured using calcium-sensitive dyes and a fluorescence plate reader. The FLIPR™ instrument has a cooled CCD camera imaging system which collects the signal from each well of a microplate simultaneously. The FLIPR™ can read at sub-second intervals, which enables the kinetics of

the response to be captured, and has an integrated pipettor that may be programmed for successive liquid additions. Figure 1 provides a diagram of a FLIPR^{TM} instrument and typical kinetic tracings.

The integrated pipettor capabilities of the FLIPR™ provide an opportunity to detect agonists, antagonists, and allosteric modulators of GPCRs all in one assay. In the first addition, compounds of screening interest are added. The timing can be adjusted to allow for a pre-incubation period with the compounds, and agonist activity is detected by monitoring the calcium flux response in this step. In the second addition, a small amount of a known agonist that results in ~10% of maximal response is added to detect potentiator activity. The third addition consists of a maximal concentration of known agonist (~90% of the maximal response) to test for antagonism. This experimental design can encompass either two or three additions depending on the specific responses to be detected.

The FLIPR™ has also been utilized to screen ion channel targets using membrane permeable fluorescent dyes, such as the bis-oxanol dye DiBAC4 (3), to measure changes in membrane potential (Table 1). Compared to the rapid sub-second kinetics of channel opening observed by electrophysiology approaches, redistribution of the dye often takes minutes to produce a measurable response, and has prompted the development of more rapid dyes compatible with the FLIPR™.

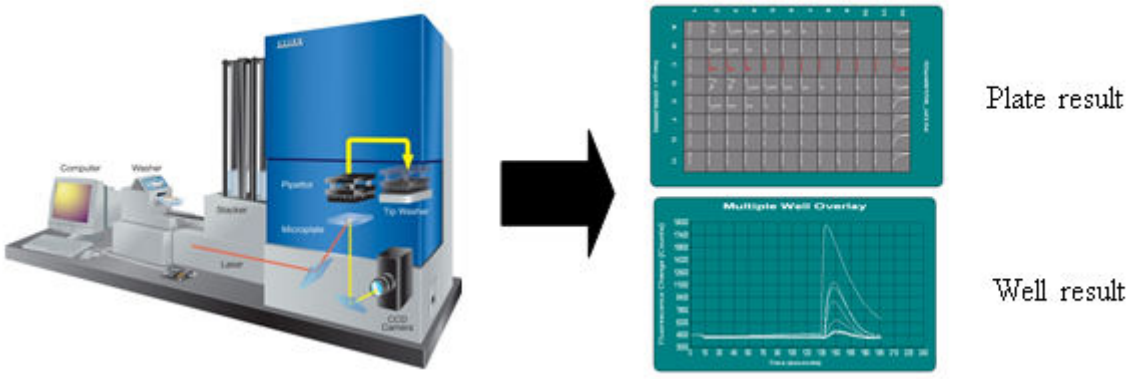


Figure 1. Diagram of a FLIPR™ instrument and typical kinetic tracings. The FLIPR™ collects a signal from each well of a multi-well plate at sub-second intervals, which captures and records a kinetic tracing of the calcium flux response. By successive additions to the same well, the FLIPR™ instrument allows one to distinguish between agonist, antagonist and allosteric modulators.

Table 1: Comparison of the Ca^{2+} Sensitive Dyes Fluo-3 and Fluo-4 used with the FLIPR® Fluorometric Imaging Plate Reader System.

Fluorescent Dye	Concentration	Loading time
Fluo-3	2 µM*	30- 60* mins
Fluo-4	1 µM	30-60 mins
Fluo-4	2 µM	30-60 mins

Suggested loading conditions (*=Standard condition). Adapted from Molecular Devices Applications.

Types of FLIPR™ Formats

GPCR Targets Coupled to Ca^{2+} Mobilization

GPCR targets that naturally couple via Gq produce a ligand-dependent increase in intracellular Ca^{2+} that can be measured using a calcium-sensitive dye. GI/o-coupled receptor activation can be "switched" to induce an increase in intracellular calcium in two ways: 1) by the use of chimeric G-proteins (Gαqi5 or Gαqo5), or 2) by engineering the cells to over-express a promiscuous G-protein (G α16 or Gα15) (Figure 2).

The integrated pipettor capabilities of the FLIPR™, as well as internal software modifications, provide an opportunity to detect agonists, antagonists, and allosteric modulators all in one assay. One-, two-, or three-addition assays may be performed depending on the desired assay format. A one-addition assay can be performed to detect agonists, where the compound of interest is added to look for a response. This mode could also be used to look for allosteric modulators or antagonists if the test compounds are added "off-line", although this is not the preferred method of operation. Until 2006, the two-addition assay was the standard assay format. In this method, the test compounds are added in the presence of an EC_{10} dose of the agonist in the first addition to detect agonists or allosteric modulators. The second addition is an EC_{90} dose of the max control to identify antagonists. While this scheme works, it requires a secondary assay to distinguish the agonists from the allosteric modulators; this need was abolished by the advent of a three-addition assay. In the three-addition mode, you can detect all three modes of activity in a single assay, saving considerable time and reagents. Another advantage found during testing of the three-addition assay was better mixing and a pre-incubation of the cells with compound resulting in better identification of potentiators.

Typical assay formats and the resulting curves are summarized below (Table 2).

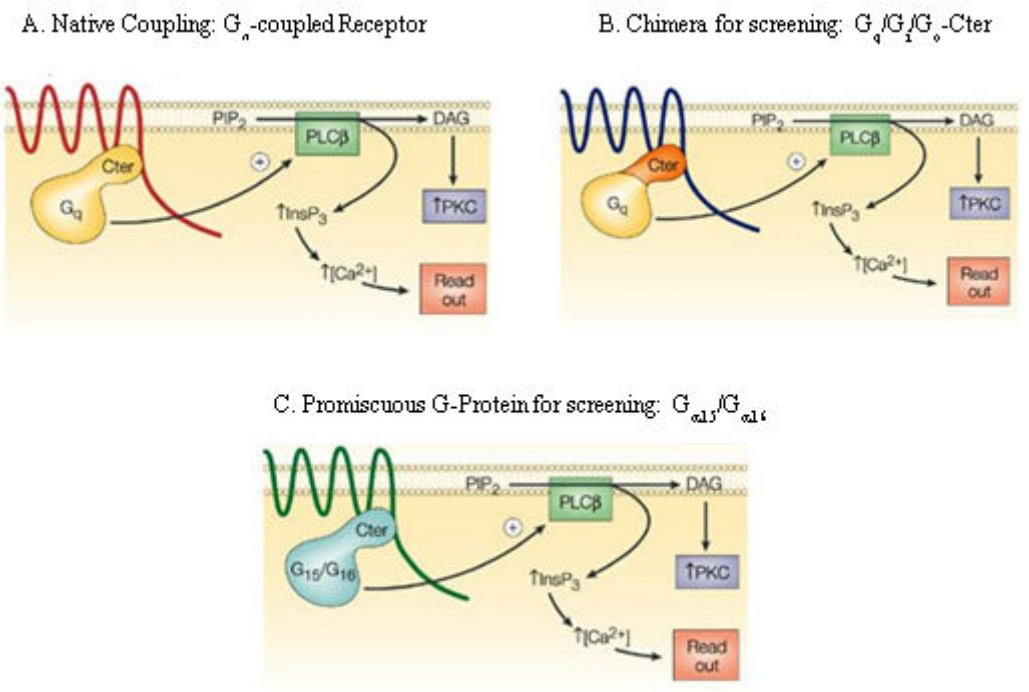


Figure 2. GPCR targets that couple via Gq naturally produce an increase in intracellular Ca^{2+} that can be measured using calcium-sensitive dyes and a FLIPR™ instrument. GPCR targets that naturally couple via GI/o can be adapted to respond to agonist with a ligand-dependent increase in intracellular calcium by the use of chimeric G-protein or by the introduction of an over-expressing promiscuous G-protein ($G_{\alpha 15}$ or $G_{\alpha 16}$). (Adapted from Nature Reviews Drug Discovery)

Ion Channels with Significant Ca^{2+} Permeability

Ion channel targets with significant Ca^{2+} permeability, such as the ionotropic glutamate receptor (iGluRs), produce an increase in intracellular calcium that can be measured using calcium-sensitive dyes and the FLIPR™ instrument. The methodology used is analogous to that for the GPCRs (Figure 3).

Ion Channels which Produce Significant Changes in Membrane Potential

Ion channel targets such as the iGluRs with ion permeability that significantly affects the membrane potential can be measured using a membrane potential dye and the FLIPR™ (Figure 4) (1).

Reagents and Buffers for Method Development

It is critical to ensure the appropriate cell lines expressing the target, control agonist and antagonist standards are available before beginning method development and validation. The minimal requirements are:

1. Transfected cell line with the G_q-coupled hGPCR target. (e.g. HEK293, CHO, THP-1 etc.). Receptors coupling through G_i, G_o, G_s or G_z can be coupled to G_q via promiscuous G−proteins as previously described.
2. Parental cell line control without the target and grown under identical conditions.
3. Agonist, antagonist, and allosteric modulator reference standards (with a wide range of potencies, if available).
4. Poly-D-lysine coated 96- or 384-well plates.
5. Appropriate cell growth media, buffer solutions, trypsinizing reagents.

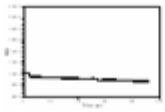
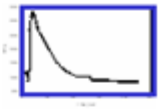
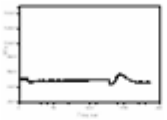
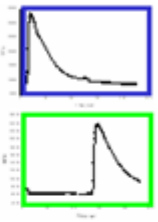
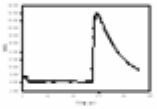
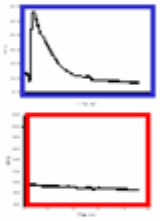
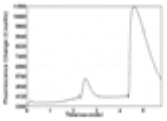
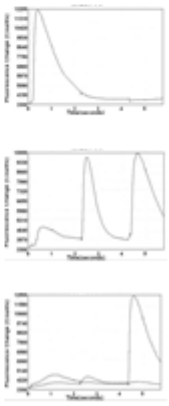
Agonist	Potentiator	Antagonist	First Addition	Second Addition	Third Addition	Inactive Cmpd Profile	"Hit" Profile
X			Compound	None	None		
X	X		Compound	10% Agonist	None		
X		X	Compound	90% Agonist	None		
X	X	X	Compound	10% Agonist	90% Agonist		

Table 2. Typical FLIPR™ Assay Formats

6. The reagents for ion channels are the same as for GPCRs, with the exception of the FLIPR™ buffer. It is recommended that 5mM calcium be used in the buffer for ion channel experiments. Since HBSS contains 1.3 mM calcium, 3.7 mM calcium chloride (Sigma) must be added prior to use.
7. Additional reagents needed for a FLIPR assay are listed in Table 3.

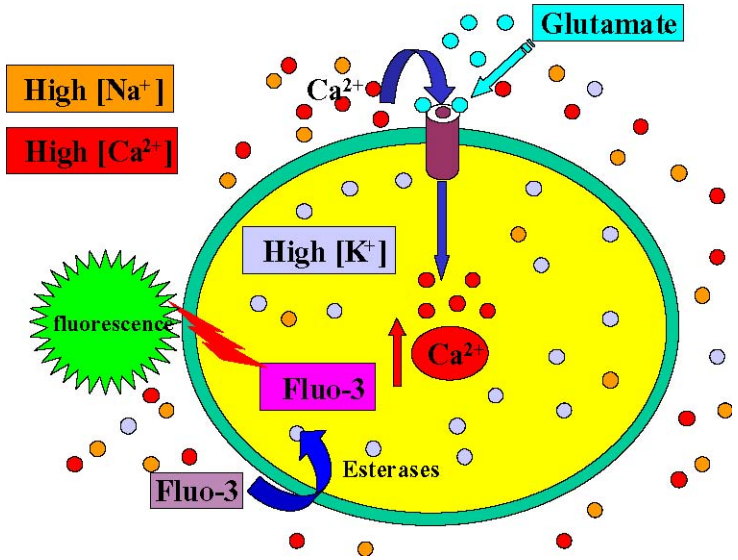


Figure 3. Schematic of the calcium flux response in ion channel targets. Fluo-3 dye ester is loaded into the cell and is cleaved by cell esterases to active dye. Ca^{2+} entering the cells bind to intra-cellular Fluo-3 and results in increased fluorescent emission at 520 nm.

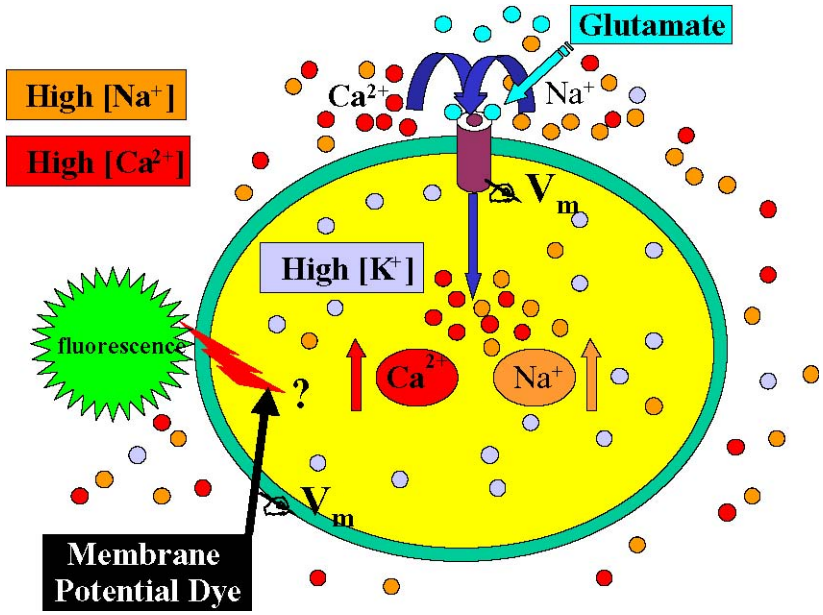


Figure 4. Measuring changes in membrane potential of ion channel targets.

Table 3: Additional reagents needed for FLIPR assay

Reagent	Manufacturer
Calcium dyes (Fluo-3, Fluo-4, Calcium 3, Calcium 4, etc)	Molecular Probes, Molecular Devices
HBSS	BioWhittaker, Invitrogen
HEPES	BioWhittaker, Invitrogen
Probenecid (if needed)	Sigma
Pluronic Acid	Sigma, Molecular Devices

Method Development and Optimization

Optimization Experiments for GPCR Targets Coupled to Ca^{2+} Mobilization

Early method development should include the following experiments to demonstrate the validity of the assay concept:

1. G_q coupling (or promiscuous G-protein coupling) of the cells expressing the GPCR should be demonstrated. Load selected cell clones with Fluo-3AM or other suitable dye, trigger Ca^{2+} flux with a known agonist, and measure fluorescence signal. Select the clones with the most robust response.
2. Determine whether cells need to be constantly maintained in culture or whether they can be prepared as frozen aliquots to be thawed and plated the day prior to the assay. The use of frozen cell stocks is a convenient and efficient alternative if it can be shown that the FLIPR™ signal is sufficiently robust and stable.
3. Conduct dye-loading experiments. Select the combination of cell line, agonist and dye concentrations that produces the most significant signal window. Use a control cell line without receptor expression to establish signal base line. Choose between use of cells in culture and frozen cell stocks.
4. Conduct preliminary experiments to establish a reasonable cell density that could be further optimized in subsequent experiments as described below.
5. Using a known antagonist or potentiator, demonstrate that the Ca^{2+} mobilization induced by the agonist can be blocked or enhanced, respectively.
6. Test poly-D-lysine coated plates with selected cell lines and conditions demonstrated in preliminary experiments. Select the plate with a stable and acceptable signal window.
7. Establish preliminary growth conditions and DMSO tolerance for the selected cell line.

Statistical experimental design can be employed to optimize these conditions and the following factors should be included:

1. Cell clones
2. Cell seeding density/well
3. Type of dye (wash vs. no-wash)
4. Dye loading concentration
5. Dye loading temperature
6. Dye loading duration
7. Coated plate type
8. Buffer additives: eg: probenecid, concanavalin A, etc.
9. Height, speed and mixing of FLIPR pipettor
10. Volume of addition

Notes on optimization experiments for GPCR targets coupled to Ca^{2+} mobilization

Some general points regarding a FLIPR™ assay for GPCRs need to be noted:

- Some receptors contain trypsin-sensitive sites in their extracellular domain that results in a loss of response if the cells are harvested by trypsinization. In these instances, cells should be harvested by either scraping or using enzyme-free dissociation buffer.
- Care should be taken when removing media and dye from the cell plate. It is common for mechanical aspiration to disrupt the cell monolayer, resulting in a deterioration of the assay performance. It is recommended to manually invert the plate and shake or “flick” the liquid out of the plate and blot onto paper towels if you are using a dye that requires washing.

Several no-wash dyes are commercially available. Testing of multiple dyes is strongly recommended, as signals differ widely. Depending on the receptor studied, media may interfere with the no-wash dyes, so testing both with and without media may be required. An example of the difference between the signal obtained from the traditional Fluo-3 dye and the new Calcium 4 no-wash dye is shown in Figure 5.

- Probenecid should be included in the dye and the buffer following dye loading whenever using CHO cells (5 mM probenecid is sufficient). This prevents the release of dye from the cells back into the medium. AV12 and HEK293 cells do not require probenecid.
- CHO cells are dye-loaded at 37°C, whereas AV12 and HEK293 cells can be dye- loaded at 25°C.
- Poly-D lysine coated plates can improve results obtained from some cell lines due to improved adhesion.
- Variability in the signal obtained on the FLIPR™ can sometimes be improved by adjusting the tip height or dispense speed on the FLIPR™.
- The standard assay buffer used in FLIPR™ experiments is HBSS with 20 mM HEPES supplemented with 0.5 mM Ca^{2+}.
- The most common fluid addition volumes for a FLIPR assay are listed in Table 4.

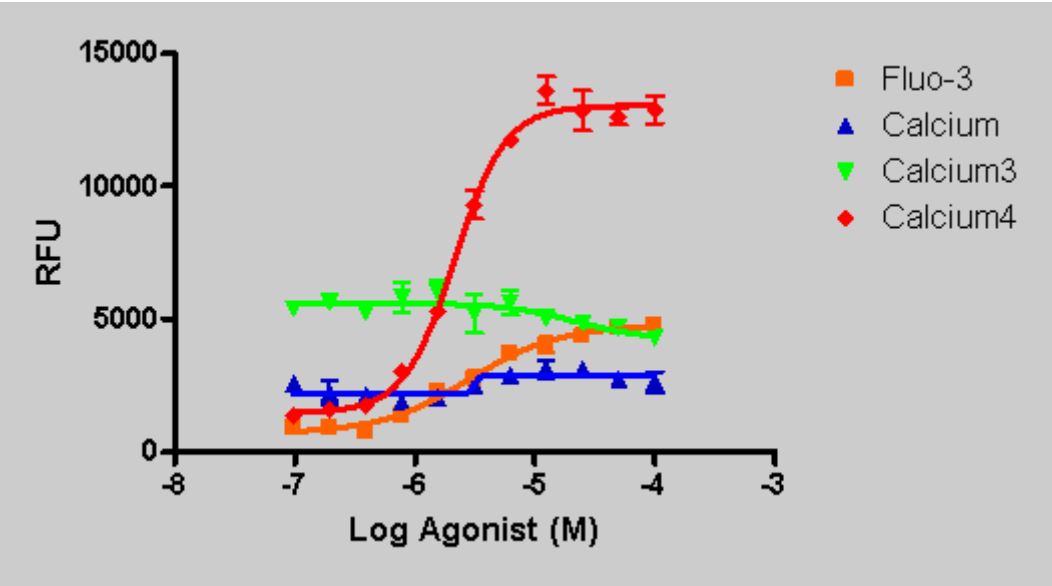


Figure 5: Comparison of different Ca^{2+} dyes on maximum response of a GPCR. In this example, a no-wash dye produced a significantly larger signal window than the traditional Fluo-3 dye. Signal windows are specific to receptors and cell lines, so it is recommended that testing be done during the initial optimization to ensure the appropriate choice of dye.

Table 4: Common fluid addition volumes for FLIPR assay

	Volume per Well	
	96 well Format	384 well Format
Dye	50 µl	20 µl
Buffer	50 µl	20 µl
1st Addition	50 µl	20 µl
2nd Addition	100 µl	20 µl

Development of a FLIPR Assay

The development of a FLIPR assay generally requires the five experiments, described in the sections below.

Experiment #1 - Cell density determination and incubation time

This is typically the first parameter that is examined. The best way to assess cell density requirements is to seed an entire assay plate at a single density; therefore, several plates are required to examine multiple cell seeding densities. The cells should be examined on the FLIPR™ using buffer in the first addition and a maximal concentration of agonist in the second addition. This will allow one to assess the extent of variability within the plate and detect any patterns in variability. The most common variability pattern we have observed is an edge effect which can usually be resolved by increasing the cell density or the humidity during incubation. We recommend examining the following cell densities for the indicated cell types listed in Table 5. Some assays will perform best with a 24-hour incubation time prior to running the assay, while others may need a 48-hour pre-incubation.

Table 5: Suggested densities for AV12, CHO, and HEK293 cell lines

	Seeding Densities (cells/well)	
Cell Line	96-well Format	384-well Format
AV12	30K, 40K, 50K, 60K	20K, 30K, 40K, 50K, 60K
CHO	10K, 20K, 30K, 40K	5K, 10K, 15K, 20K, 30K
HEK293	30K, 40K, 50K, 60K	20K, 30K, 40K, 50K, 60K

Experiment #2 - Dye loading time, dye concentration and temperature

The optimal dye loading can range from 30 minutes to 2 hours depending on the cell line and the dye used. The concentration of Fluo-3 used in the majority of FLIPR assays is 8 µM. Lower concentrations can be examined in order to reduce the cost of the assay. The no-wash dyes have been shown to be effective at lower concentrations as well. CHO cells are dye loaded at 37°C, whereas AV12 and HEK293 cells can be dye loaded at 25°C.

Experiment #3 - DMSO tolerance

DMSO can alter the response of the cells as well as shift the dose response curve for agonist. It is recommended to perform an agonist dose response curve in the presence of different concentrations of DMSO in order to assess the DMSO tolerance of the assay. Extreme care should be taken if a DMSO concentration >0.1% is required.

Experiment #4 - Agonist/antagonist dose response curves

The reproducibility of the assay can be examined by performing two independent days of agonist/antagonist/or potentiator dose-response curves. The EC_{50}/IC_{50} values should remain relatively constant over the course of the two experiments.

Experiment #5 - Full plate variability and Z′ factor determination

The variability of the assay is determined by running triplicate max/mid/min plates on three days and then calculating the Z'factor (see HTS Assay Validation).

Considerations when performing 384-well FLIPR™ assays

384-well FLIPR^{TM} assays have a number of challenges that are not apparent in the 96-well format. The first is mixing in the well. Most 96-well experiments are designed to allow a larger volume to be added to a larger space where mixing is not a concern. In a typical 96-well assay, 50 µl of test compound are added to 50 µl of buffer in the cell plate at a height of approximately 80 to 95 µl. The height is the liquid height in the well at which the tips dispense. The 384-well plate is limited to a maximum volume of a 30 µl addition in a much smaller diameter well, and using the 96-well technique will result in variable response. When adding to a 384-well plate, the tips are typically in the buffer solution of the cell plate when the dispense takes place. In a number of cases, the speed of dispense has to be increased as well. These heights and speeds should be tested with buffer to check for unwanted "pre-firing" of the cells. Another issue that arises with the 384-well format is the limited amount of diluent that can be added to the compound plate. This limitation can result in having to create intermediate dilution plates off-line, thereby slowing throughtput and adding costly consumables. This has been eliminated by using an in-tip dilution on the FLIPR™ (Figure 6). Although the final DMSO concentration is the same, the bolus of DMSO in the bottom of the tip can have an effect on the cells (Figures 7A and 7B). In our hands, a ratio of 15 µl buffer/5 µl compound was found to have the least DMSO effect. However since this result can be variable, different combinations should be tested during development. This in-tip dilution method can be used in both the two- and three-addition FLIPR™ methods.

Notes on tip washing: The FLIPR™-2 and FLIPR™-3 have tip wash stations that can be incorporated into the assay to eliminate the need to change tips. This allows one to use reservoirs without fear of cross contamination among the test compounds. In addition, a DMSO pre-wash can be performed at the tip load station with the proper adapter. When running a single-point screen of more than 100K compounds, tip washing should be tested first to minimize cost and maximize throughput. Occasionally, the compound used for the EC_{90} addition cannot be washed off the tips, resulting in significant carry-over of active compounds in to the subsequent plate (example in Figure 8A and 8B); in these cases, the tips will have to be changed. This typically happens when peptides are added as the EC_{90} dose.

Optimization Experiments for Ion Channel Targets with Ca^{2+} Permeability

Some ion channels (e.g. ionotropic glutamate receptors) differ from GPCRs in that they desensitize very quickly to agonist exposure, and in most cases, it is not possible to see a response in FLIPR™ with agonist alone. Such targets require the use of agents that decrease the rate of desensitization, which are called channel modulators or "clamps". The choice of which channel modulator to use is dependent upon the receptor. Table 6 provides a brief summary of modulators that we have used.

Since ion channel modulators are needed to decrease the rate of desensitization of the channel to agonist, the assay design is somewhat different than for GPCRs. Like for GPCRs, the ability of the FLIPR™ to make two fluid additions to the cells enables the detection of agonists, antagonists, and allosteric modulators in one assay. Representative kinetic profiles for iGluR1 flip and flop are shown in Figure 9A. Test compounds are added in the first addition along with a 90% dose of the known agonist, in this case glutamate, which normally does not generate a measurable Ca^{2+} response because the rate at which the receptor desensitizes is too fast to be detected on the FLIPR™. A response in the first read will indicate that the test compound is either a non-desensitizing agonist or a positive allosteric modulator (Figure 9B). The second addition consists of an optimal concentration (~90%) of a known allosteric modulator which results in maximal response by clamping the channel open and decreasing receptor desensitization. A reduced response in the second read will indicate that the compound is an antagonist (Figure 9C). The question of whether the compound is a non-desensitizing agonist or an allosteric modulator will be answered in the secondary assay in which the compound is added in the absence of any glutamate in the first read. If the compound alone elicits a response, it is a non-desensitizing agonist. Alternatively, if the compound only gives a response in the presence of glutamate (read 2), then it is a potentiator.

In the case of the kainate receptor iGluR6, the allosteric modulator ConA needs to be incubated on the cells for a minimum of 5 minutes prior to adding agonist. ConA takes longer to bind and has an effect on receptor desensitization.

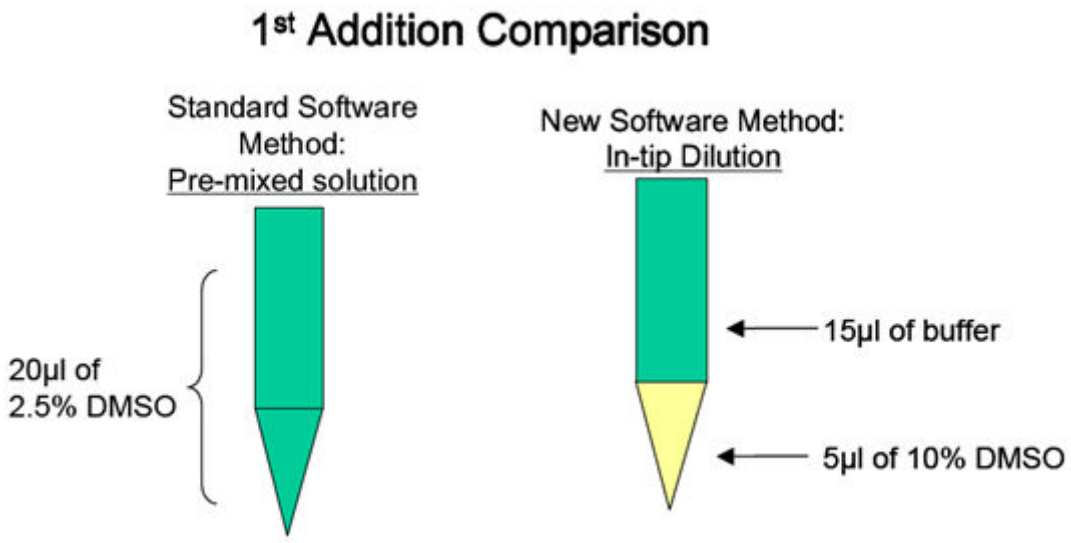


Figure 6. Schematic of in-tip dilution method.

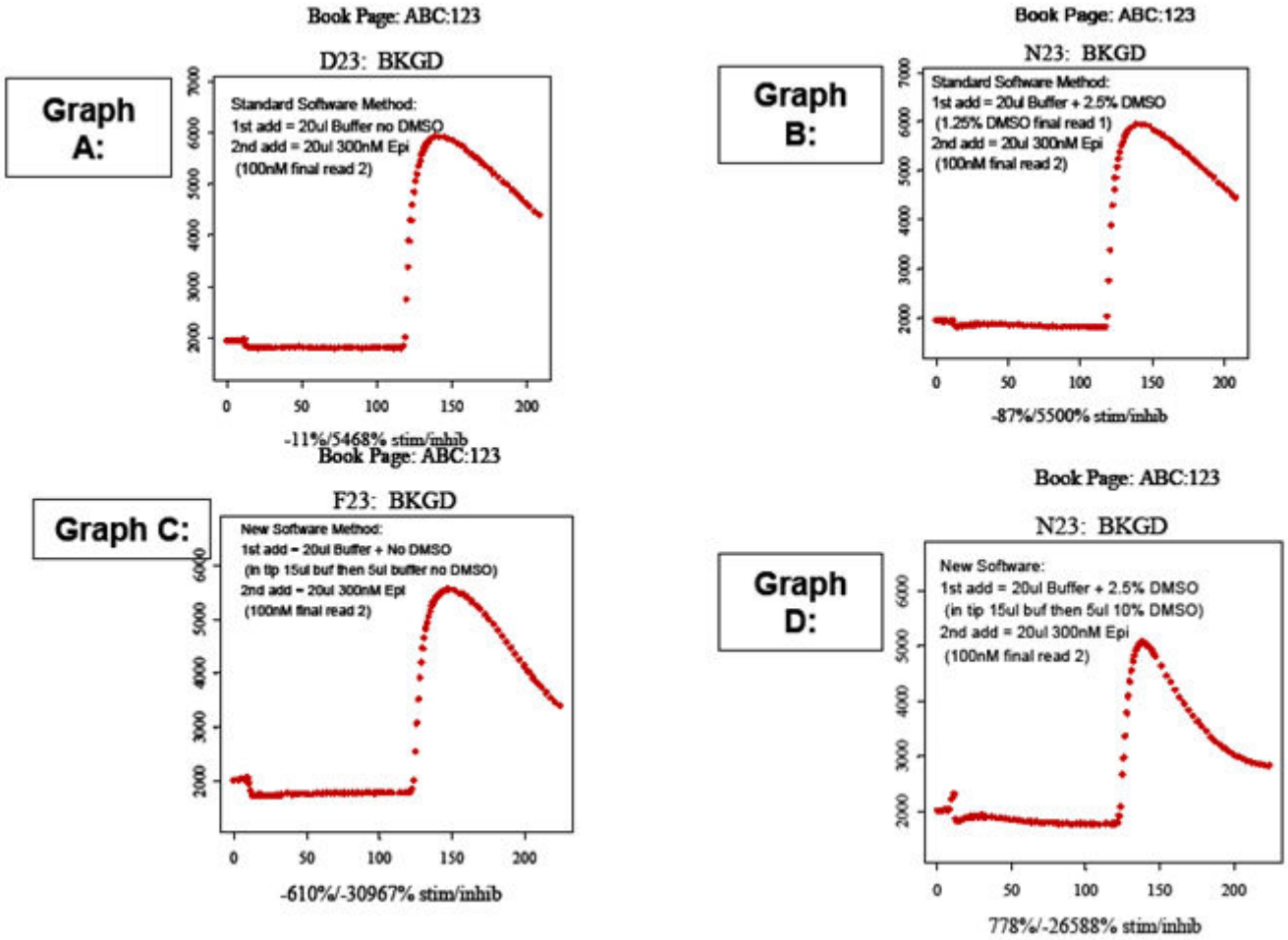


Figure 7A. Effects of bolus of DMSO on shapes of kinetic tracings.

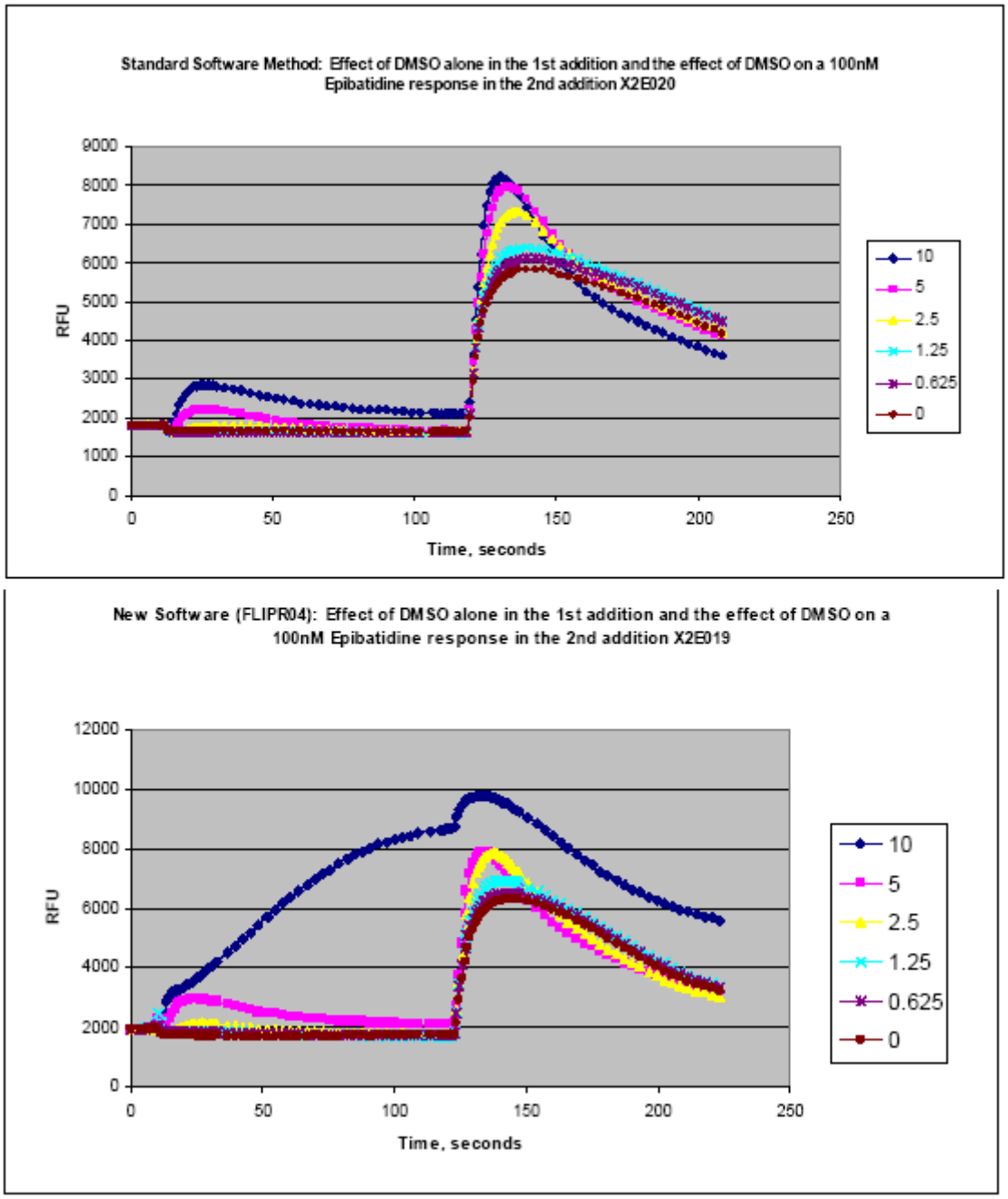


Figure 7B. Effects of bolus of DMSO on shapes of kinetic tracings. Note that between 5 and 10% DMSO the response changes, possibly due to loss in membrane integrity

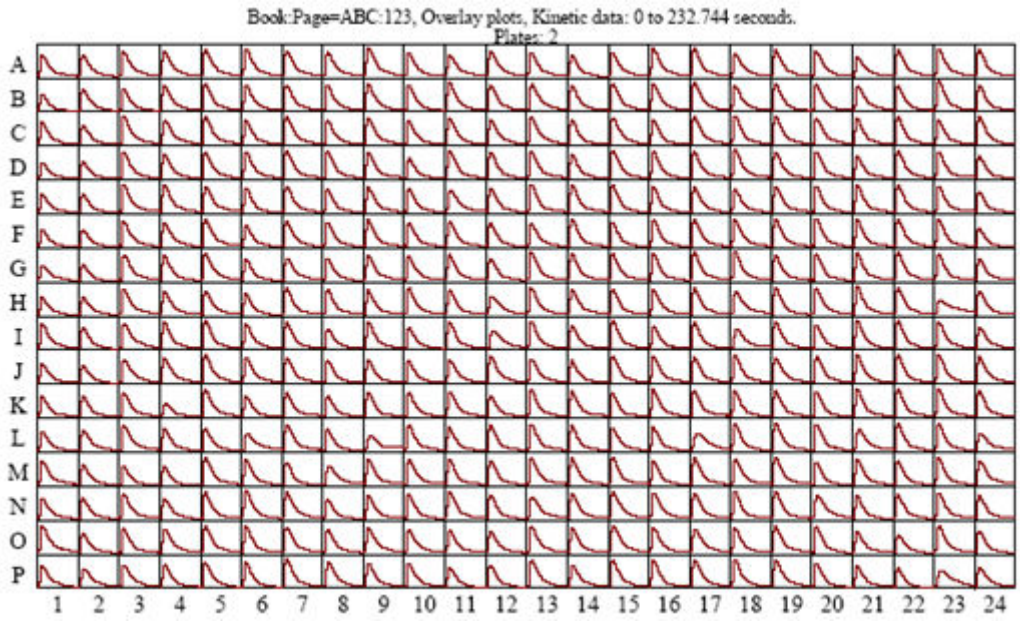


Figure 8A. Example of max addition with tip wash in agonist/potentiator assay.

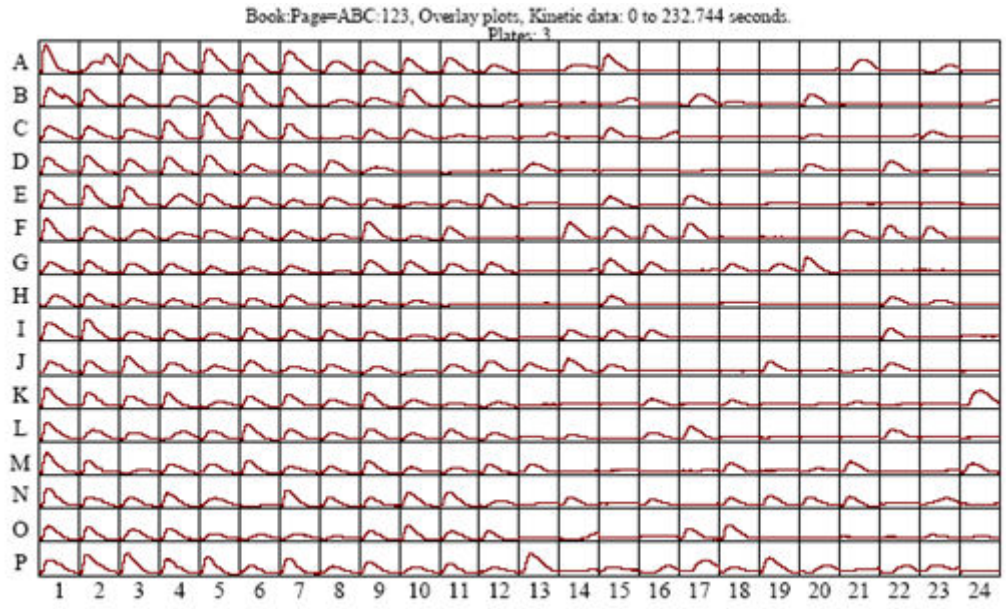


Figure 8B. Carry-over from tips in (a) in subsequent plate (buffer addition only).

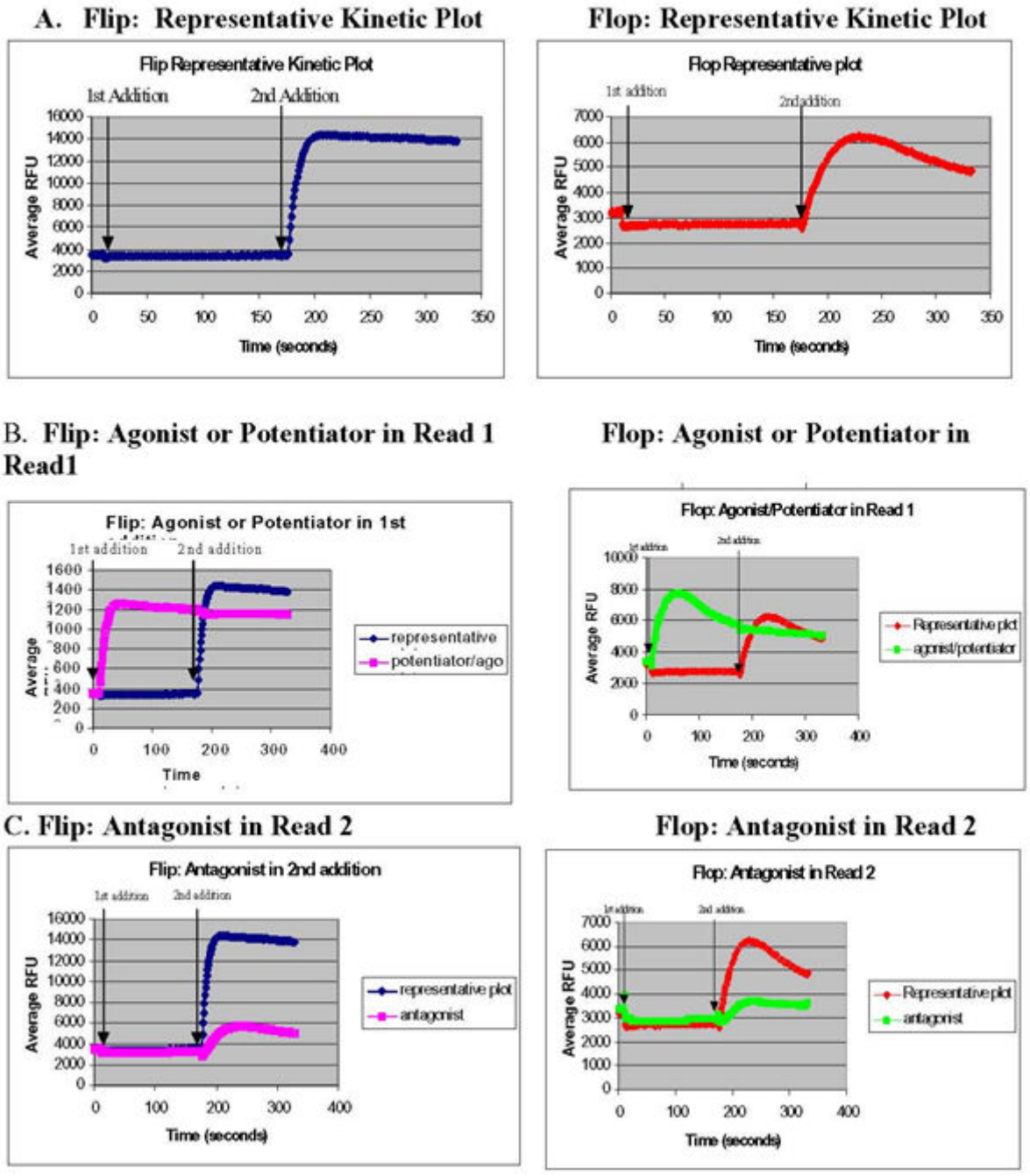


Figure 9. Expected kinetic profiles of iGluR1 Flip and Flop receptors.
(A) Expected kinetic profile of 0.5 mM glutamate (agonist) in the 1st addition followed by 20 µM LY (allosteric modulator) in the 2nd addition. (B) Expected kinetic profile of an agonist or an allosteric modulator where 20 µM LY (control potentiator) and 0.5 mM glutamate are added in 1st addition. (C) Expected kinetic profile of an antagonist where 10 µM NBQX (control inhibitor) and 0.5 mM are added in the 1st addition, followed by 20 µM LY in the second addition. In B and C, the test compounds will be added at the 1st addition with 0.5 mM glutamate, followed by 20 µM LY in the 2nd addition.

Table 6: Summary of modulators

Receptor	Channel modulator
iGluR1 flip	Cyclothiazide (CTZ)
iGluR1 flop	LY compound

Table 6 continued from previous page.

Receptor	Channel modulator
iGluR4 flip	Cyclothiazide (CTZ)
iGluR4 flop	LY compound
iGluR5 & 6	Concanavalin A (Con A)

Optimization Experiments for Ion Channel Targets with Ion Permeability that Significantly Impacts Cell Membrane Potential

Changes in membrane potential associated with ion channel activity may be measured on the FLIPR™ instrument using a voltage-sensitive dye available from Molecular Devices. The following are some of the parameters that need to be considered in developing a FLIPR™-based membrane potential assay:

***Cell Density*:**
Optimal cell conditions for the FLIPR membrane potential assay require the creation of a confluent cell monolayer. The cell seeding density depends on the cell type and the time in culture following the plating of the cells. Receptor expression levels can change with the cell passage number or as a result of the drug-selection conditions used for cell maintenance. Thus, it is critical to monitor changes in functional activity over time. Refer to the previous in this chapter for optimizing the cell seeding density.

Assay Buffer:
HBSS + 20 mM HEPES + added $CaCl_2$ (5 mM final concentration).

Preparation of Membrane potential dye:
We recommend dissolving the dye in assay buffer. After formulation, the loading buffer can be stored frozen in aliquots for several months without loss of activity.

Method of Dye Loading Cells:
Dilute the loading buffer 1:1 with assay buffer. Aspirate the media from the cells and add 100 µl of diluted buffer per well for 96-well plates. (Note: We have not had success following the Molecular Devices recommendation of adding the dye directly to the media with the iGluR targets.) The dye:buffer ratio can be optimized to reduce cost of the assay. Dye-loading the cells should be tested at 37°C and at ambient temperature. The optimal dye loading time, on average, for HEK293 cells is 60 minutes, but the range can be wide (5-60 minutes).

Antagonist Assays – Results Export Range:
The kinetic profile of the calcium response to ion channel activation is prolonged when compared to the typical profiles generated by GPCR activation. As a result, agonists introduced in the first addition, read frame I, will lead to a baseline shift which will not return to baseline prior to the second addition, read frame II (see Figure 9B). This baseline shift within read frame II is due to the prolonged activation of receptor when agonists are introduced. Because the EC_{90} challenge dose for antagonist assays is added within the initial portion of read frame II, the read frame I baseline shift due to agonists will lead to antagonist assay interference if exporting data from read frame II only (Max-Min). For this reason, one should consider exporting both read frames I and II for ion channel antagonist assays, which includes the pre-compound addition portion of read frame I, to capture the pre-compound addition or actual assay baseline (Figure 9B, time 0-350 seconds). By utilizing the pre-compound addition baseline of read frame I, false positive agonist interference in antagonist ion channel targets can be avoided.

Clamp:
Clamping agents such as Concanavalin A may be required to prevent rapid desensitization of ion channels.

Depending on the incubation time required for the clamp, it could either be added with the loading buffer or it could be added with the compound.

FLIPR setting:
Choose filter #2 in the experiment setup of the FLIPR™ software to measure membrane potential. Set the background reading ~ 20000 RFU. Table 7 lists some of the recommended setup parameters for the compound (1st addition) and agonist (2nd addition) additions to a 96-well plate.

Control:

We recommend running a KCl dose curve as a positive control to measure changes in membrane potential independent of the ion channel activity. The following is an example of time course tracings observed with the iGluR6 assay (Figure 10).

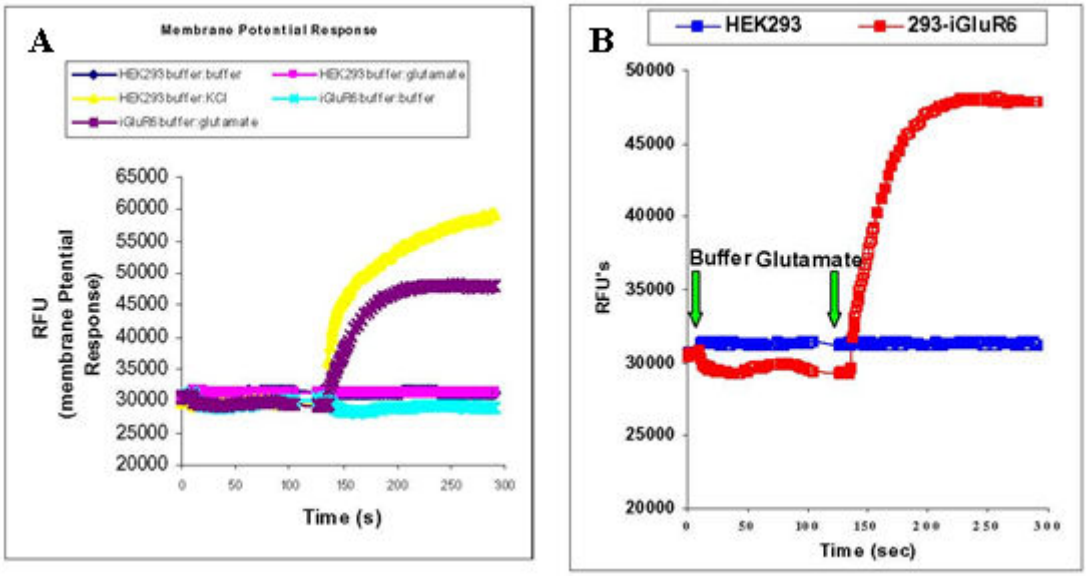


Figure 10. A) The HEK293 response to KCl vs the 293-iGluR6 response to glutamate. (B) HEK293 and 293-iGluR responses to glutamate.

Table 7: Recommended setup parameters for compound and agonist additions to a 96-well plate.

	Volume	Addition Speed	Pipettor Height
1st Addition	50 µl	50 µl/sec	100 µl
2nd Addition	50 µl	50 µl/sec	150 µl

Performing FLIPR™ using a non-adherent cell line:

So far, we have been describing methods appropriate for adherent cells cultures. In these cases, dye can be loaded directly onto cells grown to confluency in microtiter plates. In contrast, when the transfected cell line is weakly adherent or grows in suspension culture the following procedures should be followed:

1. Remove growth media from cell culture flask.
2. Add 10 ml PBS to each flask to rinse.
3. Remove PBS and repeat rinse step.
4. Add 10 ml cell dissociation buffer to each flask.
5. Rock flask gently.
6. Add 10 ml Alpha-MEM and discard the rinse.
7. Transfer cells to 50 ml centrifuge tube.
8. Add 30 ml buffer.
9. Pellet cells for 5 min at 2000 rpm.
10. Remove supernatant.
11. Add 30 ml buffer with 30 µl Fluo-3 AM (1:1000 dilution) and 30 µl pluronic acid.
12. Cover tube with foil and shake gently.
13. Place on shaker for 60 min at 180 rpm at room temperature
14. Fill up tube with buffer and spin for 5 min at 2000 rpm and remove supernatant.
15. Repeat step #14.
16. Resuspend cells at 1 x106 cells/ml.
17. Plate 50 µl/well of Poly-D-Lysine pre-coated plates.
18. Wait 20 min and centrifuge plates for 3 min at 1500 rpm.

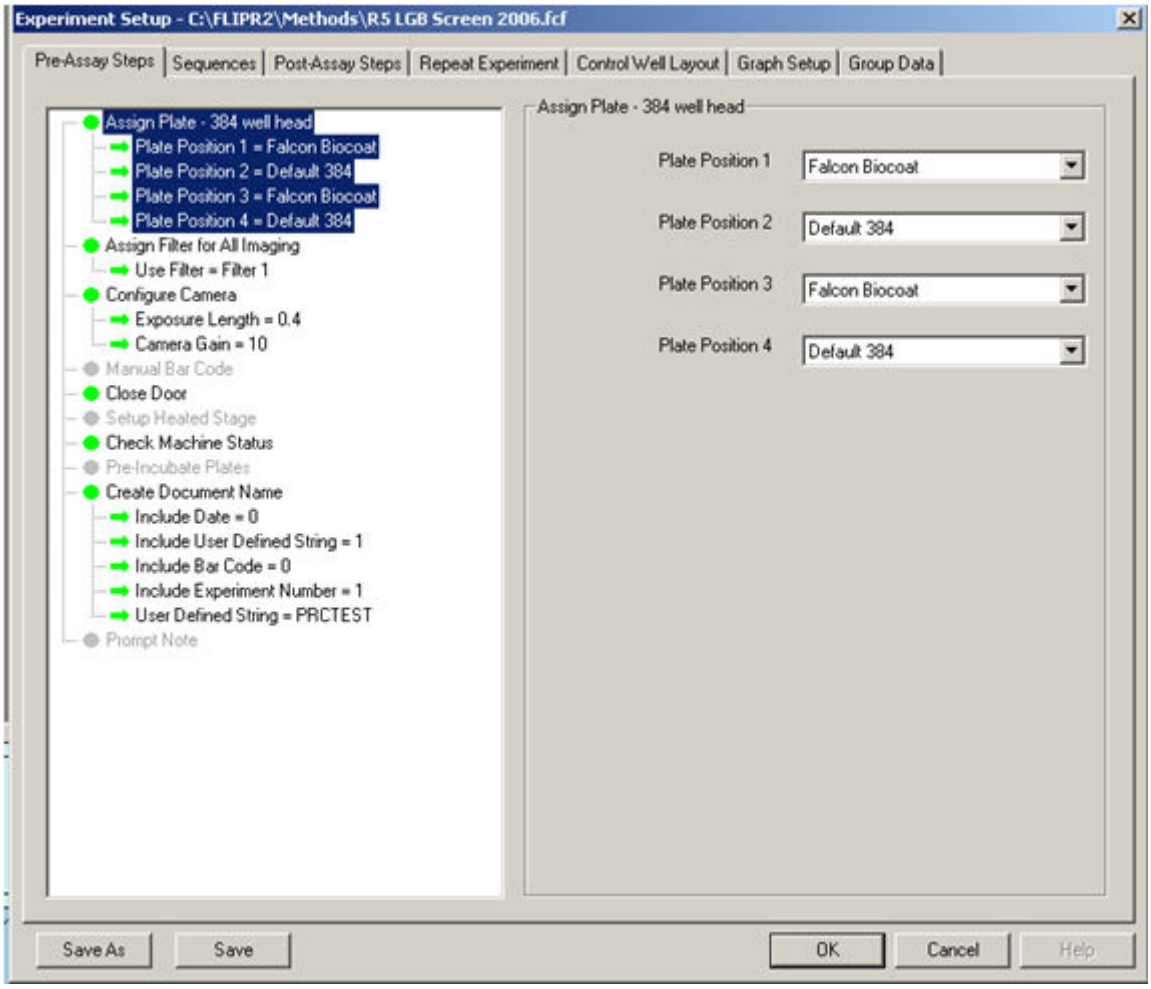
19. Place plates in FLIPR until ready for use.

Notes:

- If cells are weakly adherent, start at step #1.
- If cells are in suspension, start at step #7.
- If using a no-wash dye, skip steps #14-15.

FLIPR Instrument Setup

Pre-Assay Setup for FLIPR™-2 and -3:



In this screen, which is the same for 96- or 384-well assay set-up, the user defines the labware used in the experiment from a drop-down list. The other options on this screen are the filter selection, camera configuration, and the output file setup.

1. Assign plate: This is where the user configures the deck layout. If the plate you are using is not included, there is a default 96-well and default 384-well that can be used until the correct plate is defined.
2. Camera configuration: The exposure length is typically set to 0.4 seconds. The gain is only applicable to the FLIPR™-3 with the Andor camera.

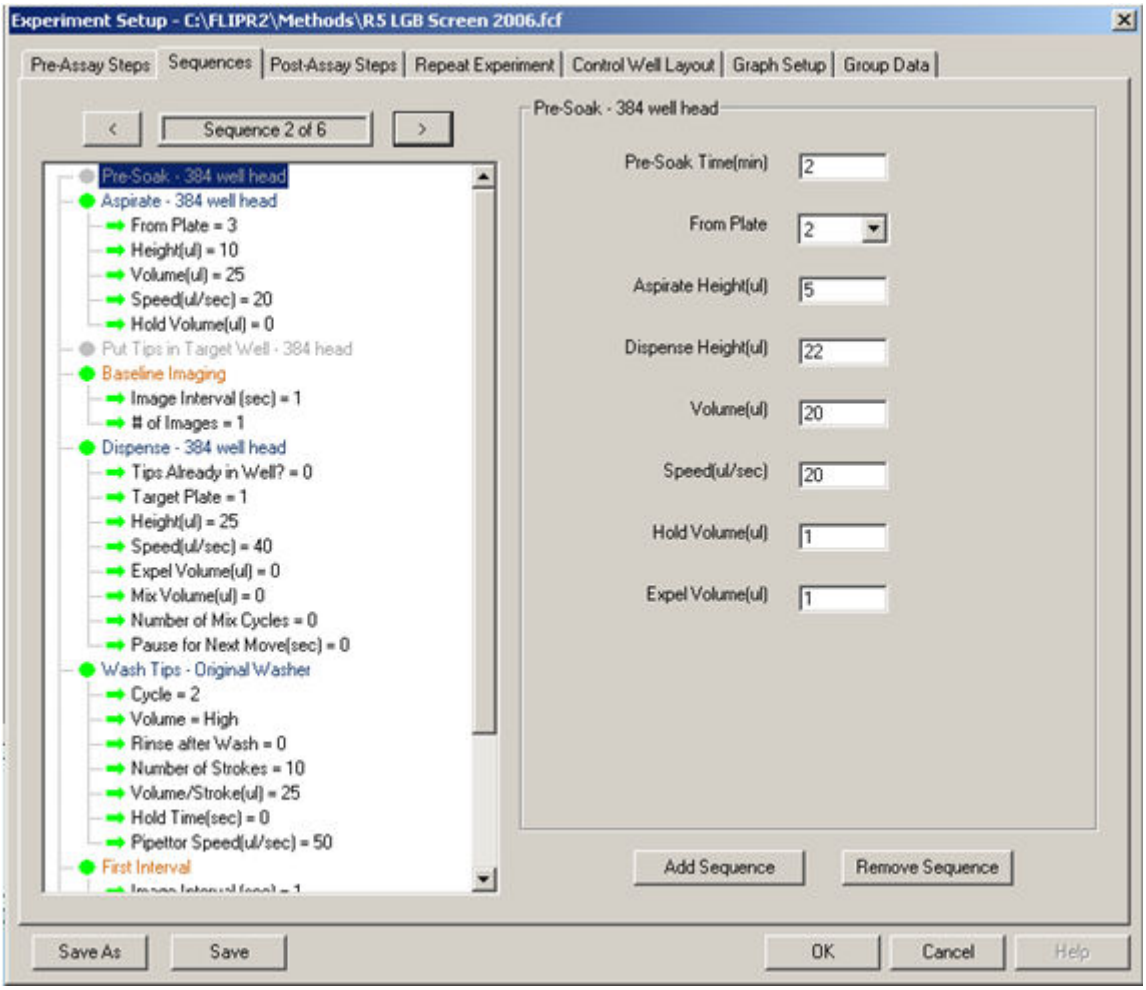
Note: To adjust the baseline signal of the plate, first adjust the laser intensity from the keypad before adjusting the exposure time. This should be done for each plate to set the same baseline over a run.

3. Filter selection: The FLIPR™ has a two-position filter slide. Typically, filter #1 is a 488-nm filter used for calcium assays, and filter #2 is either blank or a 535-nm filter for membrane potential assays.

4. Create document name: This is where the filename is created. A "1" in the field means this will be included in the file name and a "0" means it will not. A few issues deserve a warning here: If you use the date only, it is very possible that the data generated will be overwritten if another run is made on the same date. Therefore, it is a good practice to include a user-defined string in your file name. ALWAYS include the experiment number in the output. This is the flag that assigns the _n1,_n2, etc to the plates in the run. Failure to include this will result in every plate being labeled _n1, thereby overwriting all previously generated data. The best practice here is to use a lab notebook number and page as the filename. An example would be: D00567_143, where D00567 is the notebook number and 143 is the page.

Sequences Setup:

The sequence setup is where the entire experiment is defined. This includes defining the number of reads to be taken as well as all liquid handling steps, wash sequences, automated tip unload, etc. These settings should be done with the assistance of an automation engineer or an experienced FLIPR™ user.

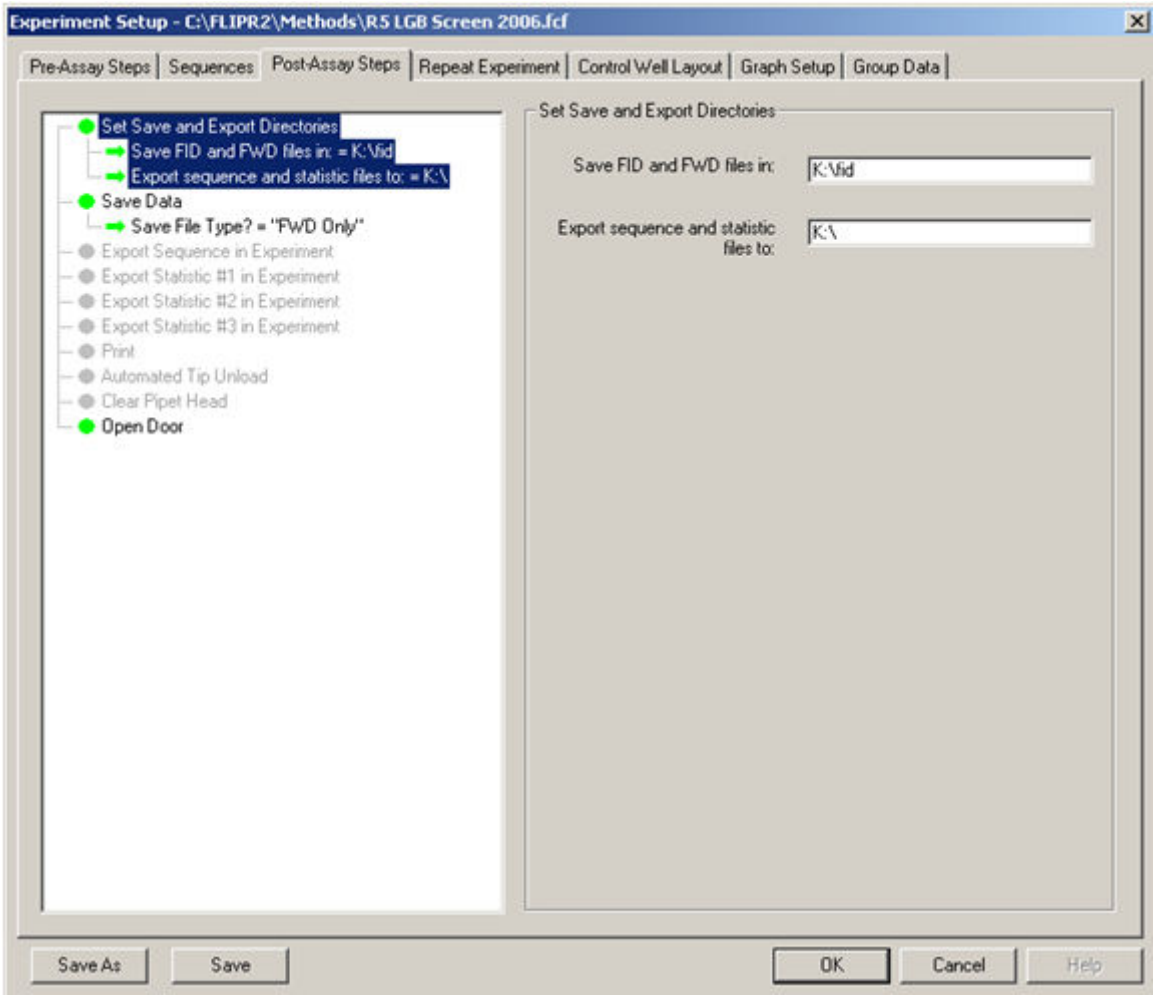


By double clicking on the circle beside each step, the user can activate/deactivate that part of the sequence. A green circle indicates the step is active while grey indicates inactive. By single clicking on the sequence step, the step's setup box appears on the right side of the window with all parameters that can be accessed by the user.

1. Pre-Soak: This is typically not used.

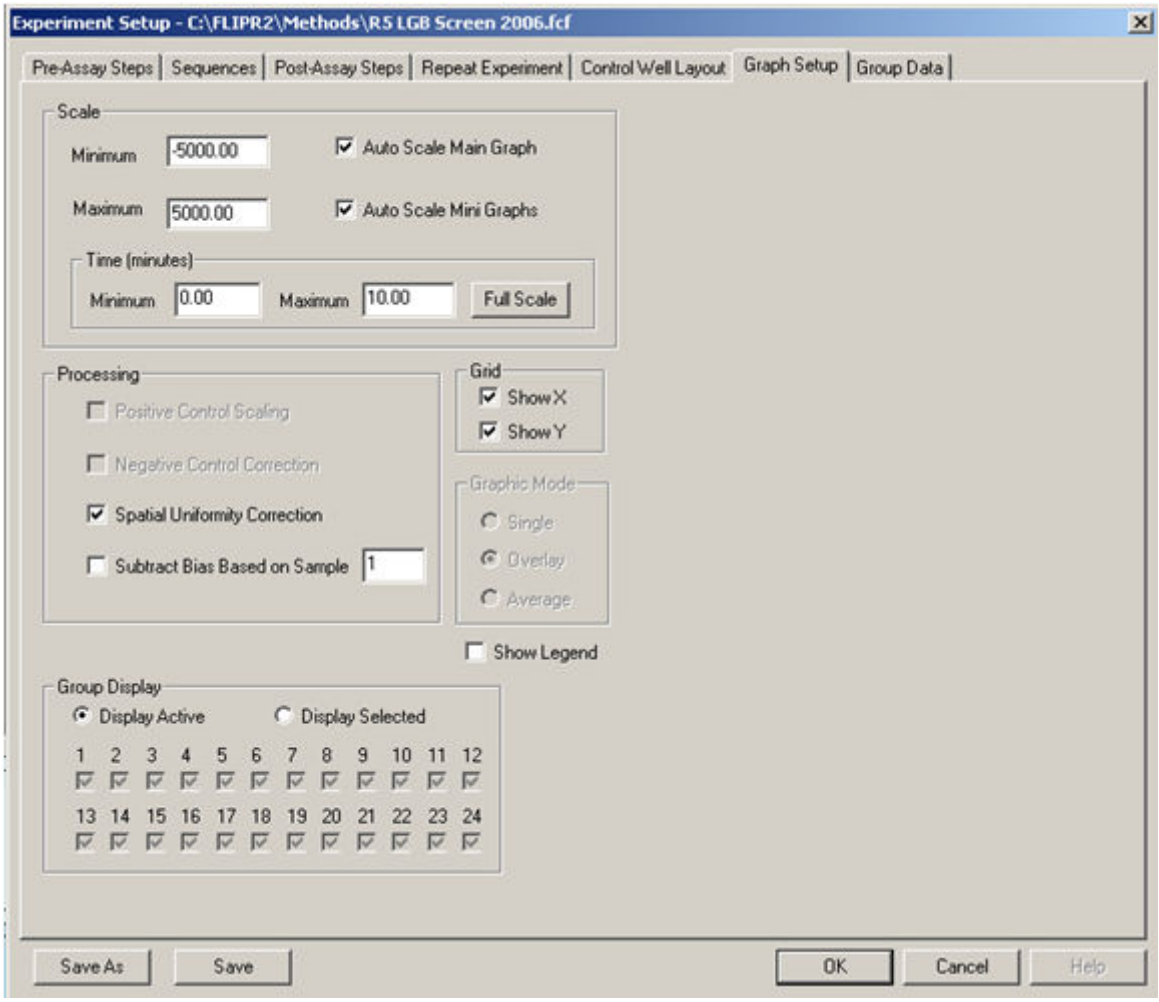
2. Aspirate: The FLIPR™ can aspirate from any of the four deck positions as long as a plate has been defined there in the initial setup page.
3. Put tips in target well: This will move the tips into the target plate before dispensing. Typically not used. NEVER use this if dispensing at a low height where the tips are in contact with the buffer. We have observed that this can cause a response from the compound on the outside of the tips.
4. Baseline imaging: The pipettor head will not move to the cell plate until the baseline imaging is complete. A typical setting is 1 to 5 secs.
5. Dispense: The FLIPR can dispense to any of the four deck positions as long as a plate has been defined there in the initial setup page.
6. Wash tips: This will wash tips in the wash station at position 6 if the unit has a wash station installed. A pre-wash can be performed at position 5 by clicking the "rinse after wash" button. This will use the same wash parameters defined, only perform them at position 5.
7. First Interval: This sets the number of images to be acquired and the interval between each image. Typically, the interval is short (1 sec) and the number of images are 30 to 60 to capture the compound addition. This should be set long enough to capture past the peak response.
8. Second Interval: This set the number of images to be acquired and the interval between each image. Typically, the interval time is longer (3-5 secs) and the number of images is sufficient to capture when the response decreases to background. In some cases, the signal will never return to background and it is the judgment of the scientist to set this range.
9. Automated Tip Unload: This will automatically unload the tips to the rack when all pipetting steps are completed. This should only be done in the last sequence.
10. Clear Pipette Head: This return the pipettor head to the home position.

Post Assay Setup:



In the post-assay setup section, the user selects where data will be saved, what type of data to save, and considers the option to automatically export and print data at the end of each plate. When setting the save location, you must type in the exact path to the save directory. The software will generate an error if the location is invalid or if it is a network location that is not available. In most instances, only FWD files should be saved. This saves storage space, as the FID files are larger image files. In some instances, such as when a heated stage is used, the open door may need to be turned off to maintain better temperature control in the FLIPR™.

Graph Setup:



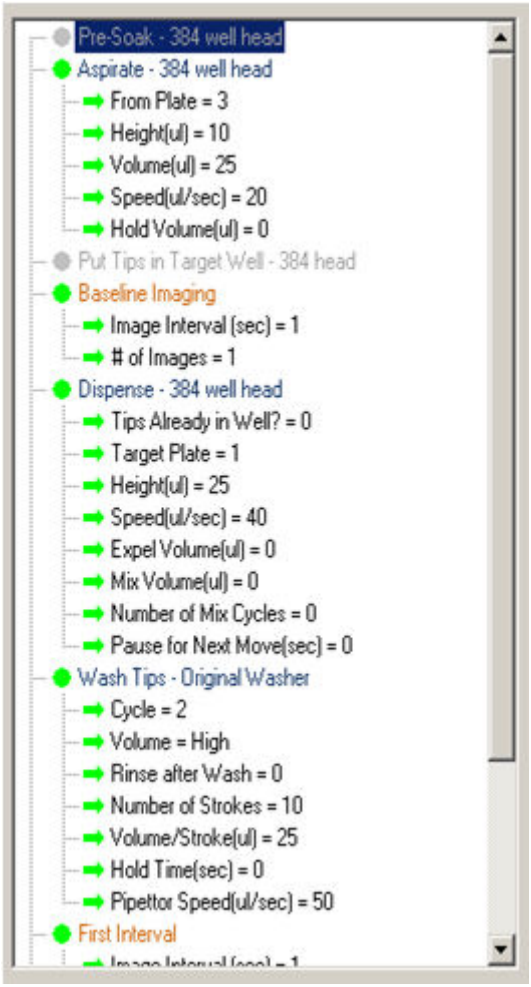
Typically, Spatial Uniformity Correction is used without subtracting the background. Spatial Uniformity Correction is basically a software normalization that sets all wells to the average RFU of the plate when starting the experiment.

In most cases, subtract bias is not used. This will background subtract the data set which can mask the assay window. An example would be to start with a baseline of 5000 RFU and the max signal response being 6000 RFU. In most situations, this is not a screenable window, but if the 5000 RFU background is subtracted, the window "looks" good (0 to 1000).

One-, Two- and Three-Addition Assay Examples:

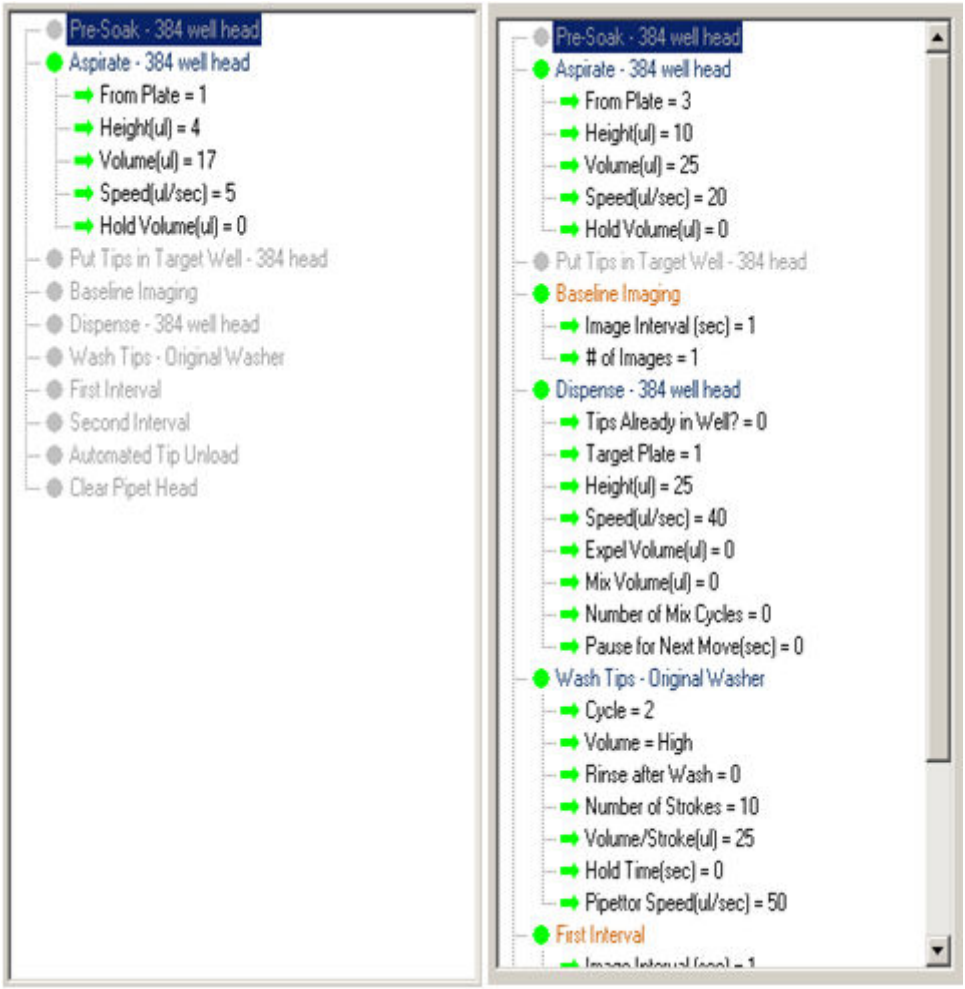
All three of these formats will require the same initial setup described above.

One-addition assays will need one or two sequences dependent upon the use of an in-tip dilution. The example below shows a 384-well aspiration from position 3 with a dispense into the cell plate at position 1 (Read Position), followed by a wash.

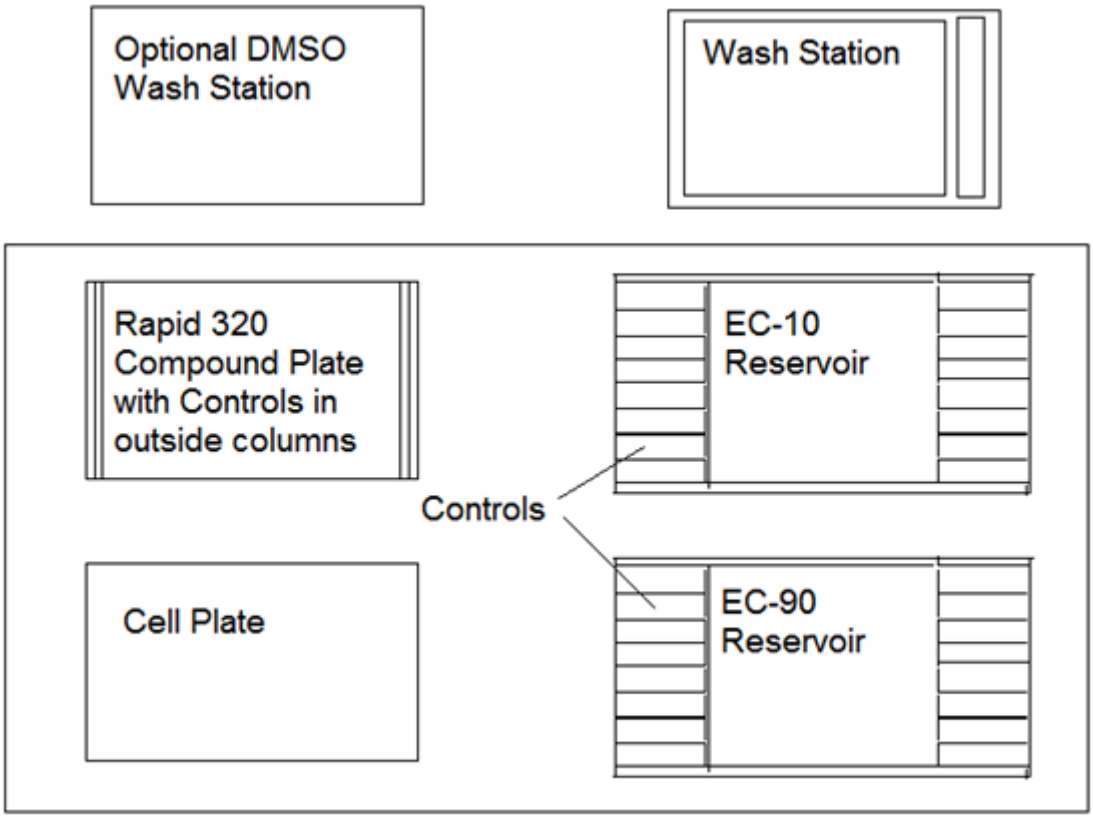


A one-addition assay with an in-tip dilution is shown below. The first step aspirates 17 µl from plate 1 and then 8 µl from plate 3.

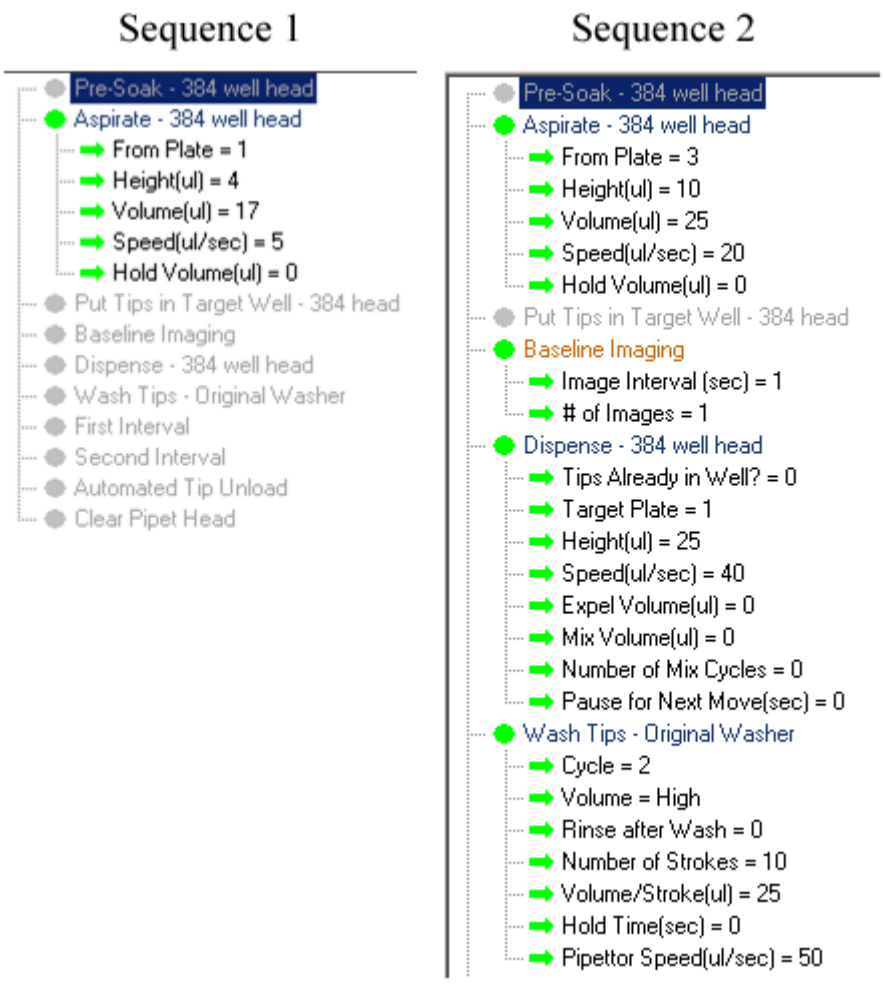
Note: When performing an in-tip dilution, the volume in the second step is the final total volume aspirated (17 µl + 8 µl). This is a result of the way the FLIPR™ software keeps track of the pipettor head.



A two-addition or three-addition assay can be run by simply adding sequences. It is recommended that if the assay is targeting potentiators, the in-tip dilution and pre-incubation time be used to maximize the sensitivity of the assay. Below is the complete liquid handling setup for a three-addition assay. Volumes and read times will vary.



Deck Layout for a three-addition assay


Sequence 1
Pre-Soak - 384 well head
Aspirate - 384 well head
From Plate = 1
Height(ul) = 4
Volume(ul) = 17
Speed(ul/sec) = 5
Hold Volume(ul) = 0
Put Tips in Target Well - 384 head
Baseline Imaging
Dispense - 384 well head
Wash Tips - Original Washer
First Interval
Second Interval
Automated Tip Unload
Clear Pipet Head
Sequence 2
Pre-Soak - 384 well head
Aspirate - 384 well head
From Plate = 3
Height(ul) = 10
Volume(ul) = 25
Speed(ul/sec) = 20
Hold Volume(ul) = 0
Put Tips in Target Well - 384 head
Baseline Imaging
Image Interval (sec) = 1
of Images = 1
Dispense - 384 well head
Tips Already in Well? = 0
Target Plate = 1
Height(ul) = 25
Speed(ul/sec) = 40
Expel Volume(ul) = 0
Mix Volume(ul) = 0
Number of Mix Cycles = 0
Pause for Next Move(sec) = 0
Wash Tips - Original Washer
Cycle = 2
Volume = High
Rinse after Wash = 0
Number of Strokes = 10
Volume/Stroke(ul) = 25
Hold Time(sec) = 0
Pipettor Speed(ul/sec) = 50



Note that in sequence 3 and 5, the order of aspiration is reversed. This is due to the fact that unknown test compounds have been added to the cell plate and to aspirate from there first would be a source of contamination to the EC_{10} reservoir. This is not the case for the 4^{th} and 6^{th} sequence as the tips have been washed.



Potential Artifacts

Although the FLIPR™ has facilitated advances in cellular calcium mobilization screens, these assays remain difficult to configure, relatively slow, and fraught with potential artifacts. Blocked FLIPR™ tips will lead to false positives in an inhibitor screen, or false negatives in an agonist screen. Fluorescent compounds, Ca^{2+} ionophores, and compounds that permeabilize the cell membrane can all contribute to false positives in the agonist read (Figure 11). These types of nuisance or interference compounds can often be identified from the kinetic traces of the response, but this kind of in depth data review is time consuming and requires experience to correctly recognize strange response profiles. In addition, compounds with agonist activity may interfere with antagonist reads due to desensitization or internalization of the receptor, resulting in false positives.

The utility of the FLIPR™ and calcium dye approach for screening GPCR targets has been greatly enabled by the use of over-expression of promiscuous and chimeric G-proteins that provide a method to "switch" GI/o-coupled receptor activation to an increase in intracellular calcium. However, screens designed to detect receptor activity against a backdrop of stable, high-level promiscuous G-protein expression are also susceptible to artifacts - - false positives derived presumably from other cell surface receptors hi-jacking the promiscuous G-proteins. Indeed, even in the absence of a promiscuous G–protein, any endogenous GPCR that couples through G_q and induces a Ca^{2+} response may show up as an agonist or interfere with antagonist reads. It is well documented that GPCRs, particularly those in heterologous expression systems, can activate multiple signal transduction pathways, and indeed there is also evidence for cross-talk between recombinant and native receptors that may

also complicate the responses to compounds. Thus, we recommend routinely performing a secondary screen against the parent cell line that lacks the receptor of interest in order to definitively identify false positives.

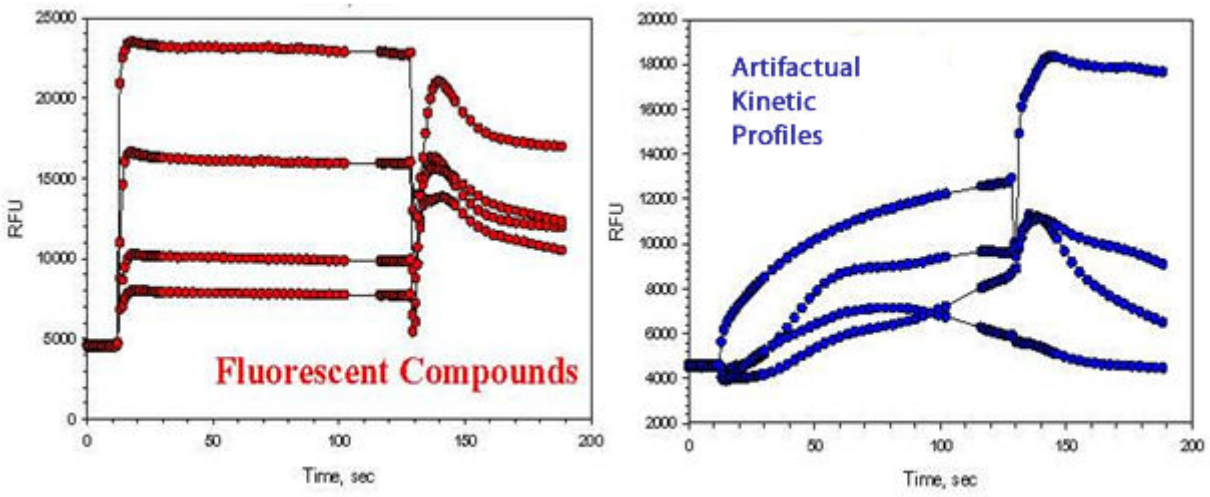


Figure 11. Typical kinetic traces that can result from FLIPR^{TM} artifacts.

References

Primary Reference

1. Baxter D. F., et al. A novel membrane potential-sensitive fluorescent dye improves cell-based assays for ion channels. J. Biomolecular Screening. 2002;7:79–85. PubMed PMID: 11897058.

Additional Reading

Benjamin E. R., et al. Pharmacological characterization of recombinant N-type calcium channel ($Ca_v2.2$) mediated calcium mobilization using FLIPR. Biochemical Pharmacology. 2006;72:770–782. PubMed PMID: 16844100.

Coward P., et al. Chimeric proteins allow a high-throughput signaling assay of GI-coupled receptors. Analytical Biochemistry. 1999;270:242–248. PubMed PMID: 10334841.

Hodder P., et al. Miniaturization of intracellular calcium functional assays to 1536-well plate format using a fluorometric imaging plate reader. J. Biomolecular Screening. 2004;9:417–426. PubMed PMID: 15296641.

Jensen A. Functional characterization of human glycine receptors in a fluorescence-based high throughput screening assay. European J. Pharmacology. 2005;521:39–42. PubMed PMID: 16182281.

Liu A.M.F., et al. G-$_{\alpha16/z}$ chimeras efficiently link a wide range of G protein-coupled receptors to calcium mobilization. J. Biomolecular Screening. 2003;8:39–49. PubMed PMID: 12854997.

Liu E.C-K., And Abell L. M. Development and validation of a platelet calcium flux assay using a fluorescent imaging plate reader. Analytical Biochemistry. 2006;357:216–224. PubMed PMID: 16889745.

Lubin M., et al. A nonadherent cell-based HTS assay for N-type calcium channel using Calcium 3 dye. Assay and Drug Development Technologies. 2006;4:689–694. PubMed PMID: 17199507.

Miret J., et al. Multiplexed G-protein-coupled receptor Ca^{2+} flux assays for high-throughput screening. J. Biomolecular Screening. 2005;10:780–787. PubMed PMID: 16234348.

New D.C., Wong Y. H. Characterization of CHO cells stably expressing a $G_{\alpha16/z}$ chimera for high throughput screening of GPCRs. Assay and Drug Development Technologies. 2004;2:269–280. PubMed PMID: 15285908.

Reynen P. H., et al. Characterization of human recombinant α2A-adrenoreceptors expressed in Chinese hamster lung cells using Ca^{2+} changes: evidence for cross-talk between recombinant α2A- and native α1A-adrenoreceptors. British J. Pharmacology. 2000;129:1339–1346.

Robas N.M., Fidock M.D. Identification of orphan G protein-coupled receptor ligands using FLIPR assays. Methods in Molecular Biology. 2005;306:17–26. PubMed PMID: 15867462.

Schroeder K. S., Neagle B. D. FLIPR: a new instrument for accurate, high throughput optical screening. J. Biomolecular Screening. 1996;1:75–80.

Wolff C. Comparative study of membrane potential-sensitive fluorescent probes and their use in ion channel screening assays. J. Biomolecular Screening. 2003;8:533–543. PubMed PMID: 14567780.

Zhang Y., et al. Evaluation of FLIPR Calcium 3 Assay Kit—a new no-wash fluorescence calcium indicator reagent. J. Biomolecular Screening. 2003;8:571–577. PubMed PMID: 14567785.

Ion Channel Screening

Owen B McManus, Ph.D.,[1,*] Maria L Garcia, Ph.D.,[2] David Weaver, Ph.D.,[3] Melanie Bryant, Ph.D.,[4] Steven Titus, Ph.D.,[5] and James B Herrington, Ph.D.[6]

Created: October 1, 2012.

Abstract

Ion channels regulate a wide range of physiological processes including rapid electrical signaling, fluid, hormone and transmitter secretion, and proliferation. As such, ion channels are common targets for toxins and therapeutics. Ion channel screening assays have traditionally utilized indirect or low throughput approaches. Recent improvements in sensor technologies and instrumentation have provided fresh opportunities for ion channel screening that afford higher throughput, improved information content, and access to novel ion channel targets. Ion channels subtypes can display a variety of functional differences in gating and permeability mechanisms, which necessitates use of assay technologies that selected and adapted for a specific channel type. In order to successfully implement improved ion channel screening assays that provide pharmacologically relevant data, it is critical to carefully evaluate and control a variety of assay parameters. In this chapter, we provide an overview and assessment of some of the assay technologies commonly used in ion channel pharmacology and drug discovery efforts.

1. Introduction

Ion channels act as molecular transistors. Powered by ion concentration gradients, ion channels transduce a variety of signals into transmembrane ion fluxes. Ion channels have traditionally been classified according to the mechanisms that control opening-closing transitions (gating) and the types of ions that can pass through a channel (selectivity). These functional characteristics, along with control of expression and localization, determine the effector activities of each channel type. Classification of ion channels based on functional characteristics has been, in large part, supported by sequence analysis of cloned channels and by available structural studies.

1.1. Gating and selectivity affect assay design

A variety of gating mechanisms are utilized in different channels to enable responses to a range of physiological stimuli including membrane potential, neurotransmitters, hormones, ions, metabolites, other proteins, temperature, lipids, pH, mechanical forces and other factors not yet identified. Multiple response capabilities may be combined such that, for instance, a single channel can gate in response to intracellular calcium and membrane potential. Some ion channels can respond rapidly to gating stimuli providing a basis for fast electrical signaling. When open, ion channels catalyze movement of (usually) charged ions across the hydrophobic barriers formed by membranes. Ion channels contain pore regions, which span the membrane, and provide a pathway for ions to traverse cell membranes following electrochemical gradients. The pore region structure provides a mechanism for distinguishing ions and thereby generating a selectivity profile for each channel type. A distinguishing characteristic of ion transport in a channel is a high flux rate, which can provide a net flux of

Author Affiliations: 1 Johns Hopkins University; Email: Owne_mcmanus@jhmi.edu. 2 Kanalis Consulting; Email: marialgarcia@gmail.com. 3 Vanderbilt University; Email: David.weaver@vanderbilt.edu. 4 University of Maryland; Email: Melbryant1@gmail.com. 5 GE Healthcare; Email: satitus@yahoo.com. 6 Genentech; Email: Herrington.james@gene.com.

Corresponding author.

* Editor

millions of ions per second. This high transport rate can be achieved, for some channels, while also stringently selecting for a single ion type among others physiologically present.

An understanding of ion channel function is needed to effectively design and implement ion channel-specific assays. The two key issues that need to be addressed when setting up an ion channel assay are, how to control channel gating and how to measure channel activity. The mechanisms controlling channel gating and ion permeation can be best determined using electrophysiological methods, which allow rapid control of membrane potential and bath solution composition and also permit direct measurement of ion flux. For this reason, conventional voltage clamp methods are often used in early stages of ion channel drug discovery and assay development to characterize factors that control channel gating and to determine ion selectivity. This information can then be used to design assays in higher density formats that afford higher throughput at the expense of reduced flexibility, control and resolution.

Controlling channel gating can be a key challenge in designing plate-based, high density ion channel assays which often use a mix-and-read format and do not permit washout steps. Gating of ligand-gated channels with slow kinetics can be reliably triggered in this format by agonist addition, but other channel classes can require more complex approaches to trigger channel activation. For instance, voltage-gated channels respond to changes in membrane potential, which cannot be directly controlled in non-electrophysiological assays. A variety of approaches have been used to trigger voltage-gated channel opening in plate-based biochemical assays including electrical field stimulation, addition of potassium or channel modulators to the bath solution (see below) or optical triggering of membrane potential changes via co-expression of light-activated channels. A further complicating feature of assays for voltage-gated channels is that membrane potential controls channel gating, which, in turn, affects membrane potential. This feedback relationship leads to difficulties in achieving reliable channel activation in high density formats, which can be overcome by applying careful control of channel expression levels and assay parameters.

Three common measures of ion channel activity are widely used in ion channel assays. Measurements of ionic currents using voltage clamp electrophysiological methods provide a direct and linear reflection of ion channel fluxes and are still the most reliable indicators of ion channel activities. Development of automated electrophysiology instruments using planar arrays now provides a means to produce medium throughput data on thousands of compounds per day. A variety of instruments and approaches have been developed with specific advantages in either throughput or flexibility or resolution. Ion fluxes through channels affect membrane potential, which provides a second approach for following ion channel activity. Membrane potential can be measured reliably using electrophysiological methods, but few automated electrophysiology instruments provide this capability. Biochemical assays for membrane potential (see below) combining bright dye systems with fluorescent plate readers with kinetic capabilities have provided high-throughput approaches to ion channel targets that were previously inaccessible. Some limitations of this approach result from the nonlinear relation between ion channel activity and membrane potential and from sensitivity of membrane potential to alteration by a wide range of processes that are not related to the channel of interest. A more widely applied approach relies on measuring changes in ion concentration on one side of a membrane (usually the intracellular compartment) resulting from ion channel activity (see below). The ion concentrations can be measured directly using atomic absorption spectroscopy or labeled isotopes, or more commonly by using sensor molecules to detect ion concentration changes. Recent developments in chemical and genetic sensors have enabled high-throughput, robust assays for a new array of ion channels that were not previously accessible. Non-physiological ions that permeate a specific channel may be substituted for the physiological ion in some assays to provide enhanced signal-to-background ratios. For example, thallium readily permeates many potassium channels and can be detected with fluorescent probes that can be loaded into cells. This approach provides an effective surrogate for potassium flux, which would be more difficult to do by measuring potassium influx due to high background levels.

Ion channels present special challenges and opportunities for assay design. Many ion channels undergo conformational changes during gating that can provide a basis for pharmacological modulation of specific states. In some cases, a specific state may be associated with a disease condition or can present an opportunity for specific therapeutic modulation. In this way, a channel that is widely expressed may be preferentially modulated in a pathological tissue or condition. Assay formats that can control channel gating are required in order to identify compounds with functional selectivity targeting specific conditions. Recent developments in automated electrophysiology, biochemical sensors, and plate readers provide a range of options for implementing ion channel assays that can detect state-specific, or state-independent, channel modulation. Typically no single assay format can offer the ideal combination of high throughput, low cost and high information content. Ion channel drug discovery projects then typically employ a combination of assays including high throughput biochemical assays and lower throughput electrophysiological assays. A key consideration when establishing these assays is pharmacological validation of the assay such that the assay results provide a direct and reliable measure of compound effects on the channel. Ideally, the assay results can then be used to predict compound effects in cells and tissues. For novel ion channel targets, pharmacological standards will likely not exist. An iterative approach can then be used to identify adequate pharmacological standards. An initial HTS assay format can be used in a pilot screen to identify a set of potential modulators. Mechanistic evaluation of this hit set using a different assay technology (usually electrophysiology) can be used to select appropriate pharmacological standards for further optimization of an HTS assay.

2. Fluorescence Assays Using Membrane Potential Sensing Dyes

2.1. Assay Overview

Ion channels represent a class of proteins with potential for therapeutic intervention. Human genetic studies have identified ion channel targets that are relevant for treating specific diseases with clearly unmet clinical needs. In addition, pharmacological validation exists for other ion channel targets related to medical conditions that are not well treated with current medications. The challenge for the ion channel field is to identify potent and selective ion channel modulators with appropriate features that will allow their evaluation in clinical trials. The significant improvement in technology over the last few years with automated electrophysiology instruments has provided additional platforms that can support ion channel drug development. However, none of these instruments can yet support screening of large chemical libraries (i.e. > 1 M compounds) that are typically required to identify new lead candidates for ion channel targets which lack viable probes or leads. In addition, the high cost of automated electrophysiology consumables necessitates a quest for, alternative technologies for measuring ion channel activities in high density formats. Although these technologies cannot substitute for electrophysiological evaluation of more advanced drug candidates, they can play an important role in lead identification and optimization.

Because ion channels permeate ions at a high rate when they open, the activity of these proteins can therefore cause changes in the membrane voltage. When properly tuned, the activity of ion channels expressed in mammalian cell systems can be indirectly monitored with the use of membrane potential sensing dyes that provide a fluorescence signal. These assays can operate in 96-, 384-, or 1536-well plate formats at a lower cost and higher throughput than the automated electrophysiological platforms currently available. However, for membrane potential-based assays to be useful, rigorous validation criteria must be implemented to ensure that the fluorescence signal provides a reliable measurement of channel activity. Fluorescence resonance energy transfer (FRET) with the use of a pair of dyes, a phospholipid-anchored coumarin and a hydrophobic oxanol that rapidly redistributes in the membrane according to the transmembrane field, can provide robust and reproducible signals when studying the activity of voltage-gated sodium, potassium and other channels. Indeed, the assay can be tuned to identify either activators or inhibitors of a given ion channel. The general concept when designing assays for inhibitors of potassium channels is illustrated below in Figure 1.

Cell lines expressing the potassium channel of interest are constructed. In these cells, the stably expressed channel sets the resting potential at ~ -90 mV. Under control conditions, addition of a high potassium solution will cause cell depolarization, and this change in voltage can be measured with the FRET dyes. In the illustrated example, the blue and red fluorescence signals represent the emission of N-(6-Chloro-7-hydroxycoumarin-3-carbonyl)-dimyristoylphosphatidylethanolamine (CC2−DMPE) and bis-(1,3-dithylthiobarbituric acid)trimethine oxonol ($DiSBAC_2$ (3)), respectively, whereas the green signal represents the ratio of CC2−DMPE to $DiSBAC_2(3)$. It can be seen that upon addition of high potassium solution (top panels of Figure 1), the emission intensity of $DiSBAC_2(3)$ decreases due to the movement of the dye to the inner leaf of the membrane. As a consequence, the emission of CC2−DMPE increases and a new fluorescence ratio is established. When cells are pre-incubated with a potassium channel inhibitor (bottom panels of Figure 1), cell depolarization will occur and further addition of the high potassium solution will not affect the FRET signal. Thus, a large assay signal can be established for identifying channel inhibitors. This assay design works well with both voltage- and non-voltage-gated potassium channels.

For identifying potassium channel activators the following assay concept can be used as shown in Figure 2.

Cell lines expressing the channel of interest are constructed. In these cells, the expressed potassium channel is not capable of setting the resting potential due to a combination of low expression levels and/or low open probability, and cell membrane potential is established near zero mV. However, in the presence of a channel activator (agonist) which increases channel open probability, the cell membrane potential will become hyperpolarized by shifting towards the potassium equilibrium potential. Upon addition of a high potassium solution, control cells will not display a change in the FRET signal, whereas a large change in FRET will be observed in those wells in which a channel activator is present. In the illustrated example, the blue and red fluorescence signals represent the emission of CC2−DMPE and $DiSBAC_2(3)$, respectively, whereas the green signal represents the ratio of CC2−DMPE to $DiSBAC_2(3)$.

An assay used for identification of inhibitors of voltage-gated sodium (Nav) channels can be implemented using the following scheme shown in Figure 3.

In mammalian cell lines, stably expressed Nav channels reside mostly in the non-conductive inactivated state due to the depolarized cell resting membrane potential (-20 to -50 mV), as sodium channels rapidly open then inactivate and remain closed in response to membrane depolarization. However, this conformation of the channel is thought to represent the high affinity state for interaction with some classes of inhibitors, and is also thought to be more prominent in some disease states. Exposure of the cells to a Nav agonist, such as veratridine, removes inactivation and allows entry of sodium ions into the cells through open, unblocked channels, causing depolarization of cells towards the sodium equilibrium potential, with a consequent change in the FRET signal. In the illustrated example, the blue and red fluorescence signals represent the emission of CC2−DMPE and $DiSBAC_2(3)$, respectively, whereas the green signal represents the ratio of CC2−DMPE to $DiSBAC_2(3)$, and individual well responses to increasing concentrations of veratridine are shown. In the presence of a Nav inhibitor, the FRET signal will be unaltered after addition of the Nav agonist because the channel equilibrium would have been shifted toward the inactivated-drug bound state, which may not open until inhibitor dissociates. It is important to determine an optimal concentration of veratridine that affords a robust signal while not significantly affecting sensitivity to inhibitors. This assay format works well for several Nav1.X channels, although the actual agonist used to initiate sodium influx varies depending on the channel under study.

2.2. General Considerations

The assays described above can provide robust, reproducible signals and operate with high Z' factors in 96-, 384-, and 1536-well plates. Particular attention to cell culture conditions is critical for the success of the assay. Cells should be confluent, but not overgrown, for the assay to work properly. The operator needs to identify cell

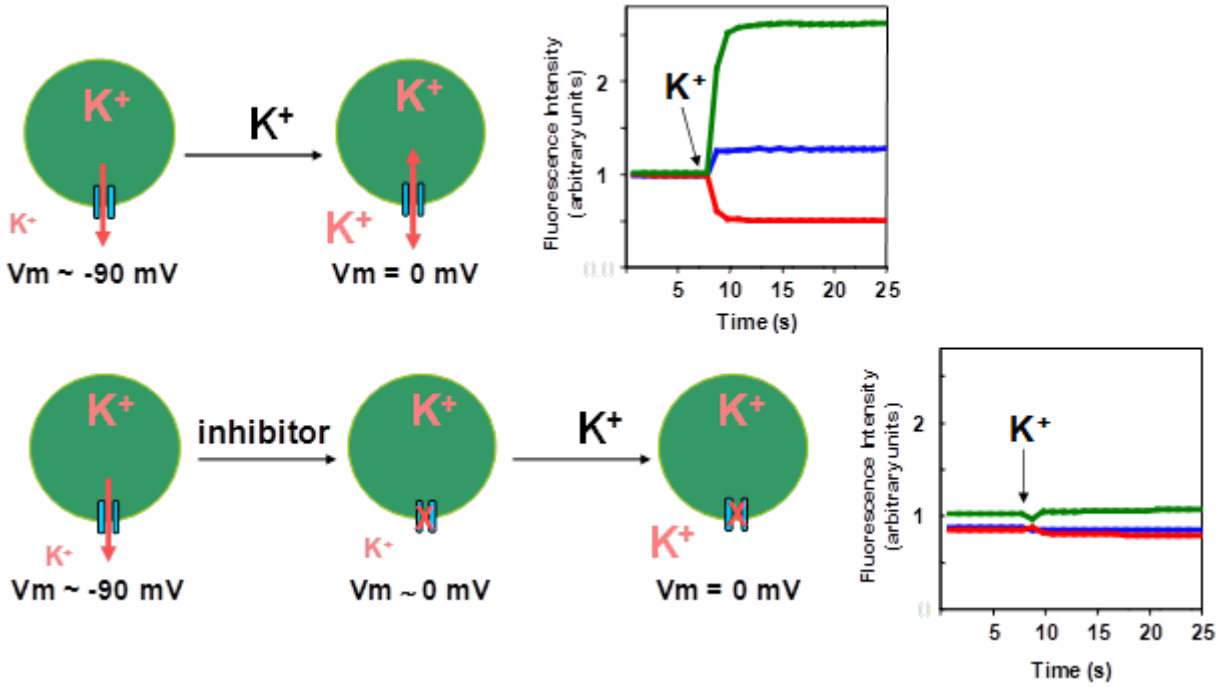


Figure 1: Fluorescence-based Membrane Potential Assay Format for Detecting Potassium Channel Inhibitors. Fluorescent dyes are used to measure cell depolarization following addition of high potassium concentration to the extracellular solution. A large depolarization and fluorescent signal occur in the absence of an inhibitor (top panels), while a reduced depolarization is seen after preincubation with an inhibitor.

growth conditions and cell plating density that are appropriate for providing a good assay signal. The handling of the dyes is also important since these molecules are lipophilic in nature and sometimes are difficult to put into solution. Binding of these reagents to plastic surfaces has been observed and therefore it is better to use glass surfaces for preparation of the dyes' solutions.

2.3. Cell Lines

The assays described above can provide robust, reproducible signals and operate with high Z' factors in 96-, 384-, and 1536-well plates. Particular attention to cell culture conditions is critical for the success of the assay. Cells should be confluent, but not overgrown, for the assay to work properly. The operator needs to identify cell growth conditions and cell plating density that are appropriate for providing a good assay signal. The handling of the dyes is also important since these molecules are lipophilic in nature and sometimes are difficult to put into solution. Binding of these reagents to plastic surfaces has been observed and therefore it is better to use glass surfaces for preparation of the dyes' solutions.

2.4. Assay Parameters

During assay optimization, a key initial experiment is to evaluate a matrix of dye concentrations to identify those that are optimal for the particular cell line and assay under consideration. In addition to reproducibility and high Z' factors any assay needs to be further validated with the use of pharmacological channel modulators. Different structural classes and mechanisms of action agents should display effects that match the properties observed in electrophysiological or other well-defined biochemical experiments. If not, changes in the assay parameters should be explored to achieve the most optimal conditions. For instance, for Nav channels, agonist concentration is critical to ensure a pharmacological readout that correlates well with electrophysiological values. When the agonist concentration is too high, a shift in the concentration-response curves of inhibitors to

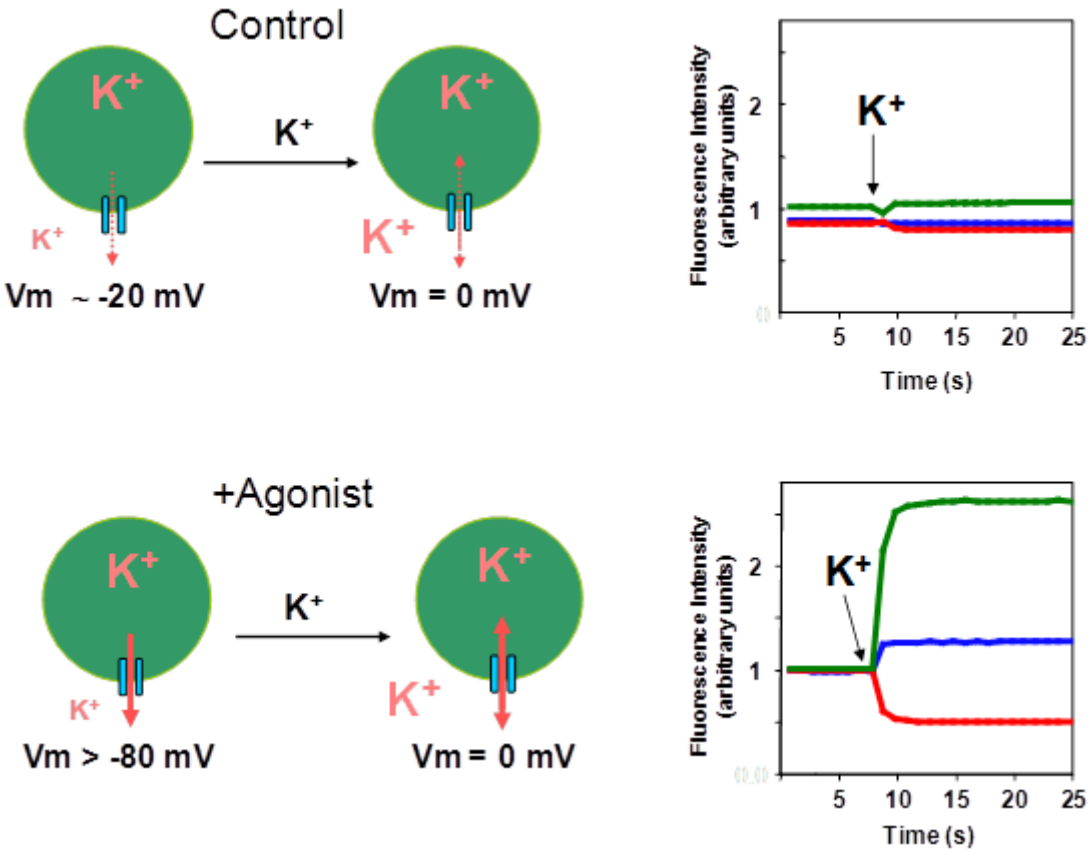


Figure 2: Fluorescence-based Membrane Potential Assay Format for Detecting Potassium Channel Activators. Fluorescent dyes are used to measure cell depolarization following addition of high potassium concentration to the extracellular solution. Potassium induces only a minimal change in membrane potential in control (top panels), while a large depolarization and fluorescent signal are seen after preincubation with an agonist.

higher IC_{50} values will occur, and it may even significantly affect the response of certain structural classes of inhibitors in such a way that the assay becomes insensitive to the presence of these agents. A concentration-response curve to agonist, such as in the above illustrated example with veratridine, should be performed in a daily basis to identify the condition that provides a robust but not saturated signal. Because the concentration-response curves to agonist are quite steep it is not possible to guess the optimal agonist concentration for a given assay since other factors such as the particular state of the cells may influence the response. In general, a pre-incubation time of 30 minutes with test compound appears to be optimal. Longer incubation times than 45 minutes may start to compromise the fidelity of the assay most likely because of toxicity-related issues from the use of the dyes.

All assay plates should always contain appropriate controls. Plates that do not comply with a minimum Z' factor should be discarded. During lead optimization, concentration-response curves to standard channel modulators must be included to ensure that the pharmacological responses of novel compounds are meaningful. Particular attention must be paid to the wells positioned at the edges of the plate. If there are any issues with the assay signals from these edge wells, then the problem needs to be fixed or otherwise these wells should not be considered when calculating data. The use of several replicates per data point provides a higher accuracy when using a four parameter Hill equation to calculate IC_{50} or EC_{50} values.

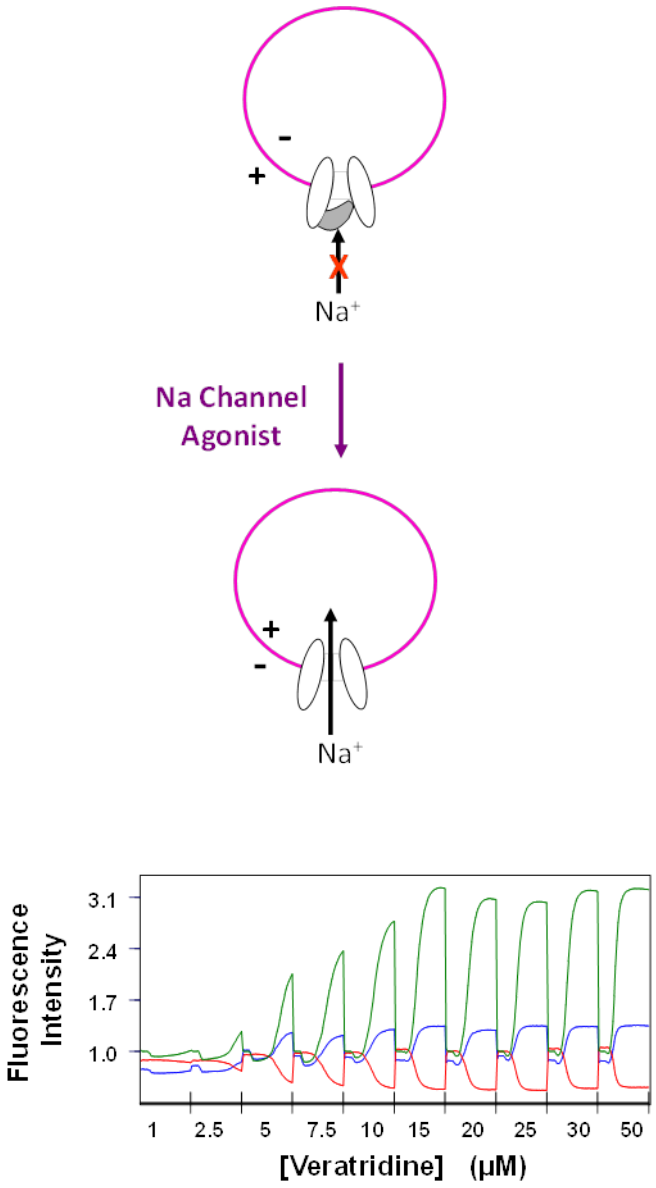


Figure 3: Fluorescence-based Membrane Potential Assay Format for Detecting Voltage-gated Sodium Channel Inhibitors. A sodium channel agonist (veratridine) is used remove channel inactivation leading to sodium influx and cell depolarization measured with a fluorescent dye pair. Concentration-dependent depolarization by veratridine is shown at bottom right for 10 wells in a plate-based assay. A sodium channel inhibitor may reduce the depolarization caused by veratridine.

2.5. Data Analysis

In the potassium channel assays, the FRET signal responses to the addition of a high potassium solution are a reflection of the membrane potential of the cells before this addition. Thus, in these assays, the plateau fluorescence ratio signal is used to calculate the IC_{50} or EC_{50} values for channel inhibitors or activators. In general, the plateau fluorescence ratio signal remains stable for a significant amount of time so there are no issues when using this approach. When assaying Nav channels, the situation is different. In this case, the change in membrane potential is triggered by the addition of the particular Nav activator. Ideally, one would want to measure the initial rate of signal change which should be related to the number of functional Nav channels. However, the slope of the FRET signal may not be strictly related to the number of modified functional channels and could be limited by the time response of the dyes and/or the instrument. For this reason, a 3 second time

interval is identified in control wells where the signal starts approaching (~95%) plateau level. This same time interval is then used to determine the effect of test compounds.

All commonly used criteria to calculate statistically significant parameters from concentration-response curves of compounds should be applied to data calculation.

3. Ion Flux Assays

Ion channels are integral membrane proteins that conduct ions across cell membranes. Ion channels have preferences for different species of ions with some channels exhibiting a preference for cations while others prefer to pass anions. Within a given subfamily of ion channels (e.g. cation channels), some channels show preference for divalent cations versus monovalent cations, and some channels still show further specificity resulting in channels (e.g. voltage-gated sodium channels) with a high-degree of specificity for sodium over potassium, for instance.

When a concentration differential exists for an ion across a cell membrane and an open channel of appropriate specificity exists in that membrane, ions may pass through the channel down their electrochemical gradient resulting in ion flux. These ion fluxs have been used for decades as a means to measure the activity of ion channels. Early work in this are was primarily focused on radionuclide-based flux assays using ions like $^{45}Ca^{2+}$ and $^{22}Na^{+}$. However, in the 1980's the development of ion-selective fluorescent dye-based indicators revolutionized the measurement of ion flux. These indicators improved the ease of use, as well as spatial and temporal resolution of ion flux measurements. The 1980's and 1990"s also witnessed the advent of genetically encoded ion flux indicators including the chemiluminescent calcium sensor, aequorin and a variety of engineered fluorescent proteins including the calcium-sensitive chameleons and anion-sensitive yellow fluorescent proteins (YFPs). More recently, the use of automated flame photometry-based ion flux assays has been proven effective as an alternative to fluorescent and radionuclide-based techniques for some ion channel assays (Figure 4).

Ion flux assays can be divided into two main categories: those that measure the flux of physiological ions (e.g. calcium, sodium, magnesium, zinc, and protons) and those that measure the flux of surrogate ions (e.g. thallium, cobalt, and iodide). For years fluorescent indicators were useful primarily for Ca^{2+} and other divalent cations while radionuclide-based approaches remained the best options for monovalent cation channels and anion channels. Recently, the new fluorescent sodium indicator, Asante Natrium Green (ANG) is showing promise as an intracellular sodium indicator. Other ions have proven more challenging; namely potassium and chloride. The discovery that the potassium congener, thallium, is capable of affecting the fluorescence of a variety of fluorescent dyes, most importantly FluoZin-2, has enabled the development of HTS-compatible assays for numerous potassium channels. Similarly, the use of surrogate anions (e.g. iodide) has allowed the development of HTS-compatible assays for chloride channels, particularly via engineered yellow fluorescent protein-based anion sensors.

In this article the main focus will be on fluorescent dye-based techniques because these are the most commonly used and most easily applied to HTS. However, many of the general principles of ion flux assay design may apply to other ion flux assay techniques. In addition, since ion channels are often effectors of signal transduction pathways, ion flux assays can be used as indirect measures of the activity of these pathways. The most common use of ion flux assays in this regard is the measurement of intracellular calcium flux mediated through the IP3 receptor downstream of G_q-couple seven transmembrane receptors (aka GPCRs).

3.1. General Considerations

Ion flux assays can have very broad utility for HTS. They are adaptable to a wide range of formats including 96, 384, and 1536 well plates. However, great care is required to establish appropriate cell culture and assay

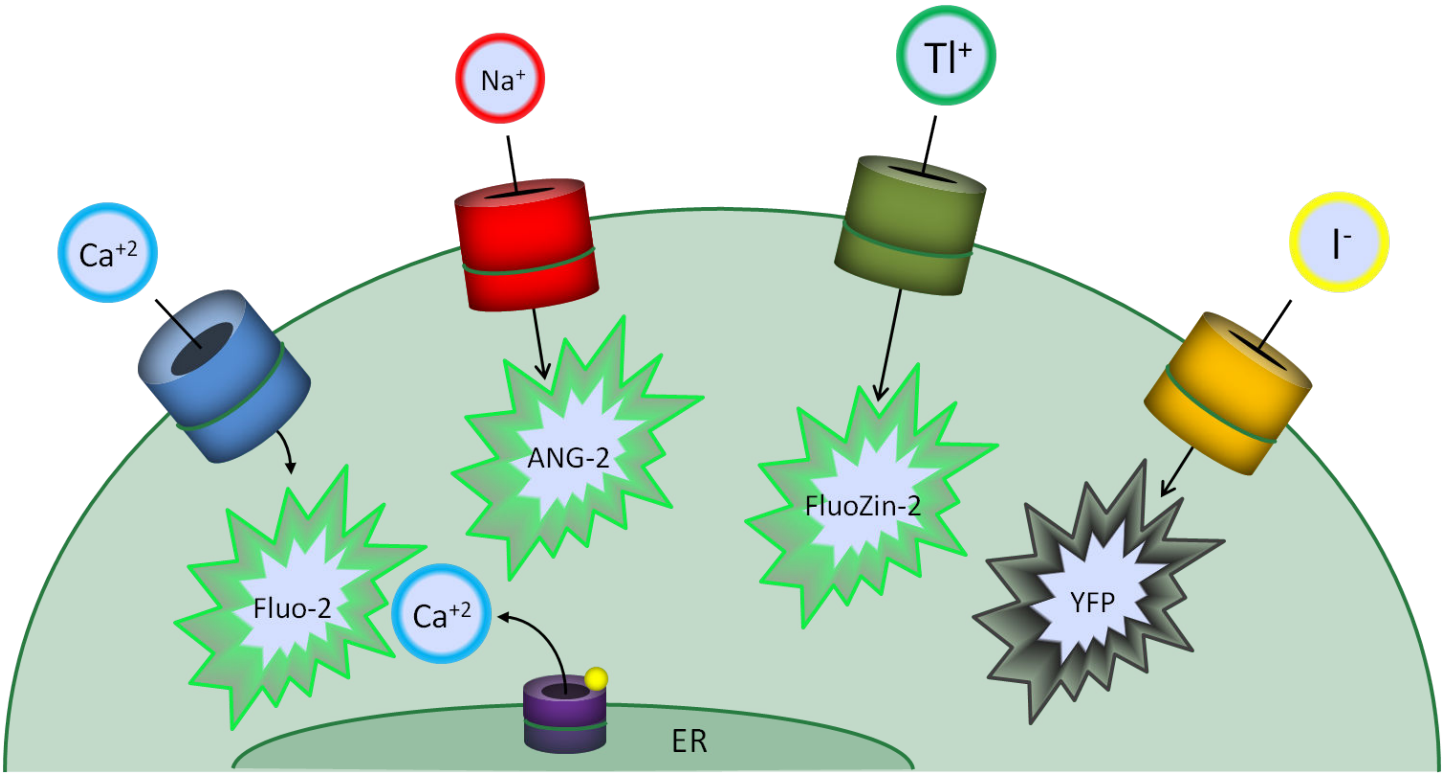


Figure 4: Fluorescence-based Ion Flux Assay Formats. Shown from left to right are examples of fluorescence-based ion flux assays. Plasma membrane calcium permeable channels (**BLUE**) and endoplasmic reticular (ER) calcium permeable channels (**PURPLE**) can be measured with a variety of fluorescent calcium indicator dyes like Fluo-2 and Fura-2 (not shown). Sodium permeable channels (**RED**) can be measured by sodium sensitive fluorescent dyes. Potassium channels (**GREEN**) can be assayed using a surrogate ion approach and the thallium sensitive dye, FluoZin-2. Unlike the other fluorescent dyes mentioned above, the mutant yellow fluorescent protein (YFP)-based sensor has its fluorescence effectively quenched by the surrogate ion, iodide, fluxing through a chloride channel (**YELLOW**).

conditions in order to achieve highly reproducible assays capable of identifying and correctly categorizing different structural classes and modes of ion channel modulators. Special attention should be paid when non-physiological conditions are used to develop assays including but not limited to the use of surrogate ions, altered ionic gradients, compounds to promote dye retention (e.g. probenecid), and extracellular quench dyes used to establish homogenous "no-wash" assay conditions. While no-wash conditions are attractive from the point of view of speed and simplicity, some targets may be sensitive to quench dyes, while others may be affected by the presence of signaling molecules in the assay medium which may necessitate the use of assay protocols that include wash steps.

In all cases, it is important to realize that changes in assay signals resulting from the addition of test compounds or other changes in assay conditions may not be due to a direct interaction with the ion channel but may instead be an indirect affect on some other component of the assay system. Thus, as part of an HTS screening tier, proper control experiments are necessary to establish which test compounds directly affect the ion channel target of interest, which are acting by indirectly modulating the target of interest, and which are affecting the assay signal through mechanisms unrelated to the target of interest.

3.2. Cell Lines

The best overall cell line for ion flux assay development will depend on the specific ion channel that is being assayed and the goals of the assay design (e.g. discovery of ion channel activators). In some cases, cell lines derived from a particular tissue of interest may be useful, particularly when the ion channel of interest is

expressed in high abundance. However, it is still most common to use "reagent" cell lines as a background to over-express the ion channel target of interest. These cell lines are most commonly, but not limited to, HEK-293 and CHO cells.

In order to generate large, robust signals in flux assays, it is often advantageous to have a high level of channel expression. However, high levels of expression of some channels can be detrimental to cell health and thus may make the establishment of highly expressing stable cell lines difficult. In the event that high levels of expression pose problems for establishment for highly expressing stable cell lines, a number of strategies may be pursued. One approach is the use of inducible systems (e.g. tetracycline inducible systems). These systems use an inducible promoter to drive the expression of the ion channel of interest. Under these conditions, expression of the channel is tonically suppressed during normal propagation of the cells. On the day before/day of the assay, expression is induced to allow transient high levels of ion channel expression. Inducible systems are not perfectly controlled, however, and promoter "leakiness" can limit their utility in certain instances. In addition, care should be taken to make sure that the cell culture medium is free of the inducing agent (e.g. tetracycline). The use of certified tetracycline-free serum is recommended. In cases where inducible systems are ineffective or insufficient, ion channel inhibitors are sometimes a useful way to limit over-expression-related toxicity. In these cases, the cells are grown in the presence of the inhibitor up until just before the time of assay when the inhibitor is removed by washing. While effective in some cases, the additional manipulation required to remove inhibitors can be inconvenient in an HTS context. For some ion channels whose activity is regulated by cellular membrane potential, co-expression of a "helper" potassium channel, such as a tonically active inward rectifying potassium channel, may be useful to set the cellular membrane potential strongly negative values, as low as -90 mV, to promote a low activity state of the target. Finally, in cases where the target is completely refractory to generation of a stable cell line, transient transfection may be pursued. While generally not as convenient as stably expressing cell lines, transiently transfected lines have proven a viable alternative to stable cell lines in some HTS assay settings.

3.3. Assay Parameters

There are a multitude of reagents and assay conditions to consider when developing an ion flux assay. These include plate format/density, cell number and confluence, level of channel expression, choice of indicator/assay technology, indicator concentration and loading parameters, method of activation of the ion channel, ionic composition of assay buffers, and wash versus no-wash formats. With so many variables to consider, a thorough knowledge of the ion channel target of interest, appropriate control compounds when available, an alternative reference method for measuring the ion channel's activity (e.g. electrophysiology), and a systematic approach using matrices of assay conditions are all important to the goal of establishing an assay that possesses a large signal, low background, good dynamic range, and the ability to properly detect, measure and classify ion channel modulators.

Particularly important to appropriate assay development is the selection of the best indicator, the best ionic composition, and the best mechanism of channel activation. It is important to choose indicators of the appropriate affinity and permeant ionic concentrations that are capable of producing robust signals without saturating the detector or the indicator. Conditions that result in saturation may result in left-shifted concentration response curves for channel activators and right-shifted concentration response curves for inhibitors. As a general guideline, indicator and ion concentration pairs should produce ~80% of the fully achievable signal magnitude for a given indicator/detector combination under conditions of maximal channel activation. Conditions that produce "square" wave signal profiles indicative of a saturated indicator or detector (Figure 5A) should be avoided. Also of great importance is the mechanism and degree to which a channel is activated. As shown in (Figure 5B), the concentration of extracellular potassium during test compound incubation can have a dramatic effects on the apparently potency of ion channel modulators and the amount of extracellular potassium added at the time of initiating a flux experiment with a surrogate ion can have a

dramatic effect on the level of ion flux observed (Figure 5C). In these examples, potassium can affect compound potency indirectly via altering cell membrane potential or by direct interactions with the ion channel.

As described below in HTS Assay Considerations**,** many ion flux assays are amenable to no-wash formats. However, care must be taken to carefully validate the assays to ensure that the chosen format is most capable of detecting and correctly categorizing modulators of the target of interest. Excessive dye loading time, the use of organic ion transport inhibitors, and extracellular quench dyes should be avoided when convenient since all of these can adversely affect cell health and ion channel activity/pharmacology.

In some systems, particularly when the system shows ion flux that is rectified during the time course of the assay (e.g. calcium flux assays), multiple addition protocols can be a useful way to measure more than one activity level of the system during the same experiment. The use of multiple addition protocols can be particularly beneficial for assays where there is a desire to detect positive and negative ion channel modulators. Figure 6 shows an example of a multiple addition protocol for a potassium channel using a fluorescent thallium indicator. The **GREEN** trace is representative of a vehicle control condition or the flux obtained in the presence of an inactive test compound. The **RED** and **BLUE** traces represent data that would be expected in the presence of an agonist and an inhibitor "hit", respectively. By using a multiple addition protocol, conditions after the first addition favor the detection of activators while conditions after the second addition favor the detection of inhibitors.

Both the ability to resolve relevant levels of channel activity as judged by Z' and other HTS assay metrics, as wells as the ability to measured potency and efficacy values for known classes of modulators for a target of interest are important for proper assay validation. Ideally, optimized assay conditions for ion flux assays will be calibrated against electrophysiological measures using a set of compounds that are known to be active on the ion channel target of interest and possess varying structures, potencies, and modes of efficacy. When applicable, comparison of ion flux assay performance to activity measured with control compounds in native preparations can lend further confidence that the assay conditions are able to detect and correctly classify modulators for the ion channel target of interest. As with other assay technologies, the inclusion of relevant control compounds and conditions throughout a screen are critical to monitoring assay performance and helping ensure the best data quality and the best ability to detect active compounds.

3.4. Data Analysis

A variety of analytical methods can be used for ion flux assays. The most appropriate analytical methods should be selected based on specific knowledge of assay system including limitations of the indicators, detectors, and properties of the ion channel target. Ideally, data obtained using a particular data analysis method should be compared to data obtained on an identical set of test compounds using another assay method (e.g. electrophysiology). Typical methods, depending on the in channel target, cellular background, and type of indicator used, are: amplitude, rate of change, area under the curve, and in regularly oscillating systems, frequency.

The most commonly used method is to measure signal amplitude relative to a relevant baseline at a specific time during an experimental protocol. In some cases, when data acquisition rates and indicator response time are appropriately fast, the rate of change in the initial assay signal can be an excellent way to obtain ion channel activity measurements. Finally, in assays systems where regularly spaced oscillations occur in ion fluxes, the frequency of peaks may also be a useful measure of the activity of the system. In these cases, the coordinated activity of a variety of processes results in the measured properties in the assays, thus the assay may be susceptible to a great many modes of modulation many of which are not directly affecting a single specific ion channel target of interest.

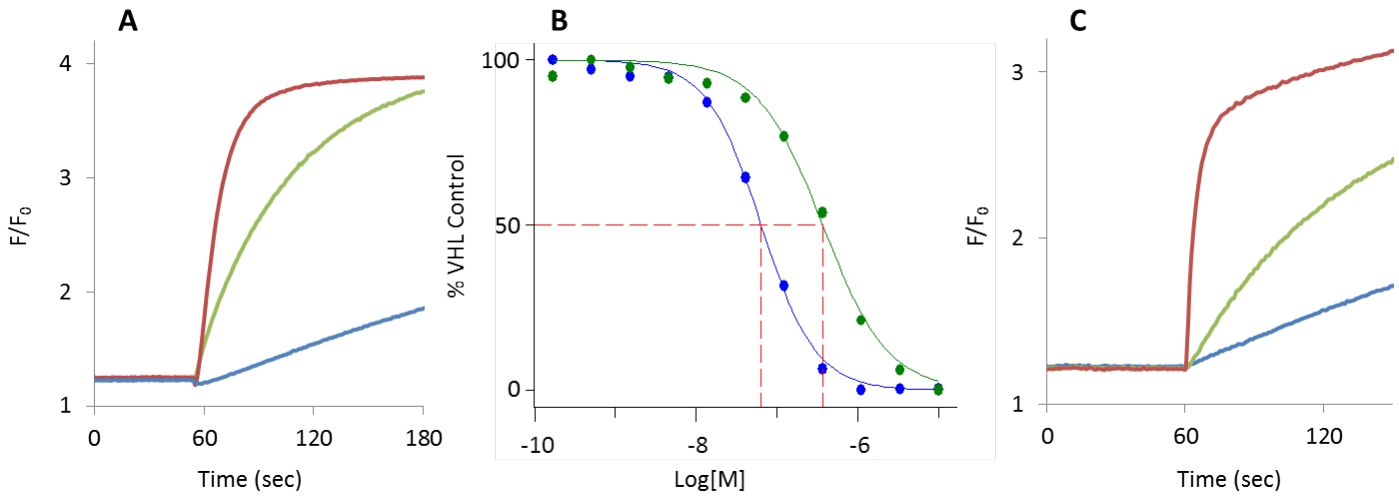


Figure 5. Optimization of Ion Flux Assay Parameters Shown in panel **A** are representative data demonstrating the effect of varying the concentration of permeant ion (Tl^+) in a potassium channel assay. The **RED** trace is at a nearly saturating concentration of Tl^+ while the **GREEN** trace is a concentration producing a large, but not saturating response. The **BLUE** trace is from untranfected cells treated with the higher of the two Tl^+ concentrations. Panel **B** shows the effects of varying extracellular K^+ in the assay buffer on the potency of a voltage-gated potassium channel inhibitor. The **GREEN** curve corresponds to the compound pre-incubated in assay buffer containing 30 mM K^+ while the **BLUE** curve was obtained when the compound was pre-incubated in 60 mM K^+-containing assay buffer. The difference in measured potency is >10-fold. Panel **C** shows the effects of varying the K^+ concentration in a Tl^+-containing stimulus buffer when assaying a voltage-gated potassium channel. The **GREEN** trace was obtained by stimulating the cells with a Tl^+ containing stimulus buffer containing 5 mM K^+. The **RED** trace was obtained with a stimulus buffer containing the same concentration of Tl^+ and 30 mM K^+. The **BLUE** trace was obtained from untransfected cells with the 30 mM K^+ stimulus buffer.

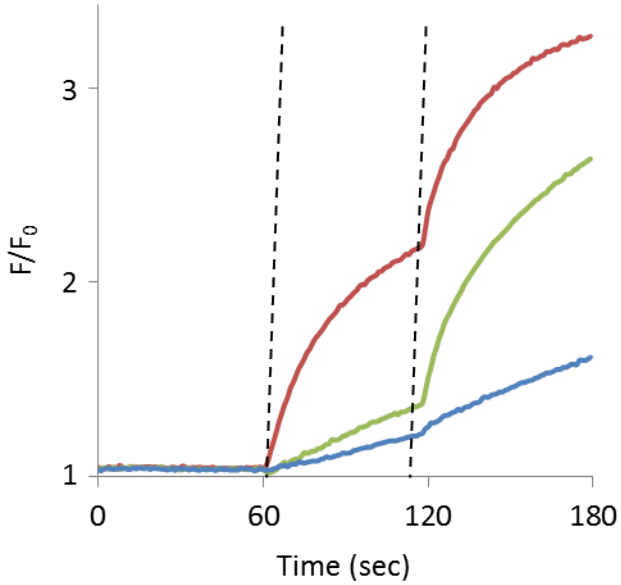


Figure 6. Multiple Addition Assays. Shown are data obtained using a multiple addition assay protocol for a ligand-gated potassium channel. The **BLUE** trace shows the flux in the presence of a channel inhibitor. The **GREEN** trace shows the flux resulting from first the addition of ~EC_0 concentration of agonist in thallium stimulus buffer followed by the addition of an ~EC_{70} concentration of agonist. The **RED** trace shows the flux resulting from the addition of an agonist "hit" followed by an ~EC_{70} concentration of agonist. The dotted lines, from left to right, mark the points of the first and second additions.

In some instances, as part of the analytical process, it is valuable to subtract a relevant control waveform from a waveform that results from assaying a test compound. Subtraction of this control waveform may reveal subtle differences that may not be readily observed in raw the waveforms. Control wave subtraction may also provide a useful way to determine the time point where peak differences occur between two different assay conditions and thereby may help define the optimal time window from which to extract amplitude information (Figure 7).

When practical, it is useful to obtain measurements before and after the addition of unknown compounds in order to detect and take into account any optical properties of the test compound (e.g. fluorescence) that might affect the analysis or interpretation of the data. For instance, in the common practice of ratio normalization (e.g. division of all data points in a wave by the initial data point in the same wave, F/F_0) is used when a fluorescent compound has been added before the first data point has been obtained, the resultant normalized values may be badly skewed resulting a false assessment of the compound's activity (Figure 7).

In all cases, standard protocols for determining well-to-well, and plate-to-plate variability can be used. Standard methods can also be used for obtaining fits and parameter estimates for concentration-response relationships.

4. HTS Assay Considerations

High-throughput screening is a leading method for identifying compounds for drug development, and ion channels are excellent targets for a wide range of health conditions. When optimizing cell based ion flux assays for use in HTS, there are many parameters to consider. Here we provide a list of several important assay parameters that can be examined to optimize signal to background ratio and Z-factors. We also include data and anecdotal evidence showing the effectiveness of manipulating these parameters in optimizing an HTS with a variety of cell lines.

4.1. Cell Growth and Harvesting

Most cell growth and harvesting parameters are specific to the cell line used for a particular assay, and are not changed when adapting an assay to high-throughput screening format. Nevertheless, changing the cell growth media, the growth temperature, the confluency at which you harvest cells, the passage number, and the method of harvesting (use of a non-proteolytic cell removal method such as versene versus trypsin) can have a significant effect on your signal. Many cell lines have been observed to stop expressing a reporter gene after reaching confluency. Additionally, some ion channels and GPCRs with large extracellular domains may be partially cleaved during incubation with trypsin, both of which can significantly affect signaling performance. Engineered cell lines can lose expression of the target of interest over time, so the use of low passage cells may be critical. In certain cases, a change in growth media or temperature the day before plating cells can favorably affect cells such that a higher signal is achieved (Figure 8).

4.2. Cell Plating

Altering conditions of cell plating can dramatically affect the signal in an HTS assay, and these parameters are typically the first to alter when optimizing an HTS assay. Parameters we have often changed include: plating media, cell density, incubation time, incubation temperature, plating volume, and the use of coated plates. The plating media and cell plating density will both be very dependent on the cell type used, although for 1536-well plates, 500-4000 cells per well is a good starting point. Certain cells types will yield a higher signal in low-serum media or after incubating at 32°C (Figure 9, left panel). The effect of temperature on efficient trafficking of ion channels to the plasma membrane has been described in multiple publication [1, 2]. Some cell types and receptors are less affected by low confluency, so more cells can yield higher signal amplitudes. In other cases, cells need to be very healthy and dividing to give a high signal, in which case a lower cell number, regular media, and regular growth temperature would be suggested. When using less adherent cells, consider the use of poly-D-lysine coated plates (Figure 9, right panel).

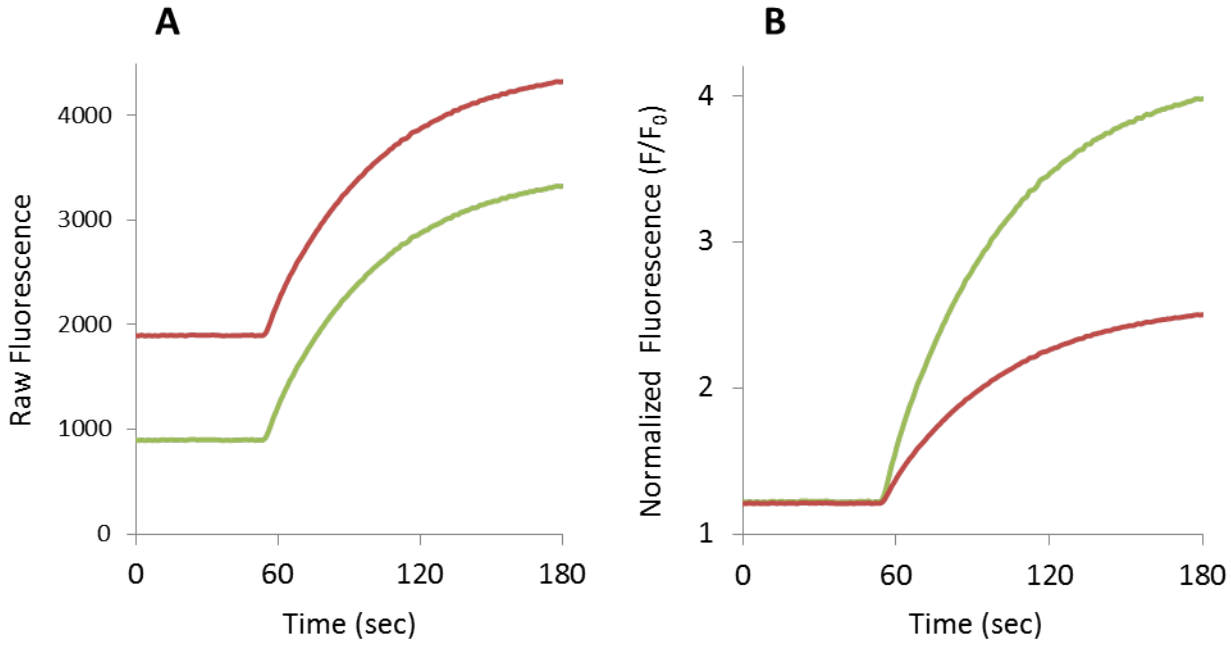


Figure 7. Ratio Artifacts in Ion Flux Data Shown in **A** are two waves obtained by testing a potassium channel with two compounds that are inactive at the channel. One compound is fluorescent (**RED** trace) and the other compound is non-fluorescent (**GREEN** trace). Both compounds were added before the assay was initiated and baseline values prior to compound addition were not obtained. When a commonly used data normalizing function F/F_0 (aka static ratio) is performed as shown in **B**, the **RED** trace is mis-normalized and superficially appears to be an inhibitor.

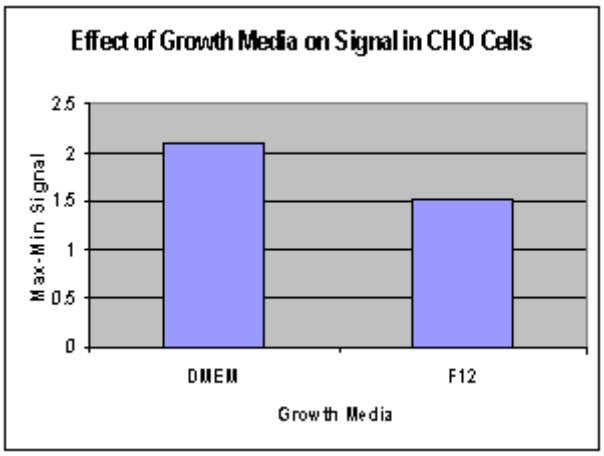
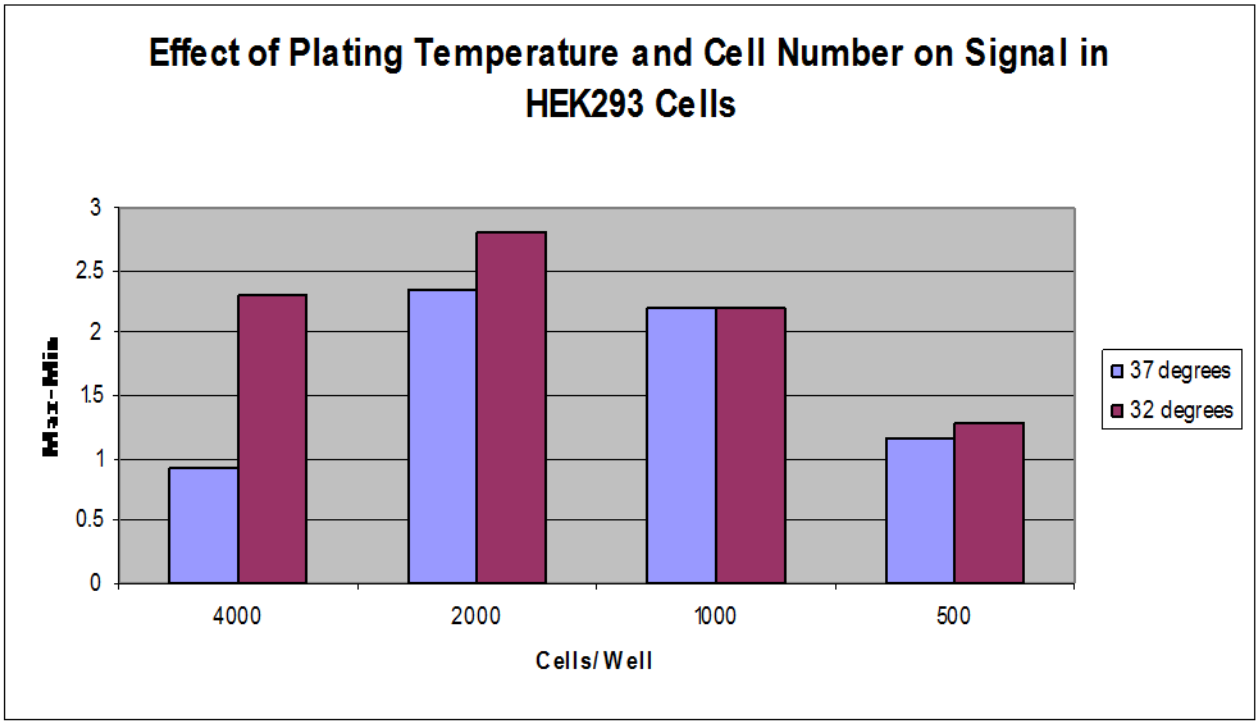


Figure 8 CHO cells were grown in DMEM and F12 media for several days prior to plating and running. Both solutions were supplemented with 10% FBS, pen/strep, and NEAA.

4.3. Dyes

For cell based ion flux assays, the dyes employed play a large role in assay performance. Fluorescent dyes are compounds that emit a particular wavelength of light after excitation by another (usually shorter) wavelength of light. There are two main types of dyes used in ion flux assays: membrane potential dyes and ion binding dyes (see above). Membrane potential dyes, such as $DiBAC_4$, respond to changes in membrane potential via redistribution within the cell membrane. This redistribution of the dye results in detectable changes in fluorescence. Ion binding dyes, in contrast, are dyes that fluoresce upon binding particular ions, such as calcium.



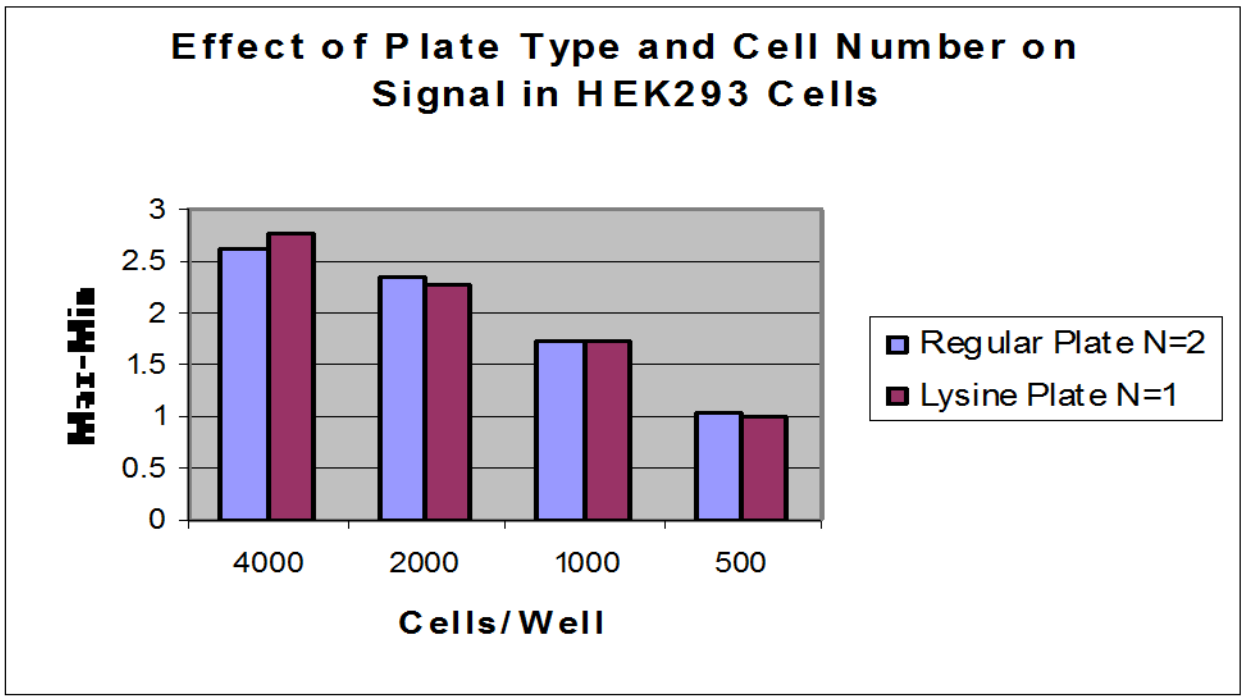


Figure 9 Left- Effects of seeding density and outgrowth temperature on signaling in a HEK293 cell line. Cells were plated at various densities at either 32°C or 37°C overnight. Right- Effects of seeding density and plate coating. HEK293 cells were plated in either regular or poly-d-lysine coated plates at various cell densities. HEK293 cells were stimulated with a ligand causing internal calcium release.

Fluo8, from AAT Bioquest, is an example of one such calcium binding dye. Many ion binding dyes contain aminomethyl (AM) ester groups; these compounds are uncharged and membrane permeable. Once in the cytosol, the AM ester groups are cleaved by intracellular esterases, resulting in charged species that are not membrane permeable, and stay trapped inside the cell. AM ester dyes are particularly useful in ion flux assays since they help prevent background fluorescence and allow detection of changes primarily within the cell. In

optimizing ion flux assays, multiple dyes can be tested and their concentration changed. A typical final concentration range of dye is 10 µM to 100 µM. Increasing concentration of dye can increase the signal window up to a point; however, upon reaching the upper detection limit of the instrument, any increase in dye after that point will increase the background signal and result in a lower signal window.

4.4. Quenchers

Fluorescent quenching agents are cell impermeable compounds that absorb fluorescence in a particular range of wavelengths [3]. Quenchers are often used in cell based ion flux assays to eliminate background fluorescence originating outside the cell membrane, thus providing a higher signal window. This is generally only necessary in no-wash assay protocols, as the wash steps are typically designed to rinse any extracellular dye out of the media. In high density format plates such as 384- and 1536-well plate assays, however, wash steps can be challenging to implement in an automated fashion and can also introduce well-to-well variations and sometimes remove less adherent cells. Therefore no-wash assays are often preferable in high density automated HTS formats. In this case, the use of quenchers can significantly improve the signal by reducing background fluorescence, although effects of quenchers on assay pharmacology should be monitored.

There are several different types of quenchers available, both from vendors and home-made. In certain intracellular calcium assays, home-made quenchers, such as Red 40 in HBSS buffer, can equal or surpass performance of commercially available quenchers. This is an important assay parameter to test when optimizing an ion flux assay. Additionally, the optimal concentration of quencher should be evaluated, since it can dramatically affect the signal window. A typical final concentration range of quencher is 10 µM to 100 µM (Figure 10).

4.5. Other Factors

There are several other parameters to relating to dyes and quenchers that require optimization in HTS ion flux assays. These parameters include incubation time, incubation temperature, and the use probenecid in the media. Since many dyes are toxic to cells, incubation time should be kept to a minimum while allowing adequate absorption time. The temperature at which cells are incubated with dye is specific to the dye and will be indicated in the manufacturer's instructions, however this may be altered to increase signal amplitude. In some cases, incubating at 30°C or 37°C can increase (or decrease) the signal amplitude compared with room temperature incubation, depending on the assay. Probenecid is a pan multidrug resistance-associated protein (MDR) blocker and an inhibitor of organic anion transport. Although toxic to cells at high concentrations, it can be added to dyes in low concentrations to increase signal by preventing the active removal of dye from the cytosol. We have found a final concentration of 1mM to 10mM effective in various assays in increasing the signal window (Figure 11).

The parameters suggested in this section are all good starting places for optimizing an ion channel assay for use in an HTS format, however there are other ways to increase signal amplitude and robustness. Changes in instrument settings, such as increasing or decreasing sensitivity, adjusting pinning or pipetting settings, altering times of incubation, temperature of reading, and other factors can have substantial impact on signal robustness and assay performance. Identifying the best parameters from the list above will likely improve signal to basal ratio and Z-scores to prepare an assay for HTS.

5. Preparation of Cells for Automated Electrophysiology

5.1. Overview

The introduction of automated electrophysiological instruments has made possible the screening of large compound sets on ion channels [4]. Numerous platforms are now commercially available with varied features

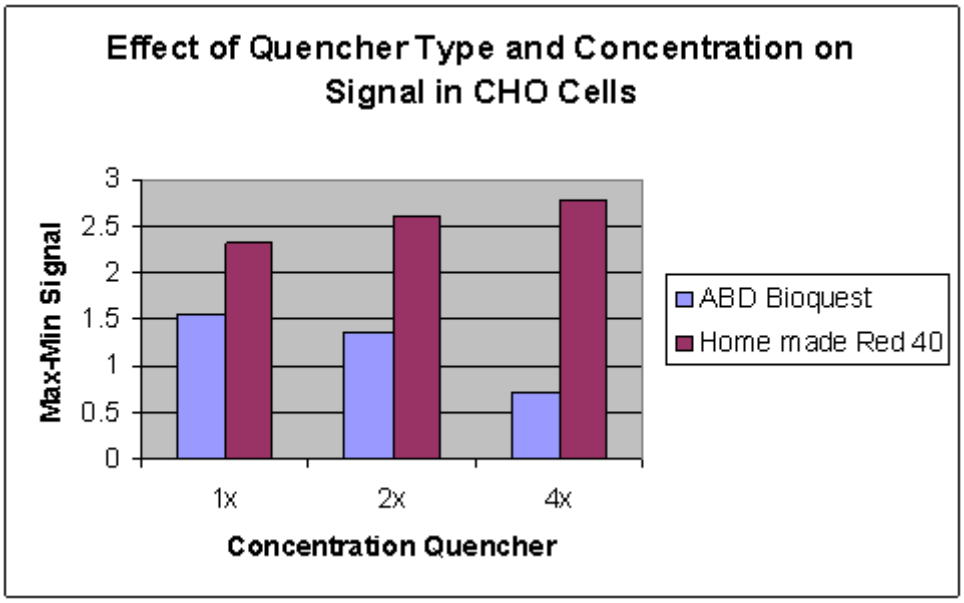


Figure 10 CHO cells were tested with three different concentrations of two different quenchers. The signal window after stimulation of calcium release is shown.

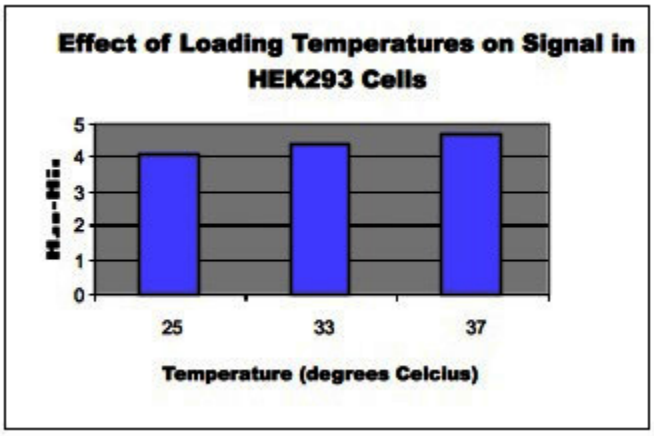


Figure 11 HEK cells were tested after loading dye at room temperature, 33°C, and 37°C.

and potential throughputs. These systems generally employ a planar recording site where a cell suspension is added, then suction is applied to form a seal between the cell(s) and the substrate. Patch clamp whole-cell recording in either the dialyzed or perforated patch recording configuration is achieved and automated fluidics is employed to apply compound(s) to the cells.

Despite the significant advancement in throughput these systems offer relative to manual electrophysiology, a key factor in assay performance is cell preparation. A prerequisite for the creation of a robust automated electrophysiology assay is a method to reproducibly obtain suspensions of healthy, single cells. Given that there is no user-based selection of which cells to record from, as in manual electrophysiology, the need for high viability cell preparations with minimal cell debris is even more important for automated electrophysiology.

This section will describe approaches for obtaining healthy, high density cell suspensions for automated electrophysiology. Since most researchers express ion channels in either Chinese Hamster Ovary (CHO) or Human Embryonic Kidney (HEK) cells, protocols for each will be given.

5.2. Cell line development

Prior to the creation of a cell line for automated electrophysiology, it is advisable to consider if the host cell line performs well on the instrument regarding electrophysiological parameters (seal quality, duration of recordings, etc.). A cell line that performs on one instrument platform may not be optimum on another platform. Ideally, the instrument to be used for the electrophysiology assay is also used to evaluate clones for functional expression [5]. Most devices now have the capability of recording from multiple cell stocks in a single assay, thus allowing the direct comparison of several clones in a single experiment. In this way, clones can be ranked not only for expression but also for performance on the instrument.

5.3. General Detachment Considerations

Detachment of most adherent cell lines from a culture flask to yield suspensions of predominantly single cells usually requires protease treatment. In general, enzyme treatment should be minimized to achieve this aim as cells that have been excessively treated with enzymes tend to be fragile and yield unstable recordings. If over-digestion is suspected, the enzyme solution can be diluted and/or the incubation time shortened. Cell viability following detachment should be very high (>95% as measured by trypan blue exclusion).

One of the major obstacles in obtaining cell suspensions that perform well on automated electrophysiology platforms is cell clumping. Since most recording systems require a high cell density in the final suspension (at least 1 million cells/ml), cell clumping can be significant. If clumping is due to the death of cells, DNAse can be added to the enzyme solution to minimize cells sticking to the free DNA in solution. Another approach is to remove the cell clumps by passing the cell suspension through a small (40-100 uM) nylon mesh filter (BD Biosciences). Keeping the cell suspension in serum-free media prior to use minimizes the formation of cell clumps.

All dissociation protocols require some degree of manual trituration of the cell suspension. As a general rule, trituration should always be gentle with a large bore Pasteur pipette (5 or 10 ml). Introduction of bubbles and frothing should be avoided. Only a few trituration steps should be needed to resuspend a cell pellet. If more are needed, this is an indication that enzyme treatment should be increased.

5.4. CHO cells

5.4.1. Example CHO Protocol

CHO cells are often the host cell line of choice for automated electrophysiology since they divide rapidly and have modest endogenous channel expression. Obtaining suspensions of single CHO cells is usually straightforward. As a general rule, CHO cells perform best when they are detached with a non-tryspin based enzyme treatment such as Detachin™ (Genlantis) or Accutase (Innovative Cell Technologies). Success has also been achieved with non-enzyme dissociation buffers containing EDTA (e.g. Versene).

Protocol:

1. Culture cells to 50-90% confluence in flasks. Typically, a confluent T150 flask can yield up to 40 million cells.
2. Rinse cells 1-2 times with Phosphate-Buffered Saline (PBS) without added calcium and magnesium.
3. Add Detachin™ (4 ml for T150 flask) and incubate for 5-15 minutes at 37°C until detached.
4. Once detached, add serum-free media (such as CHO SFM II; Invitrogen) supplemented with 25 mM HEPES, gently triturate the cells, and count the cell suspension and estimate viability. Viability should be very high (>98%) and the suspension should be mostly single cells. Centrifuge the cell suspension at 800 x g for 3 minutes.

5. Resuspend the cells at the appropriate cell density and place on a room temperature rotator (or the on-board cell handling station, if present on the instrument).
6. Allow the cells to recover for approximately 30 minutes prior to use. Cell suspensions can be kept for up to 4 hours in serum free media and aliquots taken for use.

5.4.2. Example data from CHO cell line

CHO cells were grown in F-12 media in a T-150 flask (Figure 12). Confluence was monitored with an imaging system located inside a standard tissue-culture incubator (IncuCyte™, Essen Bioscience). At near confluency (98%, Figure 12), cells were detached with Detachin™ using the standard protocol. The cell suspension was analyzed for viability (98.9%), average cell diameter (13.4 microns, Figure 13), and average circularity (0.91) with an automated cell viability analyzer (Vi-CELL™, Beckman Coulter). Example images of the cell suspension are shown in Figure 14.

5.5. HEK Cells

5.5.1. Example HEK Protocol

HEK cells typically perform better on automated electrophysiology platforms when a trypsin-based enzyme solution is used. Some HEK cell lines have the tendency to form clumps which will require special precautions.

Protocol:

1. Culture cells to 50-90% confluency in flasks. If clumping is a problem, harvest the cells at lower density (may require pooling cells from more than one flask).
2. Rinse cells 1x with Phosphate-Buffered Saline (PBS) without added calcium and magnesium. Some HEK lines detach quite easily especially at higher confluency, so this step needs to be done quickly.
3. Add 1x (0.05%) trypsin-EDTA solution (4 mL for a T150 flask) and incubate at 37°C for the minimum time required for cell detachment (usually <3 minutes).
4. Add growth media, gently triturate the cells, count the cell suspension, estimate viability, and spin the suspension at 800 x g for 3 minutes. Viability should be very high (>95%) and the suspension should be mostly single cells. If clumping is an issue, quench the enzyme with serum-free media containing soybean trypsin inhibitor.
5. Resuspend the cells at the appropriate cell density in serum-free media (with 25 mM HEPES added) and place on a room temperature rotator (or the on-board cell handling station, if present).
6. Allow the cells to recover for approximately 30 minutes prior to use. Cell suspensions can be kept for up to 4 hours in serum free media.

5.5.2. Example Data from HEK cell line

HEK cells were grown in high glucose DMEM media in a T-150 flask. At approximately 90% confluency, cells were treated with 1x trypsin using the standard protocol. The cell suspension was analyzed for viability (98.8%), average cell diameter (17.0 microns), and average circularity (0.62) with an automated cell viability analyzer (Vi-CELL™, Beckman Coulter). Example images of the cell suspension are shown in Figure 15.

5.6. Growing cells in suspension

Use of non-adherent (or weakly adherent) cell lines alleviates much of the difficulty associated with obtaining high quality cell suspensions. For example, RBL-1 is a basophilic leukemia cell line that grows in suspension that can easily be prepared for automated electrophysiology with a simple centrifugation and wash with recording saline. This line expresses an endogenous inwardly rectifying potassium channel and is quite useful for checking the performance of the recording instrument (including speed of fluid exchange) [6].

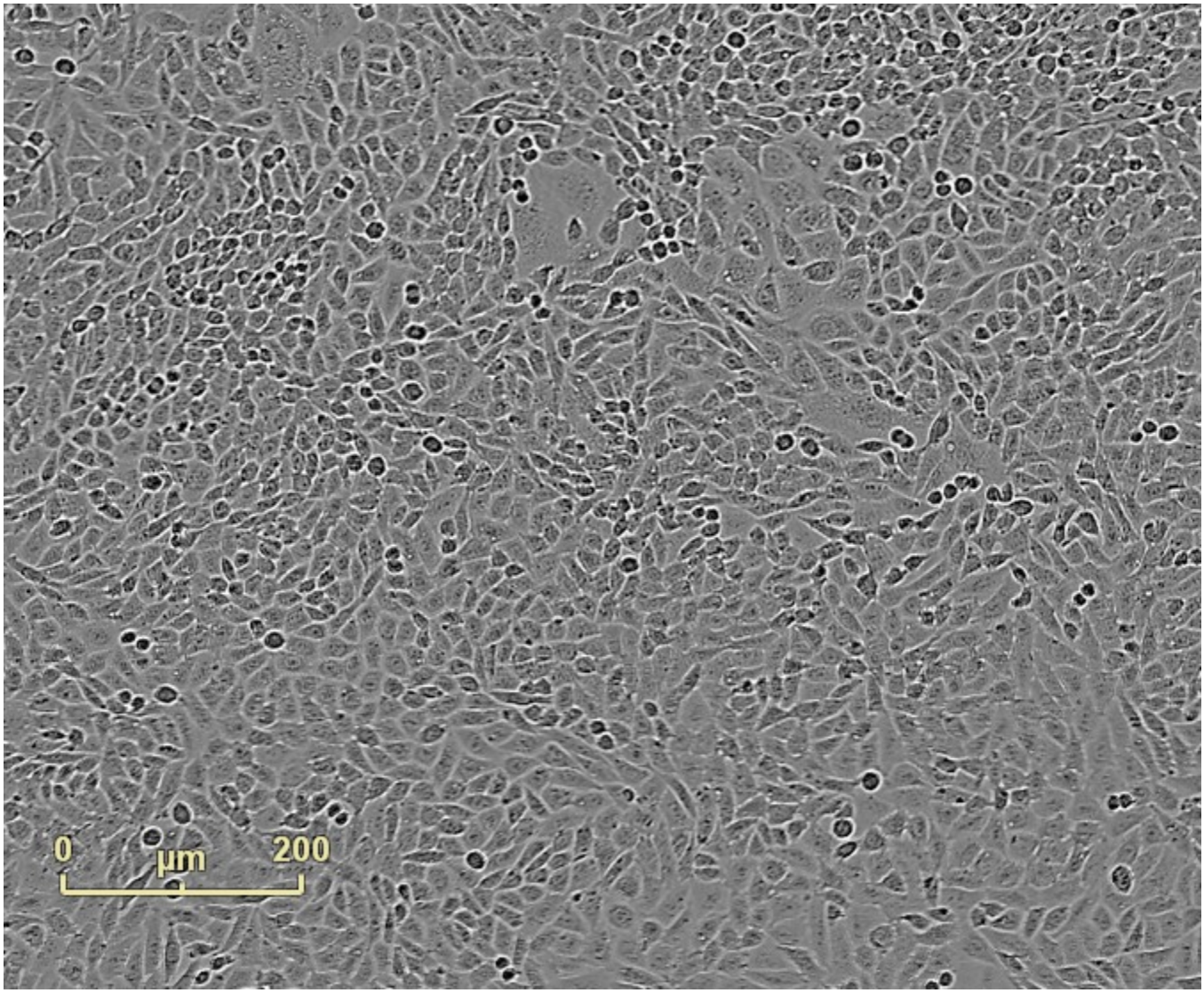


Figure 12: CHO cells grown to near confluency in a T-150 flask.

In cases where preparing a quality suspension of adherent cells is very difficult, an option to consider is converting an adherent cell line to a suspension culture. This is a time-consuming process that involves gradually reducing the amount of serum in the culture media. However, a prerequisite for this approach is that the existing adherent cell line demonstrates stable channel expression over many passages.

5.7. Use of acutely thawed cells

Another approach to obtaining consistent cell suspensions is to freeze ready-to-use vials of cells in liquid nitrogen. In one variation, a single vial containing up to 12 million cells per ml is rapidly thawed and resuspended in serum free media. After a period of at least 30 minutes of recovery, the cell suspension is washed with recording solution and used for recording. In general, such an approach yields lower quality recordings than the standard protocol. This approach has the advantage of allowing quick counterscreening on various channels without the need of keeping the cell line in culture regularly. In another variation, a vial of cell is thawed and cultured for 1-2 days prior to use. This approach gives the cells more time for recovery from the thaw while maintaining the advantage of using cells regularly at a particular passage. Since cells grown on culture for only 1-2 days are less likely to clump upon harvesting, this approach can also be useful for cell lines where single cell suspensions are difficult to obtain.